ornl

ORNL-6879

OAK RIDGE
NATIONAL
LABORATORY

MARTIN MARIETTA

FUSION ENERGY DIVISION

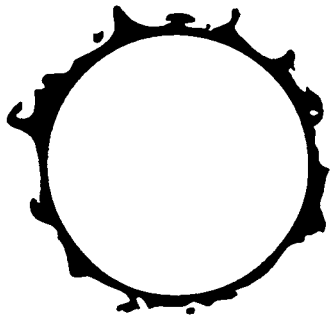

PROGRESS REPORT

Period from
January 1, 1992,
to
December 31, 1994

MANAGED BY
MARTIN MARIETTA ENERGY SYSTEMS, INC.
FOR THE UNITED STATES
DEPARTMENT OF ENERGY

DISTRIBUTION OF THIS DOCUMENT IS UNLIMITED

This report has been reproduced directly from the best available copy.

Available to DOE and DOE contractors from the Office of Scientific and Technical Information, P.O. Box 62, Oak Ridge, TN 37831; prices available from (615) 576-8401, FTS 626-8401.

Available to the public from the National Technical Information Service, U.S. Department of Commerce, 5285 Port Royal Rd., Springfield, VA 22161.

This report was prepared as an account of work sponsored by an agency of the United States Government. Neither the United States Government nor any agency thereof, nor any of their employees, makes any warranty, express or implied, or assumes any legal liability or responsibility for the accuracy, completeness, or usefulness of any information, apparatus, product, or process disclosed, or represents that its use would not infringe privately owned rights. Reference herein to any specific commercial product, process, or service by trade name, trademark, manufacturer, or otherwise, does not necessarily constitute or imply its endorsement, recommendation, or favoring by the United States Government or any agency thereof. The views and opinions of authors expressed herein do not necessarily state or reflect those of the United States Government or any agency thereof.

DISCLAIMER

Portions of this document may be illegible electronic image products. Images are produced from the best available original document.

ORNL-6879
Dist. Category UC-420

FUSION ENERGY DIVISION PROGRESS REPORT

Period from January 1, 1992, to December 31, 1994

J. Sheffield
C. C. Baker
M. J. Saltmarsh
T. E. Shannon

Fusion Energy Division Staff

Date Published: September 1995

Prepared for the Office of Fusion Energy
Budget Activity No. 2 19 00 00 0

Prepared by the
OAK RIDGE NATIONAL LABORATORY
Oak Ridge, Tennessee 37831-6285
managed by
LOCKHEED MARTIN ENERGY SYSTEMS, INC.
for the
U.S. DEPARTMENT OF ENERGY
under contract DE-AC05-84OR21400

MASTER

DISTRIBUTION OF THIS DOCUMENT IS UNLIMITED

Report previously issued in this series are as follows:

ORNL-2693	Period Ending January 31, 1959
ORNL-2802	Period Ending July 31, 1959
ORNL-2926	Period Ending January 31, 1960
ORNL-3011	Period Ending July 31, 1960
ORNL-3104	Period Ending January 31, 1961
ORNL-3239	Period Ending October 31, 1961
ORNL-3315	Period Ending April 30, 1962
ORNL-3392	Period Ending October 31, 1962
ORNL-3472	Period Ending April 30, 1963
ORNL-3564	Period Ending October 31, 1963
ORNL-3652	Period Ending April 30, 1964
ORNL-3760	Period Ending October 31, 1964
ORNL-3836	Period Ending April 30, 1965
ORNL-3908	Period Ending October 31, 1965
ORNL-3989	Period Ending April 30, 1966
ORNL-4063	Period Ending October 31, 1966
ORNL-4150	Period Ending April 30, 1967
ORNL-4238	Period Ending October 31, 1967
ORNL-4401	Period Ending December 31, 1968
ORNL-4545	Period Ending December 31, 1969
ORNL-4688	Period Ending December 31, 1970
ORNL-4793	Period Ending December 31, 1971
ORNL-4896	Period Ending December 31, 1972
ORNL-4982	Period Ending December 31, 1973
ORNL-5053	Period Ending December 31, 1974
ORNL-5154	Period Ending December 31, 1975
ORNL-5275	Period Ending December 31, 1976
ORNL-5405	Period Ending December 31, 1977
ORNL-5549	Period Ending December 31, 1978
ORNL-5645	Period Ending December 31, 1979
ORNL-5674	Period Ending December 31, 1980
ORNL-5843	Period Ending December 31, 1981
ORNL-5919	Period Ending December 31, 1982
ORNL-6015	Period Ending December 31, 1983
ORNL-6111	Period Ending December 31, 1984
ORNL-6234	Period Ending December 31, 1985
ORNL-6332	Period Ending December 31, 1986
ORNL-6452	Period Ending December 31, 1987
ORNL-6528	Period Ending December 31, 1988
ORNL-6624	Period Ending December 31, 1989
ORNL-6714	Period Ending December 31, 1991

CONTENTS

LIST OF FIGURES xi

LIST OF TABLES xv

INTRODUCTION xvii

1. TOROIDAL CONFINEMENT PROGRAM 1
SUMMARY OF ACTIVITIES 3
1.1 THE ATF PROGRAM 5
1.1.1 ATF Research Activities 5
1.1.1.1 Experimental configuration 5
1.1.1.2 Results of long-pulse, dimensionless-parameter scans 6
1.1.1.3 Results for pulse lengths of more than 1 h 6
1.1.1.4 Summary 11
1.1.2 Repair and Upgrades of the ATF Facility 12
1.1.2.1 Helical coil and vacuum vessel repairs 12
1.1.2.2 ECH upgrade 12
1.1.2.3 Helical coil power supply upgrade 13
1.1.3 Stellarator Collaborative Research 13
1.2 EDGE PHYSICS AND PARTICLE CONTROL PROGRAM 14
1.2.1 The Collaborative Advanced Divertor Program on DIII-D 14
1.2.1.1 Helium transport and exhaust studies in enhanced confinement regimes on the DIII-D tokamak 14
1.2.1.2 Particle control and boundary studies on DIII-D 19
1.2.1.3 Global particle confinement time studies on DIII-D 22
1.2.1.4 DIII-D advanced divertor cryopump 23
1.2.2 Development of Particle and Impurity Control Techniques on Tore Supra 23
1.2.2.1 Particle control studies 23
1.2.2.2 Impurity studies 30
1.2.2.3 Detailed modeling of impurity and power fluxes 31
1.2.2.4 Rf–plasma edge interactions 34
1.2.3 Helium Transport and Exhaust Studies on the TEXTOR Tokamak 37
1.3 CONFINEMENT PHYSICS PROGRAM 39
1.3.1 The Role of Shaping in Achieving High Performance in DIII-D 39
1.3.2 PBX-M Collaboration 42
1.3.2.1 Effects of LHCD wave spectrum on runaway electron production 43

1.3.2.2 Characterization of plasma parameters for shaped PBX-M discharges 44
1.3.2.3 Equilibrium reconstruction 44
1.3.2.4 Spectroscopic studies 45
1.3.2.5 Analysis of Mirnov signals 47
1.3.2.6 AM reflectometry on PBX-M 48
1.3.2.7 Wavelet analysis of ELM signals from the PBX-M tokamak 51
1.3.3 Collaboration Between ORNL and TFTR 53
1.3.3.1 Achievements and status 54
1.3.3.2 Physics accomplishments 54
1.3.4 Feedback Control and Stabilization Experiments on TEXT 58
1.3.5 Long-Pulse Particle Control Issues in TPX 58
1.3.5.1 Wall-conditioning options for particle control 58
1.3.5.2 Overnight wall conditioning 60
1.3.5.3 Wall conditioning between discharges 60
1.3.5.4 Continuous wall conditioning during discharge 61
1.4 PHYSICS ASSESSMENT OF STELLARATORS AS FUSION POWER PLANTS 62
REFERENCES 64

2. ATOMIC PHYSICS AND PLASMA DIAGNOSTICS DEVELOPMENT 71
SUMMARY OF ACTIVITIES 73
2.1 EXPERIMENTAL ATOMIC COLLISIONS 74
2.1.1 Merged-Beams Measurements of Electron-Impact Excitation of Multicharged Ions 74
2.1.2 Crossed-Beams Measurements of Electron-Impact Ionization of Ions 75
2.1.3 Multicharged-Ion Surface Interactions 76
2.1.4 Very Low-Energy Collisions of Multicharged Ions in Merged Beams 78
2.1.5 ECR Multicharged-Ion Research Facility Upgrade Project 79
2.2 THEORETICAL ATOMIC PHYSICS FOR FUSION 80
2.2.1 Electron-Impact Excitation of Ions 80
2.2.2 Dielectronic Recombination 81
2.2.3 Electron-Impact Ionization of Ions 82
2.2.4 Statistical Quasi-Quantal Treatment of Ion-Atom Collisions 83
2.2.5 Heavy-Particle Elastic Scattering 83
2.3 CFADC 84
2.3.1 The Bibliographic Database 84
2.3.2 Data Center Network 84
2.3.3 Data Compilations 85
2.3.4 Internet-Accessible Databases 86
2.4 DIAGNOSTICS OF HIGH-TEMPERATURE PLASMAS 86

2.4.1 IR Polarimeter for Measurement of Plasma-Current Profile in the Alcator C-Mod Tokamak 86
2.4.2 CO_2 Laser Thomson Scattering Ion-Tail Diagnostic for Alcator C-Mod 90
REFERENCES 94

3. FUSION THEORY AND COMPUTING 99
SUMMARY OF ACTIVITIES 101
3.1 TURBULENCE AND TRANSPORT 101
3.1.1 Improved Toroidal Confinement Regimes 101
3.1.1.1 Interaction of flows and fluctuations 101
3.1.1.2 Phase-transition model of the L-H transition 103
3.1.1.3 Validation of phase-transition model of the L-H transition by nonlinear plasma turbulence calculations 104
3.1.1.4 Core fluctuations 105
3.1.1.5 Edge fluctuations 108
3.1.2 Advanced Toroidal Confinement Scenarios 108
3.1.2.1 Energetic particles confinement 108
3.1.2.2 MHD for advanced tokamak configurations 111
3.1.3 High-Performance Computing 111
3.1.3.1 Parallel plasma fluid turbulence calculations 111
3.1.3.2 Scientific visualization 112
3.2 EDGE PHYSICS AND PLASMA MODELING 113
3.2.1 Edge Physics 113
3.2.1.1 Reduced-impurity-flow modeling of the scrape-off plasma 113
3.2.1.2 Active divertor model 113
3.2.1.3 Influence of limiters and divertors on edge turbulence 113
3.2.2 Plasma Modeling 114
3.2.2.1 L-H bifurcation theory 114
3.2.2.2 Advanced tokamaks 115
3.2.2.3 Equilibrium reconstruction of the q profile in tokamaks 116
3.2.2.4 Confinement scaling in stellarators 116
3.2.2.5 New theoretical methods: wavelet analysis 116
3.3 RF HEATING AND CURRENT DRIVE 116
3.3.1 Full-Wave Modeling of ICRF Heating and Current Drive 117
3.3.1.1 Full-wave ICRF modeling of D-T plasmas in TFTR 117
3.3.1.2 Full-wave ICRF modeling of electron heating and current drive by mode-converted slow waves in tokamaks 118
3.3.1.3 Fast-wave current-drive modeling using the combined RANT3D and PICES code 119
3.3.1.4 Full wave modeling of ICRF heating in stellarators 119
3.3.1.5 Full-wave modeling of power deposition in high-density inductively coupled plasma tools for semiconductor processing 119

3.3.1.6 Orbit-consistent plasma simulations 120
3.3.1.7 One-dimensional global and local solution for ICRF heating 120
3.3.1.8 Effect of Alfvén resonance in low-frequency ITER current drive 120
3.3.2 ICRF Antenna Studies 120
3.3.2.1 Three-dimensional physics of ICRF launchers for fusion devices 121
3.3.2.2 Phased array antennas for fast-wave current drive and heating 121
3.3.2.3 Three-dimensional modeling of rf current-drive arrays 122
3.3.3 Basic Rf Physics Issues 122
3.3.3.1 Fast-wave poloidal flow generation in a plasma 122
3.3.3.2 Parallel forces induced by waves in ICRF 122
3.3.3.3 Spurious modes for finite Larmor radius models in ICRF 123
3.3.3.4 Numerical solution of a tunneling equation 123
3.3.3.5 Minority ion sawtooth model in TRANSP 123
3.3.3.6 Rf/kinetic studies and its application on helium ash control 123
3.4 COMPUTING AND OPERATIONS 124
3.4.1 USC 124
3.4.2 Workstation Support 124
3.4.3 Networks 125
3.4.4 PC Support 125
3.4.5 Experimental Data Acquisition 125
REFERENCES 125

4. PLASMA TECHNOLOGY 129
SUMMARY OF ACTIVITIES 131
4.1 PLASMA FUELING PROGRAM 132
4.1.1 Pellet Injector Development 133
4.1.1.1 Centrifuge injector 133
4.1.1.2 Pneumatic injectors 136
4.1.1.3 Electron-beam rocket pellet injector 142
4.1.1.4 TPOP-II experiment 145
4.1.1.5 Steady-state extruder feed system 148
4.1.2 Pellet Injector Applications 148
4.1.2.1 TFTR tritium-compatible, four-shot pneumatic injector 148
4.1.2.2 Tore Supra centrifuge injector 151
4.1.2.3 DIII-D three-barrel, repeating pneumatic injector 151
4.2 RF TECHNOLOGY 155
4.2.1 Basic Development 155
4.2.1.1 Folded waveguide 155

4.2.1.2 Advanced launcher development 156
4.2.1.3 Tuning, matching, phase control, and arc detection 157
4.2.1.4 Microwave reflectometer 157
4.2.1.5 Antenna field measurements 157
4.2.1.6 Faraday shield studies 158
4.2.2 Rf Projects 160
4.2.2.1 Tore Supra 160
4.2.2.2 DIII-D 160
4.2.2.3 JET 163
4.2.3 Rf Modeling 164
4.2.3.1 Electrical representation of antennas 164
4.2.3.2 Antenna field calculations 164
4.2.3.3 Three-dimensional electromagnetic analysis 166
REFERENCES 166

5. INTERNATIONAL THERMONUCLEAR EXPERIMENTAL REACTOR 169
SUMMARY OF ACTIVITIES 171
5.1 ITER HOME TEAM MANAGEMENT 172
5.1.1 U.S. Home Team Management Activities 172
5.1.2 Quality Assurance Plan 173
5.2 ITER JCT SUPPORT 173
5.3 ITER DESIGN AND DEVELOPMENT 173
5.3.1 Physics Studies 173
5.3.1.1 Physics design of ITER variants 173
5.3.1.2 MHD stability 177
5.3.1.3 Pumping and fueling requirements 177
5.3.2 Engineering Design 178
5.3.2.1 ITER vacuum vessel design activities 178
5.3.2.2 Disruption loads 178
5.3.2.3 Thermal/mechanical analysis of the ITER divertor vane 180
5.3.2.4 ITER PF coil optimization 182
5.3.2.5 First-wall design modeling 184
5.3.2.6 ITER systems code analysis 185
5.3.3 RH 186
5.3.3.1 Remote-maintenance design manual 186
5.3.3.2 Remote cutting and welding 187
5.3.3.3 RH-compatible electrical connectors 187
5.3.3.4 In-vessel metrology system 187
5.3.4 Vacuum Vessel 188
5.3.4.1 ITER vacuum vessel design activities 188
5.3.4.2 ITER vacuum vessel R&D activities 189
5.3.5 Magnet R&D 189
5.3.6 ITER Fueling 190
5.3.6.1 Fueling system design for ITER-CDA 190

5.3.6.2 Fuel source isotopic tailoring 190
5.3.7 ITER Rf Systems 193
5.3.7.1 Rf insulator radiation tests 193
5.3.7.2 Antenna survivability study 194
5.3.7.3 Assessment of rf sheaths and impurity generation with rf 194
5.3.8 Innovative Materials for Divertor Applications 199
5.3.9 14-MeV Neutron Source 199
REFERENCES 200

6. ADVANCED TOROIDAL SYSTEMS 201
SUMMARY OF ACTIVITIES 203
6.1 FUSION ENERGY ECONOMIC ASSESSMENTS 203
6.2 ST RESEARCH PROGRAM 204
6.2.1 ST Research 204
6.2.1.1 ST experimental research collaboration 205
6.2.1.2 ST power reactors 206
6.2.2 VNS 207
6.3 TPX COLLABORATION 208
6.3.1 Remote Maintenance 208
6.3.1.1 In-vessel vehicles 209
6.3.1.2 Transfer system 210
6.3.1.3 Mock-ups and testing 211
6.3.2 Shielding 211
6.3.3 Vacuum Pumping 213
6.3.4 Rf Systems 213
6.3.4.1 LH system 214
6.3.4.2 Ion cyclotron system 214
6.3.5 TPX Physics 217
6.3.5.1 Rf physics 217
6.3.5.2 TSC disruption simulations for the TPX β_N-l_i design space 218
REFERENCES 225

7. FUSION MATERIAL RESEARCH 227
SUMMARY OF ACTIVITIES 229
7.1 NEUTRON INTERACTIVE MATERIALS 229
7.1.1 Reduced Activation 230
7.1.2 Silicon Carbide 230
7.1.3 Vanadium Alloys 231
7.2 ITER NEUTRON-INTERACTIVE MATERIALS 231
7.2.1 Austenitic Steels 232
7.2.2 Ceramic Insulator 232
7.2.3 Carbon/Carbon Composite Materials and Beryllium 233
7.2.4 Copper Alloy 233

7.3 OTHER MATERIALS FOR ITER 234
7.4 ORNL/JAERI COLLABORATION IN HFIR 234
7.5 IFMIF 235

8. RADIATION TRANSPORT 237
SUMMARY OF ACTIVITIES 239
8.1 RADIATION SHIELDING INFORMATION CENTER 239
8.2 NEUTRON CROSS SECTION 240
8.2.1 Cross-Section Evaluation 240
8.2.2 Processing Evaluated Data into Multigroup Cross Sections 241
REFERENCES 242

9. TECHNOLOGY AND SCIENCE APPLICATIONS 243
SUMMARY OF ACTIVITIES 245
9.1 PLASMA FUELING TECHNOLOGY APPLICATIONS 245
9.1.1 Argon Pellet Cleaning 246
9.1.2 CO_2 Paint Stripping—U.S. Air Force 246
9.1.3 CO_2 Pellet Blaster Demonstration 246
9.2 PLASMA HEATING TECHNOLOGY APPLICATIONS 248
9.2.1 Microwave Decontamination Processing 248
9.2.1.1 Concrete decontamination 248
9.2.1.2 Hot polymer CRADA 248
9.2.1.3 In-drum waste handling 248
9.2.2 Rf/Microwave Materials Processing 249
9.2.2.1 Alumina postprocessing 249
9.2.2.2 Alumina green-body sintering 249
9.2.2.3 Silicon carbide processing 249
9.2.2.4 Electric-field effect studies 250
9.2.3 Plasma and Ion-Beam Material Processing 250
9.2.3.1 Plasma cleaning 250
9.2.3.2 Beam/plasma ion implantation 251
9.2.4 LDRD Advanced Combustion 252
9.3 MAGNETICS AND SUPERCONDUCTIVITY TECHNOLOGY APPLICATIONS 252
9.3.1 SPI Projects 252
9.3.2 SPP 253
9.4 PLASMA THEORY APPLICATIONS 255
9.4.1 Modeling of Plasma Reactors 255
9.4.2 Computer-Aided Design of Plasma Reactors 256
9.4.3 Modeling of Plasma-Based Materials-Processing LDRD 257
9.5 PLASMA CONFINEMENT APPLICATIONS 258
9.5.1 Advanced Metallization 258
9.5.2 Analysis and Diagnostics for Plasma Synthesis 259
9.6 FUSION WASTE TRANSMUTATION 259
REFERENCES 259

10. MANAGEMENT SERVICES, ES&H ACTIVITIES, AND QA 261
SUMMARY OF ACTIVITIES 263
10.1 MANAGEMENT SERVICES 263
10.1.1 General Administration Services 263
10.1.1.1 Personnel 263
10.1.1.2 Training and development 264
10.1.1.3 Procurement 265
10.1.1.4 International agreement and collaboration 265
10.1.2 Engineering Services 265
10.1.3 Financial Services 267
10.1.4 Library Services 269
10.1.5 Publications Services 269
10.2 ES&H ACTIVITIES 269
10.3 QUALITY ASSURANCE 270

APPENDIX 1. FED PUBLICATIONS AND PRESENTATIONS 271

APPENDIX 2. ACRONYMS AND ABBREVIATIONS 337

APPENDIX 3. FED ORGANIZATION CHART 343

LIST OF FIGURES

Figure		
1.1	Variation of normalized gyroradius (ρ_*) with constant collisionality (ν_*) and β in a single ATF helium discharge	7
1.2	Plasma parameters as function of time for ATF shot with pulse length of 4667 s, or ~1 h, 17 min	8
1.3	Electron temperature, density, and input power for long-pulse hydrogen discharge ($B_0 = 0.51$ T) with T_e of 100 to 200 eV	9
1.4	Partial pressure of three gases in vacuum vessel during ATF shot ($B_0 = 0.51$ T)	10
1.5	Partial pressures of four gases in ATF vacuum vessel as function of time since last vacuum opening	10
1.6	Comparison of measured helium density and electron density profiles	15
1.7	Comparison of D_{He} and χ_{eff} in L-mode and H-mode at same plasma current (1.6 MA) and NB power (~2.0 MW)	16
1.8	Comparison of D_{He} and χ_{eff} in ELMing H-mode at two different power levels (6 MW and 12 MW)	17
1.9	Temporal evolution of helium density (points) with argon frost pumping compared with standard MIST calculation where $R_{He} = 0.95$	18
1.10	Configuration of the cryopump inside the baffle chamber	19
1.11	Cryopump particle exhaust rate vs separatrix-ring gap	20
1.12	Peak heat flux and peak particle flux as function of line-average density	21
1.13	Particle and energy confinement time temporal evolution during ELM-free H-mode discharge	22
1.14	Effect of pump limiter exhaust in shots TS 10449 and 10450	24
1.15	Distribution of the charge-exchange flux around the horizontal pump limiter in Tore Supra	25
1.16	Ionization profile in the SOL of a pump-limiter discharge in Tore Supra	26
1.17	Simplified particle flow between plasma core, wall, and pump limiter of Tore Supra	27
1.18	Particle balance in Tore Supra for discharge 10450	28
1.19	Series of discharges normalized to density at $t = 5$ s (termination of gas puff)	29
1.20	Typical spectrum obtained in throat of pump limiter	30
1.21	Langmuir probe measurements of density and floating potential in plasma edge	35
1.22	Time history of C(III) emission from Q1 antenna and IR hot spot temperatures on Q5 antenna	36
1.23	Profile of C(III) emission across Tore Supra Q5 ICRF antenna	37
1.24	Helium density profile measured at $t = 1.5$ s with 2-D OMA on TEXTOR with full ALT-II pumping	38

1.25 Three-dimensional profile of helium density with full pumping 39
1.26 Experimental shapes and maximum $\beta \cdot \tau$ vs geometric quantity $(S^2R^2/1 + \kappa^2)$ 41
1.27 Comparison of electron temperature profiles for shapes B and D 42
1.28 Profiles of radiated power with 410-kW IBW heating introduced into H-mode plasma at 450 ms 46
1.29 Evolution of spectral line radiation during IBW heating in H-mode plasma 47
1.30 Toroidal mode numbers, PBX-M shot 310724 48
1.31 Schematic of the PBX-M AM reflectometer microwave electronics circuit 49
1.32 (*a*) AM reflectometer phase signal after subtraction of calibration phase; (*b*) reconstructed density profile plotted with Thomson scattering profile (crosses with error bars) for same time interval 50
1.33 Density profiles measured before and after L-H transition 51
1.34 Density profiles measured with and without IBW power 52
1.35 D_α emission and wavelet decomposition 53
1.36 Measured electron power deposition profile and total integrated power profile for DEH in TFTR 55
1.37 Electron and ion power deposition profiles calculated from PICES code 56
1.38 Variations of D_α, $\sim B_\theta$, and τ_E for H-mode that showed transient beam turn on at 3.19 s 57
1.39 Effects of feedback on frequency spectrum of potential fluctuations 59
1.40 Helium charge-exchange flux to inner wall as function of poloidal angle 61
1.41 Average energy of charge-exchange neutrals incident on inner wall 61
1.42 Oblique view of MATF coil set with modules not up-and-down symmetric 63
2.1 Illustration of electro-optic polarization-modulation technique used in CO_2 laser polarimeter on Alcator C-Mod 88
2.2 Frequency spectra of (*a*) modulated signal at 800 kHz with $\theta_b = 45°$ and (*b*) heterodyne beat signal at 40 MHz and sideband frequencies of ±800 kHz with $\theta_b = 0°$ 90
2.3 Schematic of scattering system showing paths of source laser and receiver beams 92
2.4 Expected contributions to scattered power for Alcator C-Mod as function of scattering angle for ion tail and electrons at frequency shift of 6.92 GHz from laser line 93
2.5 Expected scattered power as function of frequency shift from laser line center for Alcator C-Mod 93
2.6 Expected scattered power for ITER as function of frequency shift from laser line center 94
3.1 Fluctuation suppression by average poloidal shear flow in the case of negative compressibility turbulence 106

3.2 Scientific visualization of linear (top) and saturated nonlinear (bottom) TAE mode structure obtained from toroidal gyrofluid calculations with TFTR-like parameters 110
4.1 Schematic of Zamboni fabrication deuterium ice (developed at ORNL to supply ice for centrifuge injectors) 134
4.2 Details of pellet fabrication device and high-speed rotating arbor for ORNL centrifuge pellet injector 135
4.3 Schematic of ORNL repeating pneumatic pellet injector 137
4.4 Photographs of 150-pellet sequence from repeating pneumatic pellet injector (1.8-mm bore) 138
4.5 Schematic of ORNL repeating pneumatic injector test facility with ENEA Frascati two-stage light-gas gun 140
4.6 Test configuration of ORNL repeating pneumatic injector with ENEA Frascati two-stage gun 141
4.7 Schematic of Frascati repeating two-stage light-gas gun 141
4.8 Experimental data from repeating two-stage pneumatic injector (2.7-mm bore) 143
4.9 Pellet acceleration, calculated from increment of pellet velocity and applied beam pulse length, as function of electron-beam power 144
4.10 Measured and calculated burn velocities as function of beam current for beam energies of (*a*) 4 keV and (*b*) 10 keV 145
4.11 Photograph of 7.4-mm-diam by 11-mm-long deuterium pellet formed and accelerated with TPOP-II repeating pneumatic injector 146
4.12 Schematic of TPOP-II pellet injector 147
4.13 Schematic of steady-state extruder feed system under development at ORNL 149
4.14 Photograph of tritium-compatible, four-shot pneumatic pellet injector system on TFTR 150
4.15 TFTR ICRH PEP and non-PEP discharges with different plasma currents and heating schemes 152
4.16 Schematic of three-barrel, repeating pneumatic injector 153
4.17 Elevation-view schematic of three-barrel injector installation on DIII-D 154
4.18 Technique for coupling power to quarter-wavelength folded waveguide from rear 155
4.19 Measurements of toroidal component magnitude of rf magnetic field generated by JET A2 flatbed antenna 159
4.20 Magnitude of rf magnetic field calculated using ARGUS code to model JET A2 flatbed antenna 159
4.21 Long-pulse antenna for fast-wave current drive on DIII-D 162
4.22 Comparison of measurements and modeling of JET A2 flatbed antenna 165
5.1 Sensitivity of ITER EDA (at 1500 MW) and CDA (at 1 MW/m^2) performance to helium (and beryllium) content 175
5.2 ITER EDA ignition capability with (*a*) ITER89-P and (*b*) ITER89-OL L-mode scalings as function of plasma current at $P_{fus} = 1500$ MW (for $n_{He}/n_e = 0$–20%, $n_{Be}/n_e = 1$–5%) 175

5.3 Fusion power operational space (minimum and maximum) for sustained ignition as determined by confinement model, helium (beryllium) content, and beta limit 176
5.4 Partially assembled vacuum vessel chamber 179
5.5 Cross section of vacuum vessel chamber design 180
5.6 Plasma disruption effects on in-vessel blanket/shield modules 181
5.7 Reference configuration for the ITER divertor 182
5.8 Cross section of vane structure 183
5.9 ITER EDA Outline Design PF coil system and one of the operational flexibility equilibria 184
5.10 Optimal ITER EDA PF coil system and one of the operational flexibility equilibria 185
5.11 Direct costs of 1993 ITER-like designs vs size 186
5.12 Metrology probe deployment scheme 188
5.13 Tritium fraction on axis and at plasma edge as function of deuterium gas fueling level 191
5.14 Tritium fraction on axis and at plasma edge as function of normalized pellet penetration 192
5.15 Loss tangent of ceramic insulators during pulsed neutron irradiation 193
5.16 Vaporization depth and melt-layer thickness for disruptions with beryllium, carbon, or tungsten armor 195
5.17 Voltage amplitude distribution on ends of Faraday shield tubes along poloidal direction of JET A2 antenna 197
5.18 Voltage phase distribution on ends of Faraday shield tubes along poloidal direction of JET A2 antenna 198
6.1 Pictorial view of TPX tokamak 209
6.2 TPX track-mounted in-vessel maintenance system 210
6.3 TPX shielding system 212
6.4 TPX lower-hybrid launcher 215
6.5 TPX ion cyclotron launcher 216
6.6 TSC filaments for TPX disruption tour cases 219
6.7 Evolution of toroidal plasma current for TSC VDE simulations with $q_{crit} = 1.3$ for TPX high-ß, high-l_i design point 221
6.8 Overlay of TPX main plasma boundaries for current-decay phase of TSC simulation 940925C 222
6.9 Extreme pressures on the three TPX divertor pieces for 13 TSC disruption tour simulations for TPX 224
6.10 Extreme pressures on TPX stabilizers, vessel, and inner toroidal limiter for 13 TSC disruption tour simulations for TPX 225
9.1 Centrifugal turbine pellet acceleration device 247
9.2 Coil Test Facility design 254
9.3 Alternating-current loss measurement setup 255
9.4 HTS magnet 256
10.1 Fusion Energy Division professional staff by discipline 264
10.2 Fusion Program expense funding (budget outlay) 267

LIST OF TABLES

Table		
1.1	ATF parameters for five different operating regimes	11
1.2	Core impurity flux comparison	33
1.3	Power plant parameters obtained using the same assumptions	64
2.1	Design considerations for two-color interferometer/polarimeter system	87
4.1	Main parameters of the ORNL/Frascati injector	142
5.1	Summary of WHIST code runs	191
6.1	TSC group numbers, wire numbers, and constraints	220
6.2	Initial TPX plasma parameters for $\beta_N = 5$, $l_i = 0.4$	220
6.3	Initial plasma parameters, halo currents, and plasma current decay rates for TSC disruption simulations for TPX	223
6.4	Extreme pressures (kPa) for TSC disruption simulations for TPX	223
9.1	150 MVA Partial-helical stator design	253
10.1	Fusion Program expense funding (in thousands of dollars)—budget outlay	268

INTRODUCTION

This progress report for the Oak Ridge National Laboratory (ORNL) Fusion Energy Division (FED) covers the 3 years from January 1992 to December 1994. The report covers all elements of the ORNL Fusion Program, including those implemented outside the division. Non-fusion work within FED, much of which is based on the application of fusion technologies and techniques, is also discussed.

The ORNL Fusion Program includes research and development in most areas of magnetic fusion research. The program is directed toward the development of fusion as an energy source and is a strong and vital component of both the U.S. and international fusion efforts.

The research discussed in this report includes

- experimental and theoretical research on magnetic confinement concepts,
- engineering and physics of existing and planned devices,
- development and testing of plasma diagnostic tools and techniques,
- assembly and distribution of databases on atomic physics and radiation effects,
- development and testing of technologies for heating and fueling fusion plasmas, and
- development and testing of materials for fusion devices.

The activities involving the use of fusion technologies and expertise for non-fusion applications ranged from semiconductor manufacturing to environmental management.

Over the period covered by this report the character of the division's work has altered. The major focus for experimental research in the toroidal confinement area shifted from the Advanced Toroidal Facility at ORNL to collaborative efforts at facilities both in the U.S. and elsewhere in the world. Similarly, in the technology and design areas there was increasing emphasis on the national Tokamak Physics Experiment (TPX) project at the Princeton Plasma Physics Laboratory and the International Thermonuclear Experimental Reactor (ITER) Engineering Design Activity. Much of the collaborative work centered on radio-frequency (rf) heating and current drive and on edge physics and particle control, reflecting ORNL's technological, theoretical, and experimental strengths in these areas.

Although most of FED's research relates to the tokamak, a small and vigorous stellarator program has continued, relying heavily on international collaboration. In addition, support for the Spherical Tokamak (ST) concept has helped initiate several ST experimental programs around the world.

In the materials area, an international conceptual design activity for a Fusion Materials Irradiation Facility (FMIF) was started, with ORNL leading the U.S. effort, supported by Los Alamos National Laboratory, Argonne National Laboratory, and an industrial consortium.

By the end of the report period, ORNL expertise was being applied at essentially all of the major tokamak and stellarator facilities in the U.S. and abroad. Innovative confinement concepts based on ORNL work were being tested or planned at a number of places around the world, and ORNL staff members were playing a significant role in the design and planning for the next generation of major experimental facilities (i.e., TPX, ITER and FMIF). Thus the laboratory is well prepared to contribute to the future of fusion research and development.

1

TOROIDAL CONFINEMENT ACTIVITIES

P. K. Mioduszewski, Head, Confinement Program
R. J. Colchin, Head, Confinement Section

D. L Akers[1]
D. B. Batchelor[2]
L. R. Baylor[3]
R. D. Benson[4]
T. S. Bigelow[3]
C. E. Bush
B. A. Carreras[5]
I. Collazo[6]
R. A. Dory[7]
J. L. Dunlap[8]
G. R. Dyer[7]
A. C. England
D. T. Fehling[2]
C. A. Flanagan[8]
R. C. Goldfinger[9]
M. J. Gouge[3]
D. E. Greenwood[10]
K. Gulec[11]
G. R. Hanson[12]
J. H. Harris
G. R. Haste[3]
G. H. Henkel
D. L. Hillis
S. P. Hirshman[2]
D. J. Hoffman[3]
J. T. Hogan[2]
R. C. Isler
E. F. Jaeger[2]
T. C. Jernigan
C. C. Klepper
E. A. Lazarus
D. K. Lee[9]
J. F. Lyon
C. H. Ma[13]
R. Maingi[14]
M. M. Menon[15]
S. L. Milora[3]
M. Murakami
G. H. Neilson
D. R. Overbey[2]
L. W. Owen[9]
C. L. Pitner[16]
A. P. Post-Zwicker[17]
A. L. Qualls[18]
D. A. Rasmussen[3]
J. A. Rome[2]
C. R. Schaich[3]
J. E. Simpkins[7]
C. E. Thomas, Jr.[12]
S. J. Tobin[17]
T. Uckan
M. R. Wade
J. A. White[4]
J. B. Wilgen
C. T. Wilson[4]
J. L. Yarber[19]

---

1. Section secretary.
2. Plasma Theory Section.
3. Plasma Technology Section.
4. Engineering Division.
5. ORNL Corporate Fellow.
6. Georgia Institute of Technology, Atlanta.
7. Retired.
8. Part-time.
9. Computational Physics and Engineering Division.
10. Computing and Telecommunications Services.
11. University of Tennessee, Knoxville.
12. Instrumentation and Controls Division.
13. Physics Division.
14. Oak Ridge Institute for Science and Education.
15. Robotics Division.
16. Secretary.
17. Oak Ridge Associated Universities.
18. Engineering Technology Division.
19. Chemical Technology Division.

1. TOROIDAL CONFINEMENT ACTIVITIES

SUMMARY OF ACTIVITIES

In this reporting period the activities in the Toroidal Confinement Section were focused on the final Advanced Toroidal Facility (ATF) campaign, before it was mothballed; on the continuation of existing tokamak collaborations on DIII-D, the Tokamak Fusion Test Reactor (TFTR), Tore Supra, the Princeton Beta Experiment—Modified (PBX-M), the Torus Experiment for Technology Oriented Research (TEXTOR), and the Texas Experimental Tokamak (TEXT), and on a stellarator power plant assessment.

In late FY 1992, work toward restarting the ATF facility began. The efforts were concentrated in three major areas: the repair of the two helical coil segments damaged in an arc-over in 1991, the addition of a 28-GHz gyrotron for steady-state operation at 0.5 T, and an upgrade of the helical field power supply for steady-state operation at up to 0.63 T. ATF resumed operation in April 1994. Since one of the original goals of the ATF program was to demonstrate steady-state operation, it was felt that it was important to address this issue before the final shutdown of the device. In addition, dimensionless parameter scaling experiments were performed, taking advantage of the ATF long-pulse capability. In the final experiments two ATF pulses with pulse lengths in excess of 1 h were obtained. The longest ATF shot, which had a pulse length of 4667 s, or about 1 h, 17 min, was a helium discharge heated by a 28-GHz gyrotron. The electron-cyclotron heating power, 70 kW, represented the maximum power level allowable in ATF in the steady-state limit. Gas feedback control was used to maintain a constant electron line density ($\bar{n}_e \approx 3 \times 10^{18}$ m^{-3}). Impurity light intensity [C(II) line] decreased during the early portion of the discharge before leveling off at a low level. ATF is now mothballed pending funding for its restart.

The Edge Physics and Particle Control program is directed at the development of steady-state particle control. This includes (1) studies of helium transport and exhaust; (2) control of the working gas by wall pumping, pumped divertors or limiters; (3) studies of impurity evolution and transport; (4) interactions of radio frequency (rf) antennas with the edge plasma; and (5) effects of particle control on plasma performance. During the reporting period, helium transport studies were carried out for various confinement regimes on DIII-D. A figure of merit for adequate helium exhaust is the ratio τ^*_{He}/τ_E, which needs to be between 7 and 15 for successful exhaust in a reactor, and was found to be ~8 in edge-localized mode H-mode discharges in DIII-D. The ORNL group was also involved in the design and optimization of a divertor cryopump in DIII-D. This pump provides toroidally symmetric pumping at a rate of 30,000–40,000 L/s for D_2 in the pressure range of 1–4 mTorr. The divertor pump has been used for density control in H-mode discharges. The resulting changes in the divertor parameters were measured and analyzed. With a layer of argon frost, this pump was also successfully used to exhaust helium. To better understand correlations between energy and particle confinement, global particle confinement studies were initiated. Determining the ratio of τ_p/τ_E in various confinement modes is the primary result of this study. So far, values of this ratio have been found to be 2 for L-mode and 4 for H-mode discharges.

Particle control experiments on Tore Supra have clearly shown that external exhaust primarily controls the wall inventory, which, in turn, controls the plasma inventory via the changing recycling coefficient. Modeling has shown that charge-exchange fluxes, penetrating the scrape-off layer (SOL), generate mostly thermal molecules at the wall, which are largely ionized within the SOL and can subsequently be exhausted. This mechanism provides a direct path between the wall and the exhaust channel. The phase III pump limiter module (built by Sandia Laboratories, Albuquerque) was commissioned and tested. It showed excellent performance in power and particle handling, until it was damaged by runaway electrons and removed from the tokamak. To overcome the leading-edge problem of pumped limiters, new concepts such as the "vented limiter" have been tried out. For hydrogen plasmas, the pressure build-up achieved in the pumping plenum was close to that of standard pump limiters. For a more complete evaluation of particle sources and sinks, impurity studies have been included. Spectroscopic measurements inside the pump limiter throat indicated chemical sputtering as a source of hydrocarbons such as CH_4. An optical system was designed for impurity surveys of in-vessel components. The impurity production due to hydrogenic and carbon self-sputtering has been calculated and used as a source for the ORNL three-dimensional impurity transport Monte Carlo code, BBQ. The expected emission profiles of C(II) ions have been compared with spectroscopic data for the inner wall, and reasonable agreement was found. As input for BBQ, expected power and particle fluxes to the inboard wall have been calculated. These results indicate very high-power fluxes localized at leading edges of graphite tiles. To remedy this, chamfering of the tiles is recommended. At long-pulse and high-power ion cyclotron range of frequencies (ICRF) operation, it has been found that the power fluxes to the protective components of the antenna suffer from overheating. Initial results indicate that rf sheath effects are responsible for the increased power and particle fluxes. The goal of this task is to devise techniques to avoid the extra loads on the antennas.

Helium transport studies on TEXTOR continue. New features include a two-dimensional optical multichannel analyzer installed by ORNL, measurements of helium exhaust with a highly radiative layer, and studies of enhanced core transport of helium stimulated by ICRF waves.

Collaborations in the Confinement Physics area include work on DIII-D, TFTR, PBX-M, TEXT, and the Tokamak Physics Experiment (TPX). The work on DIII-D is focused on plasma shaping and beta limits. A study of the optimum plasma configuration for the radiative divertor found that shape, in particular triangularity, is the important performance parameter. In PBX-M a series of activities was carried out, including a scaling study of the neutron source strength as a function of shaping and plasma parameters and the development and application of novel computational techniques to obtain accurate and fast (real-time) reconstruction of high-beta PBX-M (and TFTR) equilibria. Furthermore, the impurity behavior with neutral beam injection and ion Bernstein wave (IBW) heating was characterized, magnetic field fluctuations were studied in both time history and frequency spectrum, and a reflectometer was built and installed to measure the edge density profile in the environment of the IBW antenna. In the TFTR collaboration, the main areas of the ORNL activities were ICRF heating, confinement experiments, and pellet injection. A microwave reflectometer edge-density diagnostic was developed and tested successfully. ICRF direct electron heating power deposition profiles were measured and found to be in good agreement with predictions of Poloidal Ion Cyclotron Expansion Solution modeling. Ion temperatures were measured with the Charge Exchange Recombination Spectroscopy System, and H-mode plasmas were characterized and documented. The pellet-enhanced performance mode, which was first discovered on the Joint European Tokamak, has been reproduced on TFTR at ICRF power levels up to 5 MW. Within smaller efforts, steady-state particle control scenarios have been developed for TPX, and plasma edge feedback experiments on TEXT have been successful in controlling the edge plasma fluctuation level.

To complement the ongoing tokamak fusion reactor studies, a physics assessment of stellarator fusion power plants has been undertaken. Stellarators have significant potential advantages over tokamaks, and the cost of electricity was comparable with that of the Advanced Reactor Innovation and Evaluation Studies (ARIES) tokamak reactor studies.

1.1 THE ATF PROGRAM

1.1.1 ATF Research Activities

T. C. Jernigan, T. S. Bigelow, R. J. Colchin, G. R. Dyer, A. C. England, D. T. Fehling, D. E. Greenwood, C. C. Klepper, M. Murakami, D. R. Overbey, D. A. Rasmussen, C. R. Schaich, J. E. Simpkins, J. A. White, J. B. Wilgen, C. T. Wilson, J. L. Yarber, and the ATF Team

The Advanced Toroidal Facility (ATF) resumed operation in April 1994 after being mothballed since 1991. Because one of the original goals of the ATF program was to demonstrate steady-state operation, it was considered important to address this issue before the final shutdown of the device. This led to the final set of experiments, which were designed to explore long-pulse discharges up to the limits imposed by the existing power and particle-handling systems.

1.1.1.1 Experimental configuration

For the experiments described in this section, the magnetic field was limited to the range of 0.5 T to 0.65 T by the existing electrical buswork for the helical field (HF) system. The electron cyclotron heating (ECH) system consisted of a 35-GHz gyrotron and a 28-GHz gyrotron, each rated at 200 kW steady state.[1] Because the proposed actively cooled, first-wall divertor system was never funded, the steady-state power was limited by the maximum allowable temperature of the uncooled vacuum vessel (150°C). The particle-handling system consisted of three 2000-L/s turbopumps. To prevent damage to the Viton™ O-rings in the gate valves of the pumps, a microwave cutoff screen was installed between each gate valve and the ATF vacuum vessel. This reduced the net pumping speed to less than 1000 L/s at the torus. All other gate valves were removed from the machine except those in the microwave waveguides whose Viton™ O-rings were replaced by silicone rubber, which proved resistant to the microwave power. In addition, all but two viewing ports were removed from the vessel after some were damaged during the long pulses. Microwave cutoff screens were installed in front of the two remaining windows. The major plasma diagnostics used were a 2-mm microwave interferometer for $\bar{n}_e$, a diamagnetic loop for stored energy, and a single channel superheterodyne microwave receiver for measuring T_e from the electron cyclotron emission (ECE). In addition, a residual gas analyzer (RGA) was used to measure the background gas composition in the vacuum vessel before each shot. For the final few shots, the RGA control system was modified to allow continuous monitoring of a number of gas species during a long-pulse shot. The only wall conditioning used after the last vacuum opening was that provided by the long-pulse discharges.

Two major additions were made to the ATF data acquisition system to enhance long-pulse operation: (1) an event-based system was instituted, and (2) a digital strip chart system was developed. For the event-based system, the standard ATF data acquisition system was used with

the added capability for retriggering the system multiple times during a shot. This allowed data for all the diagnostics to be stored from multiple time slices, or events, during a single long-pulse shot. This system allowed fast data acquisition to cover a maximum of ~33% of a shot. For those systems that required constant monitoring by the operators for safety or control reasons, a digital strip chart system was developed, which interrogated the necessary digitizers at a repetition rate of about 2 Hz and displayed the results on the operators' consoles. Both of these systems proved very useful for both control and analysis purposes.

For control of long-pulse discharges, a flexible control system was added to the existing ATF computer-controlled system for the magnetic fields, the gas inlet valves, and the ECH power. The system allowed control of chosen parameters by a preprogrammed computer waveform (practical up to ~60 s with the existing hardware), a preprogrammed analog signal, manual operation, or any combination of the three. In addition, the gas feedback system was modified so that it could use the pressure in the torus as well as $\bar{n}_e$ as a reference signal.

1.1.1.2 Results of long-pulse, dimensionless-parameter scans

Dimensionless parameter scaling experiments took advantage of the ATF long-pulse capability. Confinement scaling can be expressed in a dimensionless form[2–4]

$$\tau_E \Omega = \rho_*^{\alpha_\rho} \; \nu_*^{\alpha_\nu} \; \beta^{\alpha_\beta} \; F(R_0/a, \text{transform, shear, well, } \ldots) \; , \tag{1}$$

where τ_E is the energy confinement time, Ω is the cyclotron frequency, ρ_* is the gyroradius normalized to the minor radius, ν_* is the collisionality, β is the plasma beta, and F combines the functional dependence of other dimensionless parameters. In the previous ATF experiments[5,6] modulation of dimensionless parameters (ν_* and β) was used to determine an additional dependence to the gyro-Bohm scaling: $\tau_E/\tau_{gB} \propto \nu^{-0.18} \beta^{+0.36}$. However, ρ_* was uncontrolled in these experiments. Because the time constants for the HF coils and power supply system are in excess of 1 s, long-pulse operation afforded the additional flexibility of varying the HF (B), allowing control of three variables (B, n, P) and, correspondingly, three dimensionless parameters (ρ_*, ν_*, β). By employing two discrete ECH heating frequencies (28 GHz and 35 GHz) and by adjusting the ECH power, magnetic field, and plasma density, it has been possible to maintain fixed plasma beta and collisionality while varying the normalized gyroradius by 16%, as shown in Fig. 1.1.

For Bohm-like scaling, the predicted ratio of the confinement times for the 28-GHz and 35-GHz cases presented in Fig. 1.1 is 1.09; for gyro-Bohm scaling, the ratio is 1.3. The results, shown in Fig. 1.1, using the confinement time as measured by the diamagnetic loop, indicate this ratio is between 1.5 and 2. A similar number is obtained using the ECE measurement of electron temperature and the 2-mm interferometer measurement of density. However, limitations in the diagnostics (both the ECE radiometer and diamagnetic measurement were operating close to their noise limits) and in the plasma parameters preclude a definitive result.

1.1.1.3 Results for pulse lengths of more than 1 h

Overview

In the final experiments two ATF pulses were obtained with pulse lengths in excess of 1 h. Representative data from the longest ATF shot, which had a pulse length of 4667 s, or about 1 h, 17 min, are shown in Fig. 1.2. The helium discharge was heated by a 28-GHz gyrotron. The upper trace of Fig. 1.2 shows the vacuum vessel temperature approaching an equilibrium value of about

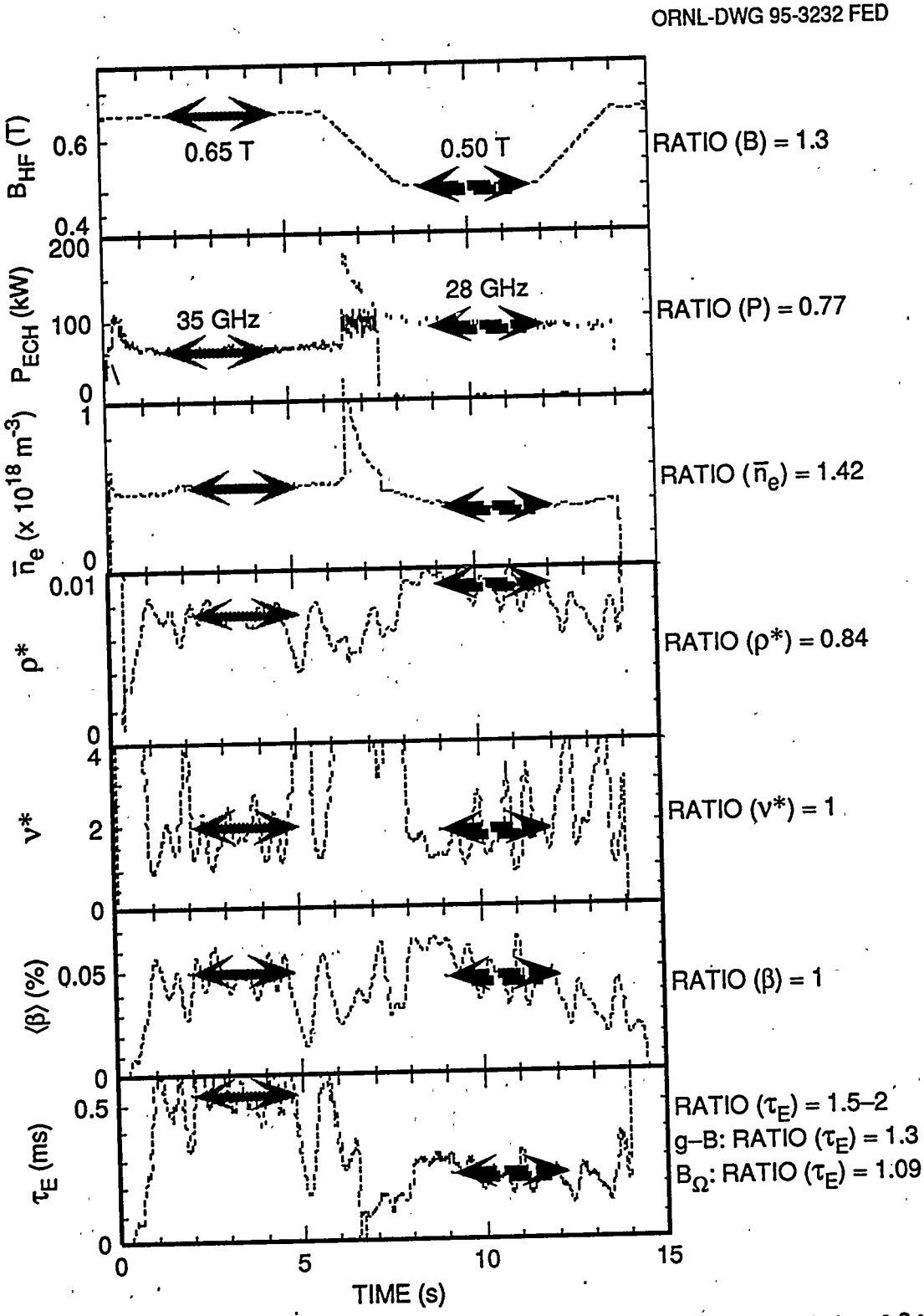

Fig. 1.1. Variation of normalized gyroradius (ρ_*) with constant collisionality (ν_*) and β in a single ATF helium discharge. The control parameters B, P_{ECH}, and $\bar{n}_e$ provide control of all three dimensionless parameters, ρ_*, ν_*, and β, allowing the functional dependence of τ_E on individual parameters to be determined.

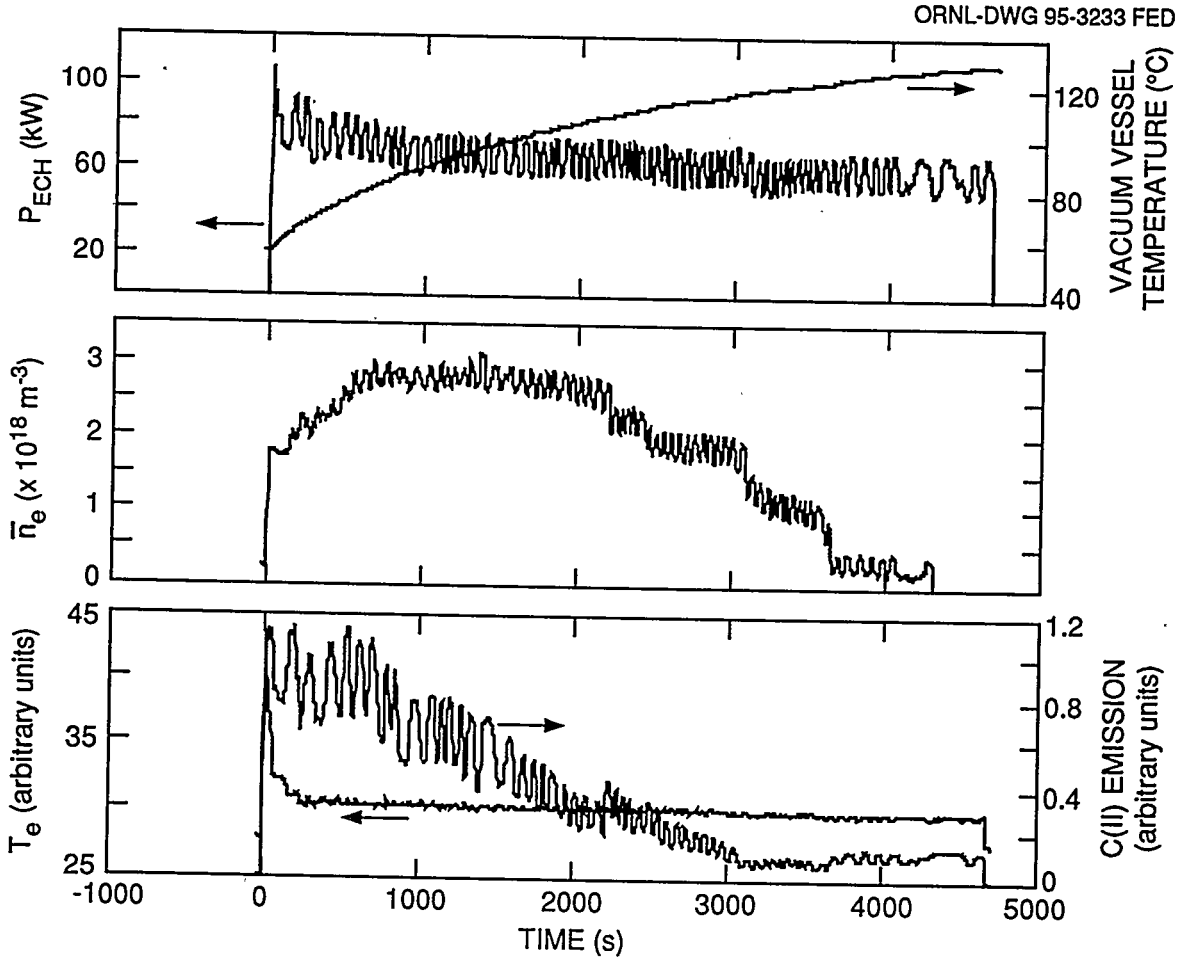

Fig. 1.2. Plasma parameters as function of time for ATF shot with pulse length of 4667 s, or ~1 h, 17 min. Helium plasma shot (B_0 = 0.51 T) probably quenched by buildup of impurities from outgassing of vacuum vessel. T_e not well calibrated, but bounds can be placed on measurement that indicate temperature lies in range of 20 to 40 eV.

150°C. The corresponding ECH power, 70 kW, represented the maximum power level allowable in ATF in the steady-state limit. Gas feedback control was used to maintain a constant electron line density ($\bar{n}_e \approx 3 \times 10^{18}$ m^{-3}). Impurity light [C(II) line] intensity decreased during the early portion of the discharge before leveling off at a low level.

Plasma control

Control of the plasma during these long shots proved challenging; it required maintaining the particle balance in the torus and keeping the power level low enough to avoid overheating the vacuum vessel while keeping the best possible plasma parameters. The electron density had to be maintained below the cutoff density (~5×10^{18} m^{-3}) of the second harmonic 28-GHz ECH. We used density feedback control with manual adjustments of the target value to maintain the vessel pressure below ~2×10^{-3} Torr. Because of the low ECH power used, power loss due to atomic processes (ionization, radiation, and charge exchange) was significant, keeping the electron temperature below the apparent radiation barrier "burn-through" threshold value. However, higher

temperature can be obtained by reducing such atomic-process–related losses, using hydrogen for the working gas, or using higher ECH power, as shown in Fig. 1.3. Feedback was controlled through both the plasma-line density and the vessel pressure during the long-pulse experiments. The vessel pressure feedback reduced the background pressure in the vessel and thus tended to reduce the neutral density in the plasma, leading to a higher electron temperature. However, plasma density feedback with manual control of the reference level provided the longest sustained discharges. Hydrogen (rather than helium) discharges also tended to have higher electron temperature because of lower ionization losses. However, hydrogen operation longer than 20 min was not possible because of lack of density control, probably caused by loading of the wall with gas.

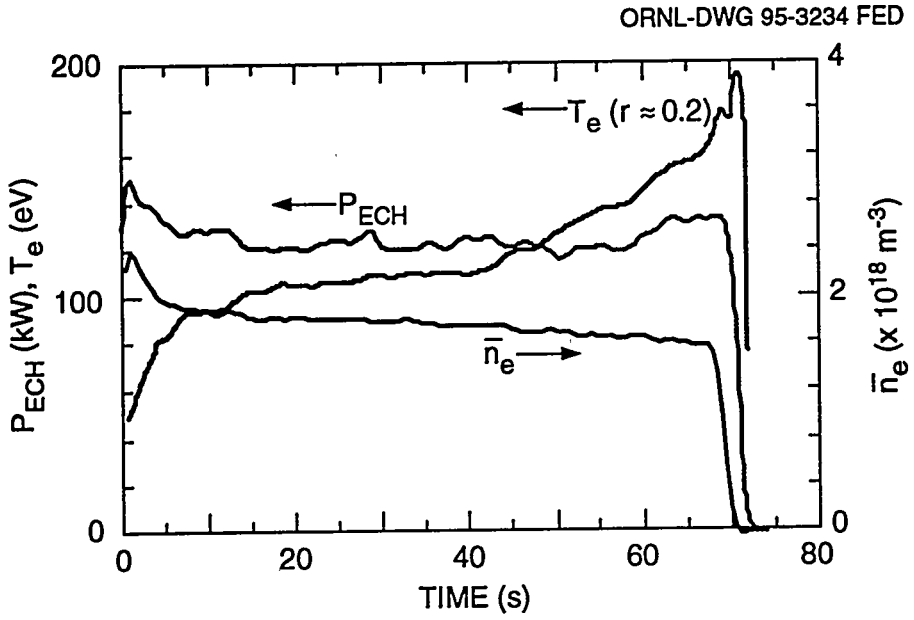

Fig. 1.3. Electron temperature, density, and input power for long-pulse hydrogen discharge (B_0 = 0.51 T) with T_e of 100 to 200 eV. Combination of higher input power (2×) and hydrogen fueling enabled discharge to "burn through" atomic processes radiation barrier.

Wall conditioning

During the long pulses, thermal equilibrium of the wall was almost obtained, as shown in the temperature trace of Fig. 1.2. However, as shown in Fig. 1.4, the hydrogen, oxygen, and water partial pressures from out-gassing of the wall gradually rose throughout the long pulses because of limitations of the torus pumping system and insufficient cleanup time. The RGA data taken over the 5-week period after the last vacuum vent showed that the mass-18 (water) level decreased to a record low level in ATF within a few days after a vent without using any gettering,[7] as shown in Fig. 1.5. Given more long-pulse discharge time, the water influx from the wall would probably have been reduced to an acceptable level, leading to truly steady-state discharges with $T_e \geq 100$ eV.

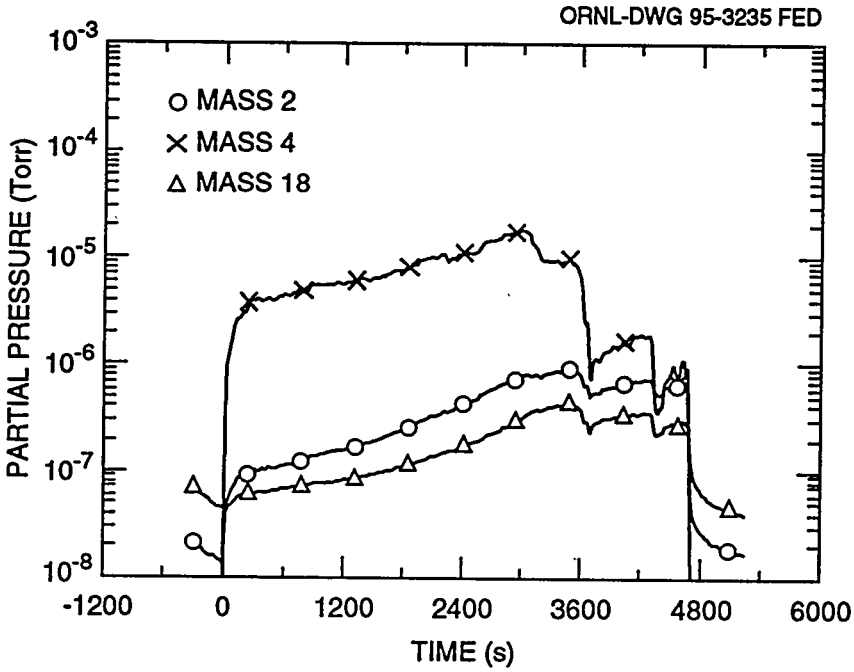

Fig. 1.4. Partial pressure of three gases in vacuum vessel during ATF shot (B_0 = 0.51 T). Steps in partial pressures are result of manual changes in plasma density reference level in attempt to offset effect of rising background pressure in vessel as temperature and outgassing increase.

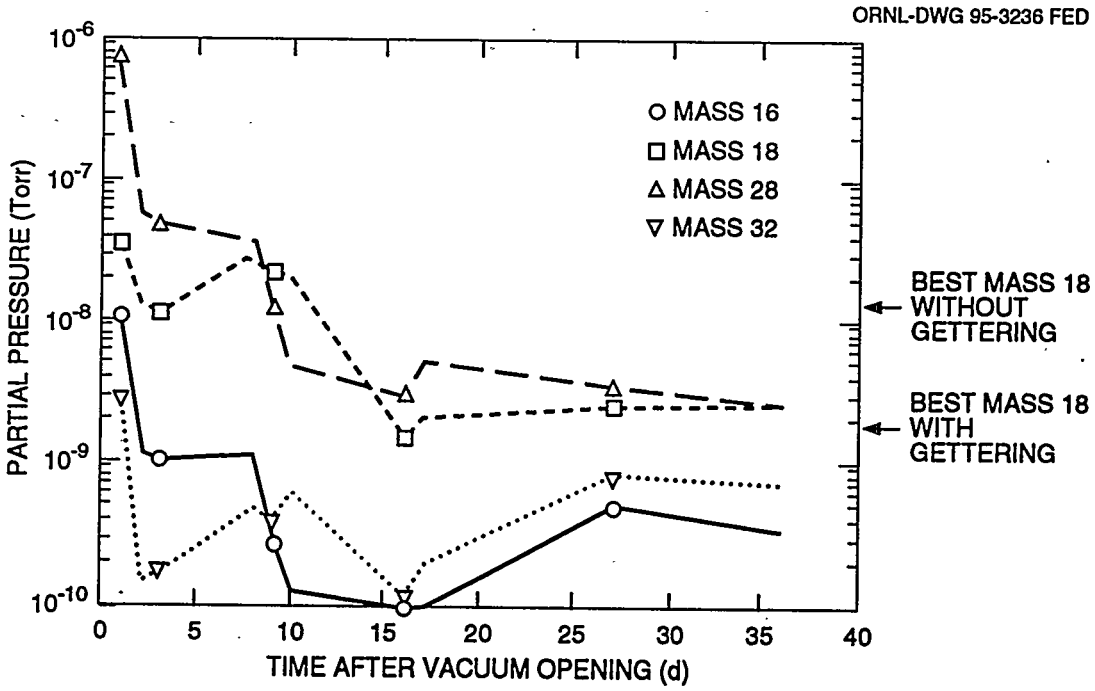

Fig. 1.5. Partial pressures of four gases in ATF vacuum vessel as function of time since last vacuum opening. Arrows on right represent best level previously achieved in ATF during short-pulse operation with (1) no gettering and (2) gettering 70% of vessel surface area with titanium.

Data handling on long-pulse experiments

The data acquisition system worked quite well throughout the long-pulse operation. The experience gained during this period indicates two areas where improvements are desirable. First, high resolution data were taken only during data acquisition events. This worked quite well for planned events where the data system could be triggered so the event time slice overlapped with the desired period. However, there were unplanned occurrences, such as the unexpected termination of the discharge, when the data system could not be triggered in advance. A suggested solution is to use a second set of digitizers that would take data continuously in the pretrigger mode and would be triggered to transmit their data for storage when an unexpected but important event occurred. The second improvement would be the addition of a filter in front of the digital strip chart digitizers to eliminate signal frequencies higher than one-half the digitization rate. Some of the ripple effects, which are seen most clearly on the ECH power and $\bar{n}_e$ traces of Fig. 1.2, are believed to be "aliasing" effects from high-frequency components.

1.1.1.4 Summary

ATF has produced shots with pulse lengths greater than 1 h (~4667 s) with zero plasma current at low power and modest plasma parameters. These discharges indicated the importance of the plasma/wall interface for steady-state operation and demonstrated data-handling techniques that are applicable to steady state. ATF parameters from a number of experiments performed over its lifetime are summarized in Table 1.1. ATF is now in a mothballed state in the event funding becomes available for its restart.

Table 1.1. ATF parameters for five different operating regimes

	High stored energy	High β	Low ν_*	Long ECH pulse (1 T)	Steady-state ECH (0.5 T)
Shot number	11740	11186	14514	16654	21380
B_0, T	1.9	0.45	1.9	0.95	0.5
$\bar{n}_e$ 10^{19} m^{-3}	11.0	4.3	0.53	0.5	0.2
P, MW	0.96	0.98	0.79	0.25	0.07
τ_E, ms	26.0	6.1	6.4	5.0	0.5
T_{e0}, keV	0.4	0.3	1.0	1.0	0.03
T_{i0}, keV	0.4	0.3	1.0	0.2	–
$\langle\beta\rangle$, %	0.4	1.7	0.1	0.15	0.05
Duration, s	0.25	0.2	0.15	20.0	4667.0

1.1.2 Repair and Upgrades of the ATF Facility

T. C. Jernigan, R. D. Benson, T. S. Bigelow, R. J. Colchin, G. R. Dyer, A. C. England, D. T. Fehling, D. E. Greenwood, C. C. Klepper, M. Murakami, D. R. Overbey, D. A. Rasmussen, C. R. Schaich, J. E. Simpkins, J. A. White, J. B. Wilgen, C. T. Wilson, and J. L. Yarber

After the ATF facility was mothballed in 1991, work toward restarting the facility began in late FY 1992. The efforts were concentrated in three major areas: repair of the two helical coil segments damaged in an arc-over in 1991, addition of a 28-GHz gyrotron for steady-state operation at 0.5 T, and an upgrade of the HF power supply for steady-state operation at up to 0.63 T.

1.1.2.1 Helical coil and vacuum vessel repairs

Two segments of the helical coil were damaged in an arc-over in 1991. A review committee determined that the most likely cause of the failure was water, which may have leaked into the joint of the HF coil from a crack in the joint tab cooling lines or from a leak in an error coil installed above the structural shell. A new design for the joint insulation was developed, which involved adding a layer of Kapton™ insulation between the turns of the joint. This insulation layer extended ~2 cm beyond the edge of the joint in all directions to provide additional "creep length" for improved voltage standoff. In addition, the water cooling lines to the joint tabs were disconnected. Removing the tab cooling limits the steady-state HF coil operation to about 0.75 T. (The precise limit must be determined by experiment.) After an outside review committee approved the new insulation scheme, it was applied to all the HF joints, and the two damaged segments were replaced.

While the machine was disassembled for the HF repairs, the opportunity was taken to improve the leak rate in the vacuum vessel. Several major leaks that resulted from cracks in welds were found and repaired. The leak rate was reduced to less than 1×10^{-5} Torr-L/s. Just before the vessel was reinstalled, it was coated with Torr-Seal™ as an additional measure to seal leaks too small to be readily detected and as a preventive measure against further leaks that may have developed because of the long-pulse operation.

1.1.2.2 ECH upgrade

Second-harmonic ECH was used to create and heat the plasma for the long-pulse experiments. Several modifications were made to the ECH system to permit lower-field long-pulse operation. A 35-GHz, 200-kW system was already available, and one of the existing 53-GHz systems was modified for a 28-GHz, 200-kW Varian gyrotron (provided by Lawrence Livermore National Laboratory from the Mirror Fusion Test Facility project). The 35-GHz waveguide system is primarily air cooled because the TE_{01} mode losses are so low. A simple, mixed-mode, water-cooled transmission line was installed for the 28-GHz system. This system is evacuated and uses a 63.5-mm aluminum waveguide with metal vacuum seals and radiused bends. The highest temperature rise measured during continuous wave (cw) operation was 70°C on an air-cooled bend bellows and ~150°C at the uncooled vacuum vessel launcher. Transmission line losses were <20%. Modifications were made to the ATF vacuum vessel to improve its cw microwave compatibility. As previously discussed, gate valves, elastomer seals, windows, and turbopumps were either removed or protected with microwave cut-off screens. The gyrotrons operated quite reliably during long pulses, with beam current leveling the most difficult problem.

1.1.2.3 Helical coil power supply upgrade

The HF power supply was modified to improve its steady-state operation capabilities at 0.5 to 0.63 T. First, the four series modules were disconnected. This lowered the maximum operation voltage of the power supply by half but improved the current control capabilities. This provides ample current for 0.63 T operation, but for 1.0 T operation, the series modules will have to be added in parallel to the existing parallel modules. In addition, the jumper connections between the modules were all water cooled for steady-state operation.

1.1.3 Stellarator Collaborative Research

Collaborations with other laboratories were an important part of our confinement program during the last period of ATF operation and, subsequently, as our research activities shifted to increased collaboration on toroidal devices at other laboratories. The stellarator collaborations involved laboratories in Japan [the National Institute for Fusion Science (NIFS) at Nagoya and the Kyoto University Plasma Physics Laboratory, Uji] and Germany (the Max-Planck-Institut für Plasmaphysik at Garching). Collaborations on domestic and foreign tokamaks are described in Sects. 1.2 and 1.3.

Oak Ridge National Laboratory (ORNL) and NIFS collaborated on long-pulse experiments on ATF. Real-time boronization was attempted for the first time in a stellarator on ATF using a small carbon-composite limiter target with 20% boron doping from Toyo Tanso. Some reduction of oxygen was seen, and deep insertion of the limiter caused an increase in carbon radiation, but a large effect was not obtained because the energy to the target was not enough to heat the surface to the 1500°C that is needed to evaporate boron. Also, 35-GHz waveguide components were fabricated at NIFS and used on ATF for long-pulse experiments.

The 200-kW, 35-GHz gyrotron on ATF was used on the Heliotron E stellarator at the Kyoto University Plasma Physics Laboratory for central heating in conjunction with 53-GHz ECH for edge heating to study the particle pumpout (degraded particle confinement) that usually occurs with ECH in Heliotron E. Particle confinement was improved by a factor of 4 to 8 with the combined edge and central heating. Turbulence-driven fluctuations inside the last closed flux surface, normally highly correlated, became decorrelated and fell in amplitude, $\Gamma_{n\phi}$ dropped by an order of magnitude, the edge density gradient steepened, the usually strong poloidal asymmetry in the potential disappeared, and the electric field in the edge region dropped to nearly zero.

Progress was also made toward developing effective ion cyclotron range of frequencies (ICRF) heating for stellarators, which requires testing various antenna designs and determining the relevant heating mechanisms. ORNL experimenters participated in the first demonstration of sustained bulk heating with ICRF in a stellarator on the Compact Helical System (CHS) at the NIFS. Boronization was used to reduce the radiation that had previously prevented the increase in stored energy produced by ICRF from being sustained for the entire ICRF pulse. The CHS ECE system was upgraded from one spatial channel to five for better time-dependent electron temperature profiles for determining heating rates and power deposition profiles. ORNL also participated in ICRF experiments with the Cattanei antenna on W7-AS.

Progress was made toward developing an effective divertor for stellarators. ORNL is collaborating with Garching on the design of a divertor for W7-AS. Improvements were made in calculations of field line and orbits and their intersections with divertor plates and the vacuum vessel walls. The German EIRENE neutrals code for divertor calculations was implemented, and a cryopump option for divertor pumping was analyzed. ORNL has also started work on a fast

pressure measurement for the CHS local island divertor experiment and calculations to model this divertor approach for both CHS and the Large Helical Device (LHD).

1.2 EDGE PHYSICS AND PARTICLE CONTROL PROGRAM

1.2.1 The Collaborative Advanced Divertor Program on DIII-D

1.2.1.1 Helium transport and exhaust studies in enhanced confinement regimes on the DIII-D tokamak

D. L. Hillis, M. R. Wade, J. T. Hogan, R. Maingi, C. C. Klepper, and the DIII-D Team

The helium transport program at ORNL began on the Tokamak Experiment for Technology Oriented Research (TEXTOR) in Jülich, Germany, in 1988. With the successful demonstration of helium exhaust on TEXTOR in 1990 using the Advanced Limiter Test II (ALT-II), considerable interest was expressed by the International Thermonuclear Experimental Reactor (ITER) conceptual design activity (CDA) to investigate whether helium could be adequately exhausted in a diverted tokamak under H-mode conditions. It was decided at ORNL to begin a collaboration with DIII-D to demonstrate helium exhaust in diverted H-mode plasmas to meet part of the ITER research and development (R&D) needs, based upon previous experience in this area of TEXTOR.

Substantial benefits can be realized in plasma performance if next-generation tokamaks, such as the ITER, can be designed to operate in an enhanced confinement regime, such as H-mode or VH-mode. One possible difficulty, however, is that the helium particle confinement time is expected to be longer for H-mode than for L-mode.[8] For burning fusion devices, continuous purging of the helium ash is essential. Estimates[9] show that newly created helium ions must be removed from the system within 7 to 15 energy confinement times to maintain a continuous burn ($7 \le \tau^*_{He}/\tau_E \le 15$). The ratio τ^*_{He}/τ_E is a global figure of merit for a reactor, where $\tau^*_{He} = \tau_{He}/(1 - R_{He})$, R_{He} is the global helium recycling coefficient, τ_{He} the particle confinement time, and τ_E is the energy confinement time. Recent measurements[10–13] on several tokamaks have demonstrated that helium can be readily exhausted from the plasma core in L-mode. The TEXTOR L-mode measurements yielded values of $\tau^*_{He}/\tau_E \approx 9$–20. More recent measurements on TEXTOR with ALT-II pumping[14] investigated an enhanced confinement regime [similar to an edge-localized mode (ELM)–free H-mode], which is produced by an edge polarization electrode. In the polarization-induced enhanced confinement regime, the ratio τ^*_{He}/τ_E increases to ~70. These measurements suggest that helium removal may be more difficult for high confinement regimes in burning plasmas; however, ELMing H-mode conditions were not investigated in TEXTOR. Reactor ignition requirements could be realized if the helium density in the core could be regulated by low-level ELMs and sawtooth activity, without undue adverse effects on energy confinement.

To simulate the presence of helium ash in DIII-D, concentrations of 10% helium (relative to n_e) were puffed into the plasma during an otherwise steady-state phase of the plasma. A lower single-null divertor configuration (double-null for VH-mode) was used with a toroidal magnetic field of 2.1 T, a major radius of 1.67 m, and a plasma current of 1.6 MA. To investigate a variety of confinement regimes, the neutral beam (NB) power was varied from modest levels of 2 MW and 4 MW to achieve the L-mode and ELM-free H-modes, respectively. At higher NB powers ELMing H-mode and VH-mode occur. The vacuum vessel walls were conditioned with boronization and helium glow discharge cleaning. The transport of helium is determined from the

temporal evolution of the absolute helium density profile in the plasma core with charge-exchange recombination (CER) spectroscopy (4686 Å transition), in conjunction with NB injection (NBI).

The helium density profile measured by CER and the electron density profile measured by Thomson scattering exhibit the same shape. Figure 1.6 displays the electron density and helium density profiles measured in L-mode, ELM-free H-mode, ELMing H-mode, and VH-mode for comparison. The profiles in each case were taken ~1.0 s after the helium gas puff, allowing the helium enough time to come into equilibrium in the discharge. This observation suggests a strong similarity between deuterium and helium transport and an encouraging absence of preferential accumulation of helium in the plasma core.

From the CER measurements, the helium particle flux Γ_{He} is evaluated by solving the continuity equation, $\partial n_{He}/\partial t = -\nabla\cdot\Gamma_{He} + S_{He}$, where n_{He} is the helium density and S_{He} is the helium source rate. The helium flux is assumed to consist of diffusive and convective flows, represented by: $\Gamma_{He}(r,t) = -D_{He}(r)\nabla n_{He}(r,t) + n_{He}(r,t)V_{He}(r)$, where D_{He} is the anomalous diffusion coefficient and V_{He} is the convective velocity. With the excellent spatial and temporal resolution of the DIII-D CER system, the helium flux Γ_{He} can then be inferred directly through the inversion of the continuity equation to determine both D_{He} and V_{He} using the method described in Refs. 15 and 16.

To compare the helium diffusivity and thermal diffusivity, a local power balance analysis is used to determine a single-fluid heat diffusivity χ_{eff} from the ONETWO transport code. A comparison of D_{He} and χ_{eff} for L-mode and ELM-free H-mode for similar configurations is shown in Fig. 1.7. The large decrease in both D_{He} and χ_{eff} between L-mode and H-mode is a clear indication of a marked improvement in both particle and energy confinement in H-mode discharges. In both cases, $D_{He}/\chi_{eff} \approx 1$ over most of the plasma radius, consistent with previous measurements on the Tokamak Fusion Test Reactor (TFTR).

As the injected power is systematically increased, ELMs become prominent, with the ELM frequency increasing at higher NB powers. These ELMs expel both plasma energy and particles

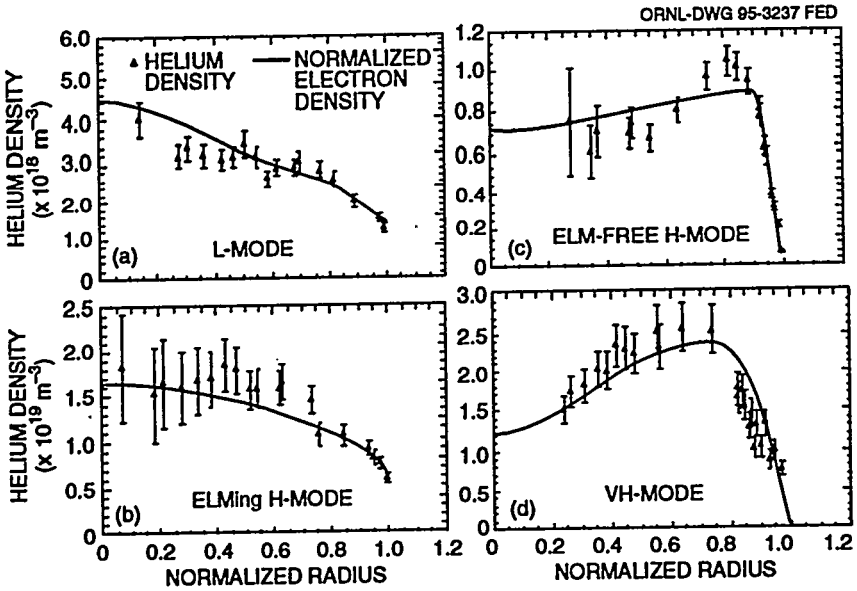

Fig. 1.6. Comparison of measured helium density and electron density profiles: (*a*) L-mode, (*b*) ELMing H-mode, (*c*) ELM-free H-mode, and (*d*) VH-mode. The solid curve is a spline fit to the measured electron density profile.

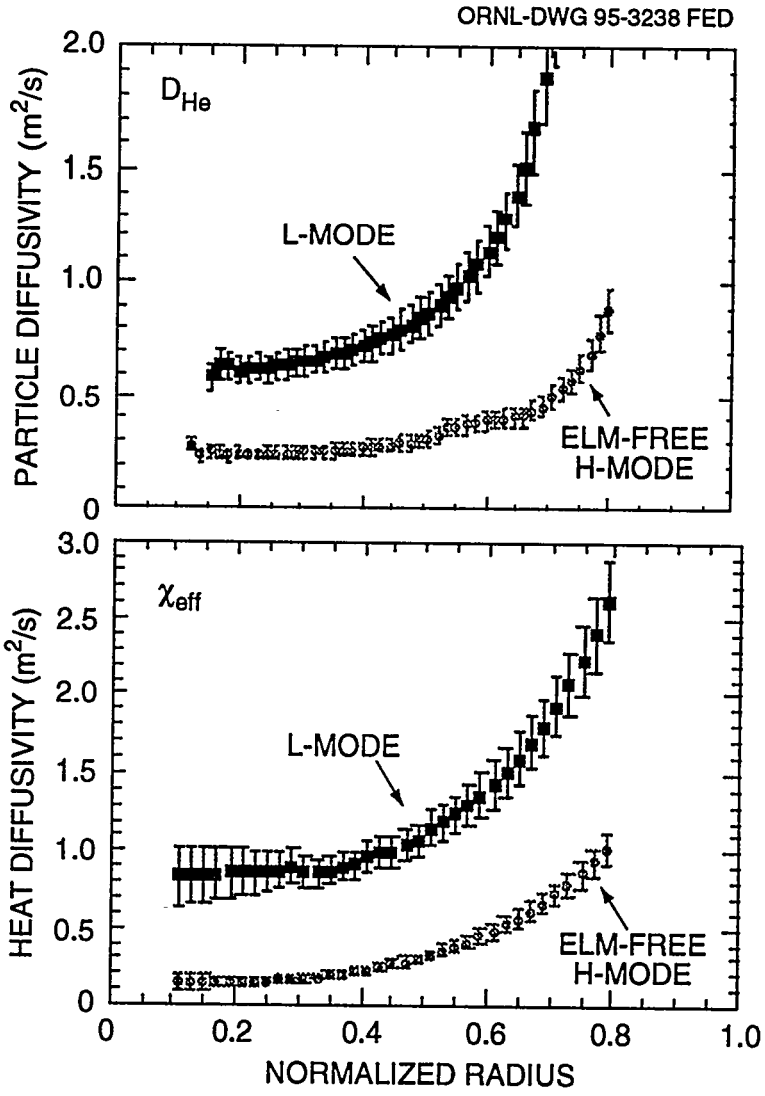

Fig. 1.7. Comparison of D_{He} and χ_{eff} in L-mode and H-mode at same plasma current (1.6 MA) and NB power (~2.0 MW).

from the plasma edge. In terms of helium transport properties within the core, both D_{He} and χ_{eff} increase as the NB power is increased. (See Fig. 1.8.) As noted earlier, this increase in auxiliary power is accompanied by an increase in ELM frequency (40 Hz at 6 MW to 120 Hz at 12 MW). However, because the ELMs are generally localized near the plasma edge, their effect on core energy and particle transport ($\rho < 0.5$) is expected to be minimal. More importantly, Fig. 1.8 suggests that $D_{He}/\chi_{eff} \approx 1$ for $\rho < 0.5$ and appears to be insensitive to changes in input power. For $\rho > 0.5$ the quantity D_{He}/χ_{eff} increases with increasing NB power, indicating that helium is more quickly transported out of the plasma, probably because of the ELMs. This suggests a favorable trend for enhancing helium transport relative to energy transport as the ELM frequency is increased and makes an ITER scenario based on ELMing H-mode conditions more feasible.

Recently, active helium pumping experiments were performed on DIII-D using the advanced divertor cryopump,[17] which was conditioned with an argon frost layer to provide helium pumping. The Advanced Divertor Program cryopump was conditioned with an

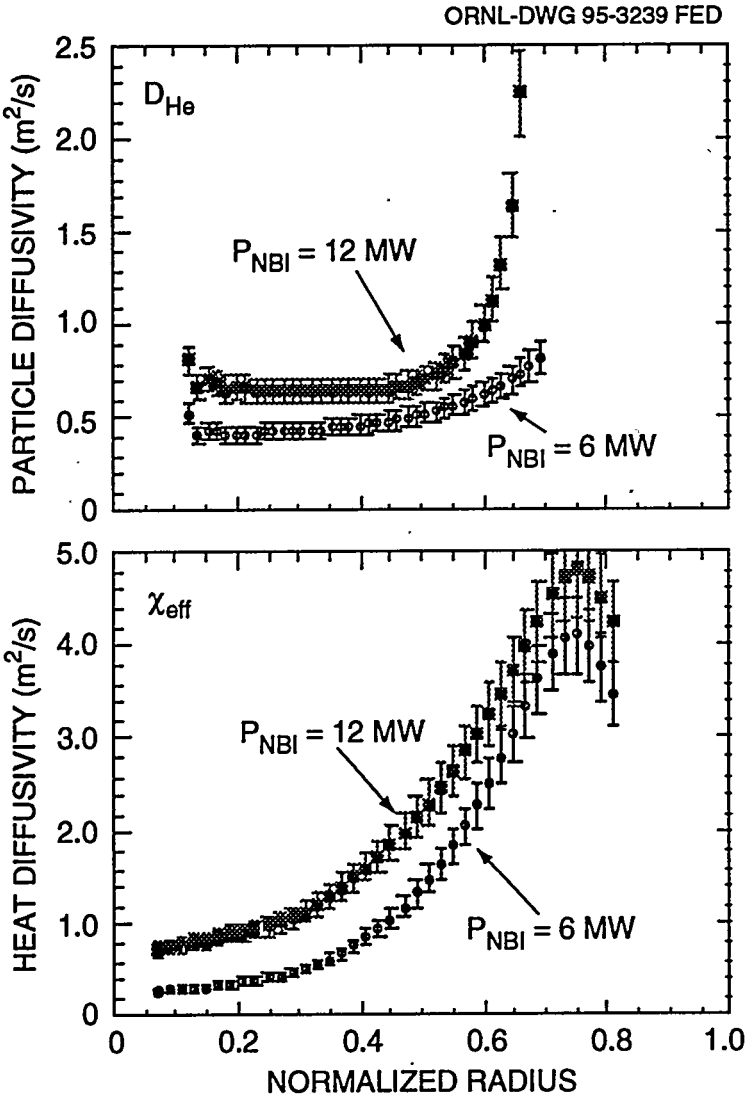

Fig. 1.8. Comparison of D_{He} and χ_{eff} in ELMing H-mode at two different power levels (6 MW and 12 MW).

argon frost layer between shots (~1500 Torr-L of argon), which provides a helium pumping speed of ~18,000 L/s when the layer is fresh. Figure 1.9 shows a typical DIII-D discharge with active helium pumping. The discharge is similar to those described earlier, but the plasma current was 1.0 MA. For the discharge in Fig. 1.9, the electron density of the background plasma was $n_e \approx 4 \times 10^{19}\ m^{-3}$ during the NB phase. As shown in Fig. 1.9, the helium density rises sharply just after the 50-ms helium gas puff (at 1.5 s), and the helium appears in the core plasma (ρ= 0.3 and 0.5) within ~200 ms. For this discharge the outer strike point (OSP) is initially well removed from the pumping baffle (no helium pumping) until 2.0 s, when the OSP is moved into the optimum pumping location. For the period without helium pumping (<2.0 s), the helium density remains constant after the initial rise, indicating full recycling ($R_{He} \approx 1.0$) of the helium. With active helium pumping, which begins at 2.0 s, the helium density drops rapidly, and ~70% of the helium found in the discharge is exhausted within ~2 s. This discharge is an ELMing H-mode discharge with an ELM frequency of ~40 Hz. The active removal of helium in this discharge is

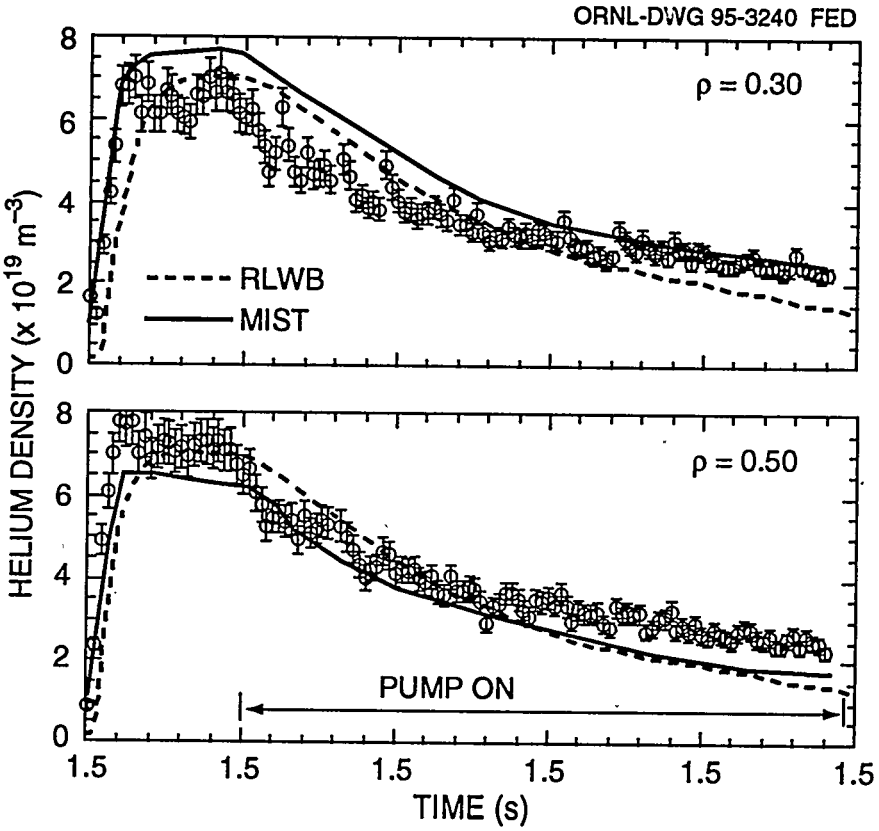

Fig. 1.9. Temporal evolution of helium density (points) with argon frost pumping compared with standard MIST calculation where $R_{He} = 0.95$. Dashed line is for RLWB model with $R_{He} = 0.97$.

very similar to the results found on TEXTOR with an L-mode discharge. Calculated from the decay of the helium density over time during the pumping phase, the helium particle confinement time in the vacuum vessel is $\tau^*_{He} \approx 1.1$ s, while diamagnetic measurements give $\tau_E \approx 0.137$ s. This yields a $\tau^*_{He}/\tau_E \approx 8$. Based on the data shown in Fig. 1.8, as the ELM frequency is increased ("grassy" ELMs), one should expect an even more favorable value for τ^*_{He}/τ_E. A limited number of ELMing H-mode discharges have been investigated on DIII-D, but for the cases studied $8 \leq \tau^*_{He}/\tau_E \leq 12$.

Comparisons with the MIST impurity transport code,[18] using anomalous transport coefficients (D_{He}, C_v) based on ELMy H-mode transport, and the Rebut-Lallia-Watkins-Boucher (RLWB) predictive particle transport model[19] are shown in Fig. 1.9. Both models show good agreement with the radial profile evolution during helium exhaust. These comparisons allow an estimate of the global helium recycling coefficient, R_{He}. The MIST calculation that fits the helium exhaust data is shown in Fig. 1.8, with D_{He} ($\rho > 0.8$) = 2 m^2/s and C_v = 1.0. Figure 1.9 shows cases with R_{He} = 0.95 (MIST) and R_{He} = 0.97 (RLWB). While the actual R_{He} is time dependent, these limiting values imply an exhaust efficiency of ~3–5%.

To summarize, helium density radial profiles were measured in DIII-D, as were the effects of enhanced confinement regimes on these radial profiles. In terms of the transport of helium within the plasma core, these experiments suggest that core transport rates for helium will probably be sufficient for ITER in either ELMing H-mode or L-mode conditions. In addition these experiments have shown that helium can be exhausted efficiently from an ELMing H-mode

plasma in a diverted tokamak with a value of $\tau^*_{He}/\tau_E \sim 8$, which is within the acceptable range for a fusion reactor like ITER. It is also encouraging that there is no preferential accumulation of helium in any of the operating regimes studied to date. Taken together, these helium transport and exhaust experiments on DIII-D encourage optimism about the use of H-mode plasmas in future fusion reactors. Future experiments on DIII-D will use NBI of helium to simulate a central source of helium in order to investigate helium transport in the presence of a radiating divertor.

1.2.1.2 Particle control and boundary studies on DIII-D

R. Maingi, P. K. Mioduszewski, J. T. Hogan, L. W. Owen, D. K. Lee, and the DIII-D Team

In early 1993, a helium-cooled cryogenic condensation pump was installed in DIII-D to provide particle exhaust. The pump plenum was formed by using a baffle to connect the toroidally symmetric ring (used for inducing electric fields in other experiments) to the outer wall. The cryopump is positioned under the baffle inside of this pumping plenum. (See Fig. 1.10.) Previous experiments on DIII-D demonstrated[20] that the static (unpumped) baffle neutral pressure was strongly dependent on the separatrix-ring gap, the minimum approach between the outer divertor leg of the magnetic separatrix and the aforementioned ring. Our experiments demonstrated that the pumped baffle neutral pressure was also strongly dependent on the separatrix-ring gap. The pumping speed of the cryopump was measured in off-line, nonplasma tests.[21] From the inferred pumping speed, the pump throughput or exhaust can be estimated as a product of the pressure and the pumping speed. Figure 1.11 shows the strong dependence[22] of the

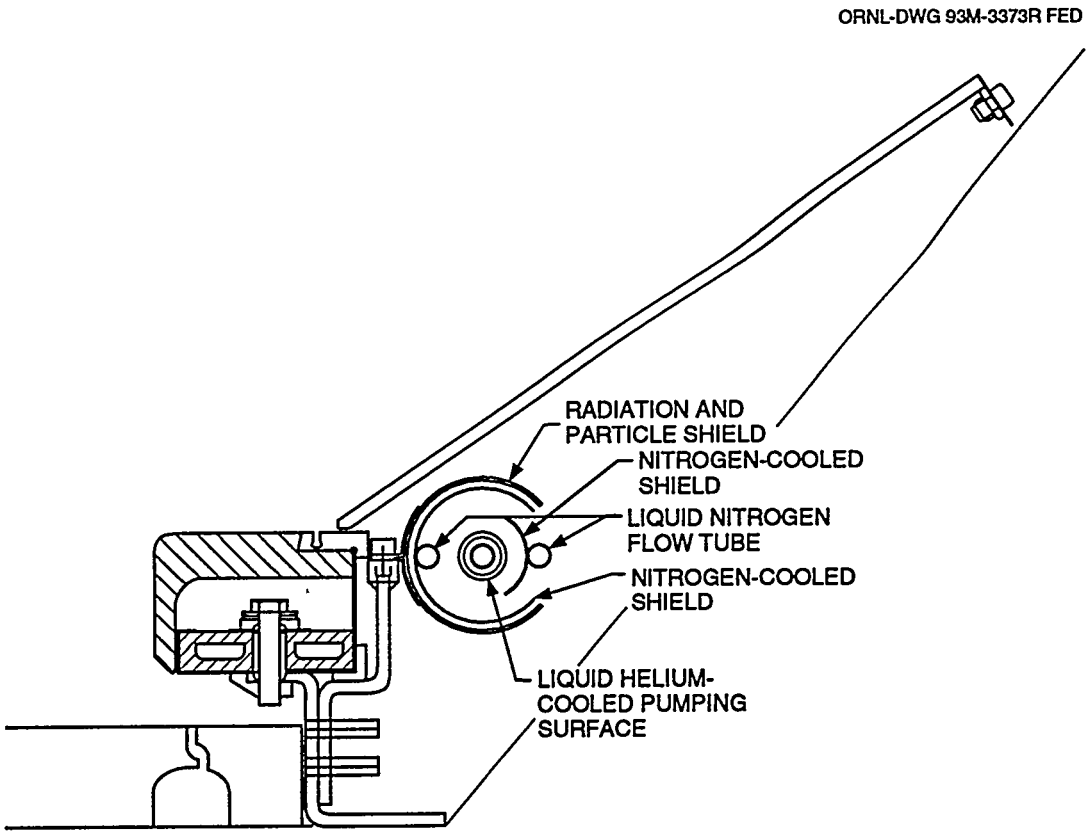

Fig. 1.10. Configuration of the cryopump inside the baffle chamber.

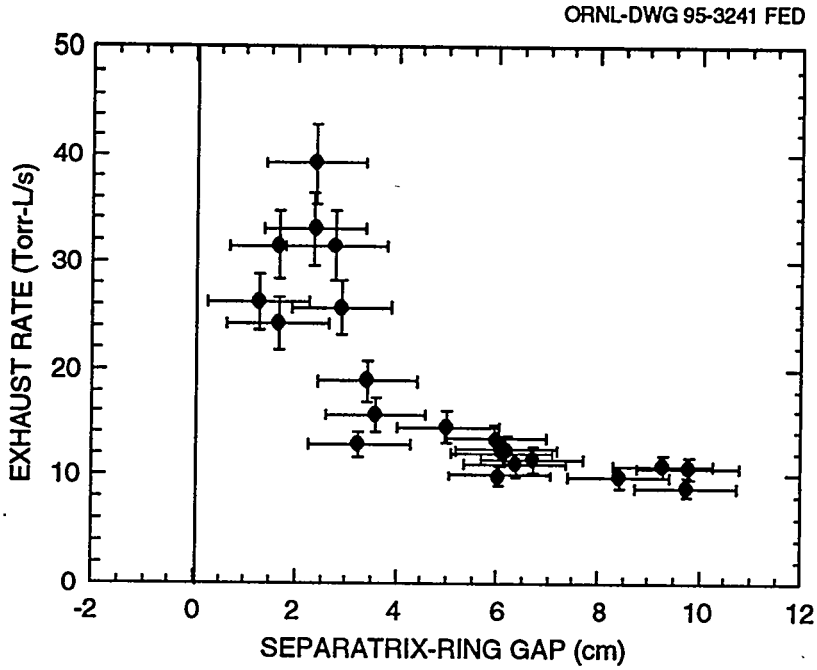

Fig. 1.11. Cryopump particle exhaust rate vs separatrix-ring gap. Exhaust rate estimated as product of baffle neutral pressure and pumping speed. *Source:* reprinted from Ref. 22.

cryopump particle exhaust rate on the ring gap. Hence, density control in H-mode has been obtained[23] in DIII-D by a variation of coil current ratios, which affects this ring gap.

Recently, the strong dependence of the unpumped and pumped baffle pressures on the ring-gap position has been modeled with the b2.5 code to simulate the edge plasma. The free parameters in the model were selected by comparison with data.[24,25] The computed plasma parameters were then put into the DEGAS code for an assessment of neutral transport in the pumping plenum and background plasma. In general, good agreement was obtained for the dependence of the baffle pressure on the ring gap with pumping, but it was difficult to reproduce the magnitude of the maximum achieved neutral pressure in the unpumped case.

The density dependence of the divertor parameters in ELMy H-mode has also been investigated on DIII-D. High-density discharges are required from the standpoint of a deuterium-based radiative divertor, but low-density discharges are required for maximum current drive efficiency. Hence, a study was initiated to investigate the electron density dependence ($\bar{n}_e$) of the divertor quantities: particle flux, heat flux, and radiation. The line-average density was varied by a factor of 2, from between 1/3 to 2/3 of the Greenwald density limit. Because of diagnostic limitations when the OSP was near the pump plenum, only the inner divertor plasma parameters could be examined at the lowest densities.

The main observations from this study were (1) the inner strike point peak heat flux increased almost linearly as the density was reduced (see Fig. 1.12); (2) the inner strike point peak particle flux was a maximum at about half of the Greenwald density limit, and it declined at both lower and higher densities; and (3) the total (core + divertor) radiation decreased as the density was reduced; this was roughly balanced by the increase in target power measured at the inner strike point. It was inferred from the data that the inner strike point was "partially detached" at the higher densities, probably because of a plasma momentum loss parallel to the magnetic field, and this detachment plays a crucial role in determining both the power conducted to the

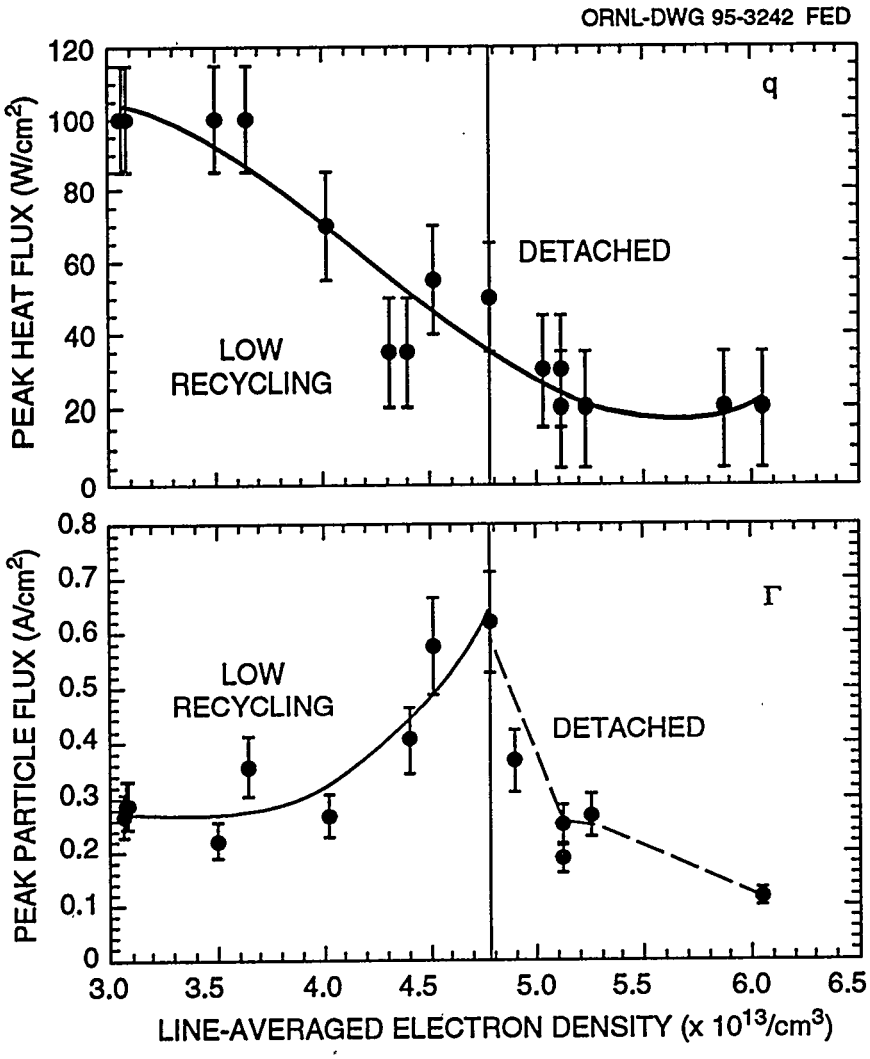

Fig. 1.12. Peak heat flux and peak particle flux as function of line-average density. Because of simultaneous decrease in peak heat flux and particle flux, it can be inferred that inner divertor is detached above 4.8×10^{13}.

inner target plate and the in/out plate target power ratio. One conclusion from this study is that tokamaks designed to operate at low density for current drive should have heat removal capabilities at the inner divertor strike point location if single-null divertor operation is desirable.

Detailed two-dimensional (2-D) edge plasma modeling was performed for three different $\bar{n}_e$ values. These simulations indicated that most of the target plate heat flux increase at low $\bar{n}_e$ was because of an increase in electron conduction, ion convection, and, to a lesser extent, radiation heat flux to the target. The electron conduction increased because of the reduced radiation source, allowing a higher T_e at the target. The radiation heat flux increased because the radiation zone moved closer to the target, even though the size of the radiation zone was reduced. In addition, the simulations indicated that the in/out target power ratio scaled inversely with the amount of radiation on the inboard leg.

1.2.1.3 Global particle confinement time studies on DIII-D

R. Maingi, P. K. Mioduszewski, J. T. Hogan, L. W. Owen, D. K. Lee, D. L. Hillis, M. R. Wade, and the DIII-D Team

The global particle confinement time, τ_p, has also been investigated on DIII-D. H-mode confinement discharges are characterized by sharp spatial gradients in both the electron density and temperature profiles in the edge plasma just inside of the separatrix. Obtaining particle transport coefficients (diffusion coefficient and pinch velocity) is difficult because the particle fluxes are dominated by the recycling source in this region. We have investigated a method to compute this recycling source. The edge plasma is modeled with the b2.5 code, using data for constraints on free parameters as mentioned previously. The computed plasma parameters were then put into the DEGAS code for core fueling calculations. A global figure that is obtained from these calculations is the particle confinement time, τ_p, defined as the ratio of the core electron particle inventory and the electron particle flux diffusing into the scrape-off layer (SOL) from the core. The latter quantity is computed by the edge plasma simulations, and the DEGAS core fueling calculations determine if the global particle balance is satisfied.

Computing the ratio of τ_p/τ_E in various confinement modes is the primary result of this study. To date, this ratio has been computed for both L-mode[26] and ELM-free H-mode discharges.[27] (See Fig. 1.13.) For L-mode, this ratio is ~2, and for ELM-free H-mode, the ratio is about 4. This analysis is very labor intensive, and more discharges need to be examined to determine if the results are confinement-mode specific or discharge specific.

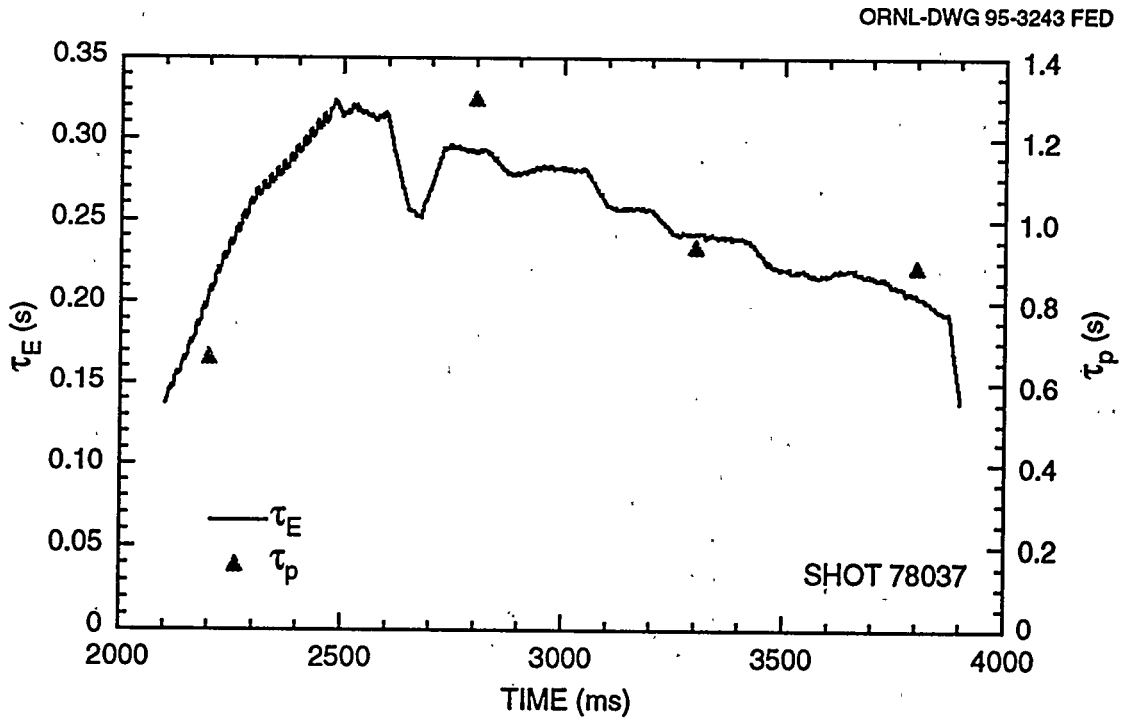

Fig. 1.13. Particle and energy confinement time temporal evolution during ELM-free H-mode discharge. *Source:* reprinted from Ref. 27.

1.2.1.4 DIII-D advanced divertor cryopump

M. M. Menon, D. L. Hillis, M. R. Wade, and the DIII-D Team

As a major collaborative effort between ORNL and General Atomics, a particle exhaust scheme in the DIII-D tokamak, employing a cryocondensation pump in the outboard divertor region under a baffle, was designed, installed, and successfully operated. The details of the design, construction, and operational characteristics have been published.[28–31] The pumping surface is made up of an 11.6-m Inconel tube, 25.4 mm in diameter, cooled by boiling liquid helium at 4.3 K. (See Fig. 1.10.) The cryopump provides toroidally symmetric pumping at a rate of 30,000–40,000 L/s for D_2 in the pressure range of 1–4 mTorr. Pressures in the 2–3-mTorr range are routinely observed under the baffle. This translates to particle exhaust throughputs of ~100 Torr-L/s. The actual exhaust throughput could be controlled by selecting the position of the plasma strike region with respect to the baffle chamber opening. The pump has been used quite effectively for plasma density control.[32]

The helium ash generated as a result of deuterium-tritium (D-T) burn in a fusion reactor must be exhausted from the plasma to avoid fuel dilution effects. In fusion plasmas, the exhaust gas will be a combination of D_2 and helium, with helium forming only a small fraction (about 10%). The pumping characteristics of pure helium and a mixture of D_2 and helium (90% D_2) were investigated using a cryosorption pump with condensed layers of argon as sorbent. The cryocondensation pump shown in Fig. 1.10 was used for the experiment. The investigation was conducted in a pressure regime that is relevant to particle exhaust from fusion plasmas. The experiment revealed that (1) the cryosorption pumping speed of pure helium drops precipitously if the argon/helium ratio falls below ~20, (2) the pumping speed for helium in a D_2/He mixture decreases exponentially with the amount of D_2 pumped, (3) increasing the thickness of argon in the range of 1–12 μm has little effect on the pumping speed for helium in a D_2/He mixture, and (4) for a pumping surface coated with a thick (>2-μm) layer of argon, surrounded by a radiation shield with a transparency factor of about 6, a helium pumping speed (in the millitorr pressure range) of 15–25 kL/s^{-1} per square meter of pumping surface, for pulse duration of about 5 s, could be obtained after pumping about 80 Torr-L of D_2. These results have been presented for publication.[33]

1.2.2 Development of Particle and Impurity Control Techniques on Tore Supra

1.2.2.1 Particle control studies

P. K. Mioduszewski, J. T. Hogan, C. C. Klepper, T. Uckan, L. W. Owen, and the Tore Supra Team

Particle balance with pump limiters

Continuous particle exhaust with pump limiters in Tore Supra has been found to behave differently than previously experienced.[34] In previous experiments, the exhausted gas would correspond closely to the decrease in plasma inventory, but plasma density control in Tore Supra was found to depend strongly on the conditions of the carbon walls. In pump limiter discharges with unconditioned walls, containing large amounts of hydrogen isotopes, the decrease in core plasma density amounted to only a small fraction of the total number of particles exhausted by the pumping system.[35] For relatively low-density ohmic discharges with $\bar{n}_e = 2 \times 10^{19}$ m^{-3} the measured particle flux removed by one pump limiter module was ~7.5 Torr-L/s for a duration of

more than 6 s flattop time (10 s total), while the maximum observed core density decay corresponded to only ~0.25 Torr-L/s. Because these plasmas were obtained with H_2 gas prefill only (i.e., without any additional external fueling during the discharge), the large amounts of exhausted gas must have originated from the walls.

In similar discharges, but with walls conditioned by prior helium glow discharges, the effect of the pump limiter exhaust on the plasma inventory was significantly different.[36] A comparison of two such discharges, one with pumping and one without pumping, is depicted in Fig. 1.14, which shows the plasma density, the gas puff, and the pressure in the pump limiter. (In shot 10499 the pressure gauge is saturated at 10 mTorr.) The pump limiter exhaust affected the plasma density behavior in two ways: (1) during the stationary phase between $t = 3$ s and $t = 5$ s, the gas puff had to be increased to achieve approximately the same density as for the nonpumped shot, and (2) after the termination of the gas puff, the density decayed much more rapidly in the

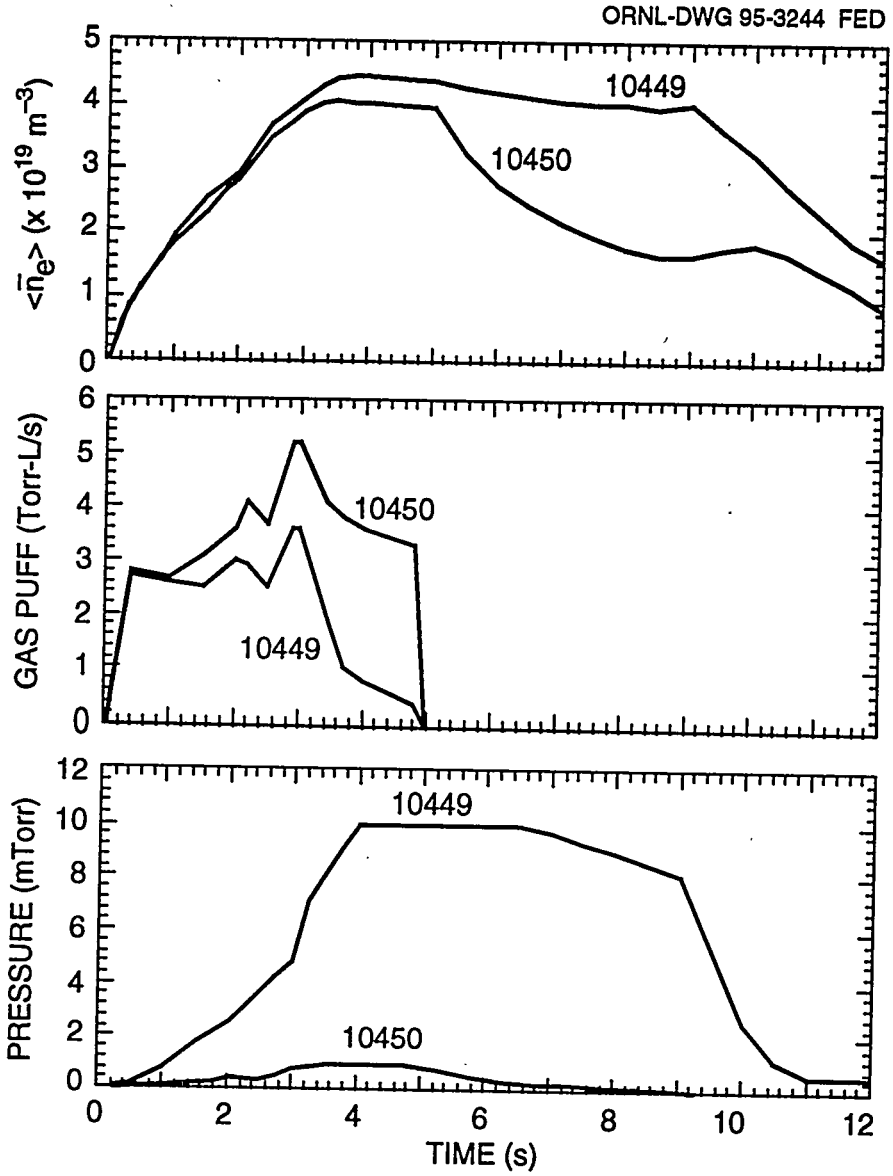

Fig. 1.14. Effect of pump limiter exhaust in shots TS 10449 and 10450.

pumped discharge. With a measured pumping speed of 23,000 L/s, the maximum exhaust rate (pressure × pumping speed) was >23 Torr-L/s. In contrast to the experience with unconditioned walls described in the previous paragraph, this was approximately balanced by the gas puff rate during the stationary phase.

As in other large devices with graphite walls, particle control in Tore Supra is dominated by wall recycling and depends on a large number of variables: wall conditioning and history, limiter configuration, fueling, heating, etc. To understand the mechanisms of core-wall particle exchange at a detailed physical level, we have modeled these Tore Supra particle exhaust experiments using the constraints provided by the measured Thomson scattering radial profiles $T_e(r,t)$ and $n_e(r,t)$ and the particle fluxes in the limiter throat measured with Langmuir probes. Based on these experimentally obtained parameters, the local effects of ionization in the SOL on the coupling between particle exhaust and plasma density have been modeled with a combination of Stangeby's model of the ionizing SOL and the DEGAS neutrals transport code.[37] These calculations indicate intense charge-exchange fluxes to the walls around the pump limiter and strong ionization of the resulting recycling fluxes within the SOL. This leads to a local flux amplification factor of ~2 in the limiter region during particle pumping and to a direct exhaust of particles originating from the wall. Figures 1.15 and 1.16 show the charge-exchange flux distribution around the limiter and the ionization profile in the SOL for a low-density ohmic discharge with $\bar{n}_e \approx 2.5 \times 10^{19}$ m^{-3} (Ref. 37).

In addition, a global particle balance between plasma core and wall has been calculated using the experimental constraints by coupling a 1 1/2-D radial transport code, a three-dimensional (3-D) Monte Carlo neutrals code, and a new 1-D code (WDIFFUSE)[38] describing the diffusion of hydrogen in the graphite layer near the limiter. The 1 1/2-D code permits an

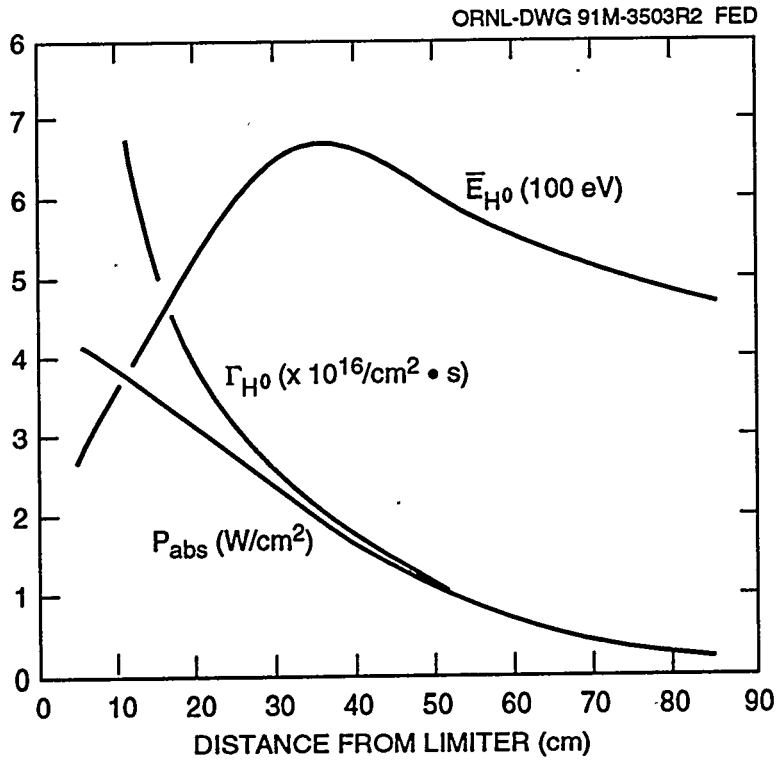

Fig. 1.15. Distribution of the charge-exchange flux around the horizontal pump limiter in Tore Supra.

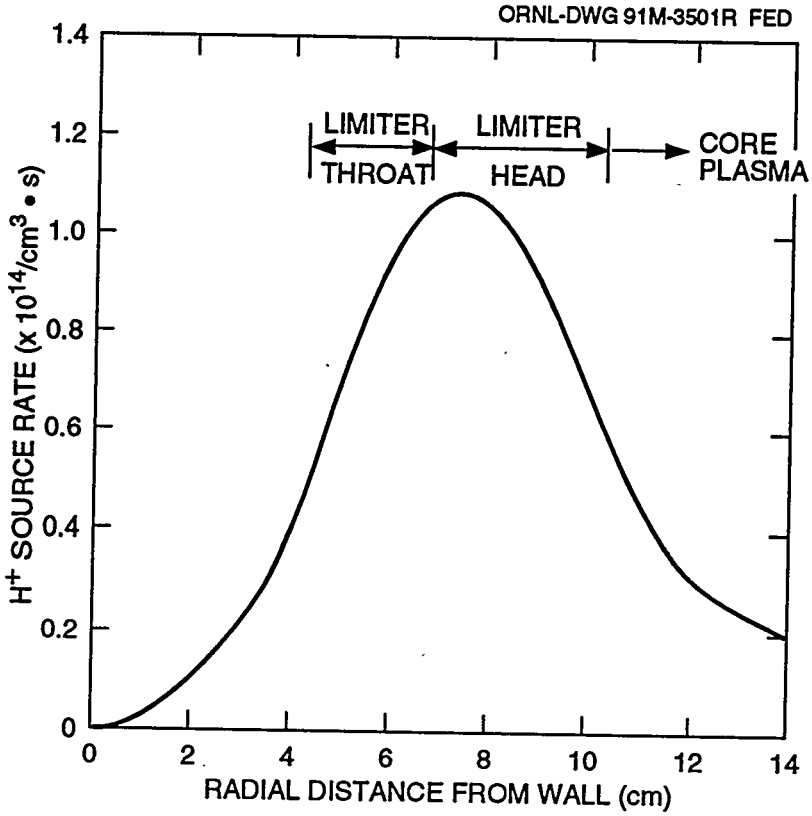

Fig. 1.16. Ionization profile in the SOL of a pump-limiter discharge in Tore Supra.

estimate of the energy spectrum (and hence implantation depth) of the charge-exchange efflux. This balance model calculates both the efflux from the wall, which is *required* to match the Thomson scattering and Langmuir probe data, and the efflux *predicted* from a saturated carbon-hydrogen layer, given the particle flux history to the layer. The main result of this modeling confirms that strong charge-exchange fluxes to the walls around the limiter mediate the core-wall particle exchange. Agreement between the required and the predicted fluxes is found if a particle source can be provided ($R > 1$). This source could result from local overheating in the near-limiter region or from particle-induced desorption caused by the charge-exchange fluxes.

For discharges with unconditioned walls and for which the pump limiter has little effect on the plasma density, the following picture emerged for ohmic discharges with $I_p = 1.2$ MA, $B_T = 4$ T, and low line-average densities of $2–3 \times 10^{19}$ m^{-3}. Due to ionizations in the SOL, the plasma efflux from the core was amplified by a factor of ~2. The characteristic decay length of the particle flux in the SOL was such that more than 90% of this amplified ion flux was incident on the limiter, while the interaction of the ion flux with the wall was negligible. The parallel ion flux in the SOL was neutralized at the limiter, and a fraction of it was subsequently ionized in the plasma to balance the efflux; the other fraction underwent charge-exchange processes, causing charge-exchange fluxes around the limiter that were similar in magnitude to the plasma efflux. It was this charge-exchange flux that caused the interaction with the wall and produced the particle flux that was exhausted by the pump limiter and led to the eventual depletion of the wall inventory.

A flow diagram of plasma and neutral particle flows in the SOL and pump limiter is shown in Fig. 1.17. The ion flux to the limiter includes the assumed core efflux (~50 Torr-L/s) and the

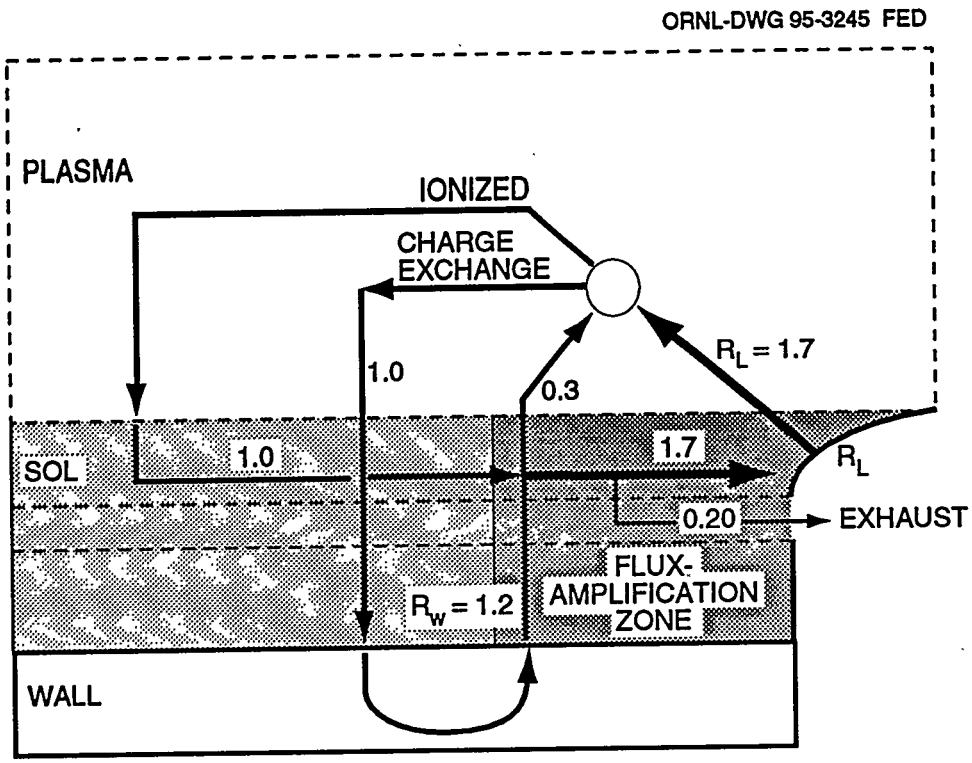

Fig. 1.17. Simplified particle flow between plasma core, wall, and pump limiter of Tore Supra.

ions that result from dissociation and ionization of the net wall efflux. Recycling particles cause this flux to be amplified by a factor of ~2 on average in the SOL and an additional factor of 2 within the throat (total amplification of ~4 for flux tubes that connect to the limiter neutralizer plate). With the small change in the plasma density, the core efflux is balanced by the core fueling rate, and the pump throughput is balanced by the net wall efflux. With the pumps active we assume that energetic charge exchange (or some other mechanism) results in the net desorption rate required to balance the pump throughput. This wall depletion by the pump limiter can be used to keep the wall conditioned (in a pumping state) for steady-state operation.

Wall conditioning with pump limiter exhaust

The wall conditioning effect of the pump limiter exhaust was demonstrated with the following experiment. After some helium glow wall conditioning, the walls were exposed to ten deuterium discharges of ~10-s pulse length each. The last discharge of this series was shot 10449, which is shown in Fig. 1.14. The very slow density decay after termination of the gas puff indicates that wall pumping had become negligible. This was then followed by six discharges with the pump limiter activated; the first of this series was shot 10450 in Fig. 1.14. The rapid density decay after the termination of the gas puff indicated the exhaust by the pump limiter. Comparison of the involved particle fluxes indicated again that the exhausted fluxes were much higher than the respective plasma decay, and the global particle balance had to include the wall inventory. This balance is shown for shot 10450 in Fig. 1.18, where the relative change in the wall inventory is taken as the difference between the gas puff and the sum of plasma inventory and pump limiter exhaust. After six pumped discharges, the pump limiter was turned off again,

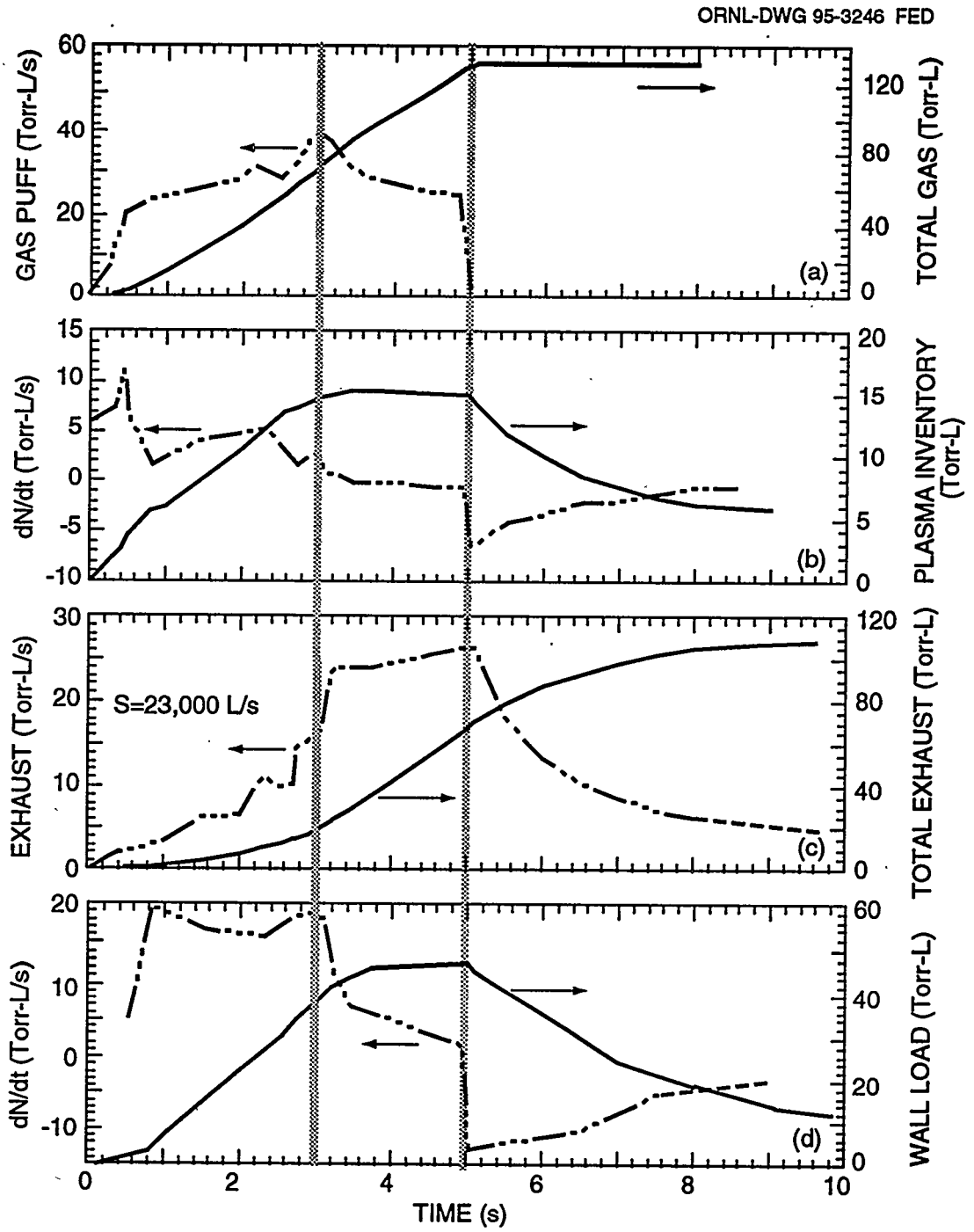

Fig. 1.18. Particle balance in Tore Supra for discharge 10450. (*a*) Gas puff, (*b*) plasma particle inventory, (*c*) exhaust, (*d*) gas loading of wall.

but the density decay after the gas puff was still fast, indicating that the wall was pumping again. The densities of the complete series of these discharges are depicted in Fig. 1.19. The figure shows the densities normalized at $t = 5$ s, the termination time of the gas puff, and the decay times $\tau_p^* = N/(dN/dt)$.

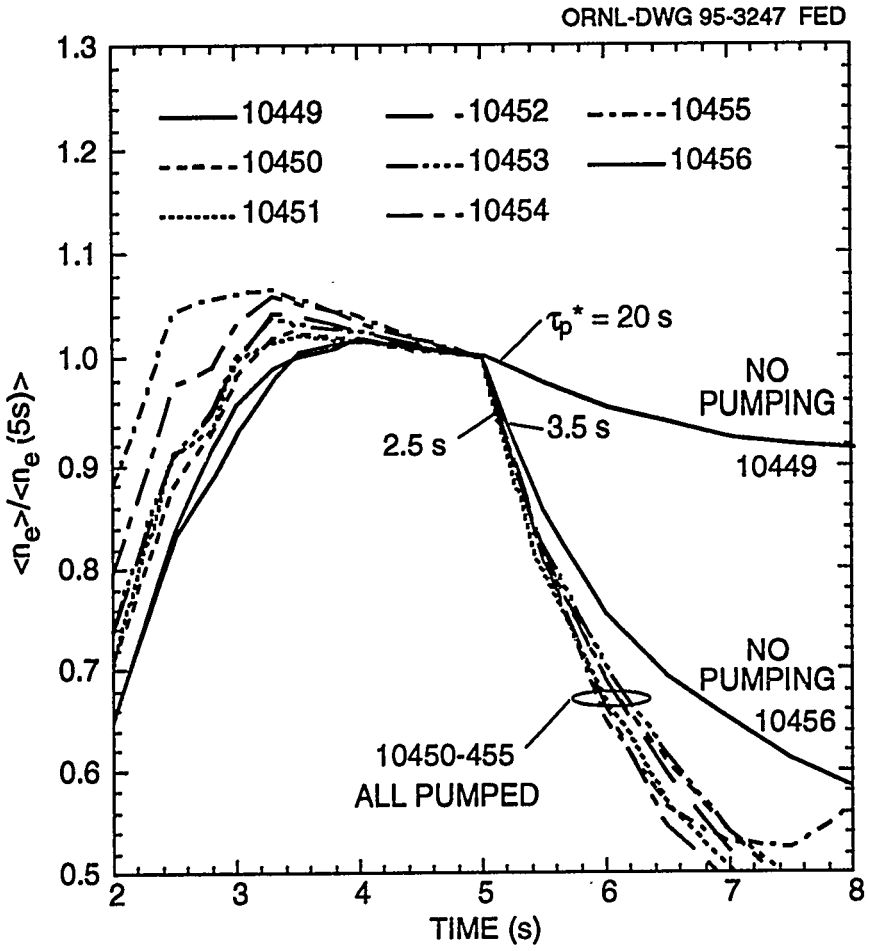

Fig. 1.19. Series of discharges normalized to density at $t = 5$ s (termination of gas puff). Shot 10449 was last shot before pumping, 10450–10455 were pumped, and 10456 was without pumping.

This mechanism offers a method for continuous wall pumping and depletion for steady-state operation in the Tokamak Physics Experiment (TPX) or ITER. Similar observations have since been made in DIII-D with the pumped divertor and will provide the basis for developing wall conditioning methods for steady-state devices.

Evaluation of new concepts for Tore Supra

A novel way of controlling the particle content in the plasma is the "vented" limiter. In this arrangement, the limiter consists of a flat plate with holes or slots. Behind the slots is a vacuum plenum. The idea is to collect mostly neutrals, created by charge exchange or Franck-Condon processes, through the slots and thus avoid leading edges, which usually present problems for high heat flux removal. Using a combination of a 1-D plasma edge code and the DEGAS code, we have performed an analysis of a vented limiter system for Tore Supra.[39] In comparison with regular pump limiters, the results indicate slightly lower efficiency for particle control, but because there was no leading-edge problem, they were encouraging enough to perform a prototype experiment. For this experiment, one of the bottom pump limiter modules was equipped with slots on the plasma-facing surface and was then used as the main limiter in an ohmic plasma. Without pumping, neutral pressures of up to 1.5 mTorr have been achieved at

volume-average densities of 4×10^{19} m^{-3}. This falls within the range resulting from DEGAS modeling.

In support of Tore Supra, a design study has been completed on the performance of a toroidal-belt pump limiter. This pump limiter has a design heat removal rate of 15 MW, with peak heat loads of 5 MW/m^2. A design study had to be performed to ensure that this pump limiter will also provide the necessary particle control. Current predictions indicate that particle removal rates of about 20 Torr-L/s can be achieved, which would be sufficient for steady-state density control in Tore Supra Continu.

Actively cooled modular pump limiter for power and particle control

Preparations of the superconducting Tore Supra tokamak for long-pulse (~30-s), high-power (~6-MW) discharges with lower hybrid (LH) heating require relatively low plasma density, $\sim 3 \times 10^{19}$ m^{-3}, in order to achieve high efficiency for the current drive experiments. To ensure stable operation during this long pulse, plasma density control is needed. One approach is to use pump limiters for the particle exhaust. In this section, the experimental observations are summarized on the particle- and power-handling characteristics of the actively cooled Phase III modular outboard pump limiter (OPL).

The toroidal extent and poloidal extent of the OPL are 0.5 m and 0.6 m, respectively. The limiter head is 2.5 cm thick and made of cooling tubes brazed with pyrolytic graphite tiles. The OPL leading edge is designed to handle heat fluxes of up to ~18 MW/m^2 and power removal of ~1.25 MW. A series of experiments was performed during the commissioning phase of the OPL, and the boronized vessel wall was prepared with an overnight helium glow discharge cleaning. Ohmically heated ~1.45-MW helium plasmas (R_0 = 2.4 m, a_p = 0.72 m, B_T = 3.8 T, I_p = 1.45 MA) were created on the inboard limiter and later moved to the OPL, and the plasmas were maintained there for ~6 s with densities of $\bar{n}_e = (3\text{–}5) \times 10^{19}$ m^{-3}. The titanium getter pumps of the OPL were not activated, but a 1-m^3/s turbomolecular pump provided the background pumping. The OPL diagnostics used were Langmuir probes and pressure gauges located in the pumping plenum of the module. The Langmuir probes are on both the ion drift and the electron drift sides of the pump limiter throat entrance, with an opening of ~2.5 cm. During these experiments, helium was pumped at the measured rate of ~0.5 Torr-L/s, resulting in a reduction of ~25% in the helium plasma density (2×10^{19} m^{-3}). This density control was possible with relatively low pumping speed because of the well-conditioned vessel wall. The OPL plenum pressure increased quadratically with the density and attained ~3 mTorr. The resulting particle collection was ~40% of the total particle flux available at the SOL ($\lambda_\Gamma \approx 2$ cm) of the OPL. Typically, the limiter leading edges reached steady-state temperatures of ~500°C in ~5 s. The estimated heat flux ($\lambda_q \approx 1.2$ cm) at the leading edges was ~15 MW/m^2. The OPL received ~50% of the heating power, which was consistent with water calorimetry measurements.

1.2.2.2 Impurity studies

A complete evaluation of particle sources and sinks needs to include a representation of impurities. The first impurity studies were performed in the pump limiter throat. For this purpose, an optical view of the neutralizer plate, consisting of ten optic fibers, was installed from the back end of the pump limiter. The ion flux to the plate was given by the Langmuir probe data in the throat. DEGAS modeling studies had shown that flux amplification between the probe and the neutralizer plate was negligible when the pump limiter was activated. The temperature of the neutralizer plate could not be measured, but the limiter front-face temperature, obtained from infrared (IR) measurements, was used with a thermal code to determine that the plate temperature

was between 450°C and 550°C. It was further assumed that the electron temperature in the sheath in front of the plate was 3 times the electron temperature measured with the Langmuir probe. The resulting ion temperatures were on the order of 100 eV. A typical spectrum obtained in the throat of the pump limiter is depicted in Fig. 1.20. It shows the band of the CD molecule as well as one of the atomic lines of the C^+ ion.

The pump limiter throat region provides a good test bed for the ORNL-developed BBQ impurities code for high-density and low-temperature divertorlike conditions. With this model, using input from the Langmuir probes, impurity generation and transport from the throat region of the Tore Supra Phase II pump limiter were estimated and compared with detailed spectroscopic measurements. Experimentally obtained evidence of chemical sputtering has been confirmed by comparison with the expected emission, which was predicted using available data for chemical sputtering with resulting CH_4 emission. Also, the modeling results indicate that <10% of the impurities generated in the throat region escape to the SOL.

The new visible-region imaging diagnostic (modified endoscope) is now optimized for measurements of the impurity source distribution on the front face of the OPL. First measurements of the front face of the Phase I ("dummy") outboard limiter were made on February 11, 1994. Detailed spatial profiles of C(II), C(III), and D_α were obtained in ohmic plasmas for a range of densities at three different plasma currents (0.8, 1.25, and 1.5 MA).

1.2.2.3 Detailed modeling of impurity and power fluxes

Detailed modeling of impurity generation and transport associated with the inner wall of Tore Supra has been carried out in collaboration with D. Guilhem, A. Seigneur, and other members of the Tore Supra team. A model of the discrete tile structure (~7500 graphite blocks) has been created, and the shadowing and overheating effects resulting from misaligned tiles have been estimated. The impurity production resulting from hydrogenic and carbon self-sputtering has

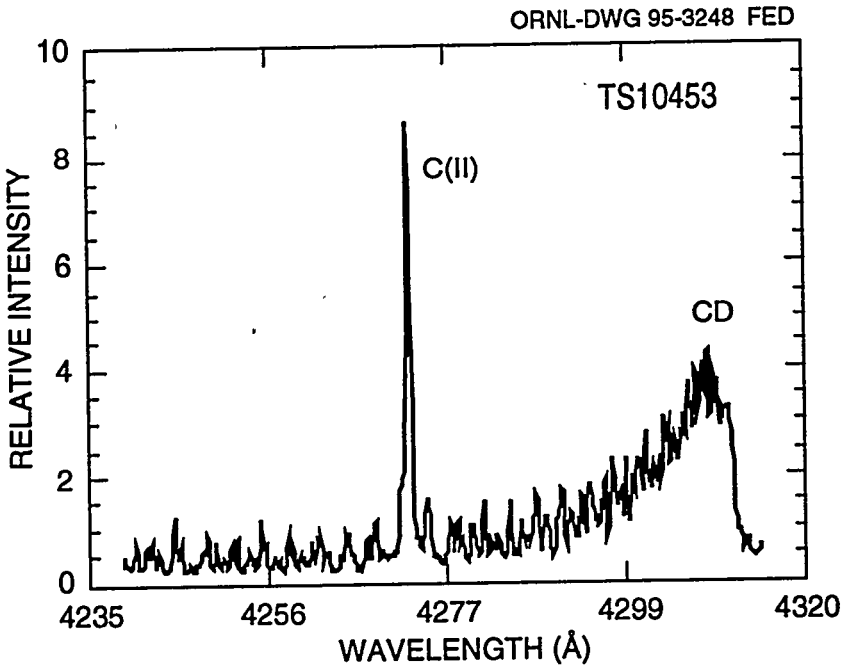

Fig. 1.20. Typical spectrum obtained in throat of pump limiter.

been calculated and used as a source for the ORNL 3-D Monte Carlo impurity transport code, BBQ. Reasonable agreement was found between the expected emission profiles of C(II) ions and the spectroscopic data for the inner wall. Based on this modeling, new experiments have been proposed, in which moderate plasma shaping ($\kappa \approx 1.1$) is to be employed to ameliorate peak heat fluxes. Calculations will be undertaken to estimate the benefits from several proposed improvements in the inner wall, such as tile chamfering. The benefits in heat removal have to be compared with possible worsening in impurity penetration efficiency, and these are to be estimated with BBQ. The interaction of impurity fluxes generated on the inner wall with other plasma-facing components [lower pump limiters, OPLs, and radio frequency (rf) antennas] are being calculated as well. Such multilimiter interactions are expected to play a key role in long-pulse heat removal experiments. Comparisons with detailed spectroscopic and IR data are being made.

BBQ SOL impurity transport code

To characterize the impurity sources in Tore Supra, it is desirable to link estimates of the impurities generation rate at plasma-facing components with the observed characteristics of the impurities in the SOL and core plasma. These characteristics are typically the spatial distributions of the spectroscopically observable impurity charge states, the thermal imaging for the SOL, and the radial transport code fits to the observed core light emission. To make this connection, it is necessary to have a code that takes into account the detailed structure of the plasma-facing components, since the impurity generation rate is critically dependent on the angle of incidence of field lines with respect to the edge structures. Further, the transport and subsequent ionization and recombination of impurities in the SOL is an inherently multidimensional process, as the impurities free-stream along the field lines and diffuse across the flux surfaces, and it depends in essential ways on the rate of heating of the particles as they interact with the background plasma. The Monte Carlo "test particle" technique is well suited to interpretation of experiments. This method assumes that impurity generation and transport take place in a given hydrogenic plasma background. While this approach has limitations for the prediction of reactor-scale conditions (e.g., for ITER), it is well suited for application to the problem of experimental interpretation because information on the plasma background is obtained from edge diagnostics, such as the reciprocating Langmuir probes in Tore Supra. Thus, the BBQ impurity transport code has been developed for Tore Supra application. At present, BBQ incorporates a detailed description of the Tore Supra plasma-facing structures for the inner wall; the Phase I, II, and III OPLs; the vertical pump limiters; the lateral protection surfaces of the ion cyclotron heating (ICH) antenna; and the LH grills.

Given an incident flux of D^+ ions and the ambient sheath condition, neutral carbon particles (for physical sputtering) or CD_4 particles (for chemical sputtering) are launched. Each particle incident from the plasma-facing component is tracked until its final disposition. The particles are assumed to diffuse in both parallel and perpendicular directions to a defined set of magnetic flux surfaces. In these calculations we use an analytic parameterization to describe the flux surfaces, although the use of exact magnetics data is also feasible. To consider the effect of plasma shape and displacement on heat and particle deposition, we adopt a simplified model for the plasma cross section. The parameters used in this description are obtained from Tore Supra magnetics fitting routines. The particles move on straight-line tracks until the first ionization or until after recombination into the neutral state. While charged, the particles move on flux surfaces as described by the magnetics model, free-stream along field lines, and diffuse by random diffusive processes. The maximum allowable step size is predetermined (usually set at $0.01 \times$ the grid resolution), and a track length estimator is used to choose a time step. The track length estimator

uses a first ionization probability of 10% to estimate the step length for neutral particles or 10% of the next stage ionization distance to estimate the step length for charged particles. Subsequent steps are handled differently, depending on whether the particles are charged.

Heat deposition on the Tore Supra inner wall

BBQ requires a calculation of the expected particle and heat fluxes to the inner wall of Tore Supra. These calculations apply the "exponential-sine" SOL heat flux deposition model to a geometry consisting of discrete tiles, located at their "ideal" (i.e., design) positions. No account is taken of possible misalignment because of cracking or installation and operational anomalies. The calculations show that the predicted heat and particle fluxes are a factor of 2 greater than those calculated using a more ideal compound circle model for the inner wall, in the absence of leading-edge considerations. Heat fluxes as large as 4 MW/m^2 are predicted for a case with 12 MW net thermal efflux. Such large "ideal" heat fluxes are caused by the infinite radius of curvature of the elements of the currently installed flat tile set. When leading-edge fluxes are included, localized heat fluxes as large as 50 MW/m^2 are predicted for the tops of tiles located near the equator, for the same total heat efflux. These spots are predicted to be very localized (~1 mm). The largest total power delivered to such an exposed face is found to be ~0.8 MW to the uppermost (leading-edge) tile. The largest value for an equatorial tile is found to be ~0.1 MW. For particle fluxes, it is estimated from these calculations that as much as 17% of the particle efflux may be collected in the gaps between the tiles. Work is in progress to estimate the results for misaligned tiles and on calculations for plasmas shifted vertically off axis.

Discrete tile geometry effects: total impurity fluxes to the core, chamfered and unchamfered cases

As an example of the combination of impurity generation and BBQ calculations, we have compared the impurity fluxes to the core from chamfered and unchamfered inner wall tiles, with a net 12 MW power efflux from the plasma. The parameters resulting from this comparison are described in Table 1.2.

Table 1.2. Core impurity flux comparison

Case	Unchamfered	Chamfered
Impurity flux from D^+ sputtering	9.73×10^{19} s^{-1}	6.75×10^{19} s^{-1} (per MW)
Core penetration efficiency	0.345	0.319
Resulting core influx	$3.36 \times 10^{19} s^{-1}$	2.16×10^{19} s^{-1}
Impurity flux from C^{n+} self-sputtering	3.9×10^{18} s^{-1}	2.76×10^{18} s^{-1}
Core penetration efficiency	0.414	0.407
Resulting core influx	1.61×10^{18} s^{-1}	1.12×10^{18} s^{-1}
Total core influx	3.52×10^{19} s^{-1}	2.27×10^{19} s^{-1}

1.2.2.4 Rf–plasma edge interactions

Experimental measurements of ICRF and edge plasma interactions on Tore Supra

J. H. Harris, C. E. Thomas, Jr., J. T. Hogan, G. R. Haste, S. Tobin, and C. C. Klepper

Experiments to explore the interaction of ICRF heating with the edge plasmas on the Tore Supra tokamak have begun. The actively cooled lateral protection (bumper limiters) on the three ICRF antennas in Tore Supra can experience overheating for power levels >2 MW per antenna and pulse lengths >2 s (depending on the power level) even when the antennas are operated in dipole mode. It appears that the local power fluxes on the lateral protection may exceed the nominally expected fluxes of 5 MW/m^2. Concentrated heat fluxes can result in hot spots with temperatures >1000°C and can result in damage to the carbon tiles that make up the armor on the lateral protection.

Initial experiments have been conducted with plasmas having I_p = 0.8–1.6 MA, $q(a)$ = 3–6, and P_{rf} = 1–2 MW to characterize the phenomena that could contribute to the overheating and to develop the diagnostic tools to be used in more comprehensive studies. Reciprocating magnetic and Langmuir probes have been used to measure the rf magnetic field amplitudes in the edge plasma and to measure the potential, electron density, and temperature on field lines connected to an antenna. Current steps are used to vary $q(a)$ during a discharge and move the field line intersecting the Langmuir probe along the antenna in the poloidal direction. Figure 1.21 shows plots of the plasma potential and density profiles determined from one series of probe movements with and without rf power. When the probe field line touches the lower corner of the ion cyclotron resonance heating (ICRH) antenna and 1 MW of ICRF power is applied to the antenna, a 50-V (differential voltage) peak in the floating potential profile and a steep density gradient appear near the last closed flux surface; these features fade when the probe field line is removed from the antenna corner. These potential structures might be evidence of an rf potential sheath.[40,41]

A charge-coupled device (CCD) camera system has been used to observe visible C(III) (4647 Å) and IR emission from the antennas. Relatively faint C(III) emission is seen from an unpowered antenna, even when ICRF power is applied to another antenna. When the antenna is powered, this emission increases markedly and is distributed across the face of the Faraday screen. Figure 1.22 shows (1) the behavior of the image-integrated C(III) emission measured using a CCD camera aimed at the Tore Supra Q1 antenna and (2) the IR temperatures of three hot spots on the Q5 antenna that were monitored using the IR camera. In this shot, the rf power was applied in two pulses, one to the Q1 antenna and one to the Q5 antenna. The C(III) emission from the Q1 antenna rises rapidly (on a time scale ≤ 100 ms, limited by diagnostic resolution time) when rf power is applied to Q1 and then decreases strongly part of the way through the heating pulse; the reduction in rf power during this pulse was caused by power-regulating circuitry in the transmitter system and is not because of a breakdown or abrupt change in antenna coupling. The C(III) emission from Q1 also increases rapidly when rf power is applied to the Q5 antenna (which is not in the field of view of the visible CCD camera) in the second rf pulse, but this increase is significantly smaller than for the first pulse. These data must be interpreted cautiously because the finite spectral bandwidth, stray light, and integration over emitting zones all add considerable uncertainty. However, the relative variations and time scales of the signals do provide preliminary information on the antenna-plasma interactions.

The IR temperature traces in Fig. 1.23 show that the temperatures of the three hot spots on the Q5 antenna change very little when power is applied to the Q1 antenna but rise significantly (with a time constant in the range of a few seconds) when rf power is applied to the Q5 antenna.

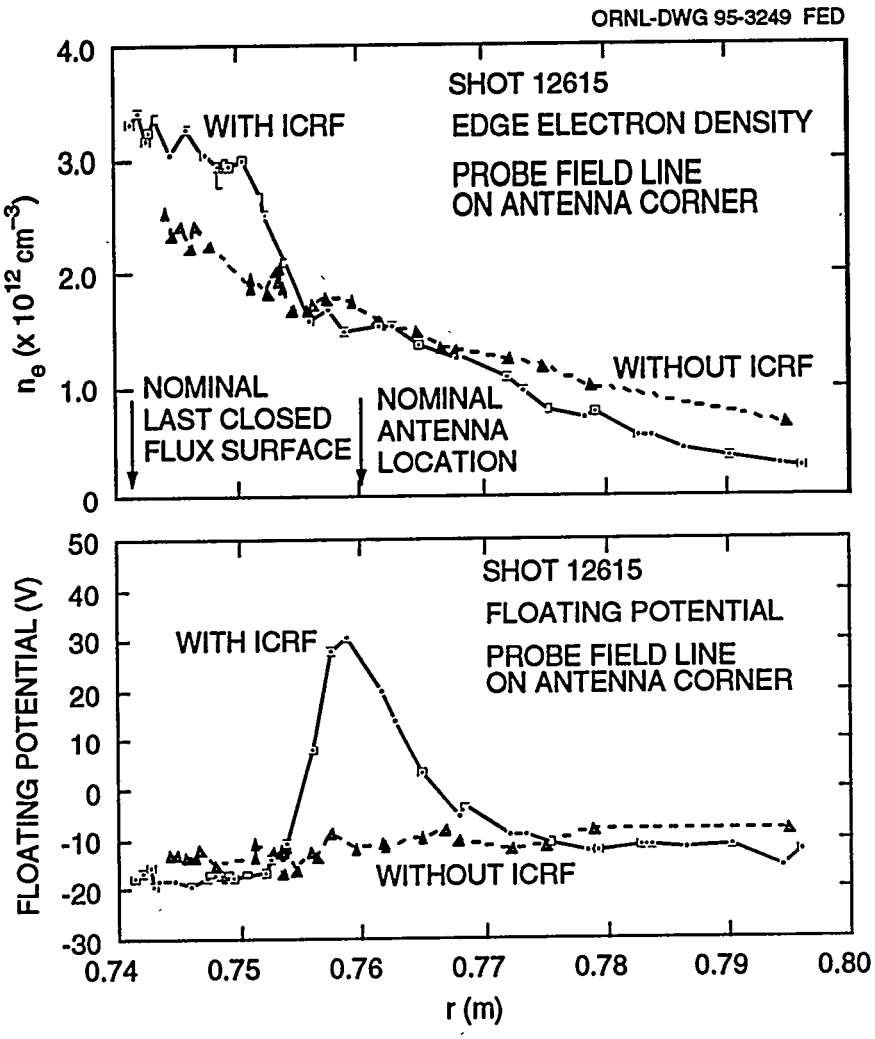

Fig. 1.21. Langmuir probe measurements of density and floating potential in plasma edge.

The surface temperature distribution (derived from the IR images) on the lateral protection can be varied significantly by using the Tore Supra ergodic divertor to modify the magnetic configuration of the edge plasma. The locations of the maximum temperatures shift along the lateral protection in response to changes in the field line connection geometry, suggesting that the hot zones are not simply "frozen" to the locations of damaged tiles or locally reduced cooling efficiency, but the contact geometry of the magnetic field lines also plays a role.

These observations suggest that the interaction of the antenna and the plasma edge involve (1) rf-plasma phenomena (both global and local to the antenna region); (2) the magnetic connections of the antenna to other plasma-facing components (e.g., inner wall, outboard limiters); and (3) thermal effects in the lateral protection. Future experiments will combine measurements of edge plasma parameters with spectroscopic studies and antenna imaging in C(II), C(III), and IR light.

We have also begun work on developing modeling techniques that will help evaluate the relative importance of the many possible physical effects in the antenna-plasma interaction. We have added the exact Tore Supra ICRF antenna geometries to the BBQ 3-D impurity transport

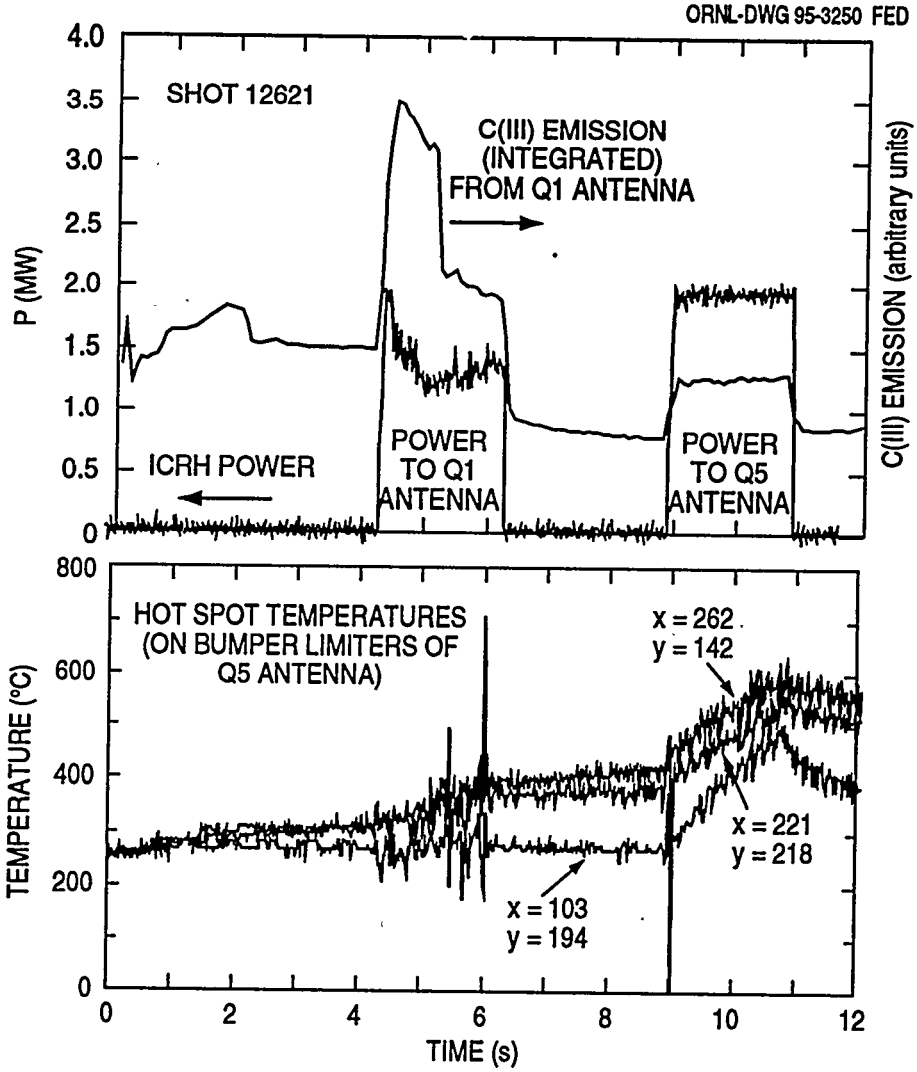

Fig. 1.22. Time history of C(III) emission from Q1 antenna and IR hot spot temperatures on Q5 antenna. Threshold level of IR system set for ~260°C. Hot spot coordinates refer to pixel locations in IR images.

code previously used to study limiter surface interactions, and we have begun model calculations. The code uses the measured SOL background plasma parameters to compute the D^+ particle flux and ambient sheath potential (typically ~50 V) at the lateral protection surface. From this flux, and the detailed geometry of the protection (angle of incidence), the predicted C(I) emission caused by physical sputtering and CD_4 emission caused by chemical sputtering is computed. Emission of C(I) resulting from self-sputtering by (assumed) C(IV) emitted from distant surfaces is also estimated. The C(I) that arises directly from physical sputtering has an assumed Thomson distribution (which can produce a high-energy tail), while the chemically produced CD_4 is assumed to be emitted with the wall temperature (0.1 eV). Thus, carbon impurities produced by physical sputtering have a broader region of localization than the carbon from the CD_4 breakup process, which may acquire a Franck-Condon energy of ~1 eV from the dissociation. The spatial distribution of other possible chemical evolutes (e.g., C_2D_2) is expected to be similar but has not yet been considered in detail. The characteristic spatial emission is shown in Fig. 1.23, with C(III)

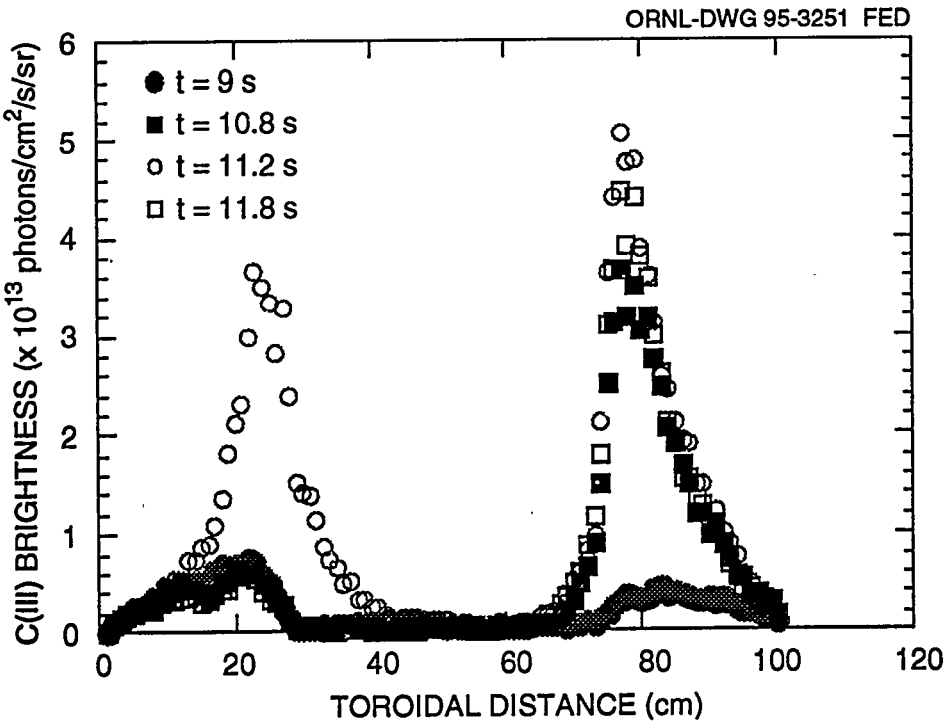

Fig. 1.23. Profile of C(III) emission across Tore Supra Q5 ICRF antenna. C(III) emission calculated by BBQ SOL impurity transport code at four times during a sample discharge, using temperature evolution data shown in Fig. 1.22. Locations of three hot spots caused by cooling defects are assumed, and C(II) emission results from combined physical and chemical sputtering.

brightness distributions calculated for $t = 9$, 10.8, 11.2, and 12 s using the hot spot temperature data in Fig. 1.22. Note that the peak temperatures in Fig. 1.22 lie at the maximum of predicted chemical sputter yield curves.

The observed temperatures at hot spots on the antenna lateral protection are near the expected maximum of chemical sputtering yields. However, the time scale of the decay of the C(III) emission predicted from model calculations of chemical sputtering (CD_4 emission) based on the observed temperatures of hot spots on the antenna bumper limiters can be much longer than seen in the experiment (~1 s vs 0.2 s). Our preliminary conclusion is that plasma-specific effects (e.g., hot particle interactions) and rf-specific effects (e.g., rf sheaths, such as those discussed in Refs. 40 and 41) must be considered further in order to explain the experimental observations fully.

1.2.3 Helium Transport and Exhaust Studies on the TEXTOR Tokamak

D. L. Hillis, J. T. Hogan, A. P. Zwicker, M. R. Wade, and the TEXTOR Team

The TEXTOR tokamak is equipped with a full toroidal-belt limiter, which is pumped by turbomolecular pumps. This belt pump limiter configuration is called the Advanced Limiter Test II (ALT-II). The necessity of understanding helium transport and exhaust mechanisms in designing ITER has continued to provide a focus for the TEXTOR helium transport program. The

current interest in L-mode discharges, as an ITER operational scenario, has provided an excellent opportunity for TEXTOR to investigate helium transport over a wide range of L-mode conditions.

To provide detailed helium transport information during either helium gas injection or helium NBI, CER spectroscopy is used to measure the helium density profile over time during the TEXTOR discharge. In collaboration with scientists at the Forschung Zentrum-Jülich, ORNL prepared a 2-D optical multichannel analyzer (OMA) system, and first measurements were performed during FY 1994. The CER spectroscopy measurements were performed with combined ICRH and NB heating. The 2-D OMA system provided measurements of the helium density profile at ten radial points along the plasma minor radius every 40 ms throughout the plasma discharge. Previously, only three radial points were available from separate spectrometer systems. The improved spatial resolution of the helium density profile permits improved modeling of the helium transport within the discharges so that the anomalous diffusivity D_α and the pinch velocity v_p can be determined more accurately. The 2-D OMA spectroscopy system has been absolutely calibrated so that absolute measurements of the helium density profile can be performed.

The first helium experiments with the new 2-D OMA system investigated helium transport and exhaust in the TEXTOR improved confinement (or I-mode) with full ALT-II pumping during ICRH and NB heating after siliconization. A typical ten-point helium profile found in these measurements at t = 1.5 s for the TEXTOR discharge is shown in Fig. 1.24. The 2-D OMA is capable of producing a ten-point helium density profile every 20 ms during the TEXTOR plasma discharge. This capability is featured in Fig. 1.25, where the helium density profile is displayed as a function of time throughout a TEXTOR discharge. Figure 1.25 shows the evolution of helium into plasma after the helium gas puff at t = 1.0 s and its subsequent exhaust via the ALT-II pump limiter. Clearly, ~90% of the injected helium has been removed from the TEXTOR discharge by ALT-II within the first second after the gas puff. These detailed measurements of the helium

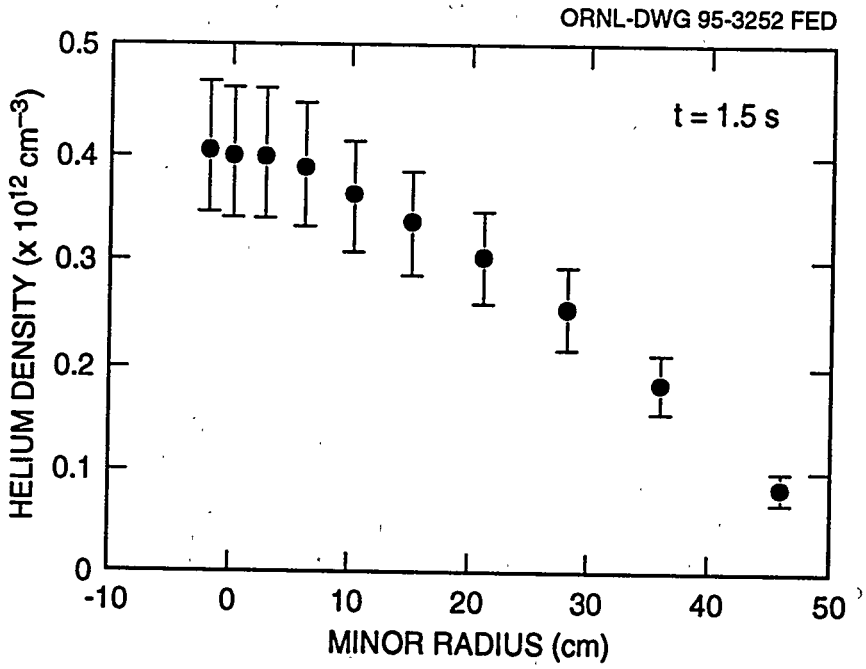

Fig. 1.24. Helium density profile measured at t = 1.5 s with 2-D OMA on TEXTOR with full ALT-II pumping. CER spectroscopy used to study helium exhaust.

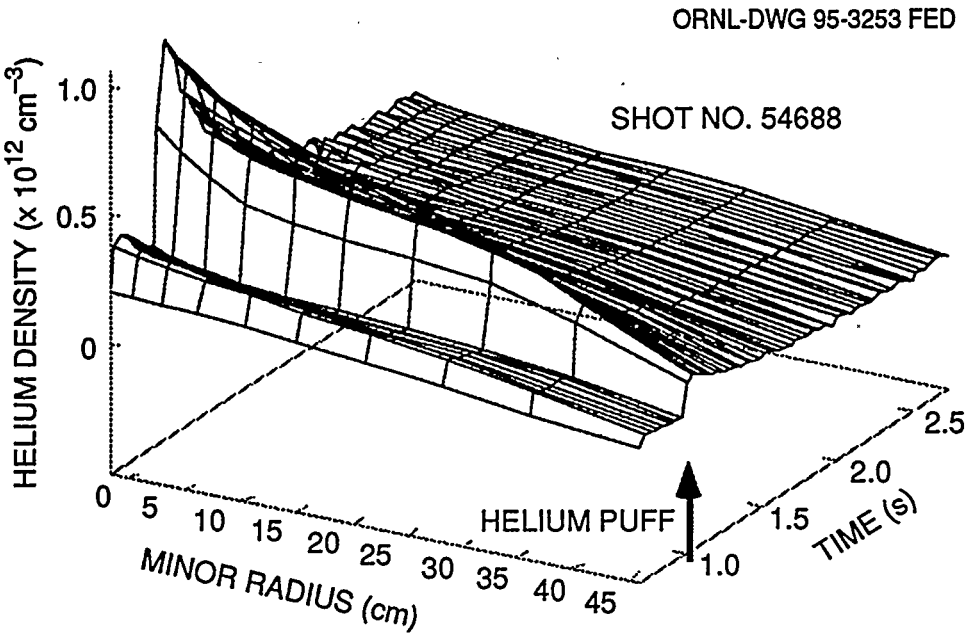

Fig. 1.25. Three-dimensional profile of helium density with full pumping. Ten-channel CER spectroscopy system on TEXTOR used to develop profile.

radial profiles will provide the necessary data to perform helium transport modeling and determine diffusivities and pinch velocities for I-mode discharges on TEXTOR.

Using the new 2-D OMA, helium transport experiments were also performed on TEXTOR to investigate the expulsion of helium from the plasma core by resonant coupling of ICRH to the helium ions. In a fusion reactor, it may be desirable to have a method of active control by expelling the helium ash or enhancing the diffusion of helium out of the plasma core. According to a proposal by C. S. Chang et al.,[42,43] it is possible to use resonant ion cyclotron waves interacting with the α particles (helium) to expel them when they have transferred ~90% of their energy to the background plasma. A coupling of the ICRH waves to this particle group is promising because it does not require a large heating power (~1 MW on TEXTOR), and the resonance frequency is still sufficiently separated from that of the deuterium. The results of these experiments are published in *Physical Review Letters*.[44] These experiments indicate that helium can be preferentially expelled by applying ICRH waves to the helium ions. Additional experiments will be necessary to determine the practicality of this method for controlling helium concentrations in the plasma core, but these initial experiments provide a possible scenario for helium expulsion if helium buildup in the plasma core of a reactor becomes a problem. Future experiments on TEXTOR will investigate helium exhaust in the presence of a neon radiating boundary.

1.3 CONFINEMENT PHYSICS PROGRAM

1.3.1 The Role of Shaping in Achieving High Performance in DIII-D

E. A. Lazarus and the DIII-D Team

While it is expected that the beta limit will depend on shape, we also find that confinement, at finite beta, depends on the plasma shape. The plasma triangularity is most important to

performance, while plasma elongation plays a weaker role. Here, we take the product $\beta \cdot \tau$ as a measure of performance. As a result of continuing improvements in the DIII-D device, a new DIII-D record triple product of $n_D(0)T_i(0)\tau_E^{th} = 4 \times 10^{20}$ (keV·s/m^3), $n_D(0)T_i(0)\tau_E = 5.6 \times 10^{20}$ (keV·s/m^3) was achieved. The particular choices of shape for this study were determined partly by physics and partly by preliminary design work on the radiative divertor.

In previous work on DIII-D, it has been shown that β depends on plasma shape in a manner consistent with Troyon scaling.[45,46] We will use the parameter $S \equiv I_p q_\psi / aB$, a measure of the toroidally weighted poloidal contour length, to characterize the plasma geometry. We have observed in a comparison of single- and double-null diverted plasmas[47] that the performance of double-null plasmas is superior to that of the single-null. Summarizing those results briefly, we found that (1) $\beta \cdot \tau$ increases with increasing S, (2) $\beta \cdot \tau$ decreases with increasing plasma current for $q_\psi < 4$, (3) $\beta \cdot \tau$ increases approximately as $\sqrt{B_t}$, and (4) for double-null plasmas good confinement is maintained with $\beta_N > 3$, whereas for single-null plasmas the confinement begins to degrade at $\beta_N = 2$.

The focus of this experimental effort was to clarify the features responsible for this improved performance, and the findings make clear that plasma shape, in particular triangularity, is the important variable. In the experiment, we investigated four double-null shapes: (1) $\kappa \approx 2.1$, $\delta \approx 0.9$, (2) $\kappa \approx 1.8$, $\delta \approx 0.8$, (3) $\kappa \approx 2.1$, $\delta \approx 0.3$, and (4) $\kappa \approx 1.8$, $\delta \approx 0.3$. For each shape, plasma current and NB power were systematically varied. All work was done at $B_t = 2.1$ T. Results discussed here were obtained during the ELM-free period, of durations 0.22–1.3 s. The termination of this phase is correlated with an uncontrolled increase in plasma density typical of H-mode plasmas. It was deemed necessary to return to the standard configuration (shape A) as a benchmark for other shapes. With the addition of carbon armor tiles to the outer wall of the DIII-D vacuum vessel, the performance was improved, as evidenced by a new DIII-D record $\beta \cdot \tau$ of 1.7 (%-s) and longer ELM-free periods than achieved previously under similar conditions.

Using DIII-D/Joint European Torus (JET) confinement scaling, $\tau_E \approx F \cdot I_p R^{3/2p-1/2}$, where F is an enhancement factor, then, below the β limit, we can write

$$\beta \cdot \tau_E = \text{const.} \left(\frac{S^2 R^2}{1 + \kappa^2} \right) \left(\frac{F}{q} \right)^2 .$$

Figure 1.26 presents the shapes used in this experiment, and for each discharge, the maximum $\beta \cdot \tau$ vs the geometric quantity $(S^2R^2/1 + \kappa^2)$. This is a reasonably good descriptor of performance. The dependence of performance on elongation is somewhat surprising. Note that performance is much better for shape B, $\kappa \approx 1.8$, $\delta \approx 0.8$, than for higher elongation with lower triangularity.

The separation of I_p and the safety factor q afforded by the geometric variation makes it clear that the degradation in F that occurs with increased plasma current is an effect of lowered q, not explicitly I_p.

While shaping might be thought to affect primarily the outer regions of the plasma, the most dramatic change with plasma shape lies in central heating efficiency. To illustrate this, Fig. 1.27 compares the electron temperature profiles for shapes B and D, under similar heating-power and safety-factor conditions. For the higher triangularity plasma, the temperature gradient remains large from approximately the $q = 2$ surface to the magnetic axis, whereas at lower triangularity the rise in T_e is more modest. Similar effects are seen in the T_i profiles. Density profiles are similar in both cases and are very broad, typical of DIII-D ELM-free plasmas.

A difference in the evolution of q_0 is also observed. For high-triangularity plasmas, when beam-heating commences, q_0, as measured with a motional Stark effect (MSE) diagnostic, rises

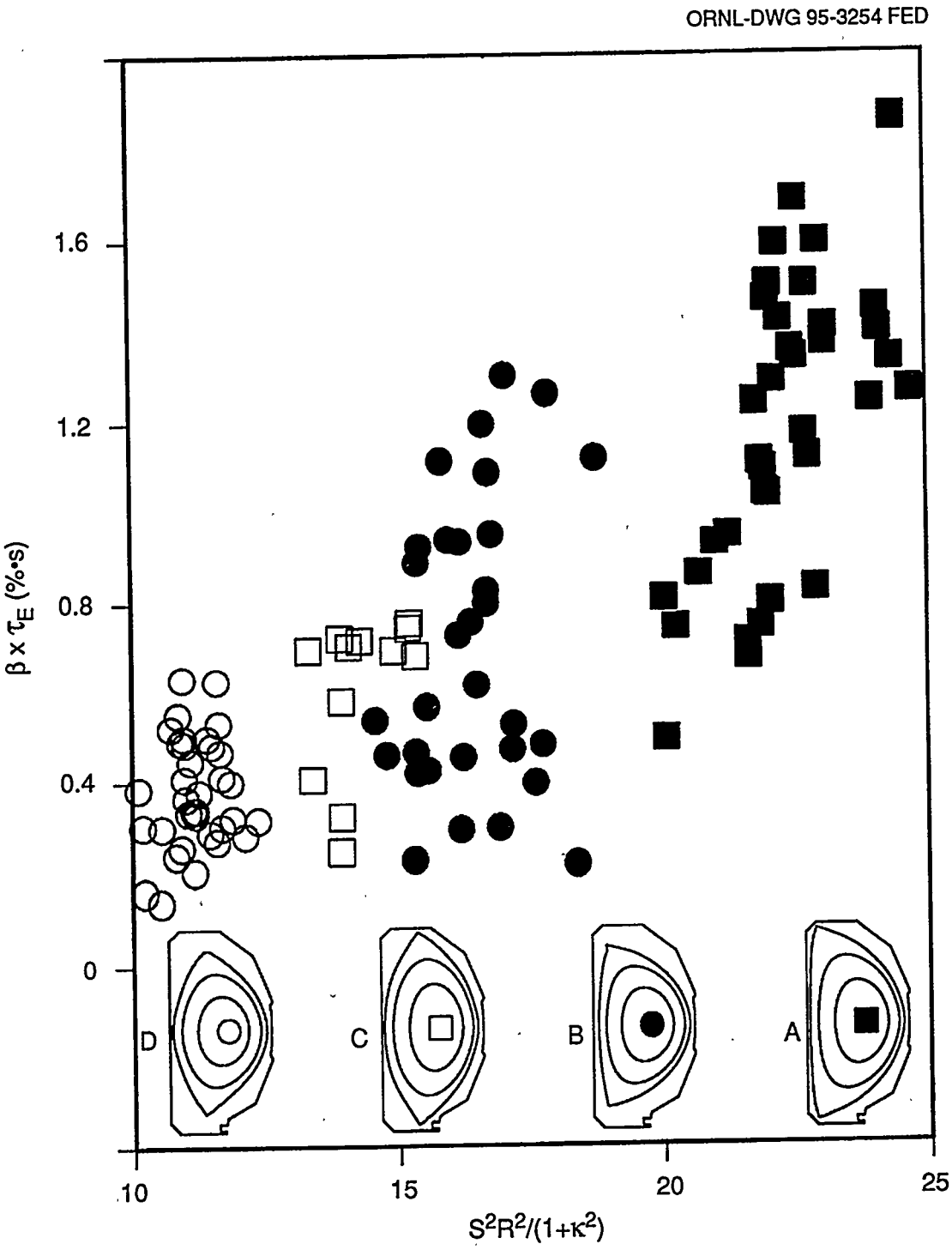

Fig. 1.26. Experimental shapes and maximum $\beta \cdot \tau$ vs geometric quantity $(S^2R^2/1 + \kappa^2)$.

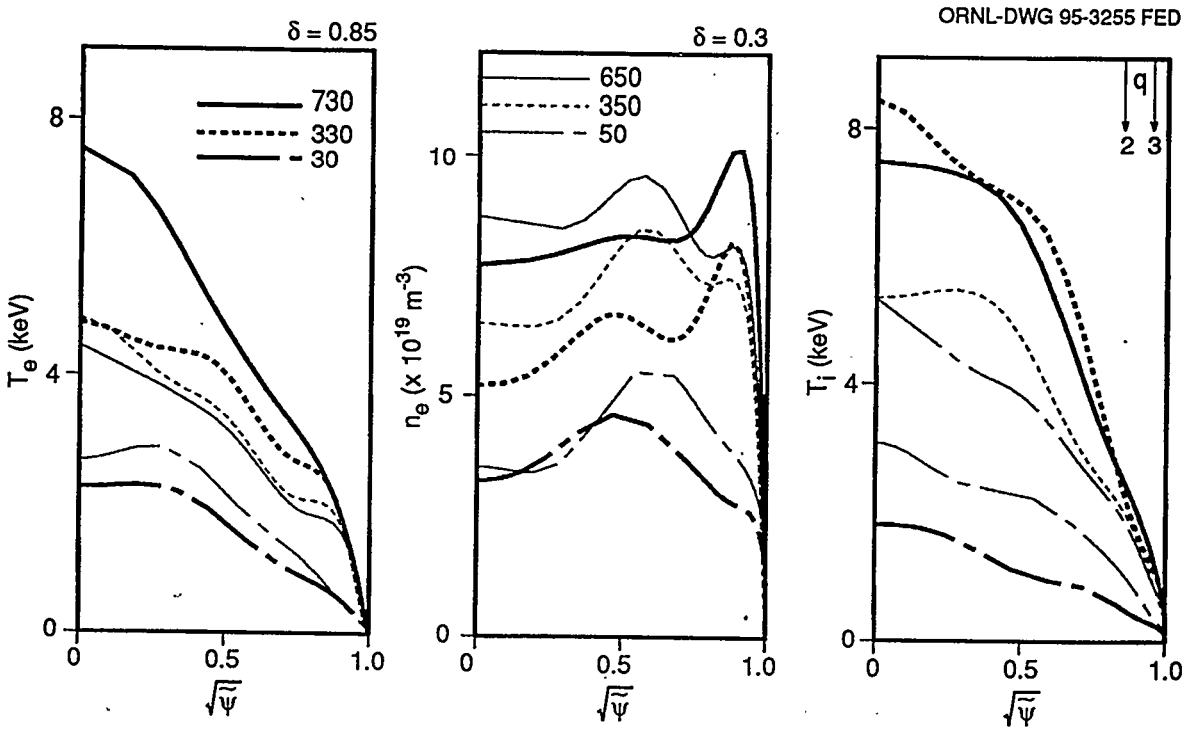

Fig. 1.27. Comparison of electron temperature profiles for shapes B and D.

above unity, typically to about 1.5. For the lower triangularity plasmas little change is seen with heating ($q_0 \lesssim 1$).

For the global results shown in Fig. 1.26, there appears to be a continuum in the quality of the discharge, to the extent that shaping merely affects the ratio of plasma current to safety factor. However, when we examine the plasma core, the results appear more as a bifurcation between those plasmas that attain Mercier stability and those that do not. High-triangularity plasmas have second-stable access. The high-performance phase is transient, and, in fact, a VH-mode.[48] The low-triangularity plasmas retain H-mode.

The dynamics of the current profile evolution has been described in detail.[49] In summary, plasmas that satisfy the Mercier criterion build central p', and a combination of bootstrap and NB current drive alters the current profile so as to remove the $q = 1$ surface from the plasma.

1.3.2 PBX-M Collaboration

R. A. Dory, J. L. Dunlap, A. C. England, D. E. Greenwood, G. R. Hanson, J. H. Harris, G. H. Henkel, S. P. Hirshman, R. C. Isler, D. K. Lee, J. B. Wilgen, A. P. Post-Zwicker, and the PBX-M Team

During this reporting period, our staff collaborated with the Princeton Plasma Physics Laboratory (PPPL) on experimental operations and physics analyses of the Princeton Beta Experiment—Modified (PBX-M) advanced tokamak program. Specific accomplishments include the following:

- Basic support of experimental operations in the areas of radiation protection, hard X-ray and neutron diagnostics, Thomson scattering, wall conditioning by boronization, impurity spectroscopy, and fluctuation measurements.
- Studies of hard X-ray production and related calculations based on parameters of the plasma and LH current drive (LHCD), leading to elucidating the effects of the LHCD wave spectrum on runaway electron production.
- Establishment and maintenance of a LOCUS data base for the neutron measurements and conducting a scaling study of the neutron source strength as a function of shaping and plasma parameters.
- Development and application of novel computational techniques (e.g., new SURFAS reconstruction code and fast VMEC equilibrium code) for prompt and accurate reconstruction of high-beta PBX-M equilibria from experimental measurements of magnetic fields, plasma profiles, and q profiles (MSE diagnostic). These techniques are being applied on both PBX-M and TFTR and form the basis of a system that could ultimately support real-time equilibrium and stability analysis for long-pulse, steady-state devices such as TPX.
- Installation and calibration of the SPRED spectrometer, and acquisition and analysis of spectroscopic data on impurity generation and transport, with particular emphasis on the effect during ion Bernstein wave (IBW) heating.
- Installation and operation of a new data acquisition system (16 channels, 256,000 samples per channel, 1-MHz sampling) for magnetic fluctuation studies, development of software for expeditious analysis, and acquisition and analyses of data from discharges with NBI, LHCD, and IBW heating. Studies of the L-H transition and ELMing.
- Coordination of two collaborative experiments proposed by Centro de Investigaciones Energéticas, Medioambientales, y Tecnológicas (CIEMAT) of Madrid, Spain, for PBX-M: (1) an AM microwave reflectometer diagnostic to measure density profiles and (2) measurements of electron temperature fluctuations in the plasma edge using a fast-sweep Langmuir probe [also in collaboration with the University of California at Los Angeles (UCLA)]. Development, design, procurement, and construction to supply a major portion of the reflectometer diagnostic and procurement to support the swept probe. Technical support and expert analysis assistance to the CIEMAT reflectometer team in its operation of the diagnostic.
- Development of protocols and computer subroutines for transparent access to PBX-M data from ORNL computers.
- Development of a novel scheme for characterizing intermittent fluctuations using the wavelet transform technique and application of this technique to H-alpha ELM data from PBX H-mode discharges. Extensions of this idea were proposed as an element in tokamak stability control.

1.3.2.1 Effects of LHCD wave spectrum on runaway electron production

Runaway electron production is expected to be influenced by the presence of a spectrum of current drive waves in the vicinity of the runaway critical energy.[50] The wave spectrum in the PBX-M LHCD current profile modification experiments consists primarily of a lobe of fast forward-running waves and a lobe of slow backward-running waves. Both lobes have a finite extent in the spectrum, because the $n_{||}$ upshift has an upper bound.[51] Correlations between the relative position of the runaway critical speed with respect to the forward and backward waves were studied using measurements of hard X-radiation from escaping runaways detected by a scintillator. When the conditions are right [LHCD phase, $n_e(r)$, $T_e(r)$, V_l, etc.], runaways from LHCD discharges are observed, whereas for similar discharges without LHCD power, no run-

aways are observed. Comparisons with the LH upshift relation have shown that a runaway condition can be predicted from the discharge parameters and the $T_e(r)$ and $n_e(r)$ profiles determined by the Thomson scattering diagnostic: if the calculated runaway critical speed is at or below the forward LH wave phase velocity, runaway production is favored.

1.3.2.2 Characterization of plasma parameters for shaped PBX-M discharges

PBX-M was operated with both elongated and bean-shaped plasmas during 1992 and 1993. Two deuterium-fed beams were used for auxiliary heating during 1992, with an average power of ≤2.5 MW. Up to four deuterium-fed beams were used during 1993, with an average power of ≤3.2 MW. The neutron source strength, S_n, showed a scaling with injected power P_b, $S_n \approx P_b^{1.9}$ in both 1992 and 1993. Extensive parameter scans were not performed during this time, because the primary focus of the PBX-M scans was to optimize plasma conditions specifically for profile modification experiments with LHCD and IBW heating. Nevertheless, it was observed that high values of S_n were obtained in bean-shaped plasmas for the highest values of $\varepsilon\beta_p$ at $q^* \approx 2.8$ for 1992. For 1993, the highest values of S_n and stored energy were obtained at $q^* \approx 2.4$, and the highest values of $\varepsilon\beta_p$ were obtained at $q^* \approx 5$. The achievement of high S_n was aided by high beam power, high toroidal field (TF), low current, strong shaping, high electron temperature, and broad profiles. The achievement of high $\varepsilon\beta_p$ was aided by low TF, high density, low triangularity, and broad profiles. The achievement of high β_T was aided by strong shaping, high density, and broad profiles. Increased operating range (higher density) was aided by low triangularity. Comparisons with scalings based on other tokamaks over a broader range of parameters are in progress.

1.3.2.3 Equilibrium reconstruction

Novel computational techniques were developed and applied to obtain accurate and fast (real-time) reconstruction of high-beta PBX-M (and TFTR) equilibria. Previously, data for external magnetic fields and internal pressure profiles have been used. These measurements did not allow good resolution of the plasma current profile. In particular, almost no information about the on-axis safety factor could be determined. With the emergence of the MSE diagnostic on PBX-M, it became possible in principle to measure the local magnetic pitch angle and, through reconstruction techniques, ascertain the internal q-profile. This capability is essential for diagnosing current profile control for advanced tokamak scenarios. For example, reconstruction of LHCD experiments in PBX-M revealed that current deposition was localized to a drop in the on-axis current and a concomitant increase in $q(0)$.

The strongly shaped (indented) plasma of PBX-M presents a numerical challenge to traditional reconstruction techniques. The current filament method, which is a fast, approximate reconstruction method, does not work well for shaped plasmas because of its sensitivity to the filament locations. In the fast SURFAS code, the filament model was generalized to allow toroidal current consistent with the equilibrium equations. To achieve real-time reconstruction speed, data base files are computed a priori from magnetohydrodynamic (MHD) equilibria with widely ranging values of currents and pressures. From these files, equilibria are identified with parameters close to the state being analyzed. A single iteration of Newton's method is carried out to determine the pressure and TF function distributions that best fit (in a least-squares sense) the measured data. This code has been validated against exact MHD equilibrium solutions and is currently in use on PBX-M.

Although SURFAS reconstructions are fast and reliable, they rely on a sufficient data base for their accuracy. The generation of this data base is generally quite time-consuming and

requires running a full MHD-equilibrium code with data-matching capabilities for a wide variety of current and pressure combinations. This process was significantly accelerated by the development of the fast equilibrium reconstruction code VMEC. This code is based on an inverse coordinate description of nested magnetic flux surfaces, which allows it to describe the strongly shaped PBX-M plasma easily. VMEC was upgraded to include data-matching to MSE, magnetic, diamagnetic, and pressure data. A least-squares minimization algorithm is used to obtain the pressure and q profiles, while an energy minimization is performed to find the MHD equilibrium state. The internal profiles were represented in terms of discrete data by using tension splines for the p and q profiles. By adjusting the spline tension, one can directly control the degree to which noisy data are allowed to influence the reconstruction. Also, by specifying the chi-squared weighting of the individual data, the reliability of the measurements can be folded into the reconstruction process.

Additional details are available in Refs. 52–54.

1.3.2.4 Spectroscopic studies

In general, no increased impurity influx or transport changes were observed with the use of LHCD in PBX-M, but severe increases in production of metal ions and very distinct changes in transport were detected when IBW heating was applied. Observations of the use of IBW heating as the sole auxiliary heating source and of its use in conjunction with NBI during L- and H-mode operation are summarized in this section. Characteristic experimental results regarding the impurity behavior in PBX-M are also presented; in general, these are consistent with previous observations in other tokamaks.

In PBX-M it is usually observed that influxes of both low-Z and high-Z impurities increase during IBW injection in all types of operation, although the rates can be minimized by boronization of the vacuum vessel. For example, 340 kW of IBW heating power can raise the iron and nickel concentrations by more than an order of magnitude above the level detected without such auxiliary heating. The central confinement of the working gas also increases, as evidenced by the narrowing of the electron density profiles. Typically, when IBW heating is unaccompanied by NBI, the radiated power profile tends to be hollow before the introduction of IBW heating but thereafter becomes continually more peaked until cessation of IBW heating or a disruption occurs. The peripheral carbon and oxygen emissions grow by factors of 5, while the metals increase until their lines are the dominant features in the vacuum ultraviolet spectrum. The data indicate that the strong increases in radiation from ions such as Fe(XVI) and Ni(XVIII) occur not only because of the increased influx, but also as a result of the impurities becoming more centrally concentrated.

Two distinct behaviors of the impurity transport are observed when IBW heating is used in conjunction with NBI, depending on whether the discharges are in the L-mode or H-mode. In a typical L-mode discharge, it is observed that 2.5 MW of NBI raises the radiation from metallic ions by about a factor of 2 over the levels observed with ohmic heating alone. The addition of 340 kW of IBW heating further increases the metallic emissions by a factor of ~5, but the transport coefficients are not distinctly altered. That is, no central impurity buildup is induced; the plasma remains in the L-mode. If a discharge makes a transition to an H-mode during NBI, the impurity confinement time appears to increase at the onset, but strong central peaking of the radiation and of the metal profiles does not occur (although such an evolution has been observed in H-modes in PBX-M under different operating conditions).[55] However, the addition of IBW heating dramatically alters the radiation pattern as the losses increase by a factor of 4, and the profile becomes very narrow; the electron temperature profile frequently evolves to a flat or slightly hollow shape in these cases. These observations are illustrated in Figs. 1.28 and 1.29,

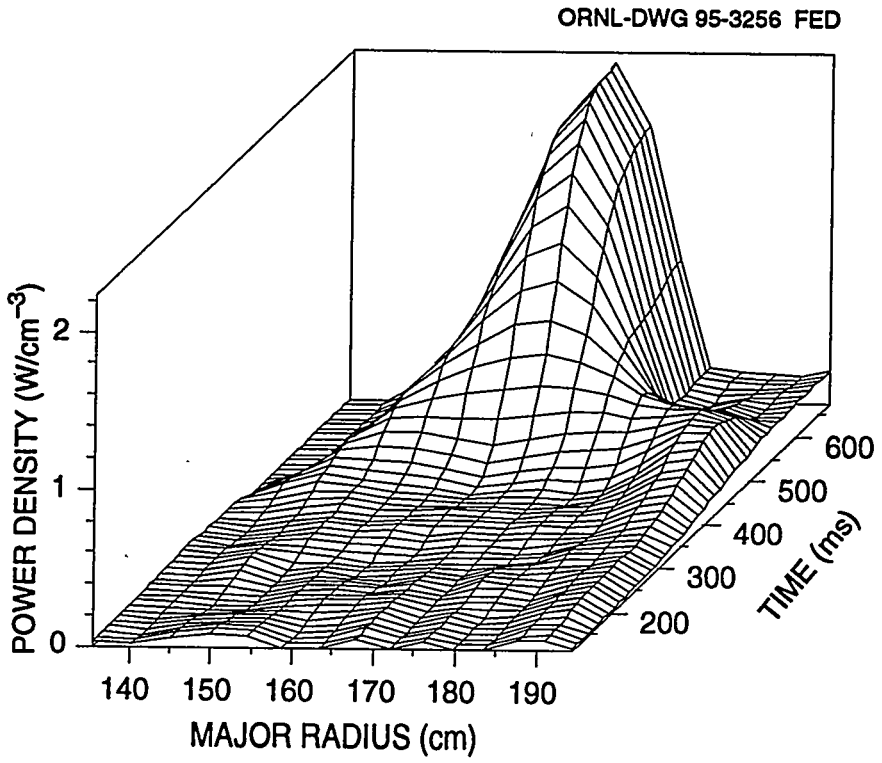

Fig. 1.28. Profiles of radiated power with 410-kW IBW heating introduced into H-mode plasma at 450 ms.

which show the effects of 410 kW of IBW heating in a discharge with 1.5–2.5 MW of NBI. Shortly after the beams are introduced at 350 ms, the plasma makes a transition to the H-mode, and emissions from peripheral ions such as O, V, and C(III) drop as the electron temperature gradient steepens. The signals then rise to pre–H-mode levels as the IBW heating apparently induces a greater influx of impurities starting around 450 ms.

In contrast, the metallic emissions show only minor changes until IBW heating is initiated; the intensities of lines of Fe(XVI) and Ni(XVIII) then grow rapidly up to 525 ms. The subsequent sharp drop in signal strength appears to result from the strong pinch that compresses the iron and nickel toward the center rather than from a decreasing influx. This interpretation is evident from the Fe(XXIII) and Ni(XXV) resonance lines (not depicted), which increase during this interval, although the central temperature is decreasing somewhat. Late in the discharge, the behavior reverses, probably because of cooling of the plasma. The tendency toward central peaking of impurities is also observed in the profiles of O^{8+} ions as deduced from charge-exchange excitation.

Finally, it should be noted that the success of the IBW heating experiments depended markedly on the fact that the machine walls were conditioned by boronization. This was accomplished by inserting doped carbon mesh probes directly into the discharges and allowing them to heat until boron was sublimated.[56] The levels of fluorine, oxygen, and (somewhat later) carbon are all substantially reduced by this procedure. It seems quite probable that without boronization, the tendency of IBW heating to raise the confinement of impurities might well have resulted in disruptions.

Additional details of the studies are given in Refs. 57 and 58.

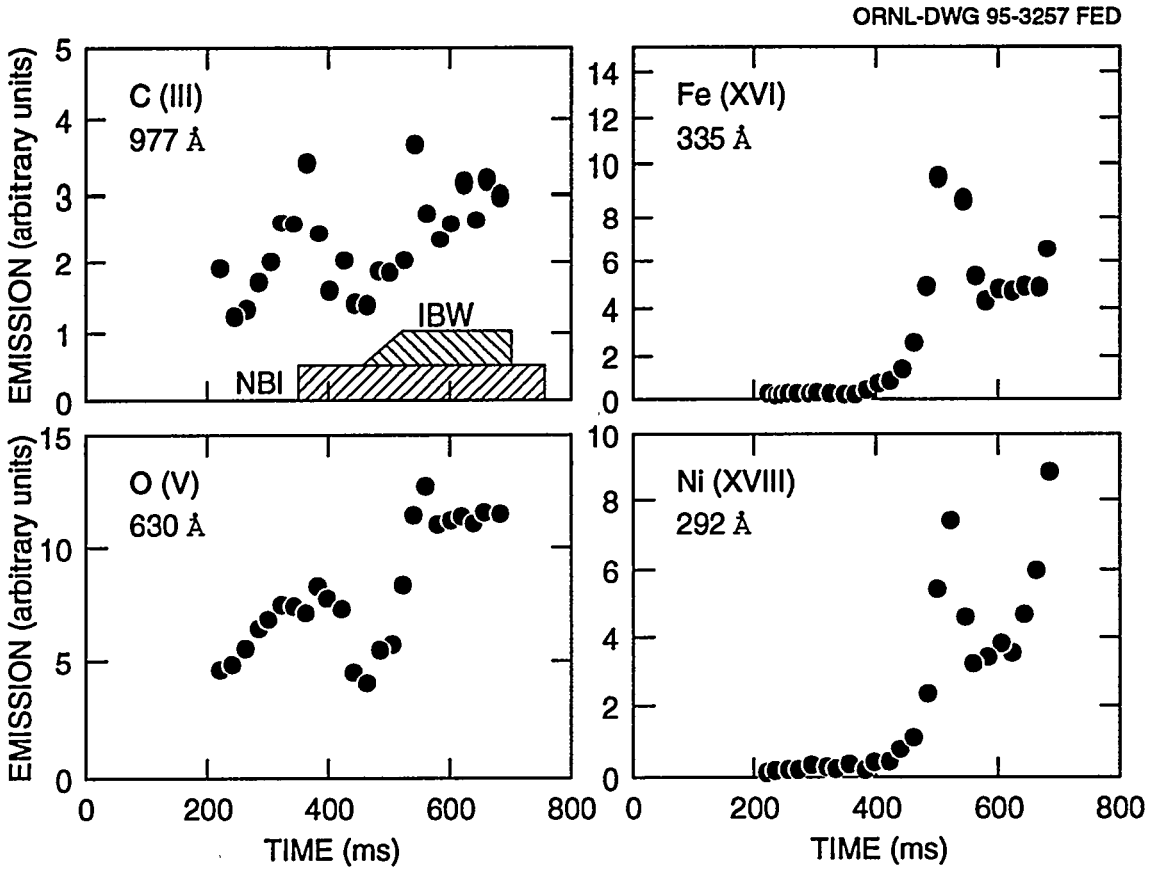

Fig. 1.29. Evolution of spectral line radiation during IBW heating in H-mode plasma.

1.3.2.5 Analysis of Mirnov signals

The magnetic field fluctuations sensed by Mirnov coil diagnostics on PBX-M are richly detailed in both time history and frequency spectrum. This detail, coupled with the large volume of data acquired, makes the analyses of these signals challenging. Two techniques that were developed to deal more effectively with these data are discussed in this section.

The cross-spectral coherence between the signals from one pair of coils was measured. Both coils are on the outer midplane of the torus, and they are separated in toroidal angle by 17°. The results clearly identify regions in time and frequency that are characterized by fluctuations with significant toroidal coherence on the length scale represented by this separation. Similar representations for two or three other separations enable classification of the fluctuations as to relative coherence lengths.

Codes have also been developed to determine the toroidal mode number automatically. The determination is constrained by two user inputs: (1) cross-spectral pairs to ignore and (2) a cutoff value of coherence. A best-fit mode number is calculated for a time-frequency cell only if for each of the remaining cross-spectral pairs that cell has a coherence that exceeds the cutoff. A display of mode numbers in time-frequency coordinates is generated. Figure 1.30 is an example of the graphics.

Details of H-mode and ELM studies are available in Refs. 59 and 60.

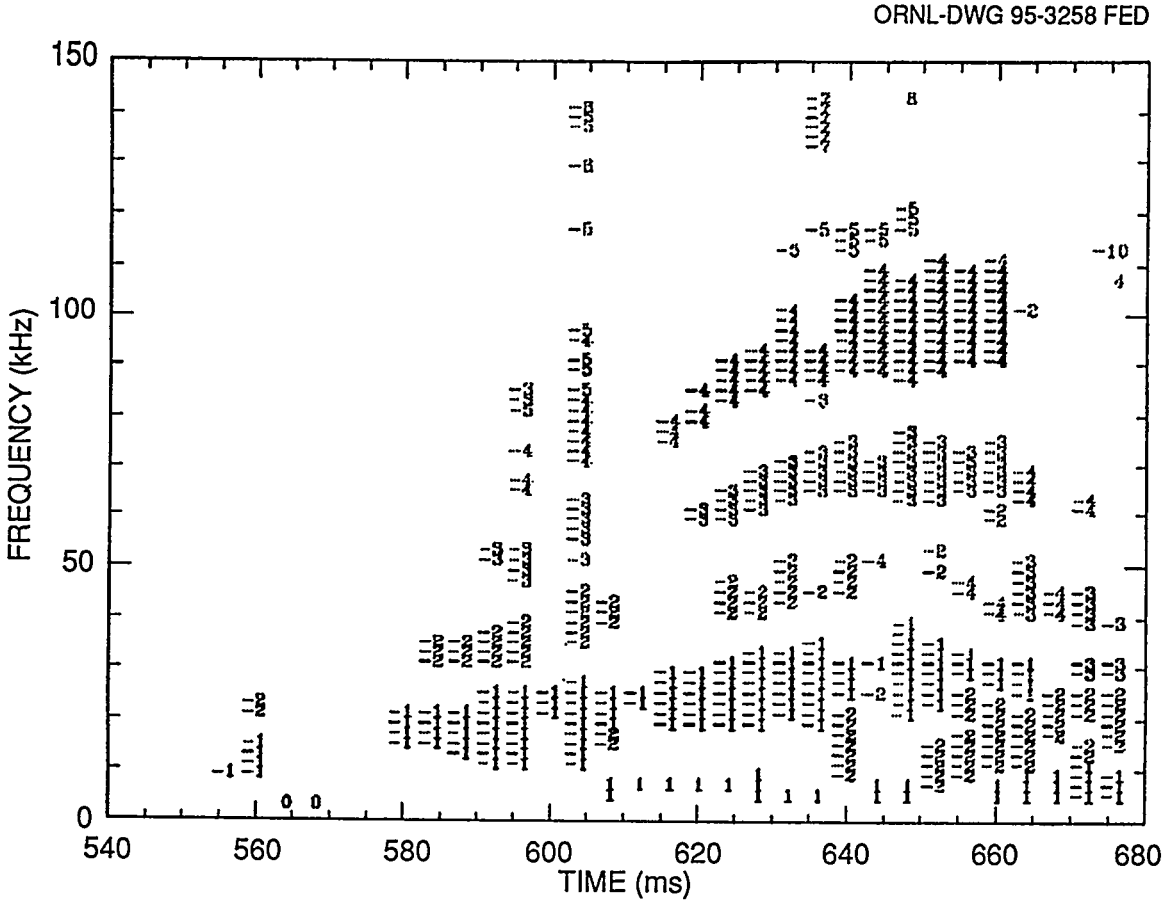

Fig. 1.30. Toroidal mode numbers, PBX-M shot 310724. Thirteen pairs of coils on outer midplane with separations in toroidal angle of 33–176° used with coherence cutoff of 0.6. Dimensions of time-frequency cells: 2 ms, 4 kHz. Error code (in color) not reproduced here.

1.3.2.6 AM reflectometry on PBX-M

Edge electron density profiles on PBX-M have been measured in the IBW antenna environment using AM-swept frequency reflectometry. This reflectometer technique, developed in a collaboration between ORNL and CIEMAT, performs a time delay measurement by the determination of the phase delay of the modulating envelope of a millimeter-wave probing beam reflected in the plasma. The effects of the large density fluctuations in the edge gradient region are overcome by reducing the multiplicity of fringes and eliminating phase excursions produced by scattering from density fluctuations at the reflecting layer. This is accomplished by using a differential phase measurement: the difference phase between the carrier and the two sidebands of the AM signal reflecting from cutoff layers separated by distances much less than the correlation length of the density fluctuations is used.

The PBX-M AM reflectometer uses 200-MHz modulation of a 32- to 50-GHz millimeter-wave signal, which probes the plasma using the extraordinary mode (X-mode) so that the edge plasma density profile can be measured in the range of $<1 \times 10^{12}$ cm^{-3} up to 1×10^{13} cm^{-3} in 1.25–1.5 T (R = 165 cm, a = 30 cm) discharges. The reflectometer microwave electronics are shown in Fig. 1.31. This system uses a swept 8- to 12.5-GHz microwave source and frequency multiplication to obtain the final 32–50 GHz output. The 200-MHz sine wave modulation is

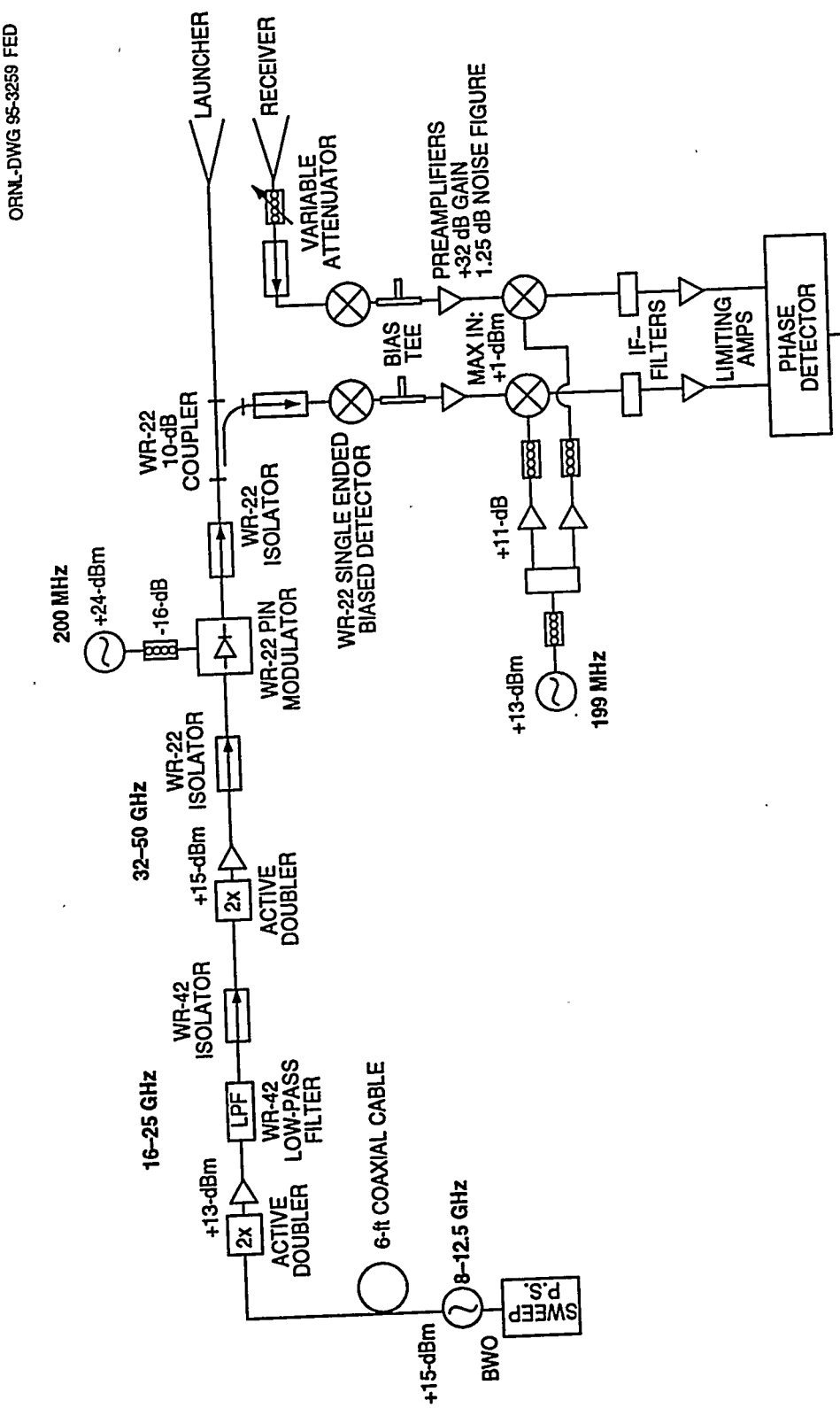

Fig. 1.31. Schematic of the PBX-M AM reflectometer microwave electronics circuit.

accomplished using a PIN diode switch that has the 200-MHz rf bias superimposed on a small dc bias. The reference signal (coupled off at the modulator output) and the received signal from the plasma are both demodulated and then converted down to 1 MHz by a high-stability 199-MHz oscillator. The 1-MHz outputs from the plasma and reference signals are filtered at 1 MHz (40-kHz band pass) and then passed through limiting amplifiers. An amplitude detector is also available to determine when the signals become too weak for accurate detection.

An AM reflectometer phase signal and the reconstructed density profile plotted with the Thomson scattering profile are shown in Fig. 1.32. In Fig. 1.33, the edge density profile evolution during the L-H transition is plotted, showing how the density gradient has increased from 2×10^{20} m^{-4} to 4×10^{20} m^{-4}. The times illustrated correspond to the closest reflectometer data, 0.5 ms before and 4.5 ms after the first observable change in the D_α signal. The data obtained by researchers from UCLA with a fast reciprocating Langmuir probe are also shown. It is observed

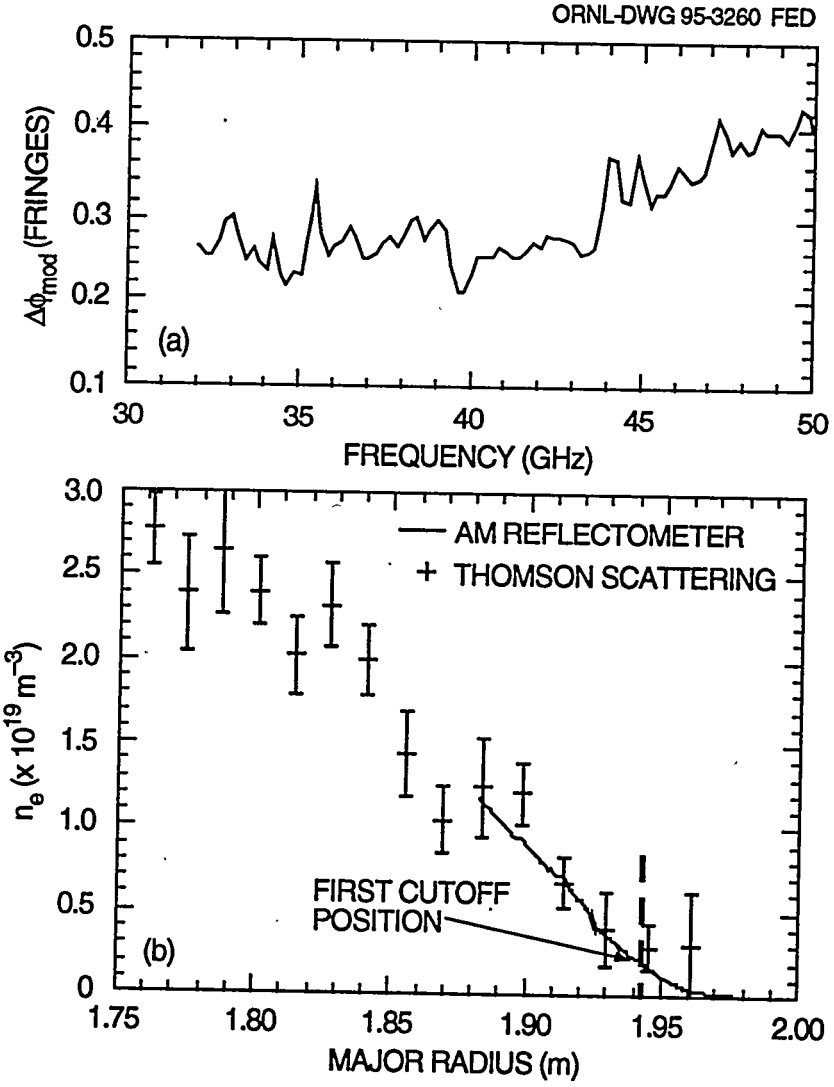

Fig. 1.32. *(a)* **AM reflectometer phase signal after subtraction of calibration phase;** *(b)* **reconstructed density profile plotted with Thomson scattering profile (crosses with error bars) for same time interval.**

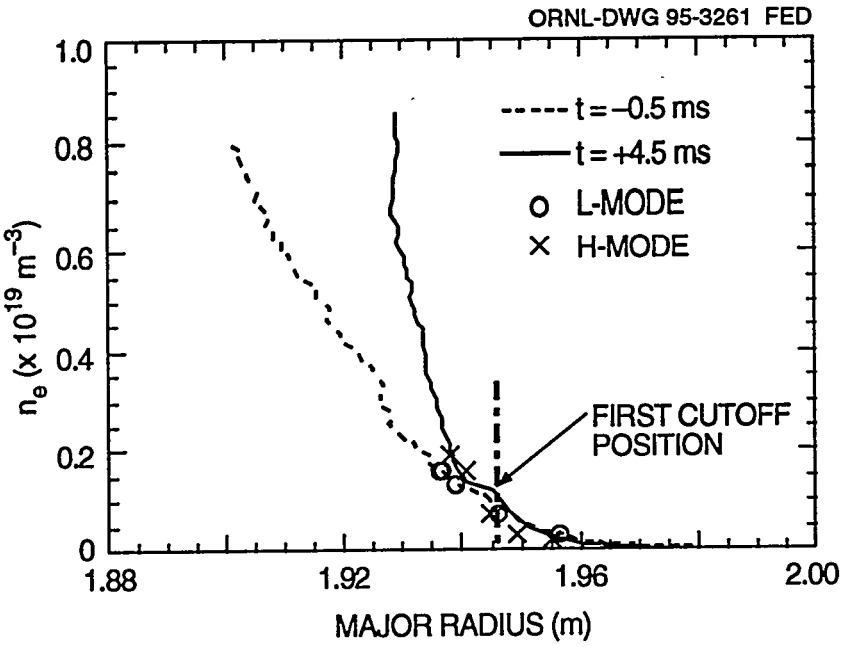

Fig. 1.33. Density profiles measured before and after L-H transition. Symbols correspond to density measurements by fast reciprocating Langmuir probe (o = L-mode, x = H-mode).

that both sets of data have good agreement. Unfortunately, with the time resolution of our system (one profile in 1 ms each 5 ms), it is not possible to follow the fast changes that take place during the transition.

In IBW heating experiments, the ponderomotive force is particularly strong because the antenna's electrical field is predominantly parallel to the magnetic field of the tokamak. If the ponderomotive force is very large, it can cause a density "hole" in front of the antenna, which then can lead to nonlinear coupling effects. Therefore, heating efficiency depends on the edge physics during IBW heating, and measurement of the edge density profile close to the antenna becomes important in understanding the wave coupling physics in IBW experiments. To study this type of phenomena in PBX-M, the reflectometer antennas (R = 202 cm) were installed immediately adjacent to the IBW antenna Faraday shield (R = 197 cm) to obtain a direct measurement of the profile modifications during the IBW heating. Edge density profiles, with and without IBW, for two discharges (I_p = 127 kA, B_0 = 1.45 T, and f_{rf} = 54 MHz) with different rf power are presented in Fig. 1.34. When the IBW power is on, a "hole" develops in front of the antenna. It can be shown that this density depletion scales with the IBW power.

Other details are available in Refs. 61–64.

1.3.2.7 Wavelet analysis of ELM signals from the PBX-M tokamak

An orthonormal wavelet basis was used to study D_α signals from the PBX-M tokamak. The goal was to identify time- and frequency-dependent features to be used for automatic detection of L-H transitions, large ELMs, and incipient terminal discharge disruptions.

Wavelet analysis is analogous to Fourier analysis combined with finite element analysis. The basis functions have limited extent in time and can therefore provide time-resolved frequency content. The basis functions are self-similarly scaled in frequency from the highest consistent with the data measurement rate to the lowest meaningful frequency, which identifies any

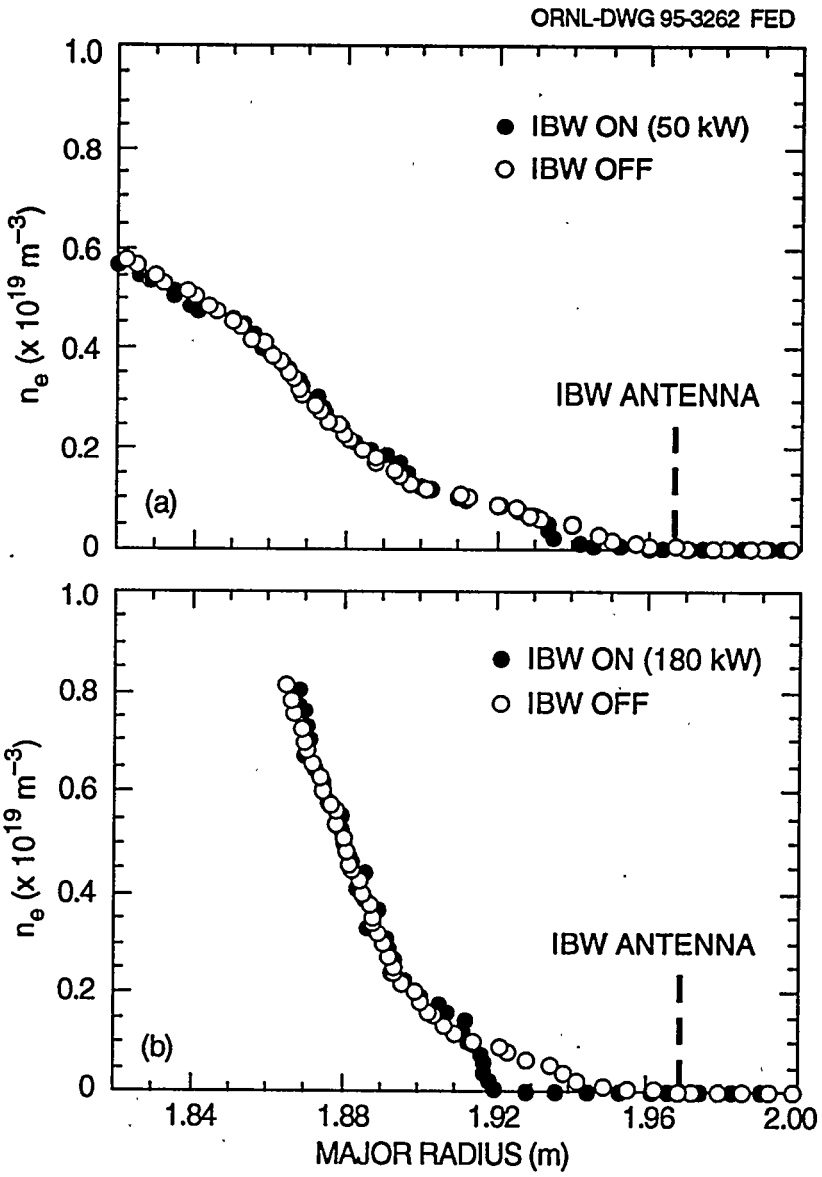

Fig. 1.34. Density profiles measured with and without IBW power. (*a*) 50 kW IBW compared to no IBW; (*b*) 180 kW IBW compared to no IBW.

time-dependent background signal. The process is analogous to a windowed Fourier analysis where the window is chosen to be just longer than the Nyquist period for each frequency.

A contour map showing the time variation of the wavelet amplitudes at several octaves gives visual clues to the interplay of frequencies at the time of the events to be detected. Since specific signal features prove to be fairly well correlated with some events, the study could be used to define how data could be analyzed in analog and digital circuitry so that the tokamak parameters could be adjusted to avoid or enhance events.

Figure 1.35 displays a time-resolved signal (lowest trace) for the amplitude of D_α emission from the PBX-M tokamak. A wavelet decomposition of that signal yields the amplitudes shown at sequentially longer periods. The duration of specific amplitude values (flattops) displays the

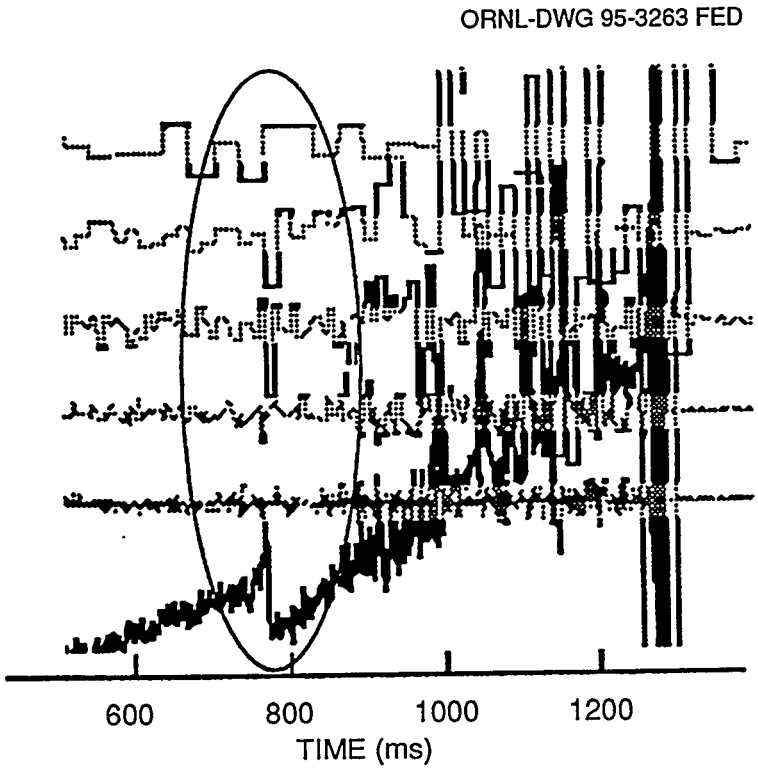

Fig. 1.35. D_α emission and wavelet decomposition.

time scale for each of the wavelet representations; progressing up from the D_α, they are 1, 2, 4, 8, and 16 ms.

The wavelet amplitudes as a function of time (x axis) and sequentially longer time scales provide recognizable patterns that could define detector circuitry so that the incidence of specific patterns of activity can be observed and acted upon. For example, the ellipse in the figure indicates the signature of an L-H transition, which is followed by grassy ELMs, moderate ELM activity, and a giant ELM crash or disruption. The greyed portions of the curves show where a threshold could be imposed in the detector circuitry to isolate periods when the amplitudes could be regarded as exceeding some "typical" background noise level.

1.3.3 Collaboration Between ORNL and TFTR

D. B. Batchelor, L. R. Baylor, T. S. Bigelow, C. E. Bush, I. Collazo, R. C. Goldfinger, M. J. Gouge, G. R. Hanson, D. J. Hoffman, E. F. Jaeger, S. L. Milora, M. Murakami, A. L. Qualls, D. A. Rasmussen, J. B. Wilgen, and the TFTR Team

The main areas of the collaborative experiments between ORNL and TFTR are ICRF heating, confinement experiments, and pellet injection. The main emphases have been (1) to incorporate microwave reflectometer to measure density profile in the edge region and (2) to apply analysis codes to ongoing experiments and use codes to predict future performance.

1.3.3.1 Achievements and status

Microwave reflectometer

A microwave reflectometer edge density diagnostic was developed and tested successfully. Measured edge density gradient profiles are in general agreement with Thomson scattering and far-infrared (FIR) interferometer measurements. The upgraded reflectometer system was installed on an ICRF antenna and began routine operation.

ICRF electron heating and modeling

ICRF direct electron heating power deposition profiles were measured and found to be in good agreement with predictions of Poloidal Ion Cyclotron Expansion Solution (PICES) modeling. Experiments to extend the electron heating in D-T plasmas were proposed. Modeling has been done with the PICES full-wave code and ORION 1-D code to evaluate the power partitioning between different plasma species for various D-T heating scenarios. Work is in progress to combine the data from high-resolution edge density profile measurements (obtained with the reflectometer) with the antenna-loading and heating results to evaluate the effectiveness of ICRF heating on TFTR more thoroughly. Projections for future D-T experiments have been made with TRANSP in extrapolations from existing deuterium-deuterium (D-D) supershot data. The effect of ICRF heating has been evaluated. Modifications to TRANSP are under way to include sawtooth-mixing of energetic tail ions.

CHERS

The Charge-Exchange Recombination Spectroscopy (CHERS) System was relocated and recalibrated for the D-T run. T_i and V_f were measured for all experimental studies during the last and current operating period.

H-mode studies on TFTR

H-mode plasmas were obtained with and without I_p ramp-down. Characteristics and phenomena of TFTR H-modes were documented. In general, they are like H-modes on other tokamaks, but some features are unique. Plans are to extend these studies to H-modes in D-T plasmas.

Pellet fueling

The pellet-enhanced performance (PEP) mode, which was first discovered on JET, has been reproduced on TFTR at ICRF power levels up to 5 MW. Similar discharge characteristics have been observed (enhanced neutron rates, decreased central transport coefficients, and elevated q).

1.3.3.2 Physics accomplishments

Edge profiles

The conclusion of a conceptual design study in FY 1992 was that a dual-frequency system measuring the differential phase of two microwave probing beams would perform best in a turbulent plasma. The reflectometer microwave electronics system was designed, built, and installed on TFTR for proof-of-principle testing. TFTR was installed and tested using the TFTR fluctuation reflectometer waveguide and launching system. The results showed that the dual-frequency

reflectometry technique allows phase measurements in the highly turbulent edge scrape-off region; however, because of limitations imposed by the TFTR fluctuation reflectometer launchers (which are not optimized for these measurements), data for only a small number of discharges could be analyzed. The comparison of the reflectometer-measured edge gradient profiles with the Thomson scattering data showed agreement in most cases inside of the limiter radius (~3.58 m). Outside of the limiter radius, the reflectometer showed the density falling off much more rapidly than the Thomson scattering data indicate. In FY 1993, the reflectometer was moved to the ICRF antenna, and the fringe offset problem was reduced by reducing the difference frequency from 250 MHz to 125 MHz. In addition, with the reflectometer launcher aperture located at the Faraday shield radius, the initial cutoff position can be >1 cm away from the aperture. This allows greater accuracy in locating the density gradient than has ever before been achieved with reflectometry.

Rf physics

The collaboration in FY 1992 and the first part of FY 1993 between ORNL and TFTR in the areas of confinement physics and ICRF has centered on conducting and analyzing experiments on ICRF direct-electron heating (DEH) in supershot plasmas. DEH, which is a basis of fast-wave current drive, has been observed in TFTR under conditions with minimal ion damping and at high electron temperature in two regimes, $B = 2.3$ T and $B = 4.6$ T, with 47-MHz rf power. Application of rf power <3 MW to NBI-heated supershot deuterium plasmas [$T_e(0) = 8$ keV and $n_e(0) = 6.4 \times 10^{19}$ with NBI power of 24 MW at $B = 4.5$ T] with no minority ions increased the central electron temperature by up to 2.5 keV. As shown in Fig. 1.36, the electron power deposition profile was measured with modulation of rf power at 5 Hz, showing strongly peaked profiles in the core with the total integrated power of up to 80% of the applied power. The magnitude and profile shape agree well with those predicted by a 3-D, full-wave ICRF modeling code (PICES), as shown in Fig. 1.37. The overall heating efficiency of DEH is similar to that of either ^{3}He-

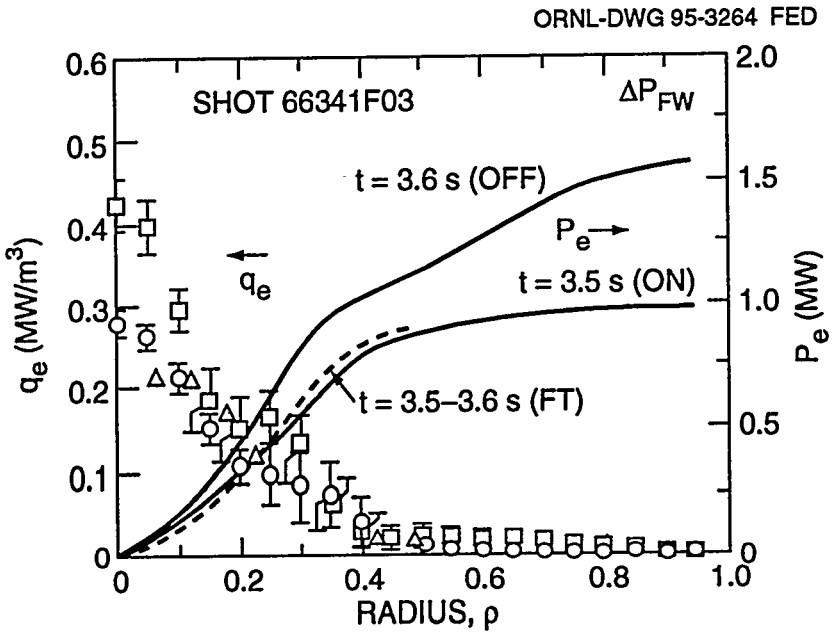

Fig. 1.36. Measured electron power deposition profile and total integrated power profile for DEH in TFTR.

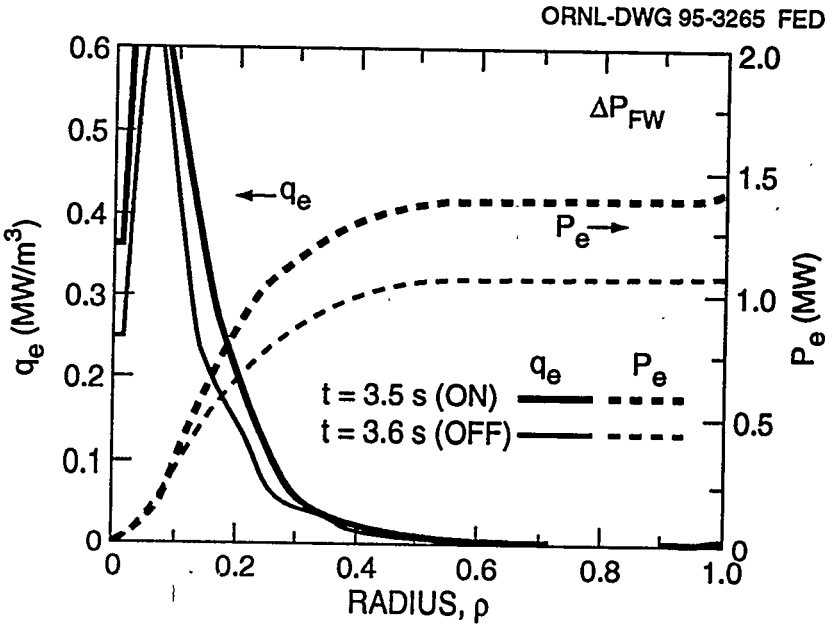

Fig. 1.37. Electron and ion power deposition profiles calculated from PICES code.

minority heating or NBI under similar conditions. Modulation of the rf power enabled an estimate of thermal diffusivity (χ_e) from the heat wave analysis that agrees with that derived from the power balance analysis ($\chi_{HW}/\chi_{PB} \approx 2$). Particle diffusivity derived from analysis of the density wave concomitant with the ICRF modulation is also in good agreement with that from the particle balance analysis. Electron transport flux was compared with that predicted by the critical temperature gradient model, which apparently failed to describe the experiment. Loss of D-D fusion products (1-MeV tritons at the cyclotron resonance) was observed to increase during the ICRF pulses without a minority tail present. This may indicate ICRF-induced transport of alpha particles in D-T plasmas and may offer a way to control alpha ash or to affect burn control. The capability of increasing the β of the alpha particles (with higher electron temperature and, thus, longer alpha-particle slow-down time) without the complication of minority ions is a significant feature of this heating method (compared with ^{3}He-minority heating during the TFTR D-T operation).

H-mode physics

During 1992 and 1993, experiments were carried out in TFTR on H-modes obtained through transitions from the supershot to the H-mode regime. The characteristics of these H-modes have been documented during this period.[65–68] They were similar to those characteristics found on other tokamaks with one main exception: the density profiles can be highly peaked. The peaked profile H-modes have been maintained in TFTR for up to ~1.5 s, limited only by the available beam pulse length, implying possible steady-state peaked density H-modes. In many cases, confinement is enhanced across the plasma; however, the largest increase is in a broad edge region of the plasma. Thus in TFTR, all of the important physics of H-modes, such as transitions, enhanced edge confinement, ELMs, and other phenomena, are studied in a large, circular limiter tokamak with the added feature of centrally peaked density profiles and the advantage of an extensive set of diagnostics. The threshold power for the transition is found[65] to be a

linear function of plasma current, $P_{th}(PW) \approx 1.1 \times I_p(MA)$. Transitions and ELMs are affected by the mix of co- and counter-NBI and by perturbations introduced by pellet injection, gas puffing, and current ramping before and during NBI. Fluctuations near both the transition and ELM events have been characterized. High-frequency magnetic fluctuations in the range ≥100–250 kHz usually decrease during the transition, as seen in Fig. 1.38. Microwave scattering spectra of density fluctuations in the plasma edge show a feature at high frequency (>1.5 MHz at $k_\perp = 5.5$ cm^{-1}) during the H-mode that is not observed in the plasma core, which is consistent with an edge poloidal rotation velocity, V_θ, of ~10^4 m/s. This spin-up is consistent with formation of a radial electric field, $-E_r$. Using data from the CHERS measurement, a Grad P_i contribution to E_r of about ~30 kV/m is found for many TFTR H-modes.[69] The shift in the fluctuation spectra begins at the transition, propagates in the direction of electron diamagnetic drift, and has modulation correlated with ELMs.[65] A modulation of the signal from fusion product probes was seen during ELMs for several discharges.[66] The ELMs appear to originate at about 15 cm within the plasma edge.[65–70] Many TFTR H-modes, such as shown in Fig. 1.38, showed a modest improvement in confinement over that of the supershots from which they originated, and an

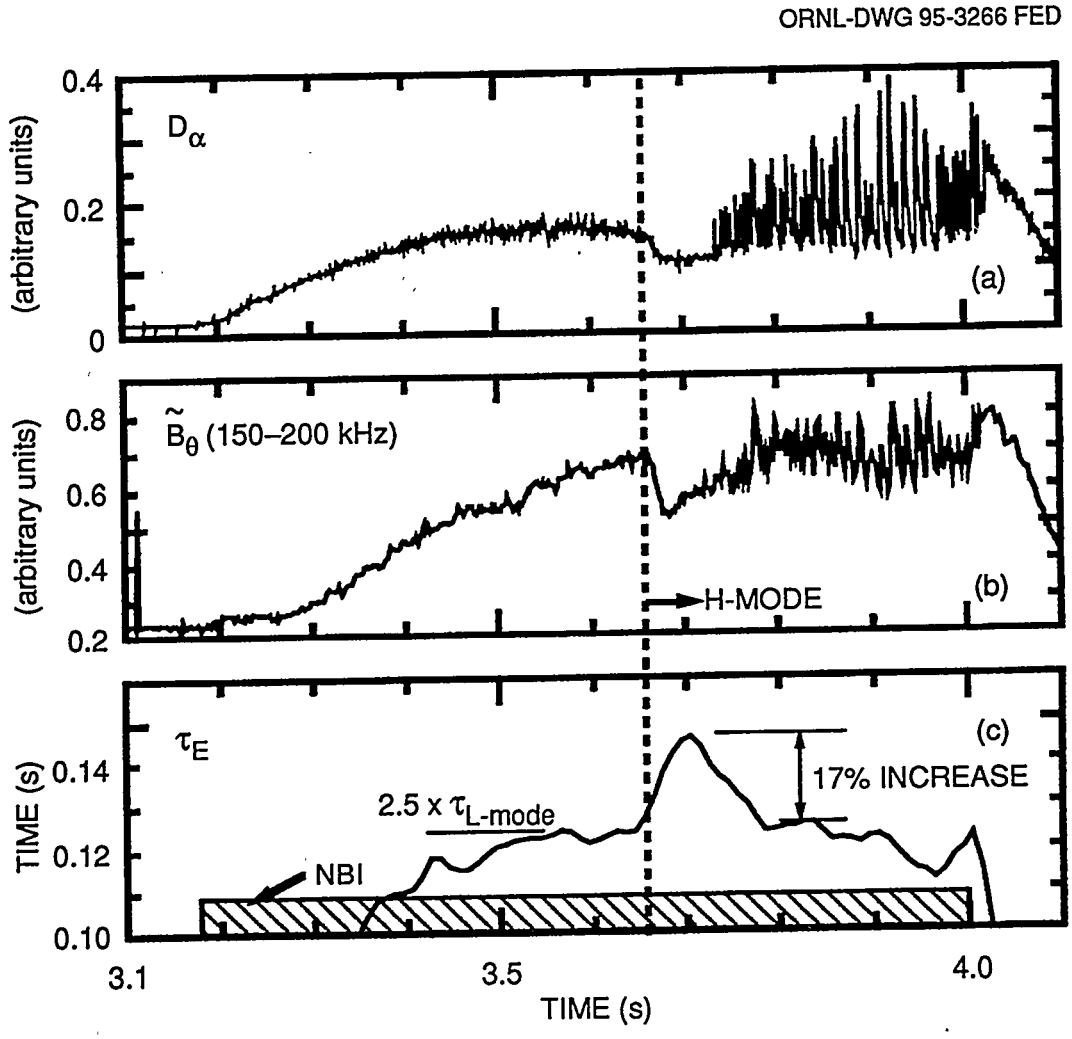

Fig. 1.38. Variations of D_α, ~B_θ, and τ_E for H-mode that showed transient beam turn on at 3.19 s. H-mode transition at ~3.66 s. $I_p = 0.85$ MA, $B_\phi = 4.8$ T, and $P_b = 12$ MW at transition.

understanding of these may eventually lead to a plasma with the combined advantages of both the supershot and the H-mode. The characteristics and physics of the TFTR H-modes are considered relevant to other tokamaks and various theoretical studies. Experimental proposals have been written, and preparations have been made for H-mode experiments in D-T plasmas during 1995.

1.3.4 Feedback Control and Stabilization Experiments on TEXT

T. Uckan, B. A. Carreras, and the TEXT Team

Plasma edge feedback experiments on the Texas Experimental Tokamak (TEXT) have been successful in controlling the edge plasma fluctuation level. The feedback launcher (FBL), consisting of two electrostatic probes located in the shadow of the limiter, is driven by the edge potential fluctuations obtained from a local sensor placed on the launcher head. The launcher probes are separated by $\lambda/2 \approx 1.8$ cm (where λ is the wavelength of the electrostatic edge fluctuations) in the poloidal direction with respect to the toroidal magnetic field. In general, a broadband frequency suppression of the edge potential fluctuations, which are the dominant fluctuations, is achieved. As shown in Fig. 1.39, for frequencies below 40 kHz the potential fluctuations can be reduced, for a phase shift between the launcher probes $\Delta\varphi_{12} = \pi$. For $\Delta\varphi_{12} = 0$ there is broadband reduction, but fluctuations around 8 kHz are strongly enhanced. This turbulence modification is observed not only locally, where the edge feedback is applied, but also at the far-field sensing probe, which is ~12 m away from the launcher along the field line, halfway around the torus. In addition, the measurements with the poloidally separated multipin, far-field sensing probe have given ~2 cm poloidal extent for the feedback excitation of the potential fluctuations. The fluctuation-induced radial particle flux and the local plasma parameters are affected by feedback phasing.

1.3.5 Long-Pulse Particle Control Issues in TPX

P. K. Mioduszewski, J. T. Hogan, and L. W. Owen

For long-pulse operation, such as the anticipated 1000-s pulses in TPX, steady-state particle control must be provided by continuous gas removal through divertor pumping. Whether divertor pumping has the same effect as wall pumping on plasma performance is not clear to date. Modeling results indicate that wall pumping removes higher-energy charge-exchange neutrals, whereas divertor pumping controls the SOL density through removal of low-energy particles in the divertor. The differences, similarities, and interrelations between wall pumping and divertor pumping are not fully understood, but recent experimental results on Tore Supra and DIII-D clearly indicate that wall recycling can be controlled by external exhaust with pump limiters or pumped divertors.

1.3.5.1 Wall-conditioning options for particle control

In most fusion devices, two different kinds of wall conditioning are employed. The first kind is for impurity control, and the second kind is for recycling control. Wall conditioning, for controlling wall recycling, can be achieved either with high-temperature walls to provide high mobility of hydrogen isotopes or with helium glow discharges to remove hydrogen implanted in a near-surface layer during operation. In machines with conventional (normal-conducting) magnets, the TF is usually ramped down after the discharge, and helium glow discharges can be applied

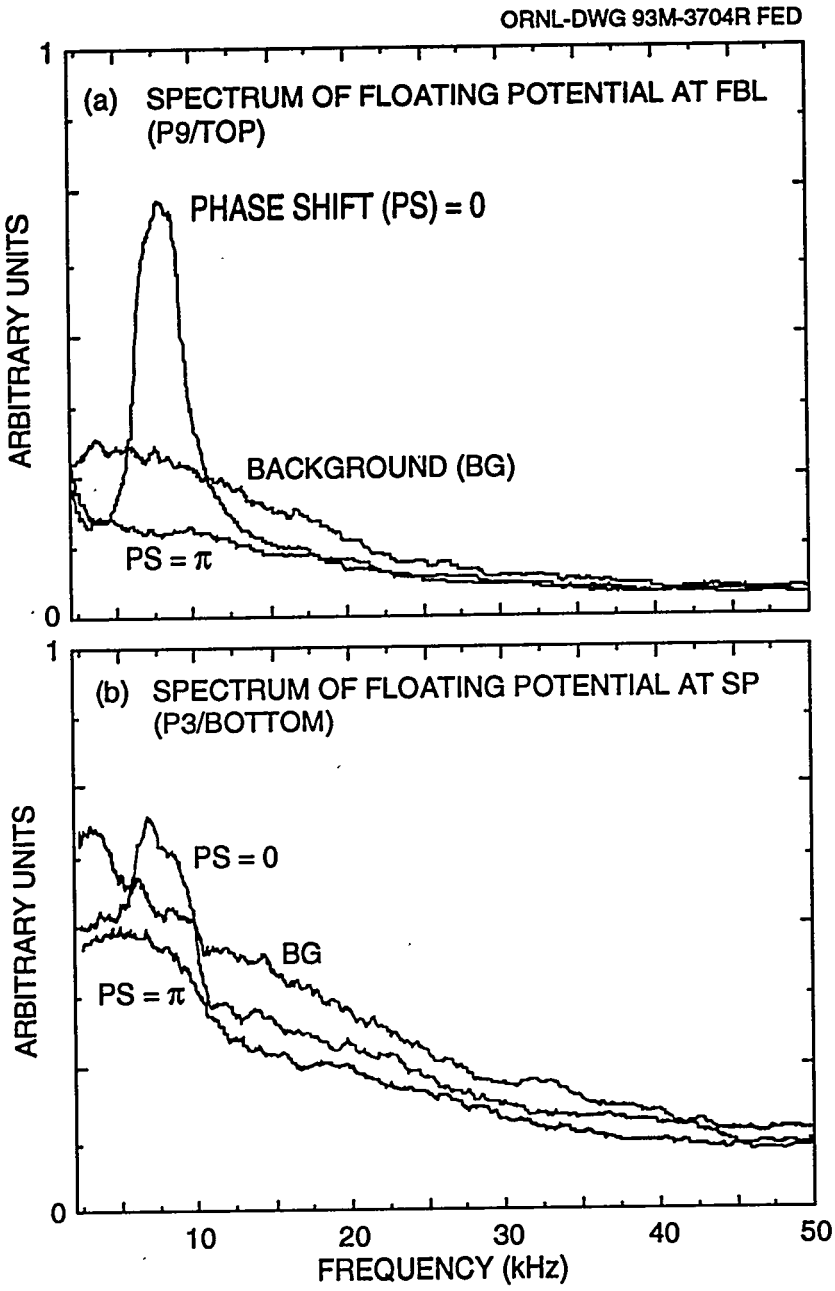

Fig. 1.39. Effects of feedback on frequency spectrum of potential fluctuations. Measured at (*a*) FBL location and (*b*) far-field sensor probe location, ~12 m from FBL along magnetic field line. Phase-shift settings of $\Delta\varphi_{12} = 0$ (positive feedback) and $\Delta\varphi_{12} = \pi$ (negative feedback) compared to no-feedback case (background).

between shots. In a machine with superconducting magnets, however, a regular glow discharge (which does not work in a TF) between discharges will not provide the necessary wall conditioning, because the presence of the toroidal magnetic field in a glow discharge leads to particle drifts that prevent a uniform bombardment of the wall surfaces. Furthermore, even if wall conditioning between discharges were possible, the static pumping capacity of the wall is not

large enough to last for pulses of 1000 s. Hence a wall-conditioning process for continuous wall-recycling control needs to be developed for steady-state operation.

To provide recycling control for long-pulse operation in TPX, techniques that work in the presence of the TF and can provide wall pumping continuously during long-pulse operation need to be developed. For the complete recycling control scenario, the wall conditioning scheme consists of wall preparation overnight, with no magnetic field; wall preparation before the discharge, with a TF; and continuous wall pumping during the discharge.

1.3.5.2 Overnight wall conditioning

The superconducting magnetic field is usually ramped down overnight. This allows application of the standard helium glow discharge at night to prepare for operation the following day. To keep the operating pressure as low as possible (because the turbomolecular pumps work more effectively near 1 mTorr than near 10 mTorr), the simple glow can be assisted by coupling low-power rf waves to the plasma, which typically lowers the operating pressure to 1 mTorr. This rf-assisted glow has been developed at TEXTOR and has become a standard technique for most tokamaks.[71] Implementation of rf-assisted glow for overnight vessel preparation should be straightforward for TPX.

1.3.5.3 Wall conditioning between discharges

Several possibilities can be explored to replace the standard glow discharge with low-power ECH or rf discharges. The effectiveness of these discharges is not obvious, because the ion fluxes to the walls are mostly parallel, guided by the magnetic field, and are not necessarily comparable to those of glow discharges. It has been shown on TFTR[72] and Tore Supra[73] that regular tokamak discharges in helium can be fairly efficient in depleting the walls of hydrogen isotopes. Even though this method is effective, it has a serious disadvantage. The total number of full tokamak discharges is usually limited by material fatigue, and using a considerable fraction of the allowable discharges for wall conditioning purposes can be very costly. Instead, we propose to explore low-power, long-pulse helium discharges on Tore Supra, driven by LH waves, which will not stress the machinery in the same way as regular discharges but will produce sufficiently large charge-exchange fluxes to the walls to remove the hydrogenic species. Wall-conditioning techniques with ECH discharges are currently being explored in TEXTOR.

During helium glow between discharges (e.g., in DIII-D), typical ion fluxes of $\sim 10^{14}$ cm^{-2} s^{-1}, with particle energies around 300 eV, impinge on the walls for 5 min. To produce similar conditions (i.e., particle fluxes and energies), we will explore low-power, long-pulse tokamak discharges generating the same helium particle fluence in the form of charge-exchange neutrals. Hence, our first goal is to determine the parameters of a low-power tokamak discharge that would generate the desired helium particle flux on the walls. For this purpose, calculations have been carried out with the DEGAS neutrals code, at a fixed plasma background, to determine the plasma parameters necessary to produce the desired charge-exchange flux. For the present cases, the core plasma parameters were fixed at $\langle n_e \rangle = 1 \times 10^{13}$ cm^{-3} and $T_e(0) =$ 1 keV. The modeling results indicate that, in addition to the charge-exchange fluxes, the helium ion fluxes on the inner wall are substantial and should contribute strongly to the wall-conditioning effect. Figures 1.40 and 1.41 show the helium charge-exchange fluxes and average energies as functions of the poloidal angle.

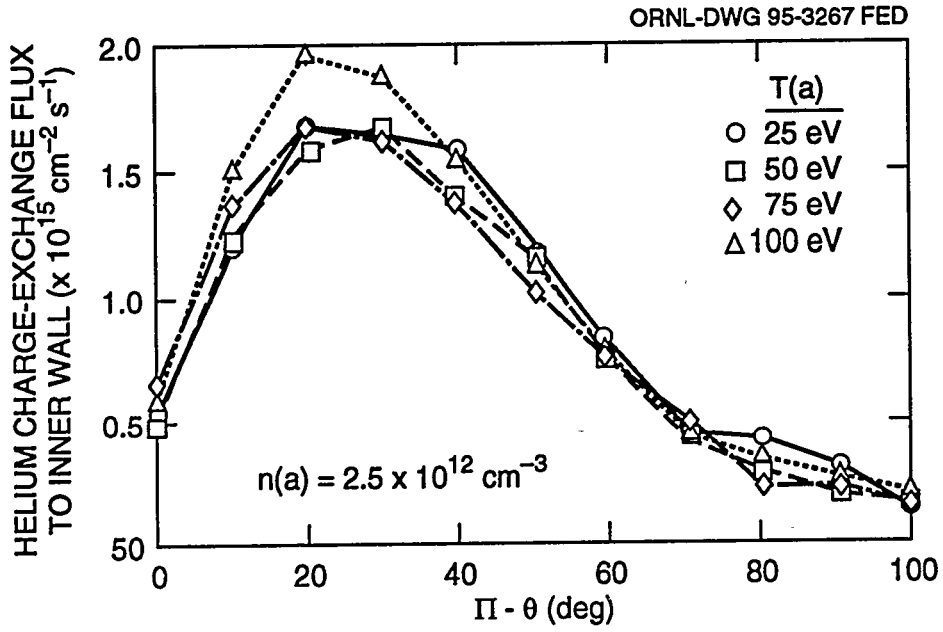

Fig. 1.40. Helium charge-exchange flux to inner wall as function of poloidal angle.

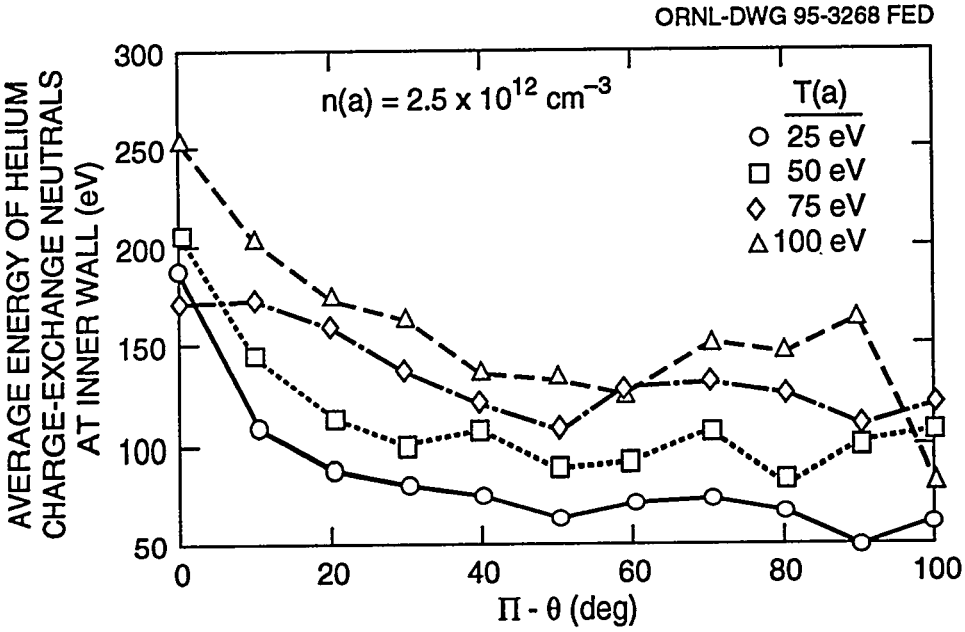

Fig. 1.41. Average energy of charge-exchange neutrals incident on inner wall.

1.3.5.4 Continuous wall conditioning during discharge

For TPX, the NB fueling rate of the full NBI heating complement alone is 43.5 Torr-L/s. So even if wall conditioning between discharges were available, the available surface area, with a capacity of several hundred torr-liters, would not last for more than ~10 s. Wall pumping, induced

by conditioning between shots, is a transient effect and not applicable for long-pulse operation in TPX. Hence, while overnight wall conditioning may be necessary for startup with a clean wall, wall conditions for long-pulse operation can only be maintained by the active exhaust system during the discharge itself.

In Tore Supra, we have performed a series of experiments in which the beginning wall recycling coefficient was reduced from 0.99 to 0.97 after five 8-s discharges with pump limiter exhaust. Pumping reduced the global confinement time τ_p^* from 20 s to 2.5 s and left the wall recycling low enough to yield $\tau_p^* = 3.5$ s even after termination of the pump limiter exhaust. This result indicates that the pump limiter had depleted the wall inventory and that the equilibrium state of the wall is probably a pumping state (i.e., wall conditioning between discharges may not be required). It has since been shown in DIII-D that divertor pumping can also deplete the wall inventory. Systematic experiments on the correlation between wall pumping and external exhaust are under way. Some of the mechanisms of wall pumping and wall depletion by external exhaust have been discussed in some detail in a recent paper.[74]

1.4 PHYSICS ASSESSMENT OF STELLARATORS AS FUSION POWER PLANTS

J. F. Lyon, J. A. Rome, and K. Gulec

Stellarators have significant potential advantages over tokamaks as fusion power plants: their operation does not involve disruptions, current drive, or a stability control system. The impression that stellarators are not attractive as fusion power plants is based on some erroneous assumptions: (1) torsatrons must have impractical continuous helical coils; (2) modular stellarators are too big; (3) a high beta limit or a large improvement in confinement is needed; (4) a large helical ripple leads to unacceptable alpha-particle energy losses and unacceptable neoclassical thermal losses; and (5) the larger major radius means that the cost of electricity (COE) for stellarators would not be competitive with that for tokamaks. Our study refutes many of these misconceptions about stellarator reactors.

The best-studied modern stellarator reactor configurations have been the CT6 Compact Torsatron[75] and the modular Helias[76] stellarator. The Helias (W7-X) configuration has better physics properties (fewer orbit losses, lower neoclassical transport, reduced bootstrap current, higher beta limit, etc.). However, its smaller plasma-coil separation leads to a larger major radius (larger blanket and shield area) and consequently to a higher-cost reactor. Recently, two new stellarator configurations have been found: a modular ATF (MATF) that removes the objection of continuous helical coils and a Modular Helias-Like Heliac (MHH)[77] that reduces the size of modular stellarators and leads to a very attractive reactor.

The CT6 Compact Torsatron configuration has good access between coils for blankets and divertor, and the large plasma-coil distance leads to moderate-sized reactors. However, the continuous helical coils would be difficult to fabricate and repair. The MATF torsatron (Fig. 1.42) was designed to overcome this drawback. The legs connecting the helical segments to the toroidal windbacks are perpendicular to the torus, which minimizes the field perturbation due to modularization. The windbacks (40° above and below the equatorial plane) provide most of the required vertical field (VF). The physical properties are similar to those of ATF, but there is a larger distance between the plasma and the coils in MATF. Field lines can still exit between coils to an exterior divertor chamber. Even the large helical-ripple loss region has relatively little effect on the reactor economics of MATF: the direct loss of energetic alpha particles is compensated by

ORNL-DWG 95-3269 FED

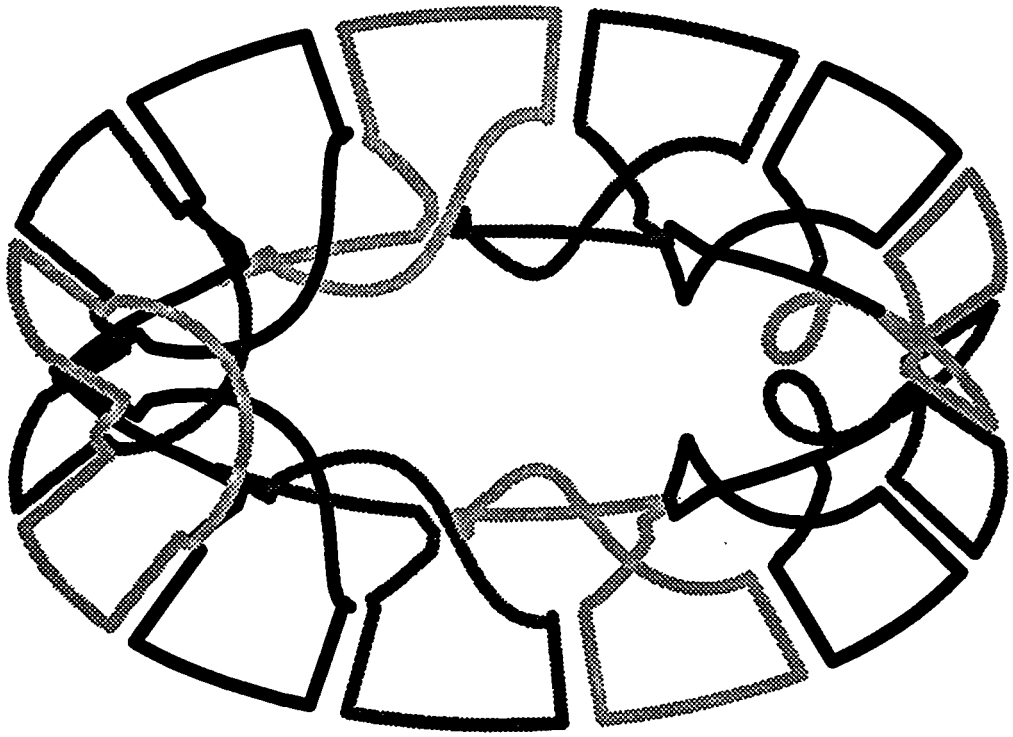

Fig. 1.42. Oblique view of MATF coil set with modules not up-and-down symmetric. Small VF coils also needed for shaping control.

avoidance of helium ash accumulation, and ripple-induced thermal losses are reduced by the resulting ambipolar radial electric field.

MHH, chosen for the U.S. Stellarator Power Plant Study, has physics properties similar to those of a Helias configuration with a larger plasma-coil separation. MHH offers excellent transport and ignition at moderate values of beta ($\langle\beta\rangle \leq 5\%$). The size of a modular stellarator reactor has been reduced dramatically in MHH by creating much of the rotational transformation with a large helical excursion of the magnetic axis. Thus, a 2-m plasma-coil gap for the blanket, shield, cryostat, coil half-thickness, and assembly gaps can be obtained in a reactor that is about 14 m in major radius. The modular coil arrangement is also convenient for reactor disassembly and maintenance. MATF has modular coils and a better divertor geometry, but its physical properties are not as good as those of MHH.

Table 1.3 shows that the CT6, MATF, and MHH configurations lead to power plants that are economically competitive with the second-stability Advanced Reactor Innovation and Evaluation Studies (ARIES)-IV tokamak,[78] given the same assumptions for materials, costing, and confinement. The device and plasma parameters for a fusion power plant were determined by minimizing the projected COE using the ARIES costing algorithms and the *same* materials assumptions (blanket, shield, coil) and constraints for all configurations: $P_{elect} = 1$ GW; $\langle\beta\rangle \leq 5\%$; and $H = \tau_E/\tau_E^{LG} \leq 2$, where $\tau_E^{LG} = 0.17 R_0 a_p^2 n^{0.6} B_0^{0.8} P^{-0.6} E^{.4}$, similar to gyro-reduced Bohm scaling.[79] One-dimensional power balance equations for $T_i(r)$ and $T_e(r)$ were solved for the same $n_e(r)$ used in the ARIES cases. Competitive power plants are still obtained as each constraint is separately varied (e.g., the COE for MHH varies <3% for $H > 1.2$ and $\langle\beta\rangle > 3\%$). Only a small

Table 1.3. Power plant parameters obtained using the same assumptions

Parameters	CT6	MATF	MHH	Helias	ARIES IV
Number of TF periods, M	6	12	4	5	1
Average plasma aspect ratio, R_0/a_p	3.8	10	9.7	13	2.8
Major radius R_0, m	11.8	13.4	13.1	23.3	6.04
Average plasma radius a_p, m	3.1	1.3	1.4	1.9	2.2
TF on axis B_0, T	4.6	5.5	5.3	4.1	7.6
Maximum field on coils B_{max}, T	14.0	13.7	15.4	8.7	15.9
Average plasma density, 10^{20} m^{-3}	1.0	2.5	2.7	1.4	2.9
Average plasma temperature, keV	8.1	6.8	7.0	8.1	10
Central ion temperature, keV	26	22	24	26	27
Volume-average toroidal beta, %	2.9	4.3	5	5	3.4
L-G confinement multiplier, H'	2	2	1.5	1.7	2.5
Fraction of power radiated	0.30	0.30	0.32	0.28	0.23
Neutron wall loading, MW/m^2	0.9	1.8	1.3	0.5	2.7
Fusion core mass, 10^3 tonnes	10.7	8.7	7.8	18.8	9.0
COE,[a] mills/kW(e)h	70	62	66	100	68

[a]In constant 1992 dollars.

change (1.5%) in R_0 occurs as P_{elect} is varied from 1 GW to 1.8 GW, but the projected COE drops significantly [from 66 to 49 mills/kW(e)h]. The alpha-particle orbit losses in MATF and CT6 and the fuel dilution due to helium ash accumulation in MHH and Helias lead to similar reductions in the alpha-particle heating; however, elimination of the 10% helium ash accumulation or introduction of a large (33%) alpha-particle energy loss has only a modest (1%) effect on the COE.

In the low-collisionality regime where neoclassical helical-ripple–induced transport can be important, electric fields drastically change the 1-D particle and heat flow equations. In configurations with significant orbit losses (CT6, MATF), a radial potential will build up to make the particle fluxes ambipolar. For fixed density and potential profiles, solutions are obtained for both signs of the resulting radial electric field; those with a negative electric field [$\phi(0)/T_i(0) \approx -3$] lead to a lower temperature and higher density than those with a positive electric field [$\phi(0)/T_i(0) \approx +4.5$], but require more initial heating to reach ignition.[80] Self-consistent solutions[81] of the 1-D heat and particle flux equations for $n_e(r)$, $n_D(r)$, $n_T(r)$, $T_e(r)$, $T_i(r)$, and the electric field $E_r(r)$ have now been found with $\phi(0)/T_i(0) \approx -3$ for relatively large values of helical ripple ($\varepsilon_h < 0.6$). As the helical ripple increases, the density profile peaks, the temperature profile broadens, and a strong electric-field shear layer develops at the edge. However, no self-consistent cases with a positive electric field have been found.

REFERENCES

1. T. S. Bigelow, C. R. Schaich, C. T. Wilson, and J. A. White, *Bull. Am. Phys. Soc.* **39**, 1627 (1994).

2. B. B. Kadomtsev, *Sov. J. Plasma Phys.* **1**, 295 (1975).

3. J. W. Connor and J. B. Taylor, *Nucl. Fusion* **17**, 1047 (1977); J. W. Connor, *Plasma Phys. Controlled Fusion* **30**, 619 (1988).

4. J. P. Christiansen, J. G. Cordey, and K. Thomsen, *Nucl. Fusion* **30**, 1183 (1990).

5. M. Murakami et al., "Dimensionless Scaling of Confinement in ATF," pp. 391–402 in *Plasma Physics and Controlled Fusion Research 1992*, Vol. 2, Proceedings of the Fourteenth International Conference on Plasma Physics and Controlled Nuclear Fusion Research, held in Würzburg, Germany, 1992, International Atomic Energy Agency (IAEA), Vienna, 1993.

6. J. B. Wilgen et al., *Phys. Fluids B* **5**, 2513 (1993).

7. R. C. Isler, G. L. Bell, T. S. Bigelow, E. C. Crume, A. C. England, J. C. Glowienka, L. D. Horton, T. C. Jernigan, R. A. Langley, P. K. Mioduszewski, M. Murakami, D. A. Rasmussen, J. E. Simpkins, J. B. Wilgen, and W. R. Wing, *J. Nucl. Mater.* **176&177**, 332 (1990).

8. *ITER Physics*, ITER Documentation Series no. 21, IAEA, Vienna, 1991.

9 D. Reiter et al., *Nucl. Fusion* **30**, 2141 (1990).

10. D. L. Hillis et al., *Phys. Rev. Lett.* **65**, 2382 (1990).

11. D. L. Hillis et al., p. 597 in *Plasma Physics and Controlled Fusion Research 1991*, Vol. 3, Proceedings of the Thirteenth International Conference on Plasma Physics and Nuclear Fusion Research, Washington, D.C., 1990, IAEA, Vienna, 1991.

12. E. J. Synakowski et al., *Phys. Rev. Lett.* **65**, 2255 (1990).

13. H. Nakamura et al., *Phys. Rev. Lett.* **67**, 2658 (1991).

14. D. L. Hillis et al., *J. Nucl. Mater.* **196–198**, 35 (1992).

15. E. J. Synakowski et al., *Phys. Fluids B* **5**, 2215 (1993).

16. M. R. Wade et al., *Fusion Technol.* **26**(3, Pt. 2), 595 (1994).

17. M. R. Wade et al., *Phys. Rev. Lett.* **74**(14), 2702 (1995).

18. R. H. Hulse, *Nucl. Technol./Fusion* **3**, 259 (1983).

19. D. Boucher et al., "Advances in Simulation and Modeling of Thermonuclear Plasmas," p. 142 in *Proceedings of the IAEA Technical Committee Meeting, Montreal, Canada, 1992*, IAEA, Vienna, 1993.

20. C. C. Klepper et al., "Divertor Neutral Pressure Enhancement with a Baffle in DIII-D," *Nucl. Fusion* **33**(4), 533 (1993).

21. M. M. Menon et al., "Performance Characteristics of the DIII-D Advanced Divertor Cryopump," p. 1047 in *Proceedings of 15th IEEE/NPSS Symposium on Fusion Engineering, Hyannis, Massachusetts, Oct. 11–15, 1993*, Vol. 2, IEEE, NewYork, 1993.

22. R. Maingi, "Effect of Low Density H-Mode Operation on Edge and Divertor Plasma Parameters," *J. Nucl. Mater.* **220–222** (*Proceedings of the Eleventh International Conference on Plasma-Surface Interactions in Controlled Fusion Devices, Mito, Japan, May 23–27, 1994*), 320 (1995).

23. M. A. Mahdavi et al., "Active Density Control in DIII-D H-mode Plasmas," *20th European Conference on Controlled Fusion and Plasma Physics*, proceedings of the 20th European Physical Society Conference on Controlled Plasma Physics, held in Lisbon, Portugal, July 26–30, 1993.

24. R. Maingi, L. W. Owen, P. K. Mioduszewski, and the DIII-D Team, "Simulation of the DIII-D Edge Plasma with the b2.5 Code," in *Proceedings of the Scrape-off Layer and Divertor Theory Meeting, Dallas, TX, March 16–17, 1994.*

25. M. J. Schaffer, R. Maingi, A. W. Hyatt, and M. A. Mahdavi, "Increased Divertor Exhaust by Electrical Bias in DIII-D," submitted to *Nucl. Fusion.*

26. L. W. Owen et al., "Modeling of Global Particle Confinement in ELM-free H-mode Discharges in DIII-D," *Bull. Amer. Phys. Soc.* **39**(7), 1653 (1994).

27. L. W. Owen et al., "Transport Modeling of Core Fueling and Global Particle Confinement in ELM-Free H-Mode Plasma in DIII-D," *J. Nucl. Mater.* **220–222** (*Proceedings of the Eleventh International Conference on Plasma-Surface Interactions in Controlled Fusion Devices, Mito, Japan, May 23–27, 1994*), 315 (1995).

28. M. M. Menon, P. M. Anderson, C. B. Baxi, A. Langhorn, J. L. Luxon, M. A. Mahdavi, P. K. Mioduszewski, L. W. Owen, M. J. Schaffer, K. M. Schaubel, and J. P. Smith, "Particle Exhaust Scheme Using an In-Vessel Cryocondensation Pump in the Advanced Divertor Configuration of the DIII-D Tokamak," *Fusion Technol.* **22**, 356–70 (1992).

29. K. M. Schaubel, C. B. Baxi, G. L. Campbell, G. L. Laughon, M. A. Mahdavi, M. M. Menon, C. C. Makariou, J. P. Smith, and M. J. Schaffer, "The Development of an In-Vessel Cryopump System for the DIII-D Tokamak," *Adv. Cryog. Eng.* **39B**, 1983–87 (1993).

30. J. P. Smith et al., "Installation and Initial Operation of the DIII-D Advanced Divertor Cryocondensation Pump," pp. 1043–46 in *Proceedings of the 15th IEEE/NPSS Symposium on Fusion Engineering, Oct. 11–15, 1993, Hyannis, Massachusetts.* Vol. 2, IEEE, New York, 1993.

31. M. M. Menon, J. T. Hogan, R. Maingi, P. K. Mioduszewski, L. W. Owen, M. R. Wade, C. B. Baxi, G. L. Campbell, G. J. Laughon, M. A. Mahdavi, E. E. Reis, M. J. Schaffer, K. M. Schaubel, J. P. Smith, and R. D. Stambaugh, "Particle Exhaust Characteristics of an In-Vessel Cryopump Used in DIII-D Diverted Plasmas," *Fusion Technol.* **27**, 355 (1995).

32. M. A. Mahdavi et al., "Application of Divertor Cryopumping to H-Mode Density Control in DIII-D," pp. 597–603 in *Proceedings of the 15th IEEE/NPSS Symposium on Fusion Engineering, October 11–15, 1993, Hyannis, Massachusetts*, Vol. 2, IEEE, New York, 1993.

33. M. M. Menon, G. J. Laughon, R. Maingi, M. R. Wade, D. L. Hillis, and M. A. Mahdavi, "Pumping Characteristics of a Cryopump with Ar Sorbent in He and in D_2/He Mixture," *J. Vac. Sci. Technol.* **13**(3) (Pt. 1) (*Papers from the 41st National Symposium of the American Vacuum Society, October 24–28, 1994, Denver, Colorado*), 551–55 (1994).

34. P. K. Mioduszewski et al., "Particle Removal With Pump Limiters in ISX-B," *J. Nucl. Mater.* **121**, 285 (1984).

35. C. C. Klepper et al., "Particle Studies in Tore Supra with a Pump Limiter," *J. Nucl. Mater.* **176&177**, 798–802 (1990).

36. T. Loarer, T. Uckan, M. Chatelier, L. D. Horton, and P. K. Mioduszewski, "Effect of Impurities on Particle Collection Studies with Modular Pump Limiter on Tore Supra," *J. Nucl. Mater.* **196–198** (*Proceedings of the Tenth International Conference on Plasma-Surface Interactions in Controlled Fusion Devices, Monterey, CA, USA, 30 March–3 April, 1992*), 1078–82 (1992).

37. L. W. Owen, M. Chatelier, J. T. Hogan, C. C. Klepper, T. Loarer, P. K. Mioduszewski, and T. Uckan, "Effects of Ionizing Scrape-Off Layers on Local Recycling in Tore Supra Pump Limiter Experiments," *J. Nucl. Mater.* **196–198** (*Proceedings of the Tenth International Conference on Plasma-Surface Interactions in Controlled Fusion Devices, Monterey, CA, USA, 30 March–3 April, 1992*), 1125–30 (1992).

38. J. T. Hogan, P. K. Mioduszewski, L. W. Owen, T. Uckan, C. C. Klepper, M. Chatelier, T. Loarer, and L. Horton, "Modeling of Core-Wall Particle Dynamics in Tore Supra Pumping Experiments," *J. Nucl. Mater.* **196–198** (*Proceedings of the Tenth International Conference on Plasma-Surface Interactions in Controlled Fusion Devices, Monterey, CA, USA, 30 March–3 April, 1992*), 1083–89 (1992).

39. L. W. Owen and P. K. Mioduszewski, "Neutrals Transport Modeling of Vented Limiter Configurations for Tore Supra," internal report, 93/7, September 30, 1993.

40. J. M. Noterdaeme and G. Van Oost, *Plasma Phys.* **11**(35), 1481 (1993).

41. C. E. Thomas, Jr., et al., *J. Nucl. Mater.* **220–222** (*Proceedings of the Eleventh International Conference on Plasma-Surface Interactions in Controlled Fusion Devices, Mito, Japan, May 23–27, 1994*), 531 (1995).

42. C. S. Chang and P. Colestock, *Phys. Fluids B* **3**, 310 (1990).

43. C. S. Chang, *Phys. Fluids B* **3**, 259 (1991).

44. K. H. Finken et al., *Phys. Rev. Lett.* **73**(3), 436 (1994).

45. E. A. Lazarus et al., *Phys. Fluids B* **3**, 2220 (1991).

46. E. J. Strait, "Stability of High Beta Tokamak Plasmas," *Phys. Fluids B* **2**(6), 1280–86 (1990).

47. E. A. Lazarus and the DIII-D Team, "Dependence of $\beta \cdot \tau$ On Plasma Shape in DIII-D," p. 195 in *Proceedings of the 20th European Conference on Controlled Fusion and Plasma Physics*, Vol. 17C, 1993.

48. G. L. Jackson et al., *Phys. Rev. Lett.* **67**, 3098 (1991).

49. E. A. Lazarus et al., *Role of Shaping in Achieving High Performance in DIII-D*, GA-A21807, General Atomics, San Diego, 1994; to be published in *Proceedings of the 15th IAEA Conference.*

50. K. Appert et al., p. 329 in *Controlled Fusion and Plasma Physics, Proceedings of the 11th European Conference, Aachen, Germany, 1983*, Vol. I, European Physical Society, Geneva, Switzerland, 1983.

51. H. Takahashi et al., p. 901 in *Controlled Fusion and Plasma Physics, Proceedings of the 20th European Conference, Lisbon, Portugal, 26–30 July 1993*, Vol. III, European Physical Society, Geneva, Switzerland, 1993.

52. D. K. Lee, S. P. Hirshman, M. Okabayashi, M. F. Reusch, and Y. C. Sun, *Method of Rapid Determination of MHD Equilibrium Properties with the Modified Version of the SURFAS Code*, PPPL-2939, Princeton Plasma Physics Laboratory, Princeton, N.J., 1993.

53. S. P. Hirshman, D. K. Lee, F. M. Levinton, S. H. Batha, M. Okabayashi, and R. M. Wieland, "Equilibrium Reconstruction of the Safety Factor Profile in Tokamaks from Motional Stark Effect Data," p. 1187 in *Proceedings of the 20th EPS Conference on Controlled Fusion and Plasma Physics, Lisbon, Portugal, 26–30 July 1993*, Vol. III, European Physical Society, Geneva, Switzerland, 1993.

54. S. P. Hirshman, D. K. Lee, F. M. Levinton, S. H. Batha, M. Okabayashi, and R. M. Wieland, "Equilibrium Reconstruction of the Q Profile in Tokamaks from Motional Stark Effect Data," *Phys. Plasmas* **1**, 2277 (1994).

55. S. F. Paul et al., *J. Nucl. Mater.* **196–198** (*Proceedings of the Tenth International Conference on Plasma-Surface Interactions in Controlled Fusion Devices, Monterey, CA, USA, 30 March–3 April, 1992*), 503 (1992).

56. H. W. Kugel, Y. Hirooka, J. Timberlake, R. Bell, A. England, R. C. Isler, S. Jones, R. Kaita, S. Kaye, R. Khandagle, M. Okabayashi, S. Paul, H. Takahashi, W. Tighe, S. Von Goeler, and A. P. Post-Zwicker, *Fusion Technol.* **25**, 377 (1994).

57. R. C. Isler, A. P. Post-Zwicker, S. F. Paul, W. Tighe, M. Ono, B. P. LeBlanc, R. Bell, H. W. Kugel, and R. Kaita, "Impurity Behavior During Ion-Bernstein Wave Heating in PBX-M," in *Proceedings of the 21st EPS Conference on Controlled Fusion and Plasma Physics, Montpelier, France, June 27–July 1, 1994* (in press).

58. A. P. Post-Zwicker, R. C. Isler, S. F. Paul, W. Tighe, M. Ono, B. P. LeBlanc, R. Bell, H. W. Kugel, and R. Kaita, "Impurity Behavior During Ion-Bernstein Wave Heating in PBX-M," *Nucl. Fusion* **35**(2), 215–23 (1995).

59. S. M. Kaye et al., "An Overview of PBX-M H-Mode Results," *Plasma Phys. Controlled Fusion* **36** [Suppl. 7A: *4th H-Mode Workshop (IAEA Technical Committee on H-Mode Physics), Ibaraki, Japan*], A51–60 (July 1994).

60. S. M. Kaye et al., "ELM-Related Fluctuations in PBX-M H-Modes," *Plasma Phys. Controlled Fusion* **36** [Suppl. 7A: *4th H-Mode Workshop (IAEA Technical Committee on H-Mode Physics), Ibaraki, Japan*], A135–40 (July 1994).

61. J. B. Wilgen, G. R. Hanson, E. de la Luna, V. Zhuravlev, J. H. Harris, J. Sanchez, and R. Kaita, "An A.M. Reflectometer on PBX-M for Edge Density Profile Measurements," *Bull. Am. Phys. Soc.* **38**(10), 2096 (1993).

62. E. de la Luna, G. R. Hanson, J. B. Wilgen, J. Sanchez, V. Zhuravlev, R. Kaita, J. H. Harris, and the PBX-M Team, "First Results with Amplitude Modulation Reflectometry," in *Proceedings of the IAEA Technical Meeting on Microwave Reflectometry for Fusion Plasma Diagnostics, Princeton*, January 1994.

63. E. de la Luna, G. R. Hanson, J. B. Wilgen, J. Sanchez, V. Zhuravlev, and R. Kaita, "First Results with Amplitude Modulation Reflectometry on PBX-M Tokamak," *Rev. Sci. Instrum.* **66**, January 1994.

64. E. de la Luna, J. Sanchez, V. Zhuravlev, G. R. Hanson, J. B. Wilgen, R. Kaita and the PBX-M Team, "Edge Density Profile Measurements on Pbx-M Using an Amplitude Modulated Reflectometer," in *Proceedings of the 21st European Conference on Controlled Fusion and Plasma Heating, Montpellier, 1994*, European Physical Society, Geneva, Switzerland, 1994.

65. C. E. Bush et al., *Characteristics of the TFTR Limiter H-Mode: The Transition, ELMs, Transport and Confinement*, PPPL-2863, Princeton Plasma Physics Laboratory, Princeton, N.J., 1992.

66. C. E. Bush, B. C. Stratton, et al., "Plasma Flows and Fluctuations During H-modes in TFTR," pp. 203–06 in *Proceedings of the 19th European Conference on Controlled Fusion and Plasma Physics, Innsbruck, 1992*, Vol. 16C, Part I, European Physical Society, 1992.

67. C. E. Bush, E. D. Fredrickson, et al., "The Supershot to H-Mode Transition in TFTR," *Bull. Am. Phys. Soc.* **38**(10), 2037 (1993).

68. C. E. Bush et al., oral presentation at the U.S.-Japan Workshop on Transient Phenomena in Toroidal Plasmas, January 20–22, 1993, San Diego, Calif.

69. C. E. Bush, N. Bretz, et al., "Supershot to Limiter H-Mode Transitions in Deuterium Plasmas in TFTR," *Plasma Phys. Controlled Fusion* **36** [Suppl. 7(A): *4th H-mode Workshop (IAEA Technical Committee on H-mode Physics), Ibaraki, Japan*], A153–58 (July 1994).

70. G. Taylor et al., "Intense Electron Cyclotron Emission Bursts During High Power Neutral Beam Heating in TFTR," *Nucl. Fusion* **32**, 1867 (1992).

71. J. Winter et al., *J. Nucl. Mater.* **93&94**, 812 (1980).

72. H. F. Dylla et al., "First-Wall Conditioning for Enhanced Confinement Discharges and the D-T Experiments in TFTR," *J. Nucl. Mater.* **162–164**, 128 (1989).

73. C. Grisolia et al., pp. 111–15C in *Controlled Fusion and Plasma Physics* **33**(13) (*18th European Physical Society Plasma Physics Division Conference, 3–7 June 1991, Berlin, Germany: Invited Papers)*, European Physical Society, Bristol, U.K.,1991.

74. P. K. Mioduszewski et al., "Particle Control Experiments in Tore Supra and DIII-D," *J. Nucl. Mater.* **220–222** (*Proceedings of the Eleventh International Conference on Plasma-Surface Interactions in Controlled Fusion Devices, Mito, Japan, May 23–27, 1994*), 91 (1995).

75. J. F. Lyon et al., *Fusion Eng. Des.* **25**, 85 (1994).

76. G. Grieger et al., *Fusion Technol.* **21**, 1767 (1992).

77. D. T. Anderson and P. R. Garabedian, *Nucl. Fusion* **34**, 881 (1994).

78. The ARIES Team, UCLA-PPG-1461, University of California at Los Angeles, 1994.

79. K. Lackner and N. A. O. Gottardi, *Nucl. Fusion* **30**, 767 (1990).
80. S. L. Painter and J. F. Lyon, *Nucl. Fusion* **31**, 2271 (1991).
81. J. F. Lyon et al., *Proceedings of the 21st EPS Conference on Controlled Fusion Plasma Physics* (1994) 380.

2

ATOMIC PHYSICS AND PLASMA DIAGNOSTICS DEVELOPMENT

C. H. Ma,[1] Plasma Diagnostics Development Program
F. W. Meyer,[1] ECR-based Atomic Collisions Program
D. R. Schultz,[1] Controlled Fusion Atomic Data Center and Fusion-Atomic Theory Programs

N. R. Badnell[2]
M. E. Bannister[1]
E. W. Bell[3]
C. A. Bennett[4]
C. Bottcher[1]
Y.-S. Chung[3]
A. S. Covington[5]
N. Djuric[3]
G. H. Dunn[3]
A. Ya. Faenov[6]
L. Folkerts[1]
H.-O. Folkerts[7]
H. B. Gilbody[8]
T. W. Gorczyca[9]
D. C. Gregory[1,10]
D. C. Griffin[11]
X. Guo[12]
J. W. Hale[1]
M. A. Haque[13]
C. C. Havener[1]
D. Hitz[14]
I. G. Hughes[1,7]
D. P. Hutchinson[15]
J. Irby[16]
M. I. Kirkpatrick[1]
T. Kojima[3]
T. Luke[16]
E. W. McDaniel[17]
T. J. Morgan[18]
S. H. Overbury[19]
F. M. Ownby[20]
R. A. Phaneuf[1,5]
M. Pieksma[21]
M. S. Pindzola[22]
R. K. Richards[1]
S. Schippers[7]
A. C. H. Smith[23]
Y. Takase[16]
E. W. Thomas[17]
J. S. Thompson[5]
D. M. Zehner[24]
P. A. Zeijlmans van Emmichoven[1,21]

1. Physics Division.
2. University of Strathclyde, Glasgow, Scotland.
3. Joint Institute for Laboratory Astrophysics, Boulder, Colorado.
4. University of North Carolina, Asheville.
5. University of Nevada, Reno.
6. Multicharged Ions Spectra Data Center, NPO National Scientific and Research Institute for Physical-Technical and Radio-Technical Measurements, VNIIFTRI, Moscow, Russia.
7. KVI Groningen, The Netherlands.
8. Consultant, Queen's University, Belfast, Northern Ireland, United Kingdom.
9. Postdoctoral fellow, Auburn University, Auburn, Alabama.
10. Environmental, Safety, and Health Compliance Division.
11. Rollins College, Winter Park, Florida.
12. Chemical and Analytical Sciences Division.
13. Alcorn State University, Lorman, Mississippi.
14. Centre d'Etudes Nucleaires, Grenoble, France.
15. Instrumentation and Controls Division.
16. Massachusetts Institute of Technology, Plasma Fusion Center, Cambridge, Massachusetts.
17. Consultant, Georgia Institute of Technology, Atlanta.
18. Consultant, Wesleyan University, Middletown, Connecticut.
19. Chemistry Division.
20. Program Secretary.
21. Utrecht University, Utrecht, The Netherlands.
22. Consultant, Auburn University, Auburn, Alabama.
23. University College London, London, United Kingdom.
24. Solid State Division.

2. ATOMIC PHYSICS AND PLASMA DIAGNOSTICS DEVELOPMENT

Summary of Activities

Atomic physics and plasma diagnostics development research is part of the Oak Ridge National Laboratory (ORNL) Fusion Program and is carried out within the ORNL Physics Division. The principal activities of this program are threefold: atomic collisions research, atomic data compilation and evaluation, and advanced plasma diagnostics development.

The atomic collisions research program focuses on inelastic processes that are critical in plasma diagnostic measurements and determining the energy balance and impurity transport in high-temperature plasmas. The objectives are to obtain a better fundamental understanding of collision processes involving highly ionized impurity atoms at kinetic energies characteristic of magnetic fusion plasmas and to determine cross sections for these processes. Close coordination of experimental and theoretical programs guides the selection of key experiments and provides both benchmarks and challenges for theory. Central to the experimental effort is an electron-cyclotron-resonance multicharged-ion source, which provides ions for colliding-beams experiments. A crossed-beams approach is applied to the measurement of cross sections for electron-impact ionization of highly ionized ions in initial charge states as high as +16. A new collaborative electron-ion merged-beams experiment to measure cross sections for electron-impact excitation of multiply charged ions by electron energy-loss spectroscopy constitutes a major part the current experimental effort. Merged beams are also being used to study charge-exchange collisions of multiply charged plasma impurity ions with hydrogen (deuterium) atoms at the lower kinetic energies relevant to the edge plasma. Ejected-electron spectroscopy is being applied as a diagnostic tool to the study of the interaction of multiply charged ions with solid surfaces. The theoretical effort has focused on the development of close-coupling methods for treating electron-impact excitation of highly charged ions, in support of the merged- and crossed-beams experiments as well as the fusion program in general. These calculations require development and implementation of sophisticated computer codes and depend heavily on the advanced computing capabilities of the National Energy Research Supercomputer Center (NERSC).

Theoretical effort has focused on addressing the most urgent needs of plasma modelers and diagnosticians studying the physics of the edge and divertor regions of present and next-step fusion devices. In particular, sophisticated computer codes have been developed to yield accurate and extensive cross sections and rates for electron impact of ions and atoms (excitation, ionization, and dielectronic recombination) as well as for heavy-particle impact (elastic scattering, ionization, and charge transfer). Development and operation of these computer codes rely heavily on the advanced computational facilities of the NERSC and, to a growing extent, the massively parallel supercomputers at the ORNL Center for Computational Science.

This theoretical work is closely coordinated with the activities of the Controlled Fusion Atomic Data Center (CFADC), whose mission is to compile, recommend, and disseminate atomic and molecular collision data relevant to fusion energy research. To this end a number of expert consultants search the current literature to maintain an up-to-date bibliography. CFADC staff query this database at the request of fusion energy researchers and use it in the production of

periodic reports and publications recommending specific evaluated cross sections and rates. In addition, CFADC participates in an international network of data centers with similar missions, coordinated through the International Atomic Energy Agency. This network shares data and information using the ALADDIN database system, a computer program and standard for the retrieval and exchange of recommended atomic data. Work has begun to make the bibliography, ALADDIN, and other resources easier for the fusion research community to access through an Internet-accessible workstation platform.

The plasma diagnostics program concentrates on the development of advanced diagnostics for magnetic fusion experiments. The current emphasis is on applying pulsed infrared (IR) lasers to the diagnostics of alpha particles produced from the fusion of deuterium and tritium. The proof-of-principle of the small-angle Thomson scattering of an IR laser beam to measure the density and velocity distribution of the alpha particles has been demonstrated on the Advanced Toroidal Facility. As a further step in the development of this alpha-particle diagnostic, a collaboration between ORNL and the Massachusetts Institute of Technology Plasma Fusion Center has been undertaken to place an ion-tail scattering experiment on the Alcator C-Mod tokamak. Also, in support of future experiments such as the International Thermonuclear Experimental Reactor that will operate with higher densities and plasma currents than present devices, a dual-wavelength IR polarimeter/interferometer is under conceptual development. As an intermediate step in this development, a 10-μm polarimeter system for plasma current-density profile measurements has been successfully developed and integrated into the interferometer system on Alcator C-Mod.

2.1 EXPERIMENTAL ATOMIC COLLISIONS

2.1.1 Merged-Beams Measurements of Electron-Impact Excitation of Multicharged Ions

M. E. Bannister, E. W. Bell, Y.-S. Chung, N. Djuric, G. H. Dunn, X. Q. Guo, T. M. Kojima, R. A. Phaneuf, and A. C. H. Smith

The Joint Institute for Laboratory Astrophysics (JILA) merged-beams electron-energy-loss apparatus was applied this period to collaborative measurements of electron-impact excitation of multiply charged ions at the ORNL electron-cyclotron resonance (ECR) Multicharged-Ion Research Facility. Following extensive apparatus modifications to improve the sensitivity of the electron-energy-loss technique and reduce the susceptibility of the apparatus to spurious beam modulation effects, absolute cross-section measurements[1] were performed for 3s-3p excitation of sodium-like Ar^{7+}. The unique merged-beams configuration makes it possible to separate inelastically scattered electrons traveling forward and backward in the laboratory frame and hence to infer gross features of the electron angular scattering in the center-of-mass frame. By measuring the apparent cross section as a function of the ion velocity (or center-of-mass velocity), over 90% of the inelastically scattered electrons were found to be ejected into the backward quadrant in the center-of-mass frame. This experimental observation of backscattering was confirmed recently[2] by close-coupling, distorted-wave, and classical-trajectory Monte Carlo (CTMC) calculations.

In a separate experiment, absolute cross-section measurements[3] were obtained for 2s-2p excitation of lithium-like O^{5+}. For this system, a nonzero cross section was observed below the excitation threshold, whose energy dependence suggested the presence of a short-lived metastable component in the incident beam, with a lifetime of ~0.9 μs. Theoretical efforts are under way to identify such a metastable component in the O^{5+} system. The measured cross sections above threshold are in good agreement with a seven-state close-coupling calculation. Both quantum-mechanical and semiclassical calculations for this system show more than 90% of the electrons causing excitation to be ejected in the backward direction in the center-of-mass frame.

Subsequent to the latter measurements, a position computer that is ten times faster was installed during the past year, along with an upgraded position-sensitive detector capable of handling higher count rates without saturation. The modification was made to reduce the significant dead-time corrections required with the original position-sensitive detector that analyzed the energy loss of the scattered electron signal. Using the fast position computer and detector, absolute cross-section measurements[4] were made of the near-threshold excitation of the $4s^2\ {}^1S \rightarrow 4s4p\ {}^3P$ intercombination transition in Kr^{6+}. The cross section was found to be dominated by resonance structures, ascribed to dielectronic capture followed by autoionization, and is the first observation of resonances in the excitation of a multicharged ion. The measured cross section will serve as a benchmark for theoretical calculations currently under way whose goal is to identify the doubly excited states responsible for the observed structure.

Most recently, the position-sensitive detector used for measuring inelastically scattered electrons was modified to increase its reliability and detection efficiency. In addition, changes were made to the digitized video camera system used to quantify the overlap of the merged electron and ion beams; this was necessary to ensure accurate absolute cross-section measurements. After completion of these modifications, the apparatus was tested thoroughly by remeasurement of the cross section for the $3s \rightarrow 3p$ excitation of Ar^{7+}, which was reproduced satisfactorily. The next measurements to be undertaken will investigate the dielectronic resonance structure predicted theoretically for near-threshold excitation of Ar^{6+}.

2.1.2 Crossed-Beams Measurements of Electron-Impact Ionization of Ions

M. E. Bannister, E. W. Bell, N. Djuric, G. H. Dunn, Y.-S. Chung, D. C. Gregory, X. Q. Guo, T. M. Kojima, R. A. Phaneuf, J. S. Thompson, and P. A. Zeijlmans van Emmichoven

A series of cross-section measurements[5,6] for electron-impact ionization of Si^{q+} ions was carried out using the electron-ion crossed-beams apparatus. Data were obtained for Si^+, Si^{2+}, Si^{6+} and Si^{7+}. Significant contributions to the total ionization cross section resulting from indirect ionization mechanisms were found only for Si^+ and Si^{2+}. This task was performed as part of a research agreement with the International Atomic Energy Agency (IAEA) through a coordinated research program on atomic data for medium- and high-Z impurities in fusion plasmas.

The performance of the electron-ion crossed-beams apparatus was subsequently upgraded by improvements to the electron gun and collector. More effective beam overlap, lower electron beam energy spread by elimination of magnetic fields (also necessary for electron spectroscopy), higher energy operation, and lower vacuum loading were the design objectives. The effect of the design changes was tested and characterized by remeasurement of the electron-impact ionization cross section for Kr^{7+}. (The previous measurements are unpublished.)

The improved apparatus was then used to measure electron-impact ionization cross sections[7] for Kr^{4+}, Kr^{5+}, and Kr^{7+} ions, which are of interest in the interpretation of the krypton beam diagnostic used on various fusion plasma devices. The measured cross sections are in good

agreement with distorted-wave calculations and show significant contributions from excitation-autoionization. Nonzero cross sections below threshold measured for the Kr^{4+} and Kr^{5+} charge states indicate significant metastable components for those two beams.

Preliminary results have also been obtained for electron-impact–induced dissociation of CD_4^+. This molecular ion is typical of the light hydrocarbons present in the low-temperature edge plasmas of fusion devices. The molecular dissociation work is part of a new collaborative initiative with JILA through which complementary measurements are being carried out to analyze the light fragments produced during the dissociative collisions. The dissociation channels leading to the heavy-fragment production (for which complete collection is expected to be less problematic) are being investigated at ORNL. The present results for molecular ion fragmentation have been summarized in a recent ORNL report,[8] which contains a compendium of all electron-impact data measured at ORNL from 1985 through 1992.

Finally, cross-section measurements were completed for electron-impact ionization of Mo^{4+} and Mo^{5+} ions using the newly developed metallic ion beam capability of the new ORNL ECR multicharged-ion source. The cross sections for Mo^{5+} ionization were measured in the 30–500 eV range with an absolute uncertainty of ~9% near the peak value of the cross section (40×10^{-18} cm^2 at 120 eV). The measurements were in good agreement with configuration-average distorted-wave (CADW) calculations of Pindzola et al.[2] The measured cross sections indicate that indirect processes such as excitation-autoionization dominate direct ionization by a 5.7 ratio near the peak of the cross section. The Mo^{5+} ion beam was found to contain ~3% metastable ions, probably in the $4p^5 4d^2\ ^4F$ state. The measured ionization cross sections for Mo^{4+} ions peaked at 60×10^{-18} cm^2 near 100 eV with an absolute uncertainty of 8%. Similar to the case for Mo^{5+} ionization, indirect processes contributed 5 times the cross section that direct ionization did near the peak. At present no distorted-wave calculations exist for comparison with the measurements.

2.1.3 Multicharged-Ion Surface Interactions

L. Folkerts, H.-O. Folkerts, I. G. Hughes, F. W. Meyer, S. Schippers, and P. A. Zeijlmans van Emmichoven

Exploratory studies of the above-surface[9] and subsurface[10] neutralization of multiply charged ions interacting with metal targets have continued, using the techniques of electron and X-ray spectroscopy. Energy- and angle-resolved and total measurements of secondary electron emission have provided new insights into the mechanisms by which the significant neutralization potential energy carried by multicharged ions is dissipated during interactions with metal surfaces. Measurements of total electron emission as a function of target crystal azimuthal orientation have permitted separation of kinetic and potential emission processes. By comparison with modeling studies of above-surface neutralization, it was deduced that Auger transitions filling inner shells of the projectile in the target bulk (i.e., after the ion has penetrated the target surface) are the dominant contributor to potential electron emission above the kinetic emission threshold.

Energy-resolved and total measurements of secondary electron emission have been performed using cesiated gold surfaces[11,12] in an attempt to determine the effect of using low–work-function surfaces on above-surface neutralization. Although cesiation reduced surface work function by up to a factor of 2, the maximum observed enhancement of above-surface K-Auger emission was ~35%. In addition, multicharged-ion–induced electron emission measurements were made using a beryllium surface, a fusion-relevant wall material that is also of interest because of the absence of loosely bound localized core levels. Projectile neutralization rates inferred for this

target were very similar to rates obtained earlier for gold and copper targets, suggesting that the primary neutralization mechanism involves projectile interactions with the delocalized valence levels of the metal target.

Scattered projectile angular and charge-state distributions have been measured for 3.75 keV/amu O^{q+} ($3 \le q \le 8$) and 1.2 keV/amu Ar^{q+} ($3 \le q \le 14$) grazingly incident on an Au(110) single-crystal target.[13] The experiment used a recently installed 2-D, position-sensitive detector in conjunction with a well-collimated incident multicharged-ion beam. Charge-state distributions were obtained by electrostatic analysis of a narrow slice of the scattered ions selected by a set of movable slits downstream of the crystal target. For beams incident along low-index target azimuthal directions, characteristic "banana-shaped" angular distributions[14] of the scattered projectiles were observed, which are indicative of surface channeling. Calculations of the projectile scattering from a simulated Au(110) lattice closely reproduce the observed angular distributions and indicate that the projectiles spend less than 30 femtoseconds within 2 Å of the gold surface and have a maximum surface penetration depth of <1 Å. Nevertheless, for incident O^{q+} ions, almost complete charge equilibration is observed in the scattered projectile charge-state distributions. These observations, along with ion trajectory modeling calculations, suggest that *at the target interface,* the projectile neutralization rates are already faster than 10^{15}/s and that strong screening effects are present as well, which facilitate electron capture directly to the L and M shells of the oxygen projectile.

Using the recently developed metal-ion production capability of the new ECR multicharged-ion source, we have measured angular scattering distributions for 150–300 keV Pb^{q+}($11 \le q \le 36$) and I^{q+}($10 \le q \le 25$) ions grazingly incident on Au(110). These measurements were taken to determine the perpendicular projectile energy gain that results from image charge acceleration before surface impact in a range of charge states overlapping earlier measurements by Winter et al.[15] using Xe^{q+} ions, also under grazing incidence conditions. These earlier measurements showed some evidence of deviation from the $q^{3/2}$ charge-state dependence[16] expected under the assumption of step-wise neutralization above the surface. For charge states up to +29, the inferred projectile energy gains were found to have the expected q dependence. Furthermore, in the region of charge-state overlap, the energy gains inferred for the I^{q+} and Pb^{q+} ions were, within the experimental uncertainty, the same. For charge states +30 and higher, however, the determined energy gains fell systematically below the expected $q^{3/2}$ trend, just as had been observed by Winter et al. In view of the different ionic species used, this effect is not likely to result from the projectile atomic structure. Energy gains inferred from studies of the saturation of potential electron emission induced by normally incident ions of charge up to +72 show no evidence[17] of such a deviation and suggest that the presence of the relatively large parallel velocity components in the case of the grazing geometry measurements may have more significant implications for the above-surface neutralization of multicharged ions than previously thought.

2.1.4 Very Low-Energy Collisions of Multicharged Ions in Merged Beams

C. C. Havener, M. A. Haque, J. S. Thompson, A. M. Covington, L. Folkerts, R. A. Phaneuf, and M. Pieksma

For very low collision energies, electron capture from hydrogen Rydberg atoms by multicharged ions is characterized by enormous cross sections; the predicted maximum is comparable to the geometric size of the Rydberg atom. Using the merged-beams apparatus, we have developed an experimental procedure[18] to quantify these cross sections for the wide range of collision

energies (0.1 to 1000 eV/amu) and charge states. Presently, a fast hydrogen (deuterium) beam containing 0.15% in n shells between 11 and 24 is produced by collisional detachment of H^- in N_2 gas. A Rydberg field stripper is used to truncate the N-shell population of the hydrogen-excited states before merger with the multicharged-ion beam. From measurements of the beam-beam signal as a function of the applied stripper electric field, we can infer the n dependence of the capture cross section ($\sigma \propto n^{\alpha}$). For collisions at the higher velocities, α is found to agree with CTMC calculations,[19] which predict $\sigma \propto n^4$ for $v/v_e \approx 1$. For collision velocities below the classical regime, α remains large and consistent with a value of four. There is no evidence for significantly larger scalings than n^4, as has recently been predicted.[20]

Measurements of hydrogen-atom ground-state cross sections have continued in order to test quantum-mechanical close-coupling calculations down to near-thermal collision energies (0.1–5000 eV/amu). Ion-atom merged-beams measurements[21] of C^{3+} + H(D) support a recent 22-state molecular orbital calculation by L. F. Errea et al., which suggests a need to renormalize previous state-selective measurements at the higher collision energies.[22] For N^{4+} + D collisions, an analysis of both the low-energy behavior and strong structure in the measured and predicted total cross sections has been performed[23] in collaboration with M. Kimura of Argonne National Laboratory. It was found that small differences in the quality of the calculated molecular states and the neglect of electron translational factors can lead to large differences in the low-energy behavior of the predicted cross section. Recent remeasurement of this system confirms previous results[24] and resolves the discrepancy between two recent calculations[25,26] whose predictions differ by an order of magnitude at 0.1 eV/amu. Preliminary measurements on Cl^{7+} + D show that the observed total electron-capture cross section is fairly constant for collisions down to 50 eV/amu, where the cross section decreases, as might be expected from the low-energy breakdown of the absorbing sphere model. The ion-atom merged-beams apparatus has also been used to take advantage of the recent metallic-ion production capability of the ECR ion source and to begin exploration of total electron-capture cross sections for Mo^{4+} + D, Mo^{5+} + D, Mo^{7+} + D, Mo^{9+} + D, and Mo^{11+} + D at collision energies between 200 and 1000 eV/amu. Electron-capture cross sections for such low-energy medium-Z ions are needed for magnetic fusion edge- and divertor-plasma modeling.

The physical mechanisms that cause ionization in low-energy ion-atom collisions are not understood. A recent experiment[27] that measured the velocity distribution of the extremely low-energy electrons emitted in 1–6 keV H^+ + H collisions found strong evidence for the existence of a saddle-point ionization mechanism at collision energies of 4 keV and higher. Identification of such mechanisms has been made possible by recent advances at ORNL using complex plane theoretical techniques. Development has begun at the ORNL ECR facility to perform such low-energy ionization measurements in a merged-beams configuration, where the relatively high center-of-mass velocities will cause electrons to travel in the laboratory frame with energies on the order of 10 eV, with resolvable deviations depending on whether emission occurs on the saddle point or centered on one of the projectiles. Because such beam-beam measurements are characterized by low signal rates, success will depend on the production of neutral beams that are a factor of 10 more intense than those that are currently being produced by the ion-atom merged-beams apparatus. An upgrade of the apparatus is under development. Initial measurements will focus on the dependence of the absolute total ionization cross sections on collision velocity and could lead to the observation of the recently proposed ionization decoupling mechanism.[27] This experimental technique is also capable of measuring the energy distribution and possibly the angular distribution of the emitted electrons for H^+ and other multicharged ions in collisions with hydrogen and should provide a critical test of complex plane theoretical techniques.

2.1.5 ECR Multicharged-Ion Research Facility Upgrade Project

F. W. Meyer, J. W. Hale, and D. Hitz

On October 22, 1992, the first multicharged-ion beam was produced using the new ECR ion source delivered from Grenoble, France. The new source was installed during a 6-week shutdown of the ORNL ECR multicharged-ion research facility that started on September 8, 1992. Initial testing of the new source was completed early in November 1992, and routine usage commenced immediately thereafter. The new source has already been used to provide more intense and stable beams than could be obtained with the old ORNL ECR source for all the on-line experiments of the multicharged-ion research facility. To illustrate the improvement in total source output, the new ECR source has produced up to 20 μA of Ar^{12+} at 17 kV source potential for argon ions (a factor of 30 improvement over what was obtained with the old source) and up to ~1 nA of Ar^{17+} (a factor of 10^5 increase over the corresponding ORNL ECR output). Similar output performance improvement for highly charged beams of second-row elements has also been documented; for example, 2.5 μA of $^{15}N^{7+}$ has already been obtained with the new source, which can be compared to 0.1 μA obtained with the old source. For ion beams of lower charge states, source output improvements of factors of 3–5 are more typical.

Measurements of *usable* beam intensity improvement made with the ion-atom merged-beams apparatus, whose beam acceptance is lowest of all the experiments now on line (because of severe constraints on beam size and divergence), showed a significant improvement in beam profile and an increase in beam intensity by a factor of at least 2–3 over that attainable with the old ECR source. Throughput tests with N^{7+} indicated that, with the new ECR source, merged-beams cross-section measurements will for the first time be possible with a fully stripped ion. The extraction system of the new source will be studied in detail to assess the possibility of reducing the emission of extracted beams, thereby increasing even further the usable source output beam fraction for collision experiments.

As the final phase of the ECR Source Facility Upgrade Project, metal-ion production capability has recently been developed for the new ECR source by installing a miniature oven into the end of the central electrode of the coaxial microwave injection waveguide, located immediately adjacent to the ECR source main plasma stage. Multicharged ions of refractory species and lower–melting-point metallic species have been produced using volatile metal-oxide and metal-chloride powders with sufficient vapor pressures for ion beam production even at moderate oven temperatures (i.e., <600–700°C). Using this technique, stable molybdenum beams in charge states up to +16 have been produced, with charge lifetimes approaching 40 h. For lower–melting-point metals, the oven has been used to generate vapor directly from the pure metal. In this mode, lead ion beams in charge states up to +36 have been produced and were used in recent surface scattering measurements described in Sect. 2.1.3 of this report.

2.2 THEORETICAL ATOMIC PHYSICS FOR FUSION

N. R. Badnell, C. Bottcher, T. W. Gorczyca, D. C. Griffin, M. S. Pindzola, and D. R. Schultz

Through interaction with the experimental atomic physics programs at ORNL, the Controlled Fusion Atomic Data Center (CFADC), fusion research centers throughout the United States, and the Atomic and Molecular Data Unit of IAEA, the theoretical atomic physics for the fusion program identifies incomplete or inaccurate atomic collision data. When such data are identified, the program strives to supply calculations to help rectify the incomplete or inaccurate

data by providing the data in a form suitable for plasma theory modeling and plasma diagnostics interpretation. The strong interaction with the ORNL experimental groups provides insight and benchmarks for the theory program and guidance for the experiments. This relationship helps maximize the amount of new information to be gained from the experimental and theoretical efforts. In particular, such close cooperation leads to improvements in the predictive power of theory for systems other than those that can be studied experimentally. Because the majority of the atomic database required for fusion research cannot be generated experimentally, this interaction is important.

In particular, research is focused on atomic collisions and the electronic structure of plasma impurity ions. The primary collision reactions include electron-impact excitation, ionization, recombination, and effects of external fields and heavy-particle impact of hydrogen, deuterium, helium, and impurity ions involving charge transfer, ionization, and elastic scattering. Calculation of atomic structure and reaction cross sections and rates for the majority of the atomic systems studied is quite computationally intensive and thus requires the facilities of the National Energy Research Supercomputer Center (NERSC) at Lawrence Livermore National Laboratory (LLNL). A collection of state-of-the-art computer codes has been developed and implemented for use in these calculations. Studies are systematized along ionic sequences to better characterize trends and improve the predictive power of theory for systems other than the limited number that can be studied experimentally.

2.2.1 Electron-Impact Excitation of Ions

Electron collisions with impurity ions are an important process in fusion plasma devices. We have developed a number of different theoretical approaches to treat electron-impact excitation of ions in both low- and high-charge states. The theoretical treatments have become increasingly robust as more detailed experimental test measurements have become available and as more detailed cross sections and rates have become of interest to fusion energy research.

Along these lines, the total and angular-differential excitation cross sections for $3s^2\ {}^1S$ to $3s3p\ {}^3P$ and $3s^2\ {}^1P$ transitions and for $3s3p\ {}^3P$ to $3s3p\ {}^1P$ transitions in magnesium-like Si^{2+} and Ar^{6+} in the near-threshold energy region have been computed using the close-coupling R-matrix method.[28] Differential cross sections were found to undergo rapid and strong variations when the incident energy is tuned through the autoionizing resonance transitions. The electrons are preferentially backscattered near the excitation threshold for the dipole-allowed transitions, but the fraction of electrons scattered in the forward direction increases dramatically with energy. The results are significant not only because of the more strenuous test of theory represented by differential cross sections, but also because the information concerning the angular distribution of electrons is crucial in determining whether and by what means experiments such as the JILA-ORNL merged-beam apparatus may detect enough of the electrons to yield accurate and reliable total cross sections.

A series of calculations has been carried out that demonstrates the breakdown of the widely used isolated-resonance approximation for electron-impact excitation of positive ions.[29–31] Resonant processes frequently dominate low-energy electron-ion scattering, and, via the tail of the Maxwellian distribution, these processes influence the populations of ions over a wide range of densities and temperatures of interest in fusion plasmas. The results have been obtained specifically for the $3s^2 \rightarrow 3s3p\ {}^3P$ transition in magnesium-like iron (Fe^{14+}) but are expected to hold for many other ions and species as well. Thus this study indicates that the consequences of overlapping resonance effects are large and commonplace for electron-impact excitation, and the standard formulation of the close-coupling approximation is not applicable.

We have also performed both quantal and quasi-classical calculations of the electron-impact excitation of argon ions ($3s \rightarrow 3p$ transition in Ar^{7+}) to explore the angular differential cross section.[32] The two approaches are in substantial agreement and elucidate the role of screening, which results in cross sections dominated by backscattering in the low-energy regime. This work highlights the ubiquitous nature of backscattering of electrons in elastic or excitation collisions with partially stripped medium- to high-Z ions. The results represent a more strenuous test of theory than consideration of only total cross sections, and they are significant for experiments with limited angular acceptance that seek to measure total excitation cross sections.

2.2.2 Dielectronic Recombination

Dielectronic recombination is important for fusion plasmas because in hot, dilute plasmas, it is the dominant recombination process. There is still great need for accurate theoretical predictions of recombination. For example, the use of low-Z metals in current and future fusion experiments has created a pressing need for extensive data on dielectronic recombination for beryllium and boron. Recently, we have calculated the zero-density rate coefficients for this process for all atomic ions of the beryllium and boron isonuclear sequences, which may be incorporated in a collisional model to obtain the level populations, ionization balance, and power loss for plasmas of interest.[33]

In addition, we have completed a calculation of the dielectronic recombination cross section between the hyperfine levels of the ground state of Bi^{82+} in anticipation of a proposed experimental measurement by A. Müller and coworkers using the Gesellschaft für Schwerionen Forschung (GSI) heavy-ion storage ring at Darmstadt, Germany. It was found that the radiative decay rates from the doubly excited resonances $1s(F = 5)nl$ are orders of magnitude larger than the autoionizing decay rates to the $1s(F = 4)$ continuum. The resulting dielectronic recombination cross sections are strongly peaked toward zero energy but are extremely small compared to the radiative background.[34]

Recent measurements completed by Müller and coworkers at the GSI storage ring (dielectronic and radiative recombination of lithium-like gold) and the Heidelberg storage ring (dielectronic recombination of lithium-like copper)[35] have been found to be in good agreement with sufficiently robust theoretical treatments. These measurements are quite significant because of the regimes of charge states made accessible by the storage-ring technology and because of their high resolution, which allowed individual resonances to be resolved. Therefore they presented a challenging test of theory. In the case of Au^{76+}, a sensitive test of calculations based on the Bethe-Salpeter approach for radiative recombination and results for dielectronic recombination from perturbative-relativistic, semirelativistic, and fully relativistic theories was made.[36]

2.2.3 Electron-Impact Ionization of Ions

Electron-impact ionization of impurity ions is also a very important process in fusion plasmas. Studies have been completed on a number of different systems of interest in fusion research. For example, the revived interest in evaluating the use of tungsten in future fusion reactors motivated consideration of the near-threshold electron-impact ionization of tungsten.[37] In a CADW calculation for the various subshells of neutral tungsten, a giant shape resonance was found, which has a large effect on the total cross section. Its signature was found most readily by examining the differential cross section, and its appearance should be characteristic in electron-impact ionization of a number of heavy atomic systems.

At the other end of the spectrum of nuclear charge, we also completed a detailed study[38] of Li^+ ionization. This study followed up an 11-state close-coupling calculation that considered contributions to ionization from double excitation followed by single autoionization and double excitation with capture followed by simultaneous double autoionization. To account more completely for the structure found in the experimental cross section found by A. Müller and coworkers, we performed a much larger, 37-state *R*-matrix calculation. Discrepancies still remain, however, possibly because of a need for more states, which might reduce the size of the resonances found with this basis set and other coupling terms. The present results show reasonable agreement with the experimental trends and cross-section magnitude in light of the complexity of the double electron transitions.

CADW calculations have also been performed[39] in support of the recent JILA-ORNL measurements of electron-impact single ionization of Si^+ and Si^{2+}. Considerable data are still lacking for the electron-impact ionization of species of importance in fusion research, and the present JILA-ORNL work is aimed at filling a gap for the silicon isonuclear series. The theoretical results consist of the sum of contributions from direct ionization and excitation-autoionization and are in good agreement with the measurements for Si^+ but somewhat less so for Si^{2+}.

A study of this process has been completed for lithium-like, beryllium-like, and boron-like iron, krypton, and xenon ions.[40] These species are currently of interest to fusion research because iron is still an important impurity originating from stainless steel components, while krypton and xenon are introduced into the plasma for diagnostic purposes. In addition, highly charged ions are among the current interests at experimental facilities such as the Test Storage Ring at Heidelberg, the Experimental Storage Ring in Darmstadt, and the Electron Beam Ion Trap at LLNL, presenting an opportunity for stringent comparisons of theory and measurements. The work has concentrated on trends along isonuclear and isoelectronic sequences, focusing on resonance contributions, and including the effects of direction ionization, excitation-autoionization, and dielectronic-capture–double-ionization.

Specifically, in a joint theoretical and experimental collaboration regarding dielectronic capture leading to ionization, the electron-impact ionization of Sc^{2+} has been computed in the close-coupling approximation and compared to new measurements in the near-threshold regime.[41] Strong resonance features are caused by the process of indirect ionization, a situation that should be common for ions with one or two electrons outside a closed subshell. In this case, the direct ionization is overwhelmed by a strong rate for excitation of autoionizing states from the many electrons of the inner subshell. The principal mechanisms are (1) excitation followed by single autoionization or (2) dielectronic capture followed by the sequential autoionization of two electrons. Investigations such as the present allow theory to predict more confidently cross sections needed for fusion, which, because of the large number of systems of interest, cannot always be investigated experimentally.

2.2.4 Statistical Quasi-Quantal Treatment of Ion-Atom Collisions

The CTMC technique, which is a statistical, quasi-quantal treatment of the initial target electronic distribution and the subsequent evolution of the projectile, target core, and electrons, continues to provide cross sections of interest to fusion research in an energy regime in which perturbative and close-coupling calculations present difficulties. A strenuous test of theory and experiment considering the differential cross sections for state-selective electron capture in 25- to 100-keV proton-helium collisions has been completed.[42] CTMC calculations were in good agreement with recent measurements of the differential cross section for capture to the 2p state

and existing measurements for capture summed over all states. The calculations provided insight concerning the origins of the differing shapes of the cross sections for capture to s- and p-states.

A significant number of works using this method have provided detailed total and differential cross sections for electron capture by heavy particles colliding with plasma components such as hydrogen, deuterium, and helium, including state-selective results. This approach has been tested even more rigorously[43,44] by computing the coherence parameters, such as the *Z*-projection of angular momentum in charge-transfer collisions of protons with helium. Through comparison with available measurements, this work has demonstrated that the approach is reasonable for intermediate collision energies.

This and several previous studies have demonstrated the utility of the CTMC method for describing total and differential, and summed and state-selective, intermediate energy charge transfer. We have also explored the applicability of the technique for much higher impact energies. We confirmed that the method overestimates the high-energy capture cross section and, in particular, demonstrated that this effect completely swamps the Thomas double-scattering mechanism, which is known to dominate.[45] However, our investigation has suggested how this overestimation might be ameliorated and suggests a technique for filtering the initial conditions in the Monte Carlo sampling to improve its efficiency for certain reactions. It is hoped that refinements suggested in this work will significantly extend the applicability of this method.

In another attempt to test the limits of applicability of the CTMC technique and to suggest ways in which it may be improved, we performed an extensive calculation of the differential cross sections for ionization of helium and deuterium by electron impact.[43,44] Perhaps surprisingly, good agreement was found with experimental measurements of the singly and doubly differential cross sections. The CTMC doubly differential cross sections lack a degree of variation with electron angle that is clearly quantum-mechanical in origin, but they reproduce the magnitude and trend of the data well, better in fact than the existing quantum-mechanical calculations of this quantity. Our conclusion is again that classical mechanics dominate the electron removal processes at intermediate collision velocities, even for light particle impact. Quantum-mechanical corrections to the CTMC model in which, for example, the phase of each trajectory is monitored, could account for the remaining discrepancies and extend the usefulness of this theory to new electron-impact collision systems.

2.2.5 Heavy-Particle Elastic Scattering

The elastic collisions between neutral and charged ions of hydrogen, deuterium, and helium in the *low-energy* regime have become a central focus of attempts to model the edge and divertor regions of next-step fusion devices. In these regions, the transport and energy exchange of these particles is important in modeling the divertor's ability to remove heat flux, recycle atomic hydrogen into the core plasma, and exhaust the helium ash of the fusion process. Because comprehensive data for these collisions do not exist in the literature, we have developed quantum-mechanical and semiclassical models and computer codes to allow calculation of the elastic differential scattering cross section. The quantum code will serve as a benchmark for the semiclassical code, which runs much faster. This speed advantage is important because of the large number of computations necessary to form a complete database and because it may be useful to distribute the codes to plasma modelers for direct interface with their codes. A preliminary set of calculations and fitting coefficients has recently been completed and published.[46]

2.3 CONTROLLED FUSION ATOMIC DATA CENTER

A. Ya. Faenov, H. B. Gilbody, D. C. Gregory, M .I. Kirkpatrick, T. J. Morgan, R. A. Phaneuf, M. S. Pindzola, E. W. McDaniel, D. R. Schultz, and E. W. Thomas

The primary mission of CFADC is to provide critically evaluated data to address the most urgent needs of fusion energy research and development. To this end a number of activities are performed, including

- maintenance of a bibliographic database of references to articles containing atomic and molecular data pertinent to fusion;
- publication of recommended data and compilations of data, including parameterizations and scalings for ease and breadth of application in fusion research and periodic assessments of the status and needs for data;
- response to user requests for bibliographic and numerical data searches; and
- establishment and dissemination of a database of recommended numerical data in cooperation with an international network of data centers coordinated by IAEA, designed to facilitate data exchange between and among data producers and users.

2.3.1 The Bibliographic Database

The bibliographic database is maintained through the efforts of a group of expert consultants who search over 100 journals for articles containing data of potential use in fusion energy research. Each entry is categorized by reaction, reactants, energy range, authors; title, and journal reference. This database contains ~26,000 entries covering the period from 1978 to the present and is accessible locally and at a number of other sites internationally in a personal-computer (PC)–based system. Hard-copy bibliographic entries covering the period from the mid-1950s to 1977 may also be searched. Efforts to convert old data tapes to modern format have been initiated so that these archival entries, which number ~45,000, may also be searched electronically. Current interest in the edge and divertor regions of fusion devices has renewed interest in reactions that were extensively explored in that period, highlighting the need to bring the older entries into a more accessible medium. Approximately two external requests to query the database are received per week.

2.3.2 Data Center Network

CFADC participates in an international network of data centers with similar missions. The goal of this network is to coordinate evaluation of the status of existing atomic and molecular data, identify needs for new or revised data, facilitate the exchange of data, and promote standardization of the data exchange format. Updates of the CFADC bibliographic database are sent to members of this network and form the basis for the periodic publication by the IAEA of the *International Bulletin on Atomic and Molecular Data for Fusion*.[47] This network has also adopted the ALADDIN database format and system as the standard for exchange of atomic and molecular data between data producers and with the user community. A number of the CFADC publications of recommended data are among the 20 ALADDIN database files currently distributed.

The data center network and IAEA also provide an important forum for meetings and workshops, for which CFADC has performed specific data evaluation and production projects, including the following:

- the IAEA consultants' meeting on Atomic and Molecular Data Base for Hydrogen Recycling and Helium Removal from Fusion Reactors in Vienna, Austria, in June 1992, where results of calculations of elastic and momentum transfer cross sections were presented and a survey of the existing data concerning these processes in the edge plasma was made;[48]
- the IAEA Advisory Group Meeting on Technical Aspects of Atomic and Molecular Data Processing and Exchange (11th Meeting of the A+M Data Centers and ALADDIN Network) in Vienna in June 1992, where recent activities and the status of CFADC were summarized;[49]
- the Fourth International Colloquium on Atomic Spectra and Oscillator Strengths for Astrophysical and Laboratory Plasmas in Gaithersburg, Maryland, in September 1992, for which a critical assessment of existing atomic collision data was performed and data requirements resulting from recent trends in fusion plasma applications were identified;[50]
- the IAEA Technical Committee Meeting on Atomic and Molecular Data for Fusion Reactor Technology in Cadarache, France, in October 1992, where the status of atomic and molecular collisional data was reviewed in an invited talk, and a poster was presented outlining the mission, activities, and plans of CFADC;[51]
- the IAEA Research Coordination Meeting on Atomic Data for Medium- and High-Z Impurities in Fusion Plasmas, held in Vienna on September 22–24, 1993, where, to increase ORNL participation in international efforts to produce data of immediate relevance to fusion, a detailed summary of the Atomic Physics for Fusion experimental program was presented, including descriptions of the ongoing efforts to measure electron-impact ionization of multicharged ions, electron excitation of ions, low-energy charge transfer processes, ion-surface interactions, and symmetric charge transfer in ion-ion collisions; and[52]
- the IAEA Advisory Group Meeting on Technical Aspects of Atomic and Molecular Data Processing and Exchange (12th Meeting of the A+M Data Centers and ALADDIN Network) in Vienna on September 20–21, 1993, where recent activities of CFADC were reported and progress reports were made regarding data projects.[53]

Other critical assessments of data status and needs were made at national and international meetings as well.[50,54]

2.3.3 Data Compilations

In addition to data assessment projects associated with meetings and workshops, CFADC periodically compiles data from the literature, which are analyzed by experts on the particular processes, and, based on these analyses, CFADC recommends specific cross sections and rate coefficients. They are published as journal articles or ORNL technical reports such as the current "Redbook" series "Atomic Data for Fusion." For example, because of the recent intense interest in low-Z materials for plasma-facing components, a critical assessment of the available data for beryllium and boron ion impact of hydrogen, deuterium, and helium was performed.[55] Also, recommended data for state-selective electron capture in collisions of C^{6+} and O^{8+} with hydrogen were published because of the importance of these reactions in CER spectroscopy.[56] To tap into the large amount of atomic data available in the former Soviet Union but not readily accessible in the West, Dr. A. Ya. Faenov, director of the Multicharged-Ion Spectral Data Center, NPO VNIITFRI in Moscow, joined CFADC as a consultant and is producing ALADDIN-formatted

data files for excitation and dielectronic recombination regarding low-Z systems, which have the most significant needs.

2.3.4 Internet-Accessible Databases

In response to CFADC users' growing need to receive bibliographic and numerical data in electronic format over the widely used Internet, the CFADC databases are being converted to a form that will allow any interested party to access them directly. The bibliographic and ALADDIN databases will be made available first, and more sophisticated data packages will be made available later.

2.4 DIAGNOSTICS OF HIGH-TEMPERATURE PLASMAS

2.4.1 IR Polarimeter for Measurement of Plasma-Current Profile in the Alcator C-Mod Tokamak

C. H. Ma, D. P. Hutchinson, R. K. Richards, J. Irby, and T. Luke

A collaboration between the Electro-Optics Laboratory (EOL), Physics Division, and the Massachusetts Institute of Technology (MIT) Plasma Fusion Center has been undertaken to measure the electron-density and plasma-current profiles in the Alcator C-Mod tokamak by using a two-color interferometer and an IR polarimeter. For high-density and high–plasma-current tokamaks, the poloidal magnetic field distribution can be determined by probing the plasma with an array of CO_2 laser beams and measuring the plasma-induced Faraday rotation θ_f of the plane of polarization. The rotation angles are proportional to the line integrals of the electron density multiplied by the magnetic field component along the probing beam paths. With the electron density distribution, determined from a phase shift (ϕ) measurement with the concomitant interferometer, and by using the close relation between the plasma current and the resulting poloidal magnetic field, the integrals can then be inverted to obtain the current-density distribution.[57] Because of similarities between the Alcator C-Mod and ITER in their expected phase shifts and Faraday rotations (shown in Table 2.1), an additional objective of the program is to determine the feasibility of this interferometer and polarimeter system for ITER. The polarimeter is a modification of a previous system developed for the Compact Ignition Tokamak.[58] An electro-optic polarization modulator has been developed to achieve the high sensitivity (≤0.01°) and time resolution (≤0.1 ms) required for measuring the Faraday rotation. The polarimeter has been successfully designed, constructed, and calibrated at EOL and has been integrated into the existing two-color interferometer on C-Mod.[59] Detailed analyses and experiments of the previous systems have been reported,[58–60] so only a brief description of the modified system is presented in this section.

The two-color heterodyne interferometer consists of ten CO_2 laser (10.6-μm) channels and three HeNe laser (0.6328-μm) channels viewing the plasma vertically with a Michelson geometry. The main components are: a CO_2 laser (MPB Technologies, Inc., model GN 802-20-MES, 20-W, single line), a germanium Bragg cell (Isomet Model 1207 B-6), and an HgCdTe thermoelectrically cooled detector array (Electro-Optical System, Inc., model MCT10TE-010/10ELE). The acoustic optic Bragg cell diffracts ~50% of the CO_2 laser power into a reference beam. This cell also introduces a frequency shift (Δf) of 40 MHz in the diffracted beam. The undiffracted probing beam is passed through a ZnSe quarter-wave Fresnel rhomb, a

Table 2.1. Design considerations for two-color interferometer/polarimeter system

	C-Mod (Double pass)	ITER (Single pass)
Wavelength, μm	10.6	10.6
Major radius, m	0.65	7.75
Minor radius, m	0.2	2.75
Central density, $10^{20}/m^3$	10	1.78
Plasma current, MA	3	25
Toroidal field, T	9	6
Faraday rotation, deg	1.4	1.4
Ellipticity	7.6×10^{-6}	1.3×10^{-5}
Phase shift, fringes	2.5	2.7

CdTe electro-optic modulator, and a mechanical polarization rotator. Emerging from the polarization modulator, the Gaussian beam is expanded, via cylindrical mirrors, to an elliptical beam with a profile of 1×20 cm for viewing the plasma cross section accessible by the viewing ports. The return beam in the two-pass system is decollimated and passed through an analyzer. The reference beam is also expanded and guided to the signal detector array to mix with the probing beam. The detector signals are then filtered, amplified, and fed into digital phase-detection circuits to extract the phase shifts between the output of the signal detectors and the reference signal. These phase shifts are proportional to the line-integrated electron densities along the ten vertical chords.

Figure 2.1 is a simplified sketch of the arrangement of the polarimeter. The electro-optic modulator (II-VI, Inc., model EOM5-10.6-0450-C) consists of a ZnSe quarter-wave Fresnel rhomb and a CdTe crystal of $4 \times 4 \times 50$ mm, operating with a half-wave voltage of 4.24 kV. Initially, both the probing beam and the reference beam are linearly polarized, with their electric fields in the x direction. The ZnSe Fresnel rhomb shown in the figure causes the probing beam to be totally reflected internally twice (with an incident angle of 65.57°), thereby changing the probing beam into a circularly polarized wave.[61] The modulator is driven by an 800-KHz oscillator-amplifier system with the electric field applied in the x direction. The mechanical polarization rotator consists of three mirrors mounted on a rotatable frame such that the polarization of the probing beam changes by twice the angle of the frame rotation. Emerging from the plasma, the probing beam is passed through an analyzer. The analyzer is oriented with its axis in the x direction so that only the x component of the probing beam is mixed with the reference beam at the detector. The output of the signal detector, V_s, can be expressed by the following relation:

$$V_s = \{(RP_p)^{1/2}\,[\cos(\phi)\cos(\omega_p t - \phi - \phi_m) - \sin(\theta)\sin(\omega_p t - \phi)] + (RP_r)^{1/2}\cos(\omega_r t)\}^2$$

$$= -RP_pJ_1(\theta_m)\,\sin(2\theta)\sin(\omega_m t) + R(P_pP_r)^{1/2}\,[\cos(\theta)\cos(\Delta\omega t + \phi + \phi_m) + \sin(\theta)\sin(\Delta\omega t + \phi)]$$

$$+ \text{terms of dc and other frequencies}\ , \quad (1)$$

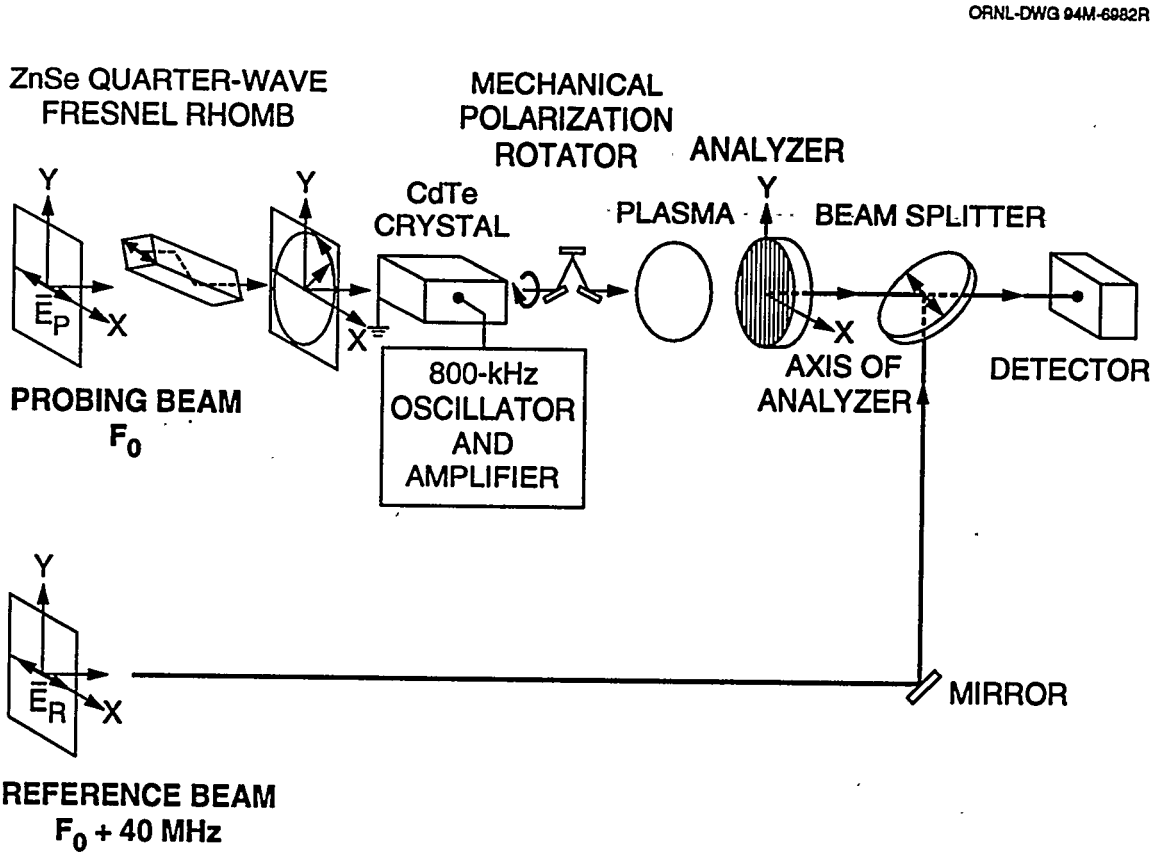

Fig. 2.1. Illustration of electro-optic polarization-modulation technique used in CO_2 laser polarimeter on Alcator C-Mod.

where

R is the responsivity of the detector;
θ is the sum of the polarization rotation angle due to the mechanical rotator, θ_b, and the Faraday rotation in plasma, θ_f;
ω_m is the modulation frequency;
ω_p is the frequency of the probing beam;
ω_r is the frequency of the reference beam;
$\Delta\omega = \omega_p - \omega_r$;
$J_1(\theta_m)$ is the Bessel function of the first kind with order 1;
P_p is the power of the probing beam at the detector; and
P_r is the power of the reference beam at the detector.

The modulation of the phase shift between the X component and the Y component of the electric field, ϕ_m, is sinusoidal and can be written

$$\phi_m = \theta_m \sin(\omega_m t) \ , \tag{2}$$

where θ_m is the amplitude of the modulation angle in degrees and is related to the modulation voltage V_m and the half-wave voltage of the CdTe crystal, V_π, by

$$\theta_m = 180\, V_m/V_\pi \ . \tag{3}$$

For small θ_f, and by setting the mechanical polarization rotator at the 45° position ($\theta_b = 90°$), Eq. (1) becomes

$$V_s = RP_pJ_1(\theta_m)\sin(2\theta_f)\sin(\omega_m t) + R\,(P_pP_r)^{1/2}\cos(\theta_f)\sin(\Delta\omega t + \phi) + \text{terms of dc and other frequencies} \ . \tag{4}$$

The phase shift ϕ is derived from the second term of Eq. (4) using the concomitant interferometer. The amplitude of this term is proportional to the laser power times $\cos(\theta_f)$ and is independent of the modulation. For angles $\theta_f \leq 5°$, the interferometer signal varies less than 0.4%; therefore, its effect on the phase measurement is negligible. The detector signal at the modulation frequency is synchronously detected by a lock-in amplifier. The output voltage of the amplifier is then

$$V_{\text{out}} = ARP_pJ_1(\theta_m)\sin(2\theta_f) \ , \tag{5}$$

where A is the voltage gain of the amplifier. The values of the individual components of Eq. (5) may be lumped into a single calibration constant V_o so that Eq. (5) becomes

$$V_{\text{out}} = V_o\sin(2\theta_f) \ , \tag{6}$$

where $V_o = ARP_pJ_1(\theta_m)$. The value of V_o can be obtained by setting the mechanical polarization rotator at a calibration angle θ_c, within 2° of its original 45° position, and measuring a calibration voltage V_c at the output of the lock-in amplifier before the beginning of the plasma discharge. The voltage V_o is related to V_c and θ_c by

$$V_o = V_c/\sin(4\theta_c) \ . \tag{7}$$

V_o as determined by this technique calibrates the polarimeter in a manner that does not require absolute knowledge of the laser power, the detector responsivity, the modulation angle, or the gain of the amplifier. For small rotation angles, $(\theta_f + 2\theta_c) \leq 5°$, V_{out} is a direct measure of θ_f, because $\sin[2(\theta_f + 2\theta_c)] \cong 2(\theta_f + 2\theta_c)$, and Eqs. (6) and (7) are reduced to the form

$$\theta_f = 2\theta_c(V_{\text{out}}/V_c - 1) \ . \tag{8}$$

The outputs of the lock-in amplifiers are digitized for computer storage and processing. The values of the Faraday rotation angles along the ten vertical chords are calculated according to Eq. (8).

A test bench of the polarimeter system was set up at EOL to determine the performance characteristics of the system. Because the signal at the modulation frequency is only proportional to the power of the probing beam, the first experiment was performed with the reference beam blocked. Figure 2.2(*a*) shows the frequency spectrum of the modulated signal at 800 kHz with $\theta_b = 45°$. It can be seen in this figure that the signal-to-noise ratio of the modulated signal is ~20 dB. The high signal-to-noise ratio was achieved with only 1 W of CO_2 laser power and without any beam focusing. The second experiment was performed with reference beam and $\theta = 0°$. Figure 2.2(*b*) shows the frequency spectrum of the heterodyne beat signal at 40 MHz and

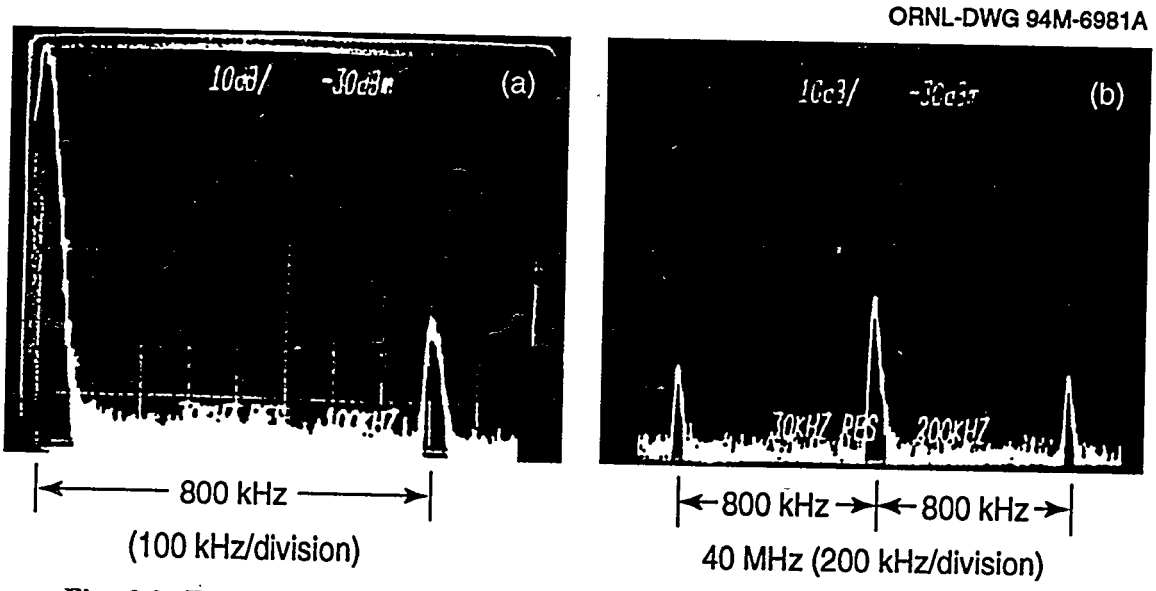

Fig. 2.2. Frequency spectra of (*a*) modulated signal at 800 kHz with θ_b = 45° and (*b*) heterodyne beat signal at 40 MHz and sideband frequencies of ±800 kHz with θ_b = 0°.

sideband frequencies of ±800 kHz. The signal-to-noise ratio of the sidebands is also ~20 dB. Finally, the calibration experiment was carried out with the mechanical polarization rotator oriented at 46°. Under this condition, a Faraday rotation of 2° was simulated. The output voltage of the lock-in amplifier was measured at ~350 mV. With both beams blocked, an output voltage in the range of 1–2 mV was observed, and a polarimeter sensitivity better than 0.01° was achieved. The sensitivity can be further enhanced by using two lock-in amplifiers connected in series. The first amplifier is synchronized at 40 MHz, and its output is fed into the second lock-in amplifier, which is synchronized to the modulation frequency of 800 kHz. The only drawback of this technique is that a reference signal detector is needed for the density measurement. The polarimeter has been added in the existing two-color interferometer system on Alcator C-Mod. The interferometer and polarimeter system has been successfully aligned and calibrated, and the measurements are under way.

2.4.2 CO_2 Laser Thomson Scattering Ion-Tail Diagnostic for Alcator C-Mod

R. K. Richards, D. P. Hutchinson, C. H. Ma, and Y. Takase

The ion velocity distribution function of high-temperature plasmas may be determined by collective Thomson scattering.[62,63] Collective Thomson scattering measurements at the CO_2 laser wavelength require operation at small angles.[64,65] For fusion-relevant plasma conditions, the scattering angle Θ between the source and receiver is typically ~1° or less. Such small angles present problems with beam alignment and stray light rejection. A proof-of-principle test of the diagnostic system has been performed on ATF with a measurement of an electron resonance feature,[66] which examined these problems and demonstrated the capability of this diagnostic. As an application for such a diagnostic, this report describes modifications made to the ATF system to allow measurement of an ICRH-produced ion tail in the Alcator C-Mod tokamak. The

diagnostic is being developed for the eventual measurement of the alpha particle velocity distribution on ITER.

The receiver system uses heterodyne detection to reduce stray light and improve the signal-to-noise ratio. The postheterodyne signal-to-noise ratio *S/N* is given by:

$$\frac{S}{N}=\frac{P_s}{P_s+P_N}\sqrt{B\tau+1}\ , \tag{9}$$

where B is the receiver bandwidth, τ is the integration time, P_S is the scattered signal power, and P_N is the system noise. A large signal-to-noise ratio requires a large product of bandwidth multiplied by integration time. The bandwidth is set by the Doppler broadening of the ions, and the integration time is limited to the laser pulse length. For this experiment, the bandwidth of each receiver is 1 GHz; the Doppler width of the ion tail is ~10 GHz. With a laser pulse length of 1 μs, the signal-to-noise ratio for each channel will have a maximum value of 32.

A schematic of a single channel of the diagnostic system is given in Fig. 2.3. Both the source laser and the receiver systems are located in a diagnostic room well away from the plasma. Having common optics for both systems helps maintain the intersection of the beams. The beam path is vertical through the plasma and requires both top and bottom ports for this experiment. Because of the magnetic coil configuration on Alcator C-Mod, these ports have limited access and restrict the view of the scattered laser radiation to ~1°.

The source laser is a modified Lumonics TEA-103. It was previously used in a proof-of-principle test of the scattering system on ATF. For the ATF test, the laser consisted of three cells with unstable resonator optics and was controlled by a cw injector laser. The injector was used to set the wavelength and polarization and lengthen the pulse width; it also provided a means of continuously monitoring the beam direction of the pulsed laser for alignment purposes. For the C-Mod experiment, the source laser has been modified by lengthening the active lasing volume from three cells to four to increase the output energy to 10 J and by adding a small amount of tripropylamine to the gas mix. The tripropylamine allows the discharge to remain stable with increased quantities of nitrogen, which produces longer pulse lengths.[67] For this laser system the pulse length was found to increase from the 1 μs demonstrated in the ATF test up to 5 μs.

The single-channel receiver system used in the ATF test has been modified to five channels. These five channels view the plasma at different scattering angles ranging from 0.5° to 0.9°. A single local oscillator is used to set the detection frequency for all five channels. An N_2O laser line displaced 6.92 GHz from the source CO_2 laser frequency has been chosen for the local oscillator. The five channels are set along a viewing line through the plasma at an angle of 60° with respect to the magnetic field axis. This angle avoids resonant magnetic effects produced by magnetized electrons when viewed at angles nearly perpendicular to the magnetic field, yet it is near enough to perpendicular to make use of a scattering enhancement caused by anisotropies in the ion-tail velocity distribution. The 60° angle was selected to accommodate the oblong ports on Alcator C-Mod, which limit the accessible view of scattering in the parallel direction to only 0.5°.

The velocity distribution is determined by measuring the shape of the scattered radiation as a function of either frequency or wave vector. These are related to the velocity component to be measured, v, by

$$\frac{\omega}{k} = v\ , \tag{10}$$

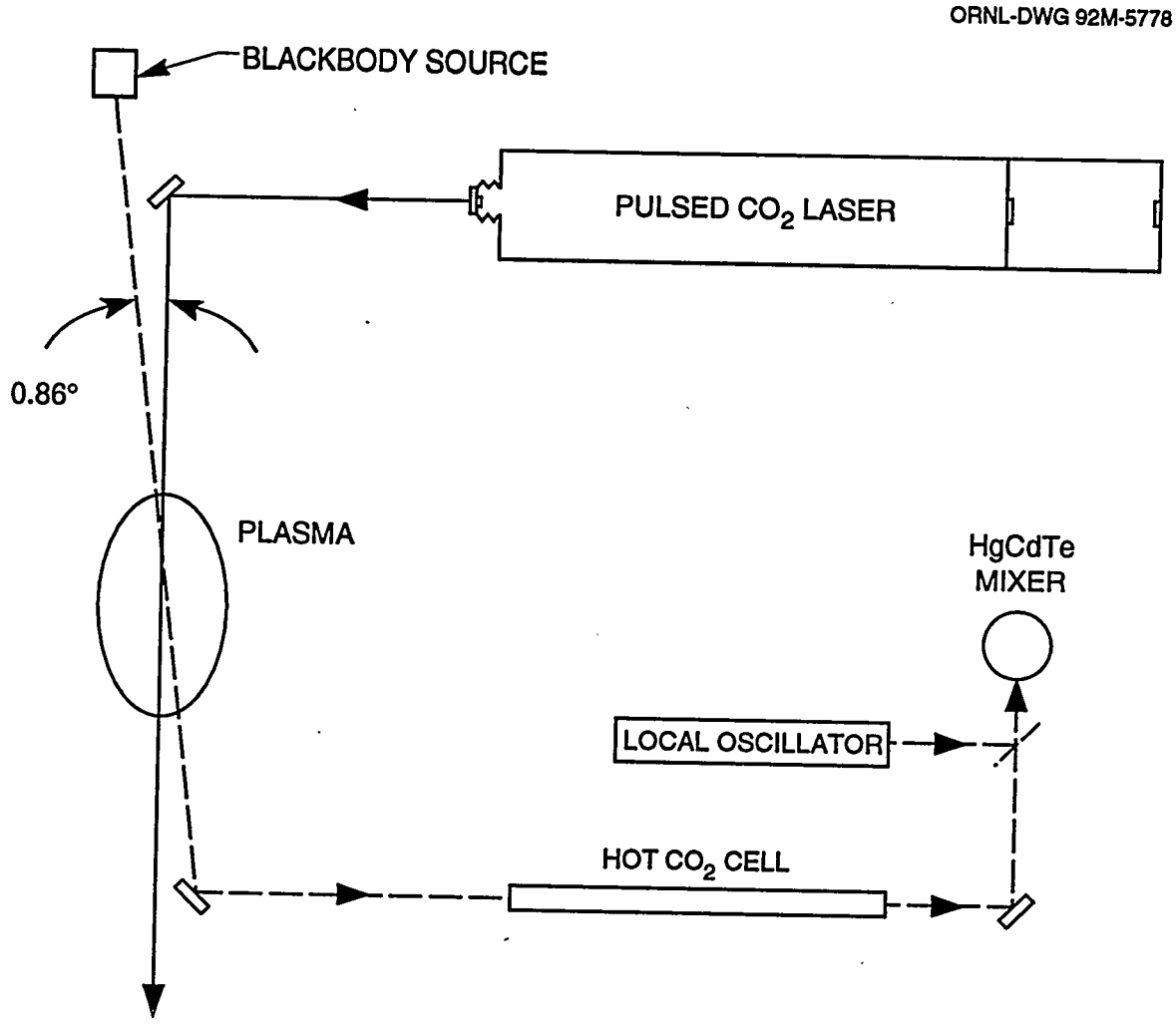

Fig. 2.3. Schematic of scattering system showing paths of source laser and receiver beams. Hot CO_2 cell serves as notch filter for stray laser radiation. Blackbody source used to align and calibrate receiver.

where ω is the frequency shift from the source generated by Thomson scattering and k is the change in wave vector. Generally, Thomson scattering is viewed as a function of frequency such as shown in Fig. 2.4 for the expected Alcator C-Mod conditions at a scattering angle of 0.75°. However, the scattering can also be viewed as a function of the change in the wave vector or, equivalently, the scattering angle Θ, which are related by

$$k = k_i 2\sin(\Theta/2) \ , \tag{11}$$

where k_i is the initial wave vector. Figure 2.5 shows the expected scattered power as a function of scattering angle for different tail temperatures in Alcator C-Mod. Note that the scattered power exhibits a temperature-dependent peak, making this measurement technique very sensitive to changes in the ion-tail temperature. The disadvantage of measuring in angle rather than frequency is that the measurement becomes more sensitive to changes in the plasma spatial distribution.

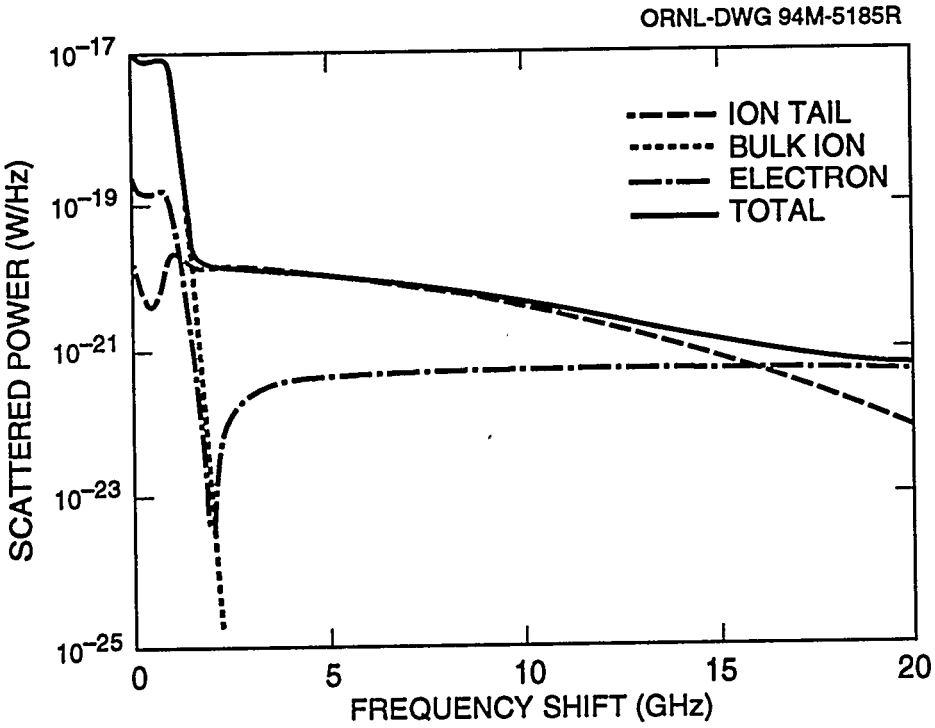

Fig. 2.4. Expected contributions to scattered power for Alcator C-Mod as function of scattering angle for ion tail and electrons at frequency shift of 6.92 GHz from laser line. Scattering angles for five channels indicated.

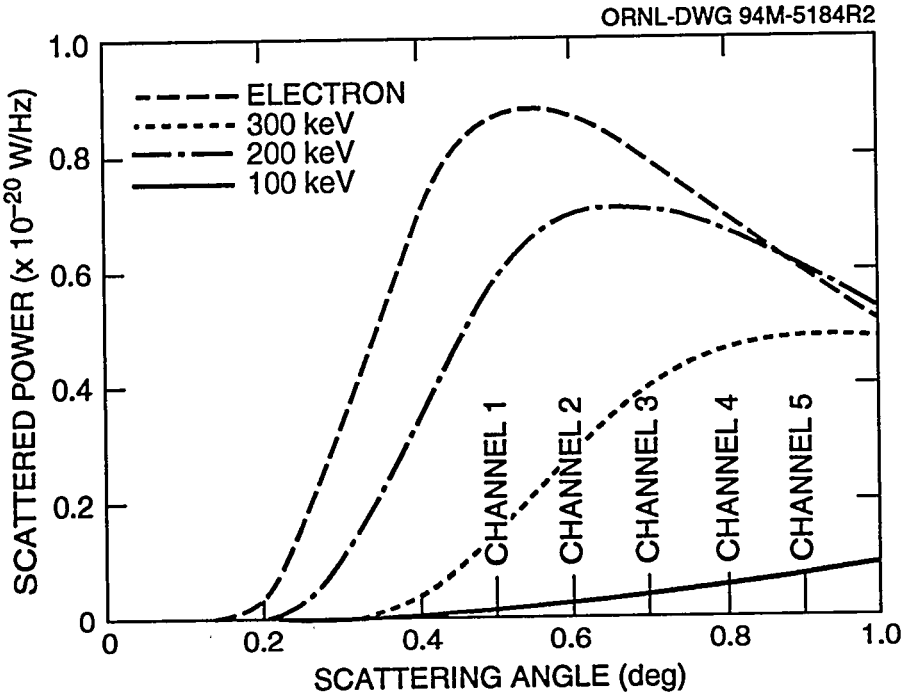

Fig. 2.5. Expected scattered power as function of frequency shift from laser line center for Alcator C-Mod. Shows individual contributions to scattering from plasma components at scattering angle of 0.75°.

The scattered power distribution expected for ITER[69] is shown in Fig. 2.6 and resembles the distribution for Alcator C-Mod (Fig. 2.4). The resemblance occurs in the velocity distributions of the alpha particles in ITER and the ion tail in Alcator C-Mod. With the higher densities expected in ITER, the expected scattered signal is larger than in Alcator C-Mod. Therefore, diagnostic development for the ion-tail measurement on Alcator C-Mod has direct application for the measurement of the alpha particle distribution on ITER.

This diagnostic system is currently under construction at Alcator C-Mod.

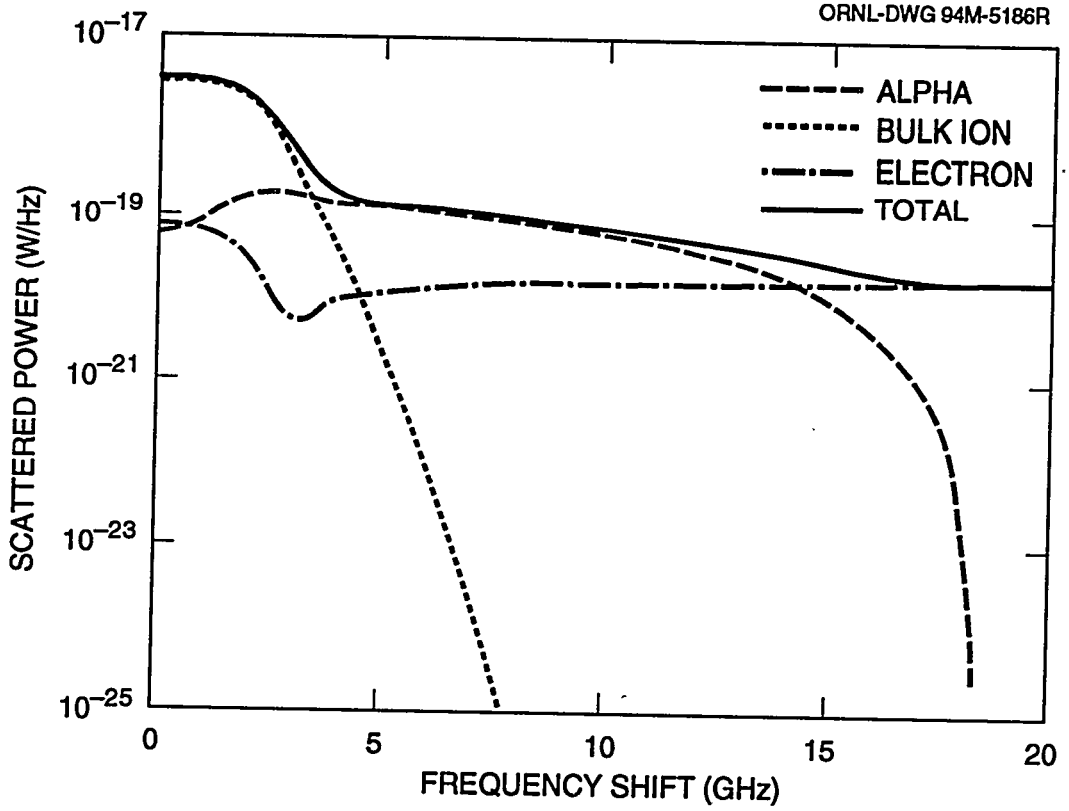

Fig. 2.6. Expected scattered power for ITER as function of frequency shift from laser line center. Shows individual contributions to scattering from plasma components at scattering angle of 0.75°.

References

1. X. Q. Guo, E. W. Bell, J. S. Thompson, G. H. Dunn, M. E. Bannister, R. A. Phaneuf, and A. C. H. Smith, "Evidence for Significant Backscattering in Near-Threshold Electron-Impact Excitation of $Ar^{7+}(3s \rightarrow 3p)$," *Phys. Rev. A* **47**, R9 (1993).

2. M. S. Pindzola, D. R. Schultz, and D. C. Griffin, *Phys. Rev. A* **48**, 4333 (1993).

3. E. W. Bell, X. Q. Guo, J. L. Forand, K. Rinn, D. R. Swenson, J. S. Thompson, G. H. Dunn, M. E. Bannister, D. C. Gregory, R. A. Phaneuf, A. C. H. Smith, A. Müller, C. A. Timmer, E. K. Wåhlin, B. D. DePaola, and D. S. Belić, "A Merged-Beams Energy-Loss Technique for Electron-Ion Excitation: Absolute Total Cross Sections for O^{5+} (2s-2p)," *Phys. Rev. A* **49**, 4585 (1994).

4. M. E. Bannister, X. Q. Guo, T. M. Kojima, and G. H. Dunn, "Resonance Structure and Absolute Cross Sections in Near-Threshold Electron-Impact Excitation of the $4s^2\ ^1S \rightarrow 4s4p\ ^3P$ Intercombination Transition in Kr^{6+}," *Phys. Rev. Lett.* **72**, 3336 (1994).

5. P. A. Zeijlmans van Emmichoven, M. E. Bannister, D. C. Gregory, C. C. Havener, R. A. Phaneuf, E. W. Bell, X. Q. Guo, J. S. Thompson, and M. Sataka, "Electron-Impact Ionization of Si^{6+} and Si^{7+}," *Phys. Rev. A* **47**, 2888 (1993).

6. N. Djurić, E. W. Bell, X. Q. Guo, G. H. Dunn, R. A. Phaneuf, and M. E. Bannister, "Absolute Cross Sections for Electron-Impact Single Ionization of Si^{+} and Si^{2+}," *Phys. Rev. A* **47**, 4786 (1993).

7. M. E. Bannister, X. Q. Guo, and T. M. Kojima, "Absolute Cross Sections for Electron-Impact Single Ionization of Kr^{4+}, Kr^{5+}, and Kr^{7+} Ions," *Phys. Rev. A* **49**, 4676 (1994).

8. D. C. Gregory and M. E. Bannister, *Electron-Impact Ionization of Multicharged Ions at ORNL: 1985–1992,* ORNL/TM-12729, Martin Marietta Energy Systems, Inc., Oak Ridge Natl. Lab., July 1994.

9. F. W. Meyer, C. C. Havener, and P. A. Zeijlmans van Emmichoven, "Above-Surface Neutralization of N^{6+} Ions During Interactions with a Cu(110) Target," *Phys. Rev. A* **48**, 4476 (1993).

10. I. G. Hughes, J. Burgdörfer, L. Folkerts, C. C. Havener, S. H. Overbury, M. T. Robinson, D. M. Zehner, P. A. Zeijlmans van Emmichoven, and F. W. Meyer, "Separation of Kinetic and Potential Electron Emission Arising from Slow Multicharged Ion-Surface Interactions," *Phys. Rev. Lett.* **71**, 291 (1993).

11. F. W. Meyer, L. Folkerts, C. C. Havener, I. G. Hughes, S. H. Overbury, D. M. Zehner, and P. A. Zeijlmans van Emmichoven, "Electron Spectroscopic Studies of the Neutralization of Slow Multicharged Ions During Interactions with a Metal Surface," Book of Invited Papers, XVIII ICPEAC, Aarhus, Denmark, 1993, *AIP Conf. Proc.* **295**, 741.

12. F. W. Meyer, L. Folkerts, I. G. Hughes, S. H. Overbury, D. M. Zehner, and P. A. Zeijlmans van Emmichoven, "Work-Function Dependence of Above-Surface Neutralization of Multicharged Ions," *Phys. Rev. A* **48**, 4479 (1993).

13. L. Folkerts, S. Schippers, D. M. Zehner, and F. W. Meyer, "On the Timescales for Charge Equilibration of O^{q+} $(3 \leq q \leq 8)$ Ions During Surface-Channeling Interactions with Au(110)," *Phys. Rev. Lett.* 74(12), 2204 (1995).

14. A. Niehof and W. Heiland, *Nucl. Instrum. Methods B* **48**, 306 (1990).

15. H. Winter, C. Auth, R. Schuch, and E. Beebe, *Phys. Rev. Lett.* **71**, 1939 (1994).

16. J. Burgdörfer and F. W. Meyer, *Phys. Rev. A* **47**, R20 (1993).

17. F. Aumayr, H. Kurz, D. Schneider, M. A. Briere, J. W. McDonald, C. E. Cunningham, and H. P. Winter, *Phys. Rev. Lett.* **71**, 1943 (1993).

18. C. C. Havener, M. A. Haque, A.C.H. Smith, X. Urbain, and P. A. Zeijlmans van Emmichoven, p. 43 in *AIP Conf. Proc.* **274**, *VIth International Conference on the Physics of Highly Charged Ions, Manhattan, Kansas, Sept. 28–Oct. 2, 1992*.

19. R. E. Olson, *J. Phys. B* **13**, 483 (1980).

20. J. Macek and S. Y. Ovchinnikov, *Phys. Rev. Lett.* **69**, 2357 (1992).

21. C. C. Havener, A. Müller, P. A. Zeijlmans van Emmichoven, and R. A. Phaneuf, "Low Energy Capture by C^{3+} from Hydrogen Using Merged Beams," *Physical Review A* **51**(4), 2982–88 (1995).

22. See H. B. Gilbody, *Adv. At. Mol. Phys.* **32**, 149 (1994).

23. L. Folkerts, C. C. Havener, N. Shimakura, and M. Kimura, "Low Energy Capture by N^{4+} Ions with H Atoms: Experimental Study by Using Merged Beams and Theoretical Analysis by Molecular Representation," submitted to *Physical Review A*.

24. M. S. Huq, C. C. Havener, and R. A. Phaneuf, *Phys. Rev. A* **40**, 1811 (1989).

25. N. Shimakura, M. Itoh, and M. Kimura, *Phys. Rev. A* **45**, 267 (1992).

26. B. Zygelman, D. L. Cooper, M. J. Ford, A. Dalgarno, J. Gerratt, and M. Raimondi, *Phys. Rev. A* **46**, 3846 (1992).

27. M. Pieksma, S. Y. Ovchinnikov, J. van Eck, W. B. Westerveld, and A. Niehaus, *Phys. Rev. Lett.* **73**, 46 (1994).

28. D. C. Griffin, M. S. Pindzola, and N. R. Badnell, "Low-Energy Total and Differential Cross Sections for the Electron-Impact Excitation of Si^{2+} and Ar^{6+}," *Phys. Rev. A* **47**, 2871 (1993).

29. M. S. Pindzola, N. R. Badnell, and D. C. Griffin, "Validity of the Isolated-Resonance Distorted-Wave Approximation for Dielectronic Recombination," *Phys. Rev. A* **46**, 5725 (1992).

30. N. R. Badnell, D. C. Griffin, T. W. Gorczyca, and M. S. Pindzola, "Breakdown of the Isolated-Resonance Approximation for the Electron-Impact Excitation of Positive Ions," *Phys. Rev. A* **48**, R2519 (1993).

31. D. C. Griffin, M. S. Pindzola, F. Robicheaux, T. W. Gorcyzca, and N. R. Badnell, "Nature of Interacting Resonances in Electron-Ion Excitation," *Phys. Rev. Lett.* **72**, 3491 (1994).

32. M. S. Pindzola, D. R. Schultz, and D. C. Griffin, "Quantal and Classical Differential-Scattering Calculations for the Electron-Impact Excitation of Argon Ions," *Phys. Rev. A* **48**, 4333 (1993).

33. M. S. Pindzola and N. R. Badnell, "Dielectronic Recombination Rate Coefficients for Ions of the Be and B Isonuclear Sequence," *Nucl. Fusion Suppl.* **3** (*Atomic and Plasma-Material Interaction Data for Fusion*), 101 (1992).

34. M. S. Pindzola, N. R. Badnell, and D. C. Griffin, "Dielectronic Recombination Between Hyperfine Levels of the Ground State of Bi^{82+}," *Phys. Rev. A* **45**, R7659 (1992).

35. G. Kilgus, B. Habs, D. Schwalm, A. Wolf, N. R. Badnell, and A. Müller, "High-Resolution Measurement of Dielectronic Recombination of Lithiumlike Cu^{26+}," *Phys. Rev. A* **46**, 5730 (1992).

36. W. Spies, A. Müller, J. Linkemann, A. Frank, M. Wagner, C. Kozhuharov, B. Franzke, K. Beckert, F. Bosch, H. Eickhoff, M. Jung, O. Kleper, W. König, P. H. Mokler, R. Moshammer, F. Nolden, U. Schaaf, P. Spädtke, M. Steck, P. Zimmerer, N. Grün, W. Scheid, M. S. Pindzola, and N. R. Badnell, "Dielectronic and Radiative Recombination of Lithiumlike Gold," *Phys. Rev. Lett.* **69**, 2768 (1992).

37. M. S. Pindzola and D. C. Griffin, "Electron-Impact Ionization of the Tungsten Atom," *Phys. Rev. A* **46**, 2486 (1992).

38. D. C. Griffin, M. S. Pindzola, and N. R. Badnell, "The Contribution of Double-Excitation-Autoionization to the Electron-Impact Ionization of Li^+," *J. Phys. B* **25**, L605 (1992).

39. N. Djuric, E. W. Bell, X. Q. Guo, G. H. Dunn, R. A. Phaneuf, M. E. Bannister, M. S. Pindzola, and D. C. Griffin, "Absolute Cross Sections for Electron-Impact Single Ionization of Si^+ and Si^{2+}," *Phys. Rev. A* **47**, 4786 (1993).

40. N. R. Badnell and M. S. Pindzola, "Resonance Contribution to the Electron-Impact Ionization of Few-Electron Highly Charged Ions," *Phys. Rev. A* **47**, 2937 (1993).

41. M. S. Pindzola, T. W. Gorczyca, N. R. Badnell, D. C. Griffin, M. Stenke, G. Hofmann, B. Weissbecker, K. Tinschert, E. Salzborn, A. Müller, and G. H. Dunn, "Dielectronic Capture Processes in the Electron-Impact Ionization of Sc^{2+}," *Phys. Rev. A* **49**, 933 (1994).

42. D. R. Schultz, C. O. Reinhold, R. E. Olson, and D. G. Seely, "Differential Cross Sections for State-Selective Electron Capture in 25–100 keV Proton-Helium Collisions," *Phys. Rev. A* **46**, 275 (1992).

43. D. R. Schultz, L. Meng, and R. E. Olson, "Classical Description and Calculation of Ionization in Collisions of 100 eV Electrons and Positrons with He and H_2," *J. Phys. B* **25**, 4601 (1992).

44. C. J. Lundy, R. E. Olson, D. R. Schultz, and J. P Pascale, "Coherence Parameters for Electron Capture in H^+ + He Collisions," *J. Phys. B* **27**, 935 (1994).

45. D. R. Schultz, C. O. Reinhold, R. E. Olson, "Classical Calculation of High-Energy Electron Capture in 5-MeV Proton-Hydrogen Collisions," *Phys. Rev. A* **46**, 666 (1992).

46. D. R. Schultz, S. Yu. Ovchinnikov, and S. V. Passovets, "Elastic and Related Cross Sections for Low Energy Collisions Among Hydrogen and Helium Ions, Neutrals, and Isotopes," in *Atomic and Molecular Processes in Magnetic Fusion Edge Plasmas*, Plenum, New York, 1994.

47. J. Botero, ed., *International Bulletin on Atomic and Molecular Data for Fusion*, Vol. 46, 1993.

48. D. R. Schultz, *Towards an Elastic and Momentum Transfer Cross Section Data Base for 1 to 1000 eV Collisions Involving A^{q+} + H, H_2 and He*, IAEA,Vienna, in press.

49. D. R. Schultz, *Status and Activities of the ORNL Controlled Fusion Atomic Data Center, 1992*, IAEA,Vienna, in press.

50. R. A. Phaneuf, "Critical Assessment of Atomic Collision Cross-Section Data for Fusion Plasma Applications," *Physica Scripta* **T47**, 124–27 (1993).

51. R. A. Phaneuf, "Status of Atomic and Molecular Collisional Databases," in *Atomic and Plasma-Material Interaction Processes in Controlled Thermonuclear Fusion*, ed. R. K. Janev and H. W. Drawin, Elsevier, Amsterdam, 1993.

52. C. C. Havener, "Plasma Impurity Cross Section Data Involving e-Ion, Ion-Atom, Ion-Surface, and Ion-Ion Collisions at ORNL," in *Atomic Data for Medium- and High-Z Impurities in Fusion Plasmas*, INDC(NDS)-292, proceedings of the First IAEA Research Co-ordination Meeting on Atomic Data for Medium- and High-Z Impurities in Fusion Plasmas, IAEA, Vienna, 1994.

53. C. C. Havener and D. R. Schultz, *The Oak Ridge National Laboratory Controlled Fusion Atomic Data Center: Progress Report, 1993*, INDC(NDS)-291, IAEA, Vienna, 1994.

54. R. A. Phaneuf, "Assessment of Ion-Atom Collision Data for Magnetic Fusion Plasma Edge Modelling," *Nucl. Fusion Suppl.* **2** (*Atomic and Plasma-Material Interaction Data for Fusion*), 75 (1992).

55. R. A. Phaneuf, R. K. Janev, H. Tawara, M. Kimura, P. S. Krstic, G. Peach, and M. A. Mazing, "Status and Critical Assessment of the Database for Collisions of Be^{q+} and B^{q+} Ions with H, H_2 and He," *Nucl. Fusion Suppl.* **3** (*Atomic and Plasma-Material Interaction Data for Fusion*), 105 (1992).

56. R. K. Janev, R. A. Phaneuf, H. Tawara, and T. Shirai, "Recommended Cross Sections for State-Selective Electron Capture in Collisions of C^{6+} and O^{8+} Ions with Atomic Hydrogen," *Atomic Data and Nuclear Data Tables* **55**, 201–32 (1993).

57. F. DeMarco and S. E. Segre, *Plasma Phys.* **14**, 245 (1972).

58. C. H. Ma, D. P. Hutchinson, and K. L. Vander Sluis, *Rev. Sci. Instrum.* **59**, 1629 (1988).

59. T. Luke and J. H. Irby, *Bull. Am. Phys. Soc.* **38**, 1955 (1993).

60. C. H. Ma, D. P. Hutchinson, and J. Irby, "Calibration of an Infrared Polarimeter for Alcator C-Mod," in *Seventeenth International Conference on Infrared and Millimeter Waves*, ed. Richard J. Temkin, Proc. SPIE 1929, 368–69 (1992).

61. R. J. King, *J. Sci. Instrum.* **43**, 617 (1966).

62. J. Sheffield, *Plasma Scattering of Electromagnetic Radiation*, Academic Press, New York, 1975.

63. V. G. Zhukovsky and V. A. Rtischev, *ITER Diagnostics by IR-Scattering*, IAE-5322/8, I. V. Kurchatov Institute of Atomic Energy, Moscow, 1991.

64. D. P. Hutchinson, K. L. Vander Sluis, J. Sheffield, and D. J. Sigmar, *Rev. Sci. Instrum.* **56**, 1075 (1985).

65. R. K. Richards, C. A. Bennett, K. L. Fletcher, H. T. Hunter, and D. P. Hutchinson, *Rev. Sci. Instrum.* **59**, 1556 (1988).

66. R. K. Richards, D. P. Hutchinson, C. A. Bennett, H. T. Hunter, and C. H. Ma, *Appl. Phys. Lett.* **62**, 28 (1993).

67. D. R. Suhre, M. J. Pechersky, J. F. Lowry, and J. F. Roach, *J. Appl. Phys.* **65**, 28 (1989).

68. Personal communication, Ken Young, Princeton Plasma Physics Laboratory (1993).

3

FUSION THEORY AND COMPUTING

D. B. Batchelor

S. E. Attenberger[1]
L. A. Berry
B. A. Carreras
M. D. Carter
L. A Charlton[1]
K. R. Chen[2]
J. W. Cobb[2]
P. H. Diamond[3]
N. Dominguez
R. A. Dory
D. T. Fehling
R. H. Fowler[1]
L. García[4]
C. E. Gibson
C. A. Giles[1]
R. C. Goldfinger[1]
D. E. Greenwood
R. D. Hazeltine[5]
C. L. Hedrick
S. P. Hirshman
J. T. Hogan
J. A. Holmes[1]
W. A. Houlberg
E. F. Jaeger
K. L. Kannan[1]
J.-N. Leboeuf
D. K. Lee[1]
V. E. Lynch[1]
J. F. Lyon[6]
D. E. Newman
D. R. Overbey
L. W. Owen[1]
J. A. Rome
K. C. Shaing
K. L. Sidikman[2]
D. A. Spong
N. A. Uckan
C. Y. Wang[2]

1. Computing and Telecommunications Services.
2. Oak Ridge Associated Universities, Oak Ridge, Tennessee.
3. University of California at San Diego, La Jolla.
4. Universidad Complutense, Facultad de Ciencias Fisicas, Madrid, Spain.
5. University of Texas, Austin.
6. Toroidal Confinement Section.

3. FUSION THEORY AND COMPUTING

Summary of Activities

During the report period, theoretical activity coalesced substantially into three primary areas: turbulence and transport (primarily for tokamaks), rf heating and current drive, and plasma edge and modeling. This condensation was in reaction to two main factors: the repeated terminating of the Advanced Toroidal Facility stellarator program, and the combination of declining budget and rising cost. This coalescence has made it possible to continue to contribute technical advances at the forefront of fusion theory, within this restricted scope of activities.

A close interaction continues with Oak Ridge National Laboratory experimenters and technologists as they apply their skills and devices throughout the world fusion program through collaborations on experiments elsewhere. The Fusion Theory and Computing group has been active in the programs at the DIII-D, Tokamak Fusion Test Reactor, Joint European Tokamak, Tore Supra, and W7-AS facilities as well as those at many smaller installations, such as the Texas Experimental Tokamak, Torus Experiment for Technology Oriented Research, and Compact Helical System facilities. This combination of technology, experimental physics, and plasma theory ensures that the theoretical activity is aligned with the primary fusion programs and has adequate opportunity for validation on data from experimental devices.

3.1 TURBULENCE AND TRANSPORT

Three broad yet focused areas have been defined in which significant accomplishments have been realized over the past three years. These areas cover improved toroidal confinement regimes, advanced toroidal confinement scenarios, and high-performance computing. These accomplishments have been achieved through a synergistic combination of analytical and computational work, augmented by advanced computing, to obtain results in real time from these increasingly detailed models of plasma behavior. As a result, participation in national theory initiatives, Transport Task Force working groups, and ITER expert groups in each of these areas aimed at resolving critical physics issues for TPX and ITER has been initiated and/or broadened.

3.1.1 Improved Toroidal Confinement Regimes

3.1.1.1 Interaction of flows and fluctuations

There are several theoretical models for the L-H transition based on sheared electric field effects on turbulence. All of these models are based on the enhanced eddy decorrelation induced

by the shear electric field with the consequent turbulence and transport suppression. After the causal relation between the radial electric field and the L-H transition was first suggested, more detailed models followed. These models suggest a two-step process: (1) at a certain level of injected power in a tokamak, the edge particle losses create or modify the radial electric field, and (2) this electric field is then responsible for the reduction of the fluctuation level and transport. However, because it has been shown that turbulence can modify the profile of average flows through Reynolds stress, the electric field profile and turbulence must be calculated self-consistently.

Resistive pressure gradient turbulence is a good paradigm for studying the self-consistent coupling of turbulence and poloidal sheared flows. Resistive pressure-gradient turbulence causes a modification of the average poloidal flow profile through Reynolds stress. The poloidal flow profile modification can be induced through a diamagnetic term or a "seed flow." This leads to several results for the steady-state poloidal flow profile. If this profile is such that $V''_0 \neq 0$ at the singular surface, there is a reduction in linear growth rate and suppression of the fluctuations. When $V''_0 = 0$ and $V'_0 \neq 0$, there is linear stabilization, but the fluctuation suppression is weak. The resistive pressure-gradient–driven turbulence is not independent of the initial conditions. A systematic study based on 400 nonlinear single-helicity calculations with random initial perturbations shows that multiple nonlinear states exist at saturation. They are characterized by different poloidal wave-number values for the dominant mode in the spectrum. As a consequence, the saturated states have different levels of fluctuations and different self-consistent poloidal flow profiles. The presence of an external shear poloidal flow does not always directly change the saturation level of the fluctuations. For low-sheared flows, the probability of accessing the high saturation levels can increase. For very high flow-shear values, however, fluctuations are suppressed. A curvature poloidal flow reduces the saturation level of each state and increases the probability of accessing the low fluctuation levels. Transitions between saturated states accompanied by sudden changes in flow profile have been observed. Most of the observed transitions are from a low to a high level of fluctuations.[1]

Plasma experiments entering the "high-confinement," or H-mode, regime undergo both a decrease in fluctuation level and an increase in electric field shear at the edge. We have tried to understand the improved confinement by studying the relationship between these effects. Our turbulence model is based on long-wavelength drift waves. A fixed electric field shear, dE_r/dr, is added to their evolution through a sheared poloidal $E \times B$ rotation. We developed the nonlinear, 3-D initial-value dissipative trapped electron mode (DTEM) code for this problem. Over the past 2 years, numerical results from DTEM have provided important insights into the behavior of electrostatic turbulence and its response to electric field shear. In these calculations, the algorithm used for purely-growing modes in the Finite Aspect Ratio (FAR) code was applied to modes with a diamagnetic rotation. For characteristic plasma parameters, the rotation rate is 10 times the growth rate. The sheared poloidal rotation introduces another fast time scale and a short spatial scale. These new scales complicate the numerical calculation. We documented the performance of the DTEM code under these conditions and prepared a paper demonstrating that the algorithm calculates linear growth rates correctly in the presence of large rotation velocities. Convergence criteria for nonlinear calculations are suggested and carefully tested. Error accumulation measurements are used to gauge the accuracy of the solutions. As a result, we have outlined the proper operation of this useful numerical tool.[2]

Calculations with the DTEM code have shown that a fixed electric field shear does not reduce the steady-state fluctuation level. Linearly, the electric field shear enhances damping by increasing the rate at which energy propagates away from a rational magnetic surface to a dissipation region. However, if the turbulence level is large enough, nonlinear wave couplings can trap long-wavelength modes on the rational surface. Since these modes no longer propagate, their

nonlinear damping is insensitive to electric field shear. These results led us to consider a fixed electric field curvature, d^2E_r/dr^2. Its effect on linear damping is analogous to that of shear, with a sign dependence, but the curvature does something more. Positive curvature increases the real frequency of the wave; negative curvature decreases it. As before, wave couplings prevent the electric field curvature from affecting the nonlinear damping, but the change in the real frequency survives. An increase in frequency can feed back through the drive to reduce the growth rate and saturation level. Calculations with the DTEM code have confirmed this effect. Thus, in the nonlinear regime, most relevant to experimental observations, electric field curvature is more effective than electric field shear in reducing the fluctuation level.[3] An electric field self-consistently generated from the fluctuations should be more effective than a fixed field in regulating fluctuation growth. Since the nonlinear trapping increases with fluctuation level, the damping effects of curvature may persist if they are increased as well. We have tried to calculate this case with the DTEM code, but the fluctuations generate a field with both stabilizing and destabilizing curvature within the same eigenfunction. The use of this model has been discontinued, and the self-consistent fluctuation and flow system is now being studied with more appropriate models.

3.1.1.2 Phase-transition model of the L-H transition

With the insight gained from the studies of interaction of flows with fluctuations, a self-consistent model of the L-H transition has been derived from two coupled nonlinear envelope equations for the fluctuation level and radial electric field shear.[4] These equations exhibit a pitchfork bifurcation between dual L-mode and H-mode fixed points. They show that the L-H transition has characteristics similar to a second-order phase transition for which the order parameter is the radial electric field shear. The power threshold is determined by the requirement that the energy input rate, in absence of radial electric field gradient, exceed the poloidal flow damping that results from magnetic pumping. This criterion imposes a condition on the relevant edge gradient. Transition occurs because of a modulational instability of the L-mode fixed point. This instability is similar to a dynamo instability and amplifies the shear in the poloidal velocity and the radial electric field gradient. The instability saturates when sufficient fluctuation energy is coupled to the sheared flow to control the fluctuation amplitude through the poloidal flow-damping rather than the energy input rate. This model intimately links the power threshold for the transition to edge gradients, coupled flow and fluctuation evolution, divergence of the transition time as power input reaches the power threshold, and hysteresis. The bifurcation is of the pitchfork variety. The sign of the symmetry-breaking electric field gradient seed is probably determined by orbit loss.

The phase-transition model of the L-H transition has been used to make definite predictions for the power threshold, the transition time, the front velocity, and the effect of external torque on threshold. The power threshold scales unfavorably with density and favorably with ion mass. The dependence on TF is induced through the temperature dependence.

The basic phase-transition model for L-H transitions describes the evolution of the fluctuation energy and the poloidal velocity shear. The model is radially local and assumes modest sheared E_r in order to allow approximation of the $E \times B$ sheared flow from the poloidal sheared flow. The basic model is

$$\frac{1}{2}\frac{dE}{dt} = \gamma_0 E - \alpha_1 E - \alpha_2 U^2 E \,, \tag{1}$$

$$\frac{dU}{dt} = -\mu U + \alpha_3 U E \,, \tag{2}$$

with $E=|\tilde{n}_k/n_0|^2$ the fluctuation energy, $U=\langle V'_E\rangle$ the flow shear, and t_{ext} the external torque. The coefficients g_0, a_1, a_2, m, and a_3 are dependent on the specific fluctuation model and are examined in Refs. 1 and 2. It was shown that the dynamics of the system depended on only two parameters: $a=\alpha_3/\alpha_1$ and $b=\mu/\gamma_0$, where $a/b=1$ is the threshold for the transition. For values of $a/b<1$, all of the free energy goes into the fluctuations and no sheared flow is generated. When the parameter above the threshold value is increased, the instability saturates first at the L-mode level, and then there is a smooth transition to H-mode with generation of flow.

Several modifications to the simple phase-transition model for the L-H transition have been made and have successfully captured many of the experimentally observed characteristic dynamics. First, a number of experiments have attempted, with varying success, to influence the L-H transition through an external mechanism to force flow shear. To describe this type of experiment theoretically, an external torque is included in the phase-transition model for the L-H transition. These equations exhibit a bifurcation between an L-mode fixed point and an H-mode fixed point with variation of a critical parameter, corresponding to the edge gradient, across a threshold value. With the addition of the external torque (from a biased limiter, probe, or rf wave) the character of the transition changes in a manner analogous to the addition of an external magnetic field to a ferro-magnetic material. In addition to the change in the transition dynamics, there is a marked decrease in the threshold level. In this simple model, the decreased threshold is proportional to the torque applied to the 2/3 power, in approximate functional agreement with that seen by some experiments.

A more complete self-consistent model of the L-H transition is derived from coupled nonlinear envelope equations for the fluctuation level and radial electric field shear E'_r as determined by ion pressure gradient ∇P_i and poloidal flow. These equations extend the applicability of the phase-transition model of the L-H bifurcation by including ∇P_i effects. In this model, the transition occurs when the turbulence drive is large enough to overcome the damping of the total $E\times B$ flow. Near the critical power for transition, poloidal flow shear dominates E'_r, but at high power ∇P_i provides the main contribution. The inclusion of ∇P_i also introduces a quenched fluctuation state that is accessible at high power and may be the experimentally observed H-mode state for $P\gg P_{crit}$. In this state, the radial electric field is determined only by ∇P_i because no fluctuation energy is available to produce a turbulent Reynolds stress.

3.1.1.3 Validation of phase-transition model of the L-H transition by nonlinear plasma turbulence calculations

The basic properties of the phase-transition model are reproduced well by nonlinear single-helicity calculations for several instabilities. For the drift thermal instability, nonlinear calculations show that the basic nonlinear behavior between fluctuations and poloidal velocity shear oscillates in time and can be explained by a Volterra model. The phase-transition model does indeed reduce to a pure Volterra model without an L-mode state in this case, with the threshold between H- and L-mode fluctuation levels predicted to be zero.[5] In the case of resistive interchange modes, the control parameter used in the nonlinear calculations is the viscosity in the evolution equation for the flux-surface–averaged poloidal velocity. The calculations show that above the threshold, determined by the balance between the resistive interchange drive and the poloidal flow damping, a transition occurs, with sheared flow increasing and the fluctuation level falling. Below the threshold, no sheared flow develops, and the fluctuation level remains constant. A transition to a zero–fluctuation-level solution is observed in these nonlinear calculations under the conditions predicted by the phase-transition model for such a state to exist.

Detailed numerical studies of bifurcations and modulation interaction have also been carried out in the case of negative compressibility turbulence with sheared perpendicular (i.e.,

poloidal) flow. The turbulence model is based on the parallel ion flow gradient instability, a representative paradigm for ion drift waves. Studies of coupled turbulence and mean flow evolution indicate the existence of two distinct nonlinear states. In the first state, saturation occurs via nonlinear transfer to damped high-k modes, and sheared flow is heavily damped. In the second state, the turbulence level is controlled by the self-consistently generated sheared flow. An example of fluctuation suppression by average poloidal sheared flow is shown in Fig. 3.1.

Transition between these states is determined by the competition between instability growth and damping of rotation. The dynamics of the observed transition are well described and consistent with the two coupled envelope equations of the model of the L-H transition, modulational interaction between small-scale turbulence and large-scale $m \neq 0$ sheared flows is observed as well.[6]

3.1.1.4 Core fluctuations

Effect of rf-induced shear flow on turbulence

At the beginning of calendar year 1994, a collaborative effort was begun with the rf theory group to investigate the effect of rf-induced sheared flow on turbulence. As ICRF waves propagate inward from the plasma edge, they couple to IBWs at the ion-ion hybrid resonance. The Bernstein waves generate a Reynolds stress in the plasma fluid that drives a radially-sheared poloidal flow near the resonance. According to scaling theory,[7] this shear should suppress surrounding turbulence. The collaboration was set up to investigate this suppression and its dependence on the input ICRF power using calculations of wave propagation and flow generation and plasma response.

The calculated poloidal flow varies in radius on two different scales, with a fast radial variation within a slowly decaying envelope. The fast scale is the Bernstein wavelength $l^B = 2p/k_x^B$, where k_x^B is the radial wave number, while the longer envelope scale L_e is set by the wave-damping mechanism. Instead of scaling theory, which is not self-consistent, linear theory is used to investigate the effect of this profile on the instability growth rate. Two different plasma instabilities were considered: driftlike DTEMs and resistive pressure-gradient-driven modes. In the DTEM case, a two-scale analytic theory was used to predict the marginal stability point as a function of L_e/r_s and $k_x^B r_s$, where r_s is the ion gyroradius. Although the results agreed very well with numerical calculations, they were only applicable for $k_x^B r_s > 1$, where the model begins to break down. No reliable results could be obtained from the DTEM model in the physically realistic regime $k_x^B r_s \approx 1$. A reduction in the growth rate was observed for $k_x^B r_s \approx 1$ using modes driven by resistive pressure gradient, but marginal stability was not obtained.[8]

Despite the difficulties, an important conclusion was reached in each case. Considered individually, shear on the L_e scale is more efficient than shear on the l^B scale in reducing the instability growth rate. However, when both scales are included, the fast variation significantly enhances the reduction produced by the envelope scale, even when l^B is on the order of the mode width. Using a reasonable value of L_e to calculate the shear, it was estimated that the fast-wave antenna power available on current experiments should be sufficient to produce some reduction in the level of fluctuations.

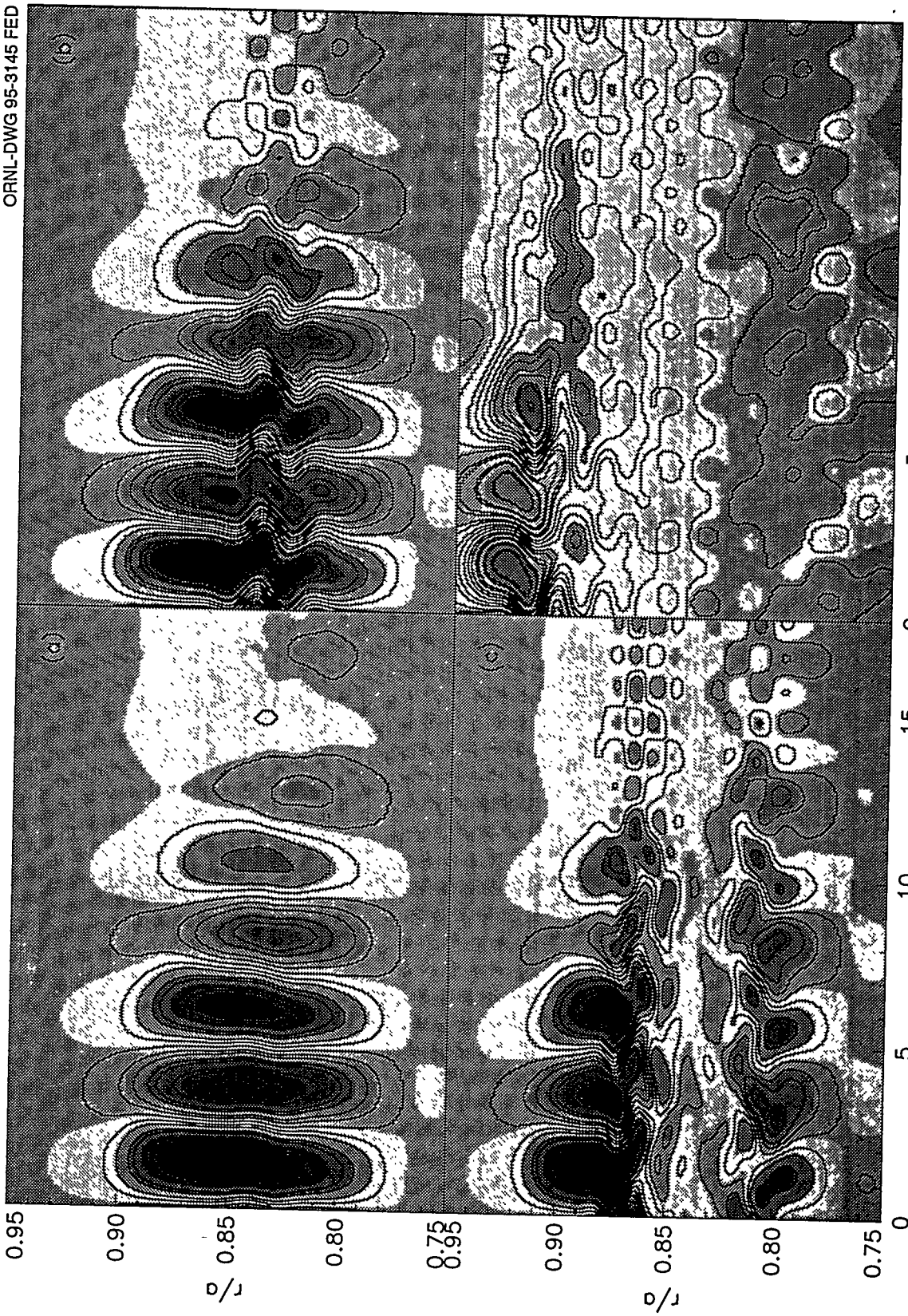

Fig. 3.1. Fluctuation suppression by average poloidal shear flow in the case of negative compressibility turbulence.

Dynamics of electrostatic turbulence in simple trapped particle models

From extensive simulations of simple local fluid models of long-wavelength drift-wave turbulence in tokamaks, a reasonably complete picture of the basic properties of spectral transfer and saturation is emerging. These studies indicate that many conventional notions about directions of cascades, locality and isotropy of transfer, frequencies of fluctuations, and stationariness of saturation are not valid for moderate to long wavelengths ($k\rho_s \leq 1$). In particular, spectral energy transfer at long wavelengths is dominated by the $E \times B$ nonlinearity, which carries energy to short scale (even in two dimensions) in a highly nonlocal and anisotropic manner. In marked contrast to the canonical self-similar cascade dynamics of Kolmogorov, energy is efficiently passed between modes separated by the entire spectrum range in a correlation time. At short wavelengths, transfer is dominated by the polarization drift nonlinearity. While the standard dual cascade applies in this subrange, it is found that finite spectrum size can produce cascades that are reverse-directed (i.e., energy to high k) and nonconservative in enstrophy and energy similarity ranges (but conservative overall). In regions where both nonlinearities are important, cross-coupling between the nonlinearities gives rise to large nonlinear frequency shifts as well as changes in the spectral dynamics. This profoundly affects the dynamics of saturation by modifying the growth rate and nonlinear transfer rates. These modifications produce a nonstationary saturated state with large amplitude and long period relaxation oscillations in energy, spectrum shape, and transport rates. Methods of observing these effects and their ramifications have been devised based on the results of these extensive simulations.[9]

Gyro-Landau fluid model of DTEM turbulence

A new physics tool has been developed for the study of turbulence and transport in the core of a tokamak, one of the major objectives of the Numerical Tokamak High-Performance Computing Center (HPCC) Grand Challenge Project. We have been aiming at two goals: (1) adding realistic kinetic effects into a drift-wave model while retaining the computational advantages of the fluid approach and (2) creating a numerical implementation that runs efficiently in the type of multiprocessing environment needed for high-performance computing. Good progress has been made on both fronts.

Fluid equations with finite Larmor radius (FLR) corrections have been derived from moments of the gyrokinetic equation. Choosing closure relations with complex coefficients causes the phase relationships between the variables to change in a way that leads to dissipation. When the coefficients are properly chosen, the linear damping rate corresponds quite closely to the exact kinetic result.[10] The coefficients we have calculated introduce both parallel (Landau) and perpendicular (ion magnetic drift) resonant damping. This gyro-Landau fluid model has been tested against the kinetic model using a shooting code to solve the radial eigenvalue problem. Excellent agreement has been obtained for both eigenvalues and eigenfunctions. The initial-value drift-wave code DTEM has been adapted to solve the new equations. Linear results from the modified DTEM code are also in excellent agreement with the shooting code and kinetic model results.

Highly resolved, low-dissipation, nonlinear calculations of DTEM turbulence have been performed in dedicated mode on the CRAY Y-MP C90 at NERSC as part of the Special Parallel Processing (SPP) allocation program. The details of the turbulent dynamics produced by these calculations, which are the largest we have ever attempted and hence have produced an enormous amount of data, are currently being analyzed. The modified DTEM code runs very efficiently on the multiprocessor C90 at NERSC. At peak performance, the code delivered 5 gigaflops while occupying all 200 megawords of available memory and using an average of 14.5 of the 16

processors. Production runs were equally efficient. While using the C90 in dedicated mode during the SPP program, our processor use was in the top four, and the code occupied 5 times as much memory as most users.

3.1.1.5 Edge fluctuations

Radiation-driven turbulence at the plasma edge in toroidal devices

Recent experimental results in TJ-1 and TEXT are shedding new light on the possible mechanisms responsible for edge turbulence. Measurements in the edge plasma (in contrast to the SOL) of TJ-1 and TEXT indicate that there is a definite phase difference close to p between density and temperature fluctuations. There are also indications that temperature fluctuations are comparable to density fluctuations in the edge plasma, at least on TJ-1. Furthermore, detailed bolometric measurements in TEXT show a mild dependence of the radiated power on electron temperature.

These experimental results have prompted reexamination of the radiation drives for plasma edge parameters. By including the electron density gradient in our impurity radiation-driven drift-wave model, it is found that the radiation power itself, rather than its derivative with respect to equilibrium electron temperature, can be strongly destabilizing through coupling to density fluctuations even in a parameter regime away from force balance. Linear and nonlinear calculations with this model show many features that compare well with the experimental results at the edge of TEXT and TJ-1. These include the opposite phase between density and temperature fluctuations, temperature fluctuations on the order of the density fluctuations, and saturation levels that do not keep increasing with radiated power. One consequence of the opposite phase between density and temperature fluctuations is that the outward energy flux is effectively reduced because the particle flux is outward while the heat flux is inward. The experimental consequence is that the fluxes should be very sensitive to temperature corrections in the edge plasma. This is also true for the interpretation of Langmuir probe data.[11]

3.1.2 Advanced Toroidal Confinement Scenarios

3.1.2.1 Energetic particles confinement

Shear Alfvén waves with Landau and collisional effects

Shear Alfvén waves can be driven unstable by hot particles, such as alpha particles in an ignited fusion device or hot ions in existing devices. Motivated by rather collisional W7-AS beam-driven global Alfvén instability experiments, we have examined the effect of electron and ion collisions on these modes. Collisions broaden and suppress the peak associated with Landau effects. This broadening makes ion damping more important, while the electron damping is suppressed. Additional resistive effects provide increased damping for the main part of the spectrum, which can have a rather high phase velocity. Of more general interest is the fact that collisional and collisionless resistivity has a numerically stabilizing effect that is known to be important for nonlinear resistive MHD. This can preclude the need for introducing, and testing the sensitivity to, similar ad-hoc effects. Numerical and analytic results for both a particle-conserving Krook collision operator and a Lorentz (pitch-angle) collision operator have also been compared.

Gyrofluid model of TAE/GAE instabilities in tokamaks

The gyrofluid model has proven to be a versatile tool for examining the stability of energetic particle-excited shear Alfvén instabilities in tokamaks. It has been applied extensively to beam-driven toroidal Alfvén eigenmode (TAE) instabilities in TFTR and DIII-D, alpha-driven TAEs in the D-T phase of TFTR and ITER, and studies of TAE nonlinear saturation mechanisms. It is the only existing model that simultaneously includes a nonperturbative approach, the full global mode structure, continuum damping, ion/electron Landau damping, and ion FLR and can be applied nonlinearly. In addition, because the MHD spectrum is automatically included, a variety of modes can be identified, and the fastest-growing one filtered out. The latter feature has been especially useful in noting the transition from TAE to global Alfvén eigenmode (GAE) instabilities in both TFTR and ITER when the central q profile is made sufficiently flat. Profiles generated by the Princeton TRANSP transport modeling code have been incorporated into the gyrofluid code for studies of the D-T phase of TFTR. A number of possible scenarios for enhancing the observation of alpha-driven TAE modes during the D-T operation of TFTR have been identified, including: lowering the ion temperature (decreases ion Landau damping), raising the ion density (increases $v_{fast}/v_{Alfvén}$ and improves resonance coupling), and raising the central q (aligns the gap structure more closely with the instability drive). These possibilities are currently being tested experimentally on TFTR.

Our studies of GAE modes in low-shear stellarators have motivated us to search for them in the low-shear central regions of tokamaks. When the central q profiles are sufficiently flat, we have identified GAE modes in both TFTR and ITER engineering design activity (EDA) configurations, which have low thresholds and very similar characteristics to those found in W7-AS. When similar studies are carried out for ATF, the GAE mode is generally absent because of the higher magnetic shear, but the TAE instability is present.

The gyrofluid model has also been used to study the nonlinear evolution and saturation of the TAE. Its particular strength here is in the treatment of mode-coupling effects. These effects typically require good resolution and a large number of poloidal and toroidal Fourier harmonics, which are difficult to include in other approaches, such as analytical and particle-based models. Typical linear and nonlinear saturated TAE mode structure from calculations with TFTR-like parameters are shown in Fig. 3.2. Within the gyrofluid model, two nonlinear saturation mechanisms appear to be viable. They are generation of sheared velocity flows and localized current generation, which modify the q profile. The production and effects of sheared velocity flows on the TAE and GAE modes can have implications for the external control of these modes as well as L-H transition physics in ignited tokamaks.[12]

Gyrofluid model of GAE instabilities in Wendelstein W7-AS

In W7-AS, it was observed that very global instabilities with frequencies in the range of the poloidal Alfvén frequency and rotation in the ion diamagnetic direction could be driven by the neutral injection beams in certain regimes. These modes have generally been seen at lower-temperature operation and with weak magnetic shear. The gyrofluid model has played a key role in identifying these as GAE modes with positive helicity (positive toroidal and poloidal mode numbers). Both linear and nonlinear studies of the beam-driven GAE instabilities observed in W7-AS have been carried out in close collaboration with A. Weller of the W7-AS experimental group. The linear calculations have generally agreed with the observed dominant mode numbers for a range of iota profiles. Also, the observed stability threshold reasonably agrees with theory. The suppression of the mode in the normal W7-AS operational regime appears to be the result of electron Landau damping and increased magnetic shear. The nonlinear studies also show good

ORNL-DWG 95-3146 FED

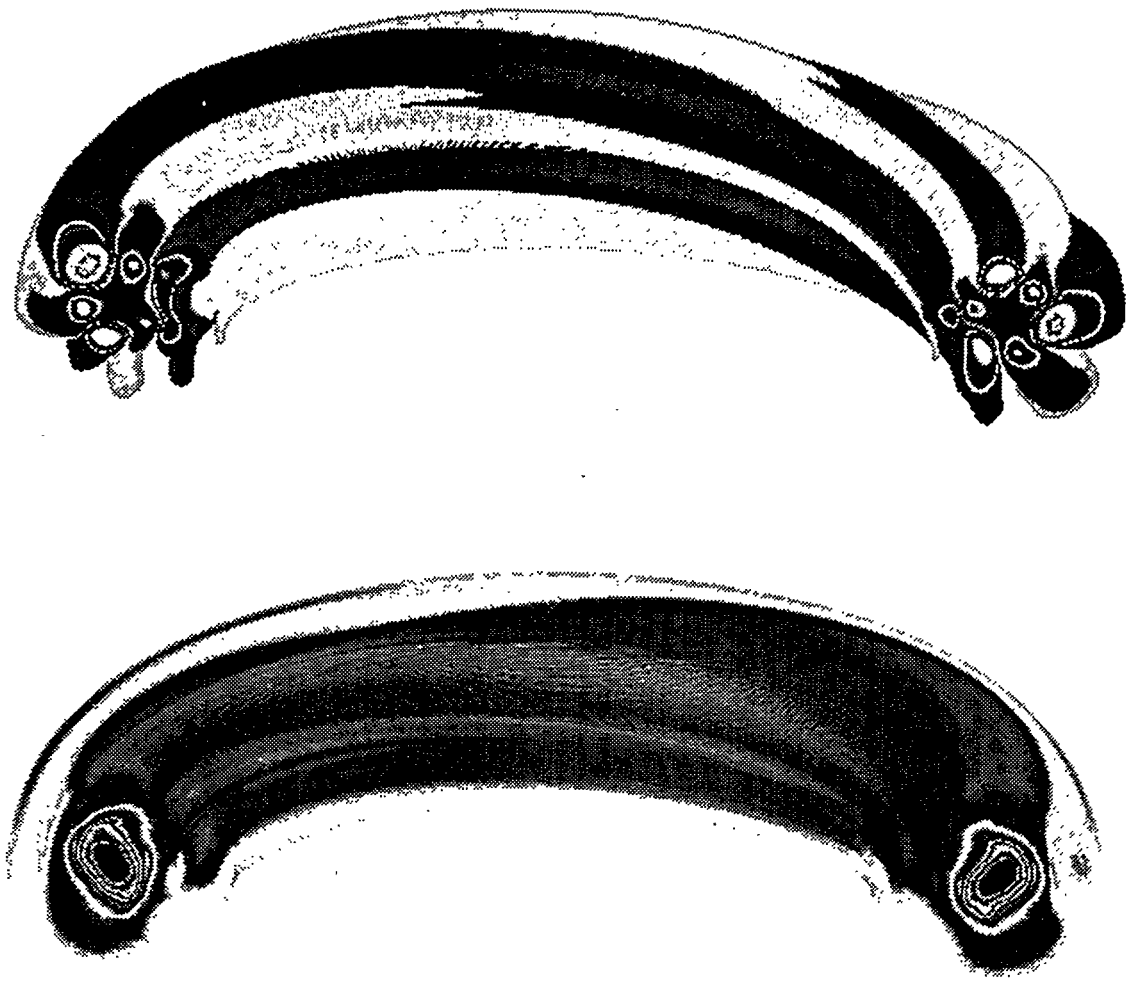

Fig. 3.2. Scientific visualization of linear (top) and saturated nonlinear (bottom) TAE mode structure obtained from toroidal gyrofluid calculations with TFTR-like parameters.

agreement with respect to the observed narrow frequency and mode spectrum and the measured magnitude of the edge magnetic fluctuations. In addition, reconstructed 2-D ECE contours of the mode structure obtained from the experiment compare well with the mode structure in the theoretical model.[13]

Preliminary calculations of pressure-driven ballooning instabilities in W7-AS have been carried out using the stellarator-averaged MHD code CHAFAR. The mode has been identified, and convergence studies are proceeding. Work has also begun on adapting the gyrofluid model of energetic particle-excited shear Alfvén instabilities to CHAFAR.

Hybrid particle fluid techniques for energetic particle instabilities

The hybrid particle alphas-fluid background plasma model developed in collaboration with MIT and applicable to 2-D slab geometry has been extended to include the evolution of the density profile of the alphas and magnetic shear. When the alpha density profile is frozen, the alpha-

driven Alfvén wave instability saturates as a result of particle velocity space diffusion, which steepens the velocity gradient of the resonant alphas. When the alpha density profile is allowed to evolve, the mode couplings arising from the $E \times B$ convection of the resonant alphas are the dominant saturation mechanism for the alpha-driven Alfvén wave instabilities. The ensuing alpha density profile in the saturated state indicates an effective displacement of the alpha particles from the core but does not necessarily indicate loss of alpha particles from the system.[14]

Fusion-produced fast-ion dynamics in magnetized plasmas

Particle-in-cell (PIC) simulation is used to study the dynamics of fusion-produced 3.5-MeV alpha particles that result from self-driven high-harmonic cyclotron waves in the LH frequency range. The waves grow according to theoretical predictions of a relativistic mass variation effect. The instability is absolute because the growth rate is larger than required for absolute instability. Some high-harmonic alpha results are similar to low-harmonic proton results, but others are quite different. The interaction becomes selective. Only those alphas with large perpendicular velocity (and/or pitch angle) are involved in the energy spreading, while there is no effect for those with small pitch angle. Large density perturbations and perpendicular energy spreading are still observed, but the average energy loss is smaller, with half of the energy being carried by thermal (not tail) deuterons. Implications for rf control of this mechanism, weakening or suppression of TAE modes, increased gyroradius of first-orbit–loss alphas (which may provide a diagnostic for this mechanism) and the need for external LH waves to tap the energy of the alpha particles are currently under investigation.[15]

3.1.2.2 MHD for advanced tokamak configurations

Standard computational linear and nonlinear MHD techniques, which have been adequate in the past to describe low-b, moderately shaped, large–aspect-ratio tokamaks, are being improved for and adapted to the more demanding TPX, ITER, and very small–aspect-ratio configurations of current interest. Collaborations with the Keldish Institute and Moscow University have been initiated, and several applicable equilibrium and linear stability codes have been obtained. The Keldish suite of codes (FRESCO and CAXE for free- and fixed-boundary equilibria, respectively, and KINX for ideal stability) is being evaluated through application to spherical torus configurations. Results obtained so far are very encouraging in that the Keldish codes can adequately describe configurations with an ultra-low aspect ratio of 1. The Moscow University equilibrium codes are well suited to the MHD stability code, FAR. Preliminary work to couple these codes to FAR has begun. At the same time, higher-order time-integration schemes for nonlinear MHD calculations are being investigated to increase their numerical stability and accuracy. A first application of the more robust nonlinear tools will be to a study of the effect of toroidal flow shear on MHD instabilities in DIII-D.

3.1.3 High-Performance Computing

3.1.3.1 Parallel plasma fluid turbulence calculations

Parallel implementation of a fluid turbulence model applicable to the collisional plasma edge, as incorporated in the KITE code, and a gyro-Landau fluid model more suitable to the hotter plasma core, as incorporated in the DTEM code, is being pursued on the CRAY Y-MP C90,[16] on the Intel family of mainframes (Intel iPSC/860, Delta, Paragon XPS/5 and XPS/35),[17] and on clusters of workstations (DEC Alphas and IBM RS6000s). This is being done not only to

improve the real-time efficiency of these calculations, thereby decreasing the wall-clock time for production calculations, but also to have access to more memory. These two elements permit inclusion of more realistic physics by evolving more plasma moments and/or using more complicated evolution equations for these moments. They also allow problem sizes and resolutions to be increased significantly, and therefore more experimentally relevant calculations can be performed. Last, but not least, parallel implementation of fluid turbulence models anticipates the next generation of production supercomputers, which are expected to be massively parallel.

While different sets of equations are solved as an initial-value problem in KITE and DTEM, both codes are spectral in the sense that a finite difference grid is used in the radial direction, and a Fourier mode expansion is adopted in the poloidal (short way around the torus) and toroidal (long way around the torus) directions. Other features common to both codes include the implicit treatment of the linear terms, requiring a block-tridiagonal matrix inversion, and the explicit treatment of the nonlinear terms, involving the (analytical) calculation of mode convolutions. The matrix operations and mode convolutions are the most time-consuming parts of the calculations, and much effort has therefore been put into their efficient parallelization. Among these parallel implementations, the greatest physics gains have been realized on the C90, where core turbulence calculations using DTEM have been performed in dedicated multiple–central-processing-unit mode and at the 200-megaword memory limit as part of the SPP allocation program. The highest aggregate speed and overlap has been achieved with DTEM during short tests in dedicated mode, namely 5 gigaflops sustained with 14.5 processors accessed simultaneously.

The KITE plasma turbulence code optimization studies on the existing Intels have continued, in preparation for the fully configured Intel Paragon with 2048 processors. Tests on the ORNL Intel Paragon XPS-5 with 66 processors have shown a 20% speedup over the Intel iPSC/860, primarily because of faster communication between nodes. Benchmarks on the Intel Paragon XPS-35 with 128 processors and 32 megabytes (MB) of memory per processor have shown 50% faster performance than the iPSC/860 for the same number of modes in the calculation. Accessing more than 128 processors on the XPS/35 has proven to be a problem because of input and output difficulties.

The massively parallel version of the KITE code developed for the Intels has also been modified to run under the parallel virtual machine (PVM) utility on a cluster of high-performance IBM RS6000 and DEC Alpha workstations. The Intel message-passing calls were simply replaced by PVM calls. The advantage of this distributed, scalar parallel environment is that the memory per node is large (from 64 to 128 MB per node) and that larger calculations may thus be possible than on the Intels where the memory per node (8 to 32 MB) is severely limiting. Efficiency has been severely limited because the communication between nodes in the cluster can only occur at ethernet speed. Communication speed cannot be improved until optical connections between the clustered workstations are established.

3.1.3.2 Scientific visualization

Scientific visualization techniques are becoming useful tools for analyzing the enormous amount of data produced by large-scale, nonlinear computer calculations. Standard packages such as PVWAVE and AVS have been incorporated in a suite of postprocessing modules. Animations of TAE nonlinear evolution have been produced using Advanced Visual Systems (AVS). Volume and surface visualization methods (with magnetic field lines) for TAE and GAE instabilities have also been developed within AVS. Some of these diagnostic calculations have in fact been found to be quite computationally intensive and better performed in a distributed manner, whereby the most computationally demanding parts of the calculations are performed on the CRAYs at

NERSC, while the more routine rendering is carried out locally on high-performance workstations.[18]

3.2 EDGE PHYSICS AND PLASMA MODELING

3.2.1 Edge Physics

3.2.1.1 Reduced-impurity-flow modeling of the scrape-off plasma

To determine the profiles of the radiation losses in the edge of a tokamak plasma, it is necessary to compute the distribution of impurities over their charge states. This distribution is affected by both the spatial diffusion along the magnetic field lines and atomic processes (impact ionization and charge exchange). An accurate description of parallel impurity transport in the short mean free path regime has been developed and includes both atomic and Coulomb collision processes. The relative impurity flows and heat fluxes are determined by generalized momentum equations. New terms (arising from atomic processes) that strongly affect the heat fluxes in the cold, dense edge plasma are retained. For high-Z impurities, a Fokker-Planck equation in charge space ($Z \gg 1$) is derived to replace the individual charge-state continuity equations. The moment method and the standard multiple-continuity equation approach are compared for representative edge conditions. The reduced charge-state model has been implemented in the computer code module FMOMBAL.

3.2.1.2 Active divertor model

A simple model for the divertor has been developed and implemented in the new 1-D computer code DTRANS. This model includes dynamic evolution of density, momentum, and energy and qualitatively describes the main properties of the divertor The particle and energy fluxes are given from the tokamak core and are taken to be boundary conditions for the model. However, they are assumed to be time dependent and to incorporate large oscillations to simulate the effect of ELMs. The injection of neutrals, the pumping rate, the injection of low-Z impurities, and particle edge diffusivity through fluctuations are used to control the divertor. The temperature and density of the plasma at the divertor plate and the neutral and impurity fluxes to the plasma are monitored. A control system based on these controls and the allowable range of the monitored quantities is being set up to optimize divertor performance and avoid "accidents" (damage to divertor plates and contamination of the main plasma).

3.2.1.3 Influence of limiters and divertors on edge turbulence

The 3-D, nonlinear, slab-geometry computer code SOL is being used to study the effect of open magnetic field lines on the stability and turbulence properties of modes driven by resistive pressure gradient. A finite difference representation is used in all three spatial dimensions, which makes boundary conditions other than periodic along and across magnetic field lines easier to incorporate than in standard turbulence models, which are spectral in the toroidal and poloidal angle. A simple two-field model for resistive pressure-gradient instabilities has been implemented in SOL, in which evolution equations for the plasma vorticity and plasma density are advanced in time using the alternative direction implicit (ADI) technique. Results from SOL agree well with those from an equivalent spectral code when the field lines are closed for all radial points. Tests in the presence of a region of field lines that are line-tied because of the presence of conducting

plates in their path are currently proceeding. The model will subsequently be applied to a study of ELMs in DIII-D.

3.2.2 Plasma Modeling

3.2.2.1 L-H bifurcation theory

Several refinements and novel applications of the L-H bifurcation theory based on the nonlinearity of the parallel (poloidal) plasma viscosity have been carried out over the past 3 years.

The relation between ion orbit loss and plasma viscosity was demonstrated by considering the effects of incompressible flow in the phase space described by the orbit-averaged Coulomb operator. This result provides a solid foundation for the theory that poloidal rotation in the edge region is driven by ion orbit loss. The rate of the ion orbit loss was also estimated for tokamak plasmas and was shown to be significant when the ion collisionality is low.[19]

The effects of shock on the L-H transition was studied. This work was motivated by the prediction of an L-H transition bifurcation theory based on the nonlinear ion viscosity. According to this theory, the $E \times B$ rotation speed has to be on the order of poloidal sonic speed in the H-mode. Under that condition, there is a possibility for a shock at poloidal Mach number $M_p = 1$. It was found that shock formation does not prevent bifurcation. A byproduct of this research is the finding that shock formation may be related to formation of multifaced asymmetric radiation from the edge of a tokamak.

When the poloidal ion diamagnetic flow is of the order of the $E \times B$ velocity, it significantly affects shock formation in a poloidally rotating tokamak plasma. The poloidal density variation in both linear and shock regimes can be weakened if the poloidal ion diamagnetic flow tends to cancel the poloidal $E \times B$ flow. The magnitude of the density variation is not symmetric with respect to the direction of the $E \times B$ poloidal rotation. The resonant condition at which strong shock occurs is also modified dramatically by the diamagnetic flow. For some cases, the poloidal density variation inside the bifurcated electric field layer in the L-H transition may not be large enough to modify significantly the plasma viscosity obtained by neglecting the compressibility effects.[20]

Convective momentum transport associated with the convective nonlinearity in the momentum equation is calculated for arbitrary values of the poloidal $E \times B$ Mach number M_p. The physics origin of the convective momentum transport is associated with the coupling of the poloidal variation of the viscosity-driven flux to that of the flow velocity in the magnetic surface. When the radial gradient scale length of the plasma velocity is on the order of the ion poloidal gyroradius, the convective momentum transport becomes comparable to the ion viscosity. At poloidal Mach numbers of order 1, the ion viscosity associated with shock (the shock viscosity) approximately balances the convective momentum transport to maintain the lowest-order ambipolarity. An extended L-H bifurcation theory that includes the effects of shock and convective momentum transport has been developed. It has been shown that the experimentally relevant plasma viscosity, effective plasma viscosity, is very similar to that obtained without including compressibility effects, even if shocks exist.

Parallel viscous force is one of the essential forces governing the poloidal momentum of the plasma. In a dynamic system, the time-dependent contribution of the viscosity can actually be more important than the direct time derivative of momentum itself in the force balance equation. The time-dependent ion parallel viscous force in the banana regime with arbitrary inverse aspect ratio e is calculated using the eigenfunction approach. The flux surface averaged viscosity is then used to study the poloidal rotation relaxation process, which leads to oscillatory relaxation

behavior. The relaxation rate ν_p is found to be approximately proportional to n_{ii}/e, where n_{ii} is the ion collision frequency.

Parallel plasma viscosity is also useful in understanding the L-H transition phenomenon observed in tokamaks. Parallel viscosity in the banana regime in a poloidally ($E \times B$) rotating plasma is calculated to include the effects of orbit squeezing and to allow the poloidal $E \times B$ Mach number M_p to have a value of order unity. The effects of orbit squeezing not only modify the size of the particle orbit, but also change the fraction of poloidally trapped particles. Resonance between the particle parallel (to B) speed u and the poloidal component of the $E \times B$ velocity can only occur for those particles with energy $(v/v_t)^2 > M_p^2$ (where v is the particle speed and v_t is the thermal speed). Thus, the resonance parallel plasma viscosity in the banana regime decreases exponentially with M_p^2 when $M_p^2 \geq 1$, and it has a local maximum of $M_p^2 \approx 1$.

The tokamak L-H transition theory can be tested in stellarators in a controlled manner by using the two or more local maxima in poloidal viscosity in these devices. Depending on the relative magnitudes of the toroidal and helical components of the magnetic field spectrum, the local maxima, and this transition, can occur either at a critical poloidal $E \times B$ Mach number M_p of the order of unity, similar to that of a tokamak, or at an M_p of the order $(m - nq)/m$, similar to that of a helically symmetric torus. Thus, by performing the L-H transition experiment on either a stellarator with an adjustable magnetic field spectrum or on several stellarators with different magnetic field spectra, we can further test the underlying tokamak L-H transition dynamics in stellarators.[21]

The mechanism for confinement improvement in the toroidal-rotation–induced VH-mode may be the turbulence suppression that results from the shear of the toroidal angular frequency associated with parallel flow. This explanation contrasts with the plausible hypothesis that H-mode confinement improvement may be caused by the turbulence suppression that results from the shear of the poloidal angular frequency associated with the $E \times B$ and parallel flows. Because it is the shear of the toroidal angular frequency, which, based on experimental observations in DIII-D, is important for the VH-mode confinement, a model toroidal momentum equation has been derived to describe the behavior of dV_t/dr, with V_t the toroidal flow velocity, in the regime where the VH-mode confinement is important. It is found that dV_t/dr can change rapidly and bifurcate, depending on the ratio of the neoclassical to the anomalous viscosity coefficient, if the toroidal momentum input is large enough.[22]

3.2.2.2 Advanced tokamaks

General expressions have been derived for the bootstrap current, ion thermal conductivity, and plasma flows that are valid for arbitrary aspect ratio, collisionality, and shaping, which can be used for interpretation of experimental data (DIII-D) and in modeling TPX and ITER. The evolution of highly shaped DIII-D plasmas has been modeled with the WHIST transport code to help interpret the role of the current profile near the axis in achieving improved confinement. In these cases the noninductive beam and bootstrap current source contributions were shown to allow access to the second-stability regime and enhanced confinement. Algorithms and models have been developed for the evaluation of current profile control through combinations of fast-wave, NB, and LH sources and have been applied to TPX and advanced tokamak reactor studies.[23] In addition, the concept of "isotopic tailoring" (separate control of the spatial variation of deuterium and tritium profiles through combination of pellet and neutral gas fueling) has been proposed and shown to be a viable means of reducing the in-vessel tritium inventory in ITER.[24]

A theory for the alpha-particle–driven bootstrap current was also developed. It was found that for low Z_{eff} (<2), the contribution of the alpha-particle bootstrap current is small and in the opposite direction from the main plasma bootstrap current.

3.2.2.3 Equilibrium reconstruction of the *q* profile in tokamaks

The MSE diagnostic has been used to obtain accurate measurements of the internal magnetic pitch angle tan-1 (*Bz/BT*) in finite-pressure tokamaks. The MSE data and external magnetic probe data are used to reconstruct self-consistently the equilibrium safety factor (*q*) profile and, hence, the plasma current density, in TFTR and PBX-M. An efficient computational scheme, based on the inverse coordinate representation of the magnetic field used in the 3-D equilibrium code VMEC, has been developed to solve the coupled nonlinear equations describing both the MHD equilibrium and the *q* profile, which best match all the experimental data.[25]

3.2.2.4 Confinement scaling in stellarators

The question of energy confinement scaling in stellarators remains of interest because of the observed similarity to tokamak confinement and because of some important differences. The gross scaling and magnitudes of losses are about as expected from either Bohm-like scaling or the gyro-reduced Bohm scaling from turbulence with radial scale lengths smaller than the plasma dimensions. This is similar to tokamaks in L-mode, although it is fairly widely believed that tokamaks favor the Bohm end of the scale, while stellarator experiments favor the gyro-reduced limit.

Development of a joint database[26] with data from the W7-AS experiment at the Max Planck Institute in Garching allowed some further definition of the scaling and indicates that net toroidal plasma current is probably an important factor in the physics of anomalous energy loss: the lower current discharges favor gyro-Bohm scaling, while inclusion of higher net toroidal current cases tilts the balance toward the less-desirable Bohm scaling. In first analyses of bulk (not spatially resolved) confinement data, it was found that confinement results in ATF and W7-AS were quite similar to each other, to similar L-mode tokamak data, and to results from Japanese experiments on Heliotron-E and CHS. One area in which similarity was not apparent pertained to the question of dependence upon the rotational transformation. This is not surprising, considering that the various machines have different geometrical properties and different transformation profiles: W7-AS has negligible shear, while the ratio of edge to central transformation value for ATF is 3:1.

3.2.2.5 New theoretical methods: wavelet analysis

Wavelet analysis is a generalization of Fourier analysis and an amalgam with the finite element method; therefore it has the potential to combine some of the advantages of both, while not simultaneously acquiring a disproportionate number of new problems. The method is analogous to an expansion in *orthogonal* wave packets in quantum mechanics and has clear benefits for study of aperiodic or intermittent phenomena such as turbulence. To that end, it has been tested on data from the PBX-M tokamak at the PPPL and has been found to have a strong chance of providing the necessary pattern recognition capability required to begin serious attempts at feedback control of phenomena such as ELMs, sawteeth, and disruptions.

3.3 RF HEATING AND CURRENT DRIVE

Radio frequency power in various frequency regimes is a key element in the U.S. fusion program. In TFTR, rf power is used to heat electrons and ions, stabilize sawtooth activity, and control energetic particle distributions for investigations of particle interactions and TAE instabilities. In the DIII-D tokamak experiment, rf is essential to development of advanced tokamak

regimes through control of pressure and current profiles. Because rf heating is essential to non-inductive current profile control in TPX, it also plays a major role in the future magnetic fusion program, and it is a leading method for heating to ignition for ITER.

Several major issues in our understanding of physics and several needs for theoretical predictive capability must be resolved for rf to fulfill its promise. These include the following:

1. Current drive efficiency, control of driven current profile, and avoidance of parasitic rf power absorption must be maximized. Full-wave models in one dimension, two dimensions, and three dimensions increase our understanding of parasitic absorption processes and possible new current-drive schemes such as mode conversion.
2. The complex interactions between the antenna and the edge plasma, the design for survivability, and the minimization of impurity generation and power loss must be better understood. Recently developed 2-D and 3-D antenna models have helped us understanding wave coupling and interactions between edge and rf in recent and ongoing experiments on DIII-D, Tore Supra, and JET.
3. The use of rf to produce enhanced confinement modes, such as H- and VH-modes, needs to be further explored, and rf systems need to be made compatible with enhanced modes.

Each of these issues requires new developments in the basic theory of rf propagation, absorption, and wave-particle interaction. Each of these issues also requires realistic computational models. In recent years, ORNL has developed sophisticated 2-D and 3-D models for wave launching and propagation in tokamak geometry. These models continue to be developed through incorporation of the latest theoretical advances, and they continue to be validated by detailed comparison with experiment.

The following have been the areas of primary emphasis in rf heating and current-drive theory over the past year:

1. Full-wave modeling of ICRF heating and current drive to understand and make best use of the D-T experiments with rf on TFTR and DIII-D.
2. Development of ICRF antenna analysis tools to study effective rf advanced tokamak scenarios for TPX and ITER and to provide design data for the antenna and rf systems for these devices.
3. Basic rf physics issues related to advanced rf current-drive techniques (such as mode-conversion current drive), coupling of power to parasitic modes at the plasma surface, and generation of plasma flows by rf power, which can affect edge turbulence and access to advanced confinement modes.

Highlights in these areas include close collaborations with experimenters on TFTR to analyze data from the first ICRF heating experiments in D-T; bringing the 3-D antenna modeling code (RANT3D) into operation, with its careful and very successful benchmarking against experimental data on TFTR; and completion and application of the minority-ion sawtooth model in the plasma transport code (TRANSP).

3.3.1 Full-Wave Modeling of ICRF Heating and Current Drive

3.3.1.1 Full-wave ICRF modeling of D-T plasmas in TFTR

Future fusion devices, such as ITER, emphasize ICRF heating and current drive. Tritium second harmonic cyclotron resonance ($2W_T$) is the proposed heating scenario in ITER operation, but until now, no experimental data have been available. TFTR has performed the first experiments on ICRF heating of D-T plasmas that show significant ion heating in the $2W_T$ regime.[27,28]

An increasing emphasis is being placed on control of the plasma current profile in order to access the advanced tokamak operating regime in future devices, such as TPX. Mode conversion to IBW has been proposed for the profile control, and, in particular, off-axis heating and current drive. The efficient mode-conversion scheme recently proposed[29] has been demonstrated for the first time in TFTR in ^{3}He-^{4}He plasmas.[30] Benchmarking of the rf computer codes (which are needed for designing future devices) with these experimental data has been facilitated by rf power modulation.

During the report period, a major effort was devoted to analyzing data from the first ICRF heating experiments in D-T plasmas on TFTR. Collaboration with TFTR experimenters Murakami, Taylor, Darrow, Majeski, and Rogers produced excellent comparisons between the results from the ORNL global wave propagation code (PICES) and measurements on D-T super-shot plasmas with ICRF heating power. These results (which were reported at several international fusion meetings) show radially resolved heat deposition profiles that agree closely with the profiles calculated by PICES. Likewise the observed power split between electrons and ions, as a function of tritium beam power, agrees with the PICES calculations.

Previous modeling calculations of direct electron heating by fast waves on TFTR[31] were extended to include the experimental configuration for D-T operation (i.e., $f = 43$ MHz with tritium fractions between 10% and 50% of the electron density). The presence of tritium allows "parasitic" ion absorption at the tritium second harmonic resonance, which competes with direct electron heating caused by Landau damping and magnetic pumping. At $B \approx 3.8$ T, this situation is similar to the 60-MHz fast-wave current-drive scenario in ITER,[32] where 30% of the rf power is absorbed by tritium. At higher fields $B \approx 4.5$ T, this situation is further complicated by the presence of the two-ion hybrid resonance layer at the extreme inboard edge of the plasma (high-field side). As the tritium fraction increases, this layer moves toward the magnetic axis, and a large fraction of the fast-wave power can be mode-converted to the IBW and subsequently absorbed by electrons in a narrow region near the plasma edge. By producing a broader current density profile than is usually produced with fast-wave current drive, this mode-converted power may be useful in current-drive applications.

3.3.1.2 Full-wave ICRF modeling of electron heating and current drive by mode-converted slow waves in tokamaks

Both 1-D and 2-D full-wave codes have been used to study possible mode-conversion and/or shear Alfvén heating scenarios in DIII-D and the associated off-axis current drive that is expected to occur in these cases. These calculations suggest possible experiments at 30 MHz with large fractions (i.e., 20%) of helium in deuterium plasmas. Based on this modeling, it has been decided to try these experiments at General Atomics.

Mode-converted slow waves in tokamak plasmas may provide an efficient means of direct electron heating and current drive.[29] One advantage over direct Landau damping of the incident fast wave is that the mode-conversion layer is quite narrow and therefore allows easy profile control for both the heat deposition and driven-current profiles. The balance between these two competing mechanisms for electron heating has been studied in ICRF experiments on TFTR with D-T-^{3}He and D-T plasmas. Numerical results have been calculated for deuterium-hydrogen operation in DIII-D geometry with $f = 30$ MHz and $B = 2.0$ T using both the 2-D reduced-order full-wave code, PICES, and the 1-D sixth-order single-pass scattering code, FAST1D. As the hydrogen concentration is increased from 5% to 50%, the separation between the hydrogen fundamental cyclotron resonance layer $\left(\omega = \Omega_{c,H}\right)$ and the mode-conversion layer $\left(n_\parallel^2 = S\right)$ increases. At the same time, there is a transition from simple minority ion heating at $\omega = \Omega_{c,H}$ for low fractions of hydrogen to significant mode-conversion heating at $n_\parallel^2 = S$ for high fractions.

One interesting characteristic of the 2-D result is that off-axis ion heating occurs near the intersection of the mode-conversion and resonant surfaces.

3.3.1.3 Fast-wave current-drive modeling using the combined RANT3D and PICES code

Fast-wave current-drive efficiency in tokamaks is critically dependent on the shape of the launched power spectrum. Recently, it has been noticed that 3-D rather than 2-D antenna models are needed to describe accurately the power spectrum launched by phased antenna arrays in present tokamaks. Therefore, to obtain the most accurate possible estimate of the driven current in these experiments, the RANT3D antenna modeling code[33] has been coupled with the PICES full-wave propagation and absorption code.[32] Detailed comparisons are being made with radially resolved current measurements from the DIII-D experiment. In these comparisons, equilibrium parameters such as plasma pressure, rotational transform, electron and ion densities, and temperatures are fit as accurately as possible to experimental values.

3.3.1.4 Full wave modeling of ICRF heating in stellarators

A major initiative during this report period has involved establishing a collaboration with Japanese fusion scientists on ICRF heating of stellarators and tokamaks. The immediate objective has been to provide guidance for, and analyze data from, the ICRF heating experiments on CHS in April 1995. In the longer term these tools will be used to analyze rf systems for LHD. The first part of this U.S.-Japanese exchange was completed in March 1994 with a visit by T. Seki to Oak Ridge, during which all Oak Ridge full-wave ICRF heating codes (PICES, ORION, and FAST1D) were ported to Japanese computers and subsequently set up to analyze Japanese ICRF heating experiments on CHS, LHD, JIPT-2U, and JT-60. This transfer involved major changes in the mathematical and graphics libraries used by these codes. At present, all of the codes and graphics programs are fully operational in Nagoya, Japan.

3.3.1.5 Full-wave modeling of power deposition in high-density inductively coupled plasma tools for semiconductor processing

Inductively coupled plasma sources, while an old concept, have found recent application in today's semiconductor industry. The high plasma density of these sources relative to parallel plate sources (10^{17-18} m^{-3} vs 10^{14-17} m^{-3}) provides a better platform for meeting future processing needs, such as ever-decreasing feature size.[34] In addition to higher densities, which allow higher flux and process rates, the new sources provide (1) lower neutral gas pressure, to reduce collisions and increase ion anisotropy; (2) lower plasma potential, to control ion bombardment energies; and (3) independent control of plasma heating power and sheath voltage (i.e., ion energy).

A computationally efficient 2-D numerical model has been developed to study power deposition in high-density inductively coupled plasma sources. Calculations include both inductive coupling, caused by plasma response to external coil currents, and capacitive coupling, caused by plasma response to external voltages on the coils and wafer. Variation in current along the induction coil is determined self-consistently from the integral constraint of charge conservation. Sheath phenomena are incorporated through previously published analytic models. The system behavior is analogous in some respects to that of a transmission line. Comparison with measurement suggests that this model provides a good description of self-consistent coil response when the electric field exhibits less than a quarter wavelength per coil turn.

3.3.1.6 Orbit-consistent plasma simulations

A kinetic plasma simulation approach has been developed and tested. A particle trajectory integrator is loosely coupled to a general (i.e., unspecified) electromagnetic field (EMF) solution algorithm. The EMF can be adjusted on each step of the trajectory integration (conventional PIC simulations) or can be held fixed for the entire trajectory integration (test particle solver) or any case in between. The solutions are self-consistent for time scales longer than the EMF-solver time scale, but details of the particle orbits are resolved for the shorter trajectory integration time scale. Simulations can be conducted that are consistent with the particle orbits but orders of magnitude less expensive than conventional PIC simulations. A specific implementation is targeted toward modeling of an rf plasma source used for semiconductor manufacturing. Orbit integration and cold plasma fluid responses have been tested.

3.3.1.7 One-dimensional global and local solution for ICRF heating

The Global and Local One-Dimensional Solution for ICRF heating (GLOSI) has been developed to solve 1-D wave equations that result from using rf waves to heat plasmas. The code uses a finite difference method. Because of its numerical stability, the code can be used to find both *global* and *local* solutions, given appropriate boundary conditions. Three types of boundary conditions are introduced to describe wave scattering, antenna wave excitation, and fixed tangential-wave magnetic field. The scattering boundary conditions are especially useful for local solutions. The antenna wave excitation boundary conditions can be used to excite fast and slow waves in a plasma. The tangential magnetic field boundary conditions are used to calculate impedance matrixes that describe plasma and antenna coupling and can be used by an antenna code to calculate antenna loading. These three types of boundary conditions can also be combined to describe various physical situations in rf plasma heating. The code also includes plasma thermal effects and calculates collisionless power absorption and kinetic energy flux. The plasma current density is approximated by a second-order Larmor radius expansion, which results in a sixth-order ordinary differential equation (ODE).

3.3.1.8 Effect of Alfvén resonance in low-frequency ITER current drive

The effect of the Alfvén resonance has been studied in low-frequency ITER current-drive scenarios using the GLOSI 1-D full-wave code. It has been found that in some cases, resonance on the low-field side can lead to mode conversion to a short-wavelength, slow wave, which can be absorbed by electrons at the plasma edge. In such cases, there is a significant parasitic power loss before the fast wave propagates into the core of the plasma.

3.3.2 ICRF Antenna Studies

The 3-D antenna modeling code, RANT3D, has evolved to a production level and is now used extensively for both 2-D and 3-D modeling. The code has been extended to permit multiple-nested recesses, thereby permitting antennas with several different septa heights to be explored. Current elements can now be specified inside arbitrary recesses, and the phase velocity effects of the strap current can be included. A simple model for the Faraday screen reduces the radial electric field caused by charge on the current strap without eliminating the parallel component of the electric field everywhere. Diagnostics have been added to provide fields in real space near the antenna and for the entire tokamak surface. Other diagnostics permit power conservation tests and calculate both loading and reactive power. The user interface to the code has been improved to

increase efficiency and accuracy in specifying complex antenna geometries. Improved visualization techniques have been incorporated to analyze the massive quantity of data obtained.

Through close work with the rf technology group, a methodology has been developed for providing an essentially complete analysis of antenna performance (including loading and spectrum radiated into plasma) in terms of practical quantities (voltage and currents in the transmission line). The methodology combines results from RANT3D for coupling to the plasma with technology codes and circuit models for strap current distribution and Faraday shield transparency.

3.3.2.1 Three-dimensional physics of ICRF launchers for fusion devices

The methodology described above has been used in a systematic and successful comparison of ten shots in TFTR using RANT3D, PLASMAIMP, density profile data from the reflectometer on TFTR, detailed magnetostatic modeling, and circuit analysis. A multilaboratory, multidisciplinary paper reporting these results has been submitted to *Nuclear Fusion*.[33]

The 3-D nature of antennas for fusion applications in ICRF requires accurate modeling in the design and analysis of new antennas. In this work, analysis and design tools for rf antennas are successfully benchmarked with experiment, and the 3-D physics of the launched waves is explored. The systematic analysis combines measured density profiles from a reflectometer system, transmission-line circuit modeling, detailed 3-D magnetostatics modeling, and a new 3-D electromagnetic antenna model that includes plasma. The results of this analysis agree very well with measured loading data from the TFTR Bay-M antenna, thus demonstrating the validity of the analysis for the design of new rf antennas. The 3-D modeling is contrasted with 2-D models, and significant deficiencies are found in the latter. The 2-D models are in error by as much as a factor of 2 in real and reactive loading, even after they are corrected for the most obvious 3-D effects. Three-dimensional effects play the most significant role at low parallel wave numbers, where the launched power spectrum can be much different from the predictions of 2-D models. For many rf designs, especially those for fast-wave current drive, 3-D effects should not be ignored.

3.3.2.2 Phased array antennas for fast-wave current drive and heating

TPX antenna design choices for six-strap and eight-strap designs with numerous phase combinations have been explored using RANT3D in both two and three dimensions. A radical reassessment of the ITER antenna concept is also now under way. RANT3D is being used as a key analytical tool for this process.

Sustained current-drive and auxiliary heating using ICRF power are essential to the operation of tokamaks, including TPX and ITER. The key issues include achieving adequate power density, controlling energy and momentum deposition profiles, providing flexibility to trade-off heating and current drive, and avoiding excessive gas or impurity production in the edge region. These issues are strongly affected by the launched power spectrum, which can be controlled by phasing the antenna array. Determination of the appropriate phasing depends upon plasma edge density gradients, return currents in the antenna structure, and the plasma modes that propagate in the edge region. A concerted effort to match experimental tests with theoretical modeling has led to a greatly improved understanding of these antennas. Proper inclusion of both return currents and poloidal asymmetries caused by plasma gradients requires 3-D modeling. Properly model the shear Alfvén wave when $\omega < \omega_{ci}$ requires parallel currents and electric fields. Recent advances using the RANT3D and PLASMAIMP codes permit realistic 3-D modeling of phased array antennas. Application of these codes has shown good agreement with loading data from TFTR

using measured density profiles, whereas earlier 2-D models did not scale properly. Implications for TPX, ITER, and C-Mod antenna designs have been studied.

3.3.2.3 Three-dimensional modeling of rf current-drive arrays

Three-dimensional modeling is necessary for a complete understanding of the rf power spectrum launched by fast-wave current-drive arrays. Return currents in the antenna sidewalls and septa are not properly handled by 2-D models. Results from the RANT3D code for the TPX 12-strap array have been studied. These results indicate that the present design produces a good spectrum, but the phase velocity of the launched waves cannot be significantly increased without degradation of the spectrum by 3-D effects. Extensions to RANT3D to handle septa with different heights have been considered. Comparisons are made with experimental vacuum measurements using RANT3D and the measured rf input (MRFI) code, which calculates the launched power spectrum using measured magnetic fields on a poloidal-toroidal plane. The MRFI code is especially useful for analyzing complex launching structures such as the folded waveguide for current-drive applications in ITER. Both the RANT3D and MRFI codes are written in the object-oriented FORTRAN 90 language.

3.3.3 Basic Rf Physics Issues

3.3.3.1 Fast-wave poloidal flow generation in a plasma

Fast-wave poloidal flow generation at the plasma edge of a tokamak has been studied with a 1-D slab model. Because of strong minority ion power absorption at the minority ion cyclotron resonance, the poloidal flow can be generated by a spatial change of plasma velocity and current-density profiles in the absence of mode conversion. The electromagnetic force plays a more important role than the plasma Reynolds stress in flow generation. In the presence of mode conversion, the flow is mainly generated by interference between the long-wavelength transmitted fast wave and the short-wavelength IBW from mode conversion. Flow shear generated in the presence of mode conversion varies spatially with a scale length similar to the IBW wavelength. With mode conversion, the plasma Reynolds stress becomes more important than the electromagnetic force in flow shear generation. For both cases, the plasma Reynolds stress and the electromagnetic force are out of phase so that the resultant flow shear is smaller than the larger of the two. The short scale-length flow shear enhances the turbulence stabilization.

3.3.3.2 Parallel forces induced by waves in ICRF

A new mechanism has been identified for rf-wave–induced force and current drive caused by a kinetic flux carried by coherent oscillations of plasma particles. The force induced along a magnetic field line by rf heating of plasmas has been calculated with a 1-D slab model and found to be contributed by the plasma power absorption and spatial inhomogeneity. The inhomogeneity term consists of a kinetic flux and a flux related to rf-wave helicity injection rate. The effect from the kinetic flux occurs only in warm plasmas, whereas, in contrast, the helicity-related flux effect occurs even in cold plasmas. The forces have been calculated for both electrons and ions in ICRF, and the effects from the ion cyclotron and the second harmonic resonance have been included.

3.3.3.3 Spurious modes for finite Larmor radius models in ICRF

Spurious resonances exist in the dispersion relations for finite Larmor radius models in ICRF plasma heating. The spurious resonances occur when the highest-order coefficient in a fourth-order equation vanishes. It has been shown that the spurious resonances cannot be removed by using a sixth-order equation because the highest-order coefficient in the sixth-order equation also vanishes at the same location as the highest-order coefficient in the fourth-order equation. However, the spurious modes are often not excited when the corresponding ODEs are solved for an incident fast wave, so the solutions from the ODEs are often accurate.

3.3.3.4 Numerical solution of a tunneling equation

A numerical method has been used to solve mode-conversion equations that result from using rf waves to heat plasmas. The solutions of the mode-conversion equations contain exponentially growing modes, and ordinary numerical techniques give large errors. To avoid the unphysical growing modes, a set of boundary conditions has been found that eliminates the unphysical modes. The mode-conversion equations are then solved with the boundary conditions as a standard two-point boundary value problem. A tunneling equation (one of the mode-conversion equations without power absorption) is solved as a specific example of this numerical technique although the technique itself is very general and can easily be applied to any mode-conversion equation. The results from our numerical calculation agree very well with asymptotic analysis results.

3.3.3.5 Minority ion sawtooth model in TRANSP

The collaboration with PPPL on rf heating continues. The major accomplishment for the report period has been completion and installation of the minority-ion sawtooth model in the TRANSP code. This project involved developing the modification to the minority distribution function in the Fokker-Planck package and then implementing these changes in TRANSP. The sawtooth effect for the minority species must be included in modeling of the electron reheating rate, power deposition profiles, and fast-ion slowdown times. The new module was applied immediately throughout the fusion community. Work on data analysis with the PPPL team and on solving some computational problems in the use of the code with the TRANSP developers continued.

3.3.3.6 Rf/kinetic studies and its application on helium ash control

The behavior of fusion-produced alphas (helium ash) that result from collective instabilities and the implications for their confinement are critically important issues in the performance of burning-fusion reactors such as TFTR and ITER and in burning-plasma physics. The super-thermal cyclotron emissions observed in some tokamaks may be a good diagnostic for exploring these issues. We have investigated a cyclotron instability that may provide a mechanism for anomalous alpha slowdown and energy-broadening. The same mechanism also explains the ion cyclotron emissions observed in JET. PIC simulation has been used to study the dynamics of fusion-produced 3.5 MeV alpha particles caused by self-driven high-harmonic cyclotron waves in the LH frequency range. According to theoretical predictions of a relativistic mass variation effect, the waves grow with an absolute instability. Depending on density gradient, the large alpha density perturbation may reduce the drive for TAE and MHD instabilities, while the pitch-angle change of alphas may affect particle transport. Because the interaction results from

cyclotron waves, rf injection at ion cyclotron wave frequency range may provide a method of controlling the process. Discussions of this work have been invited at the 1994 International Sherwood Fusion Theory Conference[35] and at the TFTR physics meeting of PPPL on February 6, 1995.

We have also been asked to help in operating TFTR and in efforts to understand its physical processes in the areas of: (1) the possible inclusion of the gyrobroadening mechanism in TRANSP calculations for understanding the alpha dynamics in TFTR's D-T operation, (2) the experimental measurements of the alpha gyrobroadening effect predicted by the mechanism, and (3) the mechanism(s) of the fast-ion–driven cyclotron emissions observed in the edge of TFTR. These activities are in support of ITER R&D high-priority task 5.4, "Helium ash control." Both theoretic and experimental efforts on the important burning-plasma issues would be helpful in the design and operation of ITER.

3.4 COMPUTING AND OPERATIONS

Computing in the Fusion Energy Division (FED) can be roughly divided into five categories: the User Service Center (USC), workstations support, experimental data acquisition, networks, and PC support. The present climate of restricted funding has placed a considerable premium on developing methods that require minimum staffing levels to provide support in all areas.

3.4.1 USC

The USC operates with only partial operator coverage during the normal work day. The USC has begun using DEC ALPHA computers running on the VMS operating system in place of the current DEC VAX computers. The helical-scan tape drives are used for regular backups of system and user disk information. Data backup is now automated and carried out regularly by the VAXes themselves, which facilitates backups on weekends or holidays and has resulted in overtime cost savings. Also, the use of helicon-scan tape units for archiving experimental data has reduced the cost and space required for storage. The write-only optical-disk jukebox continues to used for archival storage of ATF data. When fully loaded, the jukebox will provide direct access to 200 gigabytes (GB) of compressed data. It can mount an optical disk and make data available within 45 s of a request for any platter.

3.4.2 Workstation Support

Computing on UNIX workstations has increased significantly in the last 2 years. Four IBM workstations have been added to the computing environment. As a result, more than 3 times as much memory is now available (an increase from 192 MB to 640 MB), and almost 4 times the amount of disk storage is now available (an increase from 5 GB to 19.5 GB) across the IBM platforms. Currently, there are ~45 active UNIX users in addition to guests who use the workstations during short-term assignments.

One of the UNIX IBM machines serves as a central repository of more than 45 public domain programs. Notable examples are T_eX, Mosaic, Gopher, PLPLOT, and emacs. In addition, eight licensed products (AVS, Island Graphics, Mathematica, MatLab, NAG, NCAR Graphics, PV Wave, and tecPlot) are available. Much of this software is based on the X-Windows™ interface. Not only are these "X" applications easy to use, but many provide Internet access. Extensive

use of TCP/IP facilitates collaboration on projects at Princeton, in Germany and Japan, and elsewhere. Along with these benefits has come the need for heightened awareness of and attention to security issues and potential vulnerabilities to break-ins from a worldwide user community.

The UNIX file server also offers centralized storage of user files and data. This organization will eventually make the backup procedure easier and more timely. A newer-technology tape drive capable of compressing a maximum of 10 GB of data per cartridge will facilitate this task. This dual-purpose device also contains a compact disk (CD)–read-only memory (ROM) drive to read CD-ROM distribution media.

Printer management has become a priority. With the increased availability of reliable UNIX software to support graphics and desktop publishing, newer and faster Postscript printers are being added to the network. A black-and-white Postscript printer is accessible from not only the UNIX workstations but also the VAX computers and PCs. A color Postscript printer to serve all three platforms will be installed soon.

The friendliness of the UNIX X-Windows applications has increased the popularity of X terminals. Several NCD terminals have been added to the FED network to satisfy this demand.

3.4.3 Networks

The ORNL divisions (Biology, Engineering Technology, Instrumentation and Controls, and Fusion Energy) located at the Y-12 Plant have installed a fiber-distributed data interface (FDDI) network. These division are linked via the FDDI backbone. The current connection to ORNL is via a T1 circuit. A 100-megabit link from ORNL divisions' sites at the Y-12 Plant to ORNL will be installed in the near future. FED has about 250 devices on the local ethernet.

3.4.4 PC Support

Macintosh PCs are connected to the network via ethernet interfaces or Appletalk local area networks with FastPath boxes. Other PCs are connected via an ethernet interface. Most users currently use Eudora to read electronic mail. Access to the Internet is a must for Macintosh users and other PC users.

3.4.5 Experimental Data Acquisition

ATF restart and long-pulse operation was supported. Camac hardware and software to support the long-pulse experiments were brought on line. USC personnel also provided substantial support to the ORNL collaborations at TFTR, DIII-D, Tore Supra, and TEXTOR.

REFERENCES

1. B. A. Carreras, V. E. Lynch, L. García, and P. H. Diamond, "Resistive Pressure-Gradient Driven Turbulence With Self-Consistent Flow Profile Evolution," *Phys. Fluids B* **5**, 1491–1505 (1993).

2. K. L. Sidikman, B. A. Carreras, and L. García, "Drift Wave Turbulence in a Plasma with Sheared Flow," *J. Comput. Phys.* **14**, 100–12 (1994).

3. K. L. Sidikman, B. A. Carreras, P. H. Diamond, and L. García, "Theory Of Electric-Field Curvature Effects On Long-Wavelength Drift Wave Turbulence," *Phys. Plasmas* **1**, 1142–53 (1994).

4. P. H. Diamond, B. A. Carreras, Y.-M. Liang, and P. W. Terry, "Self-Regulating Shear Flow Turbulence: A Paradigm for the L to H Transition," *Phys. Rev. Lett.* **72**, 2565–68 (1994).

5. J.-N. Leboeuf, L. A. Charlton, B. A. Carreras, "Shear Flow Effects on the Nonlinear Evolution of Thermal Instabilities," *Phys. Fluids B* **5**, 2959–96 (1993).

6. L. A. Charlton, B. A. Carreras, V. E. Lynch, and K. L. Sidikman, "Bifurcations and Modulation Intercation in Negative Compressibility Turbulence," *Phys. Plasmas* **1**, 2700–10 (1994).

7. H. Biglari, P. H. Diamond, and P. W. Terry, *Phys. Fluids B* **2**, 1 (1990).

8. C. Y. Wang, E. F. Jaeger, D. B. Batchelor, and K. L. Sidikman, "Fast Wave Poloidal Flow Generation in a Plasma," *Phys. Plasmas* **1**(12), 3890–95 (1994).

9. D. E. Newman, P. W. Terry, P. H. Diamond, Y.-M. Liang, G. G. Craddock, A. E. Koniges, and J. J. Crotinger, "The Dynamics of Long Wavelength Electrostatic Turbulence in Tokamaks," *Phys. Plasmas* **1**(5), 1592–1600 (1994).

10. C. L. Hedrick and J.-N. Leboeuf, "Landau Fluid Equations for Electromagnetic and Electrostatic Fluctuations," *Phys. Fluids B* **4**, 3915–34 (1992).

11. L. A. Charlton, J.-N. Leboeuf, B. A. Carreras, and V. E. Lynch, "Radiation-Driven Turbulence at the Plasma Edge in Toroidal Devices," *Phys. Plasmas* **1**, 3871–82 (1994).

12. D. A. Spong, B. A. Carreras, and C. L. Hedrick, "Nonlinear Evolution of the Toroidal Alfvén Instability Using a Gyrofluid Model," *Phys. Plasmas* **1**(5), 1503–10 (1994).

13. A. Weller, D. A. Spong, R. Jaenicke, A. Lazaros, F. P. Penningsfeld, S. Sattler, the W7-AS Team, and the NBI Group, "Neutral Beam Driven Global Alfvén Eigenmodes in the Wendelstein W7-AS Stellarator," *Phys. Rev. Lett.* **72**, 1220 (1994).

14. F. Y. Gang and J.-N. Leboeuf, "Mode Coupling Effects on Alpha-Particle-Driven Long Wavelength Alfvén Wave Instability," *Phys. Fluids B* **5**, 2736–38 (1993).

15. K. R. Chen, "Anomalous Thermalization of Fast Ions in Magnetized Plasma," *Phys. Rev. Lett.* **72**, 3534 (1994).

16. V. E. Lynch, B. A. Carreras, J.-N. Leboeuf, B. C. Curtis, and R. L. Troutman, "Multi-CPU Plasma Fluid Turbulence Calculations on a CRAY Y-MP C90," p. 308 in *Proceedings of Supercomputing '93*, Portland, Oregon, November 15–19, 1993, IEEE Computer Society Press, Los Alamitos, Calif., 1993.

17. V. E. Lynch, B. A. Carreras, J. B. Drake, J.-N. Leboeuf, and P. Liewer, "Performance of a Plasma Fluid Code on the Intel Parallel Computers," p. 286 in *Proceedings of Supercomputing '92*, Minneapolis, Minnesota, November 16–20, 1992, IEEE Computer Society Press, Los Alamitos, Calif., 1992.

18. D. A. Spong, "Visualization of MHD Turbulence in Toroidal Magnetically Confined Plasmas," *AVS Network News* **3**, 3–5 (1994).

19. K. C. Shaing, "Ion Orbit Loss and Poloidal Rotation in Tokamaks," *Phys. Fluids B* **4**, 171–75 (1992).

20. K. C. Shaing and C. T. Hsu, "Effects of Diamagnetic Flow on Shock Formation in Poloidally Rotating Plasmas," *Phys. Fluids B* **5**, 3596–3602 (1993).

21. K. C. Shaing, "Test of Tokamak Low-Mode–High-Mode Transition Theory in Stellarators," *Phys. Fluids B* **5**, 3841–43 (1993).

22. K. C. Shaing, "Confinement Improvement Mechanism in the Very High Mode (VH Mode)," *Phys. Plasmas* **1**, 219–21 (1994).

23. W. A. Houlberg and S. E. Attenberger, "Evaluation of Current Drive Requirements and Operating Characteristics of a High Bootstrap Fraction Advanced Tokamak Reactor," *Fusion Technol.* **26**, 566–71 (1994).

24. W. A. Houlberg and S. E. Attenberger, "Evaluation of Pumping and Fueling Requirements for the ITER EDA," *Fusion Technol.* **26**, 316–21 (1994).

25. S. P. Hirshman, D. K. Lee, F. M. Levinton, S. H. Batha, M. Obayashi, and R. M. Wieland, "Equilibrium Reconstruction of the Safety Factor Profile in Tokamaks from Motional Stark Effect Data," *Phys. Plasmas* **1**, 2277–90 (1994).

26. U. Stroth, G. Kuhner, W. Massberg, M. Murakami, and R. A. Dory, *A First Step to a Joint Stellarator Data Base*, IPP III/195, Max Planck Institut für Plasmaphysik, Garching, Germany, February 1994.

27. G. Taylor et al., "ICRF Heating of Deuterium-Tritium Plasmas in TFTR," to be published in the Proceedings of the 15th International Conference on Plasma Physics and Controlled Nuclear Fusion Research, Seville, September 26–October 1, 1994.

28. C. K. Phillips et al., "Ion Cyclotron Range of Frequencies Heating and Current Drive in Deuterium-Tritium Plasmas," to be published in *Phys. Plasmas* (1994).

29. R. Majeski, C. K. Phillips, and J. R. Wilson, "Electron Heating and Current Drive by Mode Converted Slow Wave," *Phys. Rev. Lett.* **73**, 2204 (1994).

30. R. Majeski et al., "Mode Conversion Studies in TFTR," to be published in Proceedings of the 15th International Conference on Plasma Physics and Controlled Nuclear Fusion Research, September 26–October 1, 1994.

31. M. Murakami et al., "Fast Wave Direct Electron Heating in TFTR," in Proceedings of the 10th Topical Conference on Radio Frequency Power in Plasmas, Boston, *AIP Conf. Proc.* **289**, 48 (1993).

32. E. F. Jaeger, D. B. Batchelor, and D. C. Stallings, *Nucl. Fusion* **33**, 179 (1993).

33. M. D. Carter et al., submitted to *Nucl. Fusion.*

34. M. A. Lieberman and Gottsccho, in *Physics of Thin Films,* Vol. 18, *Plasma Sources for Thin Film Etching and Deposition*, ed. M. Francombe and J. Vossen, Academic Press, San Diego, 1994.

35. K. R. Chen et al., "Anomalous Thermalization of Fast Ions in Magnetized Plasma Due to Two-Gyro-Stream Instability," submitted to *Nucl. Fusion.*

4

PLASMA TECHNOLOGY

S. L. Milora

B. E. Argo
S. E. Attenberger[1]
F. W. Baity
D. B. Batchelor[6]
G. C. Barber
L. R. Baylor
G. L. Bell
T. S. Bigelow
C. E. Bush[6]
M. D. Carter[6]
J. B. Caughman
L. A. Charlton[1]
M. J. Cole[2]
I. Collazo[3]
S. K. Combs
J. F. Cox
B. E. Demps
G. R. Dyer[6]
E. G. Elliott
A. L. England[6]
A. Fadnek
D. T. Fehling[4]
P. W. Fisher[5]
C. L. Fogelman[2]
S. C. Forrester
C. A. Foster
C. R. Foust
W. L. Gardner
P. L. Goranson[2]
M. J. Gouge
R. H. Goulding
J. R. Haines
G. R. Hanson
J. H. Harris[6]
H. H. Haselton
G. R. Haste
P. P. Helton
G. H. Henkel[6]
D. J. Hoffman
W. A. Houlberg[4]
E. F. Jaeger[6]
T. C. Jernigan[6]
U. P. Lickliter[2]
R. L. Livesey
M. S. Lubell
J. W. Lue
J. N. Luton
M. Murakami[6]
W. D. Nelson
Y.-K. M. Peng
J. L. Ping[2]
A. L. Qualls
D. A. Rasmussen
P. F. Rice
P. M. Ryan
C. R. Schaich
D. E. Schechter
S. W. Schwenterly
L. K. Sharna
D. O. Sparks
D. Stallings[1]
W. L. Stirling
D. W. Swain
D. J. Taylor[2]
C. E. Thomas[6]
C. C. Tsai
J. H. Whealton
G. A. White
J. A. White[7]
T. L. White
J. B. Wilgen[6]
C. T. Wilson
J. J. Yugo[1]
H. Zhang[8]

---

1. Computing Applications Division.
2. Engineering Division.
3. Georgia Insitute of Technology, Atlanta.
4. Plasma Theory Section.
5. Chemical Technology Division.
6. Toroidal Confinement Section.
7. Management Services Section.
8. Oak Ridge Institute for Science and Education.

4. PLASMA TECHNOLOGY

Summary of Activities

The Plasma Technology Section of the Fusion Energy Division is engaged in the development and application of technologies that support fusion research. Progress in the areas of plasma fueling and radio frequency (rf) technology is described in this section. Design and physics-related activities for the International Thermonuclear Experimental Reactor (ITER) and for the Tokamak Physics Experiment (TPX) are described in Chaps. 5 and 6 of this report. Spinoffs from fusion technology with applications beyond fusion research are described in Chap. 9.

The Plasma Fueling Group participated in a broad range of research activities in support of both the U.S. magnetic fusion program and international fusion research. Work continued in the general areas of pneumatic and centrifugal pellet injector research and development (R&D) to support present and near-term applications, such as the Tokamak Fusion Test Reactor (TFTR), Tore Supra, and DIII-D, and advanced development in support of more demanding applications anticipated for the next generation of fusion devices. A major new initiative in the latter area is a joint R&D program with Ente per le Nuove Tecnologie L'energia e L'ambiente Frascati aimed at developing a high-speed, repeating, two-stage light-gas gun for fusion fueling applications. Recently, the emphasis of the development program has shifted somewhat from generic R&D and to research more focused on meeting ITER fueling needs. The activities emphasized in the ITER development program include high-reliability, long-pulse pellet feed systems; moderate-speed accelerators; and tritium pellet fabrication and acceleration tests. Particularly important in addressing the plasma fueling physics R&D needs for ITER and TPX was the development of a pellet injection system for DIII-D; the three-barrel, repeating pneumatic injector that was previously used on the Joint European Tokamak (JET) from 1987 to 1992 was modified in 1993 and installed and commissioned on DIII-D in 1994, and it is currently being used in the experimental campaign. A major objective of the experimental program will be to demonstrate greater control of the plasma density level and the shape of the plasma density profile than previously achieved on machines not equipped with adequate particle exhaust capability.

During this period, advances were made in both basic development and experimental collaborative applications in rf technology. The folded waveguide launcher was successfully tested at power levels of 1 MW in the Radio-Frequency Test Facility, and design adaptations for use on C-Mod, Tore Supra, PBX, TFTR, and ITER were studied. Other advanced launcher concepts such as the folded stripline, the stacked stripline, and the traveling-wave combline antennas were tested at low power. Microwave reflectometry was developed to measure the plasma density profile at the plasma edge and was successfully used on TFTR and DIII-D to study plasma loading and rf/edge interactions. Code development continued for the design and analysis of antenna/rf power systems, and results were validated by extensive measurements of antenna electrical characteristics and field patterns of DIII-D, JET, TFTR, Tore Supra, and Advanced Toroidal Facility antennas. Tuning, matching, phase control, and arc detection systems for such systems as DIII-D and TPX were also designed, analyzed, and tested during this period. Research on Faraday shield materials, fabrication and cooling techniques, and thermal and stress

analyses was conducted, and a small rf inductive plasma source was operated to study erosion properties of candidate Faraday shield materials.

In the area of rf collaborations, a four-strap antenna array was designed and fabricated for fast-wave current-drive experiments on DIII-D. This was installed in June 1992 and operated in excess of 1.7 MW for minority-ion heating, direct electron heating, and fast-wave current-drive experiments. Two additional arrays for operation over a wider frequency range and providing higher current-drive directivity were designed and fabricated and, in February 1994, installed on DIII-D. The Oak Ridge National Laboratory resonant double-loop antenna on Tore Supra was removed and upgraded with a long-pulse Faraday shield with cooled septum and will be installed in early 1995. This is expected to improve the pulse-length capability, increase the spectral directivity, and reduce anomalous heating of the plasma-facing components. A power compensation system was designed for the JET ICH system, and the tuning and matching system for the JET A2 antennas was developed and tested and received on-site analysis.

4.1 PLASMA FUELING PROGRAM

S. K. Combs, L. R. Baylor, P. W. Fisher, C. A Foster, C. R. Foust, M. J. Gouge, S. L. Milora, A. L. Qualls, C. C. Tsai, and D. E. Schechter

The ORNL FED Plasma Fueling Group is engaged in centrifuge and pneumatic injector development, which supports present and near-term applications, and advanced development, anticipating the greater demands expected in the future. Recently, the emphasis of the development program has shifted somewhat from generic R&D and is currently focused on meeting the fueling needs of ITER. A centrifuge pellet injector development program continues in support of the pellet fueling collaboration on Tore Supra and as a part of a broader effort for ITER. This is particularly important because the ITER EDA includes a centrifuge injection system for plasma fueling. Major objectives of the centrifuge development are to improve the performance and reliability of this type of injection system, and this includes the eventual demonstration of operating parameters and reliability applicable to ITER. Because the pellet feed system is the key component for long-pulse operation, it has received the most attention over the last few years, with an extensive development effort on the Zamboni ice machine. This unique feed device for the centrifuge accelerator is somewhat limited in performance and is not sufficient for the ITER application. A straightforward technique in which multiple extruder units of identical design operate in tandem is being developed for steady-state operation and should prove adequate for ITER. This feed system will be compatible with any acceleration scheme.

In the area of pneumatic injector development, the three-barrel, repeating pneumatic injector that was previously used on JET from 1987 to 1992 was modified in 1993 and installed on DIII-D in 1994 and has been used in several experiments. A small-bore (1.8-mm) version of the repeating pneumatic injector was specifically developed for this application. In tests at ORNL, the small gun was operated at up to 10 Hz for a pulse length of 15 s (pellet speeds of ~1 km/s). This performance represents the smallest pellet size (1.8 mm) and highest repetition rate (10 Hz) demonstrated with an ORNL repeating pneumatic pellet injector. In contrast, an 8-mm-bore version of the repeating pneumatic injector has also been constructed and successfully tested with deuterium pellets at frequencies of ~0.5 Hz and speeds of ~1.1 km/s. The 8-mm size is the largest

pellet used to date in an injector and is relevant for ITER fueling. This hardware will be used in the second phase of the tritium proof-of-principle experiment (TPOP-II) at the Tritium Systems Test Assembly (TSTA), where it will be thoroughly tested with tritium and D-T mixtures.

For long-pulse operation in a higher velocity regime (≥2 km/s), an experiment is being carried out by ORNL and Ente per le Nuove Tecnologie L'energia e L'ambiente (ENEA) Frascati of the European Atomic Energy Community (Euratom). A small ENEA Frascati two-stage gun has been installed on a repeating pneumatic injector facility at ORNL. Pellet speeds of up to 2.6 km/s have been achieved with nominal 2.7-mm-diam deuterium pellets, and results from limited testing in the repeating mode (up to ~1 Hz) have also been encouraging. The higher pellet speeds are about twice that available with conventional repeating pellet injectors. Tests of the electron-beam rocket accelerator for higher pellet speeds continued through 1993, at which time this effort was terminated with shifts in the program priorities.

The pellet fueling group participated in a number of pellet fueling experiments on several tokamak devices, including TFTR, Tore Supra, and DIII-D. On TFTR, the experimental program emphasized the fueling and confinement properties of PEP-mode discharges. The PEP modes obtained on TFTR were examined for current and power scaling and compared to earlier results from JET. The results from TFTR did not indicate the dependence of the PEP mode on core shear reversal that were indicated on JET, suggesting that another mechanism may be involved in the improved core confinement. The Tore Supra program concentrated on improved injector reliability, necessary for long-pulse particle control experiments using pellet fueling in conjunction with edge pumping. Experiments were carried out on Tore Supra with a more reliable centrifuge pellet injector to test the concept of isotopic tailoring. The results are being analyzed, and further experiments are planned. The pellet fueling program has just begun on DIII-D and will emphasize long-pulse particle control with pellet injection in a pumped divertor configuration, which is expected to be used for ITER.

4.1.1 Pellet Injector Development

4.1.1.1 Centrifuge injector

A major objective of the injector development program at ORNL is to improve the performance and reliability of the centrifuge pellet injection system; this includes pellet reproducibility and the overall pellet delivery reliability. Another development objective is to increase the number of pellets that can be provided for a single machine pulse, with the final goal of steady-state operation. A centrifuge accelerator facility at ORNL provides a test bed for experimental investigations and hardware development. During the last few years, the development effort has concentrated on improving the advanced pellet feed system referred to as the Zamboni.[1,2] A duplicate feed system is used for the pellet injector application on Tore Supra (Sect. 4.1.1.2). In these systems (Figs. 4.1 and 4.2), a rim of ice is condensed onto a rotating cryostat, and pellets are formed by chipping a piece of ice from the rim with a triangular cutting tool that moves through the ice rim from the top to the bottom. The cutting tool imparts velocity to the pellet, which pushes it to a rotating arbor for acceleration. The timing of the pellet delivery to the arbor is controlled so that it will intercept the arbor at the correct position for acceptance into an acceleration groove. The number of pellets available from this pellet feed system is limited to 100 pellets per discharge, with a typical pellet delivery rate of 4 Hz. The maximum pellet delivery rate of this system is ~8 Hz. A four-rim Zamboni system was completed at the end of 1992, with initial testing in 1993.

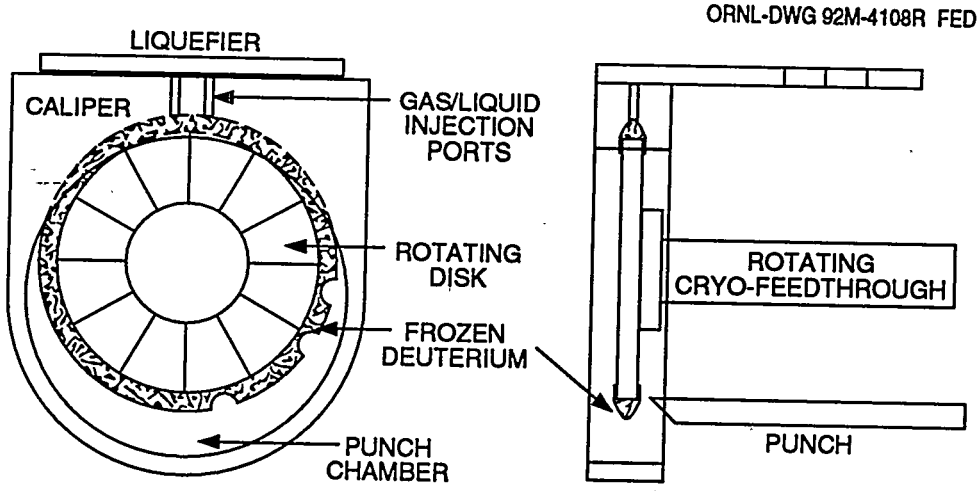

Fig. 4.1. Schematic of Zamboni fabrication deuterium ice (developed at ORNL to supply ice for centrifuge injectors). Quantity of pellets equivalent to amount of ice on the disk circumference can be punched on command.

While improvements have been made in the operations of the centrifuge injector in extensive testing in the laboratory and on Tore Supra, the feed system has not achieved greater than ~90% reliability (defined as the number of pellets that enter or would enter the plasma divided by the number of pellets requested), primarily because of a large spatial distribution of the pellets at the arbor acceptance position. Also, attempts to increase the total number of pellets available from the Zamboni device have been unsuccessful, for the most part. The Zamboni feed system has inherent limitations that make it difficult to control and unsuitable as a pellet source for future fusion applications. It cannot be extended to steady-state operation, and the time required to recharge exhausted ice rims is very long compared to the amount of time that the system is in operation. This makes it impractical when several independent feed systems are used consecutively to achieve quasi–steady-state operation. Even with optimal performance, the overall reliability of the present injector is not sufficient for the ITER application or future experiments planned for Tore Supra when active pumping becomes available.

To improve upon the present centrifuge system, alternative feed systems will be evaluated and can be retrofitted to the existing centrifuge accelerator facility. The plan for 1995 calls for adding a standard ORNL deuterium extruder (Sect. 4.1.1.2) and pellet punch mechanism to the existing centrifuge accelerator facility. The assembly will replace the Zamboni ice machine for long-pulse pellet operation. The new, punch-type pellet feed/cutter device will be close coupled to the arbor and completely adjustable, including the capability to change pellet lengths. In addition to demonstrating pellet reliability approaching that demonstrated by state-of-the-art pneumatic pellet injection systems (≥98%), the goals for the operating parameters include (1) pellet frequencies ≥10 Hz, (2) pellet speeds ≥600 m/s, (3) pellet sizes in the range of 2–7 × 10^{20} atoms/pellet, and (4) extended pulse lengths with ~200 pellets available (about twice that of the present Zamboni feed system). Extensive testing will be carried out to optimize system performance and reliability. Feed systems that can provide even more pellets to the centrifuge accelerator, including steady-state operation, are also under development (Sect. 4.1.1.5).

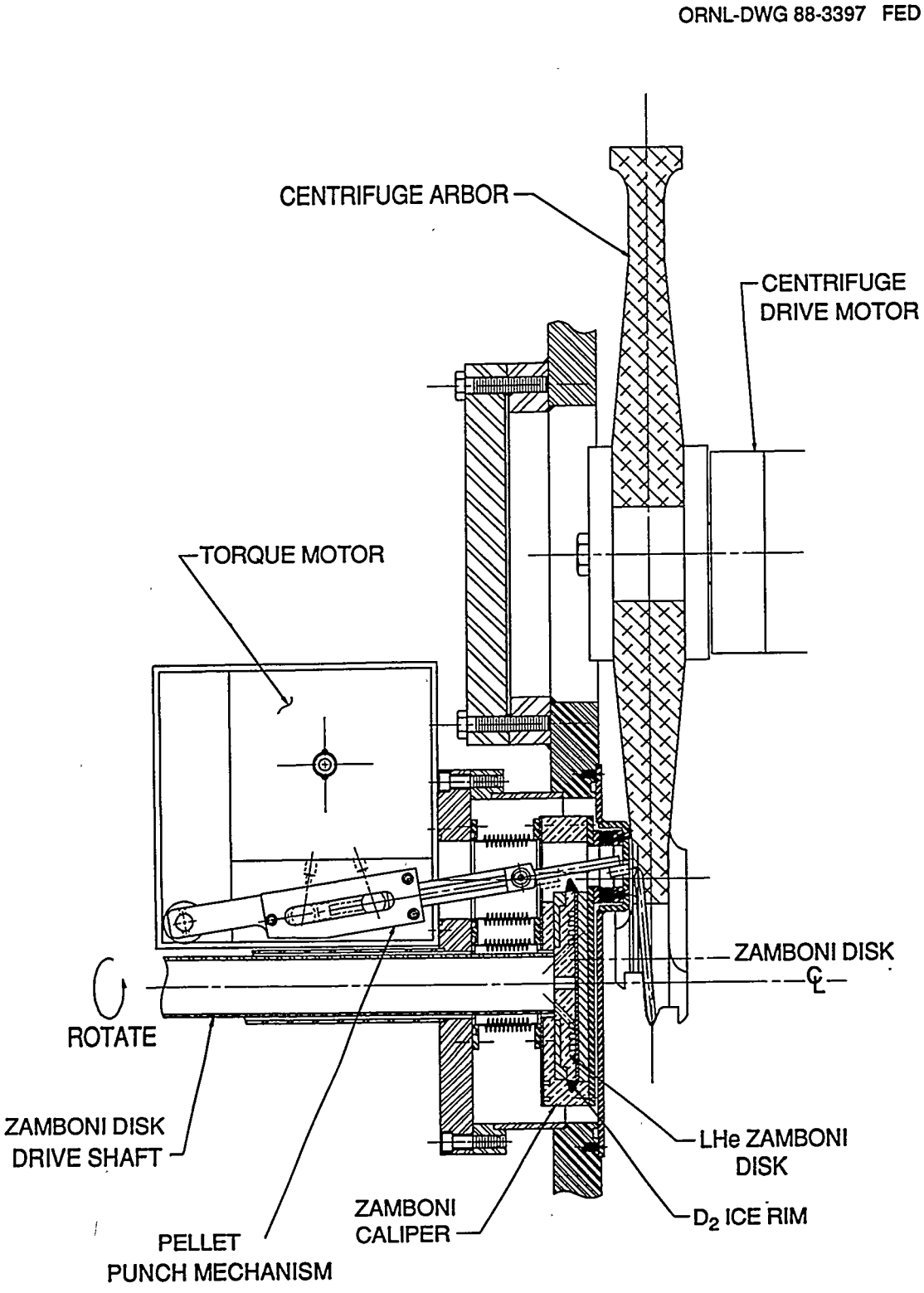

Fig. 4.2. Details of pellet fabrication device and high-speed rotating arbor for ORNL centrifuge pellet injector. Installed on Tore Supra in 1989 and used in plasma fueling experiments.

4.1.1.2 Pneumatic injectors

Small-bore, high-firing-rate pneumatic injector

Repeating pneumatic pellet injectors developed at ORNL were used for plasma fueling experiments on TFTR[3–6] and JET.[7–10] This injector type combines cryogenic hydrogen extruder and pneumatic acceleration technologies to form and propel pellets repetitively at high speed (~1 to 1.5 km/s) and is well suited for long-pulse and steady-state applications. For the plasma fueling application on the DIII-D tokamak (Sect. 4.1.2.3), a small-bore (1.8-mm) version of this injector has been developed and thoroughly tested at ORNL.[11] A general schematic of a cryogenic extruder and gun assembly is shown in Fig. 4.3; the cryogenic extruder supplies a continuous stream of frozen deuterium to the gun section, where individual pellets are repetitively formed, chambered, and accelerated. The number of pellets that can be provided by this type of device depends on the pellet size and the volume of the freezing chamber. Detailed descriptions of this class of injectors, including operations and performance, have been published previously.[3,4,6–11]

In tests at ORNL in 1993, the 1.8-mm gun was operated at up to 10 Hz for a pulse length of 15 s; photographs from a 150-pellet sequence are shown in Fig. 4.4. (Pellets were captured exiting a short guide tube downstream of the gun barrel.) The operating pressure was ~70 bar (propellant solenoid valve with helium gas), and the velocities were slightly <1 km/s. (Pellet speeds were not individually recorded for this sequence.) As estimated from the photographs, the actual pellet size is ~1.3 mm in diameter by 2.3 mm in length; slight erosion of the diameter as the pellet travels through the relatively warm barrel (which is room temperature, in contrast to the ~14 K temperature of the pellet) and some elongation during the chambering process are typical of this type of device. As illustrated in Fig. 4.4, the pellet integrity and size uniformity is exceptional, especially considering the high repetition rate. This performance represents the smallest pellet size (1.8 mm) and highest repetition rate (10 Hz) achieved with an ORNL repeating pneumatic pellet injector.

High-speed, repeating, two-stage pneumatic injector

Development of the two-stage light-gas gun technique for high-speed pellet injection has been ongoing for several years at ORNL,[12,13] including acceleration of single plastic and deuterium pellets to high speeds (5.1 and 2.8 km/s, repectively). Also, a small ORNL two-stage light-gas gun[14] previously demonstrated repetitive operation at 1 Hz and 3 km/s with plastic surrogate pellets. In a recent international collaborative study, hardware components from ORNL and ENEA Frascati have been combined on a test facility at ORNL: (1) the ORNL cryogenic hydrogen extruder[3–11] (equipped with a pellet chambering mechanism/gun barrel assembly), which has been used for long-pulse fueling experiments on several major fusion devices (DIII, TFTR, and JET) and can provide up to ~100 small pellets (2.7 mm) in a single extrusion sequence, and (2) the Frascati repeating, two-stage light-gas gun, which has been used to reliably accelerate single deuterium pellets to velocities as high as 3.3 km/s in the laboratory.[15,16] This activity is being carried out in the framework of a collaborative agreement between the U.S. Department of Energy (DOE) and ENEA. An overall schematic of the test equipment is shown in Fig. 4.5, and schematics of the ORNL extruder/gun assembly and the Frascati two-stage gun are shown in Figs. 4.6 and 4.7. The prototype repeating pneumatic injector[3,4] has been used in this study; in contrast to the breech-side chambering mechanism shown in Fig. 4.3, pellets in the prototype are cut/chambered from the extrusion by the gun barrel as shown in Fig. 4.7. Main parameters of the test equipment are listed in Table 4.1. The primary objective of this work is to

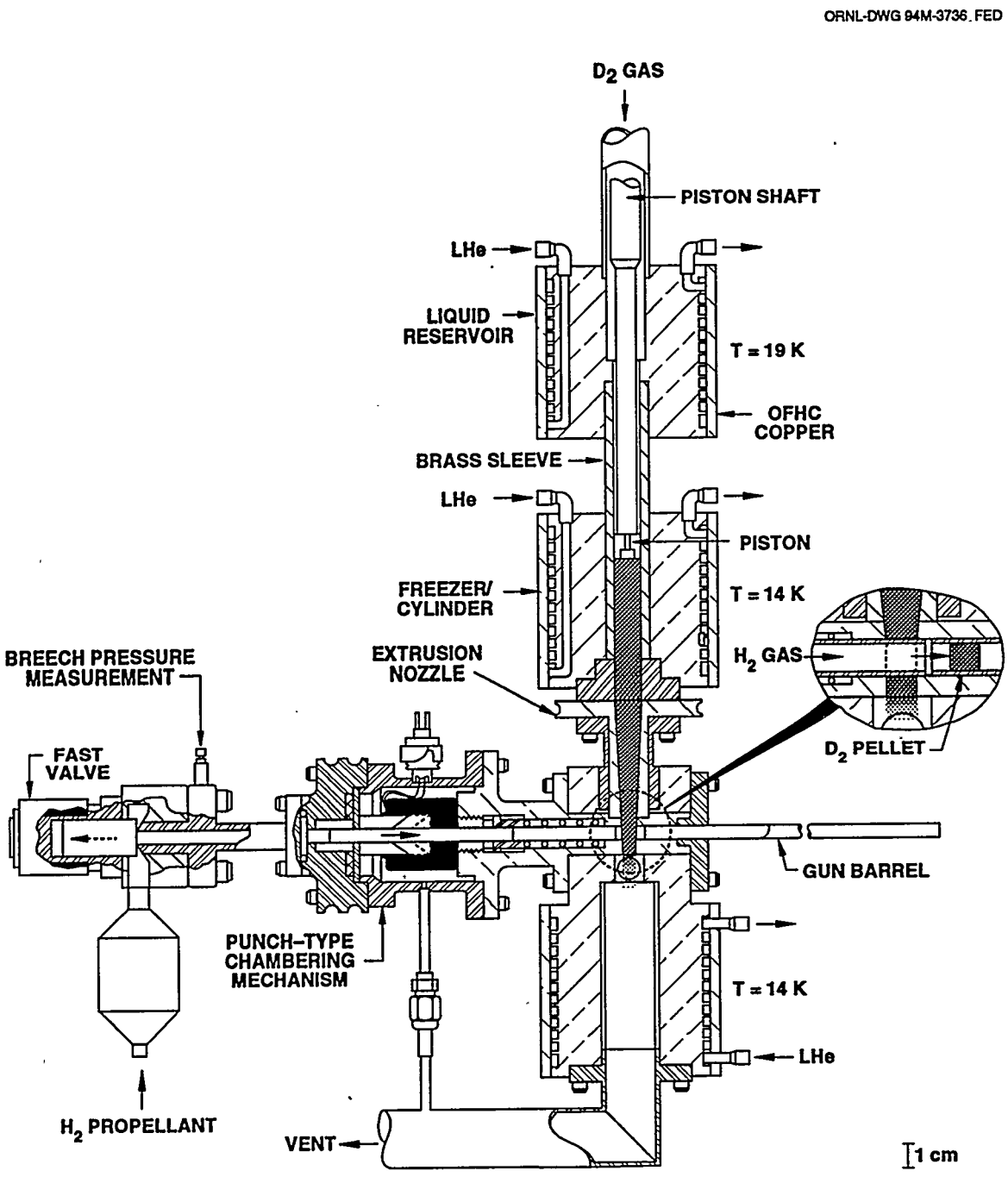

Fig. 4.3. Schematic of ORNL repeating pneumatic pellet injector.

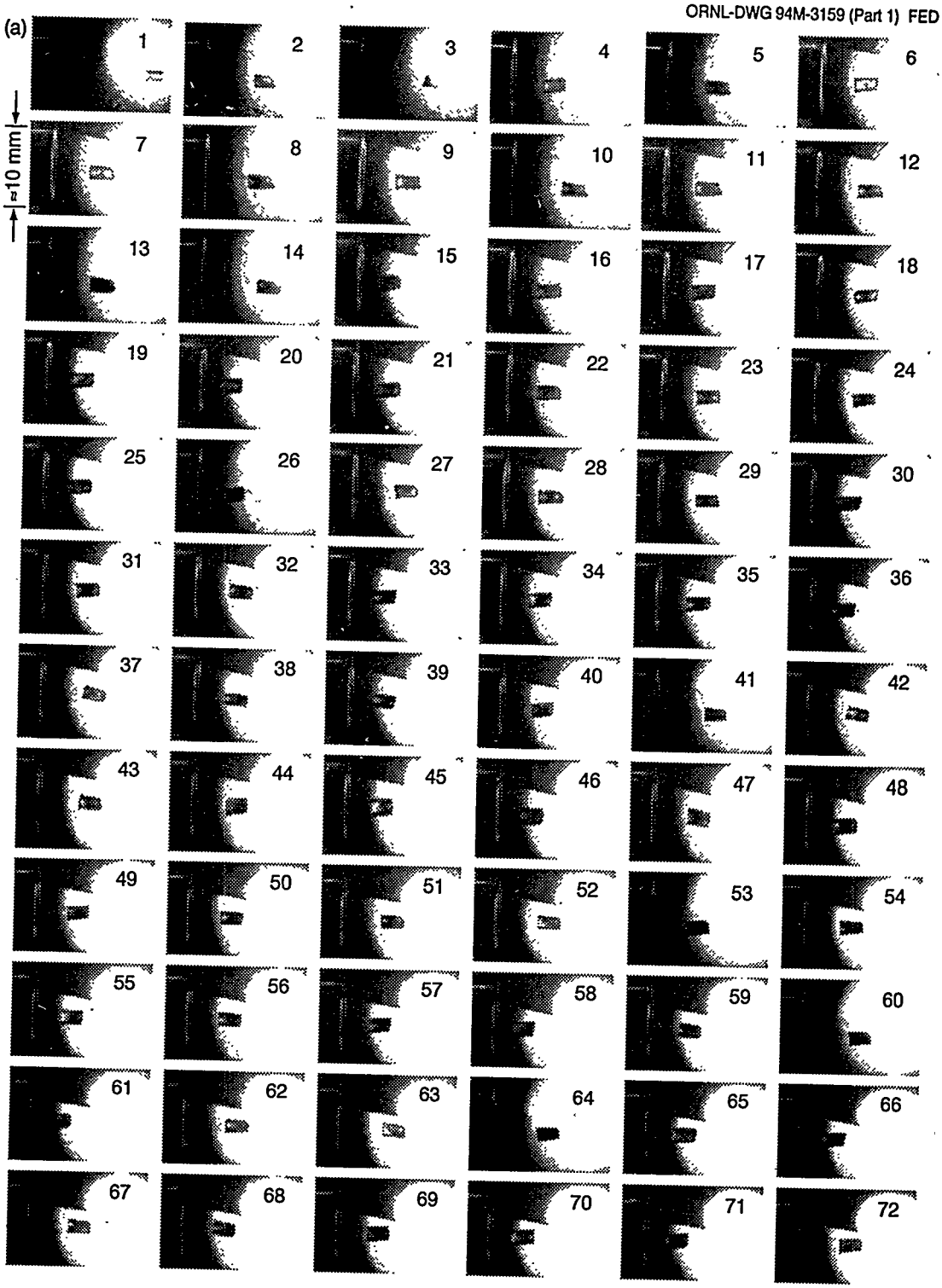

Fig. 4.4. Photographs of 150-pellet sequence from repeating pneumatic pellet injector (1.8-mm bore). Deuterium pellets shown exiting guide tube (5.3-mm ID by 9.5-mm OD) gun firing rate of 10 Hz and pellet velocities of ~1 km/s: (*a*) pellets 1–72.

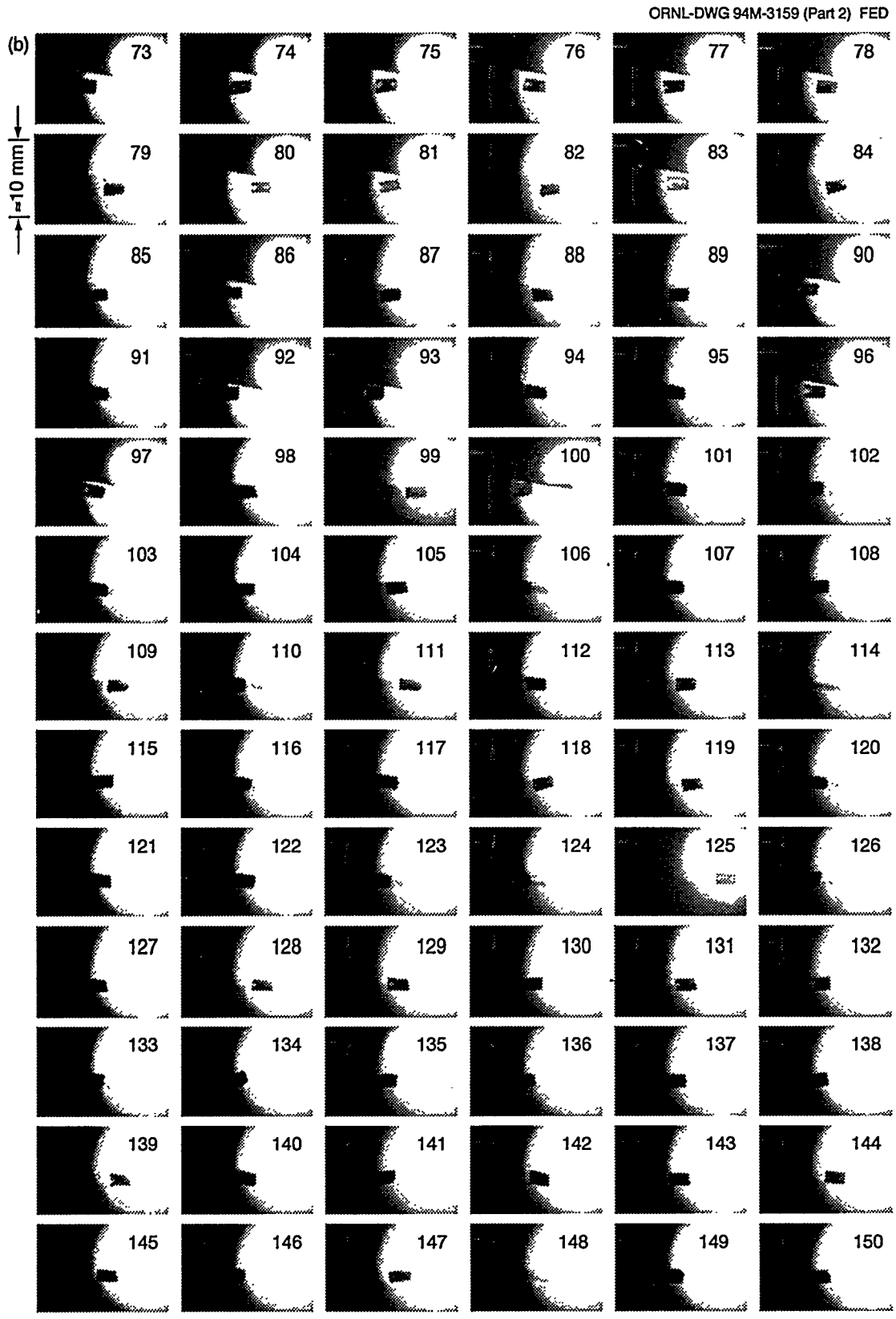

Fig. 4.4 (continued). (*b*) Pellets 73–150.

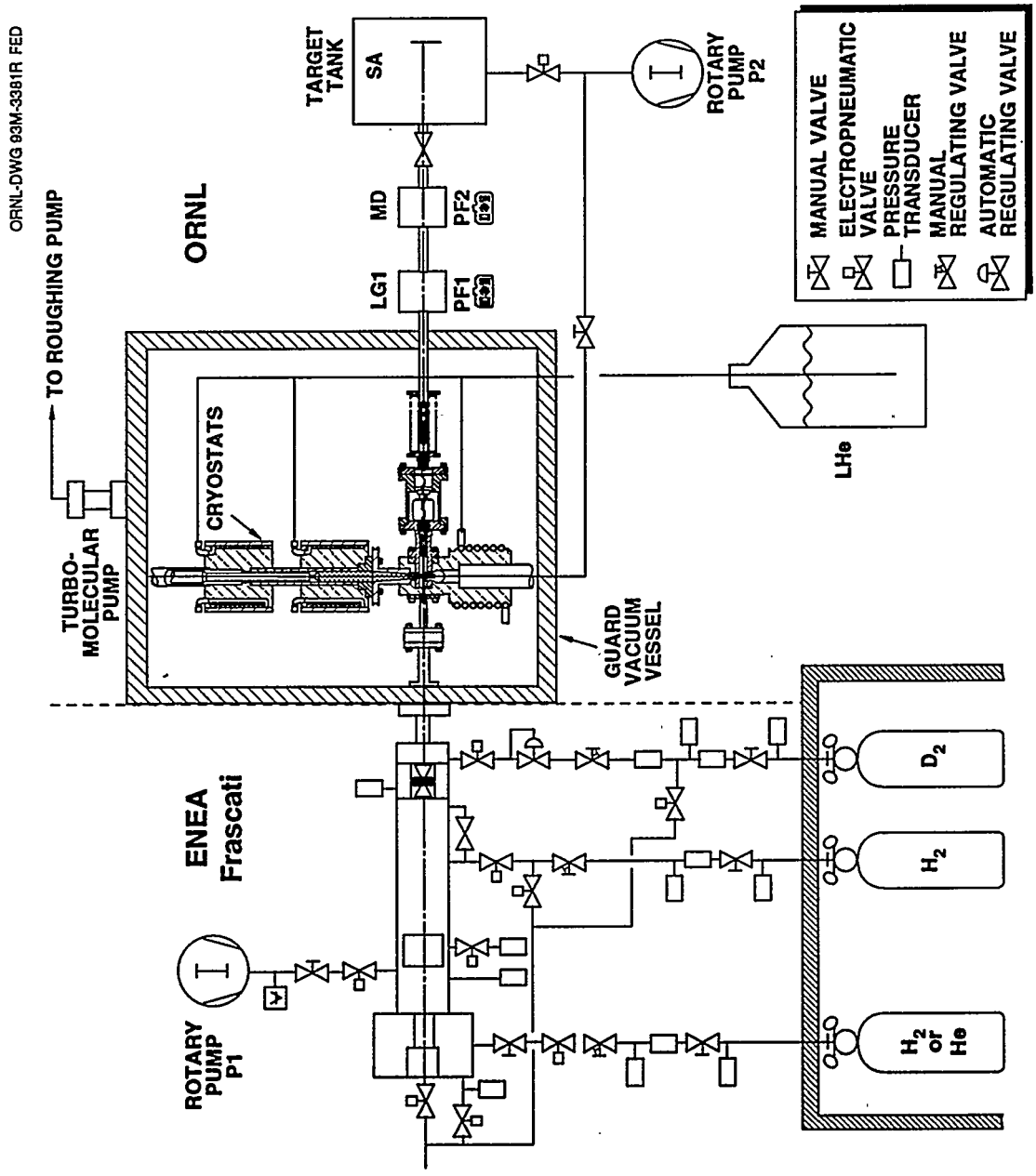

Fig. 4.5. Schematic of ORNL repeating pneumatic injector test facility with ENEA Frascati two-stage light-gas gun.

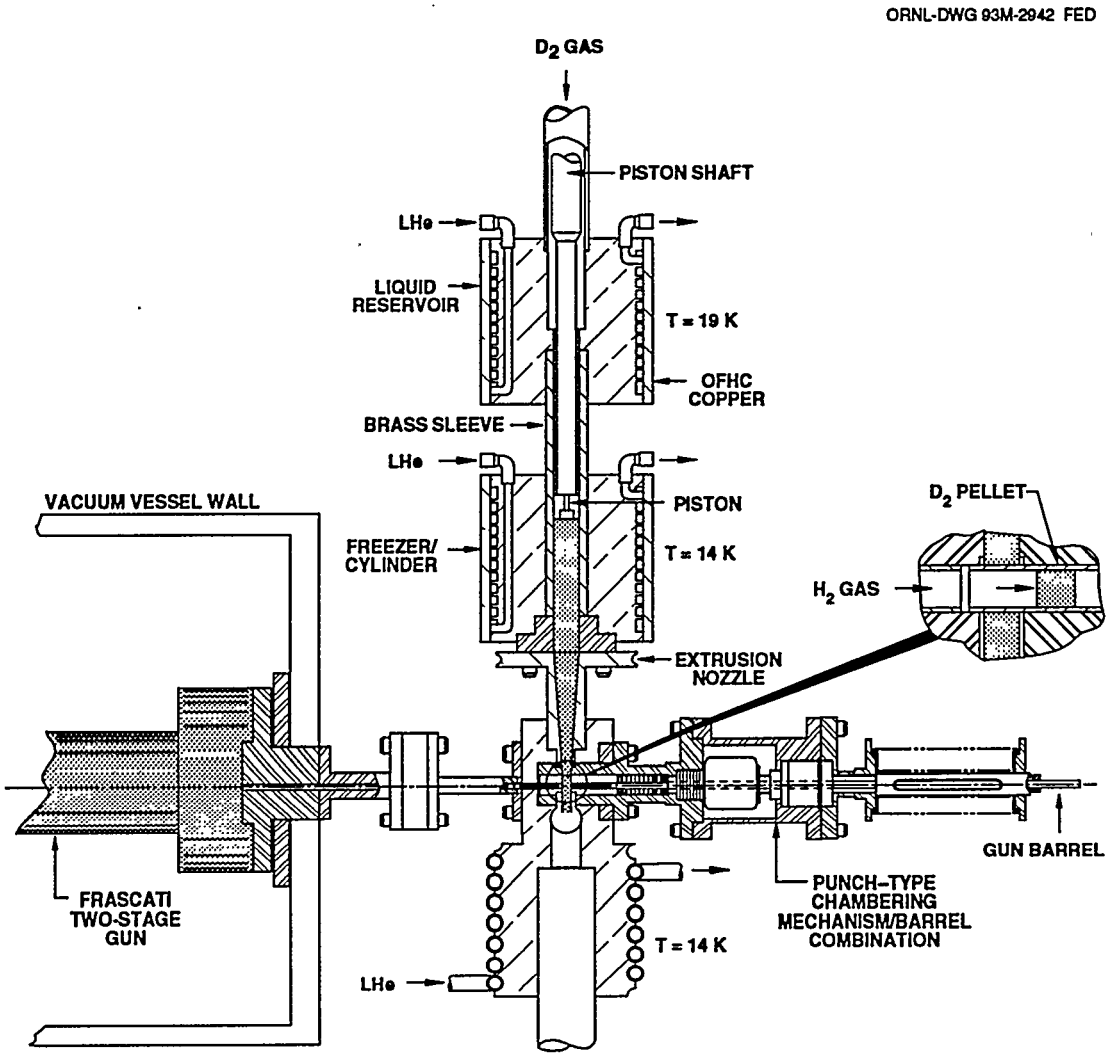

Fig. 4.6. Test configuration of ORNL repeating pneumatic injector with ENEA Frascati two-stage gun.

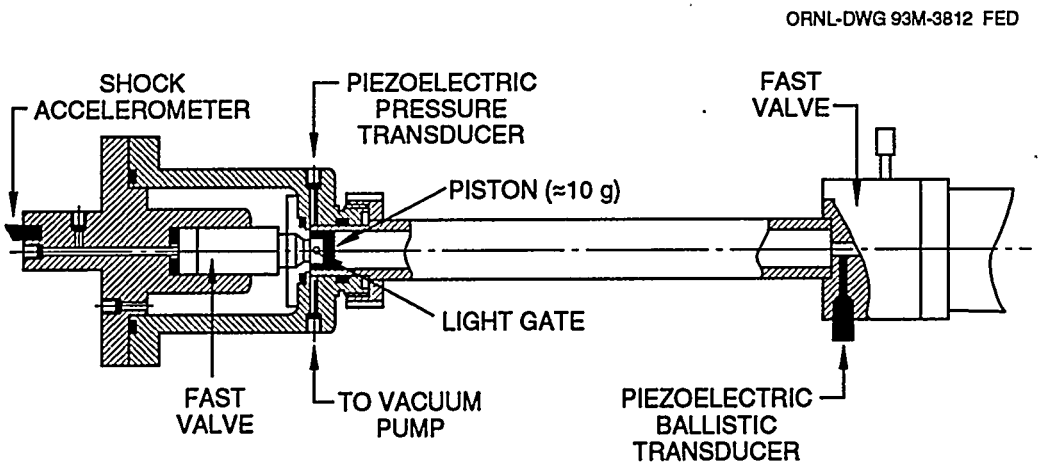

Fig. 4.7. Schematic of Frascati repeating two-stage light-gas gun.

Table 4.1. Main parameters of the ORNL/Frascati injector

Design feature	Parameters
Frascati two-stage gun	
First-stage reservoir volume	325 cm^3
Pump tube ID	25.03 mm
Pump tube length	~350–1000 mm
Piston material	Aluminum alloy (ergal)
Piston mass	~10 g
Piston length	~14 mm
Piston diameter	24.97 mm
Operating gases	Hydrogen, helium
ORNL extruder/gun assembly	
Pellet material	Deuterium
Barrel length	800 mm
Barrel ID	2.7 mm
Pellet nominal length	2.7 mm, 5.4 mm, and 8.1 mm
Pellet nominal mass	3 mg, 6 mg, and 9 mg

evaluate the capabilities of these combined technologies experimentally and to demonstrate and study repetitive operation with bare deuterium ice.[17] The test goals include operation at pellet frequencies of up to ~1 Hz and speeds in the range of 2 to 3 km/s.

The data from two experimental campaigns at ORNL[18,19] are shown in Fig. 4.8; the pellet speed is plotted against the maximum breech pressure. Pellet speeds of up to 2.6 km/s have been achieved with nominal 2.7-mm-diam deuterium pellets. During the first set of experiments, it was found that the low pellet release pressure (~5 bar) of the repeating device made it difficult to achieve speeds >2 km/s. Also, the scatter in the data from the first campaign was very large. On the basis of these results, techniques were developed to (1) prevent the pellets from accelerating until the pressure burst from the two-stage gun driver is delivered and (2) tailor the shape of the pressure pulse for optimal pellet acceleration. For the second set of experiments, the improvement in performance was dramatic, as shown in Fig. 4.8, with pellets consistently launched at speeds in the 2.0- to 2.5-km/s range. In addition, the high speeds are obtained with much lower breech pressures than for the first set of experiments, and the data scatter is greatly reduced. Most of the experiments have concentrated on optimizing single shots; however, results from limited testing in the repeating mode (0.2 to 0.5 Hz) have also been encouraging, with no significant degradation observed in the pellet speeds at equivalent breech pressures. The higher pellet speeds are about twice that available with conventional repeating pellet injectors (single-stage light-gas guns and centrifuges).

4.1.1.3 Electron-beam rocket pellet injector

While the previous high-velocity technique has been applied in other areas of research for many years, a new method of accelerating pellets to high velocity using a high-power, magnetically compressed electron beam has been under development at ORNL for the last few years.[20,21] In the electron-beam accelerator, a magnetically compressed beam of electrons (1) ablates (evaporates) a hydrogen "ice stick" and heats the resulting exhaust gas and (2) uses this heated exhaust gas to accelerate a payload pellet of deuterium or tritium to high speeds. The performance

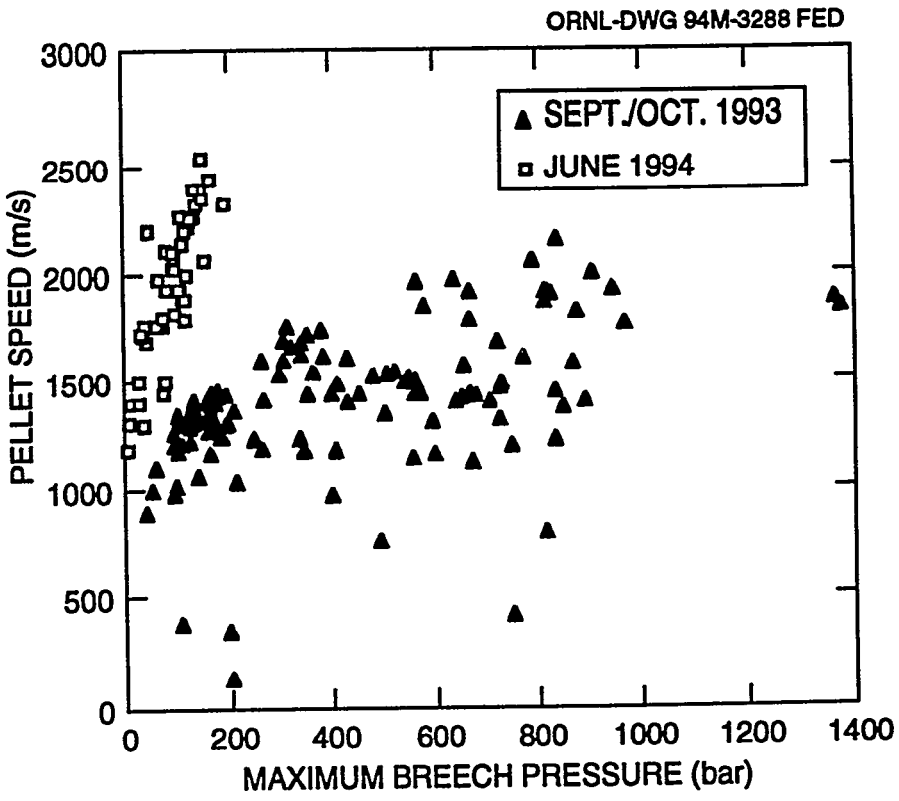

Fig. 4.8. Experimental data from repeating two-stage pneumatic injector (2.7-mm bore). Pellet muzzle velocity as function of peak breech pressure. (ORNL/ENEA Frascati collaboration.)

of an electron-beam rocket pellet accelerator depends strongly on the beam transmission efficiency, the burn velocity of the pellet, and the exhaust velocity of the propellant (or ablated) gas, which affect each other and the final pellet velocity that can be achieved. A proof-of-principle device for characterizing electron-beam rocket pellet acceleration has been developed and operated; experimental data have been collected for thousands of accelerated hydrogen pellets under a variety of beam conditions. One intact hydrogen pellet was accelerated to a speed of 578 m/s by an electron beam of 10 kV, 0.8 A, and 1 ms. The data collected reveal the significant finding that the measured burn velocity of bare hydrogen pellets increases with the square of the beam voltage in a way that is qualitatively consistent with the theoretical prediction based on the neutral gas shielding (NGS) model. The measured burn velocity increases with the beam current or power and then saturates at values two to three times greater than predicted by the NGS model. The discrepancy may result from low pellet strength and large beam-pellet interaction areas. Moreover, this feature may be the cause of the low measured exhaust velocity, which often exceeds the sonic velocity of the ablated gas. Consistent with the NGS model, the measured exhaust velocity increases in direct proportion to the beam current and in inverse proportion to the beam voltage. Some of the data from this study are shown in Figs. 4.9 and 4.10.

The results of the experiments indicate that the relatively low strength of hydrogen ice limits the acceleration to less than that needed for higher velocities in the prototype. To alleviate the pellet strength problem, experiments have been pursued with the hydrogen ice contained in a lightweight rocket casing or shell. Pellets in such sabots have the potential to withstand higher beam powers and achieve higher thrust-coupling efficiency. But the pellet speed cannot be increased effectively because of a severe weight penalty of the sabot to the rocket. Alternatively,

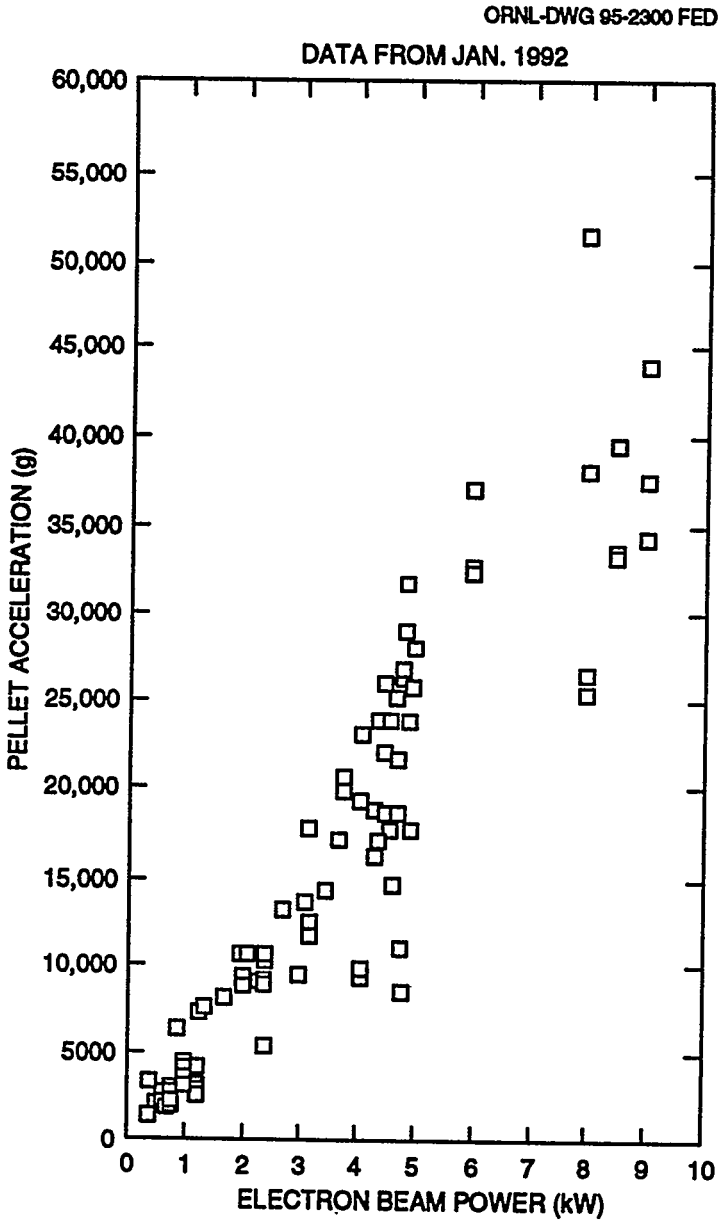

Fig. 4.9. Pellet acceleration, calculated from increment of pellet velocity and applied beam pulse length, as function of electron-beam power.

the use of lithium or lithium hydride as a substitute for hydrogen as a propellant material has been proposed and theoretically investigated. Lithium is much stronger than hydrogen and should be able to withstand greater beam acceleration. It is also denser, so the weight penalty for a casing or sabot is not as severe. Furthermore, the sonic velocity of lithium is a factor of 5 higher than that of hydrogen. This will allow the use of higher voltage (or beam energy) electron beams for pellet acceleration. Using lithium propellants with a rocket casing or sabot will require that the lithium be "burned" and the casing removed from the payload D-T pellet before injection into the fusion reactor. If successfully developed, this pellet accelerator will be suitable for an injection system

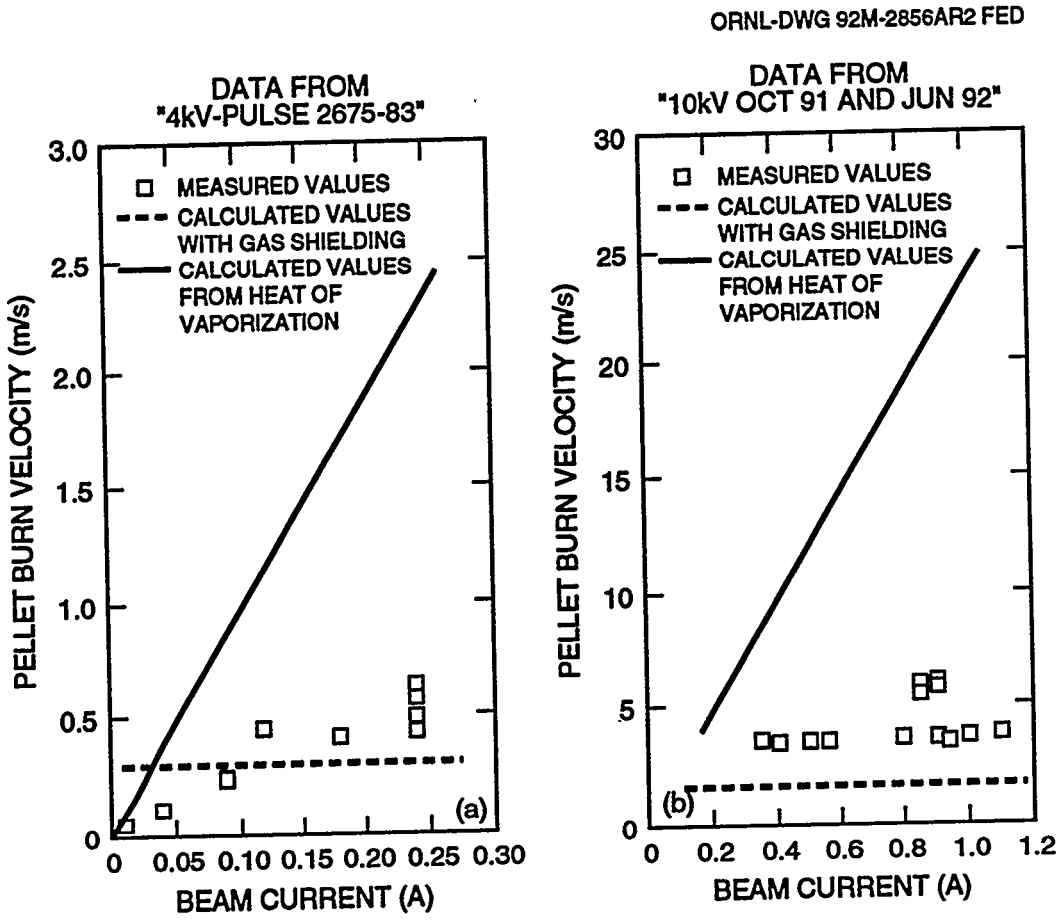

Fig. 4.10. Measured and calculated burn velocities as function of beam current for beam energies of (*a*) 4 keV and (*b*) 10 keV.

that would supply high-velocity deuterium or tritium pellets for fusion reactors. A few experiments were carried out in the prototype facility with a hydrogen pellet frozen in a lithium hydride shell. But the hydrogen pellet tends to separate from and get ahead of its sabot shell during the launching process.

While the electron-beam rocket is a potential candidate for a high-speed pellet injector, a significant amount of R&D is still needed before this technique can demonstrate the relatively high pellet speeds predicted from models and the reliability required for tests on experimental fusion devices. With recent shifts in the emphasis of the pellet injector development program, this ORNL effort was terminated in 1993.

4.1.1.4 TPOP-II experiment

The original tritium proof-of-principle (TPOP) experiment was operated in 1988 and 1989 to demonstrate the basic scientific feasibility of production and pneumatic acceleration of tritium pellets for fueling future fusion reactors.[22,23] The experiment, designed and built at ORNL, was installed and operated by ORNL personnel at TSTA at Los Alamos National Laboratory (LANL). Hundreds of 4-mm-diam pellets composed of deuterium, tritium, and D-T mixtures were made and accelerated in this device; speeds of up to 1.4 km/s were recorded. Over 100 kCi of tritium was processed through the experiment without incident. The gun for this first phase of the TPOP

program was based on the pneumatic pipe-gun concept, by which pellets are formed in situ in the barrel and accelerated with high-pressure gas. In phase II of this experiment (TPOP-II), the pipe gun will be replaced with a repeating pneumatic pellet injector similar to the design used for the three-barrel injector[7–10] that operated on JET from 1987 to 1992 and was recently installed on DIII-D (Fig. 4.3). The repetitive device will produce and accelerate 8-mm-diam pellets (twice the diameter of the original TPOP pellets), and the projected maximum repetition rate is ~0.5 to 1 Hz. The 8-mm pellets will be the largest used to date in an injector (6-mm-diam pellets were previously used on JET)[7–10] and is relevant for ITER fueling. For this large pellet size, the standard extruder can provide ~10 pellets; however, development of feed systems for longer pulses and steady-state operation is under way (Sect. 4.1.1.5).

At the end of 1994, the new TPOP-II injector had been assembled and was undergoing deuterium tests at ORNL before being shipped to and installed at TSTA, where it will be housed in a glove box. Many tests have been carried out in both the single-shot mode and the repeating mode at up to 1 Hz; the pellet speeds are nominally 1.1 km/s at an operating pressure of ~70 bar. A photograph of a typical pellet is shown in Fig. 4.11.

ORNL-DWG 94M-3667 FED

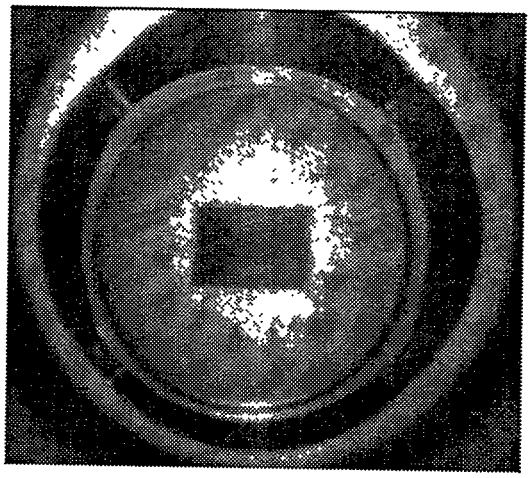

Fig. 4.11. Photograph of 7.4-mm-diam by 11-mm-long deuterium pellet formed and accelerated with TPOP-II repeating pneumatic injector. (Pellet speed 1.1 km/s.)

A schematic of the TPOP-II equipment/glovebox as it will appear during operations at TSTA is shown in Fig. 4.12. The single-stage, repeating pneumatic injector; guard vacuum enclosure; vacuum injection line; and gas-handling system are housed in a lexan/aluminum glovebox for secondary tritium containment. This is the same glovebox that was used in the original TPOP experiment. An extension has been added above one end of the TPOP glovebox to contain the tritium extruder, which is too tall to fit in the original glovebox. Below the glovebox is an ~600-L ballast volume to maintain pressure in the injection line below 30 mbar during pellet production runs. In addition to the standard components shown in Fig. 4.12, this injector includes a ^{3}He separator that removes the ^{3}He byproduct of the tritium radioactive decay from the incoming tritium supply gas stream. With very few exceptions, tritium-wetted surfaces are all metal (usually stainless steel). All interfaces between the glovebox and TSTA (tritium, deuterium, nitrogen, helium, electrical, control, vacuum connections, etc.) are through panels in the top of the

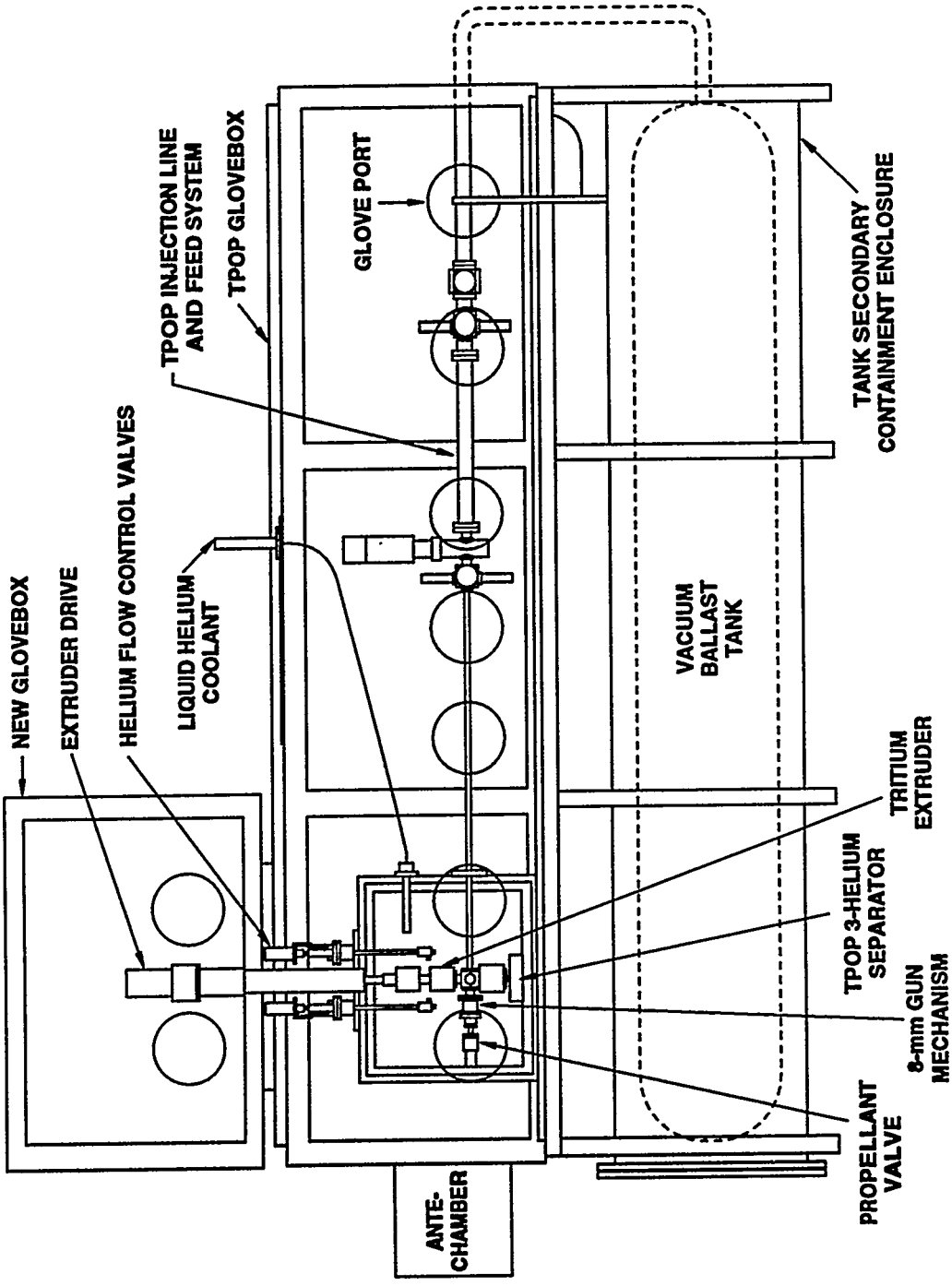

Fig. 4.12. Schematic of TPOP-II pellet injector. Repeating single-stage light-gas gun in glovebox for tritium pellet operations.

glovebox. High-speed data acquisition and fast control functions will be achieved through a MicroVAX II computer and CAMAC digitizing and timing modules.

The TPOP-II program has the following development goals: (1) evaluate the feasibility of extruding tritium and D-T mixtures for use in future pellet injection systems; (2) determine the mechanical and thermal properties of tritium and D-T extrusions; (3) integrate, test, and evaluate the extruder in a repeating, single-stage light-gas gun sized for the ITER application (pellet diameter ~7 to 8 mm); (4) evaluate options for recycling propellant and extruder exhaust gas; and (5) evaluate operation and reliability of ITER prototypical fueling systems in an environment of significant tritium inventory requiring secondary and room containment systems. Much larger D-T throughputs are required for TPOP-II than for the original pipe-gun experiment; the baseline approach will include recycling of extruder and injection line exhaust streams to maximize experimental tests within TSTA constraints on tritium supply rate and exhaust gas storage. In operation at TSTA, the repeating pneumatic injector will be thoroughly tested with tritium and D-T mixtures.

4.1.1.5 Steady-state extruder feed system

For the proposed ITER application and future steady-state fusion reactors, a feed system capable of providing a continuous supply of frozen hydrogen is required. At ORNL, a straightforward technique in which multiple extruder units of identical design operate in tandem is being developed. This approach uses a reliable ORNL technology and is illustrated in Fig 4.13. A prototype that is under construction should be able to provide a continuous source of hydrogen ice for steady-state operation. In the illustration, it is shown feeding a repeating pneumatic injector; however, the steady-state extruder feed system should be compatible with any acceleration scheme. A transition piece that accepts the three individual feeds and outputs a single feed is the key new component that must be developed for this design. Three standard ORNL extruders will be used for the prototype, each containing ~4 cm^3 of solid deuterium, for a total maximum inventory of ~12 cm^3. This equipment should be adequate to demonstrate steady-state feed rates required for pellet injector operation at frequencies of up to several hertz and pellet sizes in the 2- to 6-mm range. Preliminary designs have been carried out in which the extruder volume is doubled, and these units are an option that can be employed in a second phase of the development to accommodate larger throughput rates. The prototype steady-state extruder feed system could also be used on present long-pulse tokamaks to increase the effective fueling duration.

4.1.2 Pellet Injector Applications

4.1.2.1 TFTR tritium-compatible, four-shot pneumatic injector

The latest ORNL pellet injection system provided for TFTR (previous systems installed in 1985[4] and 1986[5]) is a tritium-compatible, four-shot pipe-gun configuration with three single-stage guns and a two-stage light-gas gun driver. This system is a modification of the TFTR eight-shot pneumatic pellet injector[5] that operated on the tokamak from 1986 to 1991. The upgraded injector[24–26] is equipped with 1-m-long gun barrels, two with a 3.4-mm ID and two with a 4.0-mm ID. The three standard guns have been operated reliably at pellet speeds of up to 1.7 km/s (using deuterium pellets). The two-stage gun can provide the high-pressure, high-temperature gas required to accelerate pellets to the 2- to 3-km/s range (as 2.8 km/s has been recorded in deuterium tests at ORNL). The size of individual pellets can be varied using techniques demonstrated in the TPOP experiment to freeze different amounts of hydrogen ice. The injector is fully

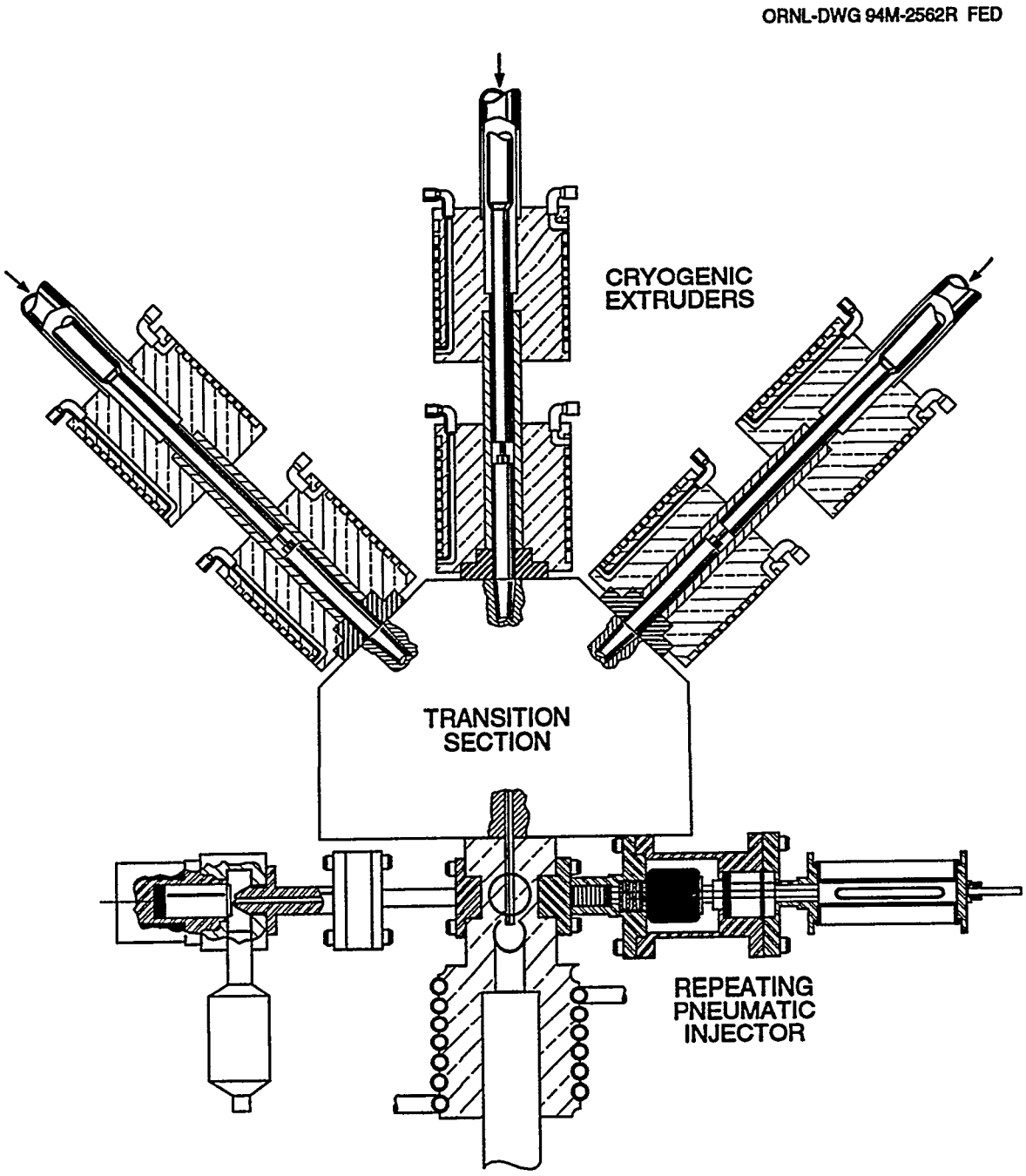

Fig. 4.13. Schematic of steady-state extruder feed system under development at ORNL. Three standard extruders operate in tandem to provide continuous source of frozen hydrogen.

tritium compatible and radiation hardened for TFTR D-T operations. The injector was installed on TFTR in 1992 (Fig. 4.14) and has been used in plasma-fueling experiments and in support of TFTR D-T experiments. In the original plan, a D-T gas manifold and two secondary containment structures were to be fitted to the pellet injection system in a second phase of work to provide full tritium pellet capability; however, the second phase was suspended indefinitely.

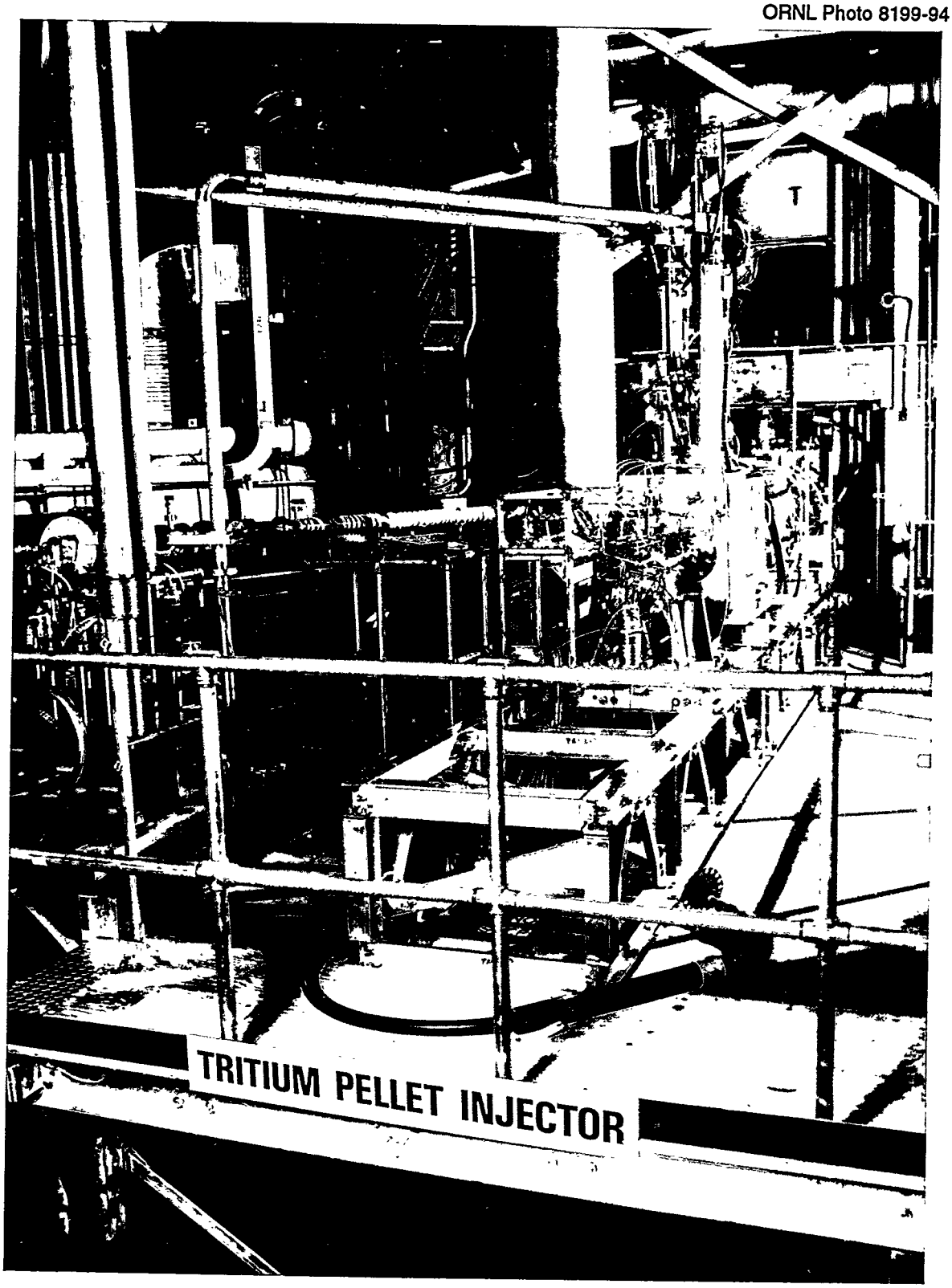

Fig. 4.14. Photograph of tritium-compatible, four-shot pneumatic pellet injector system on TFTR.

One of the primary uses of the TFTR pellet injector has been in investigating the confinement properties of the PEP-mode discharges first developed on JET.[27] In these discharges, a strongly peaked density profile is produced with pellet injection and then heated with ICRH at powers up to 6 MW. A strong transient enhancement of the central plasma parameters in these discharges is found. In particular, the fusion reactivity, central electron pressure, and plasma stored energy have been examined as a function of plasma current and heating power. Figure 4.15 shows these parameters as a function of total input power for a variety of experimental conditions. These results show the strong dependence in the neutron output on input power and an improvement of ~15% in global energy confinement over similar non-PEP discharges. The transport characteristics of these discharges have been analyzed using the TRANSP code. The core diffusivities during the enhanced phase were found to be much lower than in nonpeaked discharges. The improved confinement in these TFTR discharges has not been strongly correlated with core shear reversal as was indicated by the earlier experiments on JET, and this suggests that the improved confinement may be more dependent on high density or a strong density gradient. The enhanced confinement phase in TFTR is terminated by an MHD mode localized off-axis and not by a fast collapse of core pressure as on JET.

4.1.2.2 Tore Supra centrifuge injector

As part of an international collaboration with the Commissariat à l'Energie Atomique, ORNL supplied a centrifuge pellet injector to the Tore Supra tokamak in 1989 and continues to participate in the experiments.[1,2] As pointed out in Sect. 4.1.1.1, the centrifuge pellet injector can inject up to 100 deuterium pellets into a single plasma discharge. Up to 8 pellets/s can be injected at speeds from 0.5 to 0.8 km/s, with sizes ranging from (2–7) $\times$ 10^{20} atoms/pellet. Pellets are formed and injected into the centrifuge accelerator with the Zamboni pellet fabricator (Sect. 4.1.1.1). To date, up to 79 pellets have been injected by the injector into a single 30-s discharge, which is a record number of pellets to be injected in a tokamak plasma. The experimental program currently under way combines repetitive pellet fueling with an ergodic divertor and pump limiters to establish and study long-pulse plasmas in which the pellet fuel source is in balance with the active particle exhaust.

Experiments with the injector have been initiated to investigate the possibility of isotopic tailoring of the plasma by using continuous deuterium pellet fueling and hydrogen gas puffing. This scheme is applicable to ITER, where tritium-rich pellet fueling and deteurium gas puffing may reduce the tritium inventory of the first-wall materials.[28] In addition to the pellet fueling experiments with the centrifuge pellet injector, ORNL has participated in the analysis of PEP-mode experiments on Tore Supra using a two-stage gas gun provided by a French research group.[29] The Tore Supra PEP-mode experiments have been analyzed using the TRANSP code, and the results were compared with q-profile measurements by polarimetry.[30] As in the TFTR results discussed previously, a reduction in core diffusivities was seen, but the measured q profile shows more shear reversal than a neoclassical resistivity model would suggest; this finding requires further research on Tore Supra to determine the responsible physical mechanism for the PEP mode.

4.1.2.3 DIII-D three-barrel, repeating pneumatic injector

The three-barrel, repeating pneumatic injector (Fig. 4.16) used on JET[10–12] from 1987 to 1992 has been modified and installed on DIII-D. For the JET application, the device was equipped with gun-barrel diameters of 2.7, 4.0, and 6.0 mm and was capable of repetitive operation (at 5, 2.5, and 1 Hz, respectively, for each pellet size) under quasi–steady-state conditions

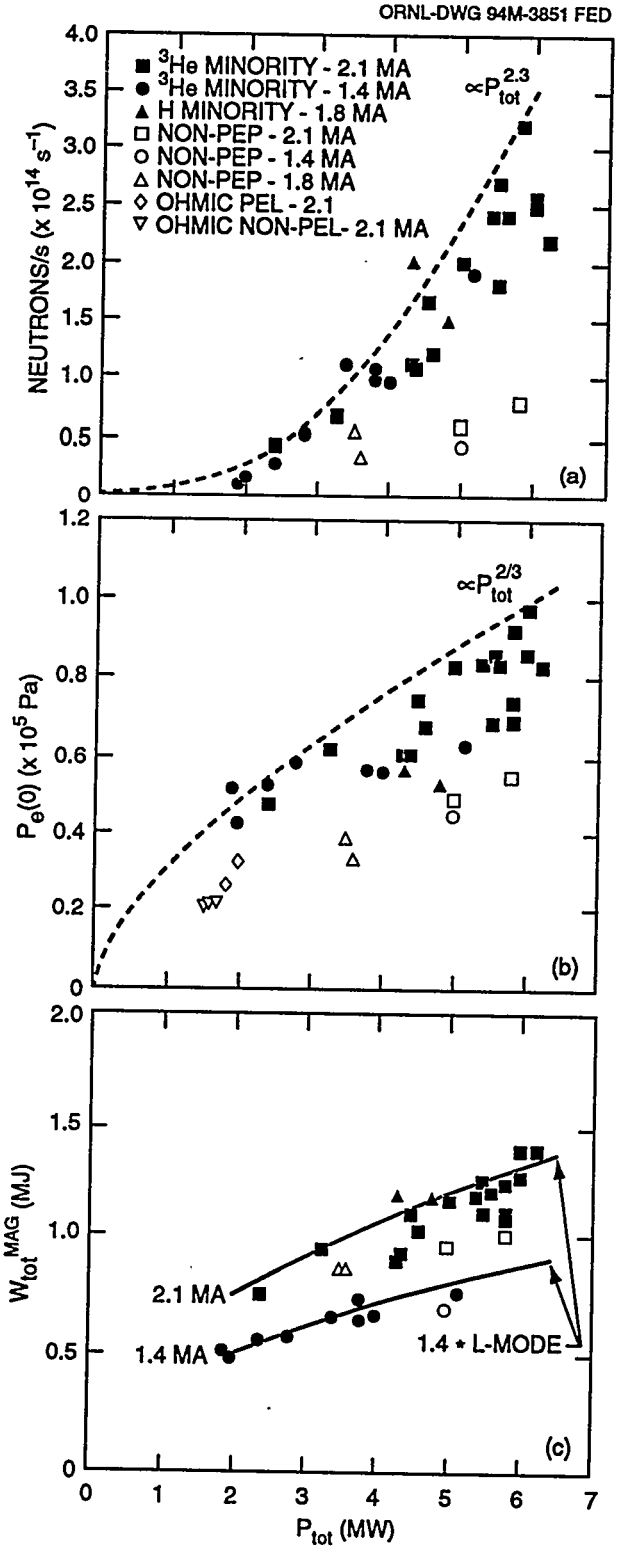

Fig. 4.15. TFTR ICRH PEP and non-PEP discharges with different plasma currents and heating schemes. (*a*) Neutron production rate; (*b*) maximum central electron pressure; (*c*) peak plasma stored energy as function of total input power. Neutron rate is peak D-D neutron emission for the discharge. Solid curves in (*c*) represent Goldston L-Mode scaling for 2.1- and 1.4-MA discharges enhanced by 40%.

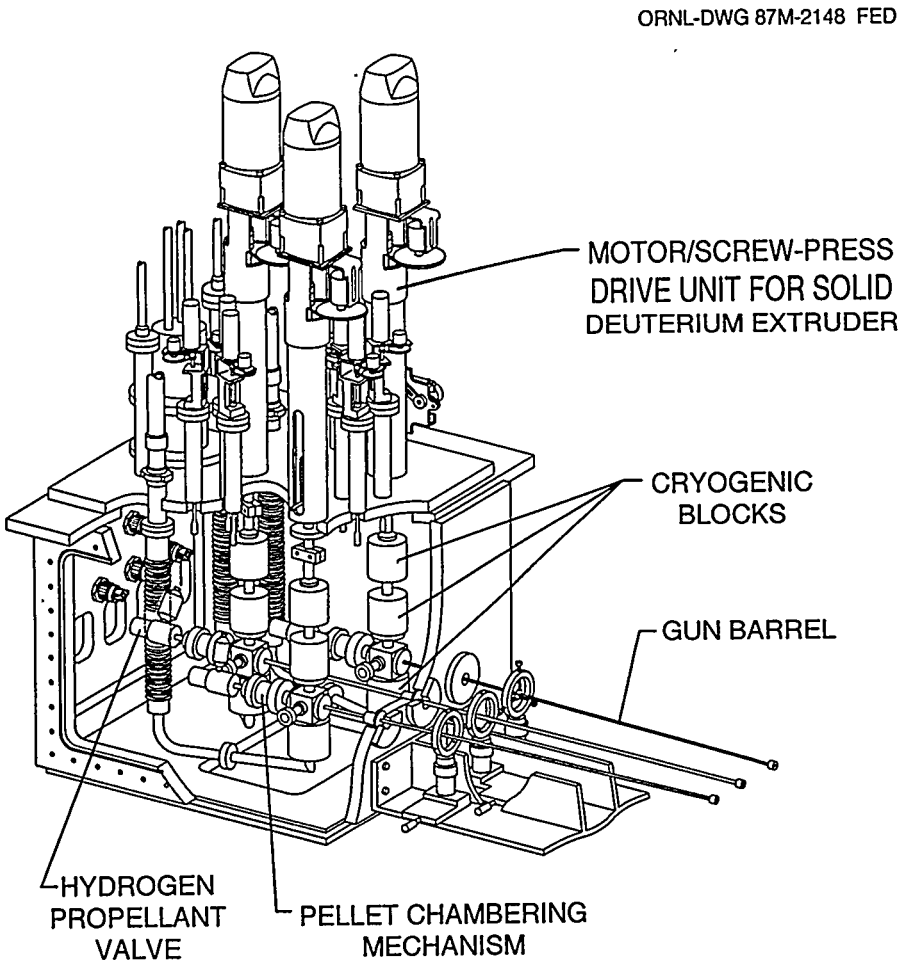

Fig. 4.16. Schematic of three-barrel, repeating pneumatic injector. Used for fueling experiments on JET from 1987 to 1992 and installed on DIII-D in 1994.

(>10 s). A schematic of a single unit and its operation is shown in Fig. 4.3. In this long-pulse fueling device, three separate cryogenic extruders provide continuous streams of frozen hydrogen isotopes to the gun sections, where individual pellets are repetitively formed, chambered, and accelerated. For the DIII-D application, the 6-mm gun was replaced by one with a 1.8-mm-ID barrel[11] and corresponding mechanisms as discussed in Sect. 4.1.1.1. Because JET did not use a conventional delivery system with guide tubes and differential pumping, the injector was also equipped with such a system, including the diagnostics equipment required for measuring pellet parameters. The installation on DIII-D is shown schematically in Fig. 4.17. The three guns have been qualified with helium propellant and deuterium pellets at velocities of ~1 km/s. As mentioned in Sect. 4.1.1.2, the small gun can operate at up to 10 Hz for a pulse length of 15 s.

The injector equipped with gun bores of 1.8, 2.7, and 4.0 mm (nominally 3×10^{20}, 9×10^{20}, and 3×10^{21} D^0 atoms/pellet) was used in some preliminary fueling experiments on DIII-D in 1994 and is scheduled for more experiments during the next few years. Pellet fueling experiments will be performed in which the fuel particle throughput is balanced by the particle exhaust rate through the use of the pellet injector in conjunction with the DIII-D pumped divertor. A major objective of the experimental program will be to demonstrate greater control of the

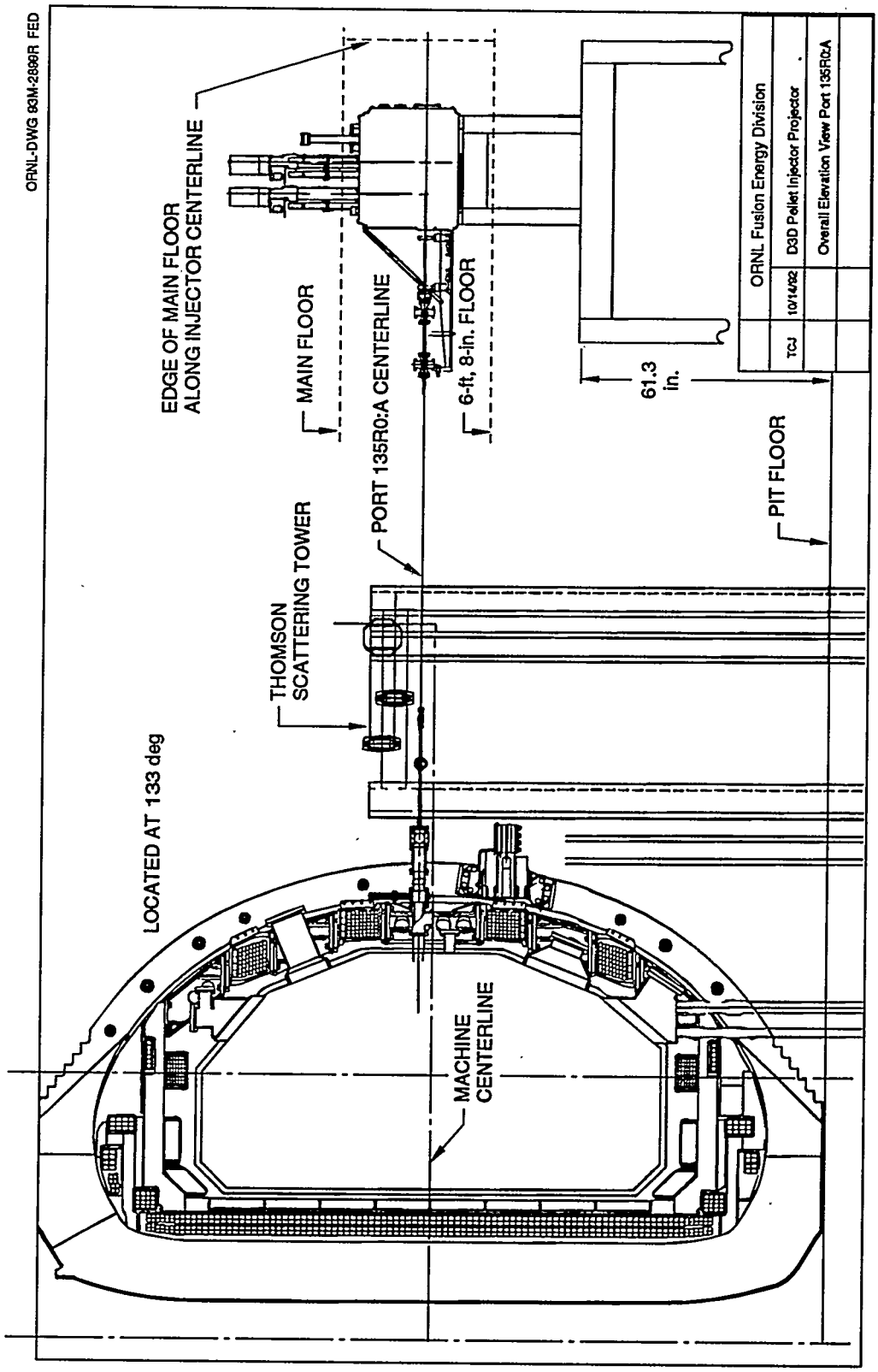

Fig. 4.17. Elevation-view schematic of three-barrel injector installation on DIII-D.

plasma density level and the shape of the plasma density profile than previously achieved under quasi–steady-state gas fueling conditions.

In the preliminary pellet fueling experiments on DIII-D, it was found that injection of pellets into H-mode plasmas triggers ELM-like events at the pellet injection time. These pellet-induced ELMs were found to have a duration and H_a divertor light magnitude similar to nonpellet ELMs. The measured diamagnetic stored energy was also found not to be appreciably affected by the pellet. This information is important for ITER pellet fueling scenarios, where there has been much concern about pellet-induced ELM damage to divertor plates. Pellet-induced ELM activity and long-pulse fueling of diverted plasmas will be studied further in support of ITER design activities.

4.2 RF TECHNOLOGY

F. W. Baity, G. C. Barker, G. L. Bell, T. S. Bigelow, J. B. Caughman, A. Fadnek, W. L. Gardner, R. H. Goulding, G. R. Hanson, G. R. Haste, D. J. Hoffman, R. L. Livesey, D. A. Rasmussin, P. M. Ryan, C. R. Schaich, D. O. Sparks, D. W. Swain, T. L. White, J. J. Yugo, and H. Zhang

4.2.1 Basic Development

4.2.1.1 Folded waveguide

The folded waveguide is an advanced launcher concept for ICRF heating and current-drive applications. Because of its nearly ceramic-free structure and its very high power capability, it has several potential advantages in ITER-like reactors. This concept has been under development at ORNL and is ready for a proof-of-principle test on a tokamak plasma. Designs for a folded waveguide launcher on C-Mod, Tore Supra, PBX, and TFTR have been advanced during this reporting period. Figure 4.18 shows a rear-feed power coupling technique envisioned for a quarter-wavelength design.

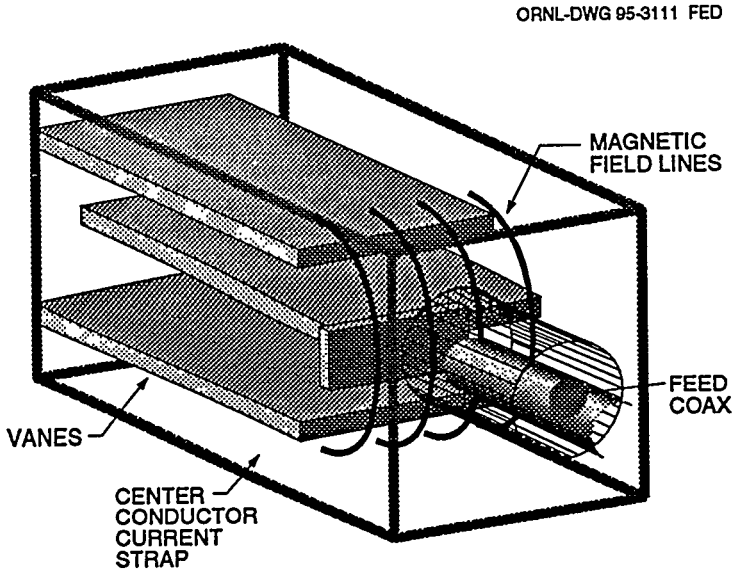

Fig. 4.18. Technique for coupling power to quarter-wavelength folded waveguide from rear. Sliding short forms loop with adjustable area to couple to waveguide magnetic field.

In tests on RFTF, the full-scale folded waveguide has been operated in plasma at power levels up 1 MW at 60 MHz. This value surpasses the previous record, held by the Tore Supra antenna, of 230 kW for a single element. Scaling the observed loading to the estimated value for a tokamak suggests that power levels of several megawatts can be attained. This performance was obtained without a Faraday shield in place to protect the openings in front of the waveguide. A calculation based on the vane toucher position gave a typical peak electric field of 26 kV/cm. Extrapolation to an SOL density of 3×10^{19} gives an incremental loading of ten times the vacuum value, corresponding to an injected power level of 10 MW. Thus, even with some reduction in the plasma density in front of the waveguide in an actual tokamak plasma, the power-handling capability of the device should be very high in comparison to a traditional loop-type launcher. The demonstrated operation without the use of a Faraday shield is very significant because heating of shield elements is likely to be the factor limiting waveguide power handling, especially in an uncooled device, given the demonstrated voltage-handling capability.

A 1/5-scale model of a two-element folded waveguide array was fabricated and operated at 350 MHz. The coupling between the two guides was measured at <1%. In comparison to loop antennas, this reduced coupling would greatly facilitate phasing and matching of an array for use in fast-wave current-drive applications.

4.2.1.2 Advanced launcher development

Identically sized, small-scale benchtop models of folded waveguide, folded stripline, and stacked stripline launchers were fabricated for comparative measurements. The folded stripline is similar to the folded waveguide but has alternate vanes electrically isolated from the cavity and connected together to form a second conductor to support transverse electromagnetic (TEM) two-conductor transmission line modes. The stacked stripline takes this concept a step further by using multiple stripline resonators and current straps stacked poloidally. The important measurement for this preliminary comparison was the relative magnetic field coupled to a loop probe at the output end of the launcher. Both of the stripline concepts seem to have better magnetic flux coupling along the vertical (poloidal) centerline than the folded waveguide. The folded waveguide, in turn, has significantly more flux linkage than loop-type designs. The stacked stripline had the best coupling, though its profile was significantly more peaked, primarily because of the nonoptimized geometry for multiply coupled resonators and the fact that only four of the five resonators were being driven. The features of both stripline designs suggest that they are hybrids of the folded waveguide and loop-type geometries. The key features that make them attractive are the low electric field at the output and the high magnetic flux coupling, which is aided by the fact that several short current straps carry the current rather than one or two long straps, as used in loop-type designs; that is, there is very small current drop because the ratio of the physical length to quarter wavelength is small.

The combline antenna concept was tested in collaboration with General Atomics. The combline antenna has several attractive features, including (1) a small number of power coupling ports, (2) relatively high port loading with concomitant low voltages along the transmission line, and (3) broad phase shift by means of small frequency variations. ORNL provided theoretical calculations, design parameters, and test equipment to General Atomics staff members to study the bench-top operation of the combline antenna at Oak Ridge. Preliminary design work was performed on a combline antenna intended to be tested in the RFTF plasma.

4.2.1.3 Tuning, matching, phase control, and arc detection

Further tests on the full-scale mockup of the DIII-D current-drive antenna array confirmed the ability of the tuning algorithm to predict correct tuner settings to within ±2 cm. A shot-to-shot matching algorithm was developed, which, according to numerical simulation, will converge to a match within two to three shots, using measurements of input impedance at the resonant loop feed points. The simulation combined ORION code calculations on the effect of current phasing on plasma-resistive and -inductive loading with a coupled lossy transmission line model of the antenna and feed circuit.

A conjugate power compensator for the JET A2 four-strap antenna arrays designed at ORNL will be operated on JET during FY 1995. The JET system configuration employs a dedicated power transmitter for each antenna strap. The compensator allows each transmitter to contribute equally to the total array power despite the power transfer between inductively coupled current straps in the antenna array. This increases the power capability of the system when operating at arbitrary relative phasing between elements. The compensator has been integrated into the JET dynamic matching systems, and appropriate control algorithms are being developed and tested. The overall system response under plasma conditions is needed to simplify the control system, improve operational reliability, and determine the necessary responsiveness to plasma variations. More details are given in Sect. 4.2.2.4.

In the area of arc detection and system protection, numerical models were developed to study the dependence of the reflection coefficient on arc characteristics and location. It was shown that up to 50% of the forward power can be coupled into an arc when the measured reflection coefficient is 0.5, and up to 10% of the forward power can be coupled to an arc when the reflection coefficient is 0.1, depending on the impedance and position of the arc. Discrimination techniques based on voltage magnitude ratios and phase shifts were investigated; initial results indicate that voltage magnitude measurement is the more sensitive technique.

4.2.1.4 Microwave reflectometer

The ORNL microwave reflectometer, designed to measure edge density profiles, began operation on TFTR. The analysis technique for the edge profile reflectometer differential phase was improved to allow more consistent inversion of the phase information into radial profiles. The density data compared favorably to the density profiles obtained from both the multichannel interferometer and the Thomson scattering system over the radial regions where the measurements overlap. A similar reflectometer was installed on the upgraded DIII-D antenna.

4.2.1.5 Antenna field measurements

Toroidal and poloidal profiles of rf magnetic field components were made for the DIII-D current-drive antenna array, the folded waveguide antenna, and a full-scale mockup of the TFTR Bay M (PPPL) antenna in 1992. A comparison of the toroidal wave number (k_z) spectra generated by a single strap of the DIII-D antenna with that generated by the folded waveguide showed a large reduction in the effect of sidewall currents in the latter case. Because these currents significantly reduce the directionality of the waves generated by an antenna, the results predict that substantially higher current-drive efficiency can be obtained with a folded waveguide array than with a loop array, which has septa between straps to reduce inductive coupling. Measurements on the Bay M mockup indicate that the sidewall slots are not very effective in increasing magnetic flux or reducing the effect of sidewall currents on the antenna k_z spectrum. These results suggested that the factor of 5–6 difference in loading observed between the Bay M and Bay L

(ORNL) antennas was primarily the result of differences in antenna cavity width, which is governed by the port size, and differences in the distance between the current strap and the plasma distance. ORNL analysis also indicated that properly designed slots can be made effective. These results were incorporated into the designs of new Faraday shields.

Radio frequency magnetic fields and scattering parameters were also measured using the JET "flatbed" A_2 antenna mockup. The amplitude and phase of the rf magnetic field in the toroidal direction (B_z) were measured at a series of 1800 grid points in a plane parallel with the Faraday shield surface and 2 cm above the shield. The measurement at this distance clearly showed significant induced currents at the septum and the ends of the antenna box at a distance 2 cm from the surface of the Faraday shield. The depressions in the field above the "doughnut holes" in the outer straps were also clearly seen. Both of these features produce modes with high poloidal or toroidal mode numbers, so they rapidly disappear with increasing distance from the antenna. Comparisons of these measurements with numerical modeling are shown in Figs. 4.19 and 4.20.

4.2.1.6 Faraday shield studies

Faraday shield losses were measured on a scaled cavity antenna model with elements composed of various materials. It was found that the loading varied as the square root of the resistivity of the surface material, which is expected from a simple model that takes skin depth effects into account. It was also found that for a "tilted" shield, with elements at an angle to the current strap of 75° rather than 90°, the losses increased by only 10 to 14%.

Good results were obtained in long-pulse tests of the bent-tube Faraday shield mounted on the single-strap Development Antenna. The goal of these tests was to operate the antenna in RFTF and observe the heating from rf losses in the uncooled shield during pulses up to 30 s. This shield has a single-tier open design with large spacing between elements, which minimizes rf losses. The shield was run with copper-plated, TiC,N-coated stainless-steel tubes for pulse lengths up to 20 s at a power level of 40 kW. In this case the shield loading is only 60 mΩ, so this amount of power corresponds to a maximum antenna voltage of >42 kV and maximum antenna current of 1050 A rms. An IR camera was used to monitor temperatures, which reached a maximum of 290°C at the end of a series of 17 pulses. The maximum temperature rise during a pulse was 50°C.

A small rf inductive plasma source was built to test erosion of candidate Faraday shield materials as a function of rf sheath potential. The source has been operated in argon and hydrogen plasmas at pressures from 0.5 to 10 mTorr. Initial experiments with copper target material showed good agreement between measured and predicted sputtering rates as a function of sheath potential. The effects of operating pressure on the sputter yield and surface morphology also agreed with published results. The erosion rate as a function of rf sheath potential will be determined for a variety of candidate Faraday shield materials. Initial emphasis will be on plasma-sprayed boron carbide and other plasma-sprayed coatings. A technique that uses surface collector probes to measure average incident ion energy will be developed on the erosion tester plasma source. The technique will then be used to measure average ion energies incident on an antenna Faraday shield in the RFTF plasma.

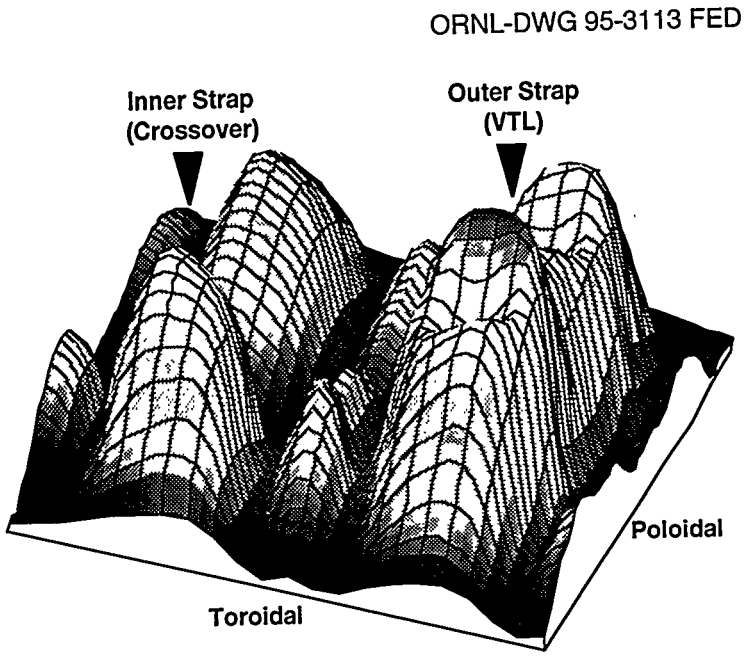

Fig. 4.19. Measurements of toroidal component magnitude of rf magnetic field generated by JET A2 flatbed antenna. Measurements made at 35 MHz, monopole phasing, 1.5 cm in front of Faraday shield.

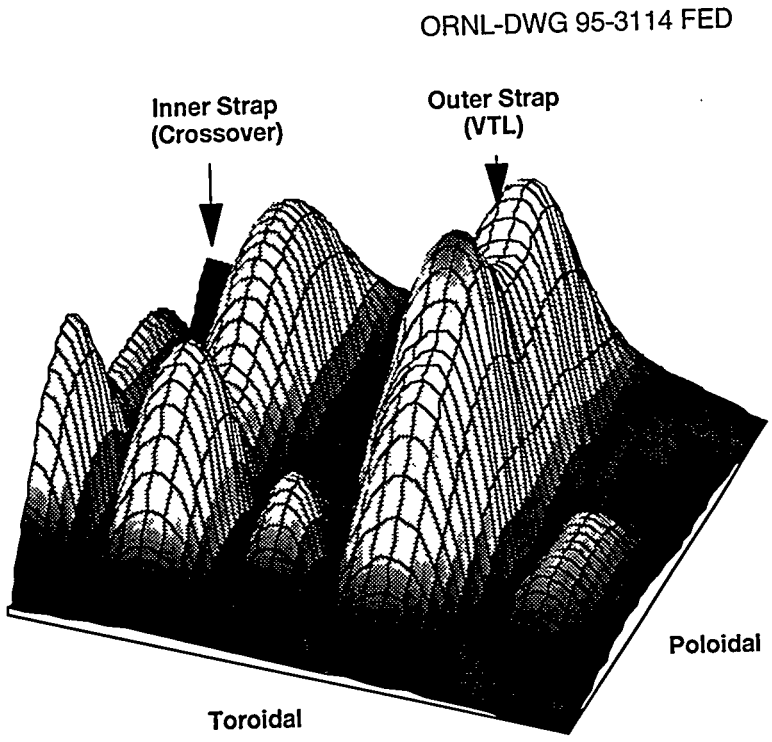

Fig. 4.20. Magnitude of rf magnetic field calculated using ARGUS code to model JET A2 flatbed antenna. Compare to measured fields in Fig. 4.19.

4.2.2 Rf Projects

4.2.2.1 Tore Supra

The ORNL antenna for Tore Supra was shipped to France during September 1989. Following extensive off-line testing and repairs that were made as a result of an accident on the test stand, the antenna was installed on Tore Supra in October 1990, along with the two French-built antennas of nearly identical design. The ORNL antenna was first operated on Tore Supra in 1991.

Up to 4 MW of rf power at 57 MHz was coupled to ohmic target plasmas in 1992, both with a single antenna and with two of the three ICRF antennas. Increases in plasma energy content resulting from both ion and electron heating were observed, along with the reduction in loop voltage expected from the lower resistivity. The Z_{eff} increased because of the higher impurity content, which was predominantly contributed by carbon, although there was a metallic contribution as well. High-power ICRF led to long-period ("monster") sawteeth. Modification of the vacuum feedthrough for the transmission line permitted replacement while the antenna was installed on the tokamak, which significantly decreased the downtime for replacement of that vulnerable item.

The high-power vacuum capacitors failed during 1992, which was a significant technical problem. The cause was determined to be vacuum leaks that resulted from water corrosion of the bellows material. In the short term, the same material will be used for the bellows, but the water-facing side will be gold-coated to extend its lifetime. In the longer term, a new material will be developed to better withstand corrosion. As a result of changes to the design of the 30-Ω Tore Supra vacuum feedthrough end caps, six feedthroughs without leaks have been produced to date, two of which have been installed and are currently operating on the ORNL long-pulse ICRF antenna at Tore Supra.

Damage to the bumper limiters of all antennas was observed during the ICRH pulses, as was heating of the uncooled septum (between the two current straps) in the ORNL antenna. Simultaneously, an increase in metal impurities in the plasma was observed. Therefore, the French antennas were upgraded using an alternative design, employing a water-cooled copper limiter with boron carbide (B_4C) coating. In addition, a long-pulse Faraday shield was designed for the ORNL antenna on the Tore Supra experiment. This shield design has improved cooling for long-pulse capability, and it has a reduced septum length, which improves the spectral directionality under phased operation and reduces anomalous rf/plasma-induced heating. The shield is coated with B_4C to reduce further any impurity generation. The reduced septum length is the major difference between this design and the upgraded French Faraday shield designs and offers the basis for direct comparison of antennas to appraise the anticipated benefits of this concept. Fabrication of the long-pulse Faraday shield was completed in 1994, and it will be installed on Tore Supra in early 1995.

4.2.2.2 DIII-D

The ORNL four-strap ICRF current-drive antenna array was installed on schedule in the DIII-D tokamak in June 1992. In initial tests it was operated at power levels up to 1.85 MW in a minority-ion heating mode (deuterium plasma with 5 to 10% hydrogen, currents phased at $0,\pi,0,\pi$, f = 32 MHz). Increases of ~300 eV in ion and electron temperatures were observed in these tests. Loading was observed to be 1.2 Ω, with a gap of 2 cm between the plasma and outside limiter. The resonant loop configuration allowed easy matching within one to two shots.

Next, the direct absorption of fast waves at 60 MHz was verified in low-density plasmas at 1 T with the antenna array phased symmetrically. It was determined that a threshold of about 1 keV in the electron temperature was required to achieve significant absorption of the rf waves. Strong single-pass absorption of the rf waves is desired for fast-wave current drive, because the directionality of the waves may be compromised by multiple passes in the plasma. The absorption of the waves increases with increasing electron temperature, so the highest current-drive efficiency is expected during high-power ECH. However, the high cost of operating the electron cyclotron system limited availability to one DIII-D run period during the phased experiments following the symmetric phasing runs.

Following these ion and electron heating experiments, the first attempts to drive current with fast waves were made with the antenna elements phased at 90°. In shots both with and without ECH, reductions in the tokamak loop voltage were observed that were in excess of expectations based on increased electron temperature and the bootstrap effect, thus indicating probable fast-wave current drive. The rf power in these experiments was mainly limited to 1.1 MW because of voltage limitations in the transmission line system, and the electron temperatures were less than optimal because of inoperative waveguides in part of the ECH system. Nevertheless, fast-wave current drive on the order of 135 kA was observed. The loop voltage drop observed in the counter-current drive phasing is thought to be the result of time-dependent profile changes in the plasma, with no rf-driven current.

The double-tier TiC,N-coated Faraday shield was removed in late 1991 for a test of operation without a Faraday shield. Experiments without a Faraday shield showed that shieldless antenna operation is possible without catastrophic impurity influx. These experiments were performed in the "heating" mode (i.e., with nondirectional phasing between straps). The plasma loading was increased somewhat over the loading with the Faraday shield installed. A key issue for operation without a Faraday shield is whether impurity generation from the antenna, chiefly copper, would be detrimental to plasma operation. The preliminary conclusion, for $0,\pi,0,\pi$ phasing, was that impurity production is insignificant. The power level achieved was less than half of the record 1.7 MW achieved with the Faraday shield in place. The antenna was next fitted with a new single-tier B_4C-coated Faraday shield with rods tilted at 12° to match the pitch of the toroidal magnetic field lines at the antenna location. The B_4C coating was used to help reduce impurity generation during current-drive experiments at 90° phasing. The new shield was designed to increase both the mutual coupling between adjacent antenna elements and the plasma loading resistance.

Preliminary tests of a decoupler for the fast-wave current-drive antenna were conducted in 1993. These tests used a 3 1/8-in., 3-dB coupler from ORNL connected to the tees in the two resonant lines. The tees are located at high-voltage points in the line, so the test was limited to power levels below 200 kW, which nevertheless was sufficient to demonstrate the principles of the concept. With the decoupler at a high-voltage point, the two feed lines both see the same impedance even for directional phasing of the antenna, so the phase should be adjustable by changing a single phase shifter. In fact, the decoupler worked as expected. The decoupler system was carefully tuned in vacuum, at minimal loading, and the only tuning required for plasma operation was to adjust the primary tuners for the increased plasma loading resistance. The two feed lines remained nearly independent and symmetric, indicating that the plasma did not change the mutual coupling of the antenna appreciably.

Following the successful operation with the prototype decoupler, a simplified high-power decoupler was installed. With this decoupler, operation at higher power (up to 1.5 MW) than achieved previously was demonstrated, and power was sustained up to the joule limit of the antenna. The array phasing was varied in 90° increments on successive shots without retuning. During this run the toroidal magnetic field was reversed from its usual direction to facilitate

low-density operation without H-mode. One consequence of reversed-field operation is that the tilt of the Faraday shield is opposite the tilt of the field lines at the antenna location; however, this did not affect heating or impurity production in any obvious way.

Two new long-pulse, fast-wave current-drive antennas (Fig. 4.21) designed by ORNL were installed on DIII-D in February 1994. The new antennas are designed to handle up to 4 MW each for pulse lengths up to 10 s. For structural strength, the antennas are constructed almost completely of Inconel 600. They are equipped with a single-tier B_4C-coated Faraday shield. All interior surfaces of the antennas are nickel plated to improve electrical conductivity and to reduce the time required (compared to copper- or silver-plated structures) for conditioning the antennas to full voltage. With the exception of the Faraday shield, all components of the antennas are water cooled to accommodate the 10-s pulse-length requirement. The new antennas operate at 30 to 120 MHz. Fabrication of these antennas was compressed to 12 months by dividing the work between ORNL and General Atomics and by foregoing any high-power rf tests before installing them on DIII-D.

ORNL-DWG 95-3112 FED

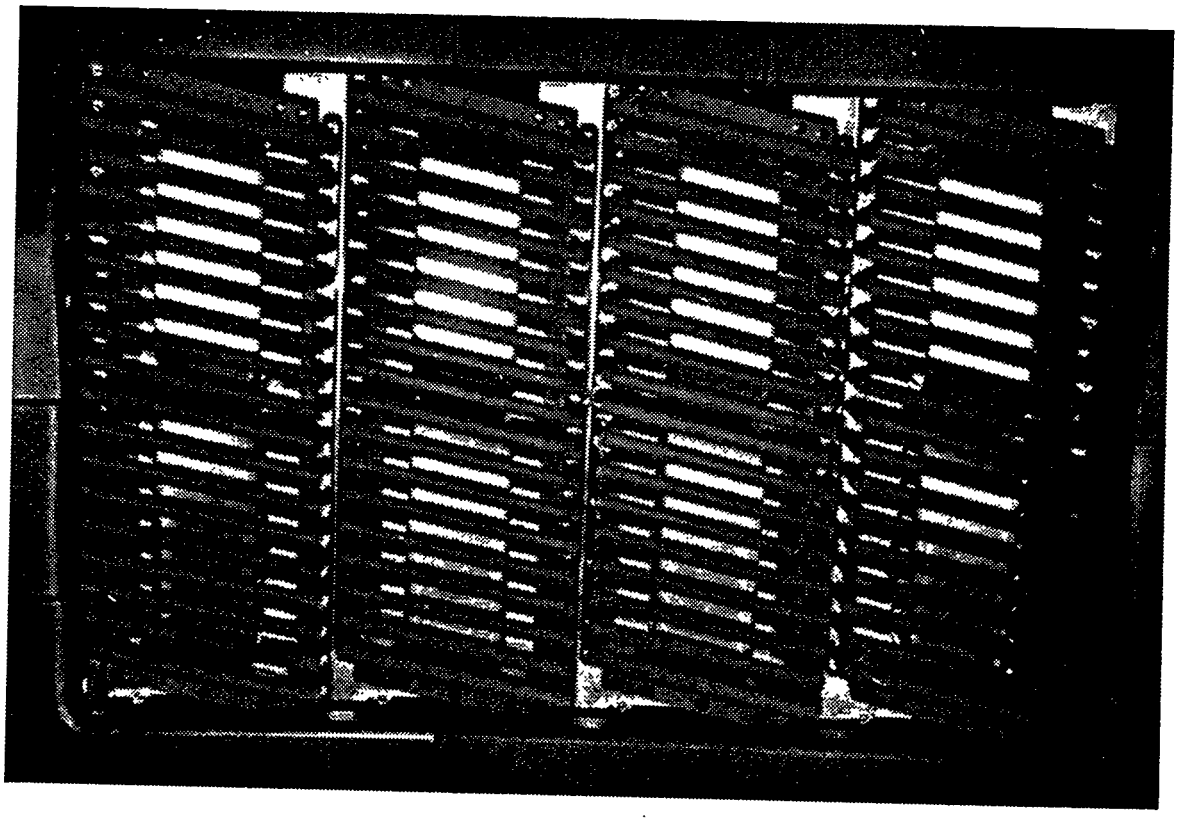

Fig. 4.21. Long-pulse antenna for fast-wave current drive on DIII-D. Array designed to operate at up to 4 MW for 10-s pulses over 30–120 MHz frequency range.

4.2.2.3 JET

JET shipped full-scale mockups of the new JET A2 antennas to ORNL for extensive electrical measurements in 1992. Scattering parameters, current distributions, magnetic field patterns, and induced Faraday shield currents were measured for a single pair of straps and, later, for the full complement of four straps. Results of these measurements were also used to test and refine antenna design codes and to provide input into the design and evaluation of the JET power compensator.

A power compensator was designed for use on the JET A2 antennas. Such a compensator will be inserted between lines 1 and 4 of each four-element strap array and will offset the power transferred along the mutually coupled antenna structure during directional phased operation. Each power compensator consists of a 3-dB directional coupler and two tuning/matching capacitors. The DIII-D four-strap mock-up antenna was bench-tested to ensure proper operation. The design was favorably received at a preliminary design review at JET in March 1992.

On-site participation at JET began in 1994. A dedicated PC was set up primarily for running SIMULINK-based, time-dependent models of the control systems for the A2 antennas. Simulations were run to check the feasibility of different techniques for system operation. For instance, the attainment of phased antenna operation by ramping the phase over a 1-s time period while maintaining a match using frequency, stub, and trombone tracking was simulated before being tested on the plant. SIMULINK was also used to test a phase correction circuit for use in the Mk II phase control circuits. The time dependence was increased considerably when the FORTRAN version of the antenna–transmission line model was linked into it.

The FOCSL code was modified so that it could be run in the control room. It has been used successfully to predict reasonable initial values for trombone settings and frequency during plasma operation. With scattering parameters measured on the torus, it was also used to predict vacuum match settings with a maximum error of 30 cm (150 kHz) during initial matching trials. An improved antenna model has been rewritten so that it can be run using PV-WAVE, and it has been incorporated into the FOCSL matching code. The model includes capacitive coupling between straps and self-coupling between different regions of the same strap. The FOCSL code was used successfully to predict the amount of phase error introduced by controlling phase on the matched section of the line and to confirm the feasibility of phase control using the phase of the forward voltage only on the unmatched line section.

Experience gained during past participation in commissioning and operating ICRF-related systems will be very helpful in further collaborative efforts in conjugate box commissioning and operation and phased antenna operations. We have participated directly in several important steps in the commissioning of the new antenna systems. These include the first high-power antenna conditioning, which was achieved using an external ramped reference waveform. Another was the first high-power antenna operation in plasma; during this session the magnetic-field–dependent multipactor "barrier" was broken for the first time, and a module input power >2 MW was achieved. A third was the first demonstration of tracking into a match starting from a large mismatch ($\rho > 0.5$) using frequency, trombone, and stub tracking. Finally, we initiated the first trial of phased operation in plasma using an A2 antenna module.

4.2.3 Rf Modeling

4.2.3.1 Electrical representation of antennas

The goal of the work on electrical representation of antennas was to model the antenna as a coupled transmission line that could reproduce the system behavior as a function of frequency, load, and phasing. Such an antenna model could be integrated into the overall power transmission system, facilitating design of the tuning, matching, phase control, and power compensation system and permitting the use of real-time control algorithms. The effort to analyze the JET A2 and the new DIII-D antenna arrays can be summarized as follows:

1. The antennas were divided into a number of coupled sections; 2-D and 3-D magnetostatic codes were used to calculate the inductance and capacitance matrixes for each section. These techniques had proved accurate in the past for calculating such parameters for simpler antenna geometries such as those used on TFTR, Tore Supra, and DIII-D. This was the first test of whether such calculations could be extended to asymmetric antenna geometries with strong internal coupling.
2. The parameters so calculated were used in a code that solved the coupled transmission line model of the antenna by iterative techniques. This code proved quite accurate over the frequency range of interest, although discrepancies with measurements on the JET A2 mock-up appeared at the higher frequencies, where the double straps approached full-wave resonance (>55–60 MHz for the JET antennas). The currents and voltages at the port were translated into scattering parameters and used to represent the antenna in the transmission system models.
3. A new transmission line code was written in MATLAB, which solved the coupled transmission line model equations analytically, permitting the antenna to be directly incorporated into the analysis of the overall transmission line system. The results of this code, using the same parameters, also agreed more closely with measurements on the JET A2 mock-up at the higher frequencies than the iterative code did. Figure 4.22 compares calculated scattering parameters with measurements.

This work showed that complex antenna geometries with a high degree of internal coupling can still be modeled as coupled transmission lines and that the techniques developed to calculate transmission line parameters in simpler geometries can be extended to these cases. The JET antenna model can easily be incorporated into the overall control system, including the power compensator and associated feedback control loop, which is modeled with the time-dependent, MATLAB-based SIMULINK program. This time-dependent system model has been used to finalize the system design and to determine the necessary control system variables and their implementation. The code has been accelerated by rewriting some sections in FORTRAN, making it likely that a version can run between shots in the JET control room.

4.2.3.2 Antenna field calculations

The magnetic field distributions of the two-strap JET A2 mockup antenna were calculated with ORNL 3-D codes and agreed well with measurements. The issue of determining the voltage distribution on antenna structures was addressed in three phases:

1. The difference in voltage distribution between adjacent Faraday shield elements was calculated from the time-varying magnetic flux that passed between them. Such a calculation was used in the design of the DIII-D Faraday shield.

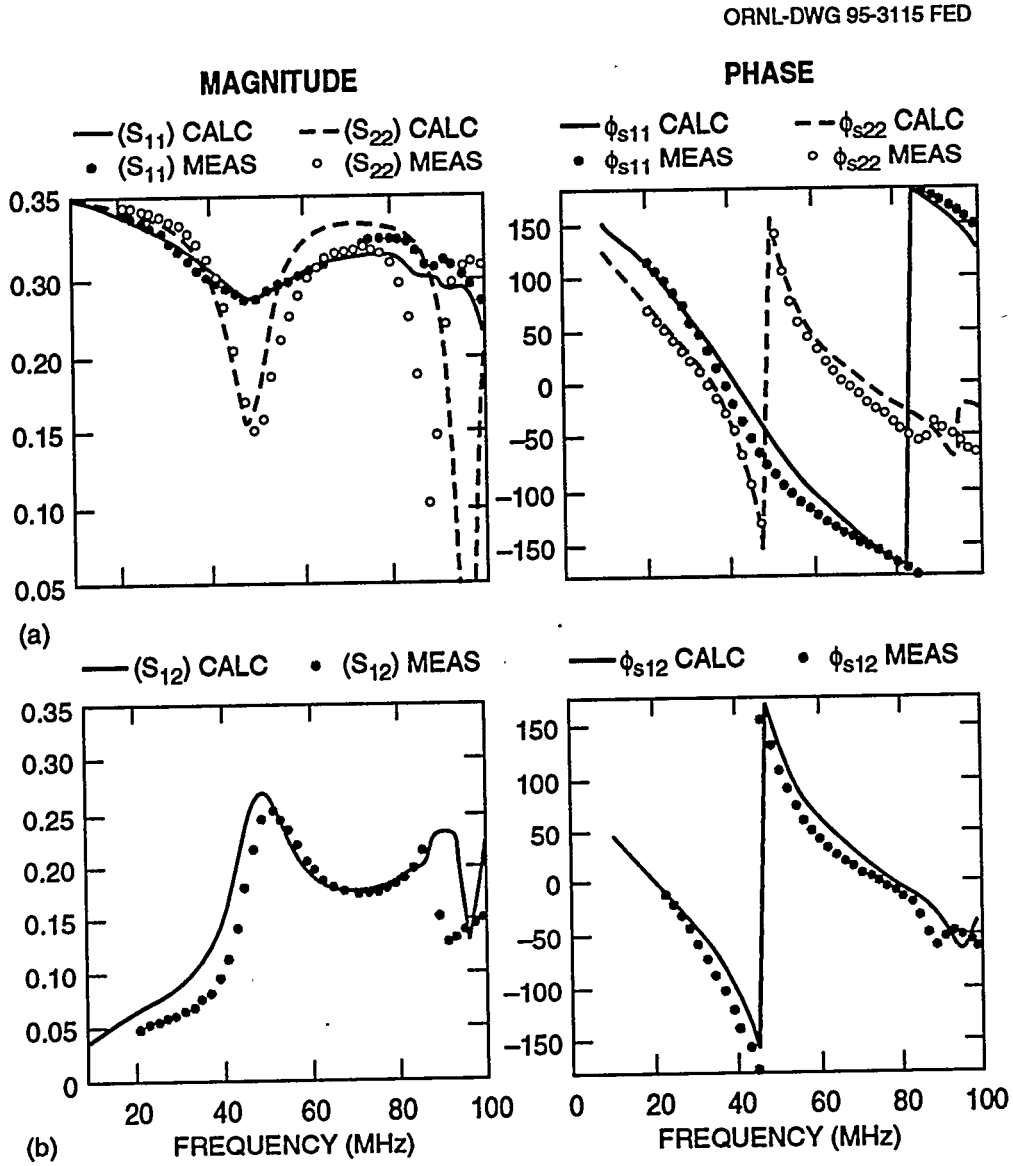

Fig. 4.22. Comparison of measurements and modeling of JET A2 flatbed antenna. (*a*) Magnitude and phase of reflection coefficients for outer (S_{11}) and inner (S_{12}) straps. (*b*) Magnitude and phase of transmission coefficient (S_{12}) between outer and inner strap.

2. The voltage distribution on the antenna frame was calculated by modeling the antenna as an unbalanced two-conductor transmission line. The frame inductance of the DIII-D mockup was calculated and used to determine the frame potential distribution, which agreed with measurements.
3. The potential distribution on the surface of the Faraday shield elements was calculated by integrating the eddy currents induced on the shield. These currents were calculated with the ORNL 3-D Faraday shield code.

The purpose of this work is to determine the voltage distribution on the antenna structure; these voltages are the driving mechanism for rf sheaths, one of the primary sources of impurity production and plasma-related antenna heating.

4.2.3.3 Three-dimensional electromagnetic analysis

Plasma-loading calculations for the TFTR ICRH antenna were performed using the density profile data obtained from the ORNL microwave reflectometer. The agreement between the measured data obtained using 2-D and 3-D analyses (RANT2D and RANT3D) was quite good for dipole phasings, provided that the 2-D results were properly modified by the "end-effects," obtained with an independent 3-D calculation. However, only a full 3-D treatment provided proper return-current paths when monopole phasing was employed. The 3-D loading agreed well with measurements; the 2-D calculations were a factor of 2 higher than the 3-D calculations. This exercise not only validated the RANT3D antenna design code but also emphasized the importance of being able to calculate all the circuit transformations required for accurate comparison with measurements.

Evaluation of the Science Applications International Corporation (SAIC) ARGUS3D electromagnetic code continued in a collaboration with Y. L. Ho of SAIC in San Diego. A new analysis technique was developed to transform the currents and voltages calculated by ARGUS into the electrical parameters required by system antenna models. The DIII-D four-strap antenna array was used as an example to demonstrate that the characteristic impedance, phase velocity, and mutual coupling parameters calculated with these transformation techniques are virtually identical with those calculated using the ORNL 3-D magnetostatic codes.

Folded waveguide modeling using the VARGUS code was carried out for the Alcator C-Mod launcher. The initial effort was to treat the folded waveguide as a closed resonant cavity and calculate the first few eigenfrequencies and their related field structure. The calculations were checked against measurements on a small mock-up waveguide and showed good agreement; the measured-to-calculated resonant frequencies were 387.68 to 386.20 MHz, 635.11 to 639.38 MHz, and 796.96 to 795.61 MHz. After this validation, the code was used to calculate resonant frequencies and internal field structures for the various C-Mod folded waveguide designs.

REFERENCES

1. C. A. Foster et al., p. 275 in *Proceedings of the IAEA Technical Meeting on Pellet Injection and Toroidal Confinement, Gut Ising, Federal Republic of Germany, 24–26 October 1988,* IAEA-TECDOC-534, IAEA, Vienna, 1989.

2. C. A. Foster et al., p. 496 in *Fusion Technology 1992*, Vol. I, proceedings of the 17th Symposium on Fusion Technology, held in Rome, Italy, 14–18 September 1992, North-Holland, Amsterdam, 1992.

3. S. K. Combs, S. L. Milora, C. R. Foust, C. A. Foster, and D. D. Schuresko, *Rev. Sci. Instrum.* **56**, 1173 (1985).

4. S. K. Combs, S. L. Milora, C. R. Foust, G. L. Schmidt, and T. P. McBride, *J. Vac. Sci. Technol. A* **4**, 1113 (1986).

5. S. K. Combs et al., *Rev. Sci. Instrum.* **58**, 1195 (1987).

6. S. K. Combs, *Rev. Sci. Instrum.* **64**(7), 1679 (1993).

7. S. K. Combs, S. L. Milora, L. R. Baylor, C. R. Foust, F. E. Gethers, and D. O. Sparks, *J. Vac. Sci. Technol. A* **6**, 1901 (1988).

8. S. L. Milora, S. K. Combs, L. R. Baylor, C. R. Foust, F. E. Gethers, and D. O. Sparks, pp. 784–86 in *Proceedings of the 12th Symposium on Fusion Engineering, Monterey, 1987,* IEEE, New York, 1987.

9. P. Kupschus, W. Bailey, M. Gadeberg, L. Hedley, P. Twynam, T. Szabo, and D. Evans, pp. 780–83 in *Proceedings of the 12th Symposium on Fusion Engineering, Monterey, 1987,* IEEE, New York, 1987.

10. S. K. Combs, T. C. Jernigan, L. R. Baylor, S. L. Milora, C. R. Foust, P. Kupschus, M. Gadeberg, and W. Bailey, *Rev. Sci. Instrum.* **60**, 2697 (1989).

11. S. K. Combs, C. R. Foust, and S. L. Milora, *Rev. Sci. Instrum.* **66**(3), 2736 (1995).

12. S. K. Combs, S. L. Milora, C. R. Foust, M. J. Gouge, D. T. Fehling, and D. O. Sparks, *J. Vac. Sci. Technol. A* 7(3), 963–67 (1989).

13. S. K. Combs, C. R. Foust, M. J. Gouge, and S. L. Milora, *J. Vac. Sci. Technol. A* **8**(3), 1814–19 (1990).

14. S. K. Combs, C. R. Foust, D. T. Fehling, M. G. Gouge, and S. L. Milora, *Rev. Sci. Instrum.* **62**(8), 1978–89 (1991).

15. A. Frattolillo et al., pp. 505–09 in *Fusion Technology 1992,* proceedings of the 17th Symposium on Fusion Technology, held in Rome, Italy, September 14–18, 1992, eds. C. Ferro, M. Gasparotto, and H. Knoepfel, Vol. I, North-Holland Elsevier Science Publishers B. V., Amsterdam, 1993.

16. A. Frattolillo et al., p. 721 in *Proceedings of the 14th Symposium on Fusion Engineering, San Diego, 1991,* Vol. 2, IEEE, New York, 1992.

17. A. Frattolillo et al., p. 500 in *Fusion Technology 1992,* Vol. I, proceedings of the 17th Symposium on Fusion Technology, held in Rome, Italy, September 14–18, 1992, North-Holland, Amsterdam, 1992.

18. S. K. Combs et al., p. 583 in *Proceedings of the 15th Symposium on Fusion Engineering, Hyannis, MA, 11–15 October 1993,* Vol. 2, IEEE, New York, 1993.

19. S. K. Combs et al., "Pellet Injector Research and Development at ORNL," p. 637 in *Fusion Technology 1994,* Vol. I, proceedings of the 18th Symposium on Fusion Technology, held in Karlsruhe, Germany, August 22–26 1994, North-Holland, Amsterdam, 1995.

20. C. C. Tsai, C. A. Foster, S. L. Milora, and D. E. Schechter, pp. 724–28 in *Proceedings of the 14th Symposium on Fusion Engineering, San Diego, 1991,* IEEE, New York, 1991.

21. C. C. Tsai, C. A. Foster, S. L. Milora, D. E. Schechter, and J. H. Whealton, *J. Vac. Sci. Technol. A* **11**, 1252–57 (1993).

22. P. W. Fisher et al., *J. Vac. Sci. Technol. A* **7**, 938 (1989).

23. P. W. Fisher, *Fusion Technol.* **21**, 794 (1992).

24. M. J. Gouge et al., *Fusion Technol.* **21**, 1665 (1992).

25. G. W. Barnes et al., *Fusion Technol.* **21**, 1662 (1992).

26. S. L. Milora et al., p. 579 in *Fusion Technol. 1992,* Vol. I, Proceedings of the 17th Symposium on Fusion Technology, held in Rome, Italy, September 14–18, 1992, North-Holland, Amsterdam, 1992.

27. The JET Team (G. L. Schmidt), p. 215 in *Plasma Physics and Controlled Nuclear Fusion Research,* proceedings of the 12th International Conference, held in Nice, France, 1988, IAEA, Vienna, 1989.

28. M. J. Gouge et al., "Fuel Source Isotopic Tailoring and Its Impact on ITER Design, Operation and Safety" accepted for publication in *Fusion Technol.*

29. J. P. Perin, G. Claudet, and F. Disdier, *Rev. Sci. Instrum.* **65**(2), 430 (1994).

30. X. Garbet et al., *Transport and Turbulence in Tore Supra,* IAEA-CN-60/A2-III-4, IAEA, Vienna, 1994.

5

INTERNATIONAL THERMONUCLEAR EXPERIMENTAL REACTOR

N. A. Uckan

C. C. Baker[1]
E. E. Bloom[2]
T. W. Burgess[3]
D. L. Conner[4]
L. Dresner
C. A. Flanagan
P. J. Fogarty[4]
J. D. Galambos[5]
M. Gildner[6]
P. L. Goranson[4]
M. J. Gouge
J. R. Haines
J. N. Herndon[3]
J. T. Hogan
W. A. Houlberg
G. Johnson[4]
T. Kring[3]
D. C. Lousteau[4]
J. W. Lue
M. S. Lubell
S. L. Milora
B. E. Nelson[1]
B. W. Riemer[4]
A. F. Rowcliffe[2]
R. T. Santoro[7]
R. O. Sayer[5]
J. H. Schneibel[3]
D. J. Strickler[5]
D. W. Swain
D. J. Taylor[4]
D. E. Williamson[4]
S. J. Zinkle[3]

1. Present address: University of California at San Diego.
2. Metals and Ceramics Division.
3. Robotics Division.
4. Engineering Division.
5. Computing and Telecommunications Services.
6. ORNL QA Program.
7. Engineering Physics and Mathematics Division.

5. INTERNATIONAL THERMONUCLEAR EXPERIMENTAL REACTOR

Summary of Activities

The International Thermonuclear Experimental Reactor (ITER) program was prompted by international agreements in 1986 for cooperation on the design of a fusion test reactor. A three-year joint conceptual design activity (CDA) among the United States, the European Atomic Energy Community (Euratom), Japan, and the Russian Federation (former Soviet Union) was successfully completed in December 1990. The CDA established a reactor configuration, agreed on by the four parties, as the basis for the next project phase, the engineering design activity (EDA), started in late 1992. The CDA also established a multiyear research and development (R&D) plan for the major reactor systems to be conducted in conjunction with the EDA. The aim of the EDA is to produce a detailed, complete, fully integrated engineering design and all technical data necessary for a decision on construction of ITER. The ITER EDA is a six-year program during which the U.S. institutions, through the U.S. Home Team, will cooperate with Euratom, Japan, and the Russian Federation and will contribute to the activities of the Joint Central Team (JCT) at one of the three joint work sites (San Diego, California; Garching, Germany; Naka, Japan).

Oak Ridge National Laboratory (ORNL) has been a major contributor to the U.S. effort during the CDA and continues to be a major contributor to the EDA. ORNL ITER program elements include engineering design, physics support, technology R&D, Home Team management support, and industrial subcontracts. The ITER design and R&D activities draw on major strengths of ORNL. The ORNL ITER program has an annual budget of about 20% of the total U.S. ITER resources and has been spread among eight divisions (Fusion Energy, Metals and Ceramics, Robotics and Process Systems, Central Engineering, Computing Applications, Atomic Physics, Instrumentation and Controls, and Engineering Physics and Mathematics) and two industrial consortia (the Rockwell-General Atomics-CIMCORP consortium for remote handling and the Pitt-Des Moines-Grumman consortium for vacuum vessel). In the Unites States, the ORNL program has been assigned leadership in several design and R&D areas, including materials, remote handling, containment structures, configuration and design integration, rf heating, pellet fueling, quality planning, plasma performance, and physics-safety interface. In addition, four ORNL employees serve as members of the JCT, each working at one of the three joint work sites.

5.1 ITER HOME TEAM MANAGEMENT

5.1.1 U.S. Home Team Management Activities

U.S. Home Team management has operated since 1991. ORNL hosted the Project Office of the U.S. Home Team during the major portion of this report period. The U.S. Home Team Leader (HTL), C. C. Baker, and Deputy HTL, C. A. Flanagan, were from ORNL.

The HTL is responsible to the ITER director for executing ITER tasks assigned to the United States and to the DOE Office of Fusion Energy (OFE), for planning and integrating the U.S. efforts in execution of assigned tasks. The U.S. HTL is responsible for planning and integrating all of the Home Team activities and is the primary point of contact with the ITER Director for the U.S. Home Team on all technical matters relating to ITER.

Specific U.S. Home Team management tasks completed during the period included the following:

- The organization of the U.S. Home Team was completed, drawing upon expertise from all of the national laboratories and universities in the United States that are significantly involved in the magnetic fusion program.
- Significant U.S. industry participation in the ITER EDA was achieved through competitively bid contracts in the major design and R&D areas of superconducting magnets, plasma-facing components, blankets, vacuum vessels, and remote handling. The latter two areas are led by ORNL.
- The U.S. Project Office at ORNL acted as the technical point of contact with the ITER Director on all matters related to tasks assigned to the U.S. Home Team.
- The necessary technical, cost, and schedule controls were implemented to complete the assigned EDA tasks within the specified constraints.
- Annual Performance Memoranda were prepared and implemented with each of the performing institutions funded to do ITER work in the United States. These memoranda described the tasks, milestones, and funding for ITER work performed at each institution. The Project Office at ORNL integrated all U.S. Home Team activities consistent with the Performance Memoranda and formal task agreements with the Joint Central Team (JCT).
- Quarterly reviews of all Home Team technical, cost, and schedule progress were organized and conducted. Quarterly Progress Reports describing work completed were issued.
- U.S. Home Team progress on all assigned tasks was monitored and reported against established plans and schedules.
- The U.S. ITER Steering Committee and the U.S. ITER Industry Council, two advisory bodies to the U.S. HTL, held approximately three to four meetings per year.
- The Project Office coordinated and administered all systems for documentation, preparation of reports, and dissemination of project information on plans, schedules, meetings, public relations, and policies. A monthly newsletter was issued to a large national and international distribution list describing activities of the U.S. Home Team.
- The Project Office established and maintained systems for monitoring and coordinating the formal task agreements with the JCT and the U.S. technical efforts to fulfill the requirements of the task agreements.
- The Project Office coordinated U.S. ITER resource activities with resource managers at other U.S. institutions, with appropriate field offices, and with OFE.
- The financial performance of all U.S. project participants was coordinated and monitored.

In mid-1994, the U.S. Home Team Project Office moved to the University of California at San Diego (UCSD), where C. C. Baker continues as the U.S. HTL.

5.1.2 Quality Assurance Plan

The ORNL Office of Quality Programs and Inspection has been preparing a quality assurance (QA) plan for the U.S. Home Team. The QA plan covers the U.S. Home Team's participation in the ITER EDA and is responsive to DOE quality requirements for design and R&D activities. The U.S. ITER QA plan is expected to be approved and implemented at the beginning of FY 1996.

5.2 ITER JCT SUPPORT

ORNL provided personnel and design support to the JCT while carrying out specific design tasks that were agreed to between the JCT, U.S. Home Team management, and DOE.

ORNL has four full-time personnel on assignment at the Garching joint work site and one part-time employee at the San Diego joint work site. ORNL activities and assignments to JCT are in the areas of vacuum vessel and blanket, electromagnetics, design integration, ITER Integrated Process Management System (IPMS), and other specialty areas that are unique to ORNL.

5.3 ITER DESIGN AND DEVELOPMENT

5.3.1 Physics Studies

5.3.1.1 Physics design of ITER variants

The ITER EDA design variants have been analyzed to evaluate the physics basis for (1) size and design trade-off issues, (2) confinement capability, (3) power levels, and (4) burn control. Highlights from each of these areas are discussed in the following paragraphs.

Size and design trade-off issues

From a radial build, the definition of q_ψ and aspect ratio A (= R/a), and the $1/R$ fall-off of the field (B $\approx 1/R$), the size of the device is specified by plasma current (I), A, safety factor $q_\psi(95\%)$, plasma shape (κ, δ), blanket-shield thickness (d_{BS}), and maximum field at the coil (B_{coil}). The choice of confinement model [Rebut-Lallia-Watkins (RLW) vs empirical power-law or offset-linear scalings], helium concentration (20% vs 10%), and elongation (1.5 vs 2) are the major design drivers. Other quantities are: $q_\psi(95\%) \geq 3$ for MHD stability, A $\approx$ 2.5–3.5 (experimental range), $d_{BS} \approx$ 1–1.2 m, and $B_{coil} \approx$ 11–13 T. The CDA ($R \approx 6$ m, $I \approx 20$ MA, $t_{burn} \approx 200$ s) and EDA ($R \approx 8$ m, $I \approx 25$ MA, $t \approx 1000$ s) designs follow from these considerations and the parameter choices for aspect ratio ($A \approx 2.8$) and elongation ($\kappa \approx 2$ for CDA and $\kappa \approx 1.5$ for EDA). For a given mission and design goal, there is sufficient room for design optimization. Especially with the RLW model, confinement is not directly a function of plasma current, and designs at significantly smaller sizes and lower currents can be found to satisfy the ignition requirement.

Confinement capability

The ignition capability of ITER EDA scenarios is evaluated using the 1-D transport simulations and zero-dimensional (0-D) global models under different confinement assumptions.

Figure 5.1 illustrates the sensitivity of ITER ignition capability to helium and impurity (beryllium) content at a nominal fusion power of 1500 MW. Figure 5.2 shows the sensitivity to plasma current. During the startup and heating to ignition (before helium buildup), there is a large operating window. During this phase ($n_{He}/n_e \approx 0$–5%, $n_{Be}/n_e \approx 0$–1%), the required L-mode enhancement factor for ITER89-P (power-law) scaling is H(ITER89-P) < 1.5 for $I \geq 22$ MA. With offset-linear scalings, H(89-OL) < 1.5 for $I \geq 19$ MA. During the burn, with H-mode-like conditions ($H \approx 2$–2.5), ignition is predicted for plasma currents as low as 16 MA, even with high helium content (10–20%). Confinement improves with current for both the power-law and offset-linear scalings, but the power-law scalings exhibit a stronger dependence on current. With $\chi(\nabla T_e)_{crit}$ (RLW model), ignition in EDA plasmas was obtained for plasma currents as low as 10–12 MA. (Note that safety factor q is higher in low-current cases, and $\nabla q/q^2$ is important.)

Power levels

Fusion power operational space (minimum and maximum) for sustained ignition is determined by an assumed confinement model, fuel dilution (helium and impurity contents), and beta limit. A typical startup, ignition, and burn scenario will evolve proceeding from an ohmic plasma state to an ignition state (with the aid of an appropriate amount of auxiliary power) to a burn equilibrium state. Possible factors influencing the burn equilibrium at a given power level include: physics considerations (confinement, MHD stability and beta limit, density limit, helium/impurity accumulation, etc.); first-wall, in-vessel divertor power-handling capability; and the ability of the poloidal field (PF) coil system to maintain equilibrium control. The question of fusion power excursions and maximum power achievable is an important design and safety assessment issue; thus, it is necessary to design robust burn control and operating-point control schemes to minimize large power excursions beyond the design capability.

Figure 5.3 shows the fusion power operational space (minima and maxima) for sustained ignition as a function of helium concentration (with 2% beryllium). With ITER89-P power-law scaling (for $H > 1.5$), the minimum power to sustain ignition at low helium content (<5%, corresponding to conditions that are expected during the startup) is only a few hundred megawatts, primarily determined by the ohmic (Neo-Alcator) scaling. Here, $t_E = \min[t_E(\text{OH}), H \times t_E(\text{ITER89-P or ITER89-OL})]$. Results from 1.5-D transport simulations show that enhancement factors of $H \geq 1.3$ allow ohmic ignition at full design current. In these simulations, the fusion power at ignition is ~300 MW in calculations that assume no threshold (L-H transition) for access to the improved confinement regime. With the power-law scalings, the minimum fusion power (to sustain ignition) shows a strong threshold-like sensitivity to helium concentration.

Predictions for minimum fusion power are nearly the same for the RLW [$c(-T_e)_{crit}$ L-mode] and ITER89-OL (offset-linear) scaling with $H \approx 2$. At low helium content (<5%, during the startup), $P_{fus\text{-}min} \approx 300$–500 MW for RLW and for ITER-OL with $H > 1.8$. In both cases, the minimum fusion power (to sustain ignition) is sensitive to helium concentration.

Fusion power operational space is limited by the effects of the MHD beta limit, either through the confinement degrading effect of a "soft" beta limit, or by the onset of a disruption at a "hard" beta limit. An initial survey of g-l_i requirements for stable operation of the EDA design showed that operation with $q_{95} < 3$ and low triangularity would impose serious limitations on performance ($g_{Troyon} < 2.2$ for the EDA l_i operating range). If the typical MHD constraint $q(0) > 1$ is relaxed by tracking (and ignoring) modes with most of the ΔW concentrated in the core (sawtooth) region, an increase in g_{Troyon} could be realized for $0.6 < l_i < 1.0$, if strong sawtoothing operation is deemed acceptable. For high helium levels of ~20% in EDA, the fusion power is limited to $P_{fus\text{-}max} \leq 2500$ MW for $g_{Troyon} \leq 2.5$.

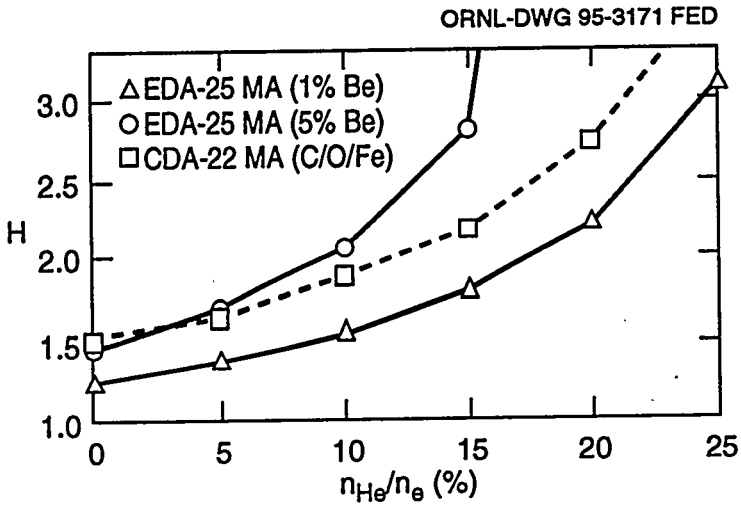

Fig. 5.1. Sensitivity of ITER EDA (at 1500 MW) and CDA (at 1 MW/m^2) performance to helium (and beryllium) content. Needed confinement improvement factor H vs helium concentration [n_{He}/n_e(%)] shown, where H = t_E(needed)/t_E(ITER89-P L-mode). Nominal profiles and <T> ≈ 10 keV used. EDA curves for 1–5% beryllium; CDA curve for CDA-specified C/O/Fe impurities.

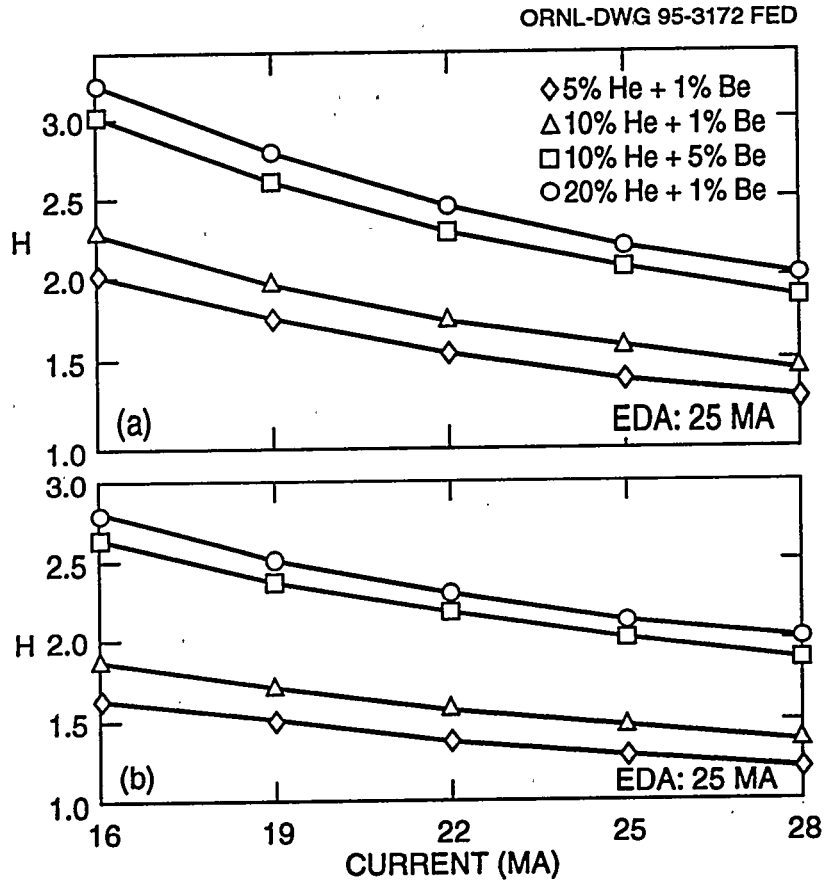

Fig. 5.2. ITER EDA ignition capability with (*a*) ITER89-P and (*b*) ITER89-OL L-mode scalings as function of plasma current at P_{fus} = 1500 MW (for n_{He}/n_e = 0–20%, n_{Be}/n_e = 1–5%). H = t_E(needed)/t_E(scaling). Nominal profiles and <T> ≈ 10 keV.

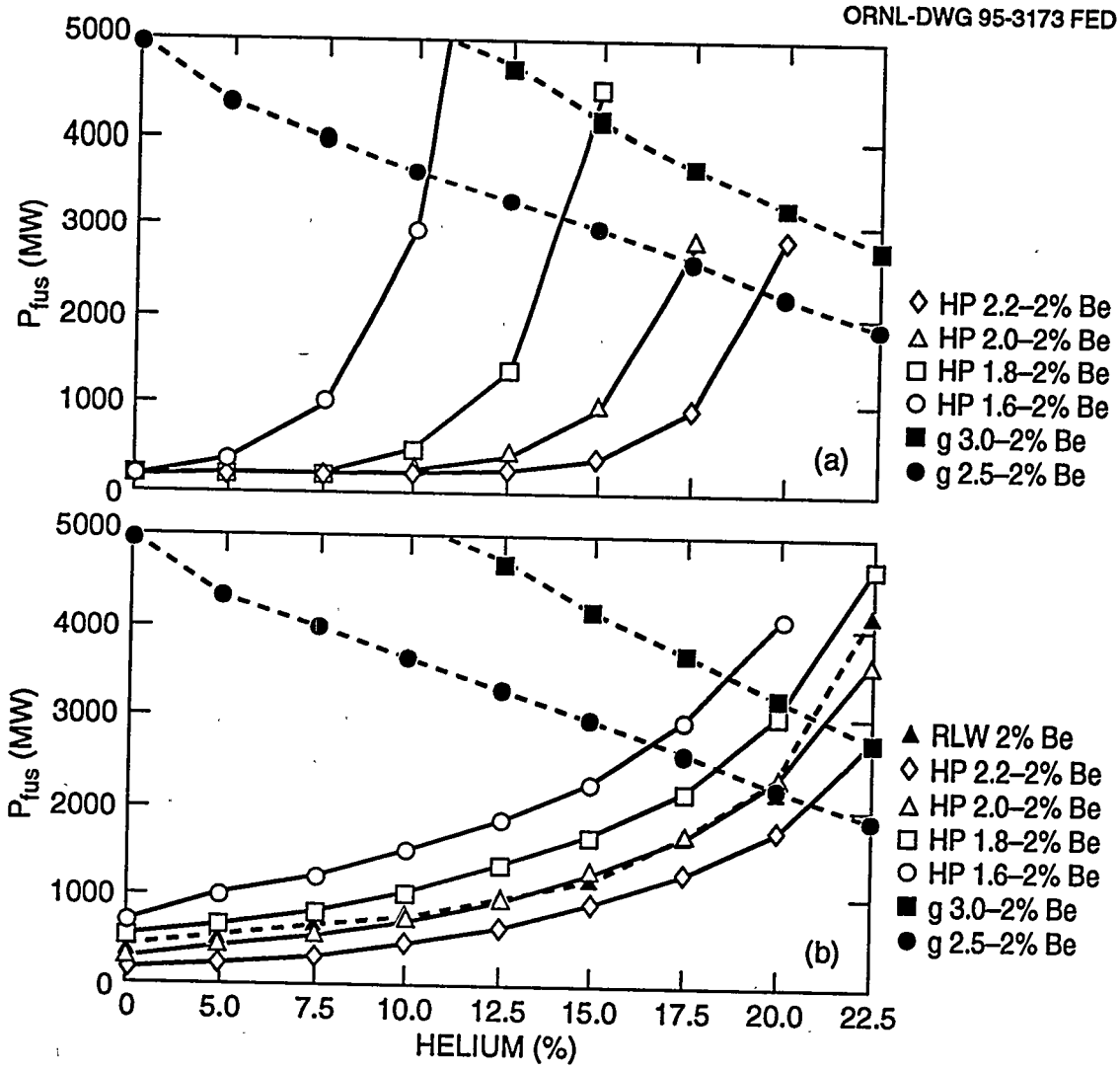

Fig. 5.3. Fusion power operational space (minimum and maximum) for sustained ignition as determined by confinement model, helium (beryllium) content, and beta limit. Confinement: (*a*) ITER89-OL and (*b*) ITER89-P scaling with various confinement improvements, $H = 1.6$–2.2. Normalized beta with $g = 2.5$–3. Beryllium content 2%. All cases developed with 0-D model using typical EDA-like (PRETOR simulation) profiles ($a_n \approx 0.25$, $a_T \approx 1.33$). Also shown (*a*): minimum fusion powers (to sustain ignition) predicted by RLW model, which correspond almost identically with ITER89-OL model, with improvement factor of 2. Operational domain above minimum power needed for ignition (curves labeled by HO, HP, and RLW) and below maximum power determined by beta limit (curves labeled $g = 2.5$ or 3).

An accurate estimate of both the magnitude and dependence on plasma parameters of H-mode threshold power P_{thr} is necessary to determine the minimum auxiliary power requirements to reach ignition in ITER. If P_{thr} is large, under empirically based scalings (ITER89-P, etc.), the H-mode conditions may not be accessed early during the startup/heating phase to ignition, and large amounts of auxiliary power (P_{aux}) are required under unfavorable L-mode conditions until $P(\alpha + \text{OH} + \text{auxiliary–radiation})$ reaches the level of P_{thr}. The ramifications are

serious if the threshold power is much above 150–200 MW, because of the auxiliary power required to access it.

Burn control

Designing and developing robust burn control and operating-point control schemes to minimize large power excursions beyond the design capability is necessary in order to ensure safety. These controls will include coupled engineering and physics scenarios and specifications for (1) operating-point definition and control, (2) burn stability control, (3) off-normal transient control, and (4) minimum diagnostic, control, and shutdown systems. The general area of burn control is an ongoing R&D area, and there are no well-established and accepted methods at this time.

5.3.1.2 MHD stability

MHD stability considerations for high–aspect-ratio design

Global MHD stability calculations using the PEST code have been carried out as part of the U.S. Home Team's high–aspect-ratio design study. Approximately 15,000 cases have been evaluated for both global and local (ballooning) modes. In addition to aspect ratio variations ($2.78 < A < 5$), a range of shapes ($1.4 < k < 2$, $0 < d < 0.6$) has been examined, and the safety factor has been varied: $1.05 < q(0) < 1.85$ and $3.1 < q_{\psi}(95\%) < 4.55$. For global aspect ratio scaling, these results show no significant increase or decrease in the normalized beta ($\beta_N = g_{Troyon}$), within the level of variation imposed by profile differences: the scaling of the maximum Troyon parameter (g_{max}) is found to be independent of A if optimal profiles are considered at each aspect ratio.

Sensitivity of ITER MHD global stability to edge pressure gradients

The stability of the ITER EDA plasma configuration to global modes places a limit on both the maximum fusion power production and the range that must be considered for fusion power transients. The global mode stability of the ITER EDA configuration has been evaluated. In view of the preliminary nature of boundary models for tokamak reactors, the sensitivity to edge gradients of the global mode MHD stability of the EDA configuration has been examined. The POLAR-2D and TORUS stability codes developed by the Keldysh Institute have been used. Transport-related profiles from the PRETOR transport code (developed by the JCT) and axisymmetric equilibria for these profiles from the TEQ code (developed by LLNL) were taken as a starting point for the study. These baseline profiles are found to have quite high global stability limits, in the range $g_{Troyon} = 4–5$. The major focus of the ORNL study has been to examine global mode stability; based on the assumption of wall variations about the baseline profiles, the pressure gradients near the boundary were changed. Such changes can be expected with an improved boundary model. Reduced stability limits and unstable cases with $g = 2–3$ are found in such cases. Thus, the assumption of ITER stability limits higher than $g = 2$ must be treated with caution.

5.3.1.3 Pumping and fueling requirements

The relationships between fueling (gas injection and pellets of various sizes and velocities), pumping in the divertor chamber (constrained by fuel processing and divertor design), core density (constrained by the desired fusion power and helium ash accumulation), separatrix density (constrained by divertor operation and density limits), and plasma confinement models

are examined for guidance in defining design requirements for ITER EDA pumping and fueling systems. Various combinations of gas and pellet injection are found to meet the constraints for operation at 1500 MW of fusion power and 1 bar-L/s (5.3×10^{22} atoms/s) of D-T pumping. Very low pumping reduces fuel processing requirements but can lead to excessive helium accumulation, depending on the particle transport properties. Isotopic tailoring of the fuel sources (e.g., 20–30% of input fuel stream as tritium pellets and the rest as deuterium gas) can maintain the core fuel species mixture in the optimum range for fusion production (at least 40–60% mixture) while reducing the tritium concentration in the edge region to 20–30%. This should reduce the tritium inventory in the plasma-facing components because that is typically governed by the fuel density mix near the plasma edge. A high-density, low-temperature ignited regime supported by deep pellet injection is shown to exist under some low (L-mode-like) confinement conditions.

5.3.2 Engineering Design

ORNL has provided leadership and/or design support in several design engineering areas in the United States, including vacuum vessel, disruption loads, thermal and mechanical analysis, PF optimization, and systems studies.

5.3.2.1 ITER vacuum vessel design activities

The vacuum vessel must provide a high-quality vacuum and, in combination with the blanket/shield, sufficient shielding to limit heat and radiation damage to the coils to tolerable levels. The vacuum vessel is also a major safety barrier and must support the electromagnetic loads resulting from plasma disruptions, vertical displacement events (VDEs), and plausible accidents, without loosing confinement.

The vacuum vessel concept was proposed and developed at ORNL. It is a double-wall structure filled with stainless-steel balls; water provides the necessary strength, nuclear shielding, and electrical resistance in a relatively simple structure. The partially assembled chamber is shown in Fig. 5.4, and a section of one 15° segment is shown in Fig. 5.5. The inner and outer shells are made of welded plates of Inconel 625, 30–40 mm thick. The total thickness of the vacuum vessel is 0.4–0.7 m, and the overall height is ~15 m. For the reference EDA design, the total toroidal resistance of the vacuum vessel and blanket is ~6 μΩ. The total heat deposited in the vacuum vessel is ~2% of the fusion power, and the maximum nuclear heating rate is calculated to be 0.04 MW/m^3.

5.3.2.2 Disruption loads

The electromagnetic loads arise during a plasma disruption or VDE, when large currents are induced in the surrounding structures. Some of the highest loads appear in the in-vessel components, including the first-wall/shield/blanket modules. A significant effort at ORNL has been directed toward accurately characterizing these loads and incorporating them into the design process for the individual components and their mounting system.

Tokamak Simulation Code (TSC) has been used to model the interaction of the plasma motion and current decay with the conducting surfaces to yield the time evolution of plasma parameters and poloidal flux. EddyCuff, a code developed for use on fusion projects, is used to calculate the resulting eddy currents and forces in the reactor components. A finite element code

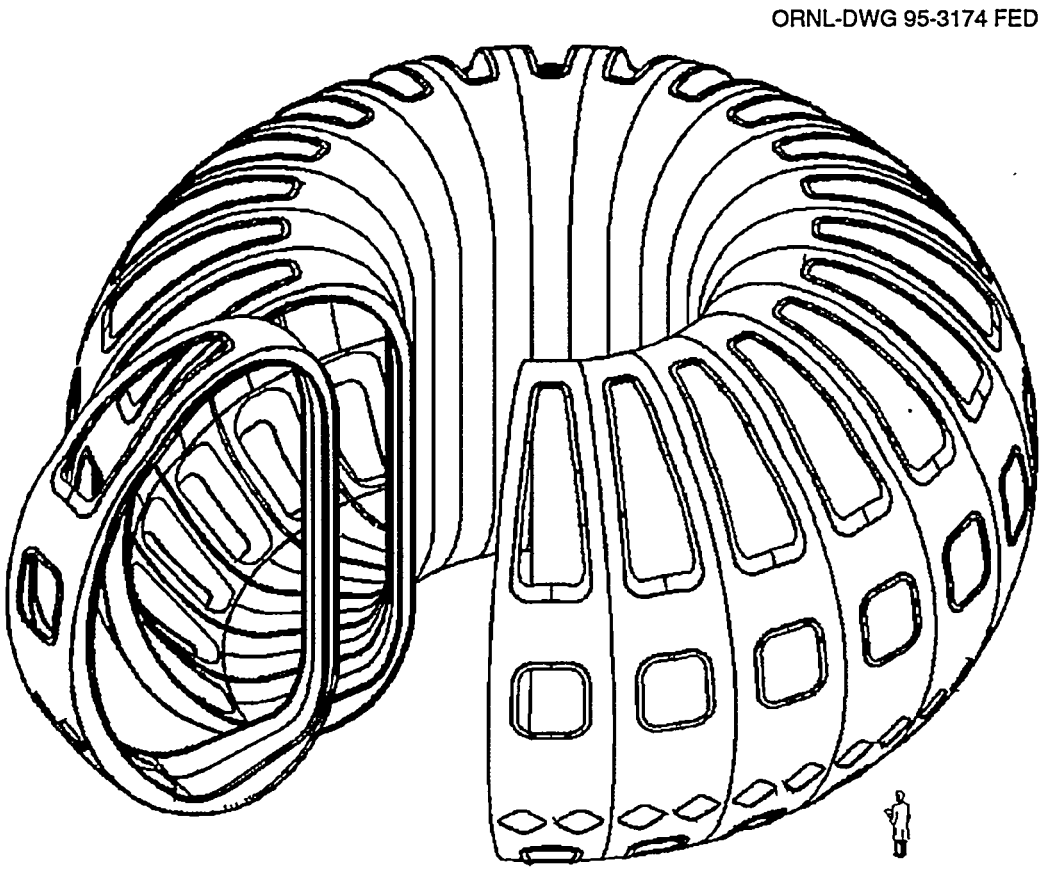

Fig. 5.4. Partially assembled vacuum vessel chamber.

is then used to analyze the resulting stresses and evaluate the reaction loads at the required interfaces. TSC has also been used to study the sensitivity of the forces to the current-decay time and to various initial conditions to determine the disruption scenario that produces the most severe loads.

Figure 5.6 shows how these codes are used to determine and analyze these effects in a typical in-vessel blanket/shield module. The plasma motion induces 3-D field effects in the module [Fig. 5.6(*a*)]; these effects result in the eddy current patterns shown in Fig. 5.6(*b*) and the load pattern in Fig. 1(*c*). Finite element stress analysis programs are then applied to determine the resulting stress and deflections in the modules, which are shown in Fig. 1(*d*).

In a typical disruption scenario, electromagnetic analyses have been carried out for centered disruptions and VDEs; a 24-MA current is assumed to decay linearly in 10 ms (decay rate 2.4 MA/ms). About 21 MA flows in the first wall at the end of the current quench, and this produces a maximum load on the first wall of 1.3 MPa. Maximum current induced in the vessel is ~3.5 MA and occurs ~200 ms after the disruption. The corresponding pressure on the vacuum vessel around the mid-plane port is ~0.4 MPa. For a typical VDE, a net downward force of 153 MN on the blanket is obtained, and an additional downward force of 54 MN is found for the vacuum vessel.

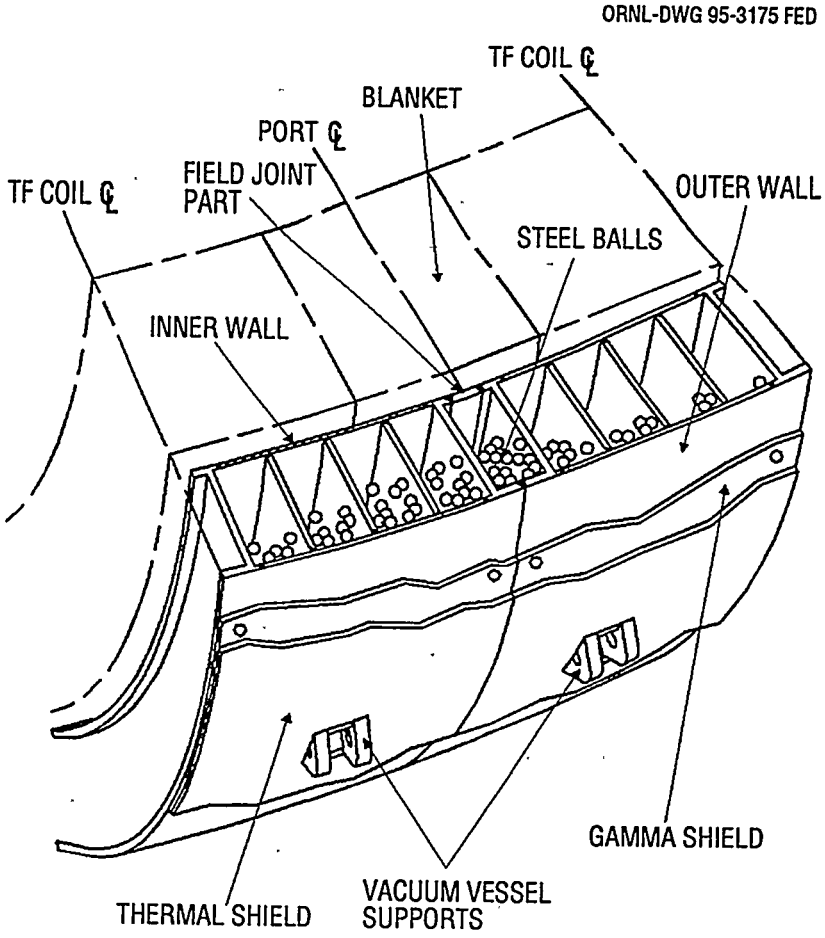

Fig. 5.5. Cross section of vacuum vessel chamber design.

5.3.2.3 Thermal/mechanical analysis of the ITER divertor vane

One of the key challenges facing ITER is the development of plasma-facing components that can withstand the severe environmental conditions at the plasma edge. The most intensely loaded plasma-facing component is the divertor, which must be designed to handle high fluxes of energetic particles and electromagnetic radiation without excessive impurity buildup in the plasma core. To determine whether the ITER divertor can be designed to withstand the intense heat loads, a series of thermal and structural analyses were performed. The reference configuration for the ITER divertor, shown in Fig. 5.7, uses a set of "vane" structures to form a "toroidally continuous/transparent wall." A cross-section of one of the vanes is shown in Fig. 5.8. The vane is constructed from a Cu-Cr-Zr alloy with beryllium or tungsten tiles bonded to the plasma-facing surfaces. Water is the coolant for the vanes. These analyses included an evaluation of the thermal hydraulic characteristics of the divertor system, as well as the use of 2-D and 3-D finite element models to determine temperature and thermal stress distributions throughout the vane structure.

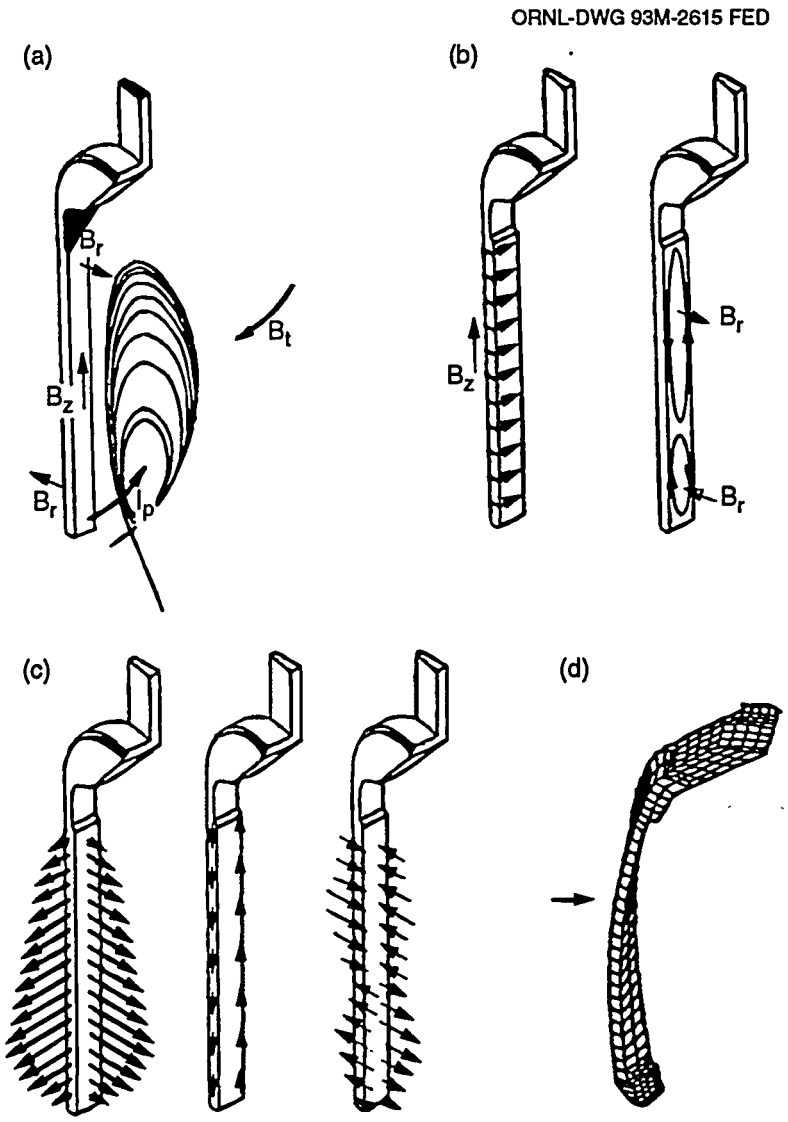

Fig. 5.6. Plasma disruption effects on in-vessel blanket/shield modules. (*a*) Blanket/shield module and plasma, (*b*) currents induced in modules by plasma motion, (*c*) force components resulting from induced currents, (*d*) deflection and stress contours.

The thermal hydraulic performance of the divertor vane concept and peak temperatures of the beryllium armor and copper alloy structure were determined to be well within acceptable limits. Although the thermal stresses are within tolerable limits for copper alloys that have not been irradiated, the lack of data on irradiation of copper alloys makes it impossible to formulate any firm conclusions regarding the ability of the copper structure to sustain these thermally induced loads. However, the vane design approach is a promising concept. Furthermore, it was recommended that irradiation testing of copper alloys be given a high priority in the ITER project.

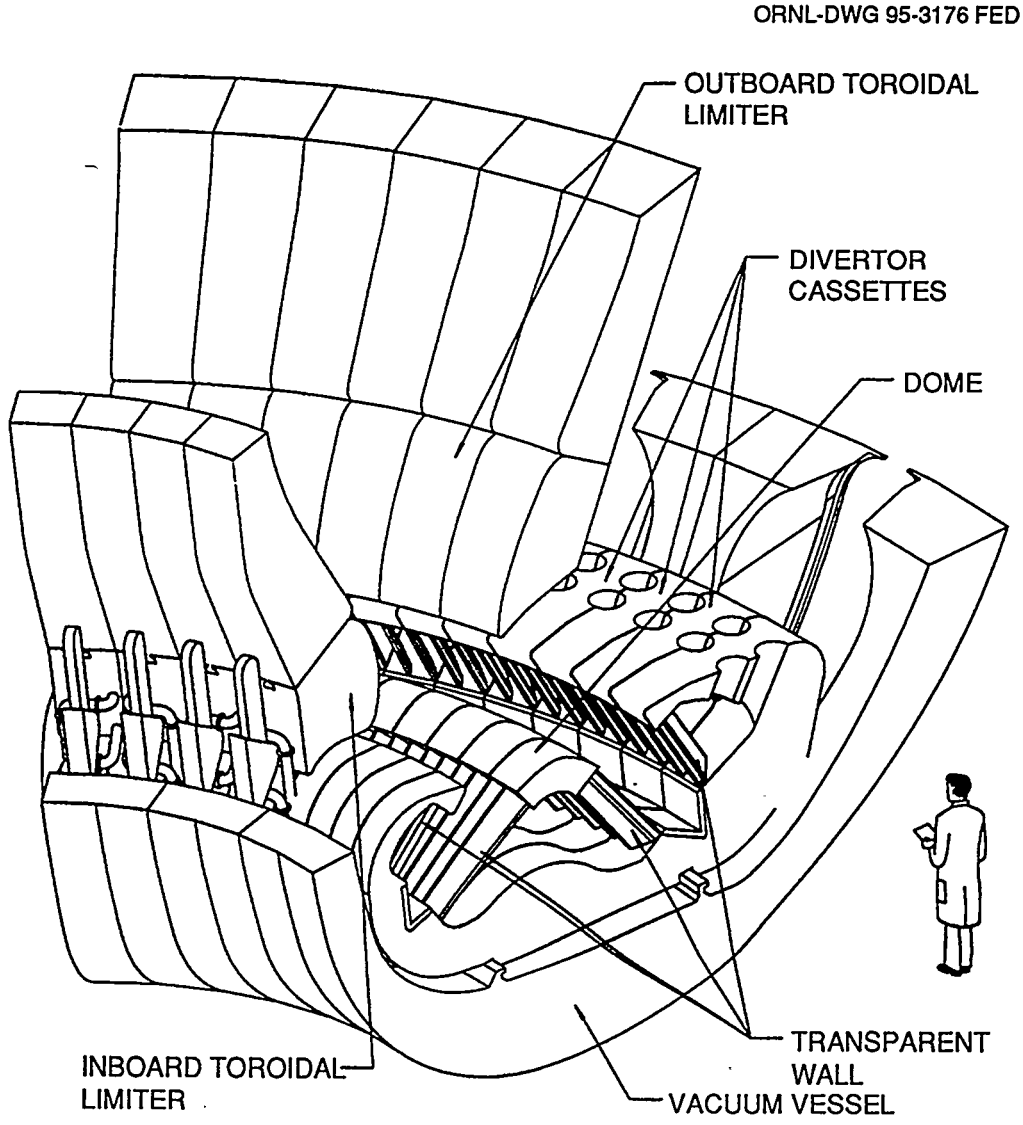

Fig. 5.7. Reference configuration for the ITER divertor.

5.3.2.4 ITER PF coil optimization

ORNL contributed to the PF design and optimization studies for ITER. The primary purpose was to establish or verify the required number of PF coils and their position and cross-sectional shape to best satisfy the plasma shape requirements. The procedure used to characterize the magnetic configuration is called an l_i survey, where l_i is the normalized internal inductance of plasma. This procedure determines the peak coil currents necessary to satisfy the plasma shape requirements over the desired operational range of current profiles, characterized by l_i. A minimization algorithm has been adopted to perform systematic optimization of PF coil positions and cross sections; this algorithm can effectively reproduce the external field of a prescribed set of MHD equilibria, while satisfying design engineering constraints. A nonlinear optimization

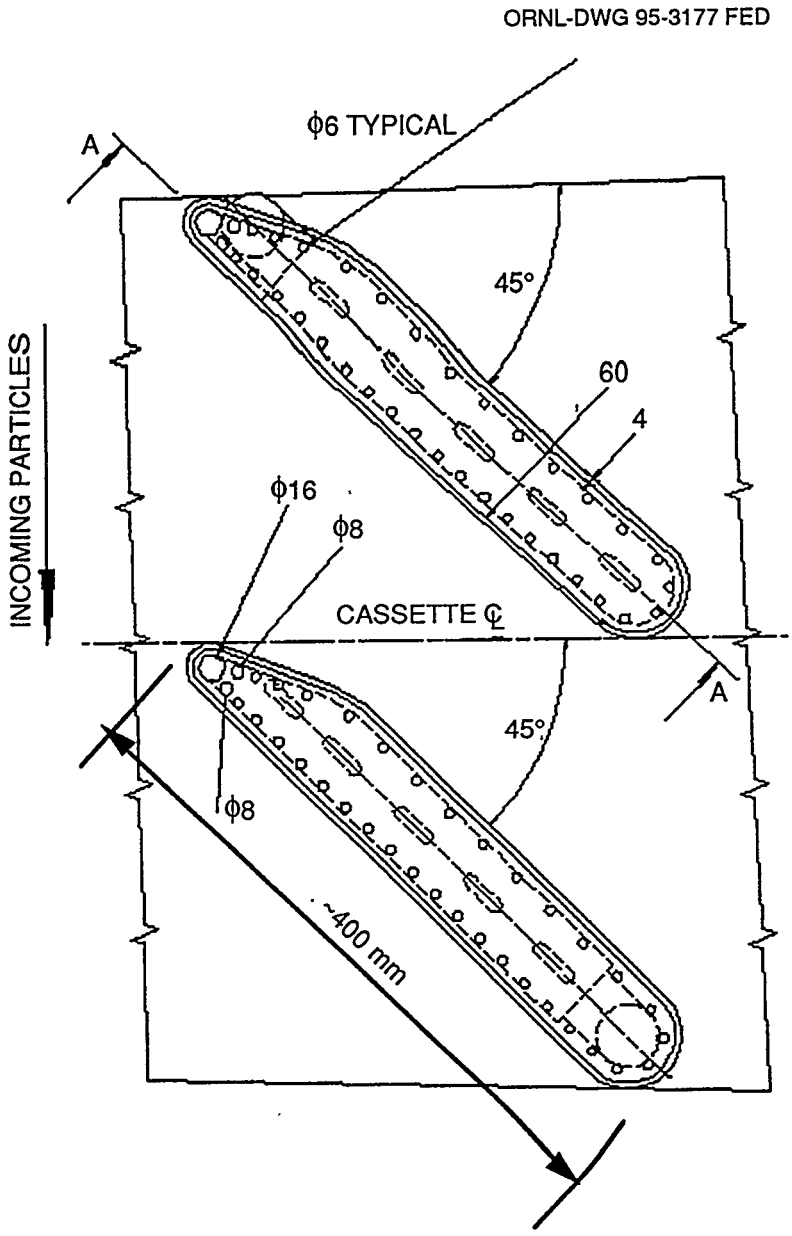

Fig. 5.8. Cross section of vane structure.

method is used to minimize PF coil volume by varying coil positions and cross-sectional shapes, within limits set by device configuration and superconducting magnet engineering constraints.

The ITER EDA Outline Design PF system and a free-boundary MHD equilibrium with nominal parameters are shown in Fig. 5.9. Corresponding optimal PF coil configuration is shown in Fig. 5.10. PF volume reductions of up to 17% are possible in the coil configuration of the ITER Outline Design, depending on device design engineering assumptions.

5.3.2.5 First-wall design modeling

The first-wall design process involves consideration of the competing effects of disruption-induced forces (which favor thicker wall solutions) and thermal loads (which favor thinner walls). As an initial guide to finding acceptable overall first-wall design, an analytic parametric scoping tool has been developed for first-wall design problems. The model included simple models for simultaneous modeling of thermal hydraulics, structural analysis, and electromagnetic-induced forces resulting from disruptions. It was used to scope out the viability of various material choices for the first wall. For example, for the high–heat-flux and high-disruption load conditions expected in the ITER device, vanadium alloy and dispersion-strengthened copper offer the best stress margins using a somewhat flattened plasma-facing configuration. Ferritic steels also appear to have an acceptable stress margin, whereas the conventional stainless steel 316 does not appear feasible. If a fully semicircular first-wall shape is required, only the vanadium and ferritic steel alloys offer acceptable solutions.

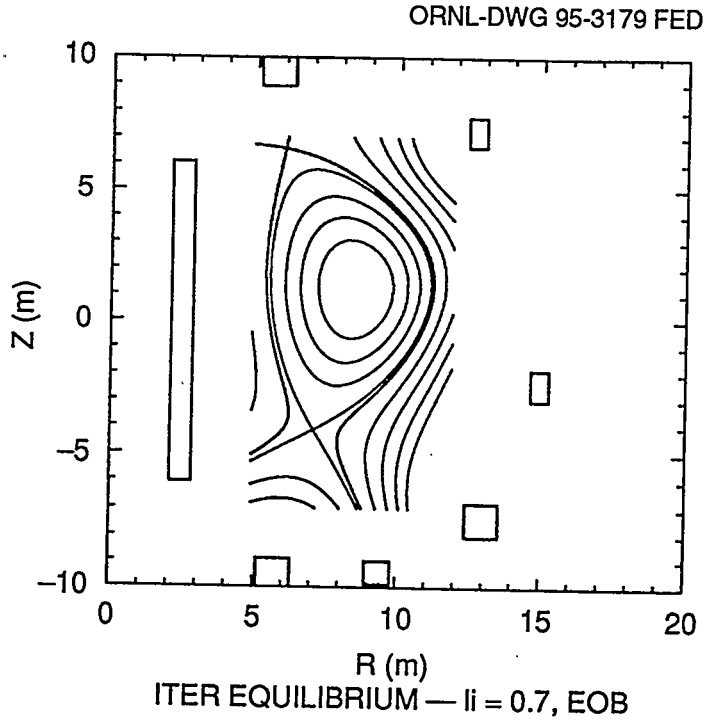

Fig. 5.9. ITER EDA Outline Design PF coil system and one of the operational flexibility equilibria.

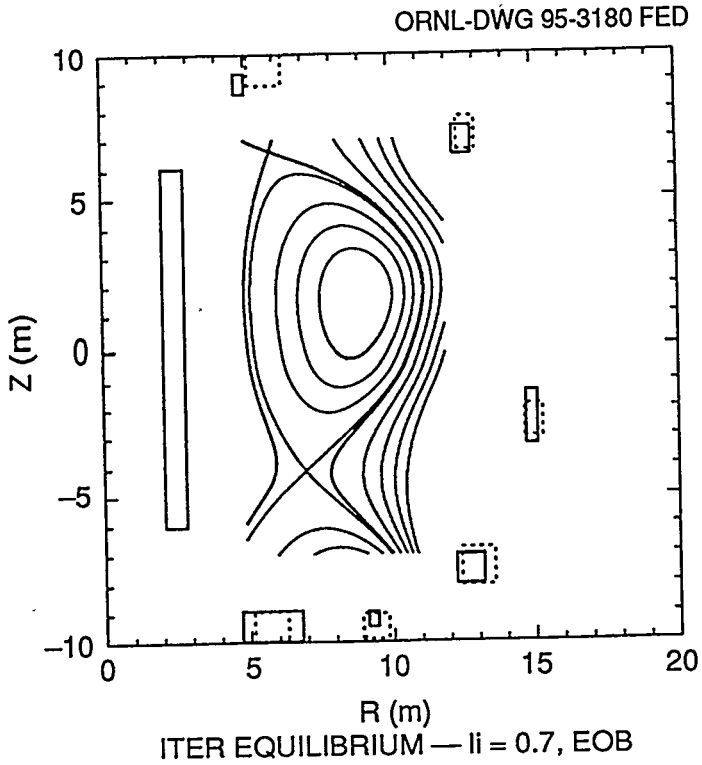

Fig. 5.10. Optimal ITER EDA PF coil system and one of the operational flexibility equilibria. Outline Design PF coil system shown in dashed lines.

5.3.2.6 ITER systems code analysis

The U.S. Home Team systems group activities consisted of defining ITER operational scenarios and carrying out cost and scoping studies for design variants. ORNL provided support for comparing initial EDA design concepts with the previous CDA design and subsequently provided cost-risk analysis of reduced-cost EDA variants. These studies were used by U.S. Home Team management, the ITER Technical Advisory Committee, and the JCT.

A major effort in this area was the development of a new systems code (SUPERCODE), which supplanted the earlier TETRA code used in the CDA. Physics modeling was improved in SUPERCODE through a fixed-boundary MHD package and 1.5-D transport modeling. ORNL played a major role in the code development. The systems studies performed in 1992–1994 include the following:

Comparison of the CDA and EDA designs: The different design assumptions and concepts of CDA and EDA were systematically investigated with regard to the impact on the required device size and cost.

Device cost: During 1993 the U.S. Home Team performed a cost estimate for the EDA design. This cost estimate was coordinated by the systems group and was used as a calibration for the SUPERCODE costing. Subsequently, the cost estimate methods of the JCT were adopted.

Ignition sensitivities: Sensitivities of the EDA design to variations in impurities, scaling laws, etc. were performed several times as the design evolved. These studies were used as input to the Technical Advisory Committee.

Number of TF coils: The effect of decreasing the number of TF coils from 24 to 12 was investigated parametrically. Of particular interest was the effect on remote-maintenance access

and ripple. Slight device-cost increases (~3%) were found if the coils were reduced from 24 to 16, which provided increased access space.

Reduced-cost EDA-like variants: The United States played a key role in the 1994 reduced-cost variant device sensitivity study, commissioned by the Technical Advisory Committee. This joint effort of the U.S. Home Team and the JCT investigated the cost benefit and ignition margin risk of adopting a smaller, lower-cost design. The cost benefit results are shown in Fig. 5.11.

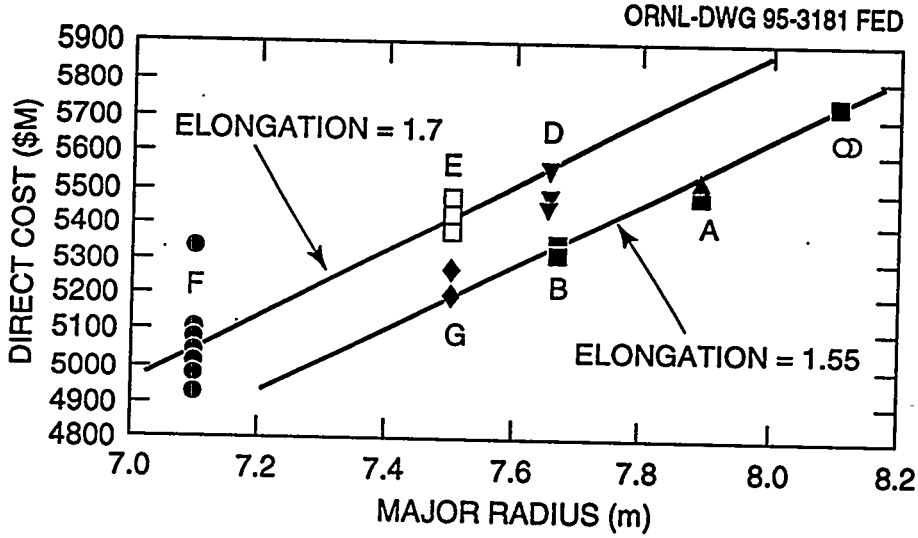

Fig. 5.11. Direct costs of 1993 ITER-like designs vs size. There is $900M/m direct cost decrease at constant elongation. Higher elongation cases increase ~$250M in cost for fixed major radius. Results shown for Outline Design and six variant devices picked for study. Costs calculated by each party shown.

5.3.3 RH

The remote handling (RH) program in the Robotics and Process Systems Division of ORNL is directed toward developing cost-effective RH technology for the ITER facility that will maximize its operational availability. The key elements of the current program are: (1) preparation of a remote-maintenance design manual; (2) development of remote cutting, welding, and weld-inspection techniques; (3) development of RH-compatible electrical connectors; and (4) development of a remote metrology system for ITER in-vessel applications. A brief synopsis of the work done under each of these areas is presented in the sections that follow.

5.3.3.1 Remote-maintenance design manual

The purpose of this task is to prepare a remote-maintenance design manual for ITER component designers. Once finalized, the manual will describe a recommended general remote-maintenance design philosophy, identify ITER RH equipment and tooling, and specify approved RH design standards and components for ITER design. A partial draft of the manual was prepared by the United States and was submitted to the Design Integration Division (DID) in January 1993. The U.S. and Euratom home teams have continued work on this task during 1994. A draft section of the manual entitled "Selection of Components and Materials to Minimize Radiation Damage" was completed and submitted to DID for review. It addresses ionizing radiation effects on

materials, the radiation hardness of materials, and their selection criteria. DID now plans to use this document as a separate materials radiation hardness manual.

5.3.3.2 Remote cutting and welding

The purpose of this task is to develop internal pipe-cutting, welding, and inspection tooling for stainless-steel service pipes ranging in diameter from 50 to 400 mm and for wall thickness up to 10 mm. Examples of ITER service pipes include the divertor- and blanket/shield-cooling water pipes. The United States is responsible for developing the weld inspection process and tooling. This work is being performed under ORNL direction by the RH task area industrial team, which is led by Rockwell International. On the basis of a comparative evaluation of different techniques, the Rockwell team has identified dry-couplant ultrasonic testing (UT) as the most promising nondestructive evaluation technique. Controlled experiments to establish the feasibility of this technique for ITER are under way at Rockwell. Preliminary test results, under induced weld-flaw conditions, indicate that proper alignment and seating pressure of the UT shoe are critical factors for the dry-couplant technique. Accurate positioning equipment and pressure-sensitive instrumentation should enhance the reliability of the technique to levels required for ITER remote maintenance.

5.3.3.3 RH-compatible electrical connectors

The purpose of this task is to develop a selection of electrical connectors that are compatible with the RH needs of ITER. Remote electrical connectors are typically used in a configuration that facilitates remote maintenance by a teleoperated, force-reflecting manipulator. Selected connectors will be listed in a standard components manual for use in the design of ITER. A survey of commercially available electrical connectors, covering a large number of manufactures, was completed. The results of this evaluation, focusing on candidate connectors of four international companies, have been documented. The documents include information on selected connectors as well as general design considerations for electrical cabling involving RH.

5.3.3.4 In-vessel metrology system

The aim of this task is to develop a remotely deployed and controlled 3-D metrology system capable of mapping in-vessel components and their support structures (i.e., vacuum vessel, blanket/shield, divertor, etc.) to submillimeter accuracy. A comparative evaluation of the various metrology techniques revealed that Frequency Modulated (FM) Coherent Laser Radar (CLR) has the most potential to meet the ITER in-vessel metrology requirements. The performance characteristics of a prototype CLR system developed for the National Aeronautics and Space Administration by Coleman Research were tested at ORNL. The results indicate that the technique is capable of meeting ITER requirements. However, because of the severity of the ITER in-vessel environment (high gamma radiation, ultra-high vacuum, etc.), some uncertainty remains in adopting this technique for ITER. Accordingly, a subcontract has been placed with Coleman Research to perform a feasibility analysis of the FM CLR technique in the ITER environment. A conceptual drawing of the metrology scheme is shown in Fig. 5.12. Three or four multiple probes will be used to map the entire in-vessel surface.

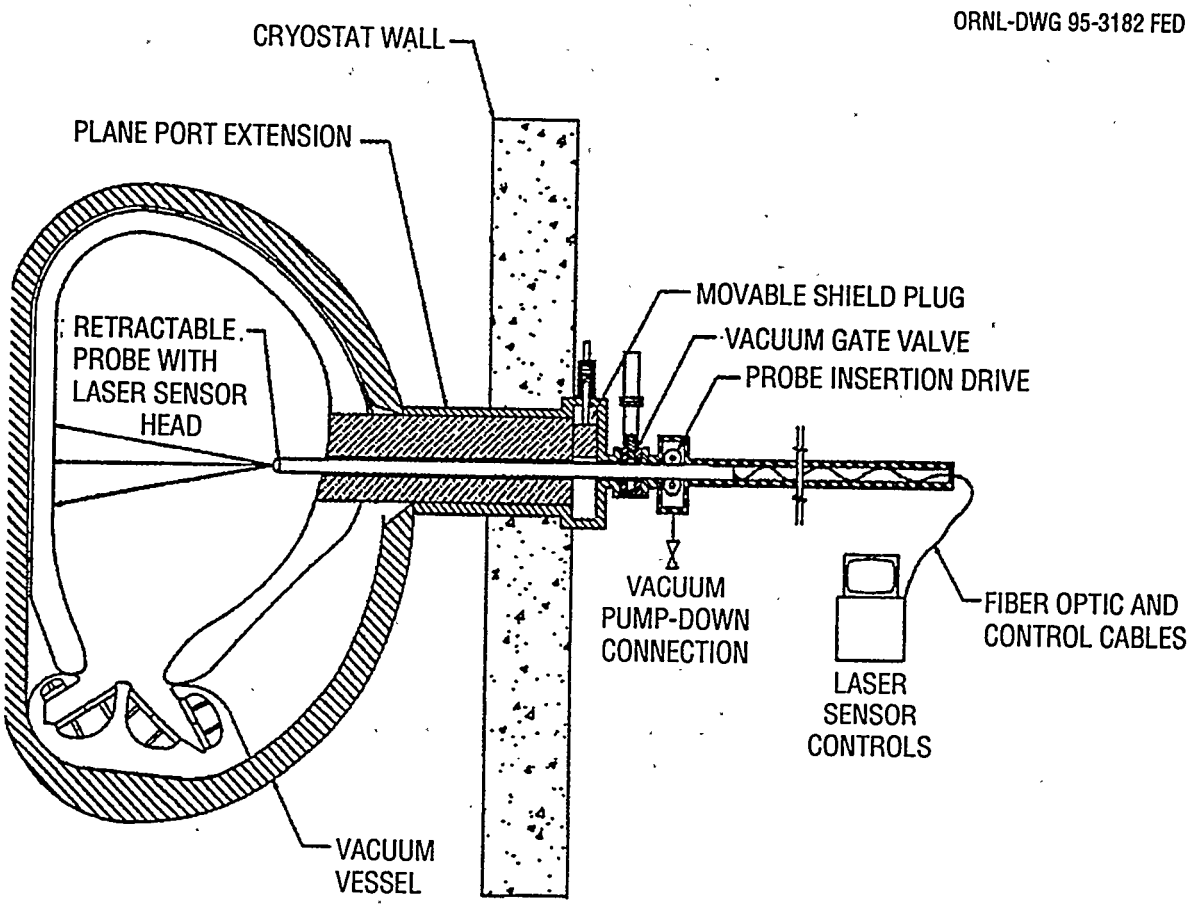

Fig. 5.12. Metrology probe deployment scheme.

5.3.4 Vacuum Vessel

ORNL has provided the leadership for the vacuum vessel design and R&D in the United States since the beginning of the ITER CDA. The vacuum vessel is a critical component because it provides the first safety barrier and must withstand large electromagnetic loads and accidental overpressure without losing confinement. In addition to the vessel itself, this task area includes the design of the structural connections between the blanket/shield modules inside the vessel.

5.3.4.1 ITER vacuum vessel design activities

The ORNL team has contributed in several key areas of the vacuum vessel design. (See Sect. 5.3.2.1.) The basic vessel concept was proposed and developed at ORNL. The double-wall structure filled with stainless-steel balls and water (see Figs. 5.4 and 5.5) provides the necessary strength, nuclear shielding, and electrical resistance in a relatively simple structure. Design features such as assembly segmentation, placement of ribs between the double shells, port duct attachment, and other details have been developed.

To evaluate the vessel design, considerable expertise has been developed for calculating electromagnetic loads. These loads arise during a plasma disruption, when large currents are induced in the surrounding structures. Some of the highest loads appear in the in-vessel

components, including the first-wall and shield/blanket modules. The interconnection of these modules for mutual support is another ORNL concept that has been adopted as the baseline ITER design. To verify and optimize the design concept, dynamic structural analysis of the coupled vacuum vessel and shield/blanket assembly has been performed, incorporating the complex electromagnetic loading during a plasma disruption.

5.3.4.2 ITER vacuum vessel R&D activities

The purpose of the ITER vacuum vessel R&D program is to develop the relevant technology database for the vacuum vessel and structural attachment hardware for the internal components.

During the interim between completion of the CDA and the formal start of the EDA, ORNL engineers formulated plans and began to carry out the most critical vacuum vessel R&D tasks that were identified during the CDA. These include: (1) demonstrating the feasibility and methods for fabricating the large, double-wall sandwich vacuum vessel to close, stable tolerances with adequate structural integrity and minimum cost; (2) demonstrating the method and equipment needed to weld and cut the large field joints between vacuum vessel sectors remotely; and (3) developing and demonstrating a welded connection between the blanket/shield modules inside the vacuum vessel. In FY 1992, requests for proposals were released and industrial subcontractors selected for double-wall vacuum vessel fabrication and remote cutting and welding. In FY 1993, these contractors performed feasibility studies and recommended design and fabrication details for inclusion in the ITER vacuum vessel design. The contractors also developed detailed R&D plans and cost estimates and began some of the welding development work. In FY 1994, the contractors designed and began fabricating a full-scale partial prototype section of the vacuum vessel and performed welding development of narrow-gap welding processes for 3-cm-thick Inconel 625 material.

5.3.5 Magnet R&D

The design of the superconducting magnets for ITER must conform to numerous constraints. However, it is important to maintain the highest current density consistent with the stability requirements and safety of the magnet system to external perturbations. ORNL has extensive experience with cable-in-conduit conductors and knowledge of how to maximize the stability margin while maintaining the safe discharge capability for any operating conditions. It is also necessary to understand how to calculate the limiting current for stable operation and thermal hydraulic quenchback (THQ) for safe operation in extreme operating conditions.

The ORNL magnet work continues to concentrate on problems involved with the applications of cable-in-conduit superconductors for ITER-size magnets. This includes theoretical work on porous conduits for the cable-in-annulus conductor configuration, which may supplant the more conventional cable-in-conduit design in the ITER project. Protection of a magnet using cable-in-conduit conductors must also be considered, and, therefore, a small effort has been made to further understand the experimental implications of THQ, or the rapid increase by an error of magnitude of a propagating normal zone. In particular, the experiments showed thresholds for THQ, that the original theory did not predict.

5.3.6 ITER Fueling

ORNL has been involved with the design and R&D of ITER fueling systems since the beginning of the ITER CDA phase. In late 1994, ORNL was assigned full responsibility for developing the ITER fueling system for the EDA phase. The R&D activities related to ITER fueling include tritium extruder and component development in collaboration with the TSTA staff at LANL, long-pulse deuterium feed system development using multiple extruders, and improvements to centrifuge injector feed and delivery systems. These development activities are discussed in more detail in Sect. 4.1.

5.3.6.1 Fueling system design for ITER-CDA

A conceptual design of an innovative plasma fueling system for ITER was developed for the ITER CDA.[1,2] The system would use a combination of gas puffing and an advanced pellet injection system to achieve and maintain ignited plasmas. Three pellet injectors were proposed. A highly reliable, moderate-velocity (1–1.5 km/s), single-stage pneumatic injector and a high-velocity (1.5–5 km/s), two-stage pneumatic pellet injector using frozen hydrogenic pellets encased in sabots would be used for rampup to ignition. For the steady-state burn phase, a continuous, single-stage pneumatic and/or centrifuge injector is proposed, which will provide a flexible fueling source beyond the edge region to aid in decoupling the edge region (constrained by divertor requirements) from the high-temperature burning plasma. The increased efficiency of pellet fueling compared to gas injection suggests the use of pellet fueling to provide all of the tritium and a portion of the deuterium needed to sustain the fusion reaction and the use of deuterium gas injection to provide the required edge densities for optimum divertor conditions. In addition to decreasing the tritium throughput and raising the tritium burn fraction, this mode of operation allows a deuterium-rich boundary-layer gas at the edge, which could significantly lower tritium inventories in plasma-facing components. This concept is presented in more detail in Sect. 5.3.6.2.

5.3.6.2 Fuel source isotopic tailoring

An effort was initiated to investigate the potential to reduce tritium inventories and throughputs by innovative use of baseline ITER systems, including the plasma fueling, fuel processing, and isotope separation systems, to control the hydrogen isotope content of separate fueling sources. This process is called isotopic fuel tailoring. Isotopic tailoring of the deuterium and tritium density profiles in fusion reactors can lead to reduced tritium inventory in plasma-facing components and, therefore, improved safety. Isotopic tailoring uses a tritium-rich pellet source for core fueling and a deuterium-rich gas source for edge fueling.[3] Because of the improved particle confinement associated with the deeper tritium core fueling component, comparable core densities of deuterium and tritium can be maintained even when the edge deuterium fuel source is much larger than the core tritium fuel source. The fuel composition of the edge and scrape-off plasmas reflects the total throughput of all makeup fuel and would therefore be deuterium-rich. The composition of the fuel particles retained in the plasma-facing components reflects the composition of the edge plasma and would also be deuterium-rich. An evaluation was made of the ability to maintain isotopically tailored deuterium and tritium profiles with pellet injection from centrifugal and pneumatic pellet injectors supplemented by deuterium gas injection, within the limitations of the ITER EDA pumping constraint of 1 bar-L/s total throughput ($\sim 5 \times 10^{22}$ particles/s).

The WHIST 1.5-D, time-dependent transport code[4] was used to examine the variation in the deuterium and tritium core and edge densities in response to various combinations of makeup gas and pellet fueling sources. A brief overview of the WHIST code and its application to pellet fueling of reactor-scale devices is given in Ref. 4. The pellet fueling component, consisting of 90% tritium and 10% deuterium, was varied between 0.27 and 0.37 bar-L/s, while the edge deuterium gas fueling component was varied from 0.75 to 0.65 bar-L/s under a constant fusion power of ~1500 MW. Because the fueling sources and transport are specified, one of the variable outputs is the D-T mix in the plasma core. Operation with a core fuel mix of ~60% deuterium and ~40% tritium does not significantly increase operating density but provides an immediate reduction in the relative tritium fraction in both the core and edge. Results from WHIST code runs are given in Table 5.1. The tritium burn fraction given in the last column is the ratio of the amount of tritium burned (which is directly related to the fusion power) to the amount of tritium provided by the fueling system. In cases 469–471 (shown in Fig. 5.13), the 90% deuterium/10% tritium pellet is sized for an equivalent spherical radius of 0.425 cm (~2×10^{22} particles, a density perturbation of ~10%) and has a speed of 1.5 km/s; this performance is typical of existing single-stage pneumatic pellet injectors. (See Sect. 4.1.)

For case 469, the deuterium gas fueling is 0.65 bar-L/s. This results in a 63% tritium fraction on axis and a 34% tritium fraction at the edge. This tritium fraction on axis is too large, so in cases 470 and 471 the deuterium edge fueling was increased to 0.7 and 0.75 bar-L/s, respectively. Given the ITER constraint of 1.02 bar-L/s total fueling, this results in a corresponding reduction in the pellet fueling source. It can be seen in Table 5.1 and in Fig. 5.13 that the tritium fraction on

Table 5.1. Summary of WHIST code runs

WHIST code run no.	Deuterium fuel source (bar-L/s)	Pellet radius (*rp*) (cm)	Pellet speed (*vp*) (km/s)	Pellet penetration[a]	Axis tritium concentration [*ft*(0)]	Edge tritium concentration [*ft*(*a*)]	Burn fraction (%)
469	0.65	0.425	1.5		0.63	0.34	3.3
470	0.70	0.425	1.5		0.47	0.29	3.8
471	0.75	0.425	1.5		0.38	0.23	4.5
472	0.75	0.425	1.5	0.3	0.34	0.24	4.5
473	0.75	0.535	3	0.37	0.43	0.24	4.5
474	0.75	0.3	1	0.25	0.30	0.23	4.5

[a]Normalized to the ITER minor radius.

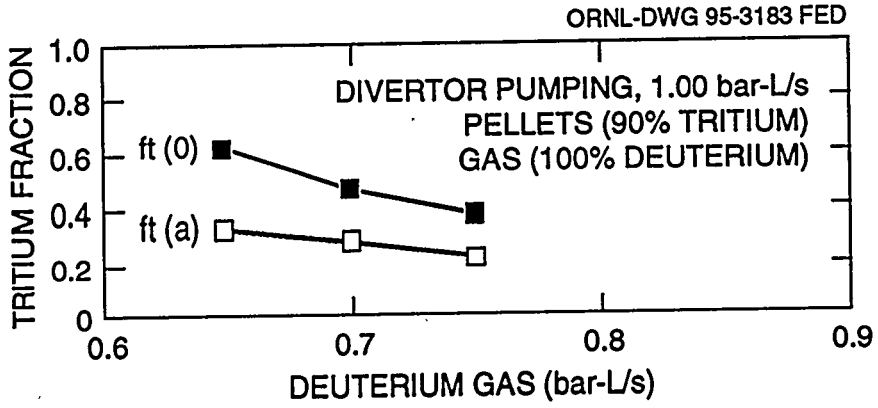

Fig. 5.13. Tritium fraction on axis and at plasma edge as function of deuterium gas fueling level.

axis and at the edge decreases at a constant fusion power of 1500 MW and fueling/pumping throughputs of ~1 bar-L/s as the edge deuterium gas source is increased.

Next, for cases 472–474, a particle pinch term is added, consisting of a neoclassical Ware pinch term and an anomalous pinch term. This results in more effective core fueling by the edge deuterium source and reduces the core tritium fraction relative to case 471. For cases 472–474, the edge fueling by deuterium gas was held constant at 0.75 bar-L/s, and the pellet fueling source was constant at 0.27 bar-L/s. For case 473, the pellet size was increased to an equivalent spherical radius of 0.535 cm (a 15% density perturbation), and the speed increased to 3 km/s. This performance is typical of two-stage pneumatic injectors without sabots or, alternatively, may be viewed as a single-stage pneumatic injector technology with enhanced shielding mechanisms, such as magnetic shielding. For case 474, the pellet size was decreased to an equivalent spherical radius of 0.3 cm (a 1% density perturbation), and the speed decreased to 1 km/s. This parameter range is typical of centrifuge injectors. It can be seen from Table 5.1 that the penetration relative to the minor radius ranged from 25 to 37% for cases 472–474. The effect of penetration on the edge and core tritium concentrations is shown in Fig. 5.14. It can be seen that edge tritium concentration is nearly constant with increasing pellet penetration, while the core tritium concentration increases from 30% to 43%. This is expected and allows the flexibility to decrease the tritium-rich pellet fueling fraction as the pellet penetration increases.

A key conclusion from these results is that it is feasible with baseline ITER systems to maintain a tritium concentration gradient in going from the core to the edge of a D-T plasma. It is possible to maintain core tritium concentrations in the 40–50% range while maintaining edge tritium concentrations in the 20–30% range. The edge D-T ratios are typical of the vacuum vessel exhaust stream isotopic fractions and directly affect lower tritium inventory of plasma-facing components. The flux of deuterium and tritium ions and atoms to these in-vessel components is directly related to the relative inventory of these hydrogen isotopes in the solid matrix. By reducing the edge tritium concentration to 20–30%, this innovative fueling concept results in a reduction by a factor of ~2 in the tritium inventory of plasma-facing components. The higher tritium burn fraction allows a significant reduction in tritium gas flows into and out of the vacuum vessel and, for fusion reactors, implies lower required tritium breeding ratios.

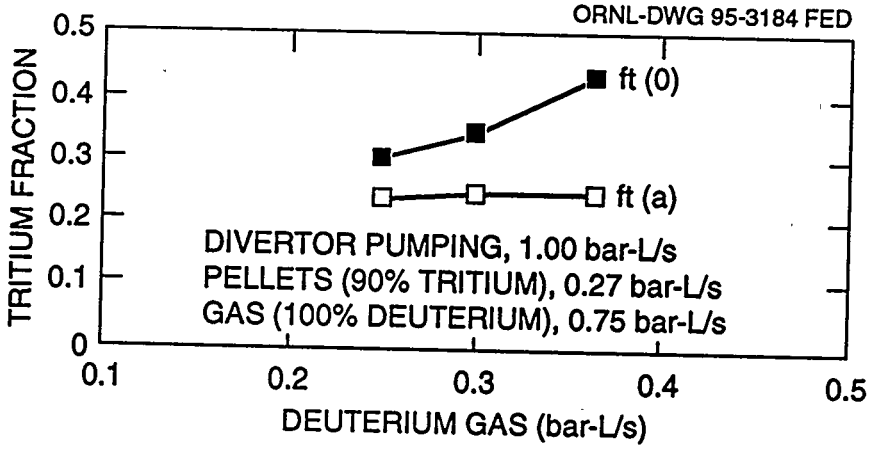

Fig. 5.14. Tritium fraction on axis and at plasma edge as function of normalized pellet penetration.

5.3.7 ITER Rf Systems

ORNL has been actively involved in design and R&D for the ITER ion cyclotron system. Some of the ITER-specific design and R&D activities are summarized here. See Sect. 4.2 for detailed discussion of rf development. Many of these tasks were carried out by ORNL; several were collaborations with other institutions.

5.3.7.1 Rf insulator radiation tests

A resonant cavity technique was used to measure the dielectric constant and loss tangent of ceramic insulators at a frequency near 100 MHz during pulsed fission reactor irradiation near room temperature. Tests were performed on single-crystal and several different grades of polycrystalline Al_2O_3, $MgAl_2O_4$, AlN, and Si_3N_4. Lead shielding experiments were performed for some of the irradiations in order to examine the importance of gamma-ray effects, as opposed to neutron irradiation effects. With the exception of AlN, the dielectric constant of all the ceramics decreased slightly during the pulsed fission reactor irradiation. The dielectric constant of AlN was observed to increase during irradiation. As shown in Fig. 5.15, significant transient increases in the loss tangent to values as high as 6×10^{-3} occurred during pulsed reactor irradiation with peak displacements per atom (dpa) and ionizing radiation fields of 2.4×10^{-6} dpa/s and 4.2×10^{4} Gy/s, respectively. The loss tangent measured during irradiation for the different ceramics did not show any correlation with the preirradiation or postirradiation values. Analysis of the results indicates that the transient increases in loss tangent result from radiation-induced increases in the electrical conductivity. The loss-tangent increases were proportional to the ionizing dose rate in all materials except for AlN, which exhibited a dose rate dependence of ~1.6.

Theoretical calculations were performed to study the thermal conductivity of ceramic insulators during irradiation. The calculations indicate that there should not be any prompt in situ

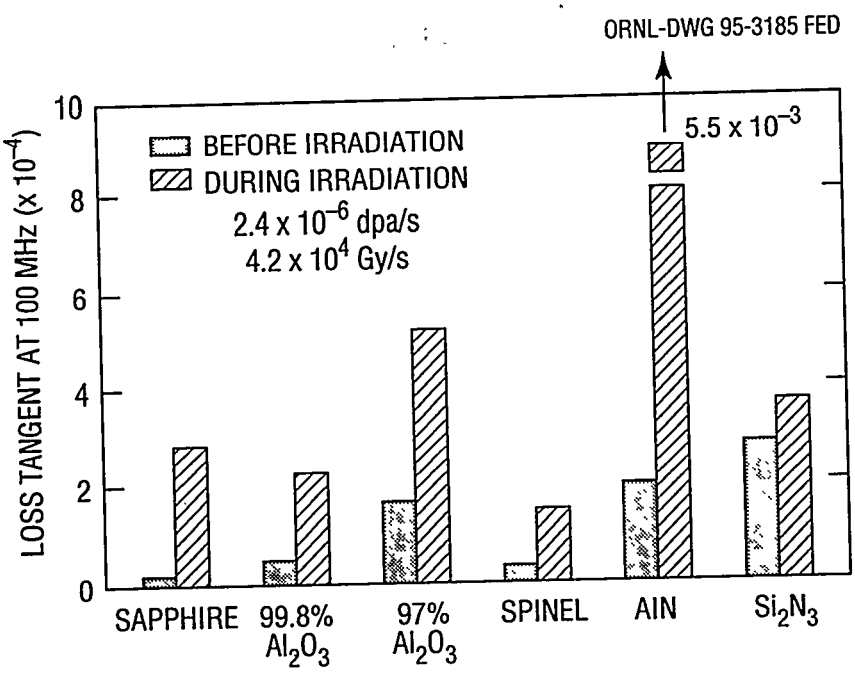

Fig. 5.15. Loss tangent of ceramic insulators during pulsed neutron irradiation.

degradation of the thermal conductivity of ceramic insulators during neutron irradiation beyond what would be detected in a postirradiation measurement, even in specimens that have suffered severe radiation-induced electrical degradation. However, it is possible that significant point defect annealing could occur in the irradiated ceramic during storage at room temperature before the thermal conductivity is measured (typically months after the irradiation). Because of this annealing effect, ITER engineering data on the thermal conductivity of irradiated ceramics should be obtained either in situ during irradiation or else shortly after irradiation. (The sample could also be stored for postirradiation measurements at cryogenic temperatures for longer periods of time.)

5.3.7.2 Antenna survivability study

The response of a prototypical Faraday shield tube to the ITER environment was analyzed. Stringent conditions (as given by the JCT) are assumed: p_{rad} = 100 W/cm^2 from plasma and rf during normal operation; dI_p/dt = 10 MA/ms during a disruption; $E_{disruption}$ = 5 MJ/m^2; and $t_{disruption}$ = 0.5–50 ms (where $E_{disruption}$ is the energy deposited on the Faraday shield during the disruption time $t_{disruption}$). Analysis results may be summarized as follows:

1. For a 50-cm-wide (and -deep) antenna, the disruption-induced stresses are much too high for any material to withstand.
2. For a 35-cm-wide (and -deep) antenna, disruption-induced stresses appear acceptable for a high-strength alloy (e.g., Inconel 625) but unacceptable for a more conventional material (e.g., 316 stainless steel).
3. Disruption thermal loads will melt a beryllium coating under almost all reasonable assumptions about the value of $t_{disruption}$.
4. Tungsten (taken as an example of a refractory metal) might survive without melting for $t_{disruption} \geq 3$ ms.
5. Carbon-coated Faraday shield rods look promising from the standpoint of withstanding the disruption thermal load.

These results were presented to the JCT in Garching, and the large amount of melting, demonstrated by Fig. 5.16, led to a reexamination of the assumptions considered by the JCT.

5.3.7.3 Assessment of rf sheaths and impurity generation with rf

The main tasks and milestones in this area were (1) for ORNL to provide calculated rf fields for the ITER antenna including Faraday screen, (2) for Lodestar to carry out ITER-specific calculations of rf sheath-driven antenna-plasma interactions (convective cells and rf-specific impurity generation), and (3) for Lodestar and ORNL to analyze the JET screenless antenna experiments.

The first milestone was addressed by ORNL in collaboration with SAIC. A simplified two-strap model of the antenna module and Faraday screen was constructed, and the rf fields were computed with the SAIC ARGUS code. The model approximates the main structural and electrical features of the ITER antenna in a simplified (planar) geometry. Further refinements in the model antenna to optimize the resonant frequencies and impedance of the antenna are in progress, but the calculated rf fields from the initial ITER antenna model are sufficient to begin the rf sheath calculations.

The third milestone, to analyze the rf fields and rf sheath effects for the ITER-funded JET screenless A2 antenna experiment, has been addressed in several ways. Lodestar has carried out estimates of the rf power dissipated in the rf sheaths for various phasings as a possible

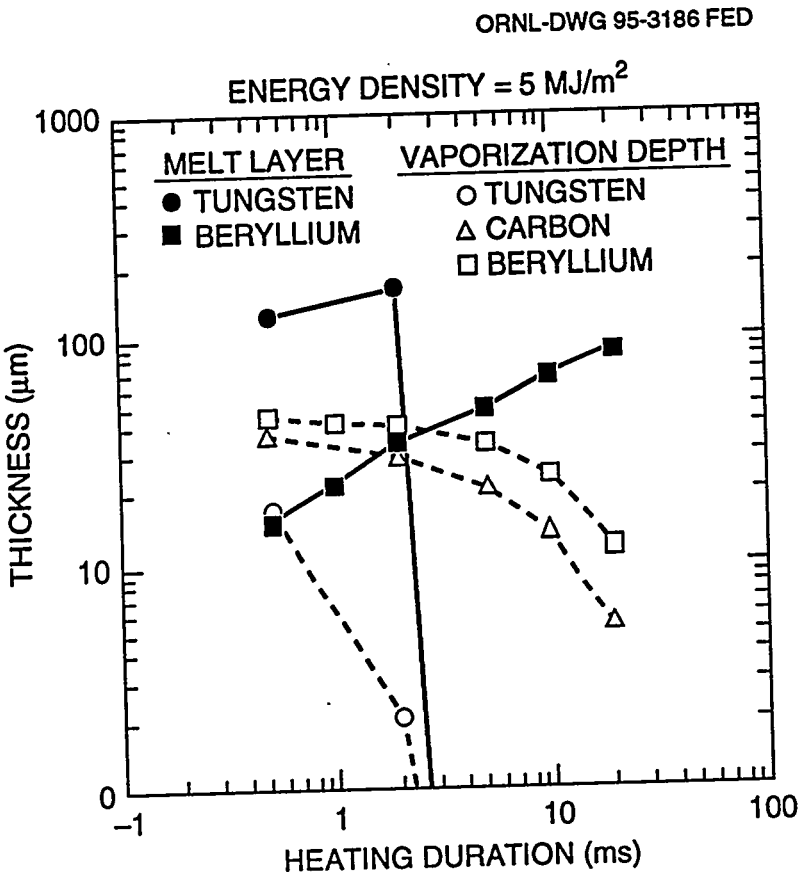

Fig. 5.16. Vaporization depth and melt-layer thickness for disruptions with beryllium, carbon, or tungsten armor.

explanation for the poor heating efficiency and limiter hot spots observed in 0-0-0-0 phasing with a Faraday screen. The results of our preliminary calculation show that rf sheath power dissipation is large in 0-0-0-0 phasing and negligible in 0-π-0-π phasing. However, these calculations do not yet agree quantitatively with the experiment. The ORNL and SAIC team is working to calculate the rf fields of the JET A2 antenna using the ARGUS code with and without the Faraday screen to provide input to the Lodestar ANSAT code for a more complete sheath analysis of the A2 antenna. Finally, measurements of the free-space voltage distribution along the Faraday screen of a full-scale mock-up of the four-strap JET A2 antenna have been carried out at ORNL. These will help benchmark the ARGUS/ANSAT calculations of sheath voltages for the A2 antenna.

ARGUS modeling of the JET A2 antenna [in collaboration with Y. L. Ho (SAIC)]

Modeling of the JET A2 antenna with the ARGUS code is proceeding in incremental stages. The prototype antenna is highly curvilinear with corrugated rear walls; the Faraday shield bars, as well as the ends of the straps and box, are angled for approximate alignment with the magnetic field lines. This complicated geometry presents some problems for accurate modeling of the structure with a Cartesian mesh, and there may be practical limits to the number of mesh nodes that can be accommodated. Therefore, the modeling effort is being undertaken in stages (described below), each one representing a more accurate, albeit more difficult, approximation of

the actual geometry. The relative accuracy of the approximations will be checked against electrical measurements.

1. The antenna will be modeled after the JET A2 "flatbed" mock-ups, which are currently undergoing electrical testing at ORNL. These mock-ups use straight sections of metal for the walls and straps, which can be aligned more easily with the solution grid. For the same reasons, the ends of the box and straps will be straight rather than slanted. The initial runs will not employ a Faraday shield, and the corrugated, curved rear wall will be replaced by a smooth, slanted wall at the appropriate position to duplicate the electrical characteristics of the antenna. This geometry is close to completion.
2. The next step is to add the Faraday shield, for which the number of mesh points will need to be tripled. The Faraday shield will be straight for these runs.
3. The final step is to slant the Faraday shields, strap ends, and box ends for alignment with the magnetic field of the machine. At this stage, corrugation may be added to the rear wall, if practical.

Voltage potential distribution measurement along JET A2 Faraday shield antenna during vacuum operation

Radio frequency voltages are induced on the frame and Faraday shield of ICH antennas by the time-varying magnetic fields produced by the current straps; these potential differences are the EMF responsible for the formation of rf sheaths. Capacitive probes have been designed and fabricated, and instrumentation to measure this potential distribution in free-space operation of antennas has been tested.

Free-space voltage measurements, although not directly applicable to plasma operation, are still important for two reasons. First, they provide additional points to test the validity of antenna design codes. Second, plasma presents only a weak load to an antenna, and the circulating power stored in the evanescent near-fields is much greater than the real power delivered to the plasma by propagating waves. ICH antennas typically operate with a Q of 20–25 (as opposed to a vacuum Q of 100–200), indicating that the reactive power and the evanescent near-fields responsible for the Faraday screen and frame voltages still dominate even in the presence of plasma. These voltages are the "open circuit" Thevenin's equivalent EMF without the plasma load.

Voltage measurements along the Faraday shields have begun on the full-scale mock-ups of the JET A2 antennas. (The mock-ups are also referred to as the "flatbed" antennas.) Each JET A2 antenna is a four-element array consisting of two double-strap modules, which are basically mirror images of each other. The power for both the inner and outer straps for each module is introduced through ports located behind the outer straps. Each transmission line feeds two poloidally-stacked, end-grounded straps connected in parallel. The parallel straps present different electrical loads at the match point because of geometrical differences between them. Currents in one section of the strap influence other sections of the same strap as well as neighboring straps because of internal inductive coupling. The lengths of the inner and outer straps differ; moreover, the inner straps are fed from ports located behind the outer straps, resulting in: (1) increased coupling between the inner and outer straps because of the long feed lines and (2) greater disparity between the electrical loads presented at the inner and outer feed ports.

One double-strap module was driven with a network analyzer, an amplifier, and a power splitter; each strap was matched at its input port to give an equal power division, and attenuators were adjusted to give equal strap currents. For some of the measurements, an additional length of line was added to the outer strap circuit to compensate for the phase shift associated with the internal crossover section, which feeds the inner straps. Voltage phase and amplitude were

monitored at a point 20 cm from the strap grounds to ensure that the straps were being driven equally with the proper phase relationship. The Faraday shield measurements have been normalized to these reference voltages. Figure 5.17 shows the voltage distribution along the poloidal direction of the antenna at 42 MHz; the measurements are taken at the end of each Faraday shield element. Strap A is the outer strap, and strap B is the inner. The shield tubes are numbered sequentially, with low numbers at the bottom and high numbers at the top of the module. The most noticeable feature is that the magnitude of the voltage induced in the Faraday shield/antenna frame is much higher for in-phase (monopole) operation than for out-of-phase (dipole) operation. The ground reference point (instrument ground) is taken as the potential of the antenna back-plane at the power feeds. The minimum Faraday shield voltage occurs at the poloidal location of the tap points on the straps, not the point at which the power enters the

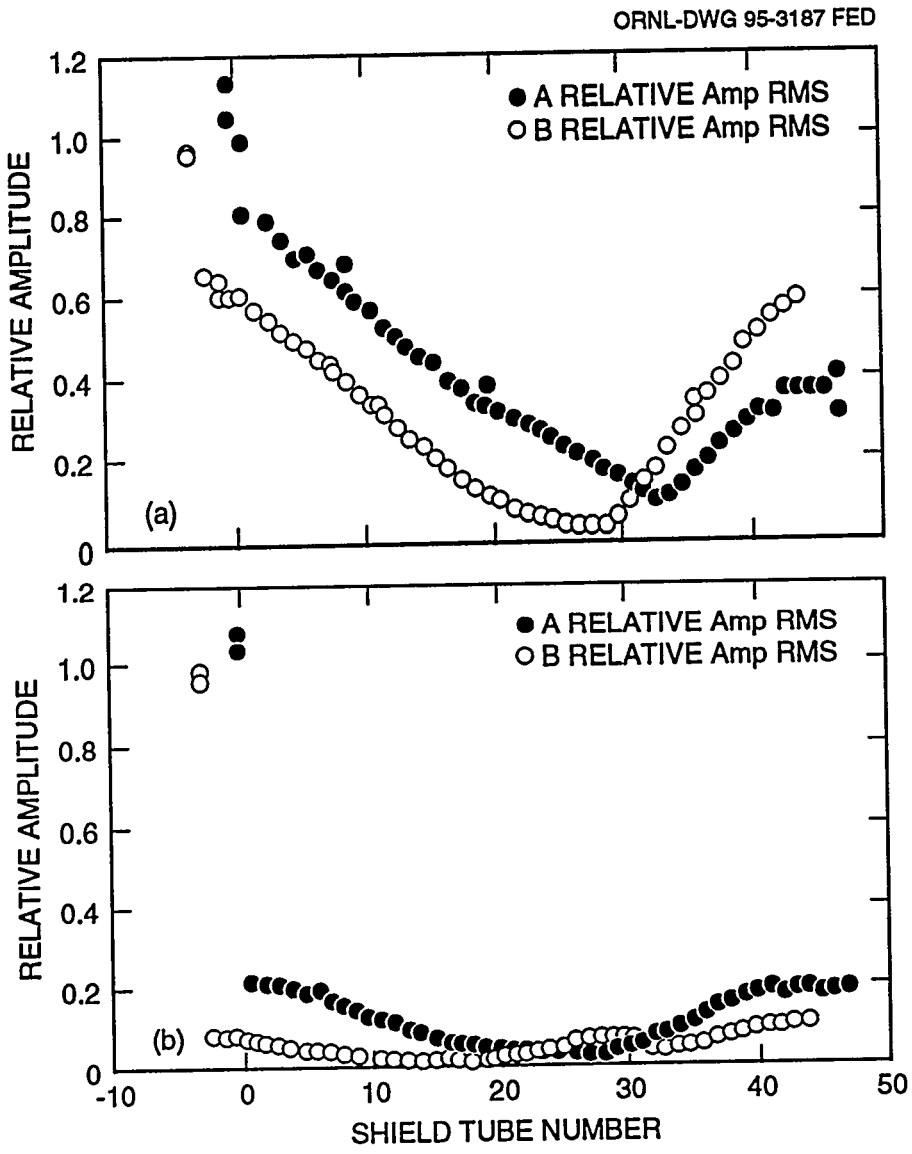

Fig. 5.17. Voltage amplitude distribution on ends of Faraday shield tubes along poloidal direction of JET A2 antenna. (*a*) Inner and outer straps driven in phase; (*b*) inner and outer straps driven out of phase.

cavity. The phase of the voltage reverses as the tap points are passed, as shown in Fig. 5.18. The phase measurements are less clean in the dipole-driven case because of the smaller amplitude of the signals.

These measurements will continue and will include the voltage distribution along the Faraday shield in the toroidal direction, as well as the frame voltage distribution in the absence of the Faraday shield. These measurements will be used in the interpretation and analysis of future operation of the JET antennas without the Faraday shield.

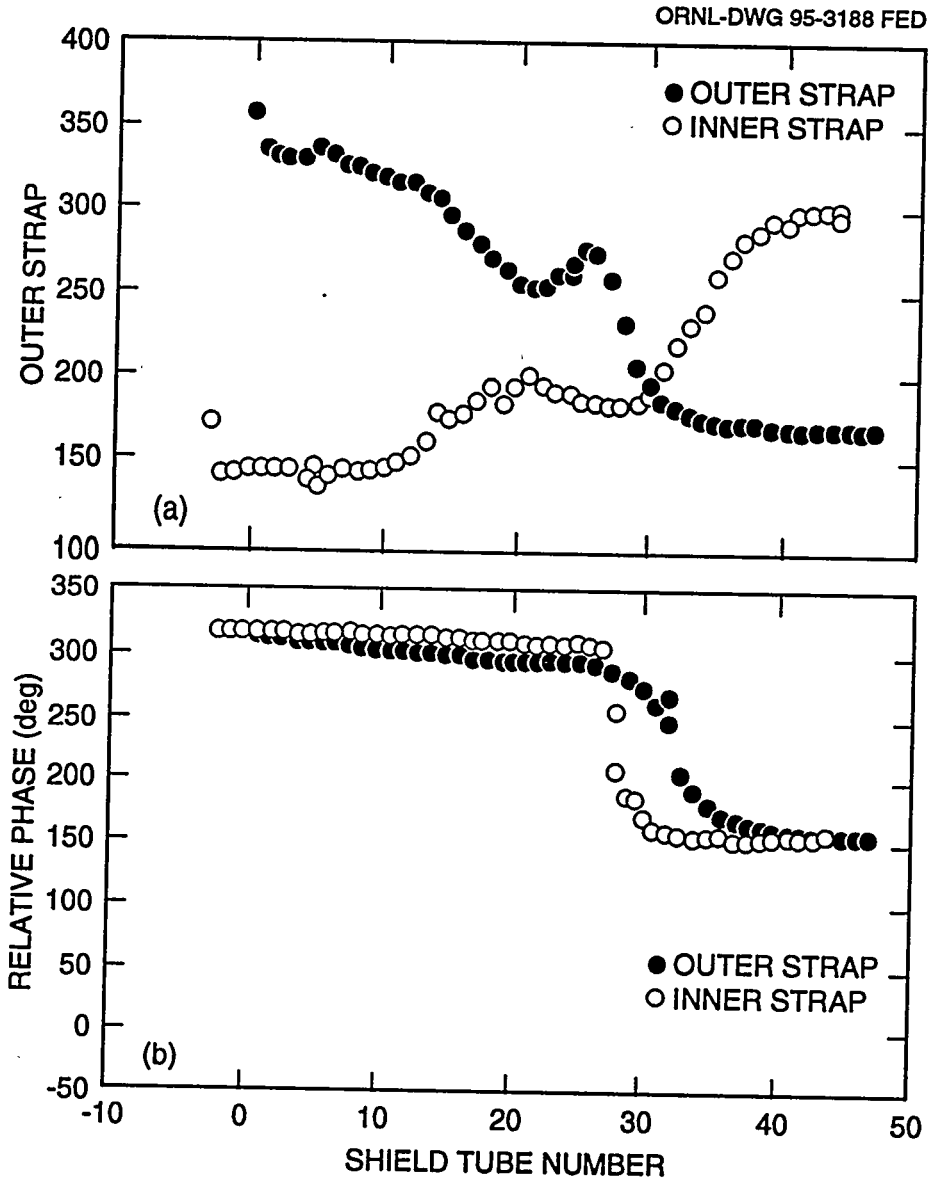

Fig. 5.18. Voltage phase distribution on ends of Faraday shield tubes along poloidal direction of JET A2 antenna. (*a*) Inner and outer straps driven out of phase; (*b*) inner and outer straps driven in phase.

5.3.8 Innovative Materials for Divertor Applications

The ITER divertor target will be constructed from beryllium armor bonded to a dissimilar metal coolant structure. Conventional joining approaches such as brazing or diffusion bonding of the beryllium to the coolant structure lead to interface stresses in the bond region caused by the mismatch in thermal expansion. These large stresses in the interface region make it challenging to reliably fabricate and maintain adequate bonding between the two materials. The purpose of this study is to develop methods to reduce these interface stresses by using graded and/or compliant interlayers of appropriate materials between the beryllium and coolant structure.

Initial activities in this area, supported with program development funds, were successful in identifying several interlayer materials to be used in joining beryllium to copper. Based on this work, funds were distributed to support the next phase of this effort—fabrication and testing of a set of beryllium-joining test specimens.

Three specimens of each of the following types were fabricated using various compliant interlayers between the beryllium armor layer and a copper or vanadium alloy substrate:

1. 5 mm Be, 0.1 mm Ag foil, 1 mm Ni, Cu alloy Elbrodur-G
2. 5 mm Be, 0.1 mm Ag foil, 1 mm Fe, Cu alloy Elbrodur-G
3. 5 mm Be, 0.1 mm Ag foil, vanadium alloy (V-5Cr-5Ti)
4. 5 mm Be, 1.6-mm layer graded from 100% Be to 60% Be/40% Al, 0.1 mm Ag foil, Cu alloy Elbrodur-G

The layers of material in each specimen were joined using hot isostatic pressing (HIP). All three of the graded layer specimens (item 4 above) were successfully joined, whereas two out of three of each of the other specimens remained intact after removal from the HIP chamber.

Future plans call for metalographic inspections of specimens and characterization of bond integrity. The use of silver foils in ITER has recently been identified as a critical issue. Silver may be unacceptable for ITER because of transmutation to cadmium. If silver is unacceptable, a substitute barrier layer will need to be identified and studied.

5.3.9 14-MeV Neutron Source

This task involves coordination of the U.S. effort to define and prepare for a "14-MeV" neutron irradiation facility for fusion materials R&D. Irradiation needs, overall facility layout, and remote-maintenance requirements will be studied as part of the coordinated U.S. effort. The task also includes coordination and possible collaboration with the various foreign programs in this area.

The need for a high-flux, high-fluence neutron irradiation facility for fusion materials R&D has long been recognized and endorsed by both the U.S. and foreign fusion programs. Because the radiation damage to materials depends upon the neutron energy spectrum, the effects of fusion neutron irradiation can be substantially different from those of fission neutron irradiations. Consequently, a fusion irradiation facility must provide the necessary spectral characteristics as well as the fluxes and fluences needed for accelerated end-of-life testing of materials. A source based on the Li (d,n) reaction, using 35- to 40-MeV deuterons from an accelerator on a flowing lithium target, is the most favored concept and formed the basis of the FMIT project, which was started in the late 1970s and later canceled.

Fusion is now preparing to enter the nuclear phase of development, as evidenced by the initial D-T operation of JET, the planned D-T operation of TFTR, the growing commitment to ITER, and the National Energy Strategy's goal of an operating demonstration in about the year

2025. Furthermore, there is increasing acceptance of the critical importance of low activation material development to the success of fusion as an energy source. All these facts increase the urgency of proceeding with the Fusion Neutron Source. There is a real possibility of international collaboration in such a facility, perhaps as part of the ITER process.

The short-term goal is to prepare for a serious CDA, possibly with international partners. A single design study team will be set up by coordinating the work of the R&D institutes currently involved and soliciting industrial participation. The objective will be to produce a preconceptual design report that represents a consensus U.S. position as a basis for an international CDA. In parallel, a case will be prepared for DOE to propose an international CDA to start in mid- to late FY 1994.

REFERENCES

1. D. Leger, P. Dinner, et al., *ITER Fuel Cycle,* ITER Documentation Series, No. 31, IAEA, Vienna, 1991.

2. M. J. Gouge, K. D. St. Onge, S. L. Milora, et al., "Pellet Fueling System for ITER," *Fusion Eng. Des.* **19**, 53–72 (1992).

3. M. J. Gouge, W. A. Houlberg, S. E. Attenberger, et al., "Fuel Source Isotopic Tailoring and Its Impact on ITER Design, Operation and Safety," to appear in *Fusion Technol.* (1995).

4. W. A. Houlberg, S. E. Attenberger, and M. J. Grapperhaus, "Density Profile Control in a Fusion Reactor Using Pellet Injection," *Nucl. Fusion* **34**, 93–108 (1994).

6

ADVANCED TOROIDAL SYSTEMS

T. E. Shannon[1]

D. B. Batchelor
K. W. Buchanan
M. D. Carter
M. J. Cole
J. G. Delene
C. H. Fogleman
P. J. Fogarty[1]
J. D. Galambos[2]
P. L. Goranson[1]
R. C. Hudson[3]
E. F. Jaeger
G. H. Jones
U. P. Lickliter
J. F. Monday[1]
J. L. Ping
B. E. Nelson[1]
Y.-K. M. Peng
M. J. Rennich
J. A. Rittenhouse
R. O. Sayer[2]
A. V. Smirnov
D. C. Stallings
J. W. Stapleton
K. D. St. Onge
D. J. Striclker[2]
D. W. Swain
D. J. Taylor
D. W. Theisen

1. Engineering Division.
2. Computing and Telecommunications Division.
3. Engineering Technology Division.

6. ADVANCED TOROIDAL SYSTEMS

Summary of Activities

The advanced toroidal systems group has been pursuing design studies for future fusion experiments. These systems include fusion energy economic assessments, spherical tokamak (ST) research, and long-pulse Tokamak Physics Experiment (TPX) engineering design and research and development (R&D) studies. The fusion energy economic assessment task provides analyses and assistance for the Magnetic Fusion Energy Program in the area of economics of fusion energy and the interrelation of the economic, safety, and environmental aspects of magnetic fusion energy. The ST research program develops *innovative* ST physics, quantifies ST applications for testing critical fusion technologies, and investigates future demonstration and power reactor concepts.

Oak Ridge National Laboratory (ORNL) is serving as a major partner in the TPX project, with design and R&D responsibility for remote maintenance, rf heating and current drive, radiation shielding, and vacuum pumping systems. ORNL is also a key partner in the TPX physics program, with task group leaders in the areas of physics integration and heating and current drive. Hutch Neilson serves as the TPX Physics Manager (as well as the Deputy Project Director). From 1992 to mid-1993, ORNL was involved in the conceptual design of the TPX device, culminating in a successful conceptual design review. The balance of 1993 was devoted to advanced conceptual design, followed by the initiation of preliminary design in 1994. Also during 1994, R&D activities to investigate key issues identified during the conceptual design were begun. This chapter describes the status of the design and R&D activities in the various areas of responsibility.

6.1 FUSION ENERGY ECONOMIC ASSESSMENTS

J. G. Delene

Magnetic fusion energy is nearing the point of demonstration feasibility. For fusion energy to be an eventual commercial success, it must deliver energy at a competitive price and have acceptable environmental and safety characteristics. A thorough understanding of the economics of fusion energy is needed in order to make choices involving the environment, safety, and economics and to guide program direction. This task has as its goals the continued improvement of the fusion costing models and methods and the consistent analysis of fusion reactor economics vis-a-vis environmental and safety goals and in comparison to other energy sources.

This task provides analyses and assistance for the Magnetic Fusion Energy Program in the area of economics of fusion energy and the interrelation of the economic, safety, and

environmental aspects of magnetic fusion energy. The scope of this work includes participation in Magnetic Fusion Energy environmental, safety, and economic programs; development of cost models and methods for fusion energy studies; review and analysis of economic studies and proposals for inertial confinement fusion; and ad hoc assistance in the general area of fusion energy economics.

An analysis of the net benefit of siting ITER in the U.S. was completed.[1] Assistance was provided to DOE programs on the economics of fusion[2] and in the review of commercial reactor studies.

6.2 ST RESEARCH PROGRAM

Y.-K. M. Peng

Low–Aspect-Ratio Spherical Tokamak (ST) Research develops *innovative* ST physics, quantifies ST applications for testing critical fusion technologies, and investigates future demonstration and power reactor concepts. Innovative ST physics deals with compact, stable, low-field plasma configurations characterized by good confinement, order-unity levels of plasma beta and self-driven current fraction, and thick outboard SOLs connected to naturally formed long-channel divertors. Research activities include

- collaborating with the University of Texas at Austin and PPPL to develop practical designs for near-term experiments in the 0.5 to 1.0 MA range and providing input as requested by other U.S. institutions interested in pursuing ST fusion research;
- studying concepts for economically competitive ST demonstration and power reactors and small-blanket test facilities volumetric neutron source (VNS) to guide the current ST research;
- collaborating with foreign institutions active in ST research such as the Small Tight Aspect Ratio Tokamak (START) at Culham, U.K.; GLOBUS-M at Ioffe, Russia; and SARIT at the University of Tel Aviv, Israel, and the possibility of collaborating with Mega-Ampere Spherical Tokamak (MAST) researchers at Culham and Superconducting Tight Aspect Ratio Experiment researchers at the Korean Basic Science Center in South Korea; and
- providing input to studies to determine the mission and the cost-effective designs for nearer-term miniature VNSs at the 5–10-MA level.

6.2.1 ST Research

Theoretical motivation for the study of the ST plasma, characterized by $1 < R_0/a < 2$, has been to obtain a more compact configuration requiring lower fields and permitting higher betas than tokamaks of standard R_0/a values.[3] The ST plasma has recently been tested in START at the 0.2-MA level and shown to possess these basic properties;[4,5] the results are generally similar to or better than projections using the standard tokamak database. If verified at the mega-ampere level for collisionless plasmas, these intrinsic features will make smaller, lower-cost ST fusion devices possible for testing advanced concept divertors under steady-state conditions, and subsequently at the multiple–mega-ampere level, for testing fusion nuclear technologies under integrated, reactor-relevant conditions. If further verified at the 30–40-MA level, these ST features may prove to be most economical for DEMO and fusion reactors.

ORNL has established a number of collaborative experimental efforts to produce ST physics data at low costs. Collaborations include active participation in the START experiment design, construction, and operation at Culham Fusion (U.K.) and an "enhanced collaboration" to

construct and perform experiments on the 0.4-MA GLOBUS-M facility with the Ioffe Institute (Russian Federation). These ST devices provide opportunities for testing the basic ST plasma properties now and in the next few years. A proposal to construct the GLOBUS-M device at the Ioffe Institute under the auspices of the International Science and Technology Center (ISTC) has just been approved.

The background for the ST option for testing ITER divertor concepts[6–8] is as follows: (1) With $I_p \approx 1.0$ MA, $B_{t0} \approx 0.5$–1.5 T, and $R_0/a \approx 1.2$–1.6, the device can provide reactor-level divertor power and particle fluxes when driven with only 5 to 10 MW of auxiliary power. (2) Such a device would provide a low-cost integrated environment for testing and verifying divertor concepts needed in future large tokamaks (such as ITER) as well as small ST applications. (3) The steady-state power supplies, heat removal systems, and basic facilities needed for the operation of such a device are available at several fusion institutions. (4) This ST experiment with $R_0/a \approx 1.2$ is capable of testing the advanced-regime physics as described in Sect. 6.2.1.2.

Finally, a high-volume, plasma-based neutron source (HVPNS)[9] for testing nuclear fusion technologies is currently accepted by the International Energy Agency (IEA) as a possible component in the world fusion program. The tokamak-based HVPNS options are included in the U.S. Volumetric Energetic Neutron User Study (VENUS), to which ORNL is making major contributions. To produce neutron wall loads in the range of $W_L \approx 1$ MW/m^2 in an ST-based HVPNS, present estimates indicate rather modest requirements: $R_0 \approx 0.8$ m, $R_0/a \approx 1.3$, $B_{t0} \approx 2$ T, $I_p \approx$ 6–8 MA, $P_{aux} \approx 20$ MW, and $Q \approx 1$. Given positive ST physics and divertor database, the ST-based HVPNS has the potential to provide a highly cost-effective integrated magnetic fusion environment for testing critical fusion nuclear technologies.

Recent studies in this research have identified a compact design concept for potentially attractive ST power reactors. The results have raised interest by the DEMO Study team led by UCSD, which recently included the ST as an option for its DEMO concepts and requested our participation in its study. The ST program will participate to ensure that the physics and design concepts are properly directed in this upcoming study of the ST DEMO option.

6.2.1.1 ST experimental research collaboration

The ST research program identifies potentially available facilities and equipment in the U.S. and elsewhere for use in carrying out near-term tests of ST physics. Collaborative arrangements with such institutions in turn bring about highly leveraged use of limited ST program funds to make significant progress. For the longer term, the program also identifies institutions with potential interest in pursuing major ST devices and solicits their participation in fusion technology development. Specific collaborations are discussed in the paragraphs that follow.

The START experiment at Culham Fusion (U.K.) was the first successful ST physics test developed with this approach. START continued to produce ST plasma parameters similar to or better than projections based on the standard tokamak data. Following upgrades to the power supply, PF coils, and central solenoid, plasma parameters have been obtained for I_p up to 0.25 MA and R_0 up to 0.32 m. Plasma beta values approaching half of the first-regime Troyon limit have been observed. Major plasma disruptions have remained absent for the nearly 25,000 plasma pulses in START as long as $R_0/a \leq 1.8$. Double-null divertor configurations have been obtained using the small-radius induction coils. Measurements of the outboard edge plasma continue to indicate a strong cross-field transport (SOL ~3 cm thick) despite relatively high electron temperatures (~50 eV) and densities (0.3×10^{14} cm^{-3}) at the last closed flux surface. The data indicate that the plasma parameters in START are comparable to those observed in standard modest-field (1–2 T) tokamaks with similar plasma currents and about 5 times the major radii. ORNL scientists will continue working as part of the START team to install and commission the

NBI system, which will permit tests of confinement, beta limits, and high-pressure–driven currents of strong auxiliary heating; ORNL scientists will also continue to contribute to the development of MAST, the next ST experiment at Culham Fusion to follow the START program.

During FY 1993, a Russian team led by the Ioffe Institute of St. Petersburg, under contract with ORNL, completed the preliminary GLOBUS-M design[10] and a joint proposal to the ISTC for construction funding. GLOBUS-M is designed to use the FT-2 tokamak experimental hall and much of the equipment at the Ioffe Institute to produce ST plasmas of $I_p \approx 0.4$ MA, $B_{t0} \approx 0.5$ T, and $R_0/a \approx 1.6$ for durations up to 0.2 s. The joint ORNL-Ioffe proposal for ISTC funds to construct GLOBUS-M was submitted to ISTC in January 1994. An international review of the proposal (and at least 46 others) was carried out during 1994. ISTC has recently approved the GLOBUS-M project, and the device is scheduled for experimental operation in the FY 1998 time frame. The contract between Ioffe and ISTC is nearly finalized. The ORNL-Ioffe collaboration will continue through construction and subsequent experimentation.

In 1994 the parameters for MAST were updated to $R_0 \approx 0.7$–0.8 m, $R_0/a \approx 1.25$–1.45, $B_{t0} \approx 0.2$–0.6 T, $q_{edge} \approx 7$–15, and $P_{drive} \approx 2$–6 MW for advanced-regime experimentation under density control ($n_{e0} \approx 0.5$–1×10^{14} cm^{-3}). This shift in the physics goal was determined by recent study results that define the advanced-regime ST physics and were reported at the 1994 IAEA Conference on Plasma Physics and Controlled Nuclear Fusion Research.[11] Whereas a mega-ampere–level ST device can be built at relatively low cost ($5–15M, depending on the pulse length and component vendor), the long-pulse auxiliary drive systems, magnet and drive power supplies, divertor power and particle-handling systems, and heat removal systems will require a larger expenditure (total $10–20M), even if steady-state facilities and equipment are assumed to be available. Three proposals have emerged during the past year: MAST (Culham, U.K.), National Spherical Tokamak Experiment (NSTX) at PPPL, and El Toro Grande (ETG) at the University of Texas at Austin). The MAST proposal has recently obtained European Community approval for its ohmic experiment phase; the proposal for the subsequent heating and longer-pulse experiment is to be reviewed at a later time. ORNL is contributing directly to the NSTX and ETG proposals, which were prepared for submission during spring 1995.

6.2.1.2 ST power reactors

A set of pioneering calculations were carried out during 1994 to define the goals for an advanced physics regime for the ST plasma for $R_0/a \approx 1.2$–1.5. The plasma is characterized by good confinement, order-unity levels of average plasma beta and self-driven current fraction, high natural elongation without vertical instabilities or major plasma disruptions, and thick outboard SOLs connected to naturally formed long-channel divertors. Such plasmas would lead to a 20–30% reduction in COE in a power plant relative to the most economic power plant based on the advanced physics regime for high R_0/a (~4.5). The status and prospects for ST research were summarized, covering the most recent results, during the Sixth Toki Conference and will be published in *Fusion Technology*.[12]

Improved parameters for the ST VNS were produced as part of the VENUS studies (ERAT942). They are: $R_0 \approx 0.8$ m, $R_0/a \approx 1.3$, $B_{t0} \approx 2$ T, $I_p \approx 6$–8.6 MA, $P_{aux} \approx 20$–30 MW, and $P_{fusion} \approx 30$ MW, to produce an average neutron wall loading of 1 MW/m^2. The range for I_p and P_{aux} reflect the impact of uncertainties in the plasma projections, which are to be clarified by the MAST experiments. The overall weight of the ST device is estimated at ~500 tonnes plus a total shield weight of about 2000 tonnes, about 1/20 of the ITER device weight.

6.2.2 VNS

ORNL participation in the U.S. VENUS program includes

1. development of a nationally based, technically and financially feasible plan for a low-cost VNS device to test nuclear technologies (such as power-producing and tritium-breeding blankets), which is critically needed by a fusion power demonstration plant (DEMO);
2. contribution to the International Fusion Technology Test Facilities Studies under the auspices of the IEA;
3. refinement of the design concepts for the tokamak-based VNS and development of the lowest-cost technically viable tokamak VNS option; and
4. establishment and management of "enhanced collaboration" subcontracts with fusion and technology institutions in the Russian Federation to maximize the progress of the VENUS program.

A recent decision by the Fusion Power Coordinating Committee (FPCC) under the aegis of IEA has identified HVPNS as a blanket test facility potentially important in developing nuclear technology for the DEMO. FPCC approved the start in 1994 of an internationally based assessment of the mission and the need for such a facility. The IEA-sponsored study of HVPNS is expected to continue in 1995. The contribution by such a facility (a fusion engineering research facility) was amply quantified by the UCLA-led FINESSE study during 1984–1986. Since then, progress in fusion research has introduced the possibility of highly attractive small versions of the tokamak for this purpose. The VENUS program was established to track this progress and reevaluate the technical and cost feasibility of the nuclear testing program as part of the DEMO R&D. ORNL is a key contributor to the VENUS program and an advocate for small, practical fusion nuclear technology such as VNS.

JET and TFTR are expected to verify driven D-T–fueled fusion burn at Q approaching 1 in tokamaks (for $I_p \approx$ 2–5 MA and $P_{DT} \approx$ 10–30 MW) by 1998. These devices and JT-60U have recently demonstrated high bootstrap current fractions (up to 80%) and full current drive via NB and rf injection. Because of the large wall areas of these devices (~200–300 m^2 with $R_0 \approx 3$ m), the fusion neutron wall loading (W_L) can only be about 0.1 MW/m^2, which is about one order of magnitude below that needed for adequate nuclear testing. Based on the driven standard tokamak physics, recent studies of the tokamak VNS envelope,[9] sponsored by IEA, have shown that a relatively sizable and costly device ($R_0 \approx 2$ m, $B_{t0} \approx 6$ T, $I_p \approx 6.4$ MA, $P_{aux} \approx 70$ MW) would be required to produce $W_L \approx 1$ MW/m^2. A much smaller, lower-field, driven tokamak producing the same wall load would be desired to make the VNS program financially feasible.

Recent advances in the physics tests of the low–aspect-ratio tokamaks (STs) have shown that this may be possible. Data from START (U.K.), the Helicity Injected Tokamak (University of Washington), and TS-3 (University of Tokyo) suggest that the plasma properties at low aspect ratio ($R_0/a \approx$ 1.3–1.5) are better than projections based on tokamak data at the standard aspect ratio. Recent analysis of plasma properties improved by the initial data also produced encouraging results. An advanced physics regime has been identified for the ST plasma, characterized by order-unity stable average beta; order-unity, self-driven current fraction; good confinement permitted by high plasma shape factor; vertical stability and disruption-free operation with high plasma elongation; and divertors with thick, long channels that do not require divertor coils. Four separate proposals for experimentation at the mega-ampere level of plasma current have emerged recently, one of which has just been approved for construction (GLOBUS-M, Ioffe Institute).

This progress points to the possibility of a highly cost-effective, steady-state ST VNS with $R_0 \approx 0.8$ m, $R_0/a \approx 1.3$, $B_{t0} \approx 2$ T, $I_p \approx 6$ MA, $P_{aux} \approx 20$ MW, $W_L \approx 1$ MW/m^2, and $Q \approx 1$. At modest fields, the TF coils can, in principle, be made demountable to permit operations at high

availability and fluence. The center leg of the TF coils can be an unshielded and actively cooled and can have a single conductor to prevent excessive insulator exposure to irradiation. The important contribution of fusion nuclear technology testing toward the goal of DEMO operation by 2025 and the strong prospect of a feasible and cost-effective ST VNS have enhanced the basis for the VENUS program.

The progress of this program is summarized in the *Phase 1 Report of the IEA Study on High Volume Plasma-Based Neutron Source (HVPNS)*,[9] which was presented recently to the international community.

6.3 TPX COLLABORATION

TPX is proposed as the next major tokamak device in the U.S. fusion program and will be built at PPPL. The TPX mission is to develop the scientific basis for a compact, continuously operating tokamak fusion reactor. To accomplish this goal, TPX will be the first tokamak to have superconducting TF and PF coils and will be designed for steady-state operation. A pictorial view of TPX is shown in Fig. 6.1.

ORNL is a major partner in the TPX project, with responsibility for design and R&D of remote maintenance, rf heating and current drive, radiation shielding, and vacuum pumping systems. ORNL is also a key partner in the TPX physics program, with task-group leaders in the areas of physics integration and heating and current drive. Hutch Neilson serves as the TPX Physics Manager and Deputy Project Director.

From 1992 to mid-1993, ORNL was involved in the conceptual design of the TPX device, culminating in a successful Conceptual Design Review (CDR). The balance of 1993 was devoted to advanced conceptual design, and preliminary design was initiated in 1994. Key issues identified during the conceptual design were also investigated in 1994. The following sections describe the status of the design and R&D activities in the various areas of responsibility.

6.3.1 Remote Maintenance

G. H. Jones, M. J. Rennich, J. A. Rittenhouse, A. V. Smirnov, J. W. Stapleton, and D. W. Theisen

The TPX machine design incorporates comprehensive planning for efficient and safe component maintenance. Three programmatic design decisions have been reached to ensure this objective is achieved. First, the tokamak will incorporate radiation shielding to reduce activation of components and limit the dose rate to personnel working on the outside of the machine. This allows most of the ex-vessel equipment to be maintained through conventional "hands-on" procedures. Second, to the maximum extent possible, low activation materials will be used inside the shielding volume. Titanium (Ti-6Al-4V) has therefore been selected for the vacuum vessel and PF coil structures. Third, the primary in-vessel components will be replaced and repaired using remote-maintenance tools specifically provided for the task. The component designers have been given the responsibility of incorporating maintenance design and proving the maintainability of the design concepts in full-scale mock-up tests before final fabrication is begun.

A design team led by ORNL will provide general-purpose tools for remote maintenance of the TPX machine. Major tools will include an in-vessel transporter, a vessel transfer system, and a large component transfer container. In addition, this ORNL-led design team will provide tools such as manipulators and remotely operable impact wrenches to the component designers. Maintenance systems will also provide the necessary controls for this equipment.

ORNL-DWG 95-3270 FED

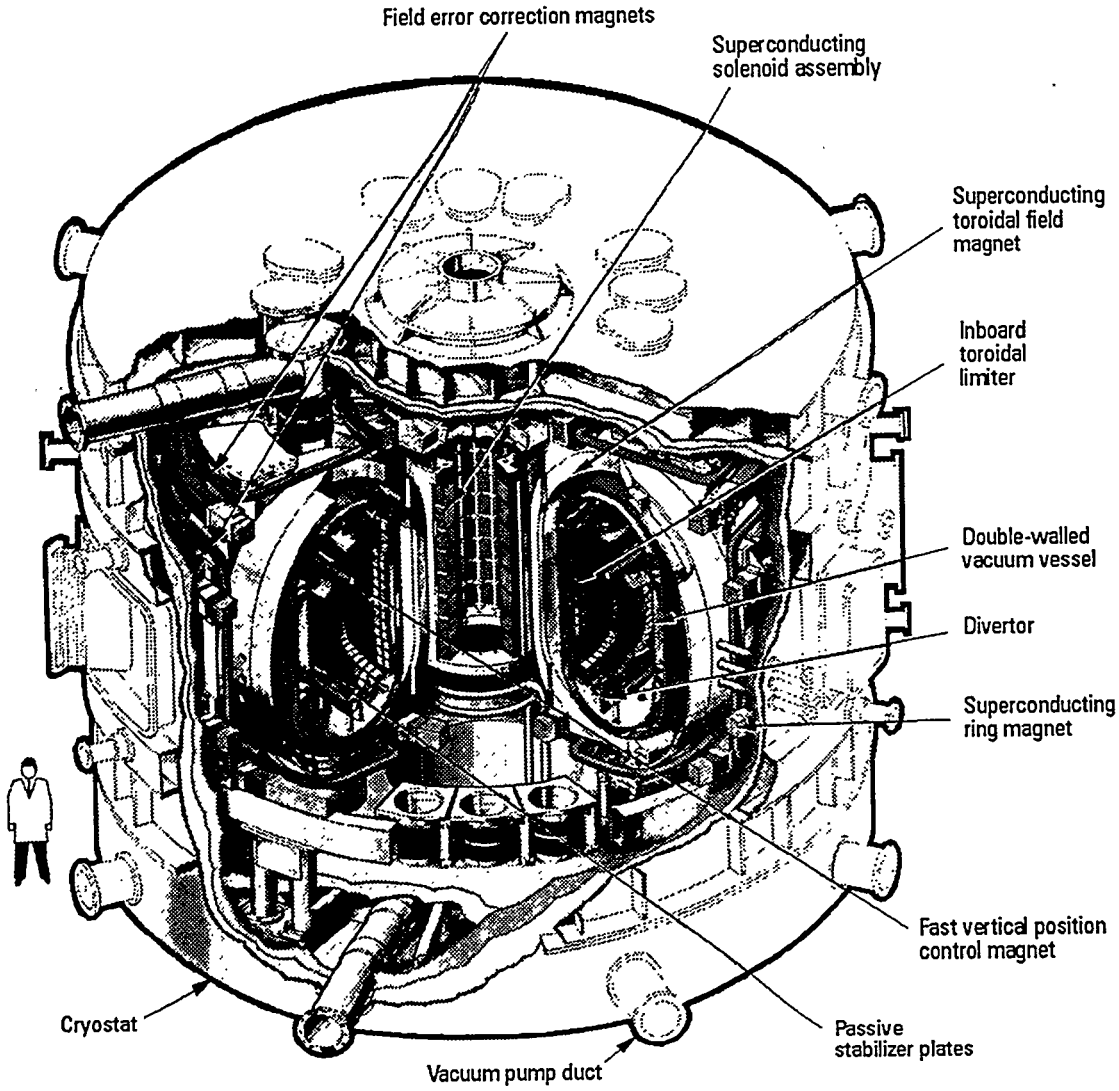

Fig. 6.1. Pictorial view of TPX tokamak.

6.3.1.1 In-vessel vehicles

A two-vehicle, track-mounted system will be used to maintain and replace the in-vessel modules. (See Fig. 6.2.) A track-mounted system was selected because of the limited working volume inside the TPX vessel and the requirements for stability under heavy loading. The functional vehicle, referred to as the tractor, will mount manipulators, lights, and cameras. All functional systems will be electric powered and will be controlled through a single umbilical cable. The cable will be deployed from access port "A" on a constant tension reel with provisions for feed in both directions. Thus the vehicles will cover the interior of the vessel by moving 180° to either side of the access port.

ORNL-DWG 95-3271 FED

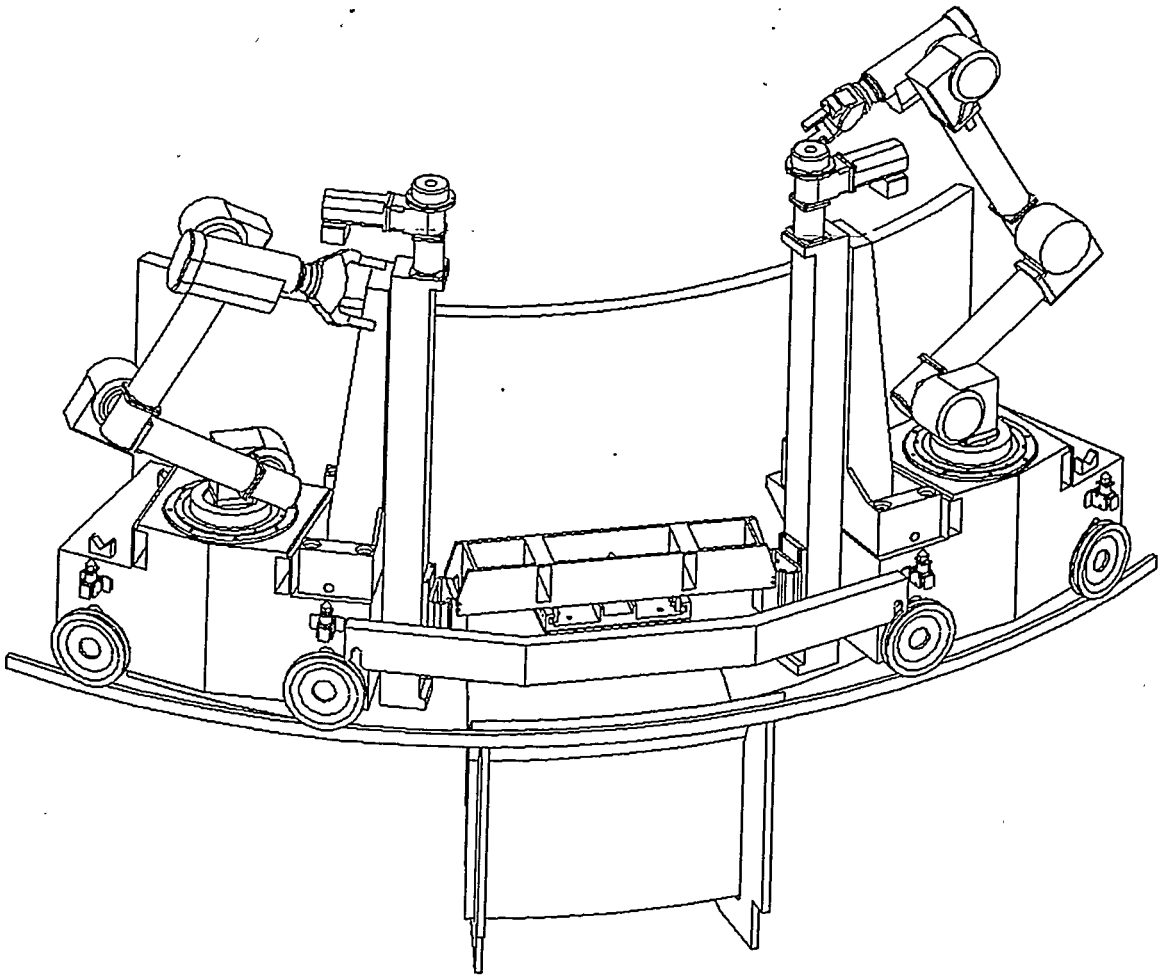

Fig. 6.2. TPX track-mounted in-vessel maintenance system.

A mating vehicle (the trailer), operating on the same track, will mount handling fixtures designed in conjunction with the PF coils. Drives and operators on the trailer will be powered by a jumper cable from the tractor, thus eliminating the need for additional umbilicals to the exterior of the vessel. The tractor, operated by remote control from the central maintenance systems control station, will position and operate the trailer.

The total weight of the in-vessel vehicle system, including a typical PF coil module, will be ~1100 kg. Consequently, the contact stress on the lower in-vessel rail is relatively high. A test program is under way to evaluate several existing titanium coating systems to select the best candidate for use inside the TPX vessel.

6.3.1.2 Transfer system

A multipurpose transfer system will be stationed at port "A" of the TPX vessel. Its primary function will be to move the in-vessel maintenance systems and components in and out of the vessel with the necessary shielding and environmental protection. A remotely operated horizontal boom will be equipped with special effectors for handling each component or tool.

A shielded transfer container with bagging capability will be integrated into the system to provide safe, noncontact movement of contaminated components to the TPX hot cell. Transfer containers will normally be constructed to match the specific requirements of the components to be handled. Thus, shielding for the actual levels of activation and contamination may range from sheet metal in the first years of operation to ~5 cm of iron in the final years.

Personnel will have access to the interior of the transfer system through an airlock entry and change room. On-board ventilation will be provided in the transfer system when the vessel entry hatch is closed. The vessel will also be equipped with a separate ventilation system as required for personnel entry to the vessel interior; personnel will be enternig the vessel primarily during the initial startup and for the first 2 years of operations.

6.3.1.3 Mock-ups and testing

Mock-up testing is crucial to the success of the maintenance systems. Consequently, all components designated for remote maintenance will be tested at each stage of design in a series of mock-ups. Two primary full-scale mock-ups will be used to verify remote maintainability. The first is located at ORNL for demonstrations of the proposed design concepts for the in-vessel components, module-handling fixtures, and maintenance systems. The frame is carbon steel, and the internal systems are fabricated from aluminum, wood, and other inexpensive materials. Emphasis will be placed on quickly trying new ideas and techniques early in the design process.

The second mock-up, located at PPPL, will include a sector of the vessel and functional features such as piping and feed-throughs. It will be operational throughout the life of the project for use in operator training and unusual-event analysis as well as verification of the final designs of the component modules and in-vessel maintenance systems.

The maintenance system will be used during PF coil installation and during the first 2 years of operation, in conjunction with hands-on repair of the TPX system. The transfer system and in-vessel vehicles will receive the most important testing and evaluation during these operations.

6.3.2 Shielding

K. W. Buchanan, M. J. Cole, and G. H. Jones

The TPX shielding system, shown in Fig. 6.3, will limit the nuclear heating of the superconducting coil set, provide a biological shield for activated materials inside the shield, and limit the neutron activation of components outside the shield to allow hands-on access to equipment. The shield will therefore reduce the size and cost of the coil cryogenic system and eliminate the need for an extensive ex-vessel remote-maintenance system.

The radiation shielding consists of a thermalizing material such as water or polyethylene to slow down the neutrons, a high–cross-section material such as boron to capture the thermalized neutrons, and a high-density material to stop the gamma radiation. The shielding is divided into three areas:

- torus shielding around the vacuum vessel,
- duct shielding around the vacuum pumping ducts and vertical diagnostic ducts, and
- penetration shielding in and around the radial ports.

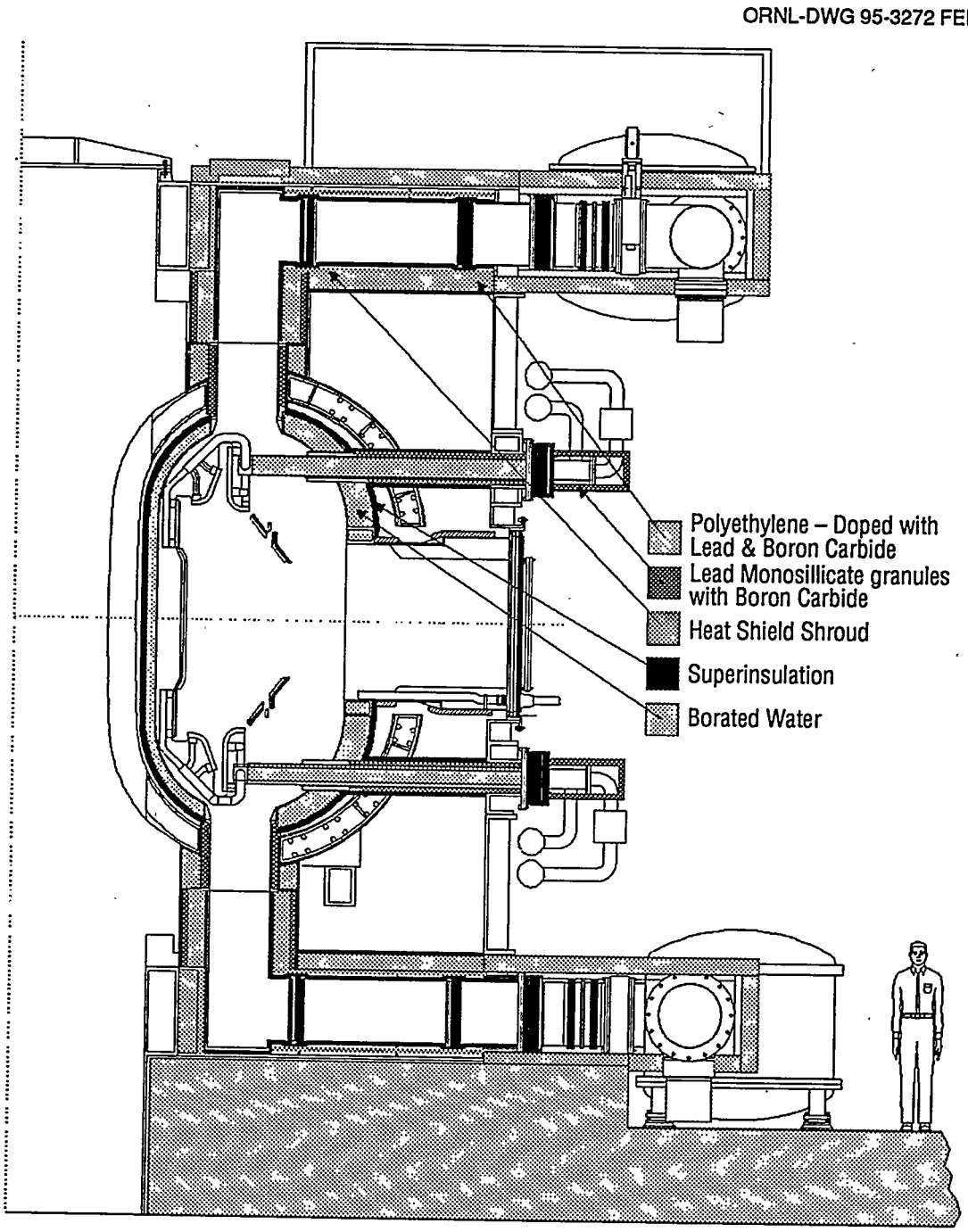

Fig. 6.3. TPX shielding system.

The CDR shielding design has been changing to reflect improved shielding configurations and lower-cost alternatives. Some of the changes are as follows:

- The torus shielding now consists of a thermalizing material provided by the water between the walls of the vacuum vessel. The thickness of the water layer varies from 14.5 cm on the inboard side of the torus to 29 cm on the outboard side. To absorb the neutrons, the

equivalent of 1 cm of boron carbide is added in the form of boric acid at a concentration of 110 g H_3BO_3/L of water.

- The duct shielding configuration has been redesigned to reduce neutron streaming. Joining of the adjacent pump ducts in a "T"-shaped configuration and a reduction in the number of horizontal ducts are among the redesigned features. The shielding between the TF coils remains the same, consisting of borated polyethylene and tungsten carbide. A borated water jacket at a concentration of 110 g H_3BO_3/L of water surrounds the upper portion of the duct.

The addition of boron to the water raised a concern about the compatibility of borated water with titanium at 150°C. A corrosion-rate study was performed to investigate this concern, and the results indicate that corrosion does not appear to be an issue.[13] Additional studies are continuing.

6.3.3 Vacuum Pumping

P. J. Fogarty and K. D. St. Onge

The TPX vacuum pumping system will be required to pump the torus, the divertors, and the cryostat; the system must also provide roughing and backing pumping for the NB injectors and various diagnostic instruments.

The salient pumping requirements set by the TPX program are as follows: (1) The desired base pressure is 10^{-9} Torr for species with $Z > 2$ and 10^{-7} Torr for other species; the gas load is assumed to be 10^{-5} Torr-L/s. (2) The divertor gas load is 100 Torr-L/s at a nominal pressure of 1 to 10 mTorr for a duration of 1000 s; peaks up to 250 Torr-L/s may be required for shorter periods. (3) The pumping speed at the interface between the torus and the vacuum ducts must be at least 85 m^3/s for deuterium at 150°C and 1 mTorr. (4) The system must support glow discharge cleaning with H_2, D_2, or helium at 350°C and 10 to 20 mTorr for indefinite periods. The vacuum pumping system concept described here is the baseline design that was presented at the TPX CDR. Since that time, several improvements and cost-reduction features have been incorporated.

The high-vacuum pumping system includes cryocondensation pumps for divertor pumping and turbomolecular pumps for pumping helium and for glow discharge cleaning. Throttling valves are used to control the pumping speed and to isolate the cryopumps.

Sixteen cryopumps are planned for TPX; the pumps are cooled with liquid helium at 4.2 K and 1 atmosphere. There is a 76-cm-diam inlet on each side of the pumps; the speed at the inlet is about 75 m^3/s for D_2 at 150°C. The pumps operate in batch mode, with eight pumps active for two shots while the others are regenerated.

Eight 3.5-m^3/s turbomolecular pump units from TFTR will be reused for TPX, along with their associated controls and roughing and backing systems.

6.3.4 Rf Systems

C. H. Fogelman, P. L. Goranson, G. H. Jones, U. P. Lickliter, J. L. Ping, D. W. Swain, and D. J. Taylor

The rf systems in TPX consist of an LH and an ion cyclotron system. ORNL has been given the responsibility for managing the design and fabrication of these systems and has worked on them since 1992. The conceptual designs for these systems were completed in 1993. In 1994, the design was continued and modified in accordance with changes in project requirements (e.g., more LH power, less ion cyclotron power) and improvements in our own concept of the design. These systems are described in the sections that follow.

6.3.4.1 LH system

The LH system is part of an overall heating and current-drive system for TPX consisting of NBs, LH, and ion cyclotron systems. The LH system is required to provide off-axis current profile control, efficient bulk current drive at low plasma temperatures, and electron heating.

The initial system at the CDR was designed to provide 1.5 MW of LH heating/LHCD power to the plasma at 3.7 GHz through one horizontal port, with the capability of upgrading to 3 MW; since the CDR, the LH power has been increased to 3 MW at startup. The LH system will make it possible to vary the wave-number spectrum dynamically in order to support flexible off-axis current profile control. Phase control will be continuous over the range of 0 to $\pm\pi$ between coupler windows.

The LH system consists of the following subsystems:

- high-voltage power supplies, which convert ac power to dc power to supply the klystrons, and associated protection circuitry;
- 3.7-GHz klystrons (with two output windows per klystron) and associated rf drivers, which convert the dc power to rf power;
- lengths of WR284 waveguide, which carry the rf power from the klystron location to the TPX area;
- boxes with power-splitting and phase-control circuitry that divide the power inputs into 64 outputs that can be phased independently (more WR284 guides carry the rf power to the launcher input);
- a radially moveable LH launcher, consisting of 256 waveguide elements, and a four-way power splitter (mounted just outside the port) that divides the 64 inputs to drive the waveguide elements; and
- an instrumentation and control system to control and monitor the operation of the LH system.

A drawing of the proposed launcher is shown in Fig. 6.4. Several R&D issues must be resolved to fabricate this launcher, and an R&D program at ORNL was initiated in FY 1994 to address these issues. A report summarizing the FY 1994 LH brazing R&D effort was prepared.[14] High-temperature brazes of a copper and a Glidcop test stack were completed using non-noble alloys. The copper test was completely successful. The Glidcop stack test was generally successful, but some small edge delamination and warping occurred. There was also evidence of diffusion of silver through the protective copper layer. The R&D program is continuing.

6.3.4.2 Ion cyclotron system

The ion cyclotron system at the CDR was designed to provide 8 MW of ion cyclotron power to the plasma through two six-strap launchers located in adjacent ports. Along with the upgraded complement of NB (24 MW) and LH (3 MW) power, it would accommodate an upgrade to 18 MW of ion cyclotron power to the plasma. The ion cyclotron power upgrade was to be coupled to the plasma through three launchers located in adjacent ports. Since the CDR, the ion cyclotron system was reduced to provide 6 MW (using three transmitters) from one six-strap antenna. The upgrade requirements remain the same.

The ion cyclotron system is designed to provide power at a single frequency in the range of 40–80 MHz with a fixed phase shift between straps. The system will operate at any of three frequencies in the range of 40–80 MHz. The system can be upgraded (by changing tuning and

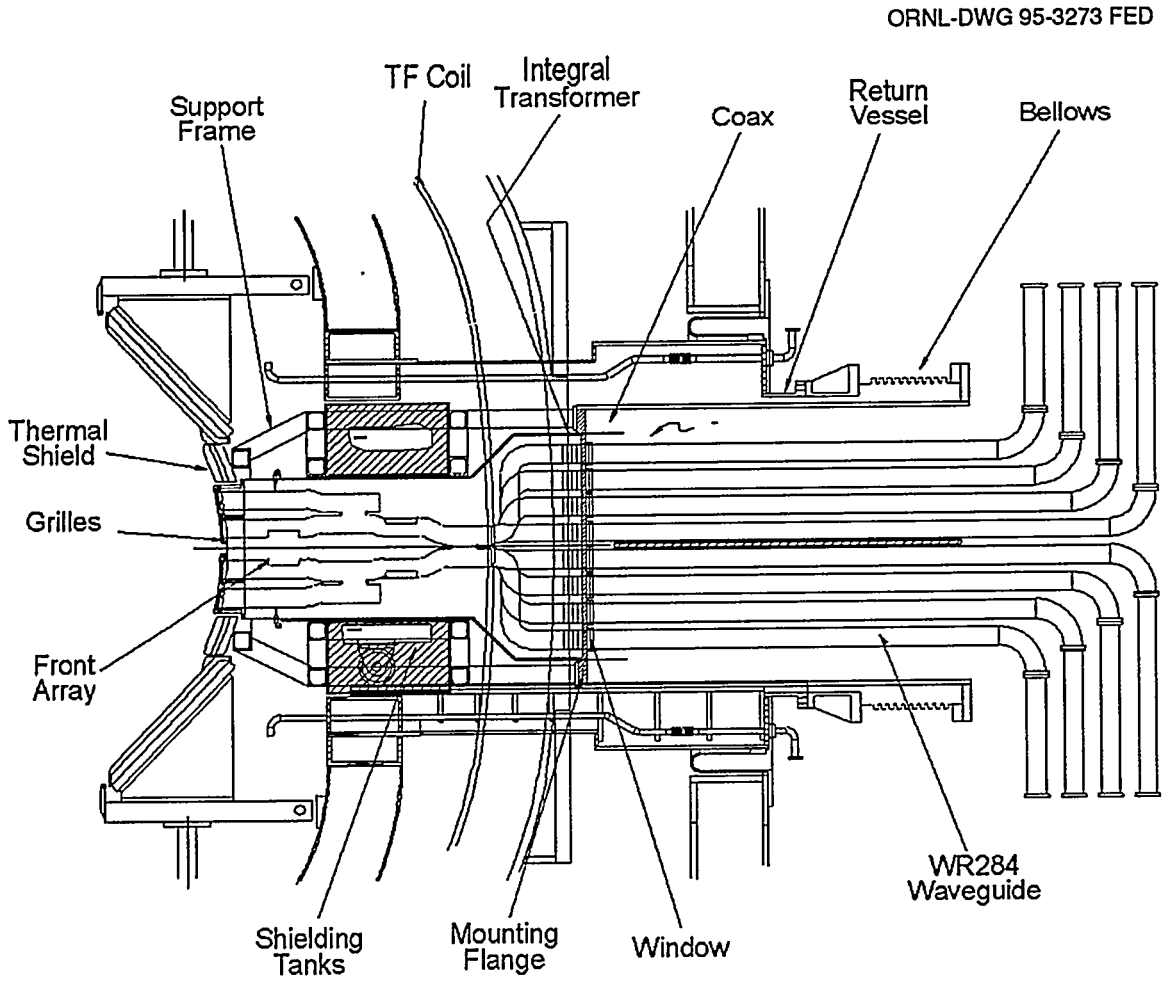

Fig. 6.4. TPX lower-hybrid launcher.

matching elements outside the plasma vacuum boundary) to operate at any frequency in the range of 40–80 MHz.

The ion cyclotron system consists of the following subsystems:

- high-voltage power supplies, which convert ac power to dc power to supply the rf power units;
- rf power units (also called transmitters), which convert the dc power to rf power;
- rf transmission lines, which carry the rf power ~800 ft from the present transmitter location to the TPX area;
- tuning and matching circuitry, which adjusts the amplitude of the currents in the antenna current straps as desired during plasma operation;
- one antenna containing six current straps, to couple the rf power to the plasma; and
- an instrumentation and control system to control and monitor the operation of the ion cyclotron system.

Figure 6.5 shows a view of the ion cyclotron launcher. The three Faraday shield elements are shown removed from the antenna frame.

ORNL-DWG 95-3274 FED

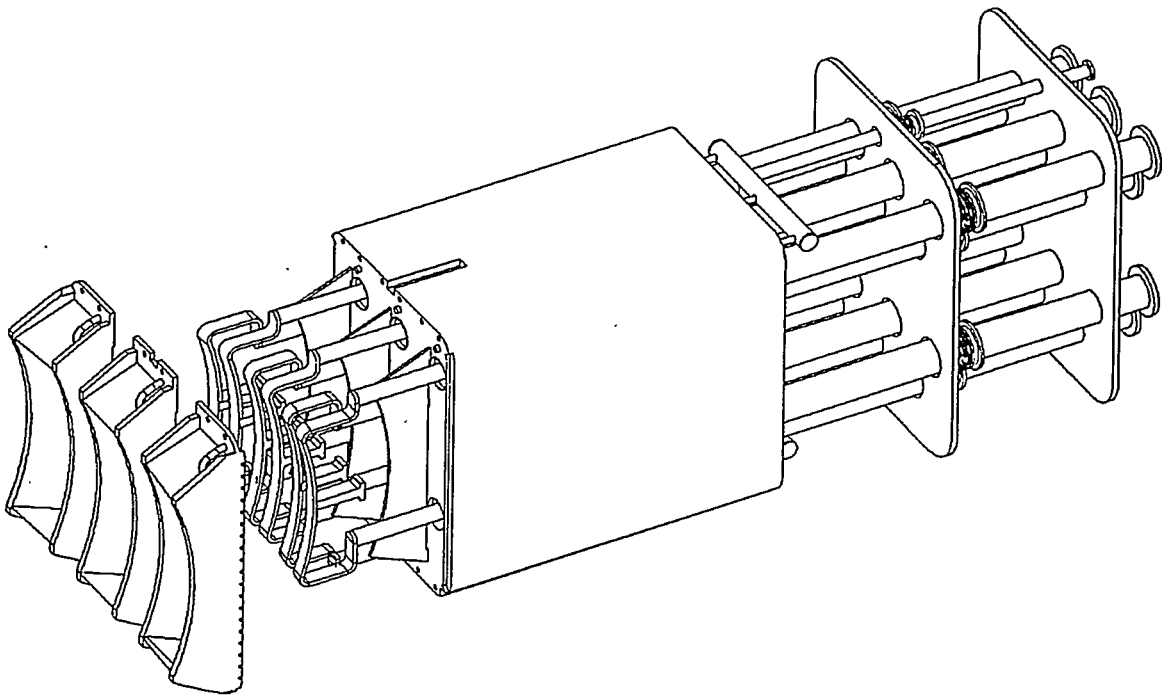

Fig. 6.5. TPX ion cyclotron launcher.

The issues for the ion cyclotron antenna revolve around the question of whether an antenna that can survive in the TPX environment can be fabricated from titanium. During FY 1994, a test-piece titanium Faraday shield specimen was fabricated by industry. Welds and tube bends appear completely satisfactory and give increased confidence that an antenna can be constructed of titanium. In addition, a successful nickel-plating technique was developed at ORNL, and an industrial vendor with the capability of plating titanium with nickel has been found.

The primary remaining issue for titanium fabrication concerns protecting the titanium from hydrogen embrittlement in the TPX environment. It is hoped that nickel plating will provide this protection, but an R&D program must be carried out to demonstrate that this technique will work. This will be done in the next year. A report summarizing the FY 1994 titanium launcher R&D effort was prepared.[15]

In addition to the launcher, the tuning and matching system plays a critical role in the ion cyclotron system's performance. ORNL has been carrying out a series of design studies for this system. Since the CDR in 1993, a series of meetings has been held with the TPX Physics group to determine what changes in requirements for the tuning and matching system are needed. As a result of these meetings, the following capability upgrades have been identified:

1. Feedback control of mismatches induced by changes in plasma loading by controlling the plasma position.
2. Feedback control of mismatches resulting from plasma-induced changes in the strap inductance through control of the rf frequency (±~100 kHz).

3. Capability to vary the current-drive efficiency between shots and to change it (within limits to be determined) during a shot, which will be accomplished by changing the phase between the transmitters that drive the antennas; how this can best be implemented will be studied in the next year.

We began a study of fast phase-shifting components, available now or under development, that could be used in the TPX ICH system to control antenna spectrum. These components might also be used in the antenna tuning and matching system. We were looking for fast phase-shifters that would operate over a range of 60° at 2 MW under high voltage standing wave ratio. We studied both electromechanical and electromagnetic units with tentative time response requirements ranging from 2 s to 20 ms. Results obtained thus far appear to indicate that the search for an electromechanical device to do fast phase shifting at high power should be discontinued, even if a 2-s response time is considered. The speed and accuracy would be impossible to attain in a reliable mechanical unit. AFT is already working to develop fusion-related components for General Atomics. In the next year, we expect to have a clearer picture of whether the active components in AFT's currently designed Fast Ferrite Tuners can be used as fast phase shifters by TPX.

6.3.5 TPX Physics

6.3.5.1 Rf physics

D. B. Batchelor, M. D. Carter, E. F. Jaeger, and D. C. Stallings

The rf theory group works in close collaboration with the rf design group (Work Breakdown Structure 23). They run various computer codes (PICES, RANT3D) to calculate the rf power deposition in the plasma, the current-drive efficiency for different TPX plasma operating parameters, and the plasma loading seen by the ion cyclotron antenna. This work is described in Sect. 3.3, which discusses the rf theory program.

Particle physics

See Sect. 1.3.5 for a discussion of the TPX work in this area.

TPX PF coil optimization

A systems optimization was used to determine a TPX PF coil configuration of minimum cost that can effectively reproduce the external field of a prescribed set of MHD equilibria while satisfying design engineering constraints. The equilibria represent different points in a TPX discharge scenario, or variations (e.g., in beta and internal inductance) about some reference solution. Nonlinear optimization was used to minimize a TPX PF cost function by varying coil positions and cross-sectional shapes, within limits set by device configuration and superconducting-magnet engineering constraints. With the optimal PF system geometry and coil current distributions, the reference free-boundary MHD equilibria[16] are accurately recomputed. Results showed that PF coil hardware cost reductions of 25% of the nonfixed cost were possible in TPX, based on device design engineering assumptions. This study, along with revisions in the radial build, formed the basis of a new TPX PF coil system design in FY 1994.

TPX magnetic diagnostic configuration studies

A relatively simple plasma shape reconstruction model provides a preliminary assessment of possible TPX magnetic diagnostic configurations. The algorithm is based on a filament representation of the plasma, and a singular value analysis illustrates the sensitivity of the plasma boundary approximation to errors in the data. The data simulating magnetic measurements consist of flux and field values derived from a symmetric free-boundary equilibrium and include asymmetric error perturbations. The resulting errors in the reconstructed plasma boundary shape are averaged over several random perturbations, of fixed magnitude, in the data. This method for computing the plasma shape from field and flux values was applied in an assessment of the TPX in-vessel magnetic diagnostics configuration described by P. Anderson et al.[17] The singular value decomposition analysis was used to examine the shape reconstruction capability of a subset of these diagnostics consisting of flux loops near the vacuum vessel and field probes both near the vessel and near the divertor and passive structure. For random error in magnetic flux and field data from a free-boundary equilibrium solution, the resulting errors in the reconstructed plasma boundary and divertor strike-point locations at critical shape control points were computed. The analysis showed that for this diagnostic configuration, average errors of 4 mm or less in the approximate boundary points and strike points were possible with additive error of up to .01 T, or 2% proportional random error in the equilibrium data.

6.3.5.2 TSC disruption simulations for the TPX β_N-l_i design space

R. O. Sayer

TPX structures must be able to withstand electromagnetic loads resulting from disruptions occurring anywhere in the required operating space in β_N and l_i. A "disruption tour" of the corners of β_N-l_i design space has been carried out with the Tokamak Simulation Code (TSC) code to determine load-limiting scenarios for the vessel and selected in-vessel components. Thirteen simulations have been completed for (β_N, l_i) = (5, 1.2), (5, 0.4), (0, 0.7), and (0, 1.2).

TSC filamentary models were built for the vacuum vessel, stabilizing plates, and divertor. The toroidal resistance of the vacuum vessel was 86.0 μΩ. Stabilizing plates were modeled as 1-in.-thick GLIDCOP at 150°C. The inner stabilizer pair was represented as a saddle structure with a gap resistor having toroidal resistance R_{gap} = 142 μΩ. The outer stabilizer pair was represented as a saddle structure with a gap resistor having toroidal resistance R_{gap} = 318 μΩ. The toroidal resistance of each member of the inner (outer) stabilizer pair was 28.6 μΩ (29.1 μΩ). Antiseries internal control coils were located at (2.8 m, 0.7 m) and (2.8 m, –0.7 m). Each of the six independent divertor structures was represented as a toroidally segmented group of filaments, with a zero net toroidal current constraint imposed on each group. The divertor material was assumed to be 1 cm of copper at 100°C. High-resistivity (titanium) elements were used to interconnect first-wall components (inboard stabilizers, divertor pieces, and outboard stabilizers) and to connect the first-wall components to the vacuum vessel, as shown in Fig. 6.6. A high-resistivity, outboard belly band (group 48 in Fig. 6.6) with zero net toroidal current constraint was included to allow poloidal current to flow in the region between ports. Table 6.1 lists the group and wire numbers for the TSC filaments.

The initial equilibria corresponded approximately to the TPX fiducial cases *except that* the magnetic axis was typically 5 cm below midplane. Selected initial plasma parameters are compared with the fiducial values in Table 6.2 for (β_N, l_i) = (5, 0.4).

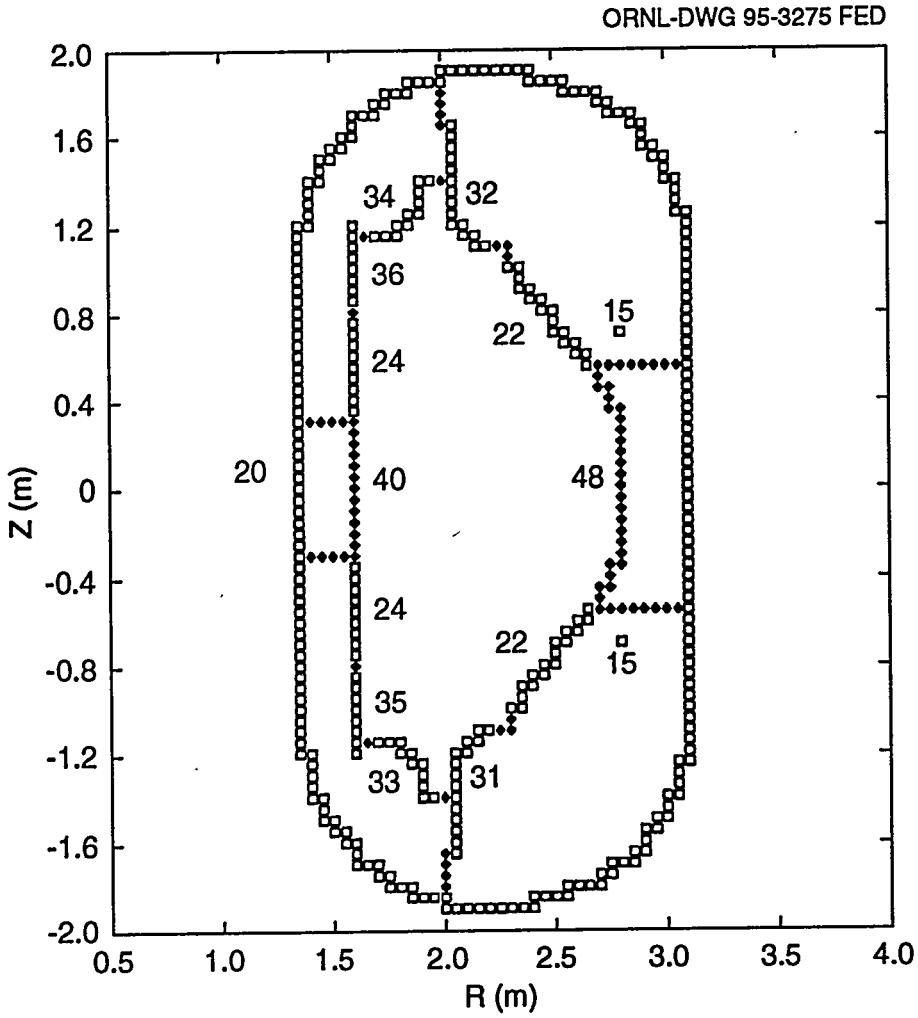

Fig. 6.6. TSC filaments for TPX disruption tour cases. High-resistivity connecting elements represented by solid symbols. TSC group numbers also shown.

Table 6.1. TSC group numbers, wire numbers, and constraints

Component	Group	Wires	Constraint
Vacuum vessel (VV)	20	1–222	None
VV belly band	48	402–426	net toroidal I = 0
Inboard stabilizer	24	257–274	R_{gap} = 142 μΩ
Outboard stabilizer	22	223–256	R_{gap} = 318 μΩ
Divertor 1 upper	32	275–289	net toroidal I = 0
Divertor 1 lower	31	290–304	net toroidal I = 0
Divertor 2 upper	34	305–315	net toroidal I = 0
Divertor 2 lower	33	316–326	net toroidal I = 0
Divertor 3 upper	36	327–334	net toroidal I = 0
Divertor 3 lower	35	335–342	net toroidal I = 0
Internal coils	15	343–344	net toroidal I = 0
Connecting elements	40–47	345–401	net toroidal I = 0

Table 6.2. Initial TPX plasma parameters for $\beta_N = 5$, $l_i = 0.4$

Quantity	Bulmer 94019 End of flattop	TSC ($Z_{mag} = 0$)	TSC ($Z_{mag} = -0.064$)
I_p, MA	2.00	2.00	2.00
R_o, m	2.250	2.240	2.254
a, m	0.500	0.494	0.495
X_{mag}, m	2.426	2.400	2.411
Z_{mag}, m	0	0	–0.064
β_N	5.0	5.7	6.4
l_i	0.40	0.41	0.45
κ_{95}	1.96	1.85	1.65
δ_{95}	0.58	0.60	0.45
q_{95}	3.90	3.51	2.76

Vertically moving disrupting plasmas with a surrounding halo were simulated for values of the plasma-halo boundary temperature T_H, ranging from 4 to 12 eV during the current-decay phase of the VDE. In the halo region the temperature was decreased linearly in ψ from the plasma-halo boundary to the halo-vacuum boundary. Different plasma-current decay rates were obtained by varying the plasma halo width and temperature during the current-decay phase. Peak decay rates ranged from 0.20 to 1.22 MA/ms, and average decay rates were 0.09 to 1.14 MA/ms. Average dI_p/dt values were based on times corresponding to I_p = 90% and I_p = 10% of the initial

I_p value. Figure 6.7 presents the evolution of the toroidal plasma current for the five VDE simulations for $(\beta_N, l_i) = (5, 1.2)$.

An initial vertical displacement was introduced, and the plasma was then evolved according to the transport equations with the vertical feedback system disconnected. During this "drift phase" the T_H values were so low (<0.5 eV) that the presence of the halo had a negligible effect on the plasma vertical motion. The drift phase evolution was continued until q at the 95% flux surface dropped to the critical value q_{crit}. At this time, the thermal quench was initiated by enhancing the radial plasma thermal conductivity by a large factor, typically 1000, producing a sudden temperature drop and enhanced plasma resistivity in the region inside the last closed flux surface.

During the ensuing current quench the plasma vertical motion accelerates until the plasma is subject to restriction by a set of limiters near the first wall and divertor locations. Motion of the plasma boundary during a disruption is illustrated in Fig. 6.8, which shows an overlay of plasma-halo boundaries for a typical VDE simulation. In some cases hyper-resistivity was turned on for a short time after the thermal quench to alter the current profile so as to increase the plasma current by about 10%. All VDE cases were run with $q_{crit} = 1.3$ to provide valid comparisons.

A postprocessor code was used to analyze the time evolution of currents and pressures for the four stabilizers (groups 22 and 24 in Fig. 6.6), six divertor pieces (groups 31–36 in Fig. 6.6), the inner toroidal limiter (group 40 in Fig. 6.6), and eight segments of the vacuum vessel. Initial plasma parameters, halo currents, plasma-current decay rates, and extreme pressures (including

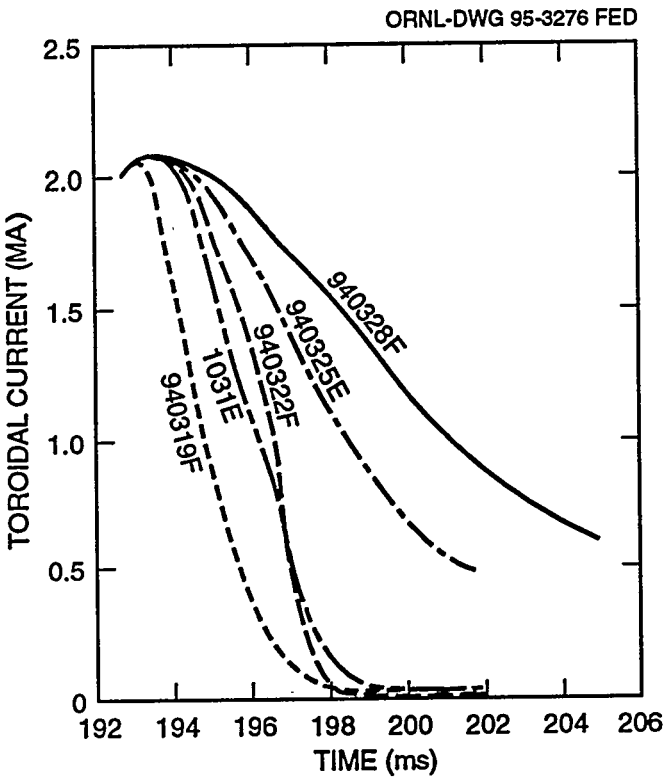

Fig. 6.7. Evolution of toroidal plasma current for TSC VDE simulations with $q_{crit} = 1.3$ for TPX high-ß, high-l_i design point.

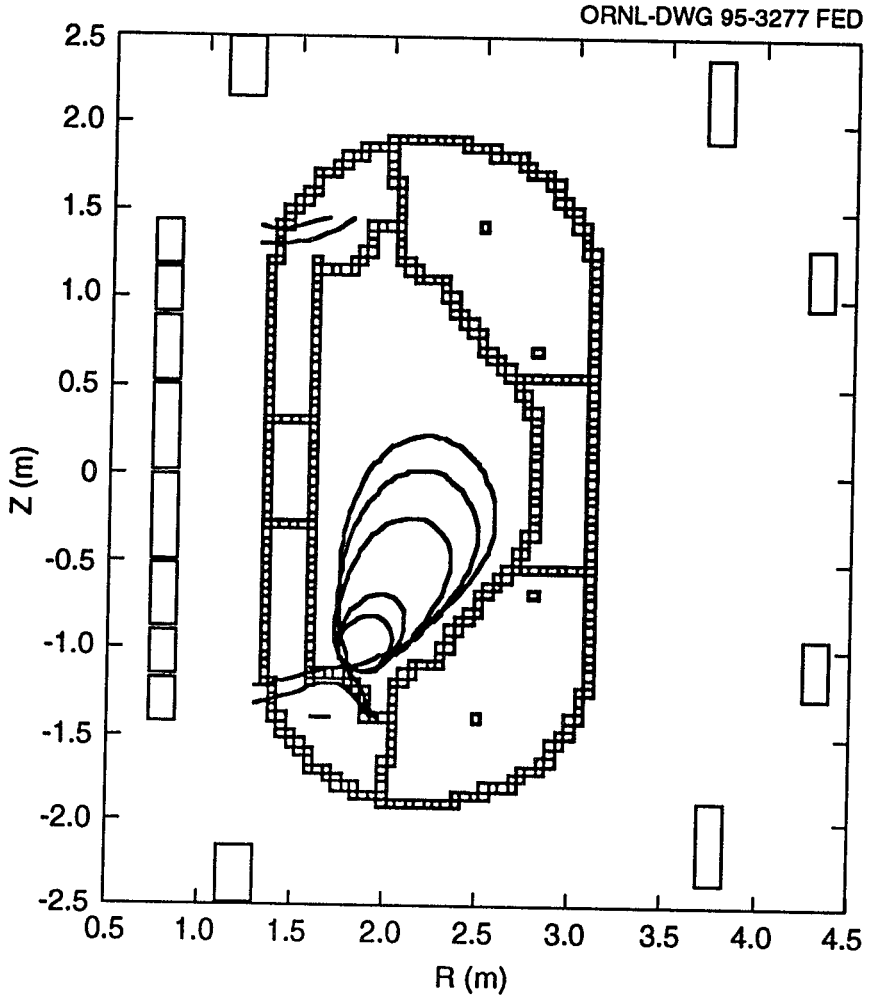

Fig. 6.8. Overlay of TPX main plasma boundaries for current-decay phase of TSC simulation 940925C.

contributions from both toroidal and poloidal currents) are listed in Tables 6.3 and 6.4. For the center divertor piece, the highest pressure occurs for the fast double-null, $\beta_N = 0$, $l_i = 0.7$, VDE case 940925C ($\langle dI_p/dt \rangle$ = –0.44 MA/ms). This case also produces the maximum poloidal halo current in the structure, 791 kA. The 9 double-null, $\beta_N = 5$, $l_i = 1.2$ cases 940322F and 1031E give the highest pressure in the outer divertor piece. However, the single-null, $\beta_N = 5$, $l_i = 1.2$ case 940919C gives the highest pressure in the inner divertor piece. It should be noted that case 940919C (with initial $I_p = 2.0$ MA) does not satisfy $q_{95} \geq 3$ or the coil allowables.

At the time of extreme pressure, the contribution from toroidal current in the stabilizers is dominant, so all the double-null, $\beta_N = 5$, $l_i = 1.2$ VDE cases with a given q_{crit} value tend to predict nearly the same extreme pressures in the stabilizers. On the other hand, the single-null, $\beta_N = 5$, $l_i = 1.2$ case 940919C predicts about 10% higher pressure in the inner stabilizer and much lower pressure in the outer stabilizer. This pressure difference is primarily attributable to the single-null plasma being a few centimeters closer to the inner stabilizer during the current decay than the double-null plasmas. For $\beta_N = 0$, and for $l_i = 0.4$, the extreme stabilizer pressures are significantly lower than the values for the high-β_N, high-l_i cases. The radial case gives much smaller extreme

Table 6.3. Initial plasma parameters, halo currents, and plasma current decay rates for TSC disruption simulations for TPX

Case[a]	Initial I_p (MA)	Initial β_N	Initial l_i	T_{halo} (eV)	Max I_{halo} (kA)	$\langle dI_p/dt \rangle$ (MA/ms)	Peak $\lvert dI_p/dt \rvert$ (MA/ms)
721E	2.00	5.0	1.2	0	0	0.63	0.63
940208A	2.00	5.0	1.2	0	0	1.14	1.14
940319F	2.00	5.0	1.2	4	448	0.57	1.22[b]
940322F	2.00	5.0	1.2	5	511	0.70	1.18[c]
1031E	2.00	5.0	1.2	4	442	0.52	0.65
940325E	2.00	5.0	1.2	8	556	0.16	0.31
940328F	2.00	5.0	1.2	12	638	0.09	0.20
940832G	2.00	5.0	0.4	5	552	0.64	1.14
940903G	2.00	5.0	0.4	12	709	0.25	0.36
940803D	1.80	0	1.2	5	619	0.46	0.65
940727D	1.80	0	1.2	12	664	0.17	0.21
940925C	2.00	0	0.7	5	791	0.44	1.20
940919C	2.00	5.0	1.2	5	549	0.29	0.42

[a]For all VDE cases, $q_{crit} = 1.3$. All cases double null except 940919C.
[b]Case 940319F : peak dI_p/dt occurs when $I_p = 1.44$ MA.
[c]Case 940322F : peak dI_p/dt occurs when $I_p = 0.65$ MA.

Table 6.4. Extreme pressures (kPa) for TSC disruption simulations for TPX

Case[a]	Vacuum vessel inboard	Outer stabilizer	Inner stabilizer	Outer divertor	Center divertor	Inner divertor	Inner toroidial limiter
721E	113	155	137	67	157	209	240
940208A	129	169	162	79	181	241	275
940319F	111	280	571	146	289	187	194
940322F	113	281	662	158	319	257	150
1031E	116	281	658	161	321	247	151
940325E	109	281	663	151	323	277	150
940328F	107	281	666	148	334	295	150
940832G	94	194	341	62	320	139	99
940903G	93	155	378	77	374	184	69
940803D	73	215	476	115	358	219	30
940727D	50	215	476	107	336	229	30
940925C	81	223	482	132	463	188	28
940919C	80	194	735	85	302	334	58

[a]For all VDE cases, $q_{crit} = 1.3$. All cases double null except 940919C.

pressures because the disrupting plasma is much farther from the stabilizers than in the VDE cases.

The 1.14 MA/ms, radial, no-halo case is limiting for the vessel and the inner toroidal limiter.

Figures 6.9 and 6.10 are plots of the extreme pressures vs case number for the 13 simulations. At least four distinct scenarios, highlighted at the bottom of the plots, are required to specify the load-limiting cases. If the single-null case 940919C is discarded because it does not satisfy $q_{95} \geq 3$ or the coil allowables, it must be replaced with case 940328F to limit the inner divertor. Case 940925C ($\beta_N = 0$, $l_i = 0.7$) still limits the center divertor even if the extreme pressure is scaled by a factor of (667/791) to reduce the extreme poloidal halo current to the reference design value of $I_p/3$.

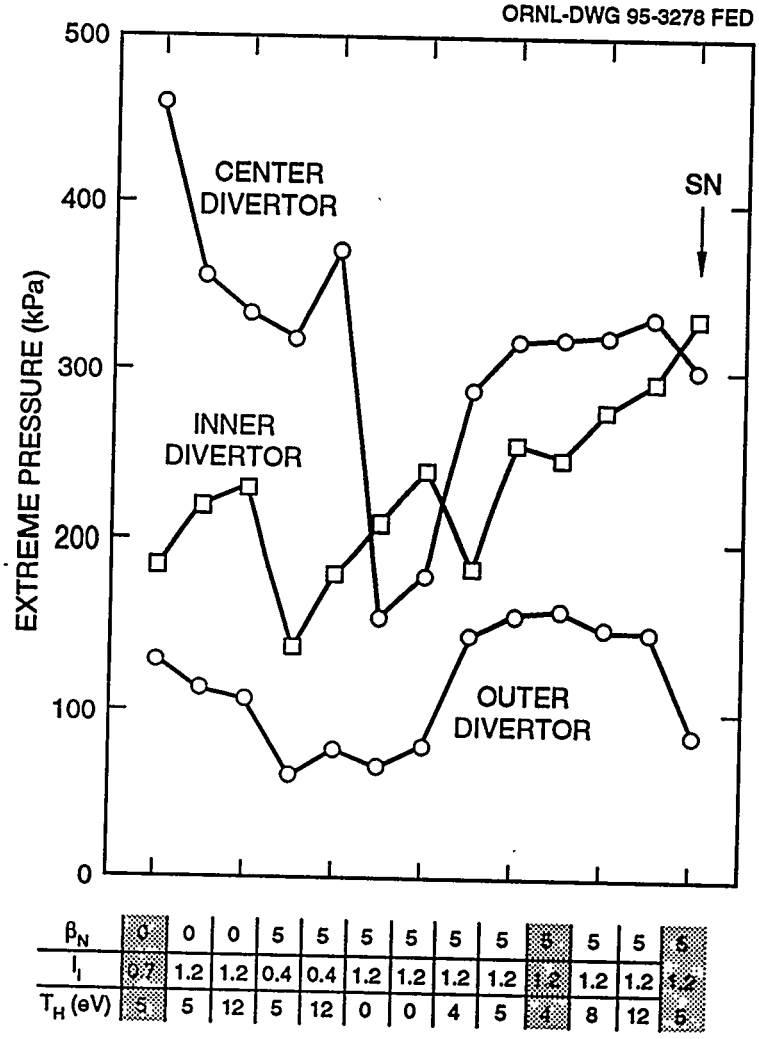

Fig. 6.9. Extreme pressures on the three TPX divertor pieces for 13 TSC disruption tour simulations for TPX.

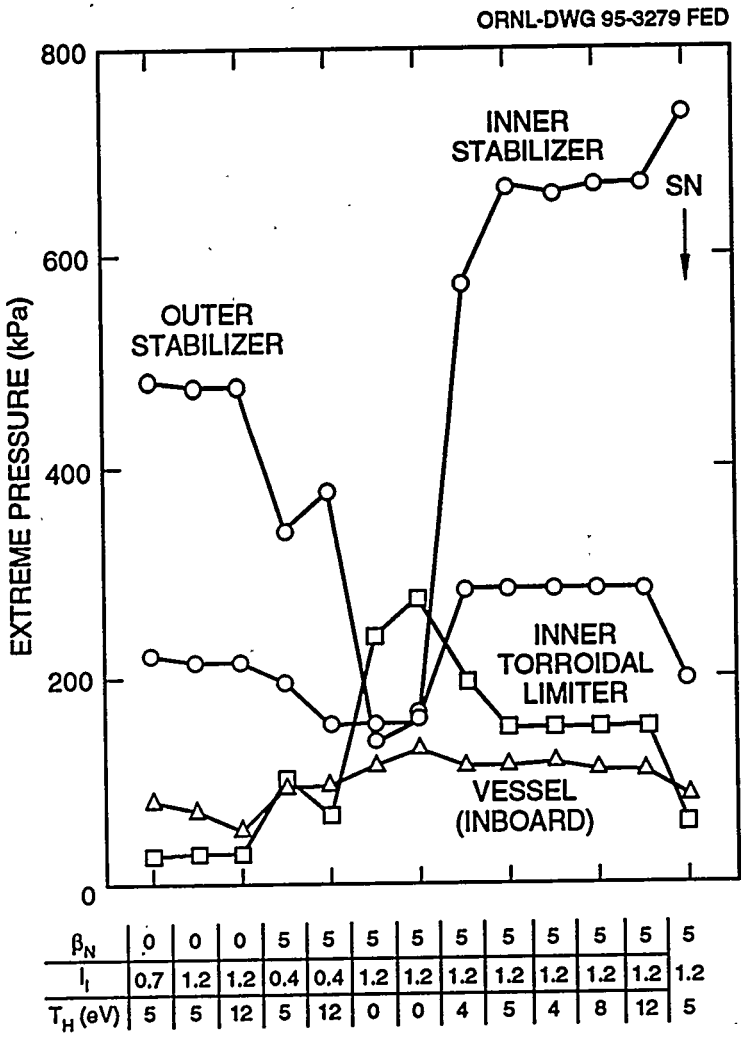

Fig. 6.10. Extreme pressures on TPX stabilizers, vessel, and inner toroidal limiter for 13 TSC disruption tour simulations for TPX.

REFERENCES

1. J. G. Delene, "Benefit of locating ITER in U.S.," letter report, 1993.

2. J. G. Delene, "Advanced Fission and Fossil Plant Economics—Implication for Fusion," *Fusion Technol.* 26(3, Pt. 2) (Suppl.: *Proceedings of the 11th Topical Meeting on the Technology of Fusion Energy, June 19–23, 1994, New Orleans*), 1105 (1994).

3. Y-K. M. Peng and D. J. Strickler, *Nucl. Fusion* **26**, 576 (1986).

4. A. Sykes et al., "First Results from the START Experiment," *Nucl. Fusion* **32**, 694 (1992).

5. A. Sykes et al., "Tight Aspect Ratio Tokamaks—Theory and Experiment," *Plasma Physics and Controlled Fusion* **35**, 1051 (1993).

6. Y.-K. M. Peng et al., "Small Tokamaks for Fusion Technology Testing," *Fusion Technol.* **21**, 1729 (1992).

7. Y.-K. M. Peng et al., *TST, Small Steady-State Tokamak for Integrated Divertor Testing*, ORNL/TM-12216, Martin Marietta Energy Systems, Inc., Oak Ridge, Tenn., 1993.

8. J. D. Galambos et al., "Scoping Studies for Small Steady-State Tokamaks for Divertor Testing," p. 1114 in *Proceedings of the 14th IEEE Symposium on Fusion Engineering, San Diego, 1991*, IEEE, New York, 1991.

9. M. Abdou et al., *Phase 1 Report of the IEA Study on High Volume Plasma-Based Neutron Source (HVPNS)*, UCLA-FNT-94, UCLA-ENG-95-111, University of California at Los Angeles, December 1994.

10. Ioffe Fusion Technology and the GLOBUS-M Design Team, *GLOBUS-M Pre-conceptual Design Study Report; Vacuum Vessel; Electromagnetic System and Power Supplies; Support Structure and Device Assembly*, Submitted to ORNL (December 1993).

11. Y.-K. M. Peng, R. J. Colchin, C. L. Hedrick, J. D. Galambos, J. Sheffield, D. J. Strickler, R. A. Blanken, A. Sykes, D. C. Robinson, A. W. Morris, J. Hugill, T. C. Hender, K. Erents, H. R. Wilson, "Physics Progress Towards Compact Tokamak Reactors with Normal Conducting Toroidal Field Coils," IAEA-CN-60/F-I-3-2(R), to appear in *Plasma Physics and Controlled Nuclear Fusion Research*, IAEA, Vienna, 1994.

12. Y.-K. M. Peng, "Prospects and Status of Low Aspect Ratio Tokamaks," paper presented at the 6th Toki International Conference, November 29–December 2, 1994, Tokishi, Japan (to be published in *Fusion Technol.*).

13. J. H. DeVan, *Stress-Corrosion Testing of Ti-Al-V Alloys in Concentrated Boric Acid*, TPX Report 18-941015-JDeVan-01, Oak Ridge Natl. Lab., 1994.

14. P. L. Goranson, *TPX WBS 241 R&D—Front Array Brazing Program*, TPX Report 24-940930-ORNL/PGoranson-01, Oak Ridge Natl. Lab., September 1994.

15. P. L. Goranson, *TPX WBS 231 R&D Low-Activation Launcher—Titanium Fabrication/ Plating Program*, TPX Report 23-940930-ORNL/PGoranson-01, Oak Ridge Natl. Lab., July 1994.

16. D. Strickler and R. Bulmer, *PF Coil Optimization*, TPX Report 14-940311-ORNL/ DStrickler-01, Oak Ridge Natl. Lab., March 1994.

17. P. Anderson et al., *Advanced Conceptual Design Review Support for TPX Magnetic Diagnostics*, TPX Report PPPL-11-931025-GA/PAnderson-01, Princeton Plasma Physics Laboratory, Princeton, N.J., November 1993.

7

FUSION MATERIAL RESEARCH

E. E. Bloom

D. J. Alexander
T. D. Burchell
J. H. DeVan
B. G. Gieseke
G. M. Goodwin
M. L. Grossbeck
A. N. Gubbi
J. R. Haines
E. A. Kenik
J. F. King
R. L. Klueh
J. E. Pawel
A. F. Rowcliffe
T. E. Shannon
K. Shiba[1]
L. L. Snead
K. R. Thoms
L. J. Turner
D. P. White
S. J. Zinkle

1. Japan Atomic Energy Research Institute.

7. FUSION MATERIAL RESEARCH

Summary of Activities

Fusion is now preparing to enter the nuclear phase of development, as evidenced by the initial D-T operation of the Joint European Torus, the recent deuterium-tritium operation of the Tokamak Fusion Test Reactor, the growing commitment to the International Thermonuclear Experimental Reactor, and the National Energy Strategy's goal of an operating demonstration reactor in about the year 2025. Furthermore, low-activation materials development is critically important to the success of fusion as an energy source. Ultimately, the economics and acceptability of fusion energy will depend heavily upon the successful performance of structural materials exposed to the combined effects of the chemical, thermal, mechanical, and neutronic environments characteristic of commercial fusion reactors. All these facts increase the urgency of pursuing research and development (R&D) study of fusion reactor materials. The R&D activities are on alloy development for neutron irradiation performance, damage analysis and fundamental studies, and special-purpose materials. The technical progress at the Oak Ridge National Laboratory during the last 3 years is further elaborated in this chapter.

7.1 NEUTRON INTERACTIVE MATERIALS

The purposes of this study are to develop an understanding of the mechanisms underlying radiation damage and corrosion phenomena in fusion reactor structural materials, to produce materials property data for application in reactor design studies, and to develop materials that allow the full economic, environmental, and safety advantages of fusion to be realized. Since fusion-like facilities do not exist, materials testing is carried out in simulation experiments that seek to produce the most critical characteristics of the fusion environment. The effects of radiation are explored using a variety of fission reactor and accelerator facilities, with the overall objective of achieving the temperature range, damage rate, fluence range, and helium generation rates typical of a fusion reactor. Corrosion studies are conducted in liquid metal gaseous and aqueous environments to assess the impact of corrosion phenomena on mechanical behavior. The rigorous operating parameters for a commercial demonstration plant require the long-term development of new ceramic and metallic materials. An important consideration for the long term is the cost and environmental impact of disposing of highly activated components. A major objective, therefore, is to develop alloy systems that will eventually permit near-surface burial and possibly increase the potential for recycling critical materials. The inventory of radioactive species and their potential for atmospheric release in accident scenarios is another important consideration in defining alloy compositions.

The principal classes of alloy and ceramic materials currently being investigated for use in fusion reactor structural application include martensitic steels, vanadium alloys, and silicon carbide (SiC)/SiC composites. The development of martensitic steels is focused on compositions with the potential to reduce levels of long-term radioactivity and create more favorable scenarios for eventual disposal of system components. A primary goal is the development of materials that will maintain adequate toughness and ductility under the combined effects of neutron damage and helium generation. The main focus of the program on SiC/SiC composite materials is to develop fibers resistant to radiation damage and to incorporate them into new composite materials. Vanadium alloys based on the V-Cr-Ti system have attractive low-activation properties. The critical areas of irradiation effects on mechanical properties and welding are being addressed.

Representative alloys are subjected to scoping studies that explore the effects of radiation on dimensional stability and mechanical and corrosion properties. Irradiation parameters investigated include temperature, fluence, and helium generation rate. Studies are conducted to assess thermomechanical behavior in various coolant media and the effects of long-term thermal exposure on mechanical performance. These experiments help define a preliminary design window for each alloy class and identify the critical phenomena that limit performance. Experiments are carried out, often in conjunction with other radiation effects programs, to determine the mechanisms that control these critical phenomena. Based upon mechanical understanding, new alloy compositions and microstructures are designed for improved performance, and their properties are explored in further scoping studies. Most of the alloy development effort is directed toward understanding radiation effects and adjusting alloy compositions to improve resistance to radiation damage. The time cycle for establishing some incremental gain in performance is on the order of 5 years, because it takes ~3 years of reactor time to accumulate a level of irradiation damage sufficient to make a full assessment of alloy response.

7.1.1 Reduced Activation

Ferritic/Martensitic Steels Charpy and tensile specimens of the eight original ORNL heats of reduced activation steels irradiated in the Materials Open Test Assembly of the Fast Flux Test Facility to 20 dpa were evaluated. Work on the IEA collaboration will begin with the characterization of a 5-ton heat and another smaller (1-ton) heat of reduced activation ferritic steels that have been obtained for the program. Two High Flux Isotope Reactor (HFIR) irradiation capsules have been designed and built to house specimens of various reduce-activation steels, including the 5-ton IEA heat. The capsules will be irradiated to 12 dpa at 300 and 400°C to investigate irradiation response and the simultaneous effect of neutron damage and helium generation. Charpy, tensile, and TEM data of irradiated specimens will be determined. To enhance helium generation, some of the steels are doped with nickel, and helium is generated by an (n, α) reaction of the thermal neutrons with ^{58}Ni. For comparison, and to obtain a larger base of data on the helium effect, conventional chromium-molybdenum ferritic steels with and without nickel additions will also be irradiated. Evaluation of new compositions of low-chromium steels developed as variations on the original eight heats will continue.

7.1.2 Silicon Carbide

Composite HFIR irradiation of composite materials fabricated from high-density SiC fibers will be completed to 1.5 dpa. Mechanical properties such as ultimate strength, interfacial strength, thermal conductivity, and microstructural evolution will be tested. Fabrication of

radiation-resistant SiC composites and development of improved interfacial structures will continue. Advanced fiber testing to identify radiation-resistant fibers will also continue.

7.1.3 Vanadium Alloys

Welding studies are being carried out on V-5Cr-5Ti alloy using 0.75-mm-thick sheet and 6-mm-thick plate. Parameters will be established for full-penetration gas tungsten arc welds, and sensitivity to hot cracking will be assessed. Weld properties are being assessed using tensile tests. The effect of oxygen concentration levels in the glove box atmosphere on the mechanical properties of welds is also being evaluated. Various shielding techniques will be studied.

Additional 50-kg heats of V-Cr-Ti alloys have been procured from Teledyne Wah-Chang to optimize the V-4Cr-4Ti prime alloy and determine sensitivity to changes in chromium, titanium, and silicon levels. A study of the relationships between fabrication history, impurity level, and impact properties of small heats of V-4Cr-4Ti alloys will be completed.

A V-4.3Cr-5.6Ti alloy has been used to measure thermal expansion, thermal conductivity, and specific heat over the range of 100 to 600°C. Fully reversed strain-controlled testing has been carried out to determine fatigue properties at 100 and 400°C.

A neutron transport calculation has been performed to determine the feasibility of creating a shielded facility in the HFIR beryllium reflector. It was found that the Eu2O3 provides satisfactory spectral tailoring to reduce production of chromium below the tolerance limit for chromium in the original alloys. The shield would have to be replaced after eight cycles or 5 dpa, but HFIR's operation schedule makes it easier to replace the shield after seven cycles. Three shields would then have to be used in order to reach 10 dpa. This facility would provide the equivalent of a low-temperature fast-neutron position in HFIR for development and preliminary qualification of vanadium alloys for fusion devices. Construction of such an irradiation facility has been proposed to DOE.

7.2 ITER NEUTRON-INTERACTIVE MATERIALS

This task is concerned with the selection and qualification of first-wall, blanket, and divertor structural materials and ceramics for diagnostics applications in ITER. During the ITER CDA, a 316-L austenitic stainless steel was recommended for the first-wall and blanket (FWB) structure. High-strength copper alloys were identified as possible candidates for the divertor structure. Selection of a specific composition and TMT for the FWB structure will be based upon characteristics such as weldability effects of irradiation on mechanical behavior and susceptibility to stress corrosion cracking.

The effects of irradiation on the tensile, fatigue, and fracture toughness properties; radiation-assisted stress corrosion cracking; and welding of irradiated materials are being addressed. The objective is to provide the basis for selecting specific compositions and TMTs and to provide the engineering database needed for a final design, component performance prediction, and construction. For the divertor structure, this task addresses the effects of neutron irradiation on the hardening, swelling, and creep properties of oxide-dispersion–strengthened copper alloys.

The task supports the *Materials Handbook for Fusion Energy Systems* through a subcontract with McDonnell-Douglas Missile Systems Company, St. Louis, Missouri.

7.2.1 Austenitic Steels

Under ITER Task T14, postirradiation measurements have been initiated on a range of austenitic stainless steels and various TMTs following irradiation to 18 dpa at 60 and 330°C in a HFIR spectrally tailored experiment. Radiation-induced hardening, ductility, irradiation creep, and density change were measured. Irradiation of a similar set of materials continues in spectrally tailored experiments operating in HFIR at 200 and 400°C. Fracture toughness property measurements have been completed on a set of U.S., European, and Japanese austenitic stainless steels following irradiation to 3 dpa at temperatures of 90 and 250°C. Data have been obtained on the influence of composition (carbon, nitrogen, titanium), TMT (SA, CW), and on weld technique (TIG, EB). Fracture properties are being correlated with changes in tensile properties and microstructure. These data will be prepared for the ITER material handbook. A second series of irradiation capsules is being planned to assess the fracture behavior of first-wall materials further.

7.2.2 Ceramic Insulator

Ionization and displacement damage to ceramic oxide materials during neutron irradiation can cause changes in electrical properties such as conductivity and loss tangent. The changes in properties can be of a magnitude that must be considered in selection and specification of materials for design of and use in ceramic components for diagnostic and plasma heating systems.

Sapphire has been proposed for insulating feedthroughs and windows in rf and microwave heating systems in fusion reactors. The degradation with irradiation of sapphire's thermal conductivity is a concern in the design of these windows. Cooling microwave windows to liquid nitrogen temperatures has been proposed in order to take advantage of the thermal conductivity peak at ~30 K in unirradiated sapphire and the lower dielectric loss tangent at these temperatures. Theoretical modeling has found that vacancy scattering can reduce thermal conductivity over a wide temperature range. For example, a vacancy concentration (resulting from neutron irradiation) of 0.01/atom leads to a 90% reduction at 77 K but only a 43% reduction at 400 K. The effects of neutron irradiation on the thermal conductivity of alumina at temperatures between 77 and 400 K have been studied.

In situ electrical conductivity measurements have been performed on polycrystalline alumina during neutron irradiation in the High Flux Beam Reactor at Brookhaven National Laboratory. In the first experiment, no radiation-induced electrical degradation (RIED) was observed in a sample at 80°C up to a damage dose of 0.11 dpa. However, there were problems related to the termination of the cable ends in the capsule for other samples. In a second irradiation, cables were sealed with glass to determine whether this would improve the cable performance. No RIED was observed in a sample at 330°C up to a damage dose of 1.4 dpa; however, there were still termination problems with some cables. A third irradiation will be performed on mineral-insulated cables and several oxide ceramic samples using braze-sealed terminations to determine if better cable performance can be obtained. The applied electric field will be about 100 V/mm in all cases.

The ion beam irradiations have been performed on oxide ceramics at room temperature and at 650°C (923 K) to examine the importance of variations in the ionizing and displacive radiation spectrum to microstructural revolution. These studies are relevant for determining whether in situ irradiation tests performed with electrons or light ions may modify some radiation-induced degradation processes that would occur in a fusion environment.

In addition, the electrical properties of ceramics have been tested and determined during fission reactor irradiations that produce ionization and displacement damage approximating that

produced in locations of diagnostic and plasma-heating components in ITER. The results will be of immediate importance in the design of ITER diagnostic and plasma-heating systems. Irradiation of HFIR target capsules CTR-60 and CTR-61 has begun. These capsules contain a wide range of ceramic materials in the form of disks and bend bars and will achieve fast neutron (E > 0.1 MeV) fluences of about 1.8 and 7.2 × 10^{26} n/m^2, respectively, (15 dpa and 60 dpa) at 100, 350, and 600°C (373, 723, and 873 K). These capsules include Al2O3 and MgAl2O4 specimens that have been isotopically tailored with 17O to achieve fusion-relevant He/dpa generation rates.

Significant progress on rf insulator radiation tests is discussed in Sect. 5.3.7.2.

7.2.3 Carbon/Carbon Composite Materials and Beryllium

The purpose of this task is to establish the feasibility and limitations on carbon/carbon composites and bulk graphite for plasma-facing applications in fusion reactors. Primary interest is in the composite materials because of their superior strength, thermal shock resistance, and design flexibility. A major problem for either composites or bulk graphites is their ability to withstand high-energy neutron irradiation without an unacceptable degradation of properties. The first objective is to provide a low-Z plasma-facing materials with neutron damage resistance that will provide a lifetime at least equal to that defined by erosion and sublimation. This task provides basic property data on graphites and carbon/carbon composites needed for selection and design of the ITER first wall and divertor.

Specimens of plasma-sprayed beryllium supplied by LANL will be subjected to thermal conductivity testing at room temperature and elevated temperature. The extent to which LANL's plasma spray process developments have improved the thermal conductivity will be elucidated. Thermal annealing studies will be performed to assess the potential for further improvements in beryllium thermal conductivity.

High conductivity unidirectional and multidirectional carbon/carbon composite materials will be irradiated in HFIR rabbit capsules. The effects of neutron irradiation on thermal conductivity will be assessed. Postirradiation thermal annealing will be employed to generate data for modeling purposes.

7.2.4 Copper Alloy

Under ITER Task T8, the development of high-strength copper alloy/stainless-steel–bonded structures has been initiated. Coordinating this task involves product fabrication at McDonnell-Douglas Aerospace, divertor development at Sandia National Laboratories, and structural design at JCT Garching.

In collaboration with PNL and the Efremov Institute RF, an irradiation experiment on high-strength copper alloys will be completed in SM-3 at doses of 1 and 4 dpa. Postirradiation tensile testing and swelling measurements will be completed for irradiation temperatures of 120, 240, and 340°C.

The relative performance of high-strength copper alloys being considered for the ITER divertor and first-wall structures will be assessed under ITER Task T7.

7.3 OTHER MATERIALS FOR ITER

Incoloy 908 was developed specifically for use as the conduit material for the ITER superconductors, with strength and coefficient of thermal expansion being major alloy design

considerations. Initial studies have indicated marginal weldability in terms of resistance to hot cracking, as measured by the sigma jig test. A typical heat of alloy 908 showed a threshold cracking stress of 11 ksi (76 MPa), which can be compared to a range of values of 15 to 50 ksi (103–345 MPa) for commercial austenitic stainless steels. This task will quantify the heat-to-heat variability that is encountered with production heats and ensure that each heat has sufficient cracking resistance to perform as expected in conduit fabrication. As additional heats are tested, a database will be established that will allow early identification of off-normal heats, thus avoiding the costs and schedule delays of rework and/or material replacement.

Sheet material from all available production heats will be obtained directly from International Nickel Company and MIT archives. It will be rolled to standard thickness (0.25 mm), and sigma jig hot crack testing will be conducted. The results will be compared with existing data for other nickel-based alloys and structure materials.

7.4 ORNL/JAERI COLLABORATION IN HFIR

The objective of this task is to conduct irradiation tests in HIFR in collaboration with the Japan Atomic Energy Research Institute (JAERI) in support of fusion material development programs in the United States and Japan. Under the collaboration all costs are equally shared. The planning, execution, review, and reporting of this work are carried out under the auspices of the Steering Committee for the Program for U.S./Japan Collaborative Testing of First Wall and Blanket Structural Materials with Mixed Spectrum Fission Reactors. The spectrally tailored experiments conducted in the HFIR removable beryllium (RB) positions provide the closest simulation of the fusion neutron damage possible in the absence of a high-flux fusion neutron source. Results of the experiments will form the foundation for design of next-step reactors such as ITER or FER. The HFIR target irradiations provide information on irradiation effects on properties at helium levels appropriate to DEMO and power reactors with concomitant displacement damage. These results are an important part of the effort to develop irradiation-resistant materials.

Two approaches are used to achieve fusion reactor damage levels (helium production and dpa levels): (1) irradiation of alloys that contain nickel (e.g., austenitic stainless steels and certain ferritic steels) in a mixed-spectrum fission reactor and (2) tailoring the isotopic composition of a material with an isotope of one of the alloying elements that has a large (n, α) cross section. Experiments of the first type, spectrally tailored experiments, are irradiated in the HFIR beryllium reflector. In these positions the damage accumulation rates are about 8 dpa/year. At the outset of the collaboration the goal was to achieve ~30 dpa for a period of 10 years. Because the HFIR was out of service for 3 years, it has been necessary to reduce this goal to 20 dpa. This damage level as well as the damage rate, irradiation temperatures, and range of properties being investigated are appropriate to ITER. To achieve higher damage levels, appropriate to a DEMO or power reactors, irradiations are performed in the HFIR target region. To achieve He/dpa ratios of a fusion spectrum, isotopic tailoring is necessary. For example, to vary the He/dpa in an austenitic or ferritic steel, we vary the ratio of 58Ni/60Ni. Essentially all properties that are of interest in evaluating the potential performance of a material in a fusion neutron environment are investigated.

Postirradiation testing and examination of the specimens from target capsules JP10, 11, 13, and 16 following irradiation to 20 dpa has been completed, as well as the postirradiation examination of JP14, irradiated to a fluence of 40 dpa. JP9, 12, and 15 completed 35 cycles on April 1, 1994, and were removed for the target region. Each capsule had accumulated a peak dose of ~57 dpa. Irradiation of JP20, 21, and 22 began in December 1993 with the start of cycle 322 in

HFIR. JP20 was removed after accumulating a peak dose of 8 dpa. As of December 7, 1994, (end of cycle 331), the remaining capsules had achieved ~12.9 dpa. Cold-worked, annealed, and welded AISI 316 from Europe, Japan, and the United States, irradiated to 3 dpa, was tested for fracture toughness, and tensile properties were measured. Quantitative fractography and TEM will be carried out on the austenitic steels from these experiments (JP17, 18, and 19) to complete the fracture toughness experiments. The spectrally tailored RB capsules 60J-1 and 330J-1 were disassembled after accumulating a peak dose of 11 dpa in HFIR, and the postirradiation measurements of tensile, creep, and swelling properties have been initiated. The 200J-1 and 400J-1 capsules continue irradiation towards their goal of 18 dpa. Density measurements have been completed on isotopically tailored specimens irradiated to 20 and 40 dpa. Swelling analyses and preliminary microscopy will be conducted with emphasis on the effects of He/dpa ratio.

7.5 IFMIF

The need for a high-flux, high-fluence neutron irradiation facility for fusion materials R&D has long been recognized and endorsed by both U.S. and foreign fusion programs. Because the radiation damage to materials depends upon the neutron energy spectrum, the effects of fusion neutron irradiation can be substantially different from those of fission neutron irradiations. Consequently, a fusion irradiation facility must provide the necessary spectral characteristics as well as the fluxes and fluences needed for accelerated end-of-life testing of materials. A source based on the Li(d,n) reaction, using 35- to 40-MeV deuterons from an accelerator on a flowing lithium target is the most favored concept and the basis of the FMIT project, which began in the late 1970s and was later canceled.

Fusion is now preparing to enter the nuclear phase of development, as evidenced by the initial D-T operation of JET, the recent D-T operation of TFTR, the growing commitment to ITER, and the National Energy Strategy's goal of an operating DEMO in about the year 2025. Furthermore, there is increasing acceptance of the critical importance of low-activation material development to the success of fusion as an energy source. All these facts increase the urgency of proceeding with the International Fusion Materials Irradiation Facility (IFMIF). There is now an international agreement for collaboration in such a facility, similar to the initial phase of ITER.

The IFMIF is a new international design study established by IEA. A 3-year CDA will begin in FY 1995, with technical work developed through a collaboration between the United States, Japan, Russia, and the European Community. Japan has been identified as the overall leader. ORNL will lead the U.S. Team. The ORNL task involves coordinating the U.S. effort to develop a conceptual design for the IFMIF. Specific studies related to design integration, the definition of irradiation needs, overall facility layout, and remote-maintenance requirements will be done by ORNL as part of the coordinated U.S. effort. The international task includes coordination with Japan to assist in the management. The task also includes coordination and possible collaboration with the various foreign programs in this area.

This task began in 1992 with discussions on the mechanisms and organization for the design study collaboration. In 1993 activities included solicitation of industry participation and a preliminary cost assessment for the project. An international workshop organized by IEA was held in Moscow to outline a technical approach for a CDA.

8

RADIATION TRANSPORT

C. Y. Fu[1]

D. M. Hetrick[2]
D. C. Larson[1]
J. B. Manneschmidt[1]
R. W. Roussin[1]
J. E. White[1]

1. Engineering Physics and Mathematics Division.
2. Computing Applications Division.

8. RADIATION TRANSPORT

Summary of Activities

The radiation transport program includes two elements: the work of the Radiation Shielding Information Center (RSIC) and cross-section evaluation and processing.

RSIC staff members continue to serve as technical consultants to the fusion energy research community, as well as a variety of other research communities, on all matters relating to radiation transport. The evaluation and processing program is directed at producing accurate cross-section data for materials that are of specific interest to fusion reactor designers. Both of these activities strongly support the International Thermonuclear Experimental Reactor (ITER) community. The development of the international Fusion Evaluated Nuclear Data File, which is the source of neutron and photon data used for the ITER project, included significant contributions from this program.

8.1 RADIATION SHIELDING INFORMATION CENTER

R. W. Roussin, J. E. White, and J. B. Manneschmidt

The Radiation Shielding Information Center (RSIC) serves an international community by responding to inquiries about radiation transport problems. Staff members provide guidance by drawing on a technical database that includes a computerized literature file, a collection of complex computer programs, and a substantial body of nuclear data libraries pertinent to the solution of such problems.

Acquiring the needed computer-based technology requires the collaboration of the neutronics community with RSIC staff members to collect, organize, process, evaluate, and package relevant technology developed in the community. This technology is disseminated to the community with a mechanism for feedback of experience through use, which results in an improved product. The resulting technology base provides an advancement of the state of the art.

A sample of some recent products of this information cycle process shows the international character of the RSIC community. The Joint Research Center in Italy, through the Nuclear Energy Association (NEA) Data Bank, Issy-les-Moulineaux, France, contributed the CCC-606/ANITA code system for the analysis of neutron-induced transmutation and activation. The Energy Research Foundation, Netherlands, provided the CCC-615/FURNACE code system for neutronic calculations in 3-D toroidal geometry. The CCC-616/BERMUDA discrete ordinates code system for shielding analysis for use with fusion and fission reactors was contributed by the Nuclear Energy Data Center of Japan. The Institute of Physics and Nuclear Engineering, Romania, through the NEA Data Bank, Issy-les-Moulineaux, France, contributed the

PSR-325/STAPRE-H code system to calculate energy-averaged cross sections of particle-induced nuclear reactions. From the Physilalisch-Technische Bundesanstalt in Braunschweig, Germany, and the Institute of Radiation Dosimetry in the Czech Republic comes the PSR-334/DIFBAS code system, which is a Bayesian approach to unfolding a neutron spectrum from a spectrum of recoiled protons.

JAERI provided the PSR-316/CASTHY statistical model calculation for neutron cross sections and capture gamma-ray spectra and the DLC-165/FSXLIB-J3 MCNP continuous energy neutron cross-section library based on JENDL-3. From IAEA in Vienna came the DLC-166/PNESD proton nucleus elastic scattering data and the DLC-170/ACTIV-FUS/INT international library of neutron activation cross-section data for fusion reactor applications.

The National Institute of Standards and Technology contributed the PSR-330/STAR CODES for calculating stopping-power and range tables for electrons, protons, and helium ions. From LLNL came the DLC-164/UNGER data library of effective dose equivalents for specific radionuclides. Sandia National Laboratories provided the PSR-345/SNL-SAND-II code system for neutron flux spectra determination by multiple foil activation using the iterative method and the DLC-178/SNLRML-recommended dosimetry cross-section compendium.

LANL updated the PSR-171/NJOY91 code system for producing pointwise and multigroup neutron and photon cross sections from Evaluated Nuclear Data File (ENDF/B) data. LANL also provided the PSR-317/TRANSX2 code system to produce neutron, photon, and particle transport tables for discrete-ordinates and diffusion codes from cross sections in MATXS format and the DLC-168/LA100-evaluated nuclear data library for transport calculations involving incident neutrons and protons of energy up to 100 MeV.

ORNL contributed the CCC-610/CALOR89 Monte Carlo code system for design and analysis of calorimeter systems, the CCC-613/VALE multigroup diffusion theory neutronics code system for solving 2-D and 3-D problems for triagonal geometries, and the PSR-315/AMPX-77 modular code system for generating coupled multigroup neutron-gamma libraries from ENDF/B.

This selection represents a small portion of the total activity of the center. Information processing (including evaluation and packaging) is a daily function. In addition to a comprehensive literature database, RSIC-packaged products include 178 data packages (DLC), 631 neutronics and shielding code packages (CCC), and 346 data processing and other miscellaneous code packages (PSR).

A number of publications[1–5] were made in support of these activities.

8.2 NEUTRON CROSS SECTION

C. Y. Fu, D. M. Hetrick, D. C. Larson, and J. E. White

This task provides evaluated and multigroup cross sections for neutron-induced reactions required for design of fusion power systems and interpretation of results from test facilities. It is divided into two subtasks.

8.2.1 Cross-Section Evaluation

This subtask provides new evaluated data to ENDF/B for materials, reactions, and energy regions of primary interest to the fusion community. Existing evaluations are upgraded through incorporation of significant new experimental data supplemented by advanced nuclear model calculations and extended to higher energies (up to 40 MeV) where required. Particular attention is focused on activation, dosimetry, and gas production cross sections; recoil nuclei spectra;

angular and energy distributions of secondary particles; and cross-section uncertainties. The subtask will result in a consistent, up-to-date, evaluated database especially tailored to fusion neutronics data needs.

Our approach will fully utilize the experimental data and advanced nuclear models made available by the Basic Energy Sciences program (now sponsored by Nuclear Physics) for fusion energy data. For the materials we evaluate, we first collect all appropriate experimental data. Then, using our TNG model code, we simultaneously reproduce cross sections for all reactions and energy ranges where experimental data are available. Model parameters are adjusted, within limits imposed by physics and previous knowledge, to achieve the most consistent set of cross sections. These techniques have been used in evaluations of the isotopes of copper, nickel, chromium, iron, and lead from 1 to 20 MeV. Success depends on the sophistication of the nuclear model codes, and we are recognized leaders in model and code development. Our familiarity with performing and analyzing measurements has led to the development of another evaluation technique, useful for measurements that were done as ratios. This method has been incorporated in a computer program and has been used to develop a database containing adjusted cross sections and associated covariance and cross-section covariance matrixes for 14 dosimetry reactions. This new method is being used to expand this database for reactions and energy ranges required for fusion energy development.

The evaluations will be produced in standardized formats, fully documented, available for general distribution, and recommended to the Cross-Section Evaluation Work Group (CSEWG) for inclusion in the ENDF/B system. Through CSEWG, the evaluators meet periodically to discuss common problems and to learn about new developments and techniques.

We also participate in development of the Fusion Evaluated Nuclear Data Library (FENDL) for use by the ITER project.

In 1992 and 1993, evaluations for ^{28}Si, ^{29}Si, and ^{30}Si have been documented, except for the resonance region. Further review work for FENDL-2 will continue. In 1994, structural material cross sections important for activation in FENDL for ITER were reviewed. Programs have been developed for comparing evaluations from different libraries (JENDL, EFF, BROND). Vanadium evaluations were reviewed.

A number of publications resulted from the neutron cross-section evaluation activities.[6–12]

8.2.2 Processing Evaluated Data into Multigroup Cross Sections

This subtask provides for the processing, testing, and packaging of a new general-purpose multigroup library, based on ENDF/B-VI. Processing will be done with state-of-the-art technology now operational at ORNL and will focus on materials of key importance for fusion neutronics applications. New or modified evaluations prepared in subtask A (Sect. 8.2.1) will also be processed in this subtask. The processed library will be tested, verified, packaged, and distributed by RSIC at ORNL and placed on the NERSC at LLNL. It will serve as a general-purpose multigroup cross-section library for fusion neutronics projects.

Specifications for the successor to VITAMIN-E indicate only minor modifications are in order. The new group structure will contain 175 neutron groups to be consistent with the European community's VITAMIN-J library, which is derived from the JEF-evaluated data files. VITAMIN-J was patterned after VITAMIN-E and designed to facilitate intercomparison of benchmark results based on analyses with different evaluated data files.

Guidance for additions and modifications will be obtained from DOE and the program for assessing magnetic fusion nuclear data needs currently being coordinated at General Atomics.

Different sequences of handling codes are needed for retrieving, manipulating, converting, editing, collapsing, self-shielding, and performing other tasks on data in CCCC or AMPX code systems. Codes for handling AMPX or CCCC format are provided in PSR-117/MARS, which is available from RSIC.

In 1992 processing capability for ENDF/B-VI was tested as evaluations in that format became available. In 1993 processing began on a new version of the VITAMIN series based on ENDF/B-VI. In 1994 processing and maintenance of the new VITAMIN library continued, based on ITER needs.

REFERENCES

1. R. W. Roussin, "Activities of the Radiation Shielding Information Center and a Report on Codes/Data for High Energy Radiation Transport," presented at Simulating Accelerator Radiation Environments Workshop, Santa Fe, N.M., January 11–15, 1993.

2. J. E. White, "Overview of Current RSIC Activities of Interest to Fusion Neutronics," presented at the 4th International Workshop on Fusion Neutronics, Los Angeles, Calif., October 20–21, 1993.

3. R. W. Roussin, "Recent Activities of CSEWG with Regard to ENDF/B-VI," oral presentation, IAEA Advisory Meeting on Review of Uncertainty Files and Improved Multigroup Cross Section Files for FENDL, Tokai, Japan, November 8–12, 1993.

4. J. E. White, "Preparation of Processed Nuclear Data Libraries for Thermal, Fast and Fusion Research and Power Reactor Applications," oral presentation, IAEA Consultants' Meeting, Vienna, December 8–10, 1993.

5. J. E. White, "Preparation of Fusion Benchmarks in Electronic Format for Nuclear Data Validation Studies," oral presentation, IAEA Consultants' Meeting, Vienna, December 13–16, 1993.

6. Z. Zhixiang, C. Y. Fu, and D. C. Larson, "Theoretical Calculation of Neutron Induced Data of F-19 and Uncertainties of Parameters," *Chinese Journal of Nuclear Physics*, **14**(1), 67–75 (1992).

7. C. Y. Fu, "Comparative Cross Section Calculation Using Exciton Level Densities Based on One and Two Kinds of Fermions," oral presentation, International Workshop on Nuclear Data for Fusion Reactor Technology, Del Mar, Calif., May 3–6, 1993.

8. D. C. Larson, "Fusion Data Measurement Capabilities at ORELA," oral presentation, International Workshop on Nuclear Data for Fusion Reactor Technology, Del Mar, Calif., May 3–6, 1993.

9. D. C. Larson, D. M. Hetrick, and S. M. Grimes, "Comparison of Recent ^{54,56}Fe Charged-Particle Emission Spectra from 8–15 MeV with ENDF/B-VI," oral presentation, International Workshop on Nuclear Data for Fusion Reactor Technology, Del Mar, Calif., May 3–6, 1993.

10. D. C. Larson, "Experimental and Theoretical Nuclear Data Work at ORELA," 1993 Symposium on Nuclear Data, Japanese Atomic Energy Research Institute, Tokai, Japan, November 8–12, 1993.

11. D. C. Larson, "Fusion Data Measurement Capabilities at the ORELA," oral presentation, 1993 Symposium on Nuclear Data, Japanese Atomic Energy Research Institute, Tokai, Japan, November 8–12, 1993.

12. D. C. Larson and C. Y. Fu, "Potential Improvements to ENDF/B-VI for Structural Materials," oral presentation, IAEA Advisory Meeting on Review of Uncertainty Files and Improved Multigroup Cross Section Files for FENDL, Tokai, Japan, November 8–12, 1993.

9

TECHNOLOGY AND SCIENCE APPLICATIONS

J. R. Haines

F. W. Baity
D. B. Batchelor
L. A. Berry
T. S. Bigelow
V. B. Campbell
J. B. O. Caughman
K. R. Chen
J. W. Cobb
L. Dresner
P. W. Fisher
S. C. Forrester
C. A. Foster
A. L. Glover
J. M. Googin
S. M. Gorbatkin
G. R. Hanson
H. H. Haselton
D. J. Hoffman
E. F. Jaeger
C. C. Klepper
J.-N. Leboeuf
E. H. Lee
M. S. Lubell
J. W. Lue
J. N. Luton
L. K. Mansur
W. D. Nelson
Y-K. M. Peng
R. Rhoades
C. R. Schaich
D. E. Schechter
S. W. Schwenterly
W. L. Stirling
L. M. Thompson
C. C. Tsai
J. H. Whealton
T. L. White
J. B. Wilgen
J. M. Williams
T. L. Wilson

9. TECHNOLOGY AND SCIENCE APPLICATIONS

Summary of Activities

Throughout the report period, Fusion Energy Division (FED) researchers have been using their unique skills, facilities, and technologies developed over years of fusion energy research in active support of the Department of Energy's technology transfer mission. Fusion program spin-offs have been so successful that they now represent about 20% of the division's funding.

The fusion spin-off program is referred to as the FED Technology and Science Applications (TSA) program. Projects within the TSA program currently include eight Cooperative Research and Development Agreements with industrial partners in the areas of microwave and plasma processing, work with the U.S. Air Force and several industrial firms on using frozen pellets to remove surface contamination, and collaboration with industry and other government agencies on projects related to the practical application of superconductivity.

The TSA program can be divided into the areas listed below:

- Plasma Fueling Technology Applications
- Plasma Heating Technology Applications
- Magnetics and Superconductivity Technology Applications
- Plasma Theory Applications
- Plasma Confinement Applications
- Fusion Waste Transmutation

Specific projects within each of these application areas are discussed in this chapter. Some of our projects that are cooperative efforts with industrial partners cannot be discussed in this report because of the proprietary nature of the work.

9.1 PLASMA FUELING TECHNOLOGY APPLICATIONS

P. W. Fisher, C. A. Foster, J. R. Haines, D. E. Schechter, and W. D. Nelson

The technology developed in FED to accelerate frozen pellets to speeds of more than 1 km/s for injection into fusion plasmas has been adapted to cleaning materials, including those for removal of paint, oxide layers, adhesives, radioactive contaminants, and grease. Conventional means of removing these surface substances often require use of solvents that can harm the environment. When surfaces are cleaned with cryogenic pellets, no solvents are necessary, and the pellet material evaporates, separating it from the surface contaminant and minimizing the amount of material in the waste stream. Three projects in this application area are discussed below.

9.1.1 Argon Pellet Cleaning

The objectives of this project were to determine the basic feasibility of removing the oxide from depleted uranium surfaces with high-velocity solidified argon (or other gases), to quantify the optimal operating conditions for the system, to fabricate and test a prototype cleaning machine, and to support development of a conceptual design for a production system. The initial effort on this project was to modify an existing FED centrifugal accelerator to test its capability to clean material surfaces using solidified gases. Both argon and CO_2 pellets were accelerated in this device; argon pellets were accelerated to ~500 m/s in cleaning tests. At these speeds the argon pellets produced severe erosion in aluminum and eroded even hard coatings from steel. A new, compact centrifuge with a 30-hp drive and capable of operating at production-scale throughputs was designed for installation in a glove box attached to a high-efficiency particulate air–filtered vacuum system for testing depleted uranium samples. Fabrication of this system, including the high-throughput argon feed, was nearly complete when the project was terminated at the end of April 1994.

9.1.2 CO_2 Paint Stripping—U.S. Air Force

The aim of this project was to design, develop, and fabricate a dry-ice pellet "blaster" to strip paint from aircraft for the U.S. Air Force. The pellet accelerator prototype built for this project includes a 0.36-m- (14-in.)-diam centrifuge capable of producing pellet speeds of up to 350 m/s (1150 ft/s) and pellet delivery rates of 450 kg/h (1000 lb/h). The centrifugal turbine acceleration method is superior to conventional pneumatic accelerators because the acceleration process is considerably more efficient, can deliver higher-velocity pellets, can easily control pellet velocity, and produces considerably less off-gas.

A picture of the turbine device, including the variable-speed motor and accelerator wheel, is shown in Fig. 9.1. The weight of this unit is 36 kg, which makes it compatible with the robotic manipulators used in the Warner Robins Air Logistics Center F-15 depaint facility. The system was demonstrated for the Air Force in February 1994. All of the significant performance specifications were met. A final report for the project was submitted in July 1994.

9.1.3 CO_2 Pellet Blaster Demonstration

The purpose of this project was to install a CO_2 pellet blaster system on a robot and demonstrate solvent-free cleaning and coating removal operations. The main elements of this system are a pellet maker and feed system, an accelerator unit, a control unit, and a robotics system. A pellet maker and feed system, including a tank to hold 1 ton of CO_2, was obtained on loan from the Air Force. The entire system is operational and has been used to demonstrate cleaning capabilities to visiting industries and government personnel. Two papers[1,2] have been presented on this work.

Fig. 9.1. Centrifugal turbine pellet acceleration device.

9.2 PLASMA HEATING TECHNOLOGY APPLICATIONS

9.2.1 Microwave Decontamination Processing

T. L. White, T. S. Bigelow, C. R. Schaich, and T. L. Wilson

9.2.1.1 Concrete decontamination

The purpose of this project is to demonstrate efficient, cost-effective removal of contaminated concrete surfaces using microwave spalling. The award fee milestone, "Complete Initial Testing of the Phase II Mobile Prototype" was completed on schedule. This phase essentially demonstrated the feasibility of mobilizing the technology. Removal rates were increased by 100% over Phase I, to 35 ft^2/h. The Phase II mobile prototype picture was operated in the "dynamic" mode at 15 kW of 18-GHz power at travel speed of 8 mm/s, and a 9-cm-wide by 5-mm-deep trench was removed continuously in a single pass. Removal depths of up to 3 mm can be achieved in multiple passes or by reducing the cart speed. Overlapping removal was also demonstrated. Removal of painted concrete surfaces and subsurface concrete was demonstrated in a single pass at a slightly reduced speed. Removal of concrete around metal anchors was also demonstrated. All microwave leakage was below the American National Standards Institute health limits. More than 95% of the debris was collected with a crude drum vacuum system.

Cooperative Research and Development Agreement (CRADA) negotiations with several companies interested in the technology are under way. Modifications to the Remotec robot carrier and vacuum system are complete. The low-speed adjustments have been refined to improve the precision of control of the carrier. The two 15-kW, 2450-MHz generators have been received. A more suitable X-Y translator has been ordered to replace the robot arm on the carrier. Detailed cost estimates for the microwave concrete decontamination system show operating costs of $\$2.50/ft^2$. Further details of this effort are described in Ref. 3.

9.2.1.2 Hot polymer CRADA

The purpose of this project is to couple the Monolith Technologies, Inc., polymer technology with state-of-the-art microwave technology, developed by ORNL, to develop a cost-effective commercial process for encapsulating radioactive waste slurry. Initial operation of the microwave/hot polymer process was completed successfully. An improved mixing arrangement is being designed by Monolith. Numerous surrogate waste-form monoliths have been processed. The overhead mixer is being fabricated so that all processing can be done in the final storage container. Preliminary throughput data suggest a microwave processing rate ~4 times greater than the conventional processing rate. Preliminary runs show improved mixing, but the overhead mixer must be redesigned to conform to the new tuning schemes being developed.

9.2.1.3 In-drum waste handling

The purpose of this project is to design, fabricate, and test a 5-L, 1/3-scale in-can microwave applicator for drying and solidifying sodium-nitrate–based transuranic liquids and sludges. A full-scale 210-L in-drum applicator is also being fabricated in parallel. The 1/3-scale system has been modified to include the latest improvements in tuning based on experience gained in building a 1.4-L system for the Oak Ridge K-25 Site. A new table-top and bellows assembly have been fabricated. The full-scale system components are being fabricated. The 1/3-scale system has been operated continuously to produce a polymer-encapsulated waste form as well as a salt cake waste form. Final machining of the full-scale system waveguide power feed

section is complete and ready for preliminary testing. A novel new tuning scheme has been developed that eliminates the need for a bellows. This new technique will be implemented on the 1/3-scale prototype before being implemented on the full-scale system.

9.2.2 Rf/Microwave Materials Processing

J. B. O. Caughman, F. W. Baity, S. C. Forrester, and D. J. Hoffman

The Rf/Microwave Sintering Program for the U. S. Army, through the administration of the Engineering Technology Division, has the goal of producing superior ceramic armor tiles of various compositions. Achievements to date are the continued progress in the sintering and postprocessing of ceramic tiles. The program has concentrated on alumina and silicon carbide. These materials have been processed with frequencies ranging from 50 MHz to 28 GHz. Material property measurements and ballistic performance of the materials have been evaluated. In addition, the interaction of the electric field at the grain boundary has been studied.

9.2.2.1 Alumina postprocessing

Presintered alumina tiles have been processed using 28-GHz microwaves. The thicknesses of the 6-in.^{2} tiles ranged from 20 to 40 cm. Material property measurements indicated a small but finite change in several properties. In addition, the statistical variance of material properties throughout each tile was smaller with the microwave-treated tiles. The ballistic performance of the tiles improved significantly, showing an 18% increase in performance over tiles that were not postprocessed with microwaves. The reason for the improved ballistic performance is still not clear. However, it is speculated that the improvement is related to the fundamental interaction of the electric fields at the grain boundaries, which is where the power is deposited.

9.2.2.2 Alumina green-body sintering

Progress has continued in processing larger samples without cracking. A 316-g sample of Coors type 995 alumina (3 in.^{2}) has been sintered (>97% dense) crack-free using rf processing at 50 MHz. This sample is twice the mass of previously sintered samples and is a record for processing in which the power coupling is caused by direct electric-field interaction with the sample. This result is encouraging because a small rf sintering furnace was used for the processing. The insulation and casket that were used are at the limit that is possible for this furnace.

A recently finished upgraded furnace will allow the processing of larger samples. The expanded rf sintering furnace chamber has been assembled, and slight modifications are being made for improved operating capability. The main chamber is 24 in. in diameter and 24 in. in height. The distance between the electrodes is variable and can accommodate casket assemblies 5–9 in. thick. A control program for automatic tuning of the cavity during operations has been written and updated.

9.2.2.3 Silicon carbide processing

Presintered silicon-carbide tiles have been processed using 2.45-GHz microwaves. Tiles were heated to 2100°C and held for 1 h. A total of 28 tiles (6 in.^{2}, 1-cm thick) have been processed and prepared for ballistic tests. As with the alumina tiles, material property tests have shown a small but finite improvement in several properties. Ballistic tests, however, have been inconclusive.

Silicon-carbide green bodies have also been processed using microwaves. Sintering densities greater that 95% have been achieved using microwaves at 2.45 GHz. Processing with lower-frequency rf power has shown some slight densification, but insulation problems with the small rf furnace have prevented temperatures from exceeding 1800°C. Processing with the upgraded furnace should allow this temperature limit to be exceeded.

9.2.2.4 Electric-field effect studies

Several experiments have concentrated on evaluating the interaction of the electric field at the grain boundary. Experiments with presintered samples of alumina (Coors 995) have been used to study this interaction. The samples have been heated to 1500°C using 50 MHz rf power and analyzed with a scanning electron microscope to look at the grain boundaries. A form of precipitant was found at some grain boundaries, but its morphology is different than conventionally processed alumina. The grain boundaries appear to have a more amorphous structure in the rf-annealed samples. The softening of grain boundaries may be a reason for improved fracture and/or ballistic performance. This characteristic may be caused by localized power deposition at the grain boundary, which is where the applied electric field is strongest.

The grain boundary precipitants do not seem to be impurities. X-ray analysis of the grain boundaries does not show anything other than alumina. This technique is sensitive to 2–5% composition, so if there are any impurities at the boundaries (magnesium or silicon), they are not detectable with this technique. However, there were places in the bulk of the grains where significant percentages of magnesium were found (up to 17%). Magnesium oxide is a common sintering additive. There is no indication at this time that there is any difference between the magnesium found in the rf-annealed samples and the samples that were not processed with rf.

9.2.3 Plasma and Ion-Beam Material Processing

9.2.3.1 Plasma cleaning

C. C. Tsai, V. B. Campbell, A. L. Glover, J. M. Googin, H. H. Haselton, W. D. Nelson, D. E. Schechter, and L. M. Thompson

In a microwave ECR plasma source, reactive plasmas of oxygen and mixtures of oxygen and argon have been used for evaluating plasma-cleaning technologies. Small aluminum samples (0.95 × 1.9 cm) were coated with thin films (≤20-μm thick) of Shell Vitrea oil and cleaned with reactive plasmas. The plasma cleanings were conducted using pulsed microwave power to create plasma. The nominal pulse width was set to 1 s at a duty factor of 10%. Pulsed rf power was applied to the sample holder to provide a desired negative bias potential. During plasma cleaning, the current of ion flux was measured using a Langmuir probe. Other operating parameters—gas pressure, gas flow rate, microwave power, magnet current, sample bias potential, and operating time (or accumulated plasma exposure time)—were also recorded. A mass spectrometer (UTI Model 100C RGA) was used to monitor the status of plasma cleaning. Signal amplitude changes of carbon monoxide can be used to indicate the cleanliness of sample surfaces being plasma cleaned. The mass loss of each plasma-cleaned sample was measured for estimating the cleaning rates. The average cleaning rates of low-pressure (0.5-mTorr) argon/oxygen plasmas were as high as 2.7 μm/min. Subsequently, test sample surfaces were studied for cleanliness using X-ray photoelectron spectroscopy (XPS) analysis.

Preliminary results[4,5] reveal that reactive plasma cleaning with a microwave ECR source works well for test samples coated with Shell Vitrea oil films with thicknesses approaching

20 μm. In low-pressure discharges (ranging from 0.3 to 5 mTorr), reactive plasmas have been created and powered by microwave energies. The small, flat aluminum samples have been plasma cleaned, and their surface cleanliness has been confirmed by XPS. Significant results are summarized below:

1. The dominant cleaning particles in oxygen and argon/oxygen plasmas are energetic ions.
2. Argon/oxygen plasmas have cleaning rates 2 to 3 times higher than those of oxygen plasmas.
3. The cleaning rates of oxygen/30%-argon plasmas can be as high as 2.7 μm/min.
4. For thick oil films (~20 μm), only samples with rf biasing can effectively be cleaned in high-pressure plasmas (~5 mTorr oxygen); samples with dc biasing cannot.
5. Samples with –200-V rf biasing can be cleaned without etch damage, but samples with –75-V dc biasing tend to have etch damage on sample surfaces.
6. XPS analysis for relative concentrations of aluminum, carbon, and oxygen on sample surfaces confirmed that the surfaces of plasma-cleaned samples can be cleaner than the surfaces of bare control samples.

9.2.3.2 Beam/plasma ion implantation

W. L. Stirling, C. C. Tsai, J. H. Whealton, E. H. Lee, L. K. Mansur, and J. M. Williams

A paper was presented at the First International Workshop on Plasma Based Ion Implantation at Madison, Wisconsin, in August 1993.[6] A summary of this paper is given below.

Surface processing techniques involving high-energy ion implantation have achieved commercial success for semiconductors and biomaterials. However, wider use has been limited in good part by economic factors, some of which are related to the line-of-sight nature of the beam implantation process. Plasma source implantation (or plasma immersion ion implantation) is intended to remove some of the limitations imposed by the directionality of beam systems and to help provide economies of scale.

Typical requirements of such beam systems are beam energies ranging from 100 eV to a few megavolts, ion currents ranging from ≤2 mA to a few amperes, current densities from ≤1 μA/cm^2 to ~1 mA/cm^2, pulse lengths from ~10's μs to cw, and ion species of gas or metal. Relevant technologies and areas of expertise for meeting future needs in materials processing exist at ORNL. Experience in generation of plasmas, control of ionization states, pulsed extraction, and sheath physics exist. Contributions to future technology can be made either for the immersion mode or for the extracted-beam mode. Existing facilities include the High-Power Test Facility, which could conservatively operate at 1 A of continuous current at 100 kV delivered to areas of 1 m^2. Higher instantaneous voltage and currents are available with a reduced duty cycle. Another facility, the High Heat Flux Facility can supply a maximum of 60 kV and currents of up to 60 A for 2 s on a 10% duty cycle. Plasma may be generated by microwaves, rf induction, or other methods, and plasma may be tailored to suit specific needs.

With material-processing expertise available through the Metals and Ceramics Division and Solid State Division, we can use our beam technology to develop advanced implantation systems for fulfilling processing requirements. In addition to ion implantation of large steel components, foreseeable applications include ion implantation of polymers, titanium alloys, aluminum alloys, and other reactive surfaces.

9.2.4 LDRD Advanced Combustion

J. B. Wilgen, T. S. Bigelow, G. R. Hanson, and J. H. Whealton

The objective of this task is to develop a pulsed, high-power microwave system for injection into an internal combustion engine chamber to investigate possible improvements in the combustion process and emission reduction.

The structure of a small-engine combustion chamber was studied as a microwave resonant cavity that would serve to couple microwave power to the combustion flame front. A resonance was found at 5.5 GHz that matched an available radar-style pulsed microwave generator. The electric fields for this resonance were mapped using cavity perturbation techniques. A 5.4–5.8 GHz, 175 kW, 2-ms pulse generator was obtained and upgraded for use in this application. A microwave window was developed to couple power to the engine cavity at near top-dead-center crank angle. The microwave behavior of the window was studied under a variety of conditions, and it was found to have a good match for most cases of interest. A waveguide system was set up to connect the generator to the engine and to monitor forward and reflected power. The system was successfully operated at high power, and several initial basic experiments were performed to study the microwave effects.

Arcing at the window limits the power level to half the generator capability. A proposed solution is to stretch the generator pulse length and thus increase the energy coupled per cycle. An alternate, low-frequency rf coupling scheme is also proposed.

9.3 MAGNETICS AND SUPERCONDUCTIVITY TECHNOLOGY APPLICATIONS

L. Dresner, M. S. Lubell, J. W. Lue, J. N. Luton, and S. W. Schwenterly

FED's Magnetics and Superconductivity (M&S) Group has dedicated its efforts primarily in three areas: (1) ITER, (2) Superconducting Partnership Initiatives (SPIs), and (3) Superconducting Partnership Program (SPP). The M&S Group has attained significant accomplishments in each. The ITER efforts are described in Chap. 5. The SPI and SPP projects are discussed in the following sections.

9.3.1 SPI Projects

An SPI project is being carried out with General Electric on Superconducting Generators. The first phase of the ORNL task was to design a more efficient type of stator. With the advent of high-temperature superconducting (HTS) materials to enhance the practical application of power system components, a partial helical stator was designed. Partial-Helical Stator Design parameters are shown in Table 9.1.

Another SPI project is in process jointly with the Electric Power Research Institute, Pirelli Cable, and the American Superconductor Corporation (ASC) on the design of a superconducting transmission line cable. ORNL's main responsibility on this project is the design of the cryogenic system and measurements of the ac losses in a 1-m-long simulated line.

Table 9.1. 150 MVA Partial-helical stator design

Core	
OD/ID, in.	74/51.1
yoke flux density, T	1.58
Armature	
slots/bars per slot	24/4
circuits/turns per coil	1/1
turns per phase	16
winding pitch	5/6
mean length of turns, in.	250
active length, in. (same bar length)	117.1
eff. current density, A/cm^2	95.5
OD/ID, in.	51.1/36.9
Subtransient reactance	
Generator losses, kW	
windage[a]	20
fan loss	38
core loss[a]	136
tooth and helical support pin loss	45
armature I^2R	288.9
extra copper loss[a]	24
stray losses[b]	300
cryocooler compressor[b]	15
total loss (excluding bearings)	867
Efficiency, %	99.36

[a]Scaled from GE-calculated value by core length ratio.
[b]Scaled from GE-calculated value by power output ratio.

9.3.2 SPP

A joint project was carried out with ASC on reducing the ac losses of its conductor and the measurements on the quench propagation velocity of a 1-T magnet. The magnet was designed and built by ASC and tested in the variable-temperature cryostat at ORNL from 4.2 K to 77 K, with background fields up to 2.5 T. The magnet met all specifications and produced 1-T self-field at 20 K. The 1-T magnet was shown to be extremely stable; operating at up to 3 times the critical current did not lead to thermal runaway. Recovery was still observed. It was shown that the ac losses could be reduced by twisting the filaments in a multifilamentary tape conductor. Figures 9.2 and 9.3 illustrate the Coil Test Facility design and the ac loss measurement setup.

A joint SPP project with the Astronautics Technology Center was carried out on magnetic refrigeration. ORNL designed and procured components for a prototype 50-W (40 K) superconducting magnet and dewar. The prototype refrigerator was successfully operated and tested as planned.

For another SPP project, a very small demonstration motor using an HTS magnet (fabricated by ASC) was designed, assembled, and successfully tested at liquid-nitrogen temperatures. With two 1.5-V batteries (in parallel) supplying current to the HTS coil and five 9-V batteries supplying the armature, the motor started itself without assistance to overcome static friction and attained speeds of several hundred revolutions per minute. (See Fig. 9.4.)

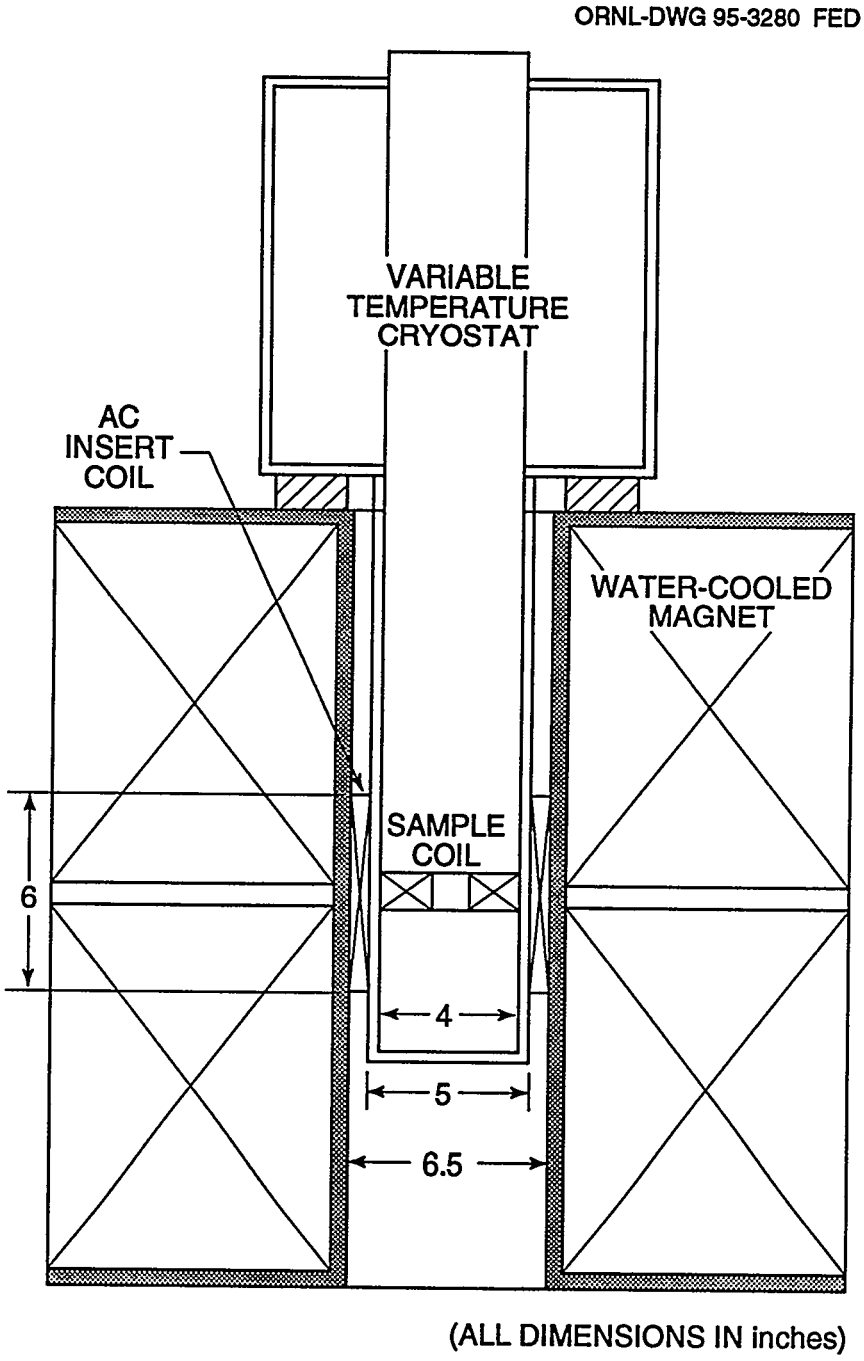

Fig. 9.2. Coil Test Facility design.

Another SPP project was a study aimed at determining the difference in the costs of a large superconducting magnetic energy storage system using a warm structure with earth support and one using a cold structure with steel supports. The crossover point lies somewhere in the range of 1–20 GJ (0.3–6 MW-h).

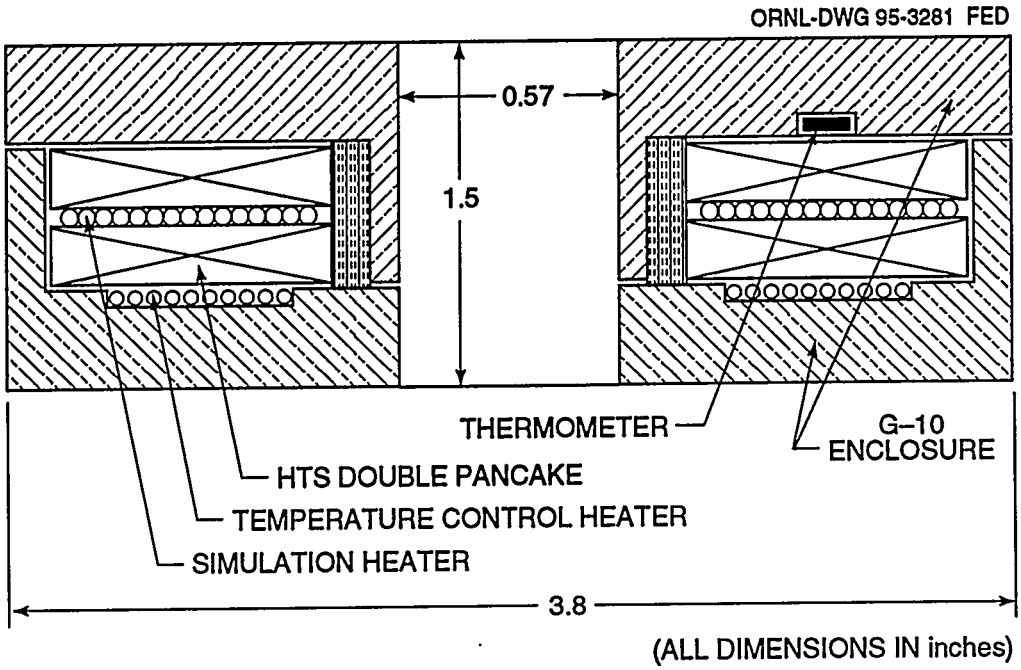

Fig. 9.3. Alternating-current loss measurement setup.

9.4 PLASMA THEORY APPLICATIONS

L. A. Berry, J.-N. Leboeuf, K. R. Chen, J. W. Cobb, E. F. Jaeger, and D. B. Batchelor

FED is applying its capabilities developed over many years of modeling fusion plasmas to modeling plasma etching and deposition processes. The plasma process modeling projects currently in progress, which include two CRADAs and one Laboratory Director's R&D project, are discussed below.

9.4.1 Modeling of Plasma Reactors

The overall purpose of this multiyear CRADA with Sandia National Laboratory and Sematech is to develop plasma models that can be used to improve and shorten the very-large-scale integrated (VLSI) circuits development cycle. The objective of the ORNL source task is to develop computer-based models of the rf currents, electric fields, and magnetic fields, as well as the resulting power deposition for high-density (primarily) inductive plasma sources. These models will be provided to those groups modeling plasma transport within the overall modeling program and, through Sematech, to member companies or vendors. The project is 2–3 years long, and continuation through the end of 1995 appears likely.

The principle issues being addressed in this project are: (1) the self-consistent calculation of inductive fields (due to changing currents) and capacitive fields (due to applied potentials) and (2) the effect of plasma sheaths on the electrostatic fields. A computationally efficient model that runs in about 12 min on a work station or high-end PC was developed. Predicted plasma source impedances agreed well with this model.

Future plans include reductions in execution time, reduced memory requirements, inclusion of coil dissipation, and development of a time domain model.

ORNL-DWG 94M-3605R FED

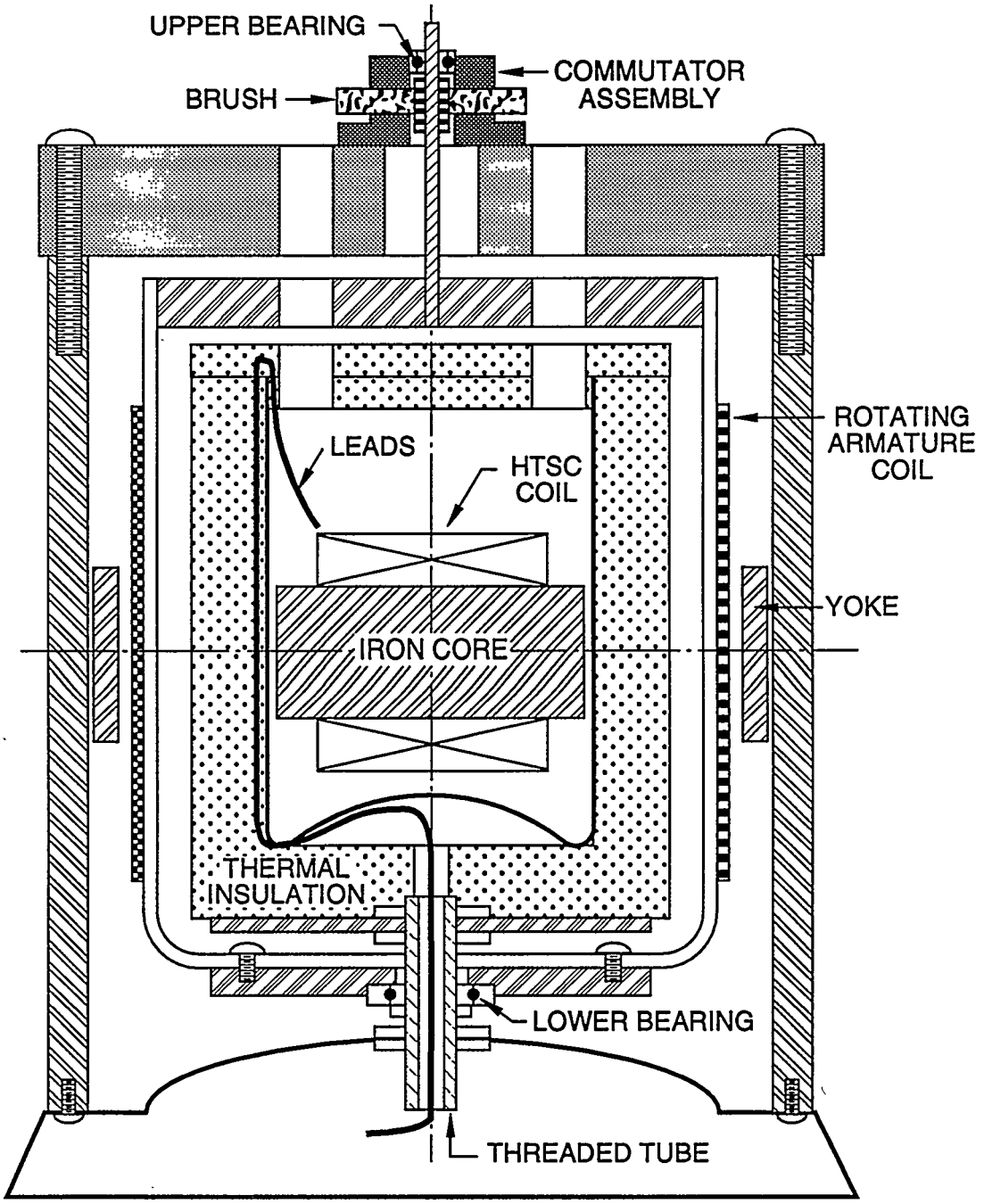

Fig. 9.4. HTS magnet.

9.4.2 Computer-Aided Design of Plasma Reactors

FED has been involved in a CRADA with LLNL, IBM, and AT&T (Bell Laboratories) to develop plasma models that can improve and shorten the VLSI circuits development cycle. ORNL's main role in this effort will be helicon wave propagation and absorption for a 2-D plasma equilibrium in cylindrical coordinates.

The model developed for this project has been checked against published work and appears to be in satisfactory agreement. Analysis of the characteristics of the helicons has shown that they have a relatively large phase velocity, several times the electron thermal velocity, and at the same time, a small parallel electric field because of the high mobility of the electrons along field lines. This makes it unlikely that Landau damping alone can account for the power deposition.

9.4.3 Modeling of Plasma-Based Materials-Processing LDRD

First-principles modeling of plasma-based materials-processing techniques (such as laser ablation for thin-film deposition and rf-ion and ECR sources for plasma etching and deposition) has been identified as a scientific area in which advances could significantly improve U.S. competitiveness. A collaborative effort in this area was initiated in September 1992 between FED, the Solid State Division, and the Engineering Physics and Mathematics Division. It is aimed at providing plasma production and transport modules in at least two space dimensions and time for massively parallel computers in order to carry out first-principles modeling of these plasma-based materials-processing techniques.

Thin-film deposition by laser ablation consists of shining a laser on a material target to produce a neutral vapor/plasma plume, which is then transported toward and deposited on a substrate of compatible material. Physics and computational modules have been developed to describe the various stages of this process. The 2-D version of the laser-material interaction code Laser8, developed by Geist, Wood, and colleagues at ORNL, has been made operational. It has been successfully benchmarked with experimental observations of flake nucleation and growth during laser annealing of silicon. The 1-D version of Laser8 has been extended to handle not only the melting of the silicon material by the laser (solid-to-liquid transition) but also its vaporization (liquid-to-vapor transition). Output from Laser8 1-D can now be used to provide input-density and temperature profiles to 1-D and 2-D gas-dynamic plasma-plume transport modules. These transport modules include atomic physics components for plasma ionization and laser absorption as well. A separate chemical kinetics module has been developed for plasma breakdown. Several physics results that are in qualitative agreement with experimental observations have been obtained with these tools. The Clausius-Clapeyron vapor pressure model implemented in Laser8 1-D has resulted in a lower energy density threshold for vaporization. The effects of a time-varying source of material on plume expansion velocity have been studied with the 1-D gas-dynamic module, and higher expansion velocities have been achieved than for other models. For plume propagation in a background gas, 1-D and 2-D transport module results show that the background gas is snowplowed by and mixed with the leading edge of the plume. This increase in pressure at the front results in a pressure gradient acting on the main body of the rarefying plume, tending to slow it down and in some cases even resulting in material going backward. A novel PIC hydrodynamic plume transport model has also been applied to the interaction of plume and background gases in two dimensions. Except for increased mixing of plume and background at the leading edge, the features of the interaction are similar to those obtained from the 1-D and 2-D gas-dynamics modules. Expansion and transport of plasma blobs in vacuum from point of formation to the substrate, including reflections therefrom, have also been modeled using the 2-D particle hydrodynamic model.

Rf sources for etching and deposition employ rf antennas on top of or around a cylindrical bucket to create a plasma that, guided by a suitable magnetic field, is transported toward an rf-biased substrate. An rf Helmholtz solver in quasi-3-D geometry (r, z, uncoupled mode expansion in q), has been specifically developed for low-density, weak–magnetic-field ECR and rf-ion plasma-processing discharges. A potential (E_q, B_q) formulation has been introduced. It is

preferable to one in terms of the three components of the electric field E, which suffers from the presence of singularities introduced by the $\nabla \times \nabla \times$ operator when all three components of the antenna current come into play. This potential formulation also alleviates the uncertainties in the boundary conditions associated with the z-component of the electric field. A final breakthrough refinement, the introduction of a staggered-space mesh, has been incorporated into the 3-D rf Helmholtz solver. The staggered grid over which current and field components are alternately evaluated allows conservation of the appropriate fluxes to machine accuracy. The rf Helmholtz solver has been successfully applied to calculate the cold-plasma response to 3-D antenna configurations, as well as the power deposition in various rf-ion and helicon reactor configurations. Another aspect of the project has focused on following plasma particles as they interact with antenna fields, in order to assess the reliability of the fluid dielectric response used in other calculations. The orbit integrator uses a syncopated leap-frog algorithm in cylindrical coordinates, which maintains second-order accuracy and minimizes computational complexity. Plasma source terms are accumulated directly in the frequency and azimuthal mode domains. Currently, the EMFs are specified by some external procedure. The source terms from particle trajectories can be compared to those from the prescribed fields as a validation for the fluid approach. This comparison will test whether the prescribed EMF is "orbit consistent," in the sense that the source terms implied by a given field agree with the source terms calculated from the orbits.

Progress has also been made in the massive parallelization of the various physics and computational modules. Parallel versions of the Laser8 1-D and 2-D laser-material interaction module have been developed for the Intel Paragons and have successfully been exercised on the XPS/5 with marked improvements in real-time efficiency. Moreover, a parallel version of the 2-D gas-dynamics transport module has been constructed using ORNL's own PVM and implemented on the Paragon XPS/5 to take advantage of the available memory to perform higher-resolution calculations than possible on workstations. In addition, a parallel version of the 3-D rf Helmholtz wave equation solver, which also uses PVM to maximize its portability, has been operational for some time on workstation clusters.

Publications resulting from this effort are listed as Refs. 7 through 14.

9.5 PLASMA CONFINEMENT APPLICATIONS

L. A. Berry, S. M. Gorbatkin, and R. Rhoades

9.5.1 Advanced Metallization

A critical step in the fabrication of integrated circuits is the deposition of metal interconnects between the various circuit elements that have been formed in earlier process steps, particularly columns of metal 2 to 3 times higher than the characteristic dimension of the circuit (about 1 to 1.5 μm high and 0.5 μm in diameter for current state of the art, headed toward a reduction in size by a factor of 2 to 5 in 5–10 years). Present commercial technologies cannot deposit such features with the process temperature, aspect ratio (height to diameter), or materials capability needed for future devices. A CRADA was negotiated with IBM to develop a commercial tool capable of depositing metal (either copper or aluminum) at temperatures below 300°C into features with sizes approaching 0.2 μm on 200-mm wafers. The capability of depositing alloys of controllable composition is also an important characteristic.

9.5.2 Analysis and Diagnostics for Plasma Synthesis

A CRADA was established to collaborate with Energy Conversion Devices on a project to improve the efficiency of solar cells by modifying the plasma processing method currently used.

9.6 FUSION WASTE TRANSMUTATION

Y-K. M. Peng

A project is under way to examine the viability of using a small, low–aspect-ratio ST fusion device producing about 1 to 30 MW of fusion power to drive a subcritical actinide fission core for eliminating long-life fission wastes while producing net electricity. Improvements to the ST version of SUPERCODE were completed to account for transmutation power blankets driven by a low–aspect-ratio, low-Q fusion neutron source. Initial economic trade-off studies have been carried out for the waste transmutation power plant. The initial results indicate that COE for the waste transmutation power plant would be about 15% below that for a pure fusion low–aspect-ratio tokamak power plant and about 15% above the best experienced pressurized-water fission power plant.

REFERENCES

1. C. A. Foster, P. W. Fisher, W. D. Nelson, and D. E. Schechter, "A Centrifuge CO_2 Pellet Cleaning System," in *Proceedings of the Second International Congress on Environmentally Conscious Design and Manufacturing, August 29–September 1, 1993, Arlington, Virginia.*

2. C. A. Foster and P. W. Fisher, "Advanced Turbine/CO_2 Pellet Accelerator," presented at the DoD/Industry Advanced Coatings Removal Meeting, New Orleans, Louisiana, May 17–19, 1994.

3. T. L. White et al., "Removal of Contaminated Concrete Surfaces by Microwave Heating—Phase I Results," *Proceedings of the 18th American Nuclear Society Symposium on Waste Management, Tucson, Arizona*, March 1992.

4. C. C. Tsai, V. B. Campbell, A. L. Glover, J. M. Googin, H. H. Haselton, W. D. Nelson, D. E. Schechter, and L. M. Thompson, *Plasma Surface Cleaning in a Microwave Plasma Source*, ORNL/TM-12495, Oak Ridge Nat. Lab., March 1994.

5. C. C. Tsai, A. L. Glover, W. D. Nelson, D. E. Schechter, and L. M. Thompson, "A Microwave Plasma Cleaning Apparatus," presented at the Conference on Aerospace Environmental Technology, August 10–11, 1994, to be published in the conference proceedings.

6. J. M. Williams, C. C. Tsai, W. L. Stirling, and J. H. Whealton, "Potential Spin-Off Applications of Fusion Neutral Beam Facilities for Advanced Material Processing," *J. Vac. Sci. Technol. B* **12**, 991 (1994).

7. J. W. Cobb and J.-N. Leboeuf, "A Syncopated Leap-Frog Algorithm for Orbit Consistent Plasma Simulation of Materials Processing Reactors," Paper 3B5, *Proceedings of the 15th International Conference on the Numerical Simulation of Plasmas, King of Prussia, Penn., USA, September 7–9, 1994.*

8. C. L. Liu, J.-N. Leboeuf, R. F. Wood, D. B. Geohegan, J. M. Donato, K. R. Chen, and A. A. Puretzky, "Computational Modeling of Physical Processes During Laser Ablation," in *Proceedings of the Engineering Foundation Conference on Materials Processing and Advanced Application of Lasers, Palm Coast, Florida, May 1–6, 1994*, to be published.

9. J.-N. Leboeuf, D. B. Geohegan, C. L. Liu, R. F. Wood, J. B. Drake, and D. W. Walker, "Modeling of Plasma Dynamics in Laser Ablation Processes," *Bull. Am. Phys. Soc.* **38**, 1900 (1993).

10. J.-N. Leboeuf, C. L. Liu, D. B. Geohegan, and R. F. Wood, "Modeling of Laser Ablation of Semiconductor Materials for Thin Film Growth," *Bull. Am. Phys. Soc.* **39**, 497 (1994).

11. C. L. Liu, J.-N. Leboeuf, R. F. Wood, B. B. Geohegan, J. M. Donato, K. R. Chen, and A. A. Puretzky, "Computational Modeling of Physical Processes During Laser Ablation," in *Proceedings of the Engineering Foundation Conference on Materials Processing and Advanced Application of Lasers, Palm Coast, Florida, May 1–6, 1994.*

12. J. M. Donato, J.-N. Leboeuf, C. L. Liu, and R. F. Wood, "Numerical Modeling of Plasma Dynamics in Laser Ablation Processes," Paper CP11:7, p. 23, *Preliminary Program, 1994 SIAM Annual Meeting, San Diego, California, July 25–29, 1994.*

13. K. R. Chen, C. L. Liu, J. M. Donato, D. B. Geohegan, J.-N. Leboeuf, A. A. Puretzky, and R. F. Wood, "Dynamical Modeling of Laser-Ablated Materials," Gordon Research Conference on Laser Ablation wi

th Surfaces, Colby Sawyer College, New London, New Hampshire, USA, August 15–19, 1994.

14. C. L. Liu, J.-N. Leboeuf, R. F. Wood, D. B. Geohegan, J. M. Donato, K. R. Chen, and A. A. Puretzky, "Numerical Modeling of Thermal, Hydrodynamic, and Electronic Processes During Laser Annealing and Ablation," Gordon Research Conference on Laser Ablation with Surfaces, Colby Sawyer College, New London, New Hampshire, USA, August 15–19, 1994.

10

MANAGEMENT SERVICES, ES&H ACTIVITIES, AND QA

Management Services
F. E. Gethers[1*]

S. B. Armstrong[1]
B. J. Beem[1]
S. A. Boatman[2]
M. E. Disney[1]
M. G. Eckerd[2]
K. A. Ensey[1]
L. J. Hickey[3]
L. W. Foley[2]
C. H. Johnson[2]
D. Y. Johnson[2]
J. D. Lentz[1]
J. C. Neeley[2]
J. C. Parrott[2]
S. J. Ping[1]
W. J. Redmond[1*]
J. O. Richardson[1]
D. G. Sharp[2]
L. K. Shaw[2]
B. J. Smith[2]
C. C. Southmayd[2]
L. W. Xiques[2]

ES&H Activities
F. E. Gethers[1*]

D. A. Rasmussen,[4*]
Laser Safety Officer

W. J. Redmond,[1*]
Environmental Protection Officer

Quality Assurance
E. B. Foster[5]

*Dual capacity.
1. Management Services Section.
2. Information Management Services.
3. Finance and Business Management.
4. Plasma Technology Section.
5. Office of Quality Programs and Inspection.

10. MANAGEMENT SERVICES, ES&H ACTIVITIES, AND QA

Summary of Activities

Broad technical and administrative support for programmatic research and development activities of the Fusion Energy Division is provided by the Management Services Section (MSS) and by the division's environmental, safety, and health (ES&H) and quality assurance (QA) programs.

MSS provides support in the following areas:

- general personnel administration, material and service procurement, subcontracting, and coordination of national and international agreements;
- nonprogrammatic engineering services for support systems and equipment; identification, planning, and coordination of General Plant Project and facility improvements; coordination of maintenance and production shop work; labor relations; and telecommunications;
- financial management;
- library services and resources; and
- publications services.

Support is provided through effective communication with division programmatic staff and through the coordination of resources from disciplines outside the division.

The division's ES&H activities include a formal safety program, environmental protection services, and self-assessment activities. The safety resource team established in 1989 continued to identify and resolve safety-related issues. A database is in place to identify and track ES&H deficiencies, which are being corrected using a graded approach.

The QA activity in the division emphasizes development and documentation of a QA program that conforms to national standards, review and approval of engineering documents, supplier surveillance, identification and documentation of nonconforming items, audits, and QA assessments and plans.

10.1 MANAGEMENT SERVICES

10.1.1 General Administration Services

10.1.1.1 Personnel

In response to declining budgets, staff levels in FED dropped from 110 employees on December 31, 1991, to 104 employees on December 31, 1992; the staffing level increased to 113

employees by December 31, 1993, but was then reduced to 92 by December 31, 1994. The composition of the division's scientific and technical staff over the past 5 years is shown in Fig. 10.1.

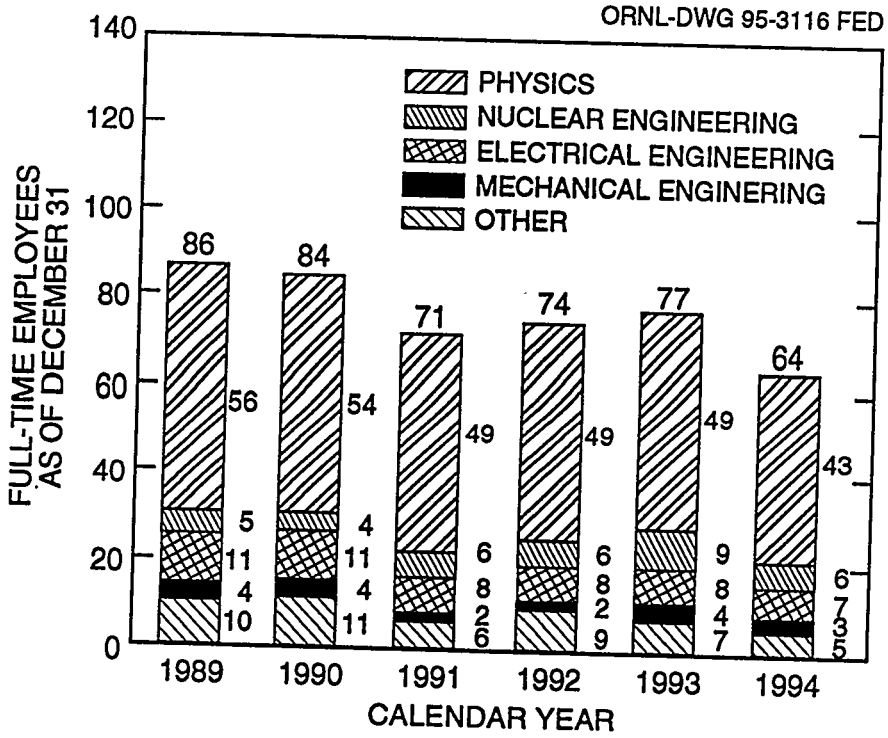

Fig. 10.1. Fusion Energy Division professional staff by discipline.

The University and College Cooperative Program sponsored one Alabama Agricultural and Mechanical University electrical engineering/physics student in 1994. University subcontracts brought four students to the division in 1992, two in 1993, and three in 1994; seven technical students participated in university programs in 1992, with four in 1993 and three in 1994. There were five postdoctoral participants in 1992, nine in 1993, and seven in 1994.

The division was host to 6 international scientific guests and 20 subcontractors in 1992, 13 international scientific guests and 19 subcontractors in 1993, and 8 international scientific guests and 14 subcontractors in 1994.

Division personnel served on long-term assignments to other laboratories; in 1992 three staff members were assigned to the Tore Supra tokamak at the Centre d'Etudes Nucleaires in Cadarache, France. In 1993, three were assigned to Tore Supra and one to the ITER project in Garching, Germany. In 1994, two were assigned to Tore Supra; one to JET in Abingdon, England, as part of the JET Joint Undertaking; and two to the ITER project in Garching, Germany. Long-term domestic assignments to General Atomics in San Diego, California, involved two staff members for 1992–1994. Three division employees were on relocation assignments to PPPL for 1992–1994.

10.1.1.2 Training and development

Since 1989 FED has maintained a training program that ensures that training requirements are fulfilled, that training desired by individual employees and their supervisors is obtained, and

that electronic and auditable hard-copy records are kept. The required training includes that mandated by the DOE Oak Ridge Operations Office, by Martin Marietta Energy Systems management, and by FED. The FED-mandated training consists primarily of a 1-h safety orientation and test for everyone who will be working unescorted in Building 9201-2 and specific safety orientation for those who will enter various hazardous areas unescorted.

At the end of 1994 there were more than 4900 records in the FED training database, where a record is one person completing one course or module. Over the past 3 years an average of 700 records have been added per year, an appreciable burden for a division of ~100 people. As far as practicable, we have attempted to contain the costs by having trainers come to FED when a sizable group of trainees is involved, by using required reading rather than lectures, by using proficiency tests, and by avoiding nonrelevant training.

10.1.1.3 Procurement

During the 1992–1994 period, the division's procurement group processed requisitions with a total value of about $5 million. This group actively monitors 150 to 200 open purchase orders.

In 1993, procurement converted to a computerized system for monitoring purchase orders. The Materials Management System links the three Oak Ridge plants as well as Purchasing, Receiving, Shipping, Stores, and Accounts Payable. In 1994, this group began receiving all information pertaining to requisitions electronically, such as receiving reports, notifications, and modifications.

10.1.1.4 International agreement and collaboration

The division participated in several personnel exchanges and collaborations during the 1992–1994 period. The Management Services Section (MSS) played a key role in organizing these activities, with responsibility for coordinating administrative, legal, and protocol matters for outbound Fusion Program representatives and inbound international guests.

In this capacity, MSS staff members worked with the ORNL Office of Guest and User Interactions, the ORNL and Y-12 Plant security organizations, the Office of General Counsel and the Office of the Comptroller and Treasurer of Martin Marietta Energy Systems, and the Washington and Oak Ridge offices of DOE, as well as other service and support organizations. Responsibilities included ensuring adherence to general laboratory and company policies and to federal laws and procedures, monitoring the processing of paperwork to ensure timeliness and accuracy, obtaining the necessary approvals, and generally supporting the satisfactory implementation of exchanges, cooperative programs, and collaborations.

10.1.2 Engineering Services

During the 1992–1994 period, the Engineering Services Group continued its tasks of managing building maintenance, providing engineering assistance in facility upgrades and improvements, providing administrative oversight in the coordination of Lock & Keys, Columbus Initiatives, Alerts, divisional meetings, dosimeter exchanges, and oversight of the division's environmental, safety, and health (ES&H) database.

In 1994 the final phase (phase III) of the Upgrade 480 V Electrical Systems General Plant Project in 9201-2 was nearly completed, with only minor work on the overhead sprinkler system remaining. Completion of this project concludes the replacement of the antiquated transformers and switch gear in the southeast transformer vault, the largest of the four building vaults.

Efforts to achieve compliance with National Pollutant Discharge Elimination System (NPDES) requirements continued at an accelerated pace in light of the anticipated revision of the plant's NPDES permit in late 1994. Several drain lines that were unnecessarily loading the Oak Ridge city sewer system were rerouted to the creek, and all lines going to the creek were reevaluated for chlorine concentrations. Tablet dechlorination units were installed on drain lines discharging into outfalls above the 0.5 mg/L limit, or, in some cases, such lines were eliminated altogether through the use of demineralized water or by source elimination. Outfall 63 was of significant concern because its source initially could not be located, but through the efforts of Environmental Restoration and Utilities personnel, the origin of the flow was located and eliminated. Other building outfalls have consistently maintained acceptable chlorine levels throughout the last few months of FY 1994, making them among the first to reduce chlorine discharge levels locally to acceptable limits.

Another NPDES compliance issue has been mercury in the creek as a result of the mercury contamination in the basement of 9201-2. Engineering Services coordinated outages and building support for the subcontractor replacement of a number of mercury-contaminated drain lines beneath the building, which was completed in mid-1994. The Interim Mercury Treatment Unit on the first floor of the building was completed toward the end of FY 1994. The treatment unit was a cooperative effort between Environmental Restoration, Y-12 Engineering, Waste Management, Facilities Management Organization personnel, and FED Engineering Services. The purpose of the unit is to remove mercury from the basement sump water before it is discharged to the creek. The unit itself was built as a prototype for gathering data and temporarily meeting the revised NPDES requirements. A permanent unit in the building is slated for 1995.

An ever-increasing amount of time has been spent in attempts to resolve outstanding ES&H deficiencies resulting from ORNL and Y-12 Plant Occupational Safety and Health Administration, Fire Protection, Industrial Safety, DOE, and other inspections. As the more easily resolved deficiencies have been closed, the costs and effort involved in closing out remaining deficiencies have gone up.

Several occurrences in the division have resulted in a number of ongoing Engineering Services efforts. A halon discharge in the Room 201 computer center in April 1992 and another in January 1994 have focused efforts on the removal of the halon and the elimination of the need for the systems throughout the building. The discovery of contamination in 1993 in the west track on the first floor of 9201-2 resulted in suggested remediation efforts, but resolution has been hampered by housekeeping problems in that area of the building. The discovery of another contamination problem with a two-person personnel lift in 1993 resulted in efforts to decontaminate the equipment, and to give the equipment to someone who could use it, but little progress has been made in either of these areas. Incidents throughout the Y-12 Plant involving procedural violations during supplied-air operations resulted in the administrative tagging-out of all breathing-air stations in the building, pending a thorough review of the distribution and use of the instrument air lines throughout the building. At present, bottled breathing air is being purchased for jobs requiring supplied air.

Energy conservation efforts have become a primary Engineering Services issue. Characterization of energy usage is under way in an effort to charge for actual energy use, rather than to approximate costs according to area size. In addition to characterization, a number of conservation measures are being evaluated. Some efforts have led to evaluation of various types of proposals, which have been submitted to the Y-12 Plant's In-House Energy Management team to determine the most cost-effective way to operate the building's chillers. At present the chillers require full-time operation of the demineralized water system, leading to a much higher-than-normal air-conditioning cost. Evaluation of other cost-saving measures will proceed as major inefficiencies are evaluated.

A variety of facility improvements have been implemented or are currently in progress. A ventilation booster has been installed in the second-floor ventilation system leading to the low northwest roof, providing positive elimination of gases and odors from experimental work. Evaluation of a ventilation fan in the basement is under way to determine if mercury levels in the basement air can be reduced. Parts have been ordered, and the request has been issued to install a conductivity meter in the demineralized water line in the building so that water quality can be monitored continuously, rather than having to request water samples to be analyzed. Requests for facility improvements by all building personnel are being evaluated and accommodated by Engineering Services based on the cost, feasibility, and effort involved and the potential benefits.

Support continues throughout the division to assist with cost-saving measures, improvements, safety concerns, housekeeping problems, and compliance issues. Primary emphasis is being placed on serving the division as a customer and assisting wherever possible to further the interests of the division.

10.1.3 Financial Services

The Finance Office is a functional part of MSS and provides financial management support for administrative, engineering, and research personnel in areas including budget preparation, cost scheduling, and variance analysis. The office also provides meaningful and appropriate accounting and cost control. Interaction with division management is an essential part of administering the budget, accounting policies, and procedures. Figure 10.2 and Table 10.1 show the funding trends for the ORNL Fusion Program.

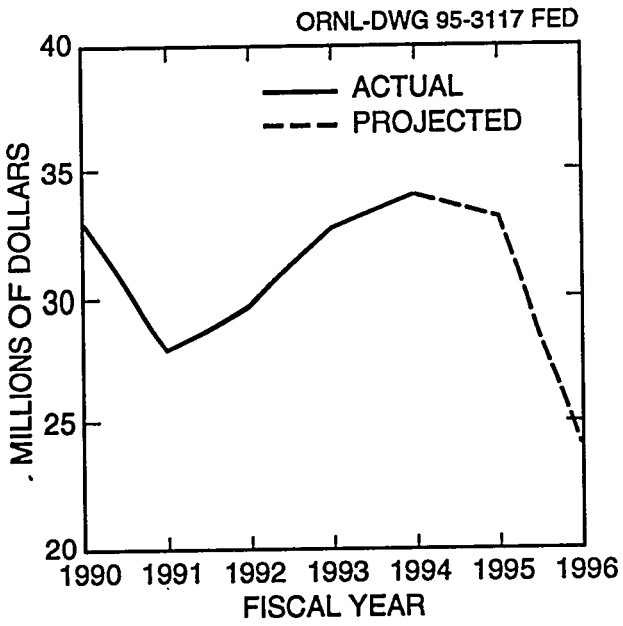

Fig. 10.2. Fusion Program expense funding (budget outlay).

Table 10.1. Fusion Program expense funding (in thousands of dollars)—budget outlay

Activity	FY 1990 Actual cost	FY 1991 Actual cost	FY 1992 Actual cost	FY 1993 Actual cost	FY 1994 Actual cost	FY 1995 Funding as of December 1994	FY 1996 Budget submission
Applied plasma physics							
Toroidal theory	$2,172	$2,152	$2,117	$2,038	$1,832	$1,868	$1,983
Alternate concept theory	0	0	144	141	141	130	138
Atomic physics theory	304	96	132	78	83	85	87
Plasma experiments	280	321	461	514	510	630	463
Diagnostics	611	487	669	398	433	415	425
Atomic physics	703	642	754	799	699	755	723
User service centers	167	401	287	290	244	350	360
Technical program support	0	101	28	0	0	0	0
	$4,237	$4,200	$4,592	$4,258	$3.942	$4,233	$4,179
Confinement systems							
Doublet III	$914	$1,106	$2,155	$2,319	$2,359	$3,300	$3,087
Confinement, other	2,575	1,966	3,311	2,906	2,422	2,481	2,622
PBX	0	0	1,348	1,373	269	0	0
Advanced toroidal research	11,436	7,605	878	3,053	4,557	140	0
ATF, other	0	0	0	0	0	2,400	2,470
TFTR physics program	0	0	1,431	1,079	1,237	800	0
TFTR heating	0	82	123	113	124	150	150
Tokamak plasma experiment	2,643	2,272	1,843	1,771	2,014	2,435	6,950
	$17,568	$13,031	$11,089	$12.614	$12,982	$11,706	$15,279
Development and technology							
High-field magnets	$24	$10	$90	$101	$119	$0	$0
ICR/LHR heating systems	2,086	2,018	1,784	498	449	125	360
ECR heating systems	133	49	0	0	0	0	0
Fueling systems	1,461	1,834	778	131	110	50	0
Blanket and shield technology	0	0	0	18	80	125	90
Nuclear analysis	85	65	56	0	0	0	0
Environmental analysis	38	40	52	23	21	0	0
Neutron source	0	0	69	102	132	1,350	1,700
Neutron-interactive materials	3,365	3,465	1,705	2,006	2,219	3,300	3,200
ITER-Magnet case materials	0	0	57	108	39	0	90
ITER-ECR heating systems	0	0	0	0	27	30	0
ITER-Plasma fueling development	0	0	470	970	1,148	700	1,800
ITER-Radiation-resistant carbon	0	0	275	294	298	225	300
ITER-ICH development	0	0	0	1,207	1,251	1,625	2,500
ITER-Neutron interactive materials	0	0	1,549	1,447	1,183	1,200	1,350
ITER-Blankets	0	0	0	117	65	60	85
ITER-Assembly and maintenance	0	0	201	571	570	800	945
ITER-Containment structures	0	0	80	335	651	970	925
ITER-Diagnostics	0	0	0	0	195	280	600
ITER-Design engineering	2,237	2,329	2,027	1,706	1,073	950	1,150
ITER-Physics design	0	0	349	322	230	230	238
ITER-Joint central team	0	0	0	0	945	1,725	1,720
ITER-Project management	0	0	482	818	1,000	300	0
Fusion system studies	221	201	90	235	231	0	0
ORR	0	0	290	14	0	0	0
U.S. Japan material collaboration	540	1,211	2,286	2,122	2,181	2,370	390
	$10,190	$11,222	$12,690	$13,145	$14,217	$16,415	$17,443
Total ORNL funding	$31,995	$28,453	$28,371	$30,017	$31,141	$32,354	$36,901

10.1.4 Library Services

The Fusion Energy Library maintains a specialized collection in plasma physics and fusion technology and is a branch of the Information Management Services Library System that serves Energy Systems. Library staff members select materials for acquisition, provide reference assistance and on-line literature searches, circulate library materials, and retrieve information in support of research activities.

Electronic access to information has increased during the past several years. FED Library patrons now have access to a CD-ROM network of various scientific and technical directories and indexes, including some with full-text retrieval capabilities. One workstation in the FED Library is dedicated to this CD-ROM network. The other workstation allows patrons to search the library system's on-line catalog, OASIS, the Internet, and the on-line catalog at the University of Tennessee in Knoxville.

A usage survey of the library's journal subscriptions was conducted to determine which journals are of greatest interest to library users. User input was also requested for acquiring new book titles, and a customer satisfaction survey was performed.

10.1.5 Publications Services

Publications and graphics services are provided to FED by the Engineering Technology/Fusion Energy Divisions Publications Office (ET/FE DPO), which serves both FED and the Engineering Technology Division (ETD). The publications office, which is part of the Information Management Services organization, provides technical editing and writing, computer and conventional graphics, composition and electronic publishing, and reproduction services. It also serves as liaison with the Laboratory Records Department for clearance of all documents prepared by FED staff.

The broad range of services available reflects the capabilities provided by the diverse skills of the 11 staff members, a wide variety of computer hardware and software, and two large copiers. The ET/FE DPO is committed to providing high-quality, cost-effective publications and graphics support to its customers.

10.2 ES&H ACTIVITIES

The division has continued to direct significant efforts toward the improvement of its ES&H programs. As part of these efforts, FED and ETD have continued the activities of mutual self-assessment teams. The primary objectives of these teams are to survey both divisions' facilities for safety hazards, document the findings, and recommend corrective actions. By the end of 1994, the two divisions had completed over a dozen self-assessments.

In response to constant changes in environmental protection regulations and DOE orders, the division continued to implement new compliance initiatives in areas including facilities, hazardous waste, transformer inventories, mercury vapor, and surveys of noise levels and air and water quality. Continued efforts were directed toward reducing the environmental concerns in the facilities, verifying that policies and procedures were in place, and keeping employees well informed about the issues. The division's intent is to minimize hazardous waste, to control effluents in and out of the facilities, and to continue to protect and preserve the environment.

A total of 2190 ES&H deficiencies have been identified and entered in the FED database. A graded approach is being used to address the 217 deficiencies that remain open.

The FED safety resource team continued to identify and resolve safety-related issues. This team is responsible for bimonthly inspections, documentation of safety and health problems, and recommendations to correct or prevent occurrences.

The division continued its promotion of safety awareness through its monthly safety meetings, facility assessments, bulletins, and basic two-way communication. The focus of the program, encouraging employees to maintain a safer attitude on and off the job, will continue to drive FED safety policies, rules, and regulations.

10.3 QUALITY ASSURANCE

The division has employed the services of one part-time QA Specialist. Noteworthy efforts include revision of the FED QA plan, which is now entitled the *FED Management Plan*; inclusion on the Energy Systems Action Management System of QA audit findings and correctives actions (originating from January 1992 to the present); dissemination of quality information and recommendations to FED personnel in oral as well as written media; adherence to the FED audit schedule; and maintenance of controlled distribution of the FED QA manual.

Appendix 1

Publications and Presentations

1992 BOOKS AND JOURNAL ARTICLES 273
1992 PRESENTATIONS 281
1992 REPORTS 294

1993 BOOKS AND JOURNAL ARTICLES 295
1993 PRESENTATIONS 301
1993 REPORTS 314
1993 CONGRESSIONAL TESTIMONY 315

1994 BOOKS AND JOURNAL ARTICLES 316
1994 PRESENTATIONS 322
1994 REPORTS 334
1994 CONGRESSIONAL TESTIMONY 335

1992 BOOKS AND JOURNAL ARTICLES

S. C. Aceto, J. D. Bell, K. A. Connor, J. C. Glowienka, R. C. Isler, M. Murakami, J. G. Schwelberger, T. Uckan, and J. J. Zielinski, "Heavy Ion Beam Probe Measurements on ATF," *Bull. Am. Phys. Soc.* 37(6), 1547 (1992)

C. Alejaldre and B. A. Carreras, ed., *Transport and Confinement in Toroidal Devices 2nd Workshop on Magnetic Confinement Fusion*, Adam Hilger Series on Plasma Physics, IOP Publishing, 1992

S. E. Attenberger, K. C. Shaing, S. P. Hirshman, and W. A. Houlberg, "Poloidal Variation of Tokamak Plasma Density," *Bull. Am. Phys. Soc.* 37(6), 1364 (1992)

F. W. Baity, D. B. Batchelor, K. C. Bills, C. H. Fogelman, E. F. Jaeger, J. L. Ping, B. W. Riemer, P. M. Ryan, D. C. Stallings, D. J. Taylor, and J. J. Yugo, "Design of Long-Pulse Fast-Wave Current Drive Antennas for DIII-D," *Bull. Am. Phys. Soc.* 37(6), 1494 (1992)

G. W. Barnes, R. Persing, G. Schmidt, M. J. Gouge, L. R. Baylor, M. J. Cole, S. K. Combs, D. Fehling, P. W. Fisher, C. Foust, S. L. Milora, and A. L. Qualls, "The TFTR Tritium Pellet Injection Facility Mechanical Design," *Fusion Technol.* 21(3, Pt. 2), 1662–64 (1992)

L. R. Baylor, G. L. Schmidt, W. A. Houlberg, S. L. Milora, C. Gowers, W. Bailey, M. Gadeberg, P. Kupschus, J. A. Tagle, D. K. Owens, D. K. Mansfield, and H. Park, "Pellet Fueling Deposition Measurements on JET and TFTR," *Nucl. Fusion* 32(12), 2177–87 (1992)

T. S. Bigelow, G. R. Hanson, J. B. Wilgen, I. Collazo, E. Mazzucato, M. McCarthy, and S. Raftopoulos, "Design of a Reflectometer System for Measurement of the Plasma Edge Density Profile on TFTR," *Bull. Am. Phys. Soc.* 37(6), 1489–90 (1992)

J. Botero, ed., *International Bulletin on Atomic and Molecular Data for Fusion*, Vols. 42–45, 1992

J. D. Callen, B. A. Carreras, and R. D. Stambaugh, "Stability and Transport Processes in Tokamak Plasmas," *Phys. Today* 45, 34 (1992)

B. A. Carreras, "Diagnostic Needs for Fluctuation and Transport Studies," *Rev. Sci. Instrum.* 63, 4589–94 (1992)

B. A. Carreras, "Problem with the Concept of Plasma Equilibrium in Tokamaks," *Revista de la Real Academia de Ciencias Fisicas, Exactas y Naturales*

B. A. Carreras, "Transport Mechanisms Acting in Toroidal Devices: A Theoretician's View," *Plasma Phys. Controlled Fusion* 34, 1285 (1992)

B. A. Carreras, J.-N. Leboeuf, D. K. Lee, J. A. Holmes, V. E. Lynch, "Effect of the Equilibrium Magnetic Field on Plasma Edge Fluctuations," p. 137 in *Research Trends in Physics: Nonlinear and Relativistic Effects in Plasmas*, AIP Conference Proceedings Series, AIP, New York, 1992

B. A. Carreras, V. E. Lynch, and L. Garcia, "Resistive Pressure-Gradient-Driven Turbulence with Self-Consistent Flow Profile Evolution," *Bull. Am. Phys. Soc.* 37(6), 1477 (1992)

B. A. Carreras, K. Sidikman, P. H. Diamond, P. W. Terry, and L. Garcia, "Theory of Shear Flow Effects on Long-Wavelength Drift Wave Turbulence," *Phys. Fluids B* 4, 3115–31 (1992)

M. D. Carter, D. B. Batchelor, and E. F. Jaeger, "Electromotive Excitation of a Plasma Sheath," *Phys. Fluids B* 4, 1081–91 (1992)

M. D. Carter, G. R. Haste, F. W. Baity, and D. J. Hoffman, "Modeling of a Folded Waveguide," *Bull. Am. Phys. Soc.* 37(6), 1604 (1992)

J. B. O. Caughman, D. J. Hoffman, and R. H. Goulding, "Arc Detection and Protection in High-Power Antenna Systems," *Bull. Am. Phys. Soc.* 37(6), 1495 (1992)

L. A. Charlton, B. A. Carreras, and P. H. Diamond, "Parallel Flow Gradient Driven Instability," *Bull. Am. Phys. Soc.* 37(6), 1476 (1992)

P. J. Christenson, N. Dominguez, and K. C. Shaing, "Tokamak Equilibrium with Steady Poloidal Flows," *Bull. Am. Phys. Soc.* 37(6), 1596 (1992)

R. J. Colchin, S. C. Aceto, A. C. England, R. C. Isler, M. Murakami, D. A. Rasmussen, T. Uckan, J. B. Wilgen, and J. J. Zielinski, "Plasma Profile Modifications in ATF Using Magnetic Field Perturbations," *Bull. Am. Phys. Soc.* 37(6), 1546 (1992)

R. J. Colchin and AEA Fusion, "Results from the START Low Aspect Ratio Tokamak," *Bull. Am. Phys. Soc.* 37(6), 1354 (1992)

K. A. Connor, S. C. Aceto, J. G. Schwelberger, and J. J. Zielinski, "Plans for Upgrades to the Heavy Ion Beam Probe Diagnostic on ATF," *Bull. Am. Phys. Soc.* 37(6), 1547 (1992)

W. A. Cooper, S. P. Hirshman, S. Merazzi, and R. Gruber, "3D Magnetohydrodynamic Equilibria with Anisotropic Pressure," *Computer Phys. Communications* **72**, 1 (1992)

E. C. Crume, Jr., P. J. Christenson, and K. C. Shaing, "Ion Collisionality and L-H Transition in Tokamaks," *Bull. Am. Phys. Soc.* 37(6), 1364 (1992)

N. Dominguez, B. A. Carareras, and V. E. Lynch, "Dissipative Trapped Electron Modes in $\ell = 2$ Torsatrons," *Phys. Fluids B* **4**, 2894–2906 (1992)

N. Dominguez, C. L. Hedrick, J.-N. Leboeuf, and L. Garcia, "Dissipative Trapped Electron Mode Turbulence with Ion Landau Damping and FLR Effects," *Bull. Am. Phys. Soc.* 37(6), 1556 (1992)

R. A. Dory and J. H. Harris, "Wavelets Characterize Aperiodic Data," *Computers in Phys.* 6(2), 198 (1992)

R. A. Dory, J. H. Harris, and S. V. Kaye, "Wavelet Analysis of ELM Signals from PBX-M Tokamak," *Bull. Am. Phys. Soc.* 37(6), 1574 (1992)

L. Dresner, "Gorter-Mellink Pulsed-Source Problem in Cylindrical and Spherical Geometry," *Cryogenics* 32, 450–54 (1992)

J. Forster, C. C. Klepper, L. A. Berry, and S. M. Gorbatkin, "Doppler Shift Measurements of Ion Energy Distribution Widths in an Electron Cyclotron Resonance/Multipole Hybrid Reactor," *J. Vac. Sci. and Technol. A* 10(5), 3114–18 (1992)

J. Galambos, C. Baker, Y-K. M. Peng, D. Cohn, M. Chaniotakis, L. Bromberg, and S. Dean, "System Studies of Copper and Superconducting Coil Pilot Plants," *Fusion Technol.* 21(3, Pt. 2), 1759 (1992)

F. Y. Gang, J.-N. Leboeuf, and D. J. Sigmar, "Nonlinear Evolutions of Energetic Alpha Particle Driven Alfvén Wave Turbulence," *Bull. Am. Phys. Soc.* 37, 1435 (1992)

F. Y. Gang, D. J. Sigmar, J.-N. Leboeuf, "Saturation of Energetic Particle Driven Alfvén Wave Instability Through Velocity Space Diffusion," *Phys. Letts. A* **161**, 517 (1992)

W. L. Gardner, F. W. Baity, R. H. Goulding, D. J. Hoffman, D. A. Rasmussen, P. M. Ryan, D. E. Schechter, and D. J. Taylor, "Comparison of Candidate ICRF Faraday Shield Materials," *Bull. Am. Phys. Soc.* 37(6), 1495 (1992)

R. C. Goldfinger, D. B. Batchelor, C. K. Phillips, R. Budny, G. W. Hammett, J. C. Hosea, D. M. McCune, J. E. Stevens, J. R. Wilson, and the TFTR Team, "DT Simulation of ICRF Heated Supershots in TFTR using TRANSP," *Bull. Am. Phys. Soc.* 37(6), 1487 (1992)

M. J. Gouge, K. D. St. Onge, S. L. Milora, P. W. Fisher, and S. K. Combs, "Pellet Fueling System for ITER," *Fusion Eng. Des.* **19**, 53–72 (1992)

M. J. Gouge, L. R. Baylor, M. J. Cole, S. K. Combs, G. R. Dyer, D. T. Fehling, P. W. Fisher, C. R. Foust, R. A. Langley, S. L. Milora, A. L. Qualls, and J. B. Wilgen, "Tritium Pellet Injector for TFTR," *Fusion Technol.* 21(3, Pt. 2), 1665 (1992)

R. H. Goulding, D. B. Batchelor, D. J. Hoffman, E. F. Jaeger, P. M. Ryan, D. C. Stallings, V. Bhatnagar, G. Bosia, A. S. Kaye, and T. J. Wade, "Phased Operation of the JET A_2 Antenna Arrays," *Bull. Am. Phys. Soc.* 37(6), 1494 (1992)

M. J. Grapperhaus, W. A. Houlberg, and S. E. Attenberger, "Pellet Fueling Options for ITER," *Bull. Am. Phys. Soc.* 37(6), 1396 (1992)

D. C. Griffin, M. S. Pindzola, and N. R. Badnell, "The Contribution of Double-Excitation-Autoionization to the Electron-Impact Ionization of Li^+," *J. Phys. B* **25**, L605 (1992)

D. C. Griffin, M. S. Pindzola, and N. R. Badnell, "Electron-Impact Excitation of Ions," p. 303 in *Electronic and Atomic Collisions*, IOP, New York, 1992

M. L. Grossbeck, P. J. Maxiasz, and A. F. Rowcliffe, "Modeling of Strenghtening Mechanisms in Irradiated Fusion Reactor First Wall Alloys," *J. Nucl. Mater.* **191–194**, 808 (1992)

J. H. Han and J.-N. Leboeuf, "Particle Simulation Model of the Lorentz Collision Operator in Guiding-Center Plasmas," *Computer Phys. Communications* **69**, 277–86 (1992)

G. R. Hanson, J. H. Harris, J. B. Wilgen, C. E. Thomas, S. C. Aceto, L. R. Baylor, J. D. Bell, J. L. Dunlap, A. C. England, C. Hidalgo, M. Murakami, D. A. Rasmussen, J. G. Schwelberger, T. Uckan, and J. J.

Zielinski, "Density Fluctuation Measurements in ATF Using Correlation Reflectometry," *Nucl. Fusion* 32(9), 1593–1608 (1992)

G. R. Hanson, J. B. Wilgen, T. S. Bigelow, I. Collazo, and C. E. Thomas, "A Swept Two-Frequency Microwave Reflectometer for Edge Density Profile Measurements on TFTR," *Rev. Sci. Instrum.* 63, 4658–60 (1992)

J. H. Harris, M. Murakami, and R. A. Dory, "Enhanced Energy Confinement in the ATF Torsatron," *Bull. Am. Phys. Soc.* 37(6), 1546 (1992)

G. R. Haste, G. Agarici, A. Becoulet, B. Beaumont, H. Kuus, and B. Saoutic, "High Power, Long Pulse ICRF in Tore Supra," *Bull. Am. Phys. Soc.* 37(6), 1412 (1992)

C. L. Hedrick and J.-N. Leboeuf, "Landau Fluid Equations for Electromagnetic and Electrostatic Fluctuations," *Phys. Fluids B* 4, 3915–34 (1992)

C. L. Hedrick, J.-N. Leboeuf, and D. A. Spong, "Alpha-Alfvén Local Dispersion Relation and Solutions," *Phys. Fluids B* 4(12), 3869–82 (1992)

C. L. Hedrick, J.-N. Leboeuf, and D. A. Spong, "Landau Fluid Model of Alpha-Alfvén Waves, Including Velocity Dependent Drift," *Bull. Am. Phys. Soc.* 37(6), 1435 (1992)

D. L. Hillis, J. T. Hogan, K. H. Finken, W. P. West, R. R. Weynants, M. R. Wade, K. Akaishi, W. Y. Baek, J. Boedo, K. H. Burrell, R. W. Conn, K. H. Dippel, R. Doerner, H. Euringer, D. Finkenthal, D. S. Gray, C. M. Greenfield, P. Gohil, R. J. Groebner, J. Kim, C. C. Klepper, A. M. Messiaen, P. K. Mioduszewski, A. Miyahara, R. Moyer, G. Van Oost, A. Pospieszczyk, D. Reiter, D. Rusbüldt, R. P. Seraydarian, R. Van Nieuwenhove, and G. H. Wolf, "Helium Transport in Enhanced Confinement Regimes on the TEXTOR and DIII-D Tokamaks," *J. Nucl. Mater.* 196–198, 35–44 (1992)

S. Hiroe, S. F. Paul, M. A. Ochando, L. R. Baylor, A. C. England, C. H. Ma, D. A. Rasmussen, A. L. Qualls, and J. B. Wilgen, "Evolution of the Radiated Power Profile and Thermal Collapse in ATF," *Nucl. Fusion* 32, 1107 (1992)

S. P. Hirshman and F. M. Levinton, "Equilibrium Analysis Incorporating the Motional Stark Effect Diagnostic," *Bull. Am. Phys. Soc.* 37(6), 1575 (1992)

D. J. Hoffman, F. W. Baity, E. Barbato, G. C. Barber, T. S. Bigelow, M. D. Carter, J. B. O. Caughman, W. L. Gardner, R. H. Goulding, G. R. Haste, P. E. Jones, and M. Ono, "The Folded Waveguide Tests on RFTF and Conceptual Designs for Tokamaks," *Bull. Am. Phys. Soc.* 37(6), 1494 (1992)

J. T. Hogan and C. C. Klepper, "BBQ: A Monte Carlo Carbon Transport Code," *Bull. Am. Phys. Soc.* 37(6), 1599 (1992)

J. T. Hogan, P. K. Mioduszewski, L. W. Owen, T. Uckan, C. C. Klepper, M. Chatelier, T. Loarer, and L. Horton, "Modeling of Core-Wall Particle Dynamics in Tore Supra Pumping Experiments," *J. Nucl. Mater.* 196–198, 1083–89 (1992)

J. T. Hogan, L. W. Owen, P. K. Mioduszewski, M. Chatelier, and T. Loarer, "A Detailed Model for Core-Wall Particle Exchange in Tore Supra Particle Control Experiments," *Bull. Am. Phys. Soc.* 37(6), 1599 (1992)

J. T. Hogan and N. A. Uckan, "MHD Stability Considerations for the High Aspect Ratio Design," submitted to *Fusion Technol.* 21(3, Pt. 2), 1397–1405 (1992)

J. T. Hogan and J. Wesley, "A Divertor Parameter Scaling Database for TPX-Class Devices," *Bull. Am. Phys. Soc.* 37(6), 1599 (1992)

J. T. Hogan, J. Wesley, and the U.S. ITER Home Team, "Scaling of Divertor Conditions (Heat Load, Temperature) with Separatrix Parameters, SOL Transport, Aspect Ratio and Divertor Geometry," *Fusion Technol.* 21(3, Pt. 2), 1406 (1992)

W. A. Houlberg, "Burning Plasma Experiment Physics Design Description—Section VII. Fueling," *Fusion Technol.* 21(3, Pt. 2), 1250 (1992)

W. A. Houlberg and S. E. Attenberger, "Transient Current Profile Behavior in TPX," *Bull. Am. Phys. Soc.* 37(6), 1397 (1992)

W. A. Houlberg, S. E. Attenberger, L. R. Baylor, M. Gadeberg, T. C. Jernigan, P. Kupschus, S. L. Milora, G. L. Schmidt, D. W. Swain, and M. L. Watkins, "Pellet Penetration Experiments on JET," *Nucl. Fusion* 32(11), 1951 (1992)

W. A. Houlberg and N. A. Uckan, "Transport Analysis of ITER Startup, Burn, and Shutdown Scenarios," *Fusion Technol.* 21(3, Pt. 2), 1421 (1992)

C. T. Hsu, K. C. Shaing, R. P. Gormley, and D. J. Sigmar, "Bootstrap Current Induced by Fusion Born Alpha Particles," *Phys. Fluids B* **4**, 3310–15 (1992)

D. P. Hutchinson, R. K. Richards, C. A. Bennett, and C. H. Ma, "Proof-of-Principle of a Diagnostic for D-T Fusion-Product Alpha Particles," *Rev. Sci. Instrum.* **63**, 4953 (1992)

The JET Team, P. H. Rebut, et al., "Fusion Energy Production from a Deuterium-Tritium Plasma in the JET Tokamak," *Nucl. Fusion* **32**(2), 187 (1992)

R. C. Isler, S. Aceto, L. R. Baylor, T. S. Bigelow, G. L. Bell, J. D. Bell, B. A. Carreras, R. J. Colchin, E. C. Crume, N. Dominguez, R. A. Dory, J. L. Dunlap, G. R. Dyer, A. C. England, R. F. Gandy, J. C. Glowienka, G. R. Hanson, J. H. Harris, S. Hiroe, L. D. Horton, T. C. Jernigan, H. Ji, R. A. Langley, D. K. Lee, K. M. Likin, J. F. Lyon, C. H. Ma, S. Morimoto, M. Murakami, H. Okada, A. L. Qualls, D. A. Rasmussen, J. A. Rome, M. Sato, J. G. Schwelberger, M. G. Shats, J. E. Simpkins, C. E. Thomas, T. Uckan, M. R. Wade, J. B. Wilgen, W. R. Wing, H. Yamada, and J. J. Zielinski, "Effects of Magnetic Geometry, Fluctuations, and Electric Fields on Confinement in the Advanced Toroidal Facility," *Phys. Fluids B* **1**, 2104–10 (1992)

E. F. Jaeger, D. B. Batchelor, M. Murakami, R. C. Goldfinger, D. A. Rasmussen, C. K. Phillips, and J. R. Wilson, "Full-Wave Modelling of Direct Electron Heating by Ion Cyclotron Waves on TFTR," *Bull. Am. Phys. Soc.* **37**(6), 1488 (1992)

T. C. Jernigan, B. A. Carreras, R. A. Dory, J. H. Harris, R. C. Isler, J. F. Lyon, P. K. Mioduszewski, M. Muradami, D. A. Rasmussen, M. J. Saltmarsh, and J. Sheffield, "ATF Program After Restart," *Bull. Am. Phys. Soc.* **37**(6), 1547 (1992)

J. A. Jimenez, A. Varias, and N. Dominguez, "Interchange Modes in Torsatrons and Heliacs," *Bull. Am. Phys. Soc.* **37**(6), 1550 (1992)

T. Kamimura, E. Montalvo, D. C. Barnes, J.-N. Leboeuf, and T. Tajima, "Implicit Particle Simulation of Electromagnetic Plasma Phenomena," *J. Comput. Phys.* **100**, 77 (1992)

F. Kazeminezhad, J. M. Dawson, J.-N. Leboeuf, R. Sydora, and D. Holland, "A Vlasov Particle Ion Zero Mass Electron Model for Plasma Simulations," *J. Comput. Phys.* **102**, 277–86 (1992)

G. Kilgus, B. Habs, D. Schwalm, A. Wolf, N. R. Badnell, and A. Müller, "High Resolution Measurement of Dielectronic Recombination of Lithiumlike Cu^{26+}," *Phys. Rev. A* **46**, 5730 (1992)

C. C. Klepper, J. T. Hogan, L. W. Owen, P. K. Mioduszewski, R. Maingi, D. N. Hill, D. Buchenauer, M. A. Mahdavi, M. J. Schaffer, T. W. Petrie, G. L. Jackson, T. E. Evans, and G. Haas, "Comparison of Transient and Stationary Neutral Pressure Response in the DIII-D Advanced Divertor," *J. Nucl. Mater.* **196–198**, 1090 (1992)

R. L. Klueh, "Developing Steels for Service in Fusion Reactors," *J. Mat.* **44**(4), 20 (1992)

R. L. Klueh and D. J. Alexander, "Embrittlement of 9Cr-1MoVNb and 12Cr-1MoVW Steels Irradiated in HFIR," *J. Nucl. Mater.* **187**, 60 (1992)

R. L. Klueh and D. J. Alexander, "Impacet Behavior of Reduced-Activation Ferrite Steels Irradiated in the Fast Flux Test Facility," *J. Nucl. Mater.* **186**, 185 (1992)

R. L. Klueh and D. J. Alexander, "Irradiation Effects on the Impact Behavior of 12Cr-1MoVW and 1 2/4 Cr-1Mo Steels," p. 1256 in *Effects of Radiation on Materials: 15th International Symposium*, ASTM STP 1125, ed. R. E. Stoller, A. S. Kumar, and D. S. Gelles, American Society for Testing and Materials, Philadelphia, 1992

R. L. Klueh and P. J. Maxiasz, "Effect of Irradiation in HFIR on Teseile Properties of Cr-Mo Steels," *J. Nucl. Mater.* **187**, 43 (1992)

T. A. Kobel, M. A. Kozyrczak, S. W. Schwenterly, and W. A. Bell, "Effects of Mounting Methods on Temperature Sensor Accuracy Below 10 K," pp. 619–26 in *Proceedings of the 4th International Industrial Symposium on the Super Collider*, Plenum, 1992

A. Kohyama, M. L. Grossbeck, and G. Piatti, "The Application of Austenitic Stainless Steels in Advanced Fusion Systems: Current Limitations and Culture Prospects," *J. Nucl. Mater.* **191–194**, 37 (1992)

M. Kwon, R. H. Goulding, T. D. Shepard, C. E. Thomas, R. J. Colchin, M. R. Wade, E. F. Jaeger, M. D. Carter, F. W. Baity, D. B. Batchelor, G. L. Bell, J. D. Bell, T. S. Bigelow, E. C. Crume, Jr., A. C. England, J. C. Glowienka, S. Hiroe, L. D. Horton, D. J. Hoffman, R. C. Isler, R. A. Langley, D. K. Lee, M. Murakami, S. L. Painter, D. A. Rasmussen, D. W. Swain, T. Uckan, J. B. Wilgen, and W. R.

Wing "Fast-Wave Heating Experiments in the Ion Cyclotron Range of Frequencies on ATF," *Nucl. Fusion* **32**(7), 1225–40 (1992)

R. A. Langley, "Simple Aluminum Gasket for Use With Both Stainless Steel and Aluminum Flanges," *J. Vac. Sci. Technol. A* **10**, 1185–87 (1992)

J.-N. Leboeuf, B. A. Carreras, and L. A. Charlton, "Drift Thermal Instability with Sheared Poloidal Flow," *Bull. Am. Phys. Soc.* **37**(6), 1477 (1992)

C. K. Lee, B. A. Chin, S. J. Zinkle, and R. C. Wilcox, "Brazing of Copper-Alumina Alloys," *J. Nucl. Mater.* **191–194**, 488–92 (1992)

D. K. Lee and S. P. Hirshman, "Rapid Determination of a Straight Magnetic Coordinate System for Stellarator Configurations," *J. Comput. Phys.* **101**(2), 330–33 (1992)

D. K. Lee, S. P. Hirshman, and H. Fishman, "Determination of MHD Equilibrium Properties from Magnetic Measurements," *Bull. Am. Phys. Soc.* **37**(6), 1575 (1992)

B. Lembege, J.-N. Leboeuf, P. Liewer, and M. Ashour-Abdalla, From Fusion to Ligth Surfing: Lectures on Plasma Physics Honoring John Dawson, ed. T. Katsouleas, Addison-Wesley Publi. Co., 1992

W. Li, M. A. Ebadian, T. L. White, and R. G. Grubb, "Heat Transfer Within a Radioactive Contaminated Concrete Slab Applying a Microwave Heating Technique"*J. Heat Transfer* **207**, 55–62 (1992)

D. C. Lousteau, J. N. Herndon, F. C. Davis, and S. L. Schrock, "Remote Maintenance Challenges for the International Thermonuclear Experimental Reactor," *Fusion Technol.* **21**(3, Pt. 2), 1389–96 (1992)

V. E. Lynch, B. A. Carreras, J. B. Drake, J.-N. Leboeuf, and J. R. Ruiter, "Plasma Turbulence Calculations on the INTEL iPSC/860 (RX) Hypercube," in *Parallel Methods on Large-Scale Structural Analysis and Physics Applications*, ed. Olaf O. Storaasli and Edward A. Carmona, Pergamon Press, 1992

V. E. Lynch, B. A. Carreras, J. B. Drake, J.-N. Leboeuf, P. Liewer, "Performance of a Plasma Fluid Code on the Intel Parallel Computer," p. 286 in *Proceedings of Supercomputing '92*, IEEE Computer Society Press, Los Alamitos, Calif., 1992

V. E. Lynch, B. A. Carreras, J. B. Drake, J.-N. Leboeuf, and P. Liewer, "Performance of a Plasma Fluid Code on the Intel Hypercubes," *Bull. Am. Phys. Soc.* **37**(6), 1556 (1992)

J. F. Lyon, "Assessment of Stellarators as Reactors," *Bull. Am. Phys. Soc.* **37**(6), 1547 (1992)

P. M. Lyster and J. N. Leboeuf, "A Fluid-Ion and Particle-Electron Model for Low-Frequency Plasma Instabilities," *Journ. Comput. Phys.* **102**(1), 180 (1992)

C. H. Ma, L. R. Baylor, D. P. Hutchinson, M. Murakami, and J. B. Wilgen, "Density Profile Measurement Using a Multichannel Difluoromethane Laser Interferometer System on ATF," *Rev. Sci. Instrum.* **63**, 4981 (1992)

L. W. Owen, J. T. Hogan, C. C. Klepper, P. K. Mioduszewski, T. Uckan, M. Chatelier, and T. Loarer, "Comparison of Inner Wall Pumping and Pump Limiter Exhaust in Tore Supra," *Bull. Am. Phys. Soc.* **37**(6), 1449 (1992)

Y-K. M. Peng, R. J. Colchin, D. W. Swain, P. T. Bonoli, and S. C. Luckhardt, "Small Steady-State Tokamak (TST) Plasma for Testing Advanced Divertors," *Bull. Am. Phys. Soc.* **37**(6), 1448 (1992)

Y-K. M. Peng, J. D. Galambos, and P. C. Shipe, "Small Tokamaks for Fusion Technology Testing," *Fusion Technol.* **21**(3, Pt. 2), 1729–38 (1992)

C. C. Petty, R. I. Pinsker, M. J. Mayberry, S. C. Chiu, T. C. Luce, R. Prater, J. C. M. de Hass, R. A. James, F. W. Baity, R. H. Goulding, D. J. Hoffman, P. T. Bonoli, and M. Porkolab, "Direct Electron Heating by 60 MHz Fast Waves on DIII-D," *AIP Conf. Proc.* **244**, 96–104 (1992)

R. A. Phaneuf, "Assessment of Ion-Atom Collision Data for Magnetic Fusion Plasma Edge Modelling," *Nucl. Fusion Suppl.* **2** (*Atomic and Plasma-Material Interaction Data for Fusion*), 75 (1992)

R. A. Phaneuf, R. K. Janev, H. Tawara, M. Kimura, P. S. Krstic, G. Peach and M. A. Mazing, "Status and Critical Assessment of the Database for Collisions of Be^{q+} and B^{q+} Ions with H, H_2 and He," *Nucl. Fusion* **3** (Suppl.: *Atomic and Plasma-Material Interaction Data for Fusion*), 105 (1992)

R. A. Phaneuf and D. R. Schultz, *The ORNL Controlled Fusion Atomic Data Center: Progress Report 1991*, INDC(NDS)-259/N7, 22 (1992)

C. K. Phillips, J. Hosea, E. Marmar, M. W. Phillips, J. Snipes, J. Stevens, J. Terry, J. R. Wilson, M. Bell, M. Bitter, R. Boivin, C. E. Bush, C. Z. Cheng, D. Darrow, E. Fredrickson, R. Goldfinger, G. W. Hammett, K. Hill, D. J. Hoffman, W. A. Houlberg, H. Hsuan, M. Hughes, D. Jassby, D. McCune, K. McGuire, Y. Nagayama, D. K. Owens, H. Park, A. Ramsey, G. Schilling, J. Schivell, D. N. Smithe,

B. Stratton, E. Synakowski, G. Taylor, H. Towner, R. White, S. Zweben, and the TFTR Group, "Ion Cyclotron Range of Frequencies Stabilization of Sawteeth of Tokamak Fusion Test Reactor," *Phys. Fluids B* 4(7), 2155–64 (1992)

M. S. Pindzola and N. R. Badnell, "Dielectronic Recombination Rate Coefficients for Ions of the Be and B Isonuclear Sequence," *Nucl. Fusion Suppl.* 3 (*Atomic and Plasma-Material Interaction Data for Fusion*), 101 (1992)

M. S. Pindzola, N. R. Badnell, and D. C. Griffin, "Comparison of Theory and Experiment for Electron-Ion Excitation and Ionization," p. 21 in *Future Directions in Electron-Ion Collision Physics*, LLNL CONF-9204186, Lawrence Livermore Natl. Lab., 1992

M. S. Pindzola, N. R. Badnell, and D. C. Griffin, "Dielectronic Recombination between Hyperfine Levels of the Ground State of Bi^{82+}," *Phys. Rev. A* 45, R7659 (1992)

M. S. Pindzola, N. R. Badnell, and D. C. Griffin, "Validity of the Isolated-Resonance Distorted-Wave Approximation for Dielectornic Recombination," *Phys. Rev. A* 46, 5725 (1992)

M. S. Pindzola and D. C. Griffin, "Electron-Impact Ionization of the Tungsten Atom," *Phys. Rev. A* 46, 2486 (1992)

M. Porkolab, D. B. Batchelor, P. T. Bonoli, M Fenstermacher, R. Goldston, S. Jardin, G. H. Neilson, W. M. Nevins, J. Ramos, and the TPX Physics Team, "Physics Design and Noninductive Current Drive Options in a Steady State Advanced Tokamak," *Bull. Am. Phys. Soc.* 37(6), 1397 (1992)

D. E. Post, S. A. Cohen, J. T. Hogan, W. M. Nevins, P. H. Rutherford, D. Sigmar, D. Stotler, N. A. Uckan, and J. C. Wesley, "Assessments of the Adequacy of the ITER Engineering Design Activity Physics R&D Program," *Fusion Technol.* 21(3, Pt. 2), 1434–43 (1992)

D. E. Post, N. A. Uckan, and the U.S. ITER Home Team, "Critical and Design Trade-off Issues for ITER," *Fusion Technol.* 21(3, Pt. 2), 1427–33 (1992)

A. L. Qualls, L. R. Baylor, S. K. Combs, G. R. Dyer, P. W. Fisher, M. J. Gouge, S. L. Milora, D. K. Owens, G. L. Schmidt, and J. B. Wilgen, "Deuterium Pellet Injection Experiments on TFTR," *Bull. Am. Phys. Soc.* 37(6), 1482 (1992)

A. L. Qualls, L. R. Baylor, J. B. Wilgen, S. K. Combs, G. R. Dyer, P. W. Fisher, M. J. Gouge, S. L. Milora, G. L. Schmidt, D. K. Owens, and D. K. Mansfield, "Pellet Ablation and Particle Deposition Studies on TFTR," *Bull. Am. Phys. Soc.* 37(6), 1482 (1992)

B. Richards, T. Uckan, A. J. Wootton, B. A. Carreras, R. D. Bengtson, et al., "First Results from the Fast Reciprocating Active Probe on TEXT," *Bull. Am. Phys. Soc.* 37(6), 1388 (1992)

G. A. Riggs, K. L. Sidikman, B. A. Carreras, and P. W. Terry, "Radial Structure of Drift Wave Turbulence," *Bull. Am. Phys. Soc.* 37(6), 1476 (1992)

J. A. Rome, *Stellarator News* (19), January 1992

J. A. Rome, *Stellarator News* (20), March 1992

J. A. Rome, *Stellarator News* (21), May 1992

J. A. Rome, *Stellarator News* (22), July 1992

J. A. Rome, *Stellarator News* (23), September 1992

J. A. Rome, *Stellarator News* (24), November 1992

P. M. Ryan, F. W. Baity, R. H. Goulding, D. J. Hoffman, D. W. Swain, and J. H. Whealton, "Comparison of One vs Two Poloidal Straps for High Frequency-ICRH Antenna Arrays," *Bull. Am. Phys. Soc.* 37(6), 1494 (1992)

D. R. Schultz (chairman), K. Katsonis, R. K. Janev, Y. Jinzhang, T. Shirai, V. A. Belyeav, V. Piksaikin, H. Tawara, V. A. Abramov, I. Komarov, P. Krstic and R. E. Olson, "Working Group Report on Atomic Data Status and Needs Concerning Plasma Impurities Colliding with H, H_2 and He," INDC(NDS)-257/N8, 20 (1992)

D. R. Schultz, L. Meng, and R. E. Olson, "Classical Description and Calculation of Ionization in Collisions of 100 eV Electrons and Positrons with He and H_2," *J. Phys. B* 25, 4601 (1992)

D. R. Schultz, C. O. Reinhold, and R. E. Olson, "Classical Calculation of High-Energy Electron Capture in 5-MeV Proton-Hydrogen Collisions," *Phys. Rev. A* 46, 666 (1992)

D. R. Schultz, C. O. Reinhold, R. E. Olson, and D. G. Seely, "Differential Cross Sections of State-Slective Electron Capture in 20–100 keV Proton-Helium Collisions," *Phys. Rev. A* 46, 275 (1992)

J. G. Schwelberger, S. C. Aceto, K. A. Connor, J. J. Zielinski, L. R. Baylor, A. C. England, R. C. Isler, C. H. Ma, M. Murakami, and T. Uckan, "Electron Density Profile Measurement with a Heavy Ion Beam Probe," *Rev. Sci. Instrum.* **63**, 4571 (1992)

S. W. Schwenterly, M. S. Lubell, et al., "Design and Testing of a Four-Pole Superconducting Motor Stator," *Adv. Cryog. Eng.* **37A**, 473–479 (1992)

K. C. Shaing, "An Estimate of the Ion Orbit Loss Rate in Tokamaks," *Phys. Fluids B* **4**, 3310–15 (1992)

K. C. Shaing, "Ion Orbit Loss and Poloidal Plasma Rotation in Tokamaks," *Phys. Fluids B* **4**, 171–75 (1992)

K. C. Shaing, "Poloidal Magnetic Field Dependence of the Edge Electric Field Layer Width in the H Mode in Tokamaks," *Phys. Fluids B* **4**, 290–91 (1992)

K. C. Shaing amd R. D. Hazeltine, "Effects of Orbit Squeezing on Ion Transport in the Banana Regime in Tokamaks," *Phys. Fluids B* **4**, 2457–51 (1992)

K. C. Shaing, R. D. Hazeltine, and H. Sanuki, "Shock Formation in a Poloidally Rotating Tokamak Plasma," *Phys. Fluids B* **4**, 404–12 (1992)

K. C. Shaing and C. T. Hsu, "Effects of Ion Diamagnetic Flow on Shock Formation in Poloidally Rotating Tokamak Plasmas," *Phys. Fluids B* **4**, 2547–51 (1992)

K. C. Shaing and C. T. Hsu, "The Effects of Shock Phenomenon on L-H Transition and MARFE Formation in Tokamaks," *Bull. Am. Phys. Soc.* **37**(6), 1364 (1992)

M. G. Shats, J. H. Harris, K. M. Likin, J. B. Wilgen, J. D. Bell, L. R. Baylor, C. H. Ma, and K. A. Sarksyan, "Microwave Scattering Measurements of Density Fluctuations in ATF," *Bull. Am. Phys. Soc.* **37**(6), 1546 (1992)

J. Sheffield, "Panel Discussion: Future Directions in Magnetic Fusion," *J. Fusion Energy* **11**(2), 67 (1992)

J. Sheffield, "Status of the New Initiative Task Force Work," *J. Fusion Energy* **11**(2), 63 (1992)

K. L. Sidikman, B. A. Carreras, L. Garcia, and P. H. Diamond, "Calculations of Drift Wave Turbulence in the Presence of a Radial Electric Field Profile," *Bull. Am. Phys. Soc.* **37**(6), 1476 (1992)

L. L. Snead, S. K. Zinkle, and D. Steiner, "Measurement of the Effect of Radiation Damage to Ceramic Composite Interfacial Strength," *J. Nucl. Mater.* **191–194**, 566–70 (1992)

L. L. Snead, S. K. Zinkle, and D. Steiner, "Radiation Induced Microstructure and Mechanical Property Evolution of SiC/SiC Composite Materials," *J. Nucl. Mater.* **191–194**, 560–65 (1992)

W. Spies, A. Müller, J. Linkemann, A. Frank, M. Wagner, C. Kozhuharov, B. Franzke, K. Beckert, F. Bosch, H. Eickhoff, M. Jung, O. Kleper, W. König, P. H. Mokler, R. Moshammer, F. Holden, U. Schaaf, P. Spädtke, M. Steck, P. Zimmerer, N. Frün, W. Scheid, M. S. Pindzola, and N. R. Badnell, "Dielectronic and Radiative Recombination of Lithium-like Gold," *Phys. Rev. Lett* **69**, 2768 (1992)

D. A. Spong, B. A. Carreras, and C. L. Hedrick, "Linearized Gyrofluid Model of the Alpha-Destabilized Toroidal Alfvén Eigenmode with Continuum Damping Effects," *Phys. Fluids B* **4**, 3316–28 (1992)

D. A. Spong, B. A. Carreras, C. L. Hedrick, N. Dominguez, L. A. Charlton, P. J. Christenson, J.-N. Leboeuf, "Alpha Destabilization of the TAE Mode using a Reduced Gyrofluid Model with Landau Closure," *Physica Scripta* **45**, 159 (1992)

D. A. Spong, C. L. Hedrick and B. A. Carreras, "Nonlinear Models of the Energetic Particle Destabilized TAE Mode," *Bull. Am. Phys. Soc.* **37**(6), 1431 (1992)

D. C. Stallings, M. D. Carter and D. B. Batchelor, "Effect of Antenna Design Parameters upon RF Antenna Performance," *Bull. Am. Phys. Soc.* **37**(6), 1604 (1992)

R. E. Stoller, R. H. Goulding, and S. J. Zinkle, "Measurement of Dielectric Properties of Ceramics Under Ionizing and Displacive Irradiation Conditions," *J. Nucl. Mater.* **191–194**, 602–06 (1992)

R. E. Stoller, M. L. Grossbeck, and L. K. Mansur, "A Theoretical Model of Accelerated Irradiation Creep at Low Temperatures by Transient Interstitial Absorption," p. 517 in *Effects of Radiation on Materials: 15th International Symposium*, ASTM STP 1125, ed. R. E. Stoller, A. S. Kumar, and D. S. Gelles, American Society for Testing and Materials, Philadelphia, 1992

D. W. Swain, F. W. Baity, D. B. Batchelor, R. H. Goulding, D. J. Hoffman, E. F. Jaeger, P. M. Ryan, and D. C. Stallings, "Optimization of Fast Wave Current Drive Systems," *Bull. Am. Phys. Soc.* **37**(6), 1603 (1992)

P. W. Terry, P. H. Diamond, B. A. Carreras, and K. Sidikman, "Tokamak Turbulence in Self-Regulated Differentially Rotating Flow and L-H Transition Dynamics," in *New Ideas in Tokamak Confinement*, ed.V. Stefan, American Institute of Physics, New York, 1992

N. A. Uckan, J. T. Hogan, D. J. Sigmar, and U.S. ITER Home Team, "U.S. ITER Plasma Physics R&D Program: Confinement Operational Limits and Alpha Particle Physics," *Bull. Am. Phys. Soc.* **37**(6), 1396 (1992)

N. A. Uckan and the U.S. ITER Home Team, "ITER Physics R&D Assessment for Confinement and Plasma Performance Projections," *Fusion Technol.* **21**, 1444 (1992)

T. Uckan, B. Richards, R. D. Bengtson, B. A. Carreras, G. X. Li, H. Lin, P. Hurwitz, W. L. Rowan, H. Y. W. Tsui, and A. J. Wootton, "Active Probing of Plasma Edge Turbulence on the Text Tokamak," *Bull. Am. Phys. Soc.* **37**, 1388 (1992)

T. Uckan, S. C. Aceto, L. R. Baylor, J. D. Bell, T. S. Bigelow, A. C. England, J. H. Harris, R. C. Isler, T. C. Jernigan, J. F. Lyon, C. H. Ma, P. K. Mioduszewski, M. Murakami, D. A. Rasmussen, J. B. Wilgen, and J. J. Zielinski, "Effects of Limiter Biasing on the ATF Torsatron," *J. Nucl. Mater.* **196–198**, 308–11 (1992)

C. A. Wang, H. T. Lin, M. L. Grossbeck, and B. A. Chin, "Suppressions of HAZ Cracking During Welding of Helium-Containing Materials," *J. Nucl. Mater.* **191–194**, 696 (1992)

A. S. Ware, P. H. Diamond, H. Biglari, B. A. Carreras, L. A. Charlton, J.-N. Leboeuf, and A. J. Wootton, "Theory of Ionization-Driven Drift Wave Turbulence," *Phys. Fluids B* **4**, 877–87 (1992)

A. S. Ware, P. H. Diamond, B. A. Carreras, J.-N. Leboeuf, and D. K. Lee, "Theory of Drift-Thermal Instability Induced Turbulence," *Phys. Fluids B* **4**, 102–16 (1992)

D. P. White and P. G. Klemens, "Thermal Conductivity of Heavily Doped Si-Ge Alloys at High Temperatures," *J. Appl. Phys.* **71**(9), 4258 (1992)

J. Wilgen, M. Murakami, J. H. Harris, T. S. Bigelow, R. A. Dory, B. A. Carreras, S. C. Aceto, D. B. Batchelor, L. R. Baylor, G. L. Bell, J. D. Bell, R. J. Colchin, E. C. Crume, N. Dominguez, J. L. Dunlap, G. R. Dyer, A. C. England, R. F. Gandy, J. C. Glowienka, R. C. Goldfinger, R. H. Goulding, C. Hidalgo, G. R. Hanson, S. Hiroe, S. P. Hirshman, L. D. Horton, H. C. Howe, D. P. Hutchinson, R. C. Isler, T. C. Jernigan, H. Ji, H. Kaneko, L. M. Kovrizhynkh, M. Kwon, R. A. Langley, D. K. Lee, K. M. Likin, J. F. Lyon, C. H. Ma, M. M. Menon, P. K. Mioduszewski, O. Motojima, H. Okada, S. Paul, A. L. Qualls, D. A. Rasmussen, R. K. Richards, J. A. Rome, M. J. Saltmarsh, K. A. Sarksyan, M. Sato, J. G. Schwelberger, K. C. Shaing, M. G. Shats, T. D. Shepard, J. E. Simpkins, C. E. Thomas, T. Uckan, K. L. Vander Sluis, M. R. Wade, W. R. Wing, H. Yamada, and J. F. Zielinski, "Fluctuation and Modulation Transport Studies in the ATF Torsatron," *Bull. Am. Phys. Soc.* **37**(6), 1591 (1992)

J. J. Zielinski, S. C. Aceto, R. C. Colchin, K. A. Connor, A. C. England, R. C. Isler, M. Murakami, J. G. Schwelberger, T. Uckan, and J. B. Wilgen, "Potential Profile Measurements During Perturbation Coil Experiments on ATF," *Bull. Am. Phys. Soc.* **37**(6), 1591 (1992)

S. J. Zinkle, "A Brief Review of Cavity Swelling and Hardening in Irradiated Copper and Copper Alloys," p. 813 in *Effects of Radiation on Materials: 15th International Symposium*, ASTM STP 1125, ed. R. E. Stoller, A. S. Kumar, and D. S. Gelles, American Society for Testing and Materials, Philadelphia, 1992

S. J. Zinkle, "Anisotropic Dislocation Loop Nucleation in Ion Irradiated $MgAl_2O_4$," *J. Nucl. Mater.* **191–194**, 645–49 (1992)

S. J. Zinkle, A. Horsewell, B. A. Singh, and W. F. Sommer, "Dispersion Stability in Cu-Al_2O_3 Alloy Under Energetic Cascade Damage Conditions," *J. Nucl. Mater.* **199**, 11–16 (1992)

1992 PRESENTATIONS

January

International Topical Conference on New Ideas in Tokamak Confinement, La Jolla, California January 27–29, 1992. Proceedings published

B. A. Carreras, V. E. Lynch, and L. Garcia, "Flow Generation by Turbulence"

P. W. Terry, P. H. Diamond, B. A. Carreras, and K. Sidikman, "Tokamak Turbulence in Self-Regulated Differentially Rotating Flow and L-H Transition Dynamics"

February

Fusion Energy Advisory Committee (FEAC) Panel 1 Meeting, Pleasanton, California, February 5, 1992

M. A. Abdou, L. A. Berry, K. H. Berkner, and D. O. Overskei, "Base Program Support for ITER"

Presentation to Representatives of the Martin Marietta Astronautics Group, Oak Ridge Y-12 Plant, February 13, 1992

J. Sheffield, "Overview of U.S. and ORNL Fusion Program"

Real Academia de Ciencias Exactas, Físicas y Naturales, Madrid, Spain, February 14, 1992. Proceedings published

B. A. Carreras, "Problems with the Concept of Plasma Equilibrium in Tokamaks"

Workshop on Fluctuations in Stellarators, Max Planck Institut fur Plasmaphysik, Garching bei Munchen, Germany, February 17–19, 1992

B. A. Carreras, N. Dominguez, V. E. Lynch, and P. H. Diamond, "Trapped Electron Modes in Stellarators"

B. A. Carreras, K. Sidikman, P. H. Diamond, and P. W. Terry, "Long Wave Length Drift Wave Turbulence"

J. H. Harris, "Fluctuation Studies on ATF"

U.S. International Thermonuclear Experimental Reactor (ITER) National Meeting, Lawrence Livermore National Laboratory, Livermore, California, February 25–26, 1992

D. A. Spong and D. J. Sigmar, "ITER Neutral Beam Stability Studies"

N. A. Uckan, "Summary of Confinement and Plasma Performance Tasks and Confinement R&D Contributions"

March

Fifth Transport Task Force (TTF) Workshop, Oak Ridge, Tennessee, March 9–12, 1992

L. A. Charlton, B. A. Carreras, J.-N. Leboeuf, and V. E. Lynch, "Role of Radiative Condensation in Tokamak Edge Turbulence"

N. Dominguez, C. L. Hedrick, and J.-N. Leboeuf, "A Model for DTEM Turbulence with Ion Landau Damping and Finite Larmor Radius Effects"

D. A. Spong, "Gyrofluid Model of the TAE Mode"

High Throughput Pellet Injection Workshop, Fusion Engineering Design Center (FEDC), Oak Ridge, Tennessee, March 11–12, 1992

W. A. Houlberg, "ITER Pellet Injection"

Ninth Topical Conference on High-Temperature Plasma Diagnostics, Santa Fe, New Mexico, March 15–19, 1992. Proceedings published in *Rev. Sci. Instrum.*

B. A. Carreras, "Diagnostic Needs for Fluctuation and Transport Studies"

G. R. Hanson, J. B. Wilgen, T. S. Bigelow, I. Collazo, and C. E. Thomas, "A Swept Two-Frequency Microwave Reflectometer for Edge Density Profile Measurements on TFTR"

D. P. Hutchinson, R. K. Richards, C. A. Bennett, and C. H. Ma, "Proof-of-Principle of a Diagnostic for D-T Fusion-Product Alpha Particles"

C. H. Ma, L. R. Baylor, D. P. Hutchinson, M. Murakami, and J. B. Wilgen, "Density Profile Measurement Using a Multichannel Difluoromethane Laser Interferometer System on ATF"

Fusion Energy Advisory Committee, Princeton Plasma Physics Laboratory, Princeton, New Jersey, March 18–19, 1992

J. Sheffield, "Report of the New Initiative Task Force"

Field Work Proposal Meeting, Germantown, Maryland, March 25–27, 1992

W. A. Houlberg, "L-H Transition Model Based on Extended Neoclassical Theory"

10th International Conference on Plasma Surface Interactons, Monterey, California, March 30–April 3, 1992. Proceedings published in *J. Nucl. Mater.* **196–198**

T. Uckan, S. C. Aceto, L. R. Baylor, J. D. Bell, T. S. Bigelow, A. C. England, J. H. Harris, R. C. Isler, T. C. Jernigan, J. F. Lyon, C. H. Ma, P. K. Mioduszewski, M. Murakami, D. A. Rasmussen, J. B. Wilgen, and J. J. Zielinski, "Effects of Limiter Biasing on the ATF Torsatron"

April

Neutron Interactive Materials Program Review Meeting, Knoxville, Tennessee, April 1–2, 1992

M. J. Saltmarsh, "U.S. Initiative on a 14-MeV Neutron Source"

J. Sheffield, "The U.S. Fusion Program: The New Initiative"

American Nuclear Society Executive Conference on Remote Operations and Robotics in the Nuclear Industry-II, Pine Mountain, Georgia, April 6–8, 1992

T. W. Burgess, F. C. Davis, G. D. Loesser, and G. R. Walton, "An Overview of Remote Handling Technology in Today's Fusion Experiments"

1992 International Sherwood Fusion Theory Conference, Sweeney Convention Center, Santa Fe, New Mexico, April 6–8, 1992. Abstracts published in *1992 International Sherwood Fusion Theory Conference Proceedings*

C. Alejaldre, E. Ascasibar, L.Garcia, A. Lopez-Fraguas, A. Varias, B. Carreras, and N. Dominguez, "Beta-Limit Evaluation for the TJ-IU Torsatron"

L. A. Charlton, B. A. Carreras, J.-N. Leboeuf, and V. E. Lynch, "Radiative Condensation and Boundary Condition Effects in Tokamak Edge Turbulence"

N. Dominguez, C. L. Hedrick, and J.-N. Leboeuf, "A Model foir Dissipative Trapped Electron Mode Turbulence with Ion Landau Damping and Finite Larmor Radius Effects"

R. A. Dory, M. Murakami, and the ATF Experimental Team, "Energy Confinement Scaling in the ATF Torsatron"

R. C. Goldfinger, D. B. Batchelor, C. K. Phillips, G. W. Hammett, D. McCune, J. R. Wilson, M. Zarnstorff, and the TFTR Group, "TRANSP Analysis of Supershots with ICRF Heating in TFTR"

C. L. Hedrick, J.-N. Lebouef, and N. Dominguez, "Approximate Model of DTEM with Ion Landau Damping and FLR Effects"

S. P. Hirshman, W. A. Cooper, S. Merazzi, and R. Gruber, "Numerical Three Dimensional Equilibria with Pressure Anisotropy"

J. A. Holmes, D. J. Strickler, and Y-K. M. Peng, "Ballooning Stability Analysis and Optimization of Tokamak Equilibria"

E. F. Jaeger, D. B. Batchelor, M. D. Carter, R. C. Goldfinger, and D. C. Stallings, "Influence of Various Physics Phenomena on Fast-Wave Current Drive Efficiency in Advanced Tokamaks"
V. E. Lynch, B. A. Carreras, J. B. Drake, J.-N. Leboeuf, P. Liewer, and D. W. Walker, "The Performance of a Fluid Code on Massively Parallel Machines"
K. C. Shaing, R. D. Hazeltine, S. E. Attenberger, S. P. Hirshman, and W. A. Houlberg, "Nonlinear Poloidal Density Variation in H-Mode Plasmas"
K. L. Sidikman, B. A. Carreras, N. Dominguez, L. Garcia, and P. H. Diamond, "Single-Equation DTEM Calculations with Two Nonlinearities"
D. A. Spong, B. A. Carreras, and C. L. Hedrick, "Fluid/Kinetic Models for Shear Alfven TAE Instabilities in Tokamaks"
P. W. Terry, P. H. Diamond, B. A. Carreras, and K. L. Sidikman, "Model Studies of L-H Transition Dynamics with Turbulently Generated Differentially Rotating Flow"

Numerical Tokamak Project Workshop (NTP), Status of NTP Technical Components, Santa Fe, New Mexico, April 8–9, 1992
J.-N. Leboeuf, N. Dominguez, C. L. Hedrick, V. E. Lynch, K. L. Sidikman, "Group #2B Progress Report on Gyro-Landau Fluid Model of Tokamak Core Fluctuations"
J.-N. Leboeuf, B. A. Carreras, N. Dominguez, J. B. Drake, C. L. Hedrick V. E. Lynch, K. Sidikman, and D. B. Walker, "Gyro-Landau Fluid Model of Tokamak Core Fluctuations"

Fusion Power Associates Annual Meeting and Symposium, Pleasanton, California, April 9–10, 1992. Proceedings published in *J. Fusion Energy*
J. Sheffield, "Panel Discussion: Future Directions in Magnetic Fusion"
J. Sheffield, "Status of the New Initiative Task Force Work"

Fifth Boulder Workshop on High Power Ion Cyclotron Range of Frequency (ICRF) Antenna Design and Physics, Boulder, Colorado, April 9–11, 1992. Abstract published
E. F. Jaeger, D. B. Batchelor, M. D. Carter, R. C. Goldfinger, and D. C. Stallings, "Influence of Various Physics Phenomena on Fast-Wave Current Drive Efficiency in Advanced Tokamaks"

Toroidal Plasma Experiments (TPX) Physics Workshop, General Atomics, LaJolla, California, April 30, 1992
W. A. Houlberg and S. E. Attenberger, "TPX Current Drive Transients"

14th Werner Brandt Workshop on Charged Particle Penetration Phenomena, Oak Ridge, Tennessee, April 30–May 1, 1992. Proceedings published in ORNL report, CONF-9204144, Oak Ridge Natl. Lab., 1992
P. A. Zeijlmans van Emmichoven, C. C. Havener, I. G. Hughes, S. H. Overbury, M. T. Robinson, D. M. Zehner, and F. W. Meyer, "Electron Emission During Multicharged Ion-Metal Surface Interactions"

May

Working Group Meeting on Edge Plasma Theory and Divertor Modeling, NYU, New York, New York, May 12, 1992
W. A. Houlberg, "Issues and Opportunities in Edge Plasma Theory"

American Physical Society Division of Atomic, Molecular and Optical Physics Meeting, Chicago, Illinois, May 20–22, 1992
C. C. Havener, P. A. Zeijlmans van Emmichoven, and R. A. Phaneuf, "Low-Energy Measurements of Electron Capture by Multicharged Ions from Excited Hydrogen Atoms"
F. W. Meyer, "The Production of 'Hollow Atoms' in Slow Multicharged Ion-Surface Interactions," invited

Third Workshop on Alpha Physics in Tokamak Fusion Test Reactor (TFTR), Massachusetts Institute of Technology, Cambridge, Massachusetts, May 28–29, 1992
D. A. Spong, "Nonlinear TAE Simulations for TFTR"

June

Nineteenth IEEE International Conference on Plasma Science, Tampa, Florida, June 1–3, 1992. Proceedings published
J. J. Zielinski, S. C. Aceto, J. G. Schwelberger, K. A. Connor, J. F. Lewis, A. Carnevali, J. C. Glowienka, H. Iguchi, I. S. Nedzelskij, and T. Uckan, "Measurements of the Plasma Potential Profile and Density Fluctuations on the ATF Torsatron Using a Heavy Ion Beam Probe"

10th Topical Meeting on the Technology of Fusion Energy, Boston, Massachusetts, June 7–12, 1992. Proceedings published in *Fusion Technol.* **21**(3)
J. Galambos, C. Baker, Y-K. M. Peng, D. Cohn, M. Chaniotakis, L. Bromberg, and S. Dean, "System Studies of Copper and Superconducting Coil Pilot Plants"
P. L. Goranson, "Hydrogen/Hydrocarbon Explosions in the ITER Vacuum Vessel"
M. J. Gouge, L. R. Baylor, M. J. Cole, S. K. Combs, G. R. Dyer, D. T. Fehling, P. W. Fisher, C. R. Foust, R. A. Langley, S. L. Milora, A. L. Qualls, and J. B. Wilgen, "Tritium Pellet Injector for TFTR"
J. T. Hogan and N. A. Uckan, "MHD Stability Considerations for the High Aspect Ratio Design"
J. T. Hogan and J. Wesley, "Scaling of Divertor Temperature and Heat Loads for TPX-Class Devices"
W. A. Houlberg and N. A. Uckan, "Transport Analysis of ITER Startup, Burn, and Shutdown Scenarios"
D. C. Lousteau, J. N. Herndon, F. C. Davis, and S. L. Schrock, "Remote Maintenance Challenges for the International Thermonuclear Experimental Reactor," invited
Y-K. M. Peng, J. D. Galambos, and P. C. Shipe, "Small Tokamaks for Fusion Technology Testing"
D. E. Post and N. A. Uckan, "Critical and Design Trade-off Issues for ITER"
N. A. Uckan and U.S. ITER Home Team, "ITER Physics R&D Assessment for Confinement and Plasma Performance Projections"
J. J. Yugo and D. E. Williamson, "A Comparison of Two Three-Dimensional Shell-Element Transient Electromagnetics Codes"

IAEA Technical Committee Meeting on Advances in Simulation and Modelling of Thermonuclear Plasmas, Montreal, Canada, June 15–17, 1992. Abstracts published
J.-N. Leboeuf, B. A. Carreras, L. A. Charlton, A. S. Ware, P. H. Diamond, Ch. P. Ritz, and A. J. Wootton, "Fluid Models for the Collisional Plasma Edge: Drift Thermal Instability with Sheared Poloidal Flow"

Toroidal Plasma Experiments (TPX) Physics Workshop, Princeton, New Jersey, June 18, 1992
W. A. Houlberg, "Current Profile Control and Reconnection Issues for TPX/SSAT"

19th International Conference on Controlled Fusion and Plasma Physics, European Physical Society (EPS), Innsbruck, Austria, June 29–July 3, 1992. Proceedings published
S. C. Aceto, J. G. Schwelberger, K. A. Connor, J. J. Zielinski, J. C. Glowienka, R. C. Isler, M. Murakami, J. D. Bell, and T. Uckan, "Results of the Heavy Ion Beam Probe Measurements on the Advanced Toroidal Facility"
C. Alejaldre, E. Ascasibar, L. Garcia, A. López-Fraguas, A. Varias, B. A. Carreras, and N. Dominguez, "Ideal MHD Studies of the TJ-IU Torsatron"
D. B. Batchelor, E. F. Jaeger, M. D. Carter, R. C. Goldfinger, and D. C. Stallings, "Influence of Various Physics Phenomena on Fast-Wave Current Drive in Advanced Tokamaks"
N. T. Besedin, D. L. Grekov, I. M. Pankratov, O. S. Pavlichenko, A. A. Shishkin, A. V. Zolotukhin, C. D. Beidler, J. Kißlinger, H. Maaßberg, F. Rau, H. Wobig, B. A. Carreras, N. Dominguez, and V. E. Lynch, "Progress in the Studies of URAGAN-2M Stability and Transport Properties"
B. A. Carreras, "Transport Mechanisms Acting in Toroidal Devices: A Theoretician's View"

L. Garcia, B. A. Carreras, V. E. Lynch, and P. H. Diamond, "Poloidal Flow Generation by Resistive Pressure-Gradient-Driven Turbulence"

J. H. Harris, J. B. Wilgen, J. D. Bell, M. Murakami, B. A. Carreras, S. C. Aceto, L. R. Baylor, T. S. Bigelow, R. J. Colchin, J. L. Dunlap, N. Dominguez, G. R. Dyer, A. C. England, G. R. Hanson, R. C. Isler, T. C. Jernigan, J.-N. Leboeuf, D. K. Lee, K. M. Likin, J. F. Lyon, C. H. Ma, D. A. Rasmussen, K. A. Sarksyan, M. Sato, M. G. Shats, C. E. Thomas, and J. J. Zielinski, "Fluctuation Studies of ECH Plasmas in the ATF Torsatron"

S. P. Hirshman, W. A. Cooper, S. Merazzi, and R. Gruber, "Numerical Three Dimensional Equilibria with Pressure Anisotropy"

M. Murakami, T. S. Bigelow, B. A. Carreras, R. A. Dory, J. B. Wilgen, L. R. Baylor, G. R. Dyer, A. C. England, D. P. Hutchinson, R. C. Isler, T. C. Jernigan, H. Ji, C. H. Ma, S. Morimoto, O. Motojima, D. A. Rasmussen, M. Sato, W. R. Wing, H. Yamada, and the ATF Group, "Transport Studies Using Modulation of Dimensionless Parameters in the Advanced Toroidal Facility"

July

Electric Power Research Institute Fusion Study Panel Meeting, Redwood City, California, July 6, 1992

Y-K. M. Peng and J. Sheffield, "EPRI Fusion Study Panel—The Spherical Torus Reactor"

Amm. Inst. Aeronaut. Astrnaut./Soc. Automat. Eng./Am. Soc. Mech. Eng./Am. Soc. for Engineering Education (AIAA/SAE/ASME/ASEE) 28th Joint Propulsion Conference and Exhibit, Nashville, Tennessee, July 6–8, 1992. Proceedings published

J. H. Whealton, D. A. Kirkman, and R. J. Raridon, "Electrostatic Ion Thruster Optics Calculations"

Europhysics Topical Conference on RF Heating and Current Drive of Fusion Devices, Brussels, Belgium, July 7–10, 1992. Abstracts published in *Europhys. Conf. Abstr.*

F. W. Baity, D. B. Batchelor, W. L. Gardner, R. H. Goulding, D. J. Hoffman, E. F. Jaeger, P. M. Ryan, J. DeGrassie, C. C. Petty, R. I. Pinsker, and R. Prater, "Comparison of Single and Double Tier Faraday Shields to Operation Without a Shield on DIII-D"

D. B. Batchelor, F. W. Baity, M. D. Carter, R. H. Goulding, E. F. Jaeger, P. M. Ryan, and D. C. Stallings, "Effect of Geometry and Plasma Parameters on Phased ICRF Antenna Array Characteristics for Heating and Current Drive"

C. C. Petty et al., "Direct Electron Absorption of Fast Waves on the DIII-D Tokamak"

Presentations at the Physics Department of the University of California at San Diego, San Diego, California, July 13, 1992

B. A. Carreras, "Poloidal Flow Profile Modification by Turbulence"

B. A. Carreras, V. E. Lynch, J.-N. Leboeuf, J. B. Drake, D. W. Walker, P. C. Liewer, and G. Tomaschke, "Impact of High Performance Computing on Tubulence Calculations"

Workshop on the IGNITRO Project, Turin, Italy, July 13–15, 1992. Presentations published

W. A. Houlberg, "Ignitor Plasma Modeling"

S. L. Milora (presented by W. A. Houlberg), "ORNL Pellet Injector Development Program Relevance to the IGNITOR Project"

DOE Fusion Computing Council Vail Workshop, Vail, Colorado, July 20–22, 1992

J.-N. Leboeuf and V. E. Lynch, "BDX and NETCDF"

Fifth Latin American Workshop on Plasma Physics, Mexico City, Mexico, July 20–31, 1992 Proceedings published by World Scientific Publishing Company

N. Dominguez and N. D. Vergara, "Review of Stellarator Research: In Search of the 'Magic Magnetic Bottle'"

August

Presentation to T-Division, Los Alamos National Laboratory, Los Alamos, New Mexico, August 10, 1992
K. L. Sidikman, "Drift Wave Turbulence at Long Wavelengths"

Ion Cyclotron Range of Frequency (ICRF) Modeling and Theory Workshop, Princeton Plasma Physic Laboratory, Princeton, New Jersey, August 17–18, 1992
D. B. Batchelor, "ICRF System for SSAT"
D. B. Batchelor, M. D. Carter, E. F. Jaeger, P. M. Ryan, D. C. Stallings, and B. Ho, "3D Antenna Modeling"
E. F. Jaeger, D. B. Batchelor, M. Murakami, R. C. Goldfinger, D. A. Ramussen, C. K. Phillips, and J. R. Wilson, "Full Wave Modelling of Direct Electron Heating by Ion Cyclotron Waves on TFTR"
E. F. Jaeger, D. B. Batchelor, and D. C. Stallings, "Full Wave Simulations of Fast Wave Current Drive on Advanced Tokamaks"

1992 Applied Superconductivity Conference, Chicago Illinois, August 23–28, 1992. Proceedings published in *IEEE Transactions on Magnetics*
J. W. Lue, L. Dresner, and S. W. Schwenterly, "Investigating Thermal Hydraulic Quenchback in a Cable-in-Conduit Superconductor"
J. W. Lue, M. S. Lubell, J. N. Luton, B. J. Frame, and F. L. Paulaskas, "The Fabrication and Test of High Current Density Cable-in-Conduit Test Coils"
S. W. Schwenterly, J. W. Lue, and C. H. Joshi, "Critical Current Measurements on a Ag/Bi-Pb-Sr-Ca-Cu-O Composite Coil as a Function of Temperature and External Magnetic Field"

Cursos de Verano de la Universidad Complutense, El Escorial, Spain, August 24–28, 1992
B. A. Carreras, "Transport Mechanisms Acting in Toroidal Devices: An Introduction. Lecture I"
B. A. Carreras, "Transport Mechanisms Acting in Toroidal Devices: An Introduction. Lecture II"

Fusión Nuclear por Confinamiento Magnético, Madrid, Spain, August 24–28, 1992. Abstract published
B. A. Carreras, "Mecanismos de Transporte en Plasmas Confinados Magneticamente"

September

ITER Home Team Meeting, Oak Ridge, Tennessee, September 1, 1992
W. A. Houlberg, S. E. Attenberger, and M. J. Grapperhaus, "Modeling Analysis of ITER Performance"

U.S. International Thermonuclear Experimental Reactor (ITER) National Meeting, Fusion Engineering Design Center, Oak Ridge, Tennessee, September 1–2, 1992
E. F. Jaeger, D. B. Batchelor, and D. C. Stallings, "Full Wave Simulations of Fast Wave Current Drive on ITER"
D. A. Spong (presented by J.-N. Leboeuf), "ITER Neutral Beam TAE Stability Studies"

International Atomic Energy Agency (IAEA) Technical Committee Meeting, Montreal, Canada, September 8–10, 1992. Proceedings published by International Atomic Energy Agency
T. Uckan, R. C. Isler, T. C. Jernigan, J. F. Lyon, P. K. Mioduszewski, M. Murakami, D. A. Rasmussen, J. B. Wilgen, S. C. Aceto, and J. J. Zielinski, "Biasing Experiments on the Advanced Toroidal Facility (ATF)"

Presentations at the University of Wisconsin, Madison, Wisconsin, September 11, 1992
B. A. Carreras, "Poloidal Flow Profile Modification by Turbulence"

17th Symposium on Fusion Technology (SOFT), Rome, Italy, September 14–18, 1992. Proceedings published

C. A. Foster, W. A. Houlberg, M. J. Gouge, S. L. Milora, A. Geraud, and M. Chatelier, "ORNL Centrifuge Pellet Fueling System"

A. Frattolillo, M. Gasparotto, S. Migliori, F. Scaramuzzi, G. Angelone, M. Baldarelli, G. Ronci, S. K. Combs, S. L. Milora, C. R. Foust, M. J. Gouge, A. Reggiori, G. Riva, R. Carlevaro, and G. B. Daminelli, "High-Speed Repetitive Pellet Injector Prototype for Magnetic Confinement Fusion Devices"

M. J. Gouge, L. R. Baylor, M. J. Cole, S. K. Combs, G. R. Dyer, D. T. Fehling, P. W. Fisher, C. R. Foust, R. A. Langley, S. L. Milora, A. L. Qualls, J. B. Wilgen, G. L. Schmidt, G. W. Barnes, and R. G. Persing, "Tritium Pellet Injector for TFTR"

R. H. Goulding, D. J. Hoffman, P. M. Ryan, V. Bhatnagar, G. Bosia, and T. J. Wade, "A Power Compensation System for Phased Operation of the JET A_2 Antenna Arrays"

J. F. Lyon, S. L. Painter, and M. J. Crouse, "Assessment of Stellarators as Reactors"

S. L. Milora, M. J. Gouge, B. E. Argo, L. R. Baylor, M. J. COle, S. K. Combs, D. T. Fehling, P. W. Fisher, C. A. Foster, C. R. Foust, A. L. Qualls, D. E. Schechter, D. O. Sparks, C. C. Tsai, and J. H. Whealton, "Pellet Injector Development at ORNL"

Y-K. M. Peng, R. J. Colchin, D. W. Swain, D. B. Batchelor, T. S. Bigelow, C. L. Hedrick, J. T. Hogan, W. A. Houlberg, E. F. Jaeger, J. F. Monday, P. K. Mioduszewski, D. A. Spong, J. A. White, S. E. Attenberger, J. D. Galambos, D. J. Strickler, B. E. Nelson, P. J. Fogarty, P. L. Goranson, D. J. Taylor, D. E. Williamson, P. Bonoli, S. Luckhardt, S. Bernabei, R. Pauletti, J. Blevins, and J. Stringer, "Small Steady-State Tokamak for Divertor Testing"

DIII-D Technical Planning Workshop, General Atomics, San Diego, California, September 15, 1992

B. A. Carreras, "TTF Needs From DIII-D"

IEA Workshop on Intense Neutron Sources, Karlsruhe, Germany, September 21, 1992

M. J. Saltmarsh, "The High Intensity D-LI Source"

Workshop on Pellet Injectors, Frascati Energy Research Centre, ENEA, Frascati, Italy, September 21–22, 1992. Abstracts published

C. A. Foster, C. C. Tsai, D. E. Schechter, and J. H. Whealton, "Electron-Beam Rocket Pellet Accelerator"

C. A. Foster, "ORNL Centrifuge Pellet Fueling System"

W. A. Houlberg, S. E. Attenberger, and M. J. Grapperhaus, "ITER Pellet Fueling Scenarios"

S. L. Milora, S. K. Combs, C. R. Foust, M. J. Gouge, L. R. Baylor, P. W. Fisher, A. L. Qualls, G. L. Schmidt, and D. T. Fehling, "Pneumatic Pellet Injector Research at ORNL"

43rd Aeroballistic Range Association Meeting, Columbus, Ohio, September 28–October 2, 1992. Proceedings published

M. J. Gouge, L. R. Baylor, S. K. Combs, P. W. Fisher, C. R. Foust, and S. L. Milora, "Tritium Pellet Injector for the Tokamak Fusion Test Reactor"

14th Internation Atomic Energy Agency (IAEA) International Conference on Plasma Physics and Controlled Nuclear Fusion Research, Würzburg, Germany, September 30–October 7, 1992. Proceedings published in *IAEA Book of Extended Synopses*

C. Z. Cheng, G. Y. Fu, H. E. Mynick, R. Budny, R. B. White, S. J. Zweben, C. T. Hsu, D. J. Sigmar, D. A. Spong, B. A. Carreras, and C. L. Hedrick, "Alpha Effects on TAE Modes and Alpha Transport"

P. H. Diamond, V. Shapiro, V. Schevchenko, Y.-B. Kim, M. N. Rosenbluth, B. A. Carreras, K. L. Sidikman, V. E. Lynch, L. Garcia, P. W. Terry, and R. Z. Sagdeev, "Self-Regulated Shear Flow Turbulence in Confined Plasmas: Basic Concepts and Potential Applications to the L → H Transition"

P. H. Diamond, V. Shapiro, V. Schevchenko, Y.-B. Kim, M. N. Rosenbluth, B. A. Carreras, K. L. Sidikman, V. E. Lynch, L. Garcia, P. W. Terry, and R. Z. Sagdeev, "Self-Regulation of Fluctuation Levels and Transport by Generation of Sheared Electric Fields"

L. Garcia, B. A. Carreras, V. E. Lynch, and P. H. Diamond, "Poloidal Flow Generation by Resistive Pressure-Gradient-Driven Turbulence"

J. H. Harris, G. R. Hanson, J. B. Wilgen, J. D. Bell, M. Murakami, B. A. Carreras, L. R. Baylor, S. C. Aceto, T. S. Bigelow, R. J. Colchin, J. L. Dunlap, N. Dominguez, G. R. Dyer, A. C. England, R. C. Isler, T. C. Jernigan, J.-N. Leboeuf, D. K. Lee, J. F. Lyon, C. H. Ma, A. L. Qualls, D. A. Rasmussen, C. E. Thomas, T. Uckan, J. Zielinski, M. G. Shats, K. M. Likin, K. A. Sarksyan, and L. M. Kovrizhnykh, "Fluctuation Studies of ECH Plasmas in the ATF Torsatron and the IMS Stellerator"

M. Kotschenreuther, B. A. Carreras, et al., "Simulations for Confinement in Near Fusion Experiments"

P. K. Mioduszewski, J. T. Hogan, L. W. Owen, and T. Uckan, "Particle Balance in Tore Supra With Controlled Particle Exhaust"

M. Murakami, R. A. Dory, T. S. Bigelow, B. A. Carreras, J. B. Wilgen, S. C. Aceto, L. R. Baylor, G. R. Dyer, A. C. England, J. H. Harris, H. C. Howe, D. P. Hutchinson, T. C. Jernigan, H. Ji, C. H. Ma, S. Morimoto, O. Motojima, D. A. Rasmussen, M. Sato, W. R. Wing, H. Yamada, J. J. Zielinski, and the ATF Group, "Dimensionless Scaling of Confinement in ATF"

D. D. Schnack, Y. L. Ho, B. A. Carreras, K. L. Sidikman, G. G. Craddock, N. Mattor, R. A. Nebel, S. C. Prager, P. W. Terry, and E. J. Zita, "Advances in Reversed Field Pinch Theory and Computation," text: published in *Plasma Physics and Controlled Nuclear Fusion Research 1992*

K. C. Shaing, S. E. Attenberger, P. J. Christenson, N. Dominguez, S. P. Hirshman, and W. A. Houlberg, "Nonlinear Poloidal Density Variation in Tokamak Plasmas"

D. J. Sigmar, F. Y. Gang, C. T. Hsu, D. A. Spong, C. L. Hedrick, J.-N. Leboeuf, B. A. Carreras, H. Biglari, and P. H. Diamond, "Nonlinear Gyrofluid and Hybrid Fluid/Particle Models of Fast Ion-Alfven Wave Interactions"

P. W. Terry, D. E. Newman, H. Biglari, R. Naxikian, P. H. Diamond, V. Lebedev, Y. Liang, V. Shapiro, V. Schevchenko, B. A. Carreras, K. Sidikman, L. Garcia, G. G. Craddock, J. Crotinger, and A. E. Koniges, "Non-Local Transport Phenomena and Long Wavelength Turbulence in Tokamaks"

4th International Colloquium on Atomic Spectra and Oscillator Strengths for Astrophysical and Laboratory Plasmas, Gaithersburg, Maryland, September 14–17, 1992

R. A. Phaneuf, "Critical Assessment of Atomic Collision Cross-Section Data for Fusion Plasma Applications," invited

VIth International Conference on the Physics of Highly Charged Ions, Manhattan, Kansas, Sept. 28–Oct. 2, 1992. Proceedings published in *AIP Conf. Proc.* **274**, *VIth International Conference on the Physics of Highly Charged Ions,* ed. P. Richard, M. Stockli, C. L. Cocke, and C. D. Lin, AIP, New York, 1993

X. Q. Guo, E. W. Bell, J. S. Thompson, G. H. Dunn, M. E. Bannister, R. A. Phaneuf, and A. C. H. Smith, "Backscattering in Electron-Impact Excitation of Multiply Charged Ions," invited

C. C. Havener, M. A. Haque, A. C. H. Smith, X. Urbain, and P. A. Zeijlmans van Emmichoven, "Low-Energy Measurements of Electron Capture by Multicharged Ions from Excited Hydrogen Atoms," invited

I. G. Hughes, C. C. Havener, S. H. Overbury, M. T. Robinson, D. M. Zehner, P. A. Zeijlmans van Emmichoven, and F. W. Meyer, "Incident Ion Charge State Dependence of Electron Emission During Slow Multicharged Ion-Surface Interactions"

F. W. Meyer, J. Burgdorfer, I. G. Hughes, S. H. Overbury, D. M. Zehner, and P. A. Zeijlmans van Emmichoven, "Neutralization of Slow Multicharged Ions Above a Cesiated Au Surface"

N. Stolterfoht, K. Sommer, F. Fremont, X. Husson, D. Lecler, J. K. Swenson, C. C. Havener, and F. W. Meyer, "Electron Correlation Effects in Collisions of Slow, Highly Charged Ions with Atoms," invited

P. A. Zeijlmans van Emmichoven, C. C. Havener, I. G. Hughes, D. M. Zehner, and F. W. Meyer, "Analysis of Low Energy Electron Emission Arising During Slow Multicharged Ion-Surface Interactions"

October

12th International Vacuum Congress, The Hague, Netherlands, October 12–16, 1992. Proceedings published
R. A. Langley and P. LaMarche, "Vacuum Pumping for Future Fusion Devices"

IAEA Technical Committee Meeting on Atomic and Molecular Data for Fusion Reactor Technology, Cadarache, France, October 12–16, 1992
R. A. Phaneuf, "Status of Atomic and Molecular Collisional Databases," invited
D. R. Schultz, M. I. Kirkpatrick, and R. A. Phaneuf, "Compilation of Atomic Data for Fusion by the ORNL Controlled Fusion Atomic Data Center"
R. A. Phaneuf and D. Post, "Atomic and Molecular Data Issues and Needs for Power and Particle Control and Plasma Diagnostics"

Eighth Joint Workshop on Electron Cyclotron Emission and Electron Cyclotron Resonance Heating, Gut Ising, Lake Chiemsee, Munich, Germany, October 19–21, 1992. Proceedings published as *Proceedings of EC-8 Conference,* IPP Report III/186, 1993
T. S. Bigelow, "Plans for Improvements to the ATF ECH System"

Edge (Fluctuations) Transport and Turbulence Workshop, Austin Texas, October 27–28, 1992
L. A. Charlton, "Radiative Condensation"
J.-N. Leboeuf and L. A. Charlton, "Ionization-Driven Drift Waves"

45th Annual Gaseous Electronics Conference, Boston, Massachusetts, Oct. 27–30, 1992
F. W. Meyer, I. G. Hughes, S. H. Overbury, D. M. Zehner, and P. A. Zeijlmans van Emmichoven, "Above-Surface Neutralization of Multicharged Ions Incident on a Cesiated Au Target"

November

Twelth International Conference on the Application of Accelerators in Research and Industry, Denton, Texas, Nov. 2–5, 1992
I. G. Hughes, "Depth Profiling of Deuterium Using Nuclear Reaction Analysis"

U.S.–Japan Bilateral Workshop, Minato-ku, Japan, November 4–6, 1992
D. J. Hoffman, "ICRF Technology Development Collaborations"

39th National American Vacuum Society (AVS) Symposium and Topical Conferences, Chicago, Illinois, November 9–13, 1992. Proceedings published
R. A. Langley, "Vacuum Equipment Needs for Research: A National Laboratory Perspective"
C. C. Tsai, C. A. Foster, S. L. Milora, D. E. Schechter, and J. H. Whealton, "Electron-Beam Rocket Acceleration on Hydrogen Pellets"

U.S.–Japan Workshop on Theory of High β Plasmas, General Atomics, San Diego, California, November 11–13, 1992
D. A. Spong, "High β Effects and Nonlinear Evolution of the TAE Instability"

59th Meeting of the Southeastern Section of the American Physical Society, Oak Ridge, Tennessee, Nov. 12–14, 1992
M. A. Haque, A. Sahibzada, P. A. Zeijlmans van Emmichoven, and C. C. Havener, "Low-Energy Measurements of Electron Capture by Multicharged Ions from Excited Hydrogen Atoms"

Supercomputing 1992, Minneapolis Convention Center, Minneapolis, Minnesota, November 16–20, 1992. Proceedings published as *Proceedings of Supercomputing '92*

V. E. Lynch, B. A. Carreras, J. B. Drake, J.-N. Leboeuf, and P. Liewer, "Performance of a Plasma Fluid Code on the INTEL Parallel Computers"

34th Annual Meeting on the American Physical Society, Division of Plasma Physics (APS/DPP), Seattle, Washington, November 16–20, 1992. Abstracts published in *Bull. Am. Phys. Soc.* 37(6) (1992)

S. C. Aceto, J. D. Bell, K. A. Connor, J. C. Glowienka, R. C. Isler, M. Murakami, J. G. Schwelberger, T. Uckan, and J. J. Zielinski, "Heavy Ion Beam Probe Measurements on ATF"

S. E. Attenberger, K. C. Shaing, S. P. Hirshman, and W. A. Houlberg, "Poloidal Variation of Tokamak Plasma Density"

F. W. Baity, D. B. Batchelor, K. C. Bills, C. H. Fogelman, E. F. Jaeger, J. L. Ping, B. W. Riemer, P. M. Ryan, D. C. Stallings, D. J. Taylor, and J. J. Yugo, "Design of Long-Pulse Fast-Wave Current Drive Antennas for DIII-D"

L. R. Baylor, G. L. Schmidt, F. C. Jobes, G. W. Hammett, S. L. Milora, D. K. Owens, H. Park, and J. E. Stevens, "Local Transport in Pellet-Fueled, ICRF-Heated Discharges in TFTR"

T. S. Bigelow, G. R. Hanson, J. B. Wilgen, I. Collazo, E. Mazzucato, M. McCarthy, and S. Raftopoulos, "Design of a Reflectometer System for Measurement of the Plasma Edge Density Profile on TFTR"

B. A. Carreras, V. E. Lynch, and L. Garcia, "Resistive Pressure-Gradient-Driven Turbulence with Self-Consistent Flow Profile Evolution"

M. D. Carter, G. R. Haste, F. W. Baity, and D. J. Hoffman, "Modeling of a Folded Waveguide"

J. B. O. Caughman, D. J. Hoffman, and R. H. Goulding, "ARC Detection and Protection in High-Power Antenna Systems"

L. A. Charlton, B. A. Carreras, and P. H. Diamond, "Parallel Flow Gradient Driven Instability"

P. J. Christenson, N. Dominguez, and K. C. Shaing, "Tokamak Equilibrium with Steady Poloidal Flows"

R. J. Colchin, S. C. Aceto, A. C. England, R. C. Isler, M. Murakami, D. A. Rasmussen, T. Uckan, J. B. Wilgen, and J. J. Zielinski, "Plasma Profile Modifications in ATF Using Magnetic Field Perturbations"

R. J. Colchin and AEA Fusion, "Results from the START Low Aspect Ratio Tokamak"

I. Collazo-Lopez, G. R. Hanson, J. B. Wilgen, T. S. Bigelow, C. E. Thomas, R. Nazikian, M. McCarthy, and E. Mazzucato, "Preliminary Results of the ORNL Swept Dual-Frequency X-Mode Reflectometer for TFTR"

K. A. Connor, S. C. Aceto, J. G. Schwelberger, and J. J. Zielinski, "Plans for Upgrades to the Heavy Ion Beam Probe Diagnostic on ATF"

E. C. Crume, Jr., P. J. Christenson, and K. C. Shaing, "Ion Collisionality and L-H Transition in Tokamaks"

N. Dominguez, C. L. Hedrick, J.-N. Leboeuf, and L. Garcia, "Dissipative Trapped Electron Mode Turbulence with Ion Landau Damping and FLR Effects"

R. A. Dory, J. H. Harris, and S. V. Kaye, "Wavelet Analysis of ELM Signals from PBX-M Tokamak"

C. A. Foster, C. C. Tsai, D. E. Schechter, and J. H. Whealton, "Electron-Beam Rocket Pellet Accelerator"

W. L. Gardner, F. W. Baity, R. H. Goulding, D. J. Hoffman, D. A. Rasmussen, P. M. Ryan, D. E. Schechter, and D. J. Taylor, "Comparison of Candidate ICRF Faraday Shield Materials"

R. C. Goldfinger, D. B. Batchelor, C. K. Phillips, R. Budny, G. W. Hammett, J. C. Hosea, D. M. McCune, J. E. Stevens, J. R. Wilson, and the TFTR Team, "DT Simulation of ICRF Heated Supershots in TFTR using TRANSP"

R. H. Goulding, D. B. Batchelor, D. J. Hoffman, E. F. Jaeger, P. M. Ryan, D. C. Stallings, V. Bhatnagar, G. Bosia, A. S. Kaye, and T. J. Wade, "Phased Operation of the JET A_2 Antenna Arrays"

M. Grapperhaus, W. A. Houlberg, and S. E. Attenberger, "Pellet Fueling Options for ITER"

J. H. Harris, M. Murakami, and R. A. Dory, "Enhanced Energy Confinement in the ATF Torsatron"

G. R. Haste, G. Agarici, A. Becoulet, B. Beaumont, H. Kuus, and B. Saoutic, "High-Power, Long-Pulse ICRF in Tore Supra"

C. L. Hedrick, J.-N. Leboeuf, and D. A. Spong, "Landau Fluid Model of Alpha-Alfvén Waves, Including Velocity Dependent Drift"

S. P. Hirshman and F. M. Levinton, "Equilibrium Analysis Incorporating the Motional Stark Effect Diagnostic"

Y. L. Ho, W. Grossmann, A. T. Drobot, M. D. Carter, P. M. Ryan, and D. B. Batchelor, "3D ICRH Antenna Modeling Using ARGUS"

D. J. Hoffman, F. W. Baity, E. Barbato, G. C. Barber, T. S. Bigelow, M. D. Carter, J. B. O. Caughman, W. L. Gardner, R. H. Goulding, G. R. Haste, P. E. Jones, and M. Ono, "The Folded Waveguide Tests on RFTF and Conceptual Designs for Tokamaks"

J. T. Hogan, L. W. Owen, P. K. Mioduszewski, M. Chatelier, and T. Loarer, "A Detailed Model for Core-Wall Particle Exchange in Tore Supra Particle Control Experiments"

J. T. Hogan and J. Wesley, "A Divertor Parameter Scaling Database for TPX-class Devices"

J. T. Hogan and C. C. Klepper, "BBQ: A Monte Carlo Carbon Transport Code"

W. A. Houlberg and S. E. Attenberger, "Transient Current Profile Behavior in TPX"

E. F. Jaeger, D. B. Batchelor, M. Murakami, R. C. Goldfinger, D. A. Rasmussen, C. K. Phillips, and J. R. Wilson, "Full-Wave Modelling of Direct Electron Heating by Ion Cyclotron Waves on TFTR"

T. C. Jernigan, B. A. Carreras, R. A. Dory, J. H. Harris, R. C. Isler, J. F. Lyon, P. K. Mioduszewski, M. Murakami, D. A. Rasmussen, M. J. Saltmarsh, and J. Sheffield, "ATF Program After Restart"

R. A. Langley, M. J. Gouge, and D. J. Santeler, "Vacuum System Design of the ITER Pellet Fueling System"

J.-N. Leboeuf, B. A. Carreras, and L. A. Charlton, "Drift Thermal Instability with Sheared Poloidal Flow"

D. K. Lee, S. P. Hirshman, and H. Fishman, "Determination of MHD Equilibrium Properties from Magnetic Measurements"

V. E. Lynch, B. A. Carreras, J. B. Drake, J.-N. Leboeuf, and P. Liewer, "Performance of a Plasma Fluid Code on the INTEL Hypercubes"

V. E. Lynch, B. A. Carreras, J. B. Drake, J.-N. Leboeuf, P. Liewer, and E. Huang, "Performance of a Plasma Fluid Code on the INTEL Parallel Computers"

J. F. Lyon, "Assessment of Stellarators as Reactors"

C. H. Ma, D. P. Hutchinson, and J. Irby, "Feasibility Study of an Infrared Polarimeter for ITER"

M. Murakami, D. A. Rasmussen, D. B. Batchelor, T. S. Bigelow, I. Collazo, R. C. Goldfinger, G. R. Hanson, D. J. Hoffman, E. F. Jaeger, J. B. Wilgen, G. W. Hammett, J. C. Hosea, R. Majeski, C. K. Phillips, J. H. Rogers, G. Schilling, S. C. Scott, J. E. Stevens, G. Taylor, J. R. Wilson, M. C. Zarnstorff, and F. G. Rimini, "ICRF Direct Electron Heating Experiments in TFTR"

L. W. Owen, J. T. Hogan, C. C. Klepper, P. K. Mioduszewski, T. Uckan, M. Chatelier, and T. Loarer, "Comparison of Inner Wall Pumping and Pump Limiter Exhaust in Tore Supra"

Y-K. M. Peng, R. J. Colchin, D. W. Swain, P. T. Bonoli, and S. C. Luckhardt, "Small Steady-State Tokamak (TST) Plasma for Testing Advanced Divertors"

M. Porkolab, D. B. Batchelor, P. T. Bonoli, M. Fenstermacher, R. Goldston, S. Jardin, G. H. Neilson, W. M. Nevins, J. Ramos, and the TPX Physics Team, "Physics Design and Noninductive Current Drive Options in a Steady State Advanced Tokamak"

A. L. Qualls, L. R. Baylor, S. K. Combs, G. R. Dyer, P. W. Fisher, M. J. Gouge, S. L. Milora, D. K. Owens, G. L. Schmidt, and J. B. Wilgen, "Deuterium Pellet Injection Experiments on TFTR"

A. L. Qualls, L. R. Baylor, J. B. Wilgen, S. K. Combs, G. R. Dyer, P. W. Fisher, M. J. Gouge, S. L. Milora, G. L. Schmidt, D. K. Owens, and D. K. Mansfield, "Pellet Ablation and Particle Deposition Studies on TFTR"

D. A. Rasmussen, R. H. Goulding, T. D. Shepard, D. J. Hoffman, F. W. Baity, R. J. Colchin, R. C. Isler, C. E. Thomas, M. R. Wade, and M. Kwon, "Ion Cyclotron Heating Experiments (ICRF) on the Advanced Toroidal Facility (ATF) with an Asymmetric Resonant Double Loop (ARDL) Antenna"

R. K. Richards, C. H. Ma, and D. P. Hutchinson, "Applications of an ITER CO_2 Laser Thomson Scattering Alpha Particle Diagnostic on Nonburning Plasma Experiments"

G. A. Riggs, K. L. Sidikman, B. A. Carreras, and P. W. Terry, "Radial Structure of Drift Wave Turbulence"

P. M. Ryan, F. W. Baity, R. H. Goulding, D. J. Hoffman, D. W. Swain, and J. H. Whealton, "Comparison of One vs Two Poloidal Straps for High Frequency ICRH Antenna Arrays"

R. O. Sayer, Y-K. M. Peng, S. C. Jardin, A. G. Kellman, and J. C. Wesley, "TSC Plasma Halo Simulation of a DIII-D Vertical Displacement Episode"

G. L. Schmidt, D. K. Mansfield, D. Mikkelsen, R. Wilson, L. R. Baylor, and S. L. Milora, "Combined Deuterium-Tritium Pellet + TF + NBI Scenario"

K. C. Shaing and C. T. Hsu, "The Effects of Shock Phenomenon on L-H Transition and MARFE Formation in Tokamaks"

M. G. Shats, J. H. Harris, K. M. Likin, J. B. Wilgen, J. D. Bell, L. R. Baylor, C. H. Ma, and K. A. Sarksyan, "Microwave Scattering Measurements of Density Fluctuations in ATF"

K. L. Sidikman, B. A. Carreras, L. Garcia, and P. H. Diamond, "Calculations of Drift Wave Turbulence in the Presence of a Radial Electric Field Profile"

D. A. Spong, C. L. Hedrick, and B. A. Carreras, "Nonlinear Models of the Energetic Particle Destabilized TAE Mode"

D. C. Stallings, M. D. Carter, and D. B. Batchelor, "Effect of Antenna Design Parameters upon RF Antenna Performance"

D. W. Swain, F. W. Baity, D. B. Batchelor, R. H. Goulding, D. J. Hoffman, E. F. Jaeger, P. M. Ryan, and D. C. Stallings, "Optimization of Fast Wave Current Drive Systems"

N. A. Uckan, J. T. Hogan, D. J. Sigmar, and U.S. ITER Home Team, "U.S. ITER Plasma Physics R&D Program: Confinement, Operational Limits, and Alpha Particle Physics"

T. Uckan, B. Richards, R. D. Bengtson, B. A. Carreras, G. X. Li, H. Lin, P. Hurwitz, W. L. Rowan, H. Y. W. Tsui, and A. J. Wootton, "Active Probing of Plasma Edge Turbulence on the Text Tokamak"

J. H. Whealton and R. J. Raridon, "The Electrohydrodynamical Ion Source: A Case Study of Self-Consistent Multiple Spatial Scale Plasma"

J. B. Wilgen and The ATF Group, "Fluctuation and Modulation Transport Studies in the ATF Torsatron"

J. J. Zielinski, S. C. Aceto, R. C. Colchin, K. A. Connor, A. C. England, R. C. Isler, M. Murakami, J. G. Schwelberger, T. Uckan, and J. B. Wilgen, "Potential Profile Measurements During Perturbation Coil Experiments on ATF"

December

Tokamak Physics Experiment (TPX) Physics Workshop, Lawrence Livermore National Laboratory, Livermore, CA, December 8–10, 1992

D. B. Batchelor, "ICRF System Physics"

W. A. Houlberg and S. E. Attenberger, "TPX Fueling Study"

3rd Annual International Workshop on Solvent Substitution, Phoenix, AZ, December 8–11, 1992

C. A. Foster, P. W. Fisher, C. C. Tsai, and D. E. Schechter, "A Centrifuge Accelerator CO_2 Pellet Cleaning System"

17th International Conference on Infrared and Millimeter Waves, Pasadena, CA, December 14, 1992. Conference digest published by SPIE

T. S. Bigelow, G. R. Hanson, R. L. Livesey, J. B. Wilgen, I. Collazo, E. J. Doyle, T. L. Rhodes, J. DeGrassie, and R. Phelps, "An ICRF Antenna Edge Plasma Density Profile Diagnostic for DIII-D"

C. H. Ma, D. P. Hutchinson, and J. Irby, "Calibration of an Infrared Polarimeter for ALCATOR C-MOD"

U.S.–Japan Workshop on Non-Inductive Current Drive and Profile Control, Princeton, New Jersey, December 14–16, 1992. Abstracts published

D. B. Batchelor, M. D. Carter, E. F. Jaeger, P. M. Ryan, D. C. Stallings, and B. Ho, "Modeling in 2D and 3D of Antenna Arrays for Fast Wave Current Drive"

R. H. Goulding, F. W. Baity, D. J. Hoffman, P. M. Ryan, C. C. Petty, R. I. Pinsker, G. Bosia, and T. J. Wade, "Design, Control, and Operation of Phased Antenna Arrays for FWCD Experiments"

E. F. Jaeger, D. B. Batchelor, and M. Murakami, "Global Wave Modeling of Electron Interactions with Fast Magnetosonic Waves"

R. K. Richards, "A CO_2 Laser Thomson Scattering Alpha Particle Diagnostic"

Presentation at the General Physics Institute, Moscow, Russia, December 18, 1992
J. H. Harris, "Confinement and Fluctuations in the ATF Torsatron"

Presentation at General Atomics, San Diego, CA, December 20, 1992
B. A. Carreras, "Fluctuations and Poloidal Flow Profile Modification"

1992 REPORTS

ORNL Reports

L. Dresner, *Design Considerations for a 1-kWh Energy Storage Magnet,* ORNL/HTSPC-2, January 1992
L. Dresner, *Preliminary Deseign of the Astronautics Refrigerator Magnets,* June 1992
L. Dresner, *Protection of a Test Magnet Wound with a Ag/BSCCO High-Temperature Superconductor,* June 1992
Ye. P. Velikhov, G. A. Yeliseyev, V. D. Ryutov, and N. S. Cheverev, *Principal Results of Research in the Area of Controlled Thermonuclear Synthesis (CTS) and Plasma Physics in the USSR During the Period Extending From July of 1990 Through July of 1991,* ORNL/OLS-92/18

ORNL Technical Memoranda

S. C. Aceto, L. R. Baylor, J. D. Bell, T. S. Bigelow, A. C. England, J. H. Harris, R. C. Isler, T. C. Jernigan, J. F. Lyon, C. H. Ma, P. K. Mioduszewski, M. Murakami, D. A. Rasmussen, J. B. Wilgen, J. J. Zielinski, *Effects of Limiter Biasing on the ATF Torsatron,* ORNL/TM-12075, September 1992
D. B. Batchelor and M. D. Carter, *An Outgoing Energy Flux Boundary Condition for Finite Difference ICRF Antenna Models,* ORNL/TM-12248, November 1992
J. F. Lyon and S. L. Painter, *Assessment of Torsatrons as Reactors,* ORNL/TM-12189, December 1992

Reports published by other institutions

W. A. Houlberg, S. E. Attenberger, L. R. Baylor, M. Gadeberg, T. C. Jernigan, P. Kupschus, S. L. Milora, G. L. Schmidt, D. W. Swain, and M. L. Watkins, "Pellet Penetration Experiments on JET"
T. E. Shannon and the FMIF Working Group, *Fusion Materials Irradiation Facility Requirements Document*
J. Sheffield, J. W. Davis, B. G. Logan, D. B. Montgomery, F. Najmabadi, G. A. Navratil, S. C. Prager, P. H. Rutherford, K. F. Schoenberg, A. M. Todd, J. C. Wesley, A. J. Wootton, and D. B. Batchelor, *Final Report of the New Initiatives Task Force*
N. A. Uckan, J. T. Hogan, D. J. Sigmar, and the U.S. ITER Home Team, *U.S. ITER Plasma Physics R&D Program: Confinement, Operational Limits, and Alpha Particle Physics,* Lawrence Livermore National Laboratory, Livermore, Calif., 1992
T. Uckan, T. Loarer, M. Chatelier, and P. K. Mioduszewski, *Plasma Effects on the Particle Collection Characteristics of the Tore Supra Modular Pump Limiter,* Cadarache, France, 1992

1993 BOOKS AND JOURNAL ARTICLES

S. E. Attenberger and W. A. Houlberg, "Extension of PEP Modes in Tokamaks to Steady-State," *Bull. Am. Phys. Soc.* 38(10), 2049 (1993)

N. R. Badnell, D. C. Griffin, T. W. Gorczyca, and M. S. Pindzola, "Breakdown of the Isolated-Resonance Approximation for the Electron-Impact Excitation of Positive Ions," *Phys. Rev. A* 48, R2519 (1993)

N. R. Badnell and M. S. Pindzola, "Resonance Contribution to the Electron-Impact Ionization of Few-Electron Highly Charged Ions," *Phys. Rev. A* 47, 2937 (1993)

N. R. Badnell, M. S. Pindzola, W. J. Dickson, H. P. Summers, D. C. Griffin, and J. Lang, "Electric Field Effects on Dielectronic Recombination in a Collisional-Radiative Model," *Astrophys. J.* 407, L91 (1993)

F. W. Baity, G. C. Barber, J. S. Degrassie, R. H. Goulding, C. C. Petty, R. I. Pinsker, and D. O. Sparks, "Transmission Line and Decoupler Testing for the DIII-D FWCD System," *Bull. Am. Phys. Soc.* 38(10) (Suppl.: *35th Annual Division of Plasma Physics of the American Physical Society Meeting, St. Louis, MO, November 1–5, 1993*), 2107 (1993)

D. B. Batchelor, L. A. Berry, E. F. Jaeger, K. C. Shaing, and J. C. Whitson, "2D Modeling of Power Deposition in Inductively Coupled Plasma Sources for Materials Processing," *Bull. Am. Phys. Soc.* 38(10), 2122 (1993)

D. B. Batchelor, D. W. Swain, E. F. Jaeger, M. D. Carter, D. C. Stallings, D. J. Hoffman, J. J. Yugo, M. Porkolab, P. T. Bonoli, P. Moroz, J. Scharer, U. Wisconsin, and T. K. Mau, "Ion Cyclotron Heating and Current Drive on TPX," *Bull. Am. Phys. Soc.* 38(10), 2049 (1993)

G. L. Bell, J. B. Wilgen, and R. F. Gandy, "Third-Harmonic Electron Cyclotron Emission Measurements on the Advanced Toroidal Facility," *Nucl. Fusion* 33(6), 875 (1993)

J. D. Bell, J. H. Harris, J. L. Dunlap, N. A. Crocker, and V. K. Paré, "Signal Analysis of Fluctuations in Toroidal Fusion Plasmas," *Rev. Sci. Instrum.* 64 , 2428–33 (1993)

S. Bernabei, S. P. Hirshamn, D. K. Lee,.et al., "Experimental exploration of profile control in the Princeton Beta Experiment-Modified (PBX-M) Tokamak," *Phys. Fluids B* 5, 2562–70 (1993)

L. A. Berry, C. A. Foster, M. S. Lubell, W. D. Nelson, J. A. Rome, J. Sheffield, and T. L. White, "Fusion Spin-Offs, An Important Part of the Oak Ridge National Laboratory Fusion Program," *J. Fusion Energy* 12(4), 393–94 (1993)

T. S. Bigelow, C. H. Fogelman, D. J. Hoffman, M. D. Carter, P. M. Ryan, S. N. Golovato, and P. Bonoli, "A Folded Waveguide ICRF Launcher for Alcator C-Mod," *Bull. Am. Phys. Soc.* 38(10), 2107 (1993)

J. Botero, ed., *International Bulletin on Atomic and Molecular Data for Fusion*, Vols. 46 and 47, 1993

J. Burgdörfer and F. W. Meyer, "Image Acceleration of Multiply Charged Ions by Metallic Surfaces," *Phys. Rev. A* 47, R20 (1993)

B. A. Carreras, "Long Wavelength Drift Wave Turbulence," *Phys. Fluids B* 5(5), 1491–1505 (1993)

B. A. Carreras, P. H. Diamond, and Y.-M. Liang, "Dynamics of the Transition to Enhanced Confinement Regimes in Magnetically Confined Plasmas," *Bull. Am. Phys. Soc.* 38(10), 1910 (1993)

B. A. Carreras, N. Dominguez, V. E. Lynch, N. T. Besedin, I. M. Pandratov, and A. A. Shishkin, "Stability Properties of the URAGAN-2M Torsatron," *Fusion Technol.* 23(1), 71–78 (1993)

B. A. Carreras, V. E. Lynch, and L. Garcia, "Effect of a Poloidal Shear Flow on the Probability of Accessing the Multiple Saturated States in the Resistive Interchange Instability," *Phys. Fluids B* 5(6), 1795–1803 (1993)

M. D. Carter, D. B. Batchelor, and D. C. Stallings, "Three Dimensional Antenna Modeling Using RANT3D," *Bull. Am. Phys. Soc.* 38(10), 2105 (1993)

J. B. O. Caughman, G. L. Bell, W. L. Gardner, and D. J. Hoffman, "The Erosion of Faraday Shield Coatings Due to RF Sheaths," *Bull. Am. Phys. Soc.* 38(10), 2107 (1993)

J. B. O. Caughman and W. M. Holber, "The Effects of Substrate Bias Frequency in an Electron Cyclotron Resonance Plasma Reactor," *J. Vac. Sci. Technol. A* 11(6), 2897–2902 (1993)

L. A. Charlton, B. A. Carreras, J. N. Leboeuf, and V. E. Lynch, "Radiation Driven Turbulence at the Plasma Edge of Toroidal Devices," *Bull. Am. Phys. Soc.* 38(10), 1912 (1993)

L. A. Charlton and J.-N. Leboeuf "Effects of Diamagnetic Drift and Compressibility on Linear Resistive Magnetohydrodynamic Stability of Stellarators," *Phys. Fluids B* 5(8), 2989–98 (1993)

R. J. Colchin, S. C. Aceto, A. C. England, R. C. Isler, M. Murakami, D. A. Rasmussen, T. Uckan, J. B. Wilgen, and J. J. Zielinski, "Plasma Profile Modifications Using Magnetic Field Perturbations in the ATF Torsatron," *Nucl. Fusion* 33(2), 323–32 (1993)

R. J. Colchin, P. G. Carolan, R. Duck, T. Edlington, S. K. Erents, J. Ferreira, S. J. Fielding, K. Gibson, D. H. J. Goodall, M. Gryaznevich, T. C. Hender, J. Hugill, I. Jenkins, J. Li, S. J. Manhood, B. J. Parham, D. C. Robinson, M. Singleton, A. Sykes, T. N. Todd, M. F. Turner, M. Valovic, M. Walsh, and H. R. Wilson, "The Small Tight Aspect Ratio Tokamak Experiment," *Phys. Fluids B* 5(7), 2481–84 (1993)

R. J. Colchin, M. R. Wade, C. E. Thomas, S. C. Aceto, J. A. Rome, A. C. England, and R. H. Fowler, "Fast Ion Behavior During Neutral Beam Injection in ATF," *Bull. Am. Phys. Soc.* 38(10), 2021 (1993)

I. Collazo-López, G. R. Hanson, J. B. Wilgen, T. S. Bigelow, D. A. Rasmussen, M. Murakami, C. E. Thomas, B. Grek, and J. R. Wilson, "Detailed Analysis of Differential Phase Reflectometer Measurements on TFTR," *Bull. Am. Phys. Soc.* 38(10), 2033 (1993)

S. K. Combs "Pellet Injection Technol.," *Rev. Sci. Instrum.* 64(7), 1679–98 (1993)

E. C. Crume, Jr., and K. C. Shaing, "Theoretical Comparisons of Tokamak and Stellarator H-mode," *Bull. Am. Phys. Soc.* 38(10), 1928 (1993)

A. Dawson, M. S. Lubell, et al., "Magnet Engineering I," *Fusion Technol.* 23, 119 (1993)

N. Djuric, E. W. Bell, X. Q. Guo, G. H. Dunn, R. A. Phaneuf, M. E. Bannister, M. S. Pindzola, and D. C. Griffin, "Absolute Cross Sections for Electron-Impact Single Ionization of Si^{+} and Si^{2+}," *Phys. Rev. A* 47, 4786 (1993)

R. A. Dory, M. Murakami, and the ATF Team, "Offset-Linear Energy Confinement Scaling in the ATF Torsatron," *Bull. Am. Phys. Soc.* 38(10), 2020 (1993)

L. Dresner, "Error Source in Cable-in-Conduit Conductors by Time of Flight," *Cryogenics* 33(10), 962–65 (1993)

L. Dresner, "Reducing the Quench Pressure by Perforating the Jacket of a Cable-in-Conduit Superconductor," *Cryogenics* 33(10), 958–61 (1993)

L. Dresner, "Stability and Protection of Ag/BSCCO Magnets Operated in the 20–40 K Range," *Cryogenics* 33(9), 900–09 (1993)

L. Dresner, "Thermomechanical Flow of He-II Through Porous Bodies," *Cryogenics* 33(9), 842–45 (1993)

J. L. Dunlap, J. H. Harris, M. F. Corneliussen, W. M. Davis, T. F. Gibney, S. M. Kaye, P. G .Roney, and S. S. Sesnic, "PBX-M Fluctuations from Mirnov Coil Diagnostics," *Bull. Am. Phys. Soc.* 38(10), 2094 (1993)

A. C. England, R. Bell, S. P. Hirshman, R. Kaita, S. Kaye, H. Kugel, D. K. Lee, B. Leblanc, M. Okabayashi, and Y. Sun, "Scaling of the Neutron Source Strength with Shaping and Plasma Parameters in PBX," *Bull. Am. Phys. Soc.* 38(10), 2092 (1993)

J. D. Galambos, Y-K. M. Peng, L. J. Perkins, S. Haney, and J. Mandrekas, "Impact of Improved Physics on Commercial Tokamak Reactors," *Bull. Am. Phys. Soc.* 38(10), 2050 (1993)

F. Y. Gang and J.-N. Leboeuf, "Mode Coupling Effects on Alpha-Particle-Driven Long Wavelength Alfvén Wave Instability," *Phys. Fluids B* 5, 2736–38 (1993)

F. Y. Gang, D. J. Sigmar, and J.-N. Leboeuf, "Mode Coupling Effects on Alpha Particle Driven Long-Wavelength Alfvén Instabilities," *Bull. Am. Phys. Soc.* 38(10), 2075 (1993)

L. M. Gomes and P. N. Stevens, "Use of Monte Carlo Procedures to Estimate First and Second Collision Sources for Discrete Ordinates Transport Codes," *Nucl. Sci. Eng.* 114, 228–37 (1993)

S. M. Gorbatkin, R. F. Burgie, W. C. Oliver, J. C. Barbour, T. M. Mayer, and M. L. Thomas, "Boron Nitride Thin Film Deposition Using Electron Cyclotron Resonance Microwave Plasmas," *J. Vac. Sci. and Technol. A* 11(4), 186369 (1993)

R. H. Goulding, D. J. Hoffman, P. M. Ryan, V. Bhatnagar, M. Bures, J. A. Dobbing, D. F. H. Start, and T. J. Wade, "Automatic Matching and Phase Control of Multiple Element ICRF Antennas," *Bull. Am. Phys. Soc.* 38(10), 2107 (1993)

D. C. Griffin, M. S. Pindzola, and N. R. Badnell, "Low-Energy Total and Differential Cross Sections for the Electron-Impact Excitation of Si^{2+} and Ar^{6+}," *Phys. Rev. A* 47, 2871 (1993)

X. Q. Guo, E. W. Bell, J. S. Thompson, G. H. Dunn, M. E. Bannister, R. A. Phaneuf, and A. C. H. Smith, "Evidence for Significant Backscattering in Near-Threshold Electron-Impact Excitation of $Ar^{7+}(3s \rightarrow 3p)$," *Phys. Rev. A* **47**, R9 (1993)

G. R. Hanson, J. B. Wilgen, T. S. Bigelow, I. Collazo, D. A. Rasmussen, D. B. Batchelor, D. J. Hoffman, E. F. Jaeger, M. Murakami, P. M. Ryan, D. C. Stallings, and J. R. Wilson, "Edge Density Profile Measurements in Front of an ICRF Antenna," *Bull. Am. Phys. Soc.* **38**(10), 2033 (1993)

C. C. Havener, M. A. Haque, A. C. H. Smith, X. Urbain, and P. A. Zeijlmans van Emmichoven, "Low-Energy Measurements of Electron Capture by Multicharged Ions from Excited Hydrogen Atoms," *AIP Conf. Proc.* **274**, 43–52 (1993)

C. L. Hedrick, J.-N. Leboeuf, and K. L. Sidikman, "Landau Fluid Equations for Dissipative Trapped Electron Mode, Including Ion Magnetic Drift," *Bull. Am. Phys. Soc.* **38**(10), 2101 (1993)

S. P. Hirshman, "Calculation of β_I and ℓ_i for Three-Dimensional Plasma Configurations," *Phys. Fluids B* **5**, 3119–21 (1993)

S. P. Hirshman, D. K. Lee, F. Levinton, S. Batha, M. Okabayashi, and R. M. Weiland, "Equilibirum Reconstruction Using Motional Stark Effect Data on PBX-M and TFTR," *Bull. Am. Phys. Soc.* **38**(10), 2038 (1993)

D. J. Hoffman, J. B. O. Caughman, G. L. Bell, F. W. Baity, R. H. Goulding, and D. A. Rasmussen, "Protection for Ion Cyclotron Heating and Current Drive Systems," *Bull. Am. Phys. Soc.* **38**(10), 2106 (1993)

J. T. Hogan, D. Guilhem, C. Klepper, and W. Hess, "Heat Deposition, Impurity Generation and Transport Calculations for Tore Supra Inner Wall Discharges," *Bull. Am. Phys. Soc.* **38**(10), 1918 (1993)

J. T. Hogan and N. A. Uckan, "Stable Operational Space for ITER Design Variants," *Bull. Am. Phys. Soc.* **38**(10), 2124 (1993)

I. G. Hughes, R. Behrisch, and A. P. Martinelli, "Depth Profiling of Deuterium Using Nuclear Reaction Analysis," *Nucl. Instrum. Methods Phys. Res.* **B79**, 487 (1993)

I. G. Hughes, J. Burgdörfer, L. Folkerts, C. C. Havener, S. H. Overbury, M. T. Robinson, D. M. Zehner, P. A. Zeijlmans van Emmichoven, and F. W. Meyer, "Separation of Kinetic and Potential Electron Emission Arising from Slow Multicharged Ion-Surface Interactions," *Phys. Rev. Lett.* **71**, 291 (1993)

R. Ito, T. Tabata, T. Shirai, and R. A. Phaneuf, *Analytic Cross Sections for Collisions of H, H_2, He and Li Atoms and Ions with Atoms and Molecules, I.*, JAERI-M, 93-117, 1993

E. F. Jaeger, D. B. Batchelor, and D. C. Stallings, "Influence of Various Physics Phenomena on Fast Wave Current Drive in Tokamaks," *Nucl. Fusion* **33**(2), 179–196 (1993)

E. F. Jaeger, M. Murakami, D. B. Batchelor, J. R. Wilson, R. Majeski, and C. K. Phillips, "Full Wave ICRF Modeling for D-T Experiments on TFTR," *Bull. Am. Phys. Soc.* **38**(10), 2034 (1993)

R. K. Janev, R. A. Phaneuf, H. Tawara, and T. Shirai, "Recommended Cross Sections for State-Selective Electron Capture in Collisions of C^{6+} and O^{8+} Ions with Atomic Hydrogen," *Atomic Data and Nuclear Data Tables* **55**, 201 (1993)

T. C. Jernigan, L. R. Baylor, S. K. Combs, C. R. Foust, S. L. Milora, J. Phillips, and R. T. Snider, "Performance of a Repeating Pellet Injector for DIII-D," *Bull. Am. Phys. Soc.* **38**(10), 2065 (1993)

J. L. Johnson, D. A. Monticello, A. H. Reiman, A. Salas, A. L. Fraguas, S. P. Hirshman, "Comparison of ATF and TJ-II Stellarator Equilibria as Computed by the 3-D VMEC and PIES Codes," *Computer Phys. Communications* **77**, 1–10 (1993)

F. Kazeminezhad, J.-N. Leboeuf, F. Brunel, and J. M. Dawson, "A Discrete Model for MHD Incorporating the Hall Term," *J. Comput. Phys.* **104**, 398–417 (1993)

C. C. Klepper, T. E. Evans, G. Haas, G. L. Jackson, and R. Maingi, "Neutral Pressure Studies with a Fast Ionization Gauge in the Divertor Region of the DIII-D Tokamak," *J. Vac. Sci. Technol. A* **11**(2), 446–50 (1993)

C. C. Klepper, W. R. Hess, J. T. Hogan, D. Guilhem, R. Guirlet, T. Loarer, S. J. Tobin, and T. Uckan, "Direct Measurement of Chemical Sputtering at the Neutralizer Plate of the Tore Supra Pump Limiter," *Bull. Am. Phys. Soc.* **38**(10), 2058 (1993)

C. C. Klepper, J. T. Hogan, D. N. Hill, R. Maingi, L. W. Owen, D. Buchenauer, L. L. Lao, M. A. Mahdavi, and M. J. Schaffer, "Divertor Neutral Pressure Enhancement with a Baffle in DIII-D," *Nucl. Fusion* **33**(4), 533–45 (1993)

R. L. Klueh and D. J. Alexander, "Low-Chromium Reduced-Activation Ferritic Steels for Fusion," *ANS Transactions* **69**, 191 (1993)

L. E. Lagos, W. Li, M. A. Ebadian, T. L. White, R. G. Grubb, and D. Foster, Jr., "Heat Transfer Within a Concrete Slab With a Finite Microwave Heating Source," *J. Heat Transfer*, HTD-Vol. 259 , 135–42, ASME (1993)

R. A. Langley and P. LaMarche, "Vacuum Pumping Requirement Considerations for Future Fusion Devices," *J. Nucl. Mater.* **200**, 326–31 (1993)

J.-N. Leboeuf, L. A. Charlton, and B. A. Carreras, "Shear Flow Effects on the Nonlinear Evolution of Thermal Instabilities," *Phys. Fluids B* **5**, 2959–66 (1993)

J.-N. Leboeuf, D. B. Geohegan, C. L. Liu, R. F. Wood, J. B. Drake, and D. W. Walker, "Modeling of Plasma Dynamics in Laser Ablation Processes," *Bull. Am. Phys. Soc.* **38**(10), 1900 (1993)

J.-N. Leboeuf, C. L. Hedrick, K. L. Sidikman, B. A. Carreras, and R. D. Sydora, "Dissipative Trapped Electron Mode Turbulence with Ion Landau Damping, FLR and Magnetic Drift Effects," *Bull. Am. Phys. Soc.* **38**(10), 2014 (1993)

D. K. Lee, S. P. Hirshman, M. Okabayashi, and Y. Sun, "Rapid Reconstruction of Tokamak MHD Equilibrium from Experimental Measurements," *Bull. Am. Phys. Soc.* **38**(10), 2093 (1993)

W. Li, M. A. Ebadian, T. L. White, R. G. Grubb, and D. Foster, Jr., "Heat Transfer in a Contaminated Porous Concrete Slab Subjected to Microwave Heating," *J. Heat Transfer*, ASME 1993

W. Li, M. A. Ebadian, T. L. White, and R. G. Grubb, "Heat Transfer Within a Concrete Slab Applying the Microwave Decontamination Process," *J. Heat Transfer*, HTD-Vol. 115 , 42–50, ASME (1993)

W. Li, M. A. Ebadian, T. L. White, R. G. Grubb, and D. Foster, Jr., "The Effect of Steel Reinforcement on Heat and Mass Transfer in a Porous Concrete Slab Subjected to Microwave Heating," *Heat Transfer Digest*, ASME 1993

W. Li, M. A. Ebadian, T. L. White, R. G. Grubb, and D. Foster, "The Effect of Steel Reinforcement on Temperature and Pressure Within a Porous Concrete Slab Subjected to Microwave Heating," *J. Heat Transfer*, HTD-Vol. 240, ASME (1993)

J. W. Lue, M. S. Lubell, et al., "Investigation of Thermal Hydraulic Quenchback in a Cable-in-Conduit Superconductor," *IEEE Trans. on Appl. Supercond.* **3**, 338 (1993)

V. E. Lynch, B. A. Carreras, J. B. Drake, J.-N. Leboeuf, and B. Curtis, "The Performance of a Fluid Code on Parrallel Computers," *Bull. Am. Phys. Soc.* **38**(10), 2015 (1993)

V. E. Lynch, B. A. Carreras, J.-N. Leboeuf, B. C. Curtis, and R. L. Troutman, "Multi-CPU Plasma Fluid Turbulence Calculations on a CRAY Y-MP C90," p. 308 in *Proceedings of Supercomputing '93, Portland, Oregon, November 15–19, 1993*, IEEE Computer Society Press, Los Alamitos, Calif., 1993

J. F. Lyon and K. Gulec, "Assessment of Stellarators as Reactors," *Bull. Am. Phys. Soc.* **38**(10), 2023 (1993)

F. W. Meyer, L. Folkerts, I. G. Hughes, S. H. Overbury, D. M. Zehner, and P. A. Zeijlmans van Emmichoven, "Work-Function Dependence of Above-Surface Neutralization of Multicharged Ions," *Phys. Rev. A* **48**, 4479 (1993)

F. W. Meyer, C. C. Havener, and P. A. Zeijlmans van Emmichoven, "Above-Surface Neutralization of Slow N^{6+} Ions during Interactions with a Cu(001) Target," *Phys. Rev. A* **48**, 4476 (1993)

A. M. Nasreldin, M. M. Ghoneim, F. H. Hammad, R. L. Klueh, and R. K. Nanstad, "Effect of Tempering on the Toughness of a Cr-Mo Bainitic Steel," *J. Materials Engineering and Performance* **2**, 413 (1993)

L. W. Owen, P. K. Mioduszewski, T. Loarer, M. Chatelier, and D. Guilhem, "Transport Analysis of a Vented Limiter for Tore Supra," *Bull. Am. Phys. Soc.* **38**(10), 2058 (1993)

Y-K. M. Peng and E. T. Cheng, "Magnetic Fusion Driven Transmutation of Nuclear Waste (FTW)," *J. Fusion Energy* **12**(4), 381–84 (1993)

R. A. Phaneuf, "Critical Assessment of Atomic Collision Cross-Section Data for Fusion Plasma Applications," *Physica Scripta* **T47**, 124 (1993)

C. K. Phillips, W. A. Houlberg, D. Q. Hwang, S. E. Attenberger, J. Tolliver, and L. Hively, "A Predictive Transport Modeling Code for ICRF-Heated Tokamaks," *Plasma Phys. Controlled Fusion* **35**(3), 301 (1993)

M. S. Pindzola, "Parity-Violation Effects on the Auger-Electron Emission from Highly Charged Atomic Ions," *Phys. Rev. A* **47**, 4856 (1993)

M. S. Pindzola, T. W. Gorczyca, and C. Bottcher, "Two-Photon Ionization of Lithium in the Time-Dependent Hartree-Fock Approximation," *Phys. Rev. A* **47**, 4982 (1993)

M. S. Pindzola, D. R. Schultz, and D. C. Griffin, "Quantal and Classical Differential-Scattering Calculations for the Electron-Impact Excitation of Argon Ions," *Phys. Rev. A* **48**, 4333 (1993)

D. E. Post and R. A. Phaneuf, "Atomic and Molecular Data: Status and Requirements," INDC(NDS)-277, 9 (1993)

R. Prater, R. A. James, C. C. Petty, R. I. Pinsker, M. Porkolab, F. W. Baity, S. C. Chiu, J. S. DeGrassie, R. H. Goulding, R. W. Harvey, D. J. Hoffman, H. Ikezi, H. Kawashima, Y. R. Lin-Liu, T. C. Luce, and V. Trukhin, "Current Drive With Fast Waves, Electron Cyclotron Waves, and Neutral Injection in the DIII-D Tokamak," *Plasma Phys. Controlled Fusion* **35**, A53–A70 (1993)

A. L. Qualls, C. A. Foster, L. R. Baylor, S. L. Milora, and D. E. Schechter, "Pellet Feed System Upgrade for the Tore Supra Centrifuge Pellet Injector," *Bull. Am. Phys. Soc.* **38**(10), 2057 (1993)

D. A. Rasmussen, S. C. Aceto, D. B. Batchelor, R. H. Goulding, D. J. Hoffman, E. F. Jaeger, D. K. Lee, and J. A. Rome, "Ion Cyclotron Heating Antenna Designs for the Advanced Toroidal Facility (ATF)," *Bull. Am. Phys. Soc.* **38**(10), 2107 (1993)

R. K. Richards, D. P. Hutchinson, C. A. Bennett, H. T. Hunter, and C. H. Ma, "Measurement of CO_2 Laser Small Angle Thomson Scattering on a Magnetically Confined Plasma," *Appl. Phys. Lett.* **62**, 28 (1993)

J. A. Rome, *Stellarator News* (25), January 1993

J. A. Rome, *Stellarator News* (27), May 1993

J. A. Rome, R. H. Fowler, J. F. Lyon, J. Sheffield, and J. D. Hanson, "Modular Stellarator Configuration Studies," *Bull. Am. Phys. Soc.* **38**(10), 2023 (1993)

J. S. Sarff, S. Assadi, A. F. Almagri, M. Cekic, D. J. Den Hartog, G. Fiksel, S. A. Hokin, H. Ji, S. C. Prager, W. Shen, K. L. Sidikman, M. R. Stoneking, "Nonlinear Coupling of Tearing Fluctuations in the Madison Symmetric Torus," *Phys. Fluids B* **5**, 2540–45 (1993)

R. O. Sayer, Y-K. M. Peng, S. C. Jardin, A. G. Kellman, and J. C. Wesley, "TSC Plasma Halo Simulation of a DIII-D Vertical Displacement Episode," *Nucl. Fusion* **33**(7), 969–78 (1993)

D. R. Schultz, "Towards an Elastic and Momentum Transfer Cross Section Data Base for 1 to 1000 eV Collisions Involving A^{q+} + H, H_2 and He," INDC(NDS)-274, 23 (1993)

D. R. Schultz, "Status and Activities of the ORNL Controlled Fusion Atomic Data Center, 1992," INDC(NDS)-275, 37 (1993)

K. C. Shaing, "Test of Tokamak Low-Mode–High-Mode Transition Theory in Stellarators," *Phys. Fluids B* **5**, 3841–43 (1993)

K. C. Shaing, "Suppression of Turbulent Fluctuations in Tokamaks," *Phys. Fluids B* **5**, 2122–24 (1993)

K. C. Shaing and P. J. Christenson, "Ion Collisionality and L-H Transition in Tokamaks," *Phys. Fluids B* **5**, 666–68 (1993)

K. C. Shaing and C. T. Hsu, "Convective Momentum Transport, Shock Viscosity, and the L-H Transition in Tokamaks," *Phys. Fluids B* **5**(8), 2981–88 (1993)

K. C. Shaing and C. T. Hsu, "Effects of Ion Diamagnetic Flow on Shock Formation in Poloidally Rotating Tokamak Plasmas," *Phys. Fluids B* **5**, 3596–3602 (1993)

K. C. Shaing and C. T. Hsu, "H-mode Bifurcation with Shock and Radial Electric Profile in Tokamaks," *Bull. Am. Phys. Soc.* **38**(10), 1928 (1993)

K. L. Sidikman, C. L. Hedrick, J.-N. Leboeuf, and B. A. Carreras, "Radially-Resolved Slab Calculations of Dissipative Trapped Electron Modes with Ion Magnetic Drift," *Bull. Am. Phys. Soc.* **38**(10), 2101 (1993)

R. N. Singh and S. J. Zinkle, "Defect Accumulation in Pure FCC Metals in the Transient Regime," *J. Nucl. Mater.* **206**, 212–29 (1993)

L. L. Snead, "Development of Silicon Carbide Composite for Fusion," *Fusion Technol.* **24**, 65–82 (1993)

L. L. Snead and R. A. Vessey, "A Moving Belt Divertor Concept," *Fusion Technol.* **24**, 83–96 (1993)

D. A. Spong, B. A. Carreras, and C. L. Hedrick, "Nonlinear Gyrofluid Models of Shear Alfvén Instabilities in Tokamaks and Stellarators," *Bull. Am. Phys. Soc.* **38**(10), 1986 (1993)

D. W. Swain, J. J. Yugo, D. B. Batchelor, C. H. Fogelman, S. E. Shipley, and E. Fredd, "Design of the Ion Cyclotron System for TPX," *Bull. Am. Phys. Soc.* **38**(10), 2107 (1993)

R. D. Sydora, J. M. Dawson J. N. Leboeuf, "Comparison of Electron Dynamic Models in 3D Gyrokinetic Simulation of Toroidal Plasmas," *Bull. Am. Phys. Soc.* **38**(10), 2099 (1993)

C. C. Tsai, C. A. Foster, S. L. Milora, D. E. Schechter, and J. H. Whealton, "Electron-Beam Rocket Acceleration of Hydrogen Pellets," *J. Vac. Sci. Technol. A* **11**(4), 1252–57 (1993)

C. C. Tsai, H. H. Haselton, W. D. Nelson, D. E. Schechter, L. M. Thompson, V. B. Campbell, A. L. Glover, and J. M. Googin, "Plasma Surface Cleaning Using Microwave Plasmas," *Bull. Am. Phys. Soc.* **38**(10), 1901 (1993)

N. A. Uckan and the U.S. ITER Home Team, "Confinement Capability of ITER-EDA," *Bull. Am. Phys. Soc.* **38**(10), 2050 (1993)

M. Ulrickson, D. N. Hill, R. Campbell, W. A. Houlberg, D. Ruzic, D. P. Stotler, and K. Werley, "Power and Particle Control for TPX," *Bull. Am. Phys. Soc.* **38**(10), 2049 (1993)

J. H. Whealton, R. J. Raridon, and R. G. Cowan, "Self-Consistent Plasma Edge Calculations for Divertor Plasmas," *Bull. Am. Phys. Soc.* **38**(10), 1921 (1993)

D. P. White, "The Effect of Ionizing and Displacive Radiation on Thermal Conductivity of Alumina," *J. Appl. Phys.* **73**(5), 2254 (1993)

J. B. Wilgen, G. R. Hanson, E. De La Luna, V. Zhuravlev, J. H. Harris, J. Sanchez, and R. Kaita, "An A.M. Reflectometer on PBX-M for Edge Density Profile Measurements," *Bull. Am. Phys. Soc.* **38**(10), 2096 (1993)

J. B. Wilgen, M. Murakami, J. H. Harris, T. S. Bigelow, R. A. Dory, B. A. Carreras, S. C. Aceto, D. B. Batchelor, L. R. Baylor, G. L. Bell, J. D. Bell, R. J. Colchin, E. C. Crume, N. Dominguez, J. L. Dunlap, G. R. Dyer, A. C. England, R. F. Gandy, J. C. Glowienka, R. C. Goldfinger, R. H. Goulding, G. R. Hanson, C. Hidalgo, S. Hiroe, S. P. Hirshman, L. D. Horton, H. C. Howe, D. P. Hutchinson, R. C. Isler, T. C. Jernigan, H. Ji, H. Kaneko, L. M. Kovizhnykh, M. Kwon, R. A. Langley, D. K. Lee, K. M. Likin, J. F. Lyon, C. H. Ma, M. M. Menon, P. K. Mioduszewski, O. Motoiima, H. Okada, S. Paul, A. L. Qualls, D. A. Rasmussen, R. K. Richards, J. A. Rome, M. J. Saltmarsh, K. A. Sarksyan, M. Sato, J. G. Schwelberger, K. C. Shaing, M. G. Shats, T. D. Shepard, J. E. Simpkins, C. E. Thomas, T. Uckan, K. L. Vander Sluis, M. R. Wade, W. R. Wing, H. Yamada, and J. J. Zielinski, "Fluctuation and Modulation Transport Studies in the Advanced Toroidal Facility (ATF) Torsatron," *Phys. Fluids B* **5**, 2513–18 (1993)

P. A. Zeijlmans van Emmichoven, M. E. Bannister, D. C. Gregory, C. C. Havener, R. A. Phaneuf, E. W. Bell, X. Q. Guo, J. S. Thompson, and M. Sataka, "Electron Impact Ionization of Si^{6+} and Si^{7+}," *Phys. Rev. A* **47**, 2888 (1993)

P. A. Zeijlmans van Emmichoven, C. C. Havener, I. G. Hughes, D. M. Zehner, and F. W. Meyer, "Emission of Low Energy Electrons from Multicharged Ions Interacting with Metal Surfaces," *Phys. Rev. A* **47**, 3998 (1993)

S. J. Zinkle, P. L. Maziasz, and R. E. Stoller, "Dose Dependence of the Microstructural Evolution in Neutron-Irrated Austenitic Stainless Steel," *J. Nucl. Mater.* **206**, 266–86 (1993)

1993 PRESENTATIONS

January

Sixth Boulder Workshop on High Power Ion Cyclotron Range of Frequency (ICRF) Antenna Design and Physics, Boulder, CO, January 20–22, 1993

D. B. Batchelor, "ICRF Issues for High Density, High Field Tokamaks"

U.S.–Japan Workshop, Transient Phenomena and Transport in Toroidal Plasmas, San Diego, California, January 20–22, 1993

J. H. Harris, R. A. Dory, S. Kaye, et al., "Wavelet Analysis: A Tool for Transient Phenomena, Joint Study of H_a Signals From the PBX-M Tokamak"

U.S. International Thermonuclear Experimental Reactor (ITER) Home Team Meeting, San Diego, California, January 25–26, 1993

D. B. Batchelor and E. F. Jaeger, "Global Wave Modeling of Fast Wave Current Drive in ITER-R"

W. A. Houlberg and S. E. Attenberger, "1-1/2-D ITER Transport Simulations"

Fusion Power Associates Annual Meeting and Symposium, La Jolla, California, January 28–29, 1993. Proceedings published in *J. Fusion Energy*

J. Sheffield, "Looking Beyond ITER: Toroidal Concept Improvement"

February

Workshop on Alpha Physics and Tritium Issues in Large Tokamaks, Princeton Plasma Physics Laboratory, Princeton, New Jersey, February 17–19, 1993

D. A. Spong, "Nonlinear Gyrofluid Simulation of TAE Instabilities in TFTR"

Sixth Transport Task Force Workshop, Newport, Rhode Island, February 21–25, 1993. Abstracts published

B. A. Carreras, "Fluctuations and Poloidal Flow Profile Modification"

R. A. Dory, M. Murakami, the ATF Team, U. Gasparino, G. Kühner, H. Maaβberg, H. Ringler, U. Stroth, and the W7AS Team, "Confinement Scaling for Stellarators: Initial Comparisons with Bohm and Gyro-Bohm Scaling for a Joint ATF–W7-AS Database"

J. H. Harris, J. B. Wilgen, J. D. Bell, L. R. Baylor, C. H. Ma, the ATF Group, M. G. Shats, K. M. Likin, and K. A. Sarksyan, "Microwave Scattering Measurements of Density Fluctuations in the ATF Torsatron"

W. A. Houlberg and S. E. Attenberger, "Evaluation of the Critical Gradient Model: Numerical Implementation"

D. A. Spong and A. Weller, "Global and Toroidicity-Induced Shear Alfvén Instabilities in Tokamaks and Stellarators"

T. Uckan, B. Richards, R. D. Bengtson, B. A. Carreras, D. B. Crockett, K. W. Gentle, G. X. Li, P. D. Hurwitz, W. L. Rowan, H. Y. W. Tsui, and A. J. Wootton, "Observations From the First Active Probing of Plasma Edge Tubulence and Feedback Experiments on TEXT"

March

JET Joint Undertaking Seminar, Abingdon, England, March 3, 1993

S. L. Milora, "Pellet Injector Technology at ORNL and Possible Pellet Injection Collaborations with JET"

Seminar at National Institute for Fusion Studies, Nagoya, Japan, March 5, 1993
J. F. Lyon, "The U.S. Stellarator Program"

Internal Japanese Workshop, National Institute for Fusion Studies, Nagoya, Japan, March 8, 1993
J. F. Lyon, "Stellarator Reactor Studies"
J. F. Lyon for J. A. Rome, "Coil Design Considerations for Stellarator Reactors"

Briefing for U.S. Technical Advisory Committee (TAC) International Thermonuclear Experimental Reactor (ITER) Members, Atlanta, Georgia, March 10, 1993
N. A. Uckan and the U.S. ITER Home Team, "ITER EDA Design: Confinement Capability"

1993 International Sherwood Fusion Theory Conference, Newport, Rhode Island, March 28–31, 1993. Proceedings published as *1993 International Sherwood Fusion Theory Conference Proceedings*
M. D. Carter, D. B. Batchelor, and D. C. Stallings, "Three Dimensional Effects for Radio Frequency Antenna Modeling"
L. A. Charlton, B. A. Carreras, and P. H. Diamond, "Parallel Flow Gradient Driven Instability"
E. C. Crume, Jr., K. C. Shaing, and C. T. Hsu, "Convective Momentum Transport, Shock Viscosity, and the L-H Transition in Tokamaks"
N. Dominguez, K. C. Shaing, and C. T. Hsu, "Resonance Parallel Viscosity in the Banana Regime in Poloidally Rotating Tokamak Plasmas"
R. C. Goldfinger, D. B. Batchelor, C. K. Phillips, R. Budny, G. W. Hammett, J. C. Hosea, D. M. McCune, J. E. Stevens, J. R. Wilson, and the TFTR Team, "DT Simulation of ICRF Heated Supershots in TFTR using TRANSP"
C. L. Hedrick, J.-N. Leboeuf, and D. A. Spong, "Global Alpha-Alfvén Wave Dispersion Relation and Rosetta Stone"
W. A. Houlberg and S. E. Attenberger, "Fuel and Helium Confinement in Fusion Reactors"
C. T. Hsu, K. C. Shaing, R. P. Gormley, and D. J. Sigmar, "Bootstrap Current Induced by Neutral Beam Injection"
E. F. Jaeger, D. B. Batchelor, and M. Murakami, "Global Wave Modeling of Electron Interactions with Fast Magnetosonic Waves"
J.-N. Leboeuf and R. D. Sydora, "Gyrokinetic iδ Particle Model of Dissipative Trapped Electron Mode Turbulence"
V. E. Lynch, B. A. Carreras, B. Curtis, J. B. Drake, and J.-N. Leboeuf, "A Comparison of the Performance of a Fluid Code on the C90 and the iPSC/860"
J. A. Rome, "Exploration of Stellarator Orbit Topology Using J^{**}"
K. C. Shaing and C. T. Hsu, "Effects of Ion Diamagnetic Flow on Shock Formation in Poloidally Rotating Tokamak Plasmas"
K. L. Sidikman, B. A. Carreras, L. Garcia, and P. H. Diamond, "Nonlinear Damping of Drift Waves by Strong Flow Curvature"
D. A. Spong, C. L. Hedrick, and B. A. Carreras, "Nonlinear Gyrofluid Models of Shear Alfvén Instabilities in Ignited and Beam Heated Toroidal Plasmas"

TPX Conceptual Design Review, Princeton, New Jersey, March 29–31, 1993
D. B. Batchelor, M. D. Carter, R. H. Goulding, D. J. Hoffman, E. F. Jaeger, P. M. Ryan, D. W. Swain, J. S. Tolliver, J. J. Yugo, J. C. Hosea, S. M. Kaye, C. K. Phillips, J. R. Wilson, T. K. Mau, and J. E. Scharer, "ICRF Physics"
D. B. Batchelor, M. D. Carter, D. J. Hoffman, E. F. Jaeger, P. M. Ryan, D. C. Stallings, D. W. Swain, M. Porkolab, and J. E. Scharer, "Plasma Physics Basis for TPX Antenna Design"

Numerical Tokamak Second Annual Symposium, Newport, Rhode Island, March 31–April 1, 1993
J.-N. Leboeuf, "Gyro-Landau Fluid Model of Dissipative Trapped Electron Mode (DTEM) Turbulence"

April

Tenth Topical Conference on Radio Frequency Power in Plasmas, Boston, Massachusetts, April 1–3, 1993. Proceedings published by American Institute of Physics

F. W. Baity, D. B. Batchelor, K. C. Bills, C. H. Fogelman, D. J. Hoffman, E. F. Jaeger, J. L. Ping, B. W. Riemer, P. M. Ryan, D. C. Stallings, D. J. Taylor, and J. J. Yugo, "Design of Long-Pulse Fast-Wave Current Drive Antennas for DIII-D"

T. S. Bigelow, D. W. Swain, and M. Sawan, "A Preliminary Engineering Assessment of the ITER CDA ECH Launcher"

M. D. Carter, D. B. Batchelor, and D. C. Stallings, "Three Dimensional Effects for Radio Frequency Antenna Modeling"

J. B. O. Caughman and D. J. Hoffman, "Arc Detection and Protection in High Power Antenna Systems"

W. L. Gardner, J. B. O. Caughman, D. J. Hoffman, and P. Probert, "Comparison of the Folded Stripline and Stacked Stripline Concepts to the Folded Waveguide Launcher"

R. C. Goldfinger, D. B. Batchelor, C. K. Phillips, R. Budny, G. W. Hammett, J. C. Hosea, D. M. McCune, J. E. Stevens, J. R. Wilson, and the TFTR Team, "DT Simulation of ICRF Heated Supershots in TFTR Using TRANSP"

R. H. Goulding, D. J. Hoffman, P. M. Ryan, G. Bosia, M. Bures, D. Start, T. Wade, C. Petty, and R. Pinsker, "Power Compensators for Phased Operation of Antenna Arrays on JET and DIII-D"

G. R. Haste, C. E. Thomas, A. Fadnek, M. D. Carter, B. Beaumont, A. Becoulet, H. Kuus, and B. Saoutic, "Effect on Antenna Structure of High Power RF During Plasma Operation"

C. L. Hedrick, J.-N. Leboeuf, and D. A. Spong, "Global Alpha-Alfvén Wave Dispersion Relation and Rosetta Stone"

D. J. Hoffman, T. S. Bigelow, C. H. Fogelman, J. J. Yugo, J. B. O. Caughman, W. L. Gardner, M. D. Carter, P. Probert, and E. Barbato, "Folded Waveguide Designs for Tokamaks"

E. F. Jaeger, D. B. Batchelor, and M. Murakami, "Global Wave Modeling of Electron Interactions with Fast Magnetosonic Waves"

M. Murakami, E. F. Jaeger, F. G. Rimini, D. A. Rasmussen, J. E. Stevens, J. R. Wilson, D. B. Batchelor, M. Bell, R. Budny, E. Fredrickson, R. C. Goldfinger, G. Hammett, D. J. Hoffman, J. C. Hosea, A. Janos, R. Majeski, D. Mansfield, C. K. Phillips, J. H. Rogers, G. Schilling, G. Taylor, and M. C. Zarnstorff, "Fast Wave Direct Electron Heating in TFTR"

P. Probert, M. D. Carter, E. Barbato, and F. Wesner, "Folded Waveguide Designs for Tokamaks"

D. A. Rasmussen, D. B. Batchelor, R. H. Goulding, D. J. Hoffman, E. F. Jaeger, and J. A. Rome, "Ion Cyclotron Heating Experiments, and Plans for the Advanced Toroidal Facility (ATF)"

P. M. Ryan, R. H. Goulding, V. Bhatnagar, A. Kaye, and T. Wade, "Electrical Characterization of the JET A_2 Antenna: Comparison of Model with Measurements"

D. W. Swain, E. Fredd, S. Shipley, J. Yugo, R. Goulding, D. B. Batchelor, and D. C. Stallings, "Design of the Ion Cyclotron System for TPX"

J. B. Wilgen, G. R. Hanson, T. S. Bigelow, D. B. Batchelor, I. Collazo, D. J. Hoffman, M. Murakami, D. A. Rasmussen, D. C. Stallings, S. Raftopoulos, and J. R. Wilson, "Microwave Reflectometry for ICRF Coupling Studies on TFTR"

J. J. Yugo, B. W. Riemer, D. J. Taylor, D. W. Swain, and R. O. Sayer, "Disruption Analysis of RF Antennas"

Oral Presentation at Columbia University, New York, New York, April 2, 1993

B. A. Carreras, "Self Consistent Interaction of Shear Poloidal Flow and Turbulence"

U.S.–Japan Workshop on the Profile and Turbulence Diagnostics on High-Beta Plasmas and Internal Magnetic Field Measurement, Princeton, New Jersey, April 13–15, 1993. Abstracts published

G. R. Hanson, "Fluctuation Studies of ECH Plasmas in ATF"

C. H. Ma, D. P. Hutchinson, R. K. Richards, J. Irby, and T. C. Luke, "A CO_2 Laser Polarimeter for Plasma Current Profile Measurement in Alcator C-Mod"

Fifth American Nuclear Society (ANS) Topical Meeting on Robotics and Remote Systems, Knoxville, Tennessee, April 26–29, 1993. Proceedings published

F. C. Davis, M. S. Walker, and T. G. Brown, "New Remote Maintenance Approach for TPX"

May

International Workshop on Nuclear Data for Fusion Reactor Technology, Del Mar, California, May 3–6, 1993

A. C. England, "A Fission Chamber for 14 MeV Neutrons"

International Atomic Energy Agency (IAEA) Technical Committee Meeting on Pellet Injection, Naka Fusion Research Establishment of Japan Atomic Energy Research Institute (JAERI), Naka, Japan, May 10–12, 1993. Proceedings published by IAEA

L. R. Baylor, G. L. Schmidt, F. C. Jobes, G. W. Hammett, D. K. Owens, and S. L. Milora, "Transport in Pellet-Fueled ICRH Discharges in TFTR"

S. K. Combs, C. A. Foster, C. R. Foust, M. J. Gouge, S. L. Milora, D. E. Schechter, C. C. Tsai, and J. H. Whealton, "High-Speed Pellet Injection Development at ORNL: Two-Stage Light Gas Guns and an Electron-Beam-Heated Rocket"

S. K. Combs, B. E. Argo, L. R. Baylor, M. J. Cole, G. R. Dyer, D. T. Fehling, P. W. Fisher, C. A. Foster, C. R. Foust, M. J. Gouge, T. C. Jernigan, R. A. Langley, S. L. Milora, A. L. Qualls, D. E. Schechter, D. O. Sparks, C. C. Tsai, J. B. Wilgen, and J. W. Whealton, "Pellet Injector Research and Development at ORNL"

P. W. Fisher, S. K. Combs, S. L. Milora, and M. J. Gouge, "Tritium Pellet Injector Development at ORNL"

C. A. Foster, L. R. Baylor, A. L. Qualls, S. L. Milora, D. E. Schechter, M. J. Gouge, A. Géraud, M. Chatelier, and G. Gros, "ORNL Centrifuge Pellet Fueling System"

A. Frattolillo, M. Gasparotto, S. Migliori, F. Scaramuzzi, G. Angelone, M. Baldarelli, M. Capobianchi, C. Domma, and G. Ronci, A. Reggiori, G. Riva, R. Carlevaro, G. B. Daminelli, S. K. Combs, S. L. Milora, C. R. Foust, and M. J. Gouge, "High-Speed Repetitive Pellet Injector Prototype for Magnetic Confinement Fusion Device"

10th International Atomic Energy Agency (IAEA) Workshop on Stellarators, IBZ Garching, Germany, May 10–14, 1993. Proceedings published in International Atomic Energy Agency (IAEA) Conference Proceedings

R. J. Colchin, S. C. Aceto, A. C. England, R. C. Isler, M. Murakami, D. A. Rasmussen, T. Uckan, J. B. Wilgen, and J. J. Zielinski, "Effects of Magnetic Field Perturbations in the ATF Torsatron"

R. A. Dory, M. Murakami, and the ATF Team, "Distinguishing Gyro-Bohm and Bohm Scaling in Stellarators"

R. C. Isler, J. H. Harris, M. Murakami, and the ATF Group, "Fluctuations and Confinement in ATF"

J. F. Lyon, "Assessment of Stellarators as Reactors"

J. F. Lyon, "Overview of the ATF Stellarator Program"

D. A. Spong and A. Weller, "Global, Toroidal and Helical-Induced Shear Alfvén Instabilities in Stellarators"

T. Uckan, R. C. Isler, T. C. Jernigan, J. F. Lyon, P. K. Mioduszewski, M. Murakami, D. A. Rasmussen, J. B. Wilgen, S. C. Aceto, and J. J. Zielinski, "Limiter Biasing Experiments on the Advanced Toroidal Facility (ATF)"

M. R. Wade, C. E. Thomas, J. A. Rome, A. C. England, and H. R. Fowler, "Fast Ion Behavior During Neutral Beam Injection in ATF"

International Atomic Energy Agency (IAEA) Technical Committee Meeting on Alpha Particles in Fusion Research, International Centre for Theoretical Physics, Trieste, Italy, May 10–14, 1993. Proceedings published by IAEA

D. A. Spong, C. L. Hedrick, and B. A. Carreras, "Nonlinear Gyrofluid Models of Shear Alfvén Instabilities in Ignited and Beam Heated Toroidal Plasmas"

Supercomputacion Vectorial Y Paralela, 93, CIEMAT, Madrid, Spain, May 10–14, 1993
V. E. Lynch, "Parallel Computing for Fusion Energy Applications"

Division of Atomic, Molecular, and Optical Physics, American Physical Society, Reno, Nevada, May 17–19, 1993
E. W. Bell, X. Q. Guo, G. H. Dunn, M. E. Bannister, A. C. H. Smith, B. D. DePaola, C. A. Timmer, and E. K. Wahlin, "Electron-Impact Excitation of O^{5+} (2s-2p) Using a Merged Beams Technique"
S. Datz, I. G. Hughes, F. W. Meyer, and J. Shinpaugh, "A Single-Source Merged-Beam Experiment to Measure Multicharged Ion - Multicharged Ion Symmetric Charge Transfer"
L. Folkerts, I. G. Hughes, and F. W. Meyer, "Observation of K Auger Electrons and K X-rays from Collisions of Ar^{17+} and Ar^{18+} with Surfaces"
M. A. Haque, L. Folkerts, P. A. Zeijlmans van Emmichoven, and C. C. Havener, "Low-Energy Measurements of Electron Capture by Multicharged Ions from Hydrogen Rydberg Atoms"
C. C. Havener and L. Folkerts, "Low-Energy Electron Capture Cross Sections for N^{4+} + H Using Merged Beams"
I. G. Hughes, J. Burgdorfer, L. Folkerts, C. C. Havener, S. H. Overbury, M. T. Robinson, D. M. Zehner, P. A. Zeijlmans van Emmichoven, and F. W. Meyer, "Potential Electron Emission above the Kinetic Emission Threshold in Slow Multicharged Ion-Surface Interactions"
F. W. Meyer, L. Folkerts, I. G. Hughes, S. H. Overbury, and D. M. Zehner, "The Effect of Work Function Reduction on Above-Surface Neutralization of Multicharged Ions"
D. R. Schultz and C. O. Reinhold, "Comparison of Classical, Quasi-Classical and Quantal Approximations for the Ejected Electron Spectrum in 1.5 MeV/u F^{9+} + He Collisions"

U.S./Globus Workshop, Ioffe Institute, St. Petersburg, Russian Federation, May 20–25, 1993
R. J. Colchin, "START Central Solenoid Design Considerations" .

June

20th Institute of Electrical and Electronics Engineers (IEEE) International Conference on Plasma Science, Vancouver, B.C., Canada, June 7–9, 1993. Abstracts published
I. Collazo-López, G. R. Hanson, J. B. Wilgen, T. S. Bigelow, C. E. Thomas, R. Nazikian, M. McCarthy, and E. Mazzucato, "Preliminary Results of the ORNL Swept Dual-Frequency X-Mode Reflectometer for TFTR"

Tennessee Valley Chapter, American Vacuum Society (TVC-AVS) Symposium and Equipment Exhibit, Oak Ridge, Tennessee, June 9–10, 1993
J. B. O. Caughman and W. M. Holber, "The Effects of Substrate Bias Frequency in an Electron Cyclotron Resonance Plasma Reactor"
S. M. Gorbatkin, R. F. Burgie, W. C. Oliver, J. C. Barbour, T. M. Mayer, and M. L. Thomas, "Electron Cyclotron Resonance Microwave Plasma Processing of BN Thin Films"

1993 Annual Meeting of the American Nuclear Society, San Diego, California, June 20–24, 1993. Proceedings published as *Proceedings of the 1993 Annual Meeting of the American Nuclear Society*
C. C. Baker, "ITER—An International Step to Fusion Energy"

U.S.–Japan Steady-State Workshop, Kyushu University, Kasuga, Japan, June 29–July 2, 1993. Proceedings published as *U.S.–Japan Steady-State Workshop Proceedings*
W. A. Houlberg and S. E. Attenberger, "Pellet Fueling and Pumping for Density Profile Control in Steady-State"
W. A. Houlberg and S. E. Attenberger, "The Applicability of PEP Modes for Steady-State"

July

International Energy Agency (IEA) Technical Workshop on Neutron Sources for Fusion, Moscow, Russia, July 12–16, 1993. Proceedings published as *IEA Fusion Neutron Source Workshop Summary,* Plenum Publishing

Y-K. M. Peng, "Initial Design Boundaries and Parameters of Small Tokamak VNS Envelope"

T. E. Shannon, "Engineering Design of a Volume Neutron Source,"

T. E. Shannon, "Facility Design and Remote Handling Considerations for the Fusion Materials Irradiation Facility"

International Cryogenic Engineering and Cryogenic Magnetic Conference, Albuquerque, New Mexico, USA, July 12–16, 1993. Proceedings published as *Advances in Cryogenic Engineering,* Plenum Publishing

L. Dresner, "Stability of an Uncooled Segment of a High-Temperature Superconductor"

J. W. Lue and L. Dresner, "Normal Zone Propagation and Thermal Hydraulic Quenchback in Cable-in-Conduit Superconductor"

J. W. Lue, S. W. Schwenterly, M. S. Lubell, J. N. Luton, C. H. Joshi, L. J. Masur, and E. R. Podtburg, "Test Results of Two High Temperature Superconducting Sample Coils"

S. W. Schwenterly and L. Dresner, "Simple Estimate of Stored Energy and Conductor Insulation Voltage-Withstand Requirements for Advanced Solenoid Magnet Designs"

XVIII International Conference on the Physics of Electronic and Atomic Collisions, Aarhus, Denmark, July 21–27, 1993. Abstracts and invited papers published in *AIP Conf. Proc.* 295

L. Folkerts, I. G. Hughes, and F. W. Meyer, "Observation of the K Auger Electron Spectra from Collisions of Ar^{17+} and Ar^{18+} with Metal Surfaces"

C. C. Havener, L. Folkerts, M. A. Haque, X. Urbain, and P. A. Zeijlmans van Emmichoven, "Low-Energy Measurements of Electron Capture by Multicharged Ions from Hydrogen Rydberg Atoms"

I. G. Hughes, J. Burgdorfer, L. Folkerts, C. C. Havener, S. H. Overbury, M. T. Robinson, D. M. Zehner, P. A. Zeijlmans van Emmichoven, and F. W. Meyer, "The Role of Below-Surface Secondary Cascade Processes in Potential Electron Emission During Multicharged Ion-Surface Interactions"

F. W. Meyer, L. Folkerts, C. C. Havener, I. G. Hughes, S. H. Overbury, D. M. Zehner, and P. A. Zeijlmans van Emmichoven, "Electron Spectroscopic Studies of the Neutralization of Slow Multicharged Ions During Interactions with a Metal Surface," invited

20th European Physical Society (EPS) Conference on Controlled Fusion and Plasma Physics, Lisboa, Portugal, July 26–30, 1993. Proceedings published in *European Physical Society (EPS) Conference Proceedings*

E. Barbato, F. De Marco, E. F. Jaeger, M. D. Carter, D. J. Hoffman, F. W. Baity, R. Goldfinger, and D. B. Batchelor, "Fast Wave at 433 MHz on FTU by a Folded Waveguide Launcher"

B. A. Carreras, P. H. Diamond, and Y.-M. Liang, "Dynamics of the L to H Transition"

B. A. Carreras, L. A. Charlton, K. Sidikman, P. H. Diamond, and L. Garcia, "Self-Regulated Shear Flow Turbulence in Confined Plasmas"

L. Garcia, B. A. Carreras, and V. E. Lynch, "Probability of Accessing the Multiple Saturated States in the Resistive Interchange Instability"

S. P. Hirshman, D. K. Lee, F. Levinton, S. Batha, S. Bernabei, R. Kaita, C. Kessel, M. Okabayashi, and R. M. Wieland, "Equilibrium Reconstruction of the Q-Profile from Motional Stark Effect Data"

C. C. Klepper, J. T. Hogan. L. W. Owen, W. R. Hess, D. Guilhem, R. Guirlet, "Impurity Generation in the Tore Supra Outboard Pump Limiter"

M. A. Mahdavi, , R. J. Groebner, D. N. Hill, F. L. Hinton, M. A. Hollerbach, J. Hogan, , C. C. Klepper, E. A. Lazarus, , M. M. Menon, P. Mioduszewski, , L. W. Owen, , M. R. Wade, J. G. Watkins, W. P. West, R. Wood, et al., "Active Density Control in DIII-D H-Mode Plasmas"

M. Murakami, E. F. Jaeger, D. A. Rasmussen, D. B. Batchelor, C. E. Bush, R. C. Goldfinger, D. J. Hoffman, E. Frederickson, J. R. Wilson, M. C. Zarnstorff, M. G. Bell, R. V. Budny, D. Darrow, J. C.

Hosea, A. Janos, R. Majeski, D. Mansfield, H. Park, C. K. Phillips, J. H. Rogers, G. Schilling, S. C. Scott, J. E. Stevens, E. Synakowski, G. Taylor, R. W. Wieland, S. Z. Zweben, F. G. Rimini, and S. Sabbagh, "ICRF Direct Electron Heating Experiments in TFTR"

M. Porkolab, D. B. Batchelor, S. Bernabei, P. T. Bonoli, M. E. Fenstermacher, R. J. Goldston, L. R. Grisham, A. Hubbard, G. H. Neilson, T. K. Mau, D. Mikkelsen, P. Moroz, W. M. Nevins, J. Ramos, D. Swain, and K. I. Thomassen, "Heating and Current Drive Scenarios in the Tokamak Physics Experiment"

A. Seigneur, D. Guilhem, J. Hogan, C. DeMichelis, Ph. Ghendrih, M. Goniche, A. Grosman, R. Guirlet, W. Hess, J. Lasalle, J. Valter, and A. Samain, "The Use of Large Surface Area for Particle and Power Deposition"

H. Takahashi, J. Dunlap, A. England, J. Harris, R. Hatcher, S. Hirshman, D. Ignat, R. Isler, S. Jardin, S. Jones, R. Kaita, S. Kaye, M. Ono, F. Paoletti, S. Paul, F. Perkins, A. P. Post-Zwicker, N. Sauthoff, et al., "Accessibility for Lower Hybrid Waves in PBX-M"

T. Uckan, B. Richards, R. D. Bengtson, B. A. Carreras, D. B. Crockett, K. W. Gentle, G. X. Li, P. D. Hurwitz, W. L. Rowan, H. Y. W. Tsui, and A. J. Wootton, "Active Probing of Plasma Edge Turbulence and Feedback Studies on the Texas Experimental Tokamak (TEXT)"

M. R. Wade, D. L. Hillis, J. T. Hogan, P. K. Mioduszewski, W. P. West, K. H. Burrell, R. P. Seraydarian, R. J. Groebner, P. Gohil, C. Greenfield, J. Kim, and D. F. Finkenthal, "Dependence of Helium Transport on Plasma Current and ELM Frequency in H-mode Discharges in DIII-D"

A. Weller, D. A. Spong, H. J. Hartfub, R. Jaenicke, A. Lazaros, F. P. Penningsfeld, S. Sattler, the W7-AS Team, and the NBI Group, "Stability of Neutral Beam Driven Alfvén Eigenmodes in the Wendelstein W7-AS Stellarator"

August

International Workshop on Plasma-Based Ion Implantation, Madison, WI, August 4–6, 1993. Proceedings published by Materials Research Society

C. C. Tsai, W. L. Stirling, and J. M. Williams, "Potential Spin-off Applications of Fusion Neutral Beam Facilities for Advanced Material Processing"

AVS Topical Conference, Second Workshop on High Density Plasmas and Applications, San Francisco, California, August 5–6, 1993. Proceedings published in *J. Vac. Sci. Technol.*

L. A. Berry and S. M. Gorbatkin, "Permanent Magnet ECR Plasma Source with Remote Window"

J. B. O. Caughman, "Plasma Characterization of a Radio Frequency Induction Source with Chamber Wall Bias Capabilities"

1993 Summer School on Turbulence and Transport, University of Wisconsin, Madison, Wisconsin, August 15–20, 1993

B. A. Carreras, "Fluctuation Level Reduction by Shear Flow"

B. A. Carreras, "Long Wavelength Drift Wave Turbulence"

B. A. Carreras, "Nonlinear Resistive MHD"

B. A. Carreras "Self-Regulated Shear Flow Turbulence"

Briefing for U.S. Technical Advisory Committee (TAC) and ISCUS Members, Los Angeles, California, August 16, 1993

N. A. Uckan, J. Hogan, W. Houlberg, J. Galambos, D. Hillis, J. Perkins, S. Haney, D. Post, and P. Rugherford, "ITER EDA Design: Physics Basis for Size, Confinement Capability, Power Levels, and Burn Control"

EPRI Fusion Working Group Meeting, Washington, D.C., August 24, 1993

J. F. Lyon, "Overview of the Stellarator Concept"

2nd International Congress on Environmentally Conscious Manufacturing, Arlington, Virginia, August 29–September 1, 1993. Proceedings published

C. A. Foster, P. W. Fisher, W. D. Nelson, and D. E. Schechter, "A Centrifuge CO_2 Pellet Cleaning System"

Workshop on Local Transport Studies in Fusion Plasmas, Varenna, Italy, August 29–September 4, 1993

B. A. Carreras, "Turbulence, E × B Flows, and Transport"

September

TPX Physics Workshop, MIT, Boston, Massachusetts, September 8–9, 1993

D. B. Batchelor, "ICRF Physics"

Advanced Tokamak Scenarios Group, Massachusettes Institute of Technology, Cambridge, Massachusettes, September 10, 1993

W. A. Houlberg and S. E. Attenberger, "Steady-State PEP Modes"

44th Aeroballistic Range Association Meeting, Munich, Germany, September 13–17, 1993. Proceedings published

M. J. Gouge, L. R. Baylor, S. K. Combs, P. W. Fisher, C. A. Foster, C. R. Foust, S. L. Milora, and A. L. Qualls, "Ballistics Considerations for Small-Caliber, Low-Density Projectiles"

IAEA Technical Committee Meeting and Workshop on Fusion Reactor Design and Technology, University of California, Los Angeles, California, September 13–17, 1993. Proceedings published

M. A. Abdou, Y-K. M. Peng, M. S. Tillack, A. Ying, and the VENUS Group, "Role, Technical Requirement and Design Envelope of Volume Neutron Source"

J. F. Lyon, K. Gulec, R. L. Miller, and L. El-Guebaly, "Status of the U.S. Stellarator Reactor Study"

9th APS Topical Conference on Atomic Processes in Plasmas, San Antonio, Texas, September 19–23, 1993. Proceedings published

M. E. Bannister, "Observation of Resonance Structure in Near-Threshold Electron-Impact Excitation of the $4s^2\ {}^1S \rightarrow 4s4p\ {}^3P$ Intercombination Transition in Kr^{6+}"

C. C. Klepper, W. R. Hess, J. T. Hogan, and D. Guilhem, "Characterization of Atomic and Molecular Impurity Sources and Transport in the Tokamak Edge"

13th International Conference on Magnet Technology, Victoria Conference Center, Victoria, British Columbia, Canada, September 20–24, 1993. Proceedings published

L. Dresner, "Stability and Protection of Uncooled Magnets Wound with High-Temperature Superconductors"

J. W. Lue, M. S. Lubell, J. N. Luton, B. J. Frame, and F. L. Paulaskas, "Development of Light Weight, High Current Density Superconducting Magnets"

J. W. Lue, J. N. Luton, S. W. Schwenterly, and C. T. Wilson, "Test Results of Superconducting AC Magnets for Magnetic Refrigeration Experiment"

5th European Fusion Theory Conference, San Lorenzo del Escorial, Madrid, Spain, September 21–24, 1993

B. A. Carreras, P. H. Diamond, and Y. M. Liang, "Dynamics of the L to H Transition"

IAEA Coordinated Research Program on Atomic Data for Medium- and High-Z Impurities in Fusion Plasmas, Sept. 22–24, 1993. Proceedings published as *IAEA Summary Report*, INDC(NDS)-292, December 1994

C. C. Havener, "Plasma Impurity Cross Section Data Involving e-Ion, Ion-Atom, Ion-Surface, and Ion-Ion Collisions at ORNL"

XXIV Reunion Bienal de la Real Sociedad de Física y Química, Jaca, España, September 27–30, 1993
B. A. Carreras, "Plasma Turbulence and Global Flows"

Multilevel Metallization Focused Technical Advisory Board Meeting, September 29–30, 1993
L. A. Berry, "Development of ECR Plasma Metallization"

October

Fusion Power Associates Annual Meeting and Symposium, Oak Ridge, TN, October 5–7, 1993
L. A. Berry, "Plasma Processing for Integrated Circuits"

15th Institute of Electrical and Electronic Engineers/Nuclear Plasma Sciences Society (IEEE/NPSS) Symposium on Fusion Engineering, Hyannis, Massachusetts, October 11–15, 1993. Proceedings published by Institute of Electrical and Electronic Engineers, Piscataway, N.J., 1994

L. R. Baylor, B. E. Argo, G. C. Barber, S. K. Combs, M. J. Cole, G. R. Dyer, D. T. Fehling, P. W. Fisher, C. A. Foster, C. R. Foust, M. J. Gouge, T. C. Jernigan, R. A. Langley, S. L. Milora, A. L. Qualls, D. E. Schechter, D. O. Sparks, C. C. Tsai, J. B. Wilgen, and J. W. Whealton, "Pellet Injector Development and Experiments at ORNL"

T. S. Bigelow, M. D. Carter, P. M. Ryan, J. J. Yugo, C. H. Fogelman, D. J. Hoffman, S. Golovato, and P. Bonoli, "RF Modeling and Design of a Folded Waveguide ICRF Launcher for Alcator C-Mod Tokamak"

M. J. Cole, B. E. Nelson, G. H. Jones, P. L. Goranson, Y. Gohar, and S. L. Liew, "Conceptual Design of the Tokamak Radiation Shielding for the Tokamak Physics Experiment (TPX)"

S. K. Combs, S. L. Milora, C. R. Foust, M. J. Gouge, A. Frattolillo, M. Gasparotto, S. Migliori, F. Scaramuzzi, G. Angelone, M. Baldarelli, M. Capobianchi, C. Domma, and G. Ronci, "High-Speed Repetitive Pellet Injector for Plasma Fueling of Magnetic Confinement Fusion Devices"

J. S. deGrassie, R. I. Pinsker, W. P. Cary, R. W. Callis, R. O'Neill, C. C. Petty, D. B. Remsen, F. W. Baity, R. H. Goulding, and S. W. Ferguson, "4 MW Upgrade to the DIII-D Fast Wave Current Drive System"

C. H. Fogelman, T. S. Bigelow, M. D. Carter, D. J. Hoffman, S. Golovato, and P. Bonoli, "Design of Folded Waveguide Antenna for Alcator C-Mod"

C. A. Foster, A. L. Qualls, L. R. Baylor, D. E. Schechter, and S. L. Milora, "A 400-Pellet Feed System for the ORNL Centrifuge Pellet Injector"

J. D. Galambos, D. L. Conner, P. L. Goranson, D. C. Lousteau, D. E. Williamson, B. E. Nelson, and F. C. Davis, "Methodology for First Wall Design"

J. D. Galambos, L. J. Perkins, S. Haney, and J. Mandrekas, "The Impact of Improved Physics on Commercial Tokamak Reactors"

R. H. Goulding, F. W. Baity, J. B. O. Caughman, D. J. Hoffman, P. M. Ryan, J. S. deGrassie, C. C. Petty, R. I. Pinsker, V. P. Bhatnagar, M. Bures, J. A. Dobbing, D. F. H. Start, and T. J. Wade, "Design and Control of Phased ICRF Antenna Arrays"

R. A. Langley, T. S. Bigelow, and D. J. Santeler, "Determination of Vacuum Pumping Characteristics for an Evaculated ECH Circular Waveguide System"

J. F. Lyon, "Overview of the U.S. Stellarator Reactor Study"

J. J. Yugo, D. W. Swain, D. B. Batchelor, G. H. Jones, C. H. Fogelman, S. E. Shipley, and E. Fredd, "Conceptual Design of the ICH System for the Tokamak Physics Experiment (TPX)"

46th Annual Gaseous Electronics Conference, Montreal, Quebec, October 19–22, 1993

R. A. Stewart, P. Vitello, D. B. Graves, E. F. Jaeger, and L. A. Berry, "A Two-Dimensional Fluid Model of High Density Inductively Coupled Plasma Sources"

6th International Symposium on Laser-Aided Plasma Diagnostics, Bar Harbor, Maine, October 25–28, 1993

D. P. Hutchinson, R. K. Richards, and C. H. Ma, "ORNL Infrared-Based Diagnostics Development for ITER"

R. K. Richards, D. P. Hutchinson, and C. H. Ma, "CO_2-Laser Collective Thomson Scattering Ion-Tail Diagnostic for C-Mod"

TPX Council Meeting, Princeton, New Jersey, October 26, 1993

W. A. Houlberg and S. E. Attenberger, "Advanced Tokamak Reactor Profile Control and Stability Assessment"

November

35th American Physical Society (APS) Annual Meeting, Division of Plasma Physics, St. Louis, Missouri, November 1–5, 1993 Abstracts published in *Bull. Am. Phys. Soc.* 38 (1993)

S. E. Attenberger and W. A. Houlberg, "Extension of PEP Modes in Tokamaks to Steady-State"

F. W. Baity, G. C. Barber, J. S. Degrassie, R. H. Goulding, C. C. Petty, R. I. Pinsker, and D. O. Sparks, "Transmission Line and Decoupler Testing for the DIII-D FWCD System"

D. B. Batchelor, L. A. Berry, E. F. Jaeger, K. C. Shaing, and J. C. Whitson, "2D Modeling of Power Deposition in Inductively Coupled Plasma Sources for Materials Processing"

D. B. Batchelor, D. W. Swain, E. F. Jaeger, M. D. Carter, D. C. Stallings, D. J. Hoffman, J. J. Yugo, M. Porkolab, P. T. Bonoli, P. Moroz, J. Scharer, U. Wisconsin, and T. K. Mau, "Ion Cyclotron Heating and Current Drive on TPX"

T. S. Bigelow, C. H. Fogelman, D. J. Hoffman, M. D. Carter, P. M. Ryan, S. N. Golovato, and P. Bonoli, "A Folded Waveguide ICRF Launcher for Alcator C-Mod"

B. A. Carreras, P. H. Diamond, and Y.-M. Liang, "Dynamics of the Transition to Enhanced Confinement Regimes in Magnetically Confined Plasmas"

M. D. Carter, D. B. Batchelor, and D. C. Stallings, "Three Dimensional Antenna Modeling Using RANT3D"

J. B. O. Caughman, G. L. Bell, W. L. Gardner, and D. J. Hoffman, "The Erosion of Faraday Shield Coatings Due to RF Sheaths"

L. A. Charlton, B. A. Carreras, J.-N. Leboeuf, and V. E. Lynch, "Radiation Driven Turbulence at the Plasma Edge of Toroida Devices"

R. J. Colchin, M. R. Wade, C. E. Thomas, S. C. Aceto, J. A. Rome, A. C. England, and R. H. Fowler, "Fast Ion Behavior During Neutral Beam Injection in ATF"

I. Collazo-López, G. R. Hanson, J. B. Wilgen, T. S. Bigelow, D. A. Rasmussen, M. Murakami, C. E. Thomas, B. Grek, and J. R. Wilson, "Detailed Analysis of Differential Phase Reflectometer Measurements on TFTR"

E. C. Crume, Jr., and K. C. Shaing, "Theoretical Comparisons of Tokamak and Stellarator H-Mode"

E. de la Luna, J. B. Wilgen, G. R. Hanson, J. Sanchez, V. Zhuravlev, R. Kaita, J. H. Harris, and the PBX-M Team, "An AM Reflectometer on PBX-M for Edge Density Profile Measurements"

N. Dominguez, Y-K. M. Peng, and K. C. Shaing, "Tokamak and Spherical Torus (ST) MHD Equilibrium for H-Mode and VH-Mode"

R. A. Dory, M. Murakami, and the ATF Team, "Offset-Linear Energy Confinement Scaling in the ATF Torsatron"

J. L. Dunlap, J. H. Harris, M. F. Corneliussen, W. M. Davis, T. F. Gibney, S. M. Kaye, P. G. Roney, and S. S. Sesnic, "PBX-M Fluctuations from Mirnov Coil Diagnostics"

A. C. England, H. Takahashi, S. Bernabei, B. LeBlanc, and S. von Goeler, "Effects of LHCH Wave Spectrum on Runaway Electron Production"

A. C. England, R. Bell, S. P. Hirshman, R. Kaita, S. Kaye, H. Kugel, D. K. Lee, B. Leblanc, M. Okabayashi, and Y. Sun, "Scaling of the Neutron Source Strength with Shaping and Plasma Parameters in PBX"

J. D. Galambos, Y-K. M. Peng, L. J. Perkins, S. Haney, and J. Mandrekas, "Impact of Improved Physics on Commercial Tokamak Reactors"

R. H. Goulding, D. J. Hoffman, P. M. Ryan, V. Bhatnagar, M. Bures, J. A. Dobbing, D. F. H. Start, and T. J. Wade, "Automatic Matching and Phase Control of Multiple Element ICRF Antennas"

G. R. Hanson, J. B. Wilgen, T. S. Bigelow, I. Collazo, D. A. Rasmussen, D. B. Batchelor, D. J. Hoffman, E. F. Jaeger, M. Murakami, P. M. Ryan, D. C. Stallings, and J. R. Wilson, "Edge Density Profile Measurements in Front of an ICRF Antenna"

R. J. Hawryluk, L. R. Baylor, T. S. Bigelow, T. Burgess, I. Coliazo, R. C. Goldfinger, M. J. Gouge, G. R. Hanson, S. P. Hirshman, D. J. Hoffman, E. F. Jaeger, S. L. Milora, M. Murakami, A. L. Qualls, D. A. Rasmussen, J. B. Wilgen, et al., "Preparations for Deuterium Tritium Experiments on the Tokamak Fusion Test Reactor"

C. L. Hedrick, J-N. Leboeuf, and K. L. Sidikman, "Landau Fluid Equations for Dissipative Trapped Electron Mode, Including Ion Magnetic Drift"

D. L. Hillis, K. H. Finken, H. Euringer, M. R. Wade, J. T. Hogan, J. Boedo, R. W. Conn, R. Doerner, D. S. Gray, G. Mank, A. M. Messien, G. Van Oost, R. Van Nieuwenhove, R. R. Weynants, and G. H. Wolf, "Investigation of Helium Transport and Exhaust with the ALT-II Pump Limiter in TEXTOR"

S. P. Hirshman, D. K. Lee, F. Levinton, S. Batha, M. Okabayashi, and R. M. Weiland, "Equilibirum Reconstruction Using Motional Stark Effect Data on PBX-M and TFTR"

D. J. Hoffman, J. B. O. Caughman, G. L. Bell, F. W. Baity, R. H. Goulding, and D. A. Rasmussen, "Protection for Ion Cyclotron Heating and Current Drive Systems"

J. T. Hogan, D. Guilhem, C. C. Klepper, and W. R. Hess, "Heat Deposition, Impurity Generation and Transport Calculations for Tore Supra Inner Wall Discharges"

J. T. Hogan and N. A. Uckan, "Stable Operational Space for ITER Design Variants"

W. A. Houlberg, S. E. Attenberger, and N. A. Uckan, "Density Excursions and Their Impact on Thermal Stability in Tokamak Reactors"

E. F. Jaeger, M. Murakami, D. B. Batchelor, J. R. Wilson, R. Majeski, and C. K. Phillips, "Full Wave ICRF Modeling for D-T Experiments on TFTR"

T. C. Jernigan, L. R. Baylor, S. K. Combs, C. R. Foust, S. L. Milora, J. Phillips, and R. T. Snider, "Performance of a Repeating Pellet Injector for DIII-D"

C. C. Klepper, W. R. Hess, J. T. Hogan, D. Guilhem, R. Guirlet, T. Loarer, S. J. Tobin, and T. Uckan, "Direct Measurement of Chemical Sputtering at the Neutralizer Plate of the Tore Supra Pump Limiter"

J.-N. Leboeuf, D. B. Geohegan, C. L. Liu, R. F. Wood, J. B. Drake, and D. W. Walker, "Modeling of Plasma Dynamics in Laser Ablation Processes"

J-N. Leboeuf, C. L. Hedrick, K. L. Sidikman, B. A. Carreras, and R. D. Sydora, "Dissipative Trapped Electron Mode Turbulence with Ion Landau Damping, FLR and Magnetic Drift Effects"

D. K. Lee, S. P. Hirshman, M. Okabayashi, and Y. Sun, "Rapid Reconstruction of Tokamak MHD Equilibrium from Experimental Measurements"

V. E. Lynch, B. A. Carreras, J. B. Drake, J.-N. Leboeuf, and B. Curtis, "The Performance of a Fluid Code on Parrallel Computers"

J. F. Lyon and K. Gulec, "Assessment of Stellarators as Reactors"

C. H. Ma, D. P. Hutchinson, R. K. Richards, J. Irby, and T. Luke, "An Infrared Polarimeter for Measurement of Plasma Current Profile in Alcator C-Mod"

R. Maingi, P. K. Mioduszewski, J. W. Cuthbertson, D. L. Hillis, J. T. Hogan, C. C. Klepper, C. J. Lasnier, M. A. Mahdavi, R. A. Moyer, L. W. Owen, M. J. Schaffer, M. R. Wade, and J. G. Watkins, "Effect of Particle Exhaust on SOL and Divertor Plasma Parameters"

P. K. Mioduszewski and L. W. Owen, "Particle Balance Modeling in Pump Limiters"

L. W. Owen, P. K. Mioduszewski, T. Loarer, M. Chatelier, and D. Guilhem, "Transport Analysis of a Vented Limiter for Tore Supra"

A. L. Qualls, C. A. Foster, L. R. Baylor, S. L. Milora, and D. E. Schechter, "Pellet Feed System Upgrade for the Tore Supra Centrifuge Pellet Injector"

D. A. Rasmussen, S. C. Aceto, D. B. Batchelor, R. H. Goulding, D. J. Hoffman, E. F. Jaeger, D. K. Lee, and J. A. Rome, "Ion Cyclotron Heating Antenna Designs for the Advanced Toroidal Facility (ATF)"

R. K. Richards, D. P. Hutchinson, and C. H. Ma, "CO_2-Laser Collective Thomson Scattering Ion-Tail Diagnostic for C-Mod"

J. A. Rome, R. H. Fowler, J. F. Lyon, J. Sheffield, and J. D. Hanson, "Modular Stellarator Configuration Studies"

P. M. Ryan, F. W. Baity, T. S. Bigelow, R. H. Goulding, and D. J. Hoffman, "Electric Potential Distributions on ICRH Launcher Structures"

G. L. Schmidt, D. Bartlett, L. R. Baylor, S. Clemens, M. Gadeberg, N. Gottardi, P. Kupschus, P. Morgan, P. Nielsen, J. O'Rourke, A. Rossi, G. Sadler, and A. Tanga, "H-Mode Perturbations Following Pellet Injection in JET"

K. C. Shaing and C. T. Hsu, "H-Mode Bifurcation with Shock and Radial Electric Profile in Tokamaks"

K. L. Sidikman, C. L. Hedrick, J.-N. Leboeuf, and B. A. Carreras, "Radially-Resolved Slab Calculations of Dissipative Trapped Electron Modes with Ion Magnetic Drift"

D. A. Spong, B. A. Carreras, C. L. Hedrick, J.-N. Leboeuf, D. J. Sigmar, A. Weller, S. J. Zweben, and R. Budny, "Nonlinear Gyrofluid Models of Shear Alfvén Instabilities in Tokamaks and Stellarators"

D. W. Swain, J. J. Yugo, D. B. Batchelor, C. H. Fogelman, S. E. Shipley, and E. Fredd, "Design of the Ion Cyclotron System for TPX"

C. C. Tsai, H. H. Haselton, W. D. Nelson, D. E. Schechter, L. M. Thompson, V. B. Campbell, A. L. Glover, and J. M. Googin, "Plasma Surface Cleaning Using Microwave Plasmas"

N. A. Uckan and the U.S. ITER Home Team, "Confinement Capability of ITER-EDA"

T. Uckan, B. Richards, R. D. Bengtson, B. A. Carreras, G. X. Li, H. Lin, P. Hurwitz, W. L. Rowan, H. Y. W. Tsui, and A. J. Wootton, "Effects of the Edge Feedback on the Texas Experimental Tokamak (TEXT)"

M. Ulrickson, D. N. Hill, R. Campbell, W. A. Houlberg, D. Ruzic, D. P. Stotler, and K. Werley, "Power and Particle Control for TPX"

J. H. Whealton, R. J. Raridon, and R. G. Cowan, "Self-Consistent Plasma Edge Calculations for Divertor Plasmas"

J. B. Wilgen, G. R. Hanson, E. De La Luna, V. Zhuravlev, J. H. Harris, J. Sanchez, and R. Kaita, "An AM Reflectometer on PBX-M for Edge Density Profile Measurements"

International Atomic Energy Agency (IAEA) Technical Committee Meeting (TCM) on High Power Radio-Frequency (RF) (Launching Physics and Technology for Fusion Devices or) Launchers for Plasma Heating and Current Drive, Naka, Japan, November 10–12, 1993. Proceedings published

F. W. Baity, D. B. Batchelor, R. H. Goulding, D. J. Hoffman, E. F. Jaeger, P. M. Ryan, J. S. deGrassie, C. C. Petty, R. I. Pinsker, and R. Prater, "Fast Wave Current Drive Technology Development at ORNL"

International Atomic Energy Agency (IAEA) Technical Committee Meeting on H-Mode Physics, Japan Atomic Energy Research Institute (JAERI), Naka, Japan, November 15–17, 1993. Proceedings published in *Plasma Phys. Controlled Fusion* (special issue)

B. A. Carreras, P. H . Diamond, and Yi Ming Liang, "Dynamics of L to H Bifurcation"

D. L. Hillis, M. R. Wade, J. T. Hogan, W. P. West, K. H. Burrell, R. P. Seraydarian, and C. M. Greenfield, "Helium Transport Studies of Enhanced Confinement Discharges in the DIII-D Tokamak"

D. L. Hillis, M. R. Wade, J. T. Hogan, W. P. West, K. H. Burrell, R. Maingi, C. C. Klepper, M. M. Menon, P. K. Mioduszewski, M. A. Mahdavi, G. L. Jackson, N. H. Brooks, and D. F. Finkenthal, "Helium Transport and Exhaust Studies of H-Mode Discharges in the DIII-D Tokamak"

K. C. Shaing, C. T. Hsu, and N. Dominguez, "L-H Transition in Tokamaks and Stellarators"

Technical Meeting on Radiation Effects on In-Vessel Components, Garching, Germany, November 15–19, 1993

R. H. Goulding, T. S. Bigelow, S. J. Zinkle, and R. E. Stoller, "Radiation Testing of Ceramic Vacuum Windows for High Power RF Feedthroughs"

American Vacuum Society (AVS) 40th National Symposium and Topical Conferences, Orlando, Florida, November 15–19, 1993. Proceedings published in *J. Vac. Sci. Technol.*

L. A. Berry and S. M. Gorbatkin, "Permanent Magnet ECR Source for Metal Deposition"

L. A. Berry and S. M. Gorbatkin, "The Influence of Microwave Coupler-Mode and Window-Size on Chlorine Etching of Polysilicon"

J. B. O. Caughman, "Boundary Condition Effects in a Radio-Frequency Induction Plasma Source"

C. C. Tsai, H. H. Haselton, W. D. Nelson, D. E. Schechter, L. M. Thompson, V. B. Campbell, A. L. Glover, and J. M. Googin, "Plasma Surface Cleaning Using Microwave Plasmas"

Supercomputing '93, Portland, Oregon, November 15–19, 1993. Proceedings published as *Proceedings of Supercomputing '93,* IEEE Computer Society Press

V. E. Lynch, B. A. Carreras, J.-N. Leboeuf, B. C. Curtis, and R. L. Troutman, "Multi-CPU Plasma Fluid Turbulence Calculations on a CRAY Y-MP C90"

Fifth International Toki Conference on Plasma Physics and Controlled Nuclear Fusion (ITC-5), Toki, Japan, November 16–19, 1993. Proceedings published

D. B. Batchelor, M. D. Carter, E. F. Jaeger, R. N. Morris, and D. C. Stallings, "Recent Results on Modeling of Fast Wave Current Drive and FWCD Antenna Arrays"

Presentation to the Fusion Power Associates Annual Meeting and Symposiuim, Oak Ridge, Tennessee, November 30, 1993. Published in *J. Fusion Energy* 12(4)

L. A. Berry, C. A. Foster, M. S. Lubell, W. D. Nelson, J. A. Rome, J. Sheffield, and T. L. White, "Fusion Spin-offs, an Important Part of the Oak Ridge National Laboratory Fusion Program"

Southeastern Section Meeting of the American Physical Society, Columbia, South Carolina, November 4–6, 1993

D. R. Schultz, "Modelling Atomic Collisions Through Time-Dependent Quantum and Statistical-Quasiclassical Methods," invited

December

Toroidal Plasma Experiments (TPX) Physics Workshop, Oak Ridge, Tennessee, December 16–17, 1993

D. B. Batchelor, "ICRF Physics"

Showcase Seminar, Oak Ridge National Laboratory, Oak Ridge, TN, December 17, 1993

T. L. White, "Microwave Processing of Radioactive Wastes"

1993 REPORTS

ORNL Technical Memoranda

B. A. Carreras, *Transport Mechanisms Acting in Toroidal Devices: A Theoretician's View*, ORNL/TM-12209, January 1993

M. D. Carter, D. B. Batchelor, and E. F. Jaeger, *Multiple Antenna Implementation System (MAntIS)*, ORNL/TM-12264, January 1993

M. D. Carter, D. B. Batchelor, and D. C. Stallings, *Three-Dimensional Effects for Radio Frequency Antenna Modeling*, ORNL/TM-12464, September 1993

L. Dresner, *On Some General Properties of Parabolic Conservation Equations*, ORNL/TM-12509, October 1993

J. D. Galambos, L. J. Perkins, S. Haney, and J. Mandrekas, *The Impact of Improved Physics on Commercial Tokamak Reactors*, ORNL/TM-12483, December 1993

Y-K. M. Peng, R. J. Colchin, D. W. Swain, B. E. Nelson, and J. F. Monday, *The TST: A Small Steady-State Tokamak for Integrated Divertor Testing*, ORNL/TM-12216, September 1993

R. K. Richards, D. P. Hutchinson, and C. H. Ma, *Optimization of a CO_2 Laser Thomson Scattering Alpha Particle Diagnostic*, ORNL/TM-12219, January 1993

R. O. Sayer, Y-K. M. Peng, S. C. Jardin, A. G. Kellman, and J. C. Wesley, *TSC Plasma Halo Simulation of a DIII-D Vertical Displacement Episode*, ORNL/TM-12281, January 1993

D. J. Strickler, R. Chester, K. Ingle, P. Payne, J. A. Rome, and K. Kertis, *Inventory Management Plan for a Research and Development Local Area Network*, ORNL/TM-12408, August 1993

T. Uckan, B. Richards, R. D. Bengtson, B. A. Carreras, D. B. Crockett, K. W. Gentle, G. X. Li, P. D. Hurwitz, W. L. Rowan, H. Y. W. Tsui, and A. J. Wootton, *Active Probing of Plasma Edge Turbulence and Feedback Studies on the Texas Experimental Tokamak (TEXT)*, ORNL/TM-12424, August 1993

Other Reports

A. Boozer, B. Braams, R. Cohen, R. Hazeltine, F. Hinton, W. Houlberg, E. Oktay, D. Post, W. Sakowski, D. Sigmar, A. Wootton, and H. Weitzner, *A Survey of Problems in Divertor and Edge Plasma Theory*, DOE/ER/53223-196

M. J. Gouge, "Plasma Fueling R&D for ITER" Discussions with ITER JCT Garching Joint Work Site

M. B. Nestor, "The U.S. Fusion Program as a Source of Technology Transfer"

1993 CONGRESSIONAL TESTIMONY

C. C. Baker, Testimony for Congressional Hearings on Fusion Energy Concepts held by the House of Representatives Committee on Science, Space, and Technology, May 1993

1994 BOOKS AND JOURNAL ARTICLES

S. E. Attenberger, S. P. Hirshman, and W. A. Houlberg, "MACH—A Computer Code for Solution of the Poloidal Asymmetry Eigenvalue Problem in Tokamaks," *Computer Phys. Communications* **79**, 341 (1994)

F. W. Baity, R. H. Goulding, D. J. Hoffman, P. M. Ryan, J. S. deGrassie, C. C. Petty, and R. I. Pinsker, "The Technology of Fast Wave Current Drive Antennas," *Fusion Eng. Des.* **24**, 91 (1994)

M. E. Bannister, X. Q. Guo, and T. M. Kojima, "Absolute Cross Sections for Electron-Impact Single Ionization of Kr^{4+}, Kr^{5+}, and Kr^{7+} Ions," *Phys. Rev. A* **49**, 4676 (1994)

M. E. Bannister, X. Q. Guo, T. M. Kojima, and G. H. Dunn, "Resonance Structure and Absolute Cross Sections in Near-Threshold Electron-Impact Excitation of the $4s^2\ ^1S \rightarrow 4s4p\ ^3P$ Intercombination Transition in Kr^{6+}," *Phys. Rev. Lett.* **72**, 3336 (1994)

L. R. Baylor, T. C. Jernigan, S. K. Combs, C. R. Foust, W. A. Houlberg, S. L. Milora, M. R. Wade, J. C. Phillips, and D. P. Schissel, "Initial Results from Deuterium Pellet Injection Experiments in DIII-D," *Bull. Am. Phys. Soc.* **39**(7), 1654 (1994)

E. W. Bell, X. Q. Guo, J. L. Forand, K. Rinn, D. R. Swenson, J. S. Swenson, G. H. Dunn, M. E. Bannister, D. C. Gregory, R. A. Phaneuf, A. C. H. Smith, A. Müller, C. A. Tanner, E. K. Wåhlin, B. D. DePaola, and D. S. Beli, "A Merged Beams Energy-Loss Technique for Electron-Ion Excitation: Absolute Total Cross Sections for O^{5+} (2s-2p)," *Phys. Rev. A* **49**, 4585 (1994)

G. L. Bell, J. M. Lohr, J. B. Wilgen, M. E. Austin, and C. B. Forest, "Initial ECE Radiometer Electron Temperature Measurements on DIII-D," *Bull. Am. Phys. Soc.* **39**(7), 1561 (1994)

T. S. Bigelow, C. R. Schaich, C. T. Wilson, and J. White, "ATF ECH System Long Pulse Operation," *Bull. Am. Phys. Soc.* **39**(7), 1627 (1994)

T. D. Burchell, W. P. Eatherly, and J. P. Strizak, "The Effect of Neutron Irradiation Damage on the Structure and Properties of Carbon-Carbon Composites," p. 1266 in *Effects of Radiation on Materials: 16th International Symposium*, ASTM STP 1175, ed. A. S. Kumar, D. S. Gelles, and R. K. Nanstad, American Society for Testing and Materials, Philadelphia, 1994

B. A. Carreras, P. H. Diamond, Y.-M. Liang, V. Lebedev, and D. E. Newman, *Plasma Phys. Controlled Fusion* **36**, A93–A98 (1994)

B. A. Carreras, D. E. Newman, P. H. Diamond, and Y.-M. Liang, "Dynamics of Low to High ("L" to "H") Bifurcation: Poloidal Flow and Ion Pressure Gradient Evolution," *Phys. Plasmas* **1**(12), 4014–21 (1994)

J. B. O. Caughman, G. L. Bell, W. L. Gardner, and D. J. Hoffman, "The Effects of RF Sheaths on the Erosion of Faraday Shield Coatings," *Bull. Am. Phys. Soc.* **39**(7), 1627 (1994)

L. A. Charlton, B. A. Carreras, V. E. Lynch, K. L. Sidikman, and P. H. Diamond, "Bifurcations and Modulational Interaction in Negative Compressibility Turbulence," *Phys. Plasmas* **1**(8), 2700–10 (1994)

L. A. Charlton, J.-N. Leboeuf, B. A. Carreras, and V. E. Lynch, "Radiation-Driven Turbulence at the Plasma Edge in Toroidal Devices," *Phys. Plasmas* **1**(12), 3871–82 (1994)

K. R. Chen, "Anomalous Thermalization of Fast Ions in Magnetized Plasma," *Phys. Rev. Lett.* **72**, 3534 (1994)

K. R. Chen, D. B. Batchelor, and J.-N. Leboeuf, "Alpha Particle Dynamics Due to Self-Driven Relativistic Lower-Hybrid cyclotron Waves," *Bull. Am. Phys. Soc.* **39**(7), 1763 (1994)

K. R. Chen, W. Horton, and J. W. Van Dam, "An Explanation for Experimental Observations of Harmonic Cyclotron Emission Induced by Fast Ions," *Phys. Plasmas* **1**(5), 1195–98 (1994)

J. W. Cobb, J.-N. Leboeuf, L. A. Berry, and E. F. Jaeger, "Orbit Consistent Plasma Processing Simulations," *Bull. Am. Phys. Soc.* **39**(7), 1728 (1994)

R. J. Colchin, J. D. Galambos, S. P. Hirshman and J. A. Rome, "Plasma Voltages, Flux Consumption, and Nuetral Beam Calculations for START," *Bull. Am. Phys. Soc.* **39**(7), 1572 (1994)

G. G. Craddock, A. E. Koniges, P. H. Diamond, D. E. Newman, and P. W. Terry, "Effects of Nonlinear Electron Dynamics in a Fluid Model of Collisionless Trapped-Electron Mode Turbulence," *Phys. Plasmas* **1**(6), 1877–81 (1994)

P. H. Diamond, B. A. Carreras, Y.-M. Liang, and P. W. Terry, *Phys. Rev. Lett.* **72**, 2565 (1994)

P. H. Diamond, Y.-M. Liang, B. A. Carreras, and P. W. Terry, "Self-Regulating Shear Flow Turbulence: A Paradigm for the L to H Transition," *Phys. Rev. Lett.* **72**, 2565 (1994)

N. Dominguez, K. C. Shaing, M. Yokoyama, M. Wakatani, and C. T. Hsu, "Approximate Analytic Expressions for Plasma Viscosity and Neoclassical Flows and Fluxes in Finite Aspect Ratio Tokamaks," *Bull. Am. Phys. Soc.* **39**(7), 1617 (1994)

L. Dresner, "On the Connection Between the Normal-Zone Voltage and the Hot-Spot Temperature in Uncooled Magnets," *Cryogenics* **34**(2), 111–18 (1994)

L. Dresner "Quench Energies of Uncooled Superconductors," *Cryogenics* **34**(1), 77–82 (1994)

A. C. England, J. B. Wilgen, G. R. Hanson, D. A. Rasmussen, M. Murakami, D. C. Stallings, J. H. Rogers, and J. R. Wilson, "Reflectometer Measurements of Edge-Density Profiles at an ICRF Antenna on TFTR," *Bull. Am. Phys. Soc.* **39**(7), 1674 (1994)

J. Galambos, Y-K. M. Peng, J. R. Haines, and J. Sheffield, "Minimun Size Q = 1 and Ignited Spherical Tokamak Devices," *Fusion Technol.* **26**(3, Pt. 2), 1196–1202 (1994)

J. D. Galambos and L. J. Perkins, "Sub-Ignited ITER-Like Designs—A Question of Confinement Margin," *Fusion Technol.* **25**(2), 176–81 (1994)

F. Y. Gang, D. J. Sigmar, J.-N. Leboeuf, and F. Wising, "Alpha-Particle Driven Alfvén Turbulence and Its Effect on Alpha-Particle Transport," *Fusion Technol.* **25**, 266–77 (1994)

T. W. Gorczyca, M. S. Pindzola, D. C. Griffin, and N. R. Badnell, "Configuration-Interaction Effects on the Electron-Impact Ionization of Ti^{3+}," *J. Phys. B* **27**, 2399 (1994)

R. H. Goulding, F. W. Baity, D. J. Hoffman, P. M. Ryan, M. J. Mayberry, C. C. Petty, and R. I. Pinsker, "Phased Operation of the DIII-D FWCD Antenna Array with a Single Power Source," *Fusion Eng. Des.* **24**, 103 (1994)

R. H. Goulding, G. L. Bell, D. J. Hoffman, P. M. Ryan, V. Bhatnagar, M. Bures, J. A. Dobbing, B. Fechner, D. F. H. Start, and T. J. Wade, "Initial FWCD Results using the JET A2 Antenna Arrays and Experience with Phased Operation," *Bull. Am. Phys. Soc.* **39**(7), 1566 (1994)

D. C. Griffin, M. S. Pindzola, F. Robicheaux, T. W. Gorczyca, and N. R. Badnell, "Nature of Interacting Resonances in Electron-Ion Excitation," *Phys. Rev. Lett.* **72**, 3491 (1994)

G. R. Hanson, J. B. Wilgen, T. S. Bigelow, I. Collazo, A. C. England, M. Murakami, D. A. Rasmussen, C. E. Thomas, J. R. Wilson, and H. K. Park, "Microwave Reflectometry for Edge Density Profile Measurements on TFTR" *Plasma Phys. Controlled Fusion* **36**(12), 2078–82 (1994)

G. R. Hanson, J. B. Wilgen, E. J. Doyle, K. W. Kim, C. L. Rettig, E. De La Luna, and J. Sanchez, "Edge Density Profile Measurements on DIII-D Using an AM Reflectometer," *Bull. Am. Phys. Soc.* **39**(7), 1560 (1994)

G. R. Haste, F. W. Baity, G. C. Barber, T. S. Bigelow, M. D. Carter, W. L. Gardner, R. H. Goulding, D. J. Hoffman, P. M. Ryan, and T. D. Shepard, "The Folded Waveguide: A High Frequency rf Launcher," *Fusion Eng. Des.* **24**, 191 (1994)

C. C. Havener, "Plasma Impurity Cross Section Data Involving e-Ion, Ion-Atom, Ion-Surface, and Ion-Ion Collisions at ORNL," INDC(NDS)-292, 35 (1994)

R. J. Hawryluk, S. P. Hirshman, et al., "Preparations for Deuterium-Tritium Experiments on the Tokamak Fusion Test Reactor," *Phys. Plasmas* **1**(5), 1560–67 (1994)

D. L. Hillis, G. Mank, K. H. Finken, H. Euringer, U. Samm, B. Unterberg, M. R. Wade J. T. Hogan, A. Post-Zwicker, J. A. Boedo, D. S. Gray, A. M. Messien, G. van Oost, J. Ongena, G. Van Wassenhove, and P. Dumortier, "Helium Transport and Exhaust in the Presence of a Neon Radiating Boundary with the ALT-II Pump Limiter in TEXTOR," *Bull. Am. Phys. Soc.* **39**(7), 1567 (1994)

S. P. Hirshman, W. A. Houlberg, S. E. Attenberger, S. I. Krasheninnikov, D. J. Sigmar, and D. Knoll, "Reduced Impurity Flow Modeling of the Scrape-Off Plasma," *Bull. Am. Phys. Soc.* **39**(7), 1713 (1994)

S. P. Hirshman, D. K. Lee, F. M. Levinton, S. H. Batha, and R. M. Wieland, "Equilibrium Reconstruction of the Q-Profile in Tokamaks from Motional Stark Effect Data," *Phys. Plasmas* **1**(7), 2277–90 (1994)

W. A. Houlberg and S. E. Attenberger, "Evaluation of Current Drive Requirements and Operating Characteristics of a High Bootstrap Fraction Advanced Tokamak Reactor," *Fusion Technol.* **26**(3, Pt. 2), 566–71 (1994)

W. A. Houlberg and S. E. Attenberger, "Evaluation of Pumping and Fueling Requirements for the ITER EDA," *Fusion Technol.* **26**(3, Pt. 2), 316–21 (1994)

W. A. Houlberg and S. E. Attenberger, "Isotopic Tailoring of Fuel Density Profiles Using Auxiliary Fueling Sources and Pumping," *Bull. Am. Phys. Soc.* **39**(7), 1595 (1994)

W. A. Houlberg, S. E. Attenberger, and M. J. Grapperhaus, "Density Control in a Fusion Reactor Using Pellet Injection," *Nucl. Fusion* **34**(1), 93–108 (1994)

C. T. Hsu, K. C. Shaing, and R. Gormley, "Time Dependent Parallel Viscosity and Relaxation Rates of Poloidal Rotation in the Banana Regime," *Phys. Plasmas* **1**, 132–38 (1994)

R. C. Isler, "An Overview of Charge-Exchange Spectroscopy as a Plasma Diagnostic," *Plasma Phys. Controlled Fusion* **36**(2), 171 (1994)

R. Ito, T. Tabata, T. Shirai, and R. A. Phaneuf, "Analytic Cross Sections for Collisions of H, H_2, He and Li Atoms and Ions with Atoms and Molecules, II," JAERI-Data/Code 94-005 (1994)

T. C. Jernigan and the ATF Team, "Long Pulse Experiments on the ATF Stellarator," *Bull. Am. Phys. Soc.* **39**(7), 1545 (1994)

R. L. Klueh and D. J. Alexander, "Charpy Impact Toughness of Martensitic Steels Irradiated in FFTF: Effect of Heat Treatment," p. 591 in *Effects of Radiation on Materials: 16th International Symposium*, ASTM STP 1175, ed. A. S. Kumar, D. S. Gelles, and R. K. Nanstad, American Society for Testing and Materials, Philadelphia, 1994

L. E. Lagos, W. Li, M. A. Ebadian, T. L. White, R. G. Grubb, D. Foster, "Two-Dimensional Finite Element Analysis of Heat Transfer within a Concrete Slab Exposed to a Microwave Source," *J. Heat Transfer* ASME Transactions, March 1994

R. A. Langley, M. J. Gouge, and D. J. Santeler, "Vacuum System Design of the International Thermonuclear Experimental Reactor Pellet Fueling System," *J. Vac. Sci. Technol. A* **12**, 1635–38 (1994)

J.-N. Leboeuf, K. R. Chen, J. M. Donato, D. B. Geohegan, C. L. Liu, and R. F. Wood, "Two-Dimensional Modeling of Plume Dynamics in Laser Ablation Processes," *Bull. Am. Phys. Soc.* **39**(7), 1763 (1994)

J.-N. Leboeuf, C. L. Hedrick, V. E. Lynch, K. L. Sidikman, D. A. Spong, and R. D. Sydora, "Nonlinear Calculations of Core Fluctuations with Gyro-Landau Fluid Models," *Bull. Am. Phys. Soc.* **39**(7), 1664 (1994)

C. K. Lee, B. A. Chin, S. J. Zinkle, and R. C. Wilcox, "Mechanical Properties of Induction Brazed GlidCop Al-15," pp. 1026–40 in *Effects of Radiation on Materials: 16th International Symposium*, ASTM STP 1175, ed. A. S. Kumar, D. S. Gelles, and R. K. Nanstad, American Society for Testing and Materials, Philadelphia, 1994

D. C. Lousteau, "The ITER In-Vessel System," *Fusion Technol.* **26**(3, Pt. 2), 284–91 (1994)

J. W. Lue, M. S. Lubell, et al., "Test Result of Two Small High Temperature Superconducting Coils," *Adv. Cryog. Eng.* **40A**, 327–34 (1994)

J. W. Lue, M. S. Lubell, et al., "Development of Lightweight, High Current Density Superconducting Coils," *IEEE Trans. Magn.* **30**, 2364 (1994)

C. J. Lundy, R. E. Olson, D. R. Schultz, and J. P. Pascale, "Coherence Parameters for Electron Capture in H^+ + He Collisions," *J. Phys. B* **27**, 935 (1994)

J. F. Lyon, K. Gulec, R. L. Miller, and L. El-Guebaly, "Status of the U.S. Stellarator Reactor Study," *Fusion Eng. Des.* **25**(1–3), 85 (1994)

J. F. Lyon, S. L. Painter, L. M. Kovrizhnykh, and K. Gulec, "Stellarator Transport Optimization With Self-Consistent Electric Fields," *Bull. Am. Phys. Soc.* **39**(7), 1603 (1994)

J. W. McKeever, C. W. Sohns, S. W. Schwenterly, et al., "Operation of a Test Bed Axial-Gap Brushless DC Rotor with a Superconducting Stator," *Adv. Cryog. Eng.* **39**, 941–48 (1994)

M. M. Menon, G. J. Laughon, R. Maingi, M. R. Wade, D. L. Hillis, and M. A. Mahdavi, "Pumping Characteristics of a Cryopump with Ar Sorbent in He and in D_2/He Mixture," *J. Vac. Sci. Tech.* **13**(3, Pt. 1), 551–55 (1994)

M. Murakami, D. B. Batcherlor, A. C. England, G. R. Hanson, E. F. Jaeger, D. A. Rasmussen, C. Wang, J. B. Wilgen, M. G. Bell, R. V. Budny, E. Fredrickson, J. C. Hosea, R. Majeski, H. Park, C. K. Phillips, J. H. Rogers, G. Schilling, S. C. Scott, J. E. Stevens, G. Taylor, J. R. Wilson, and M. C. Zarnstorff, "Modulated ICRF Heating and Transport in DT TFTR Plasmas," *Bull. Am. Phys. Soc.* 39(7), 1698 (1994)

D. E. Newman, B. A. Carreras, and P. H. Diamond, "A Computational Study of the Dynamics of Hydrodynamic Trapped Ion Temperature Gradient Driven Turbulence," *Bull. Am. Phys. Soc.* 39(7), 1655 (1994)

D. E. Newman, P. W. Terry, P. H. Diamond, Y.-M. Liang, G. G. Craddock, A. E. Koniges, and J. A. Crottinger, "The Dynamics of Long Wavelength Electrostatic Turbulence in Tokamaks," *Phys. Plasmas* 1(5), 1592–1600 (1994)

J. E. Pawel, D. J. Alexander, M. L. Grossbeck, A. W. Longest, A. F. Rowcliffe, G. E. Lucas, S. Jitsukawa, A. Hishinuma, and K. Shiba, *J. Nucl. Mater.* **212–15**, 442–47 (1994)

Y-K. M. Peng, R. J. Colchin, C. L. Hedrick. J. D. Galambos, J. Sheffield, D. J. Strickler, R. A. Blanken, A. Sykes, D. C. Robinson, A. W. Morris, J. Hugill, T. C. Hender, S. K. Erents, and H. R. Wilson, "Physics Progress Towards Compact Tokamak Reactors with Normal Conducting Toroidal Field Coils," in *Plasma Physics and Controlled Nuclear Fusion Research,* IAEA, Vienna, 1994

Y-K. M. Peng, C. L. Hedrick, K. Erents, D. Goodall, J. Hugill, and A. Sykes, "MHD Ballooning Stability Limit for Scrape-Off Layer Thickness," *Bull. Am. Phys. Soc.* 39(7), 1713 (1994)

M. S. Pindzola, T. W. Gorczyca, N. R. Badnell, D. C. Griffin, M. Stenke, G. Hofmann, B. Weissbecker, K. Tinschert, E. Salzborn, A. Müller, and G. H. Dunn, "Dielectronic Capture Processes in the Electron-Impact Ionization of Sc^{2+}," *Phys. Rev. A* **49**, 933 (1994)

D. A. Rasmussen, R. Kumazawa, K. Nishimura, S. Masuda, T. Mutoh, F. Shimbo, T. Seki, T. Watari, R. Akiyama, A. Ando, A. Ejiri, H. Idei, K. Ida, H. Iguchi, S. Kubo, K. Matsuoka, T. Morisaki, S. Morita, S. Okamura, T. Ozaki, S. Sakakibara, C. Takahashi, T. Kawamoto, K. Tanaka, J. Xu, H. Yamada, I. Yamada, M. Murakami, D. J. Hoffman, and E. F. Jaeger, "Ion Cyclotron Heating in the Compact Helical System (CHS)," *Bull. Am. Phys. Soc.* 39(7), 1627 (1994)

M. J. Rennich and B. E. Nelson, "TPX Remote Maintenance and Shielding," *Fusion Technol.* 26(3, Pt. 2), 376–80 (1994)

B. Richards, T. Uckan, A. J. Wootton, B. A. Carreras, R. D. Bengtson, P. Hurwitz, G. X. Li, H. Lin, W. L. Rowan, H. Y. W. Tsui, A. K. Sen, and J. Uglum, "Modifcation of Tokamak Edge Turbulence Using Feedback," *Phys. Plasmas* 1, 1606–11 (1994)

J. A. Rome and the SPPS Team, "Stellarator Power Plant Study," *Bull. Am. Phys. Soc.* 39(7), 1603 (1994)

P. M. Ryan, F. W. Baity, R. H. Goulding, G. R. Haste, D. J. Hoffman, K. E. Rothe, and J. H. Whealton, "Methods of Calculating Selected Geometrical Effects in the Design of ICRH Antennas," *Fusion Eng. Des.* 24, 135 (1994)

P. M. Ryan, D. W. Swain, R. H. Goulding, M. D. Carter, D. J. Hoffman, and D. B. Batchelor, "Phase Control System for the TPX ICH Antenna Arrays," *Bull. Am. Phys. Soc.* 39(7), 1569 (1994)

D. R. Schultz, "Atomic and Molecular Data Needs for Fusion," *AIP Conference Proceedings of the Ninth Topical Conference on Atomic Processes in Plasmas*, September 19–23, 1994, San Antonio, Texas

D. R. Schultz, S. Yu. Ovchinnikov, and S. V. Passovets, "Elastic and Related Cross Sections for Low Energy Collisions Among Hydrogen and Helium Ions, Neutrals, and Isotopes," in *Atomic and Molecular Processes in Magnetic Fusion Edge Plasmas*, Plenum, New York, 1994

D. R. Schultz, C. O. Reinhold, and R. E. Olson, "Two-Center Effects in the Ejected-Electron Spectra in Ion-Atom Collisions," in *Proceedings of Symposium on Two-Center Effects in Ion-Atom Collisions*, Lincoln, Nebraska, May 13–14, 1994, AIP Press, New York, 1994

K. C. Shaing, "Confinement Improvement Mechanism in Very High Mode (VH-Mode) and High-Beta-Poloidal Mode," *Phys. Plasmas* 1(2), 219–21 (1994)

K. C. Shaing, "Erratum: Test of Tokamak Low-Mode-High-Mode Transition Theory in Stellarators," *Phys. Plasmas* 1(5), 1373 (1994)

K. C. Shaing and C. T. Hsu, "Poloidal Flow and E × B Flow in H-Mode," *Bull. Am. Phys. Soc.* 39(7), 1617 (1994)

K. C. Shaing, C. T. Hsu, and N. Dominguez, "Resonance Parallel Viscosity in the Banana Regime in Poloidally Rotating Tokamak Plasmas," *Phys. Plasmas* 1(5), 1168–76 (1994)

K. C. Shaing, C. T. Hsu, and R. D. Hazeltine, "Effects of Orbit Squeezing on Poloidal Mass Flow and Bootstrap Current in Tokamka Plasmas," *Phys. Fluids B* 5, 3365–68 (1994)

J. Sheffield, "Fusion Energy and Technology Development," *Bull. Am. Phys. Soc.* 39(2), 1247 (1994)

J. Sheffield, "Magnetic Fusion Commercial Power Plants," *J. Fusion Energy*, 13(2/3), 167–70 (1994)

J. Sheffield, "The Physics of Magnetic Fusion Reactors," *Rev. Mod. Phys.* 66(3), 1015–1104 (1994)

J. Sheffield and J. D. Galambos, "Prospects for Toroidal Fusion Reactors," *Fusion Technol.* 26(3, Pt. 2), 1122–26 (1994)

K. L. Sidikman, B. A. Carreras, P. H. Diamond, and L. Garcia, "Theory of Electric-Field Curvature Effects on Long-Wavelength Drift Wave Turbulence," *Phys. Plasmas* 1(5), 1142–53 (1994)

K. L. Sidikman, B. A. Carreras, and L. Garcia, "Drift Wave Turbulence in a Plasma with Sheared Flow," *J. Comput. Phys.* 114(1), 100–12 (1994)

D. A. Spong, "Visualization fo MHD Turbulence in Toroidal Magnetically Confined Plasmas," *AVS Network News* 3, 3–5 (1994)

D. A. Spong, B. A. Carreras, and C. L. Hedrick, "Nonlinear Evolution of the Toroidal Alfvén Instability using a Gyrofluid Model," *Phys. Plasmas* 1(5), 1503–10 (1994)

D. W. Swain, F. W. Baity, D. B. Batchelor, S. C. Chiu, J. Degrassie, E. J. Doyle, G. R. Hanson, K. W. Kim, R. I. Pinsker, C. C. Petty, C. L. Rettig, and J. Wilgen, "DIII-D FWCD Antenna Operation with No Faraday Shield," *Bull. Am. Phys. Soc.* 39(7), 1649 (1994)

G. Taylor, "ICRF Heating on TFTR D-T Supershot Plasmas," *Bull. Am. Phys. Soc.* 39(7), 1673 (1994)

K. S. Toth, "Comment on 'Decays and Masses of ^{162,163}Ta and Some Neighboring Nuclides,'" *Phys. Rev. C* 50, 518–19 (1994)

N. A. Uckan, J. T. Hogan, W. A. Houlberg, J. D. Galambos, L. J. Perkins, S. W. Haney, S. Kaye, and D. E. Post, "ITER Design: Physics Basis for Size, Confinement Capability, Power Levels and Burn Control," *Fusion Technol.* 26(3, Pt. 2), 327–30 (1994)

T. Uckan, M. Chatelier, A. Grlsman, T. Loarer, P. K. Mioduszewski, and L. W. Owen, "Power and Particle Handling Studies for the Tore Supra Toroidal Belt Pump Limiter," *Bull. Am. Phys. Soc.* 39(7), 1757 (1994)

T. Uckan, R. C. Isler, T. C. Jernigan, J. F. Lyon, P. K. Mioduszewski, M. Murakami, D. A. Rasmussen, and J. B. Wilgen, "Biased Limiter Experiments on the Advanced Toroidal Facility (ATF) Torsatron," *Nucl. Fusion* 34(2), 295–99 (1994)

M. R. Wade, J. T. Hogan, D. L. Hillis, R. Maingi, M. M. Menon, K. H. Burrell, R. J. Groebner, M. A. Mahdavi, W. P. West, D. F. Finkenthal, and the DIII-D Team, "Helium Transport and Exhaust Studies in DIII-D," *Fusion Technol.* 26(3, Pt. 2), 595–602 (1994)

M. Wakatani and K. C. Shaing, "Shock Formation in Poloidally Rotating Helically Symmetric Plasmas," *Bull. Am. Phys. Soc.* 39(7), 1617 (1994)

C. Y. Wang, D. B. Batchelor, and E. F. Jaeger, "Parallel Forces Induced by Waves in Ion Cyclotron Range of Frequency," *Bull. Am. Phys. Soc.* 39(7), 1617 (1994)

C. Y. Wang, E. F. Jaeger, D. B. Batchelor, and K. L. Sidikman, "Fast Wave Poloidal Flow Generation in a Plasma," *Phys. Plasmas* 1(12), 3890–95 (1994)

A. S. Ware, P. H. Diamond, and B. A.. Carreras, "Comment on 'Critique of Atomic Physics Instability Mechanisms :Ionization-Driven and Radiative Microinstbilities in the Tokamka Edge Plasmas' [*Phys. Plasmas* 1, 2630 (1994)]," *Phys. Plasmas* 1, 2806–07 (1994)

C. Watts, D. E. Newman, and J. C. Sprott, "Chaos In Reversed-Field-Pinch Plasma Simulation and Experiment," *Phys. Rev E* 49(3), 2291–2301 (1994)

A. Weller, D. A. Spong, R. Jaenicke, A. Lazaros, F. P. Penningsfeld, S. Sattler, the W7-AS Team, and the NBI Group, *Phys. Rev. Lett.* 72, 1220 (1994)

J. B. Wilgen, A. C. England, T. S. Bigelow, G. R. Dyer, D. E. Greenwood, M. Murakami, C. R. Schaich, J. A. White, and J. L. Yarber, "ECE Radiometer Measurement of Electron Temperature on the ATF Stellarator," *Bull. Am. Phys. Soc.* 39(7), 1603 (1994)

S. J. Zinkle, E. V. Nesterova, V. R. Barabash, V. V. Rybin, and A. V. Naberenkow, "Effect of Ion Irradiation on the Structure Stability of Commercial Dispersion-Strengthened Copper Alloys," *J. Nucl. Mater.* **208**, 119–27 (1994)

1994 PRESENTATIONS

January

SPIE—International Conference on Millimeter and Submillimeter Waves and Applications, San Diego, California, January 10–14, 1994. Proceedings published as *Special SPIE Proceedings*

T. S. Bigelow, "A Quasi-Optical Resonant Ring for High Power ECH Window Testing"

Workshop on Ion Cyclotron Range of Frequency (ICRF) Heating & Current Drive in Deuterium-Tritium (DT) Plasmas, PPPL, Princeton, New Jersey, January 13–15, 1994

E. F. Jaeger, M. Murakami, C. Y. Wang, J. R. Wilson, R. Majeski, and C. K. Phillips, "Full Wave ICRF Modeling for D-T Experiments on TFTR"

ITER Technical Meeting on Fueling and Pumping, Garching ITER Co-center, Garching, Germany, Seminar at CEA Cadarache, France, January 19–26, 1994 . Proceedings published

D. L. Hillis, DIII-D Team, and TEXTOR Team (presented by W. A. Houlberg), "Helium Transport and Exhaust Studies in the DIII-D and TEXTOR Tokamaks"

W. A. Houlberg and S. E. Attenberger, "Particle Control Aspects of Fueling and Pumping for the ITER EDA Design"

IAEA Technical Meeting on Microwave Reflectometry for Fusion Plasma Diagnostics, Princeton Plasma Physics Laboratory, Princeton, New Jersey, January 25–February 7, 1994. Proceedings published as *Proceedings of the International Atomic Energy Agency (IAEA) Technical Meeting on Microwave Reflectometry for Fusion Plasma Diagnostics, Princeton, NJ, January 1994*

G. R. Hanson, J. B. Wilgen, T. S. Bigelow, I. Collazo, D. A. Rasmussen, D. B. Batchelor, D. J. Hoffman, E. F. Jaeger, R. Majeski, M. Murakami, H. K. Park, J. H. Rogers, P. M. Ryan, D. C. Stallings, and J. R. Wilson, "Results from the TFTR Edge Profile Reflectometer"

E. de La Luna, G. R. Hanson, J. B. Wilgen, J. Sanchez, V. Zhuravlev, R. Kaita, J. H. Harris, and the PBX-M Team, "First Results with Amplitude Modulation Reflectometry"

Oral Presentation at Auburn University, Auburn, Alabama, January 28, 1994

B. A. Carreras, "Plasma Turbulence and Global Flows"

February

Technical Meeging and Workshop on ITER Divertor Physics Design, Garching, Germany, February 21, 1994

Y-K. M. Peng and L. Hedrick, "MHD Ballooning Stability Limit for Scrape-Off Layer Thickness"

March

Workshop on Deuterium and Tritium (DT) Experiments, Princeton Plasma Physics Laboratory, Princeton, New Jersey, March 2–4, 1994

D. A. Spong, B. A. Carreras, C. L. Hedrick, and J.-N. Leboeuf, "TAE Stability Thresholds in the TFTR DT Experiments"

Seventh Transport Task Force Workshop, Dallas, Texas, March 8–12, 1994. Abstracts published

W. A. Houlberg and S. E. Attenberger, "The Reactor Potential of TPX Advanced Physics Regimes"

D. E. Newman, B. A. Carreras, and P. H. Diamond, "External Control of the Power Threshold for L-H Transitions"

15th Werner Brandt Workshop, Gainesville, Florida, March 10–11, 1994

L. Folkerts, S. Schippers, and F. W. Meyer, "Charge State Distributions from Highly Charged Ions Channeled at a Metal Surface"

U.S. Stellarator Powewr Plant Study Workshop, Dallas, Texas, March 13, 1994

R. A. Dory, "Energy Confinement in Stellarators—τ_E Scaling"

1994 International Sherwood Fusion Theory Conference, Dallas, Texas, March 14–16, 1994. Proceedings published

L. A. Charlton, B. A. Carreras, V. E. Lynch, and P. H. Diamond, "Parallel Ion Flow Gradient-Driven Instability and the L-H Transition"

M. D. Carter, D. B. Batchelor, T. S. Bigelow, G. L. Bell, and D. J. Hoffman, "Three Dimensional Modeling of RF Current Drive Arrays"

K. R. Chen, D. B. Batchelor, J.-N. Leboeuf, V. H. Wong, and W. Horton, "Anomalous Thermalization of Fast Ions in Magnetized Plasma due to Two-Gyro-Stream Instability"

C. L. Hedrick, J.-N. Leboeuf, and K. L. Sidikman, "Fitting Eigenfunctions and Suppressing Noise in a Landau Fluid Approach to Dissipative Trapped Electron Modes"

W. A. Houlberg and S. E. Attenberger, "A High Density, Low Temperature Ignition Regime for the International Tehrmonuclear Experimental Reactor (ITER)"

E. F. Jaeger, M. Murakami, C. Y. Wang, D. B. Batchelor, R. Majeski, C. K. Phillips, and J. R. Wilson, "Full-Wave ICRF Modeling of Electron Heating and Current Drive by Mode Converted Slow Waves in Tokamaks"

Y. R. Lin-liu, F. L. Hinton, C. F. F. Karney, and S. P. Hirshman, "A Numerical Study of the Neoclassical Bootstrap Current Using Adjoint Functions"

V. E. Lynch, B. A. Carreras, J.-N. Leboeuf, and B. C. Curtis, "The Performance of Fluid Codes on a Dedicated Cray Y-MP C90"

D. E. Newman, B. A. Carreras, and P. H. Diamond, "The Dymanics of Front-Like and Uniform Transitions from L to H or VH Modes"

J. A. Rome, "New Stellarator Reactor Concepts"

K. C. Shaing, C. T. Hsu, and R. D. Hazeltine, "Effects of Orbit Squeezing on Poloidal Mass Flow and Bootstrap Current in Tokamak Plasmas"

K. L. Sidikman, C. L.Hedrick, and J.-N. Leboeuf, "Nonlinear Calculations of Dissipative Trapped Electron Modes with Ion Magnetic Drift"

D. J. Sigmar, S. I. Krasheninnikov, and S. P. Hirshman, "Simplified Description of High-Z Impurity Transport in Tokamak Edge Plasma"

D. A. Spong, C. L. Hedrick, and B. A. Carreras, "Excitation of TAE/GAE Shear Alfvén Modes by an Energetic Alpha Population in the TFTR DT Experiments"

M. Wakatani and K. C. Shaing, "Shock Formation in Poloidally Rotating Helically Symmetric Plasmas"

C. Y. Wang, E. F. Jaeger, D. B. Batchelor, and K. L. Sidikman, "Fast Wave Poloidal Flow Generation in a Plasma"

Scrape-Off Layer and Divertor Theory Meeting, Dallas, Texas, March 16, 1994

W. A. Houlberg and S. E. Attenberger, "Evaluation of Pumping and Fueling in Coupled Core, Scrape-Off Layer and Divertor Chamber Calculations"

K. R. Chen, D. B. Batchelor, J.-N. Leboeuf, V. H. Wong, and W. Horton, "Anomalous Thermalization of Fast Ions in Magnetized Plasma Due to Two-Gyro-Instability"

Third Annual Numerical Tokamak Symposium, Dallas, Texas, March 16–17, 1994

J.-N. Leboeuf, C. L. Hedrick, V. E. Lynch, K. L. Sidikman, D. A. Spong, J. Dawson, V. Decyk, and R. Sydora, "Gyro-Landau Fluid Models of Dissipative Trapped Electron Mode Turbulence and Toroidal Alfvén and Global Alfvén Instabilities"

J.-N. Leboeuf, V. E. Lynch, B. A. Carreras, J. Donato, C. L. Hedrick, K. L. Sidikman, D. A. Spong, and B. Curtis, "The Performance of Fluid Codes on a Dedicated Cray Y-MP C90 and on the Intel Paragons"

April

7th Boulder International RF Workshop on RF Current Drive and Profile control for Advanced tokamaks, Boulder, Colorado, April 6–8, 1994

M. D. Carter, D. B. Batchelor, G. L. Bell, T. S. Bigelow, A. C. England, G. R. Hanson, J. H. Harris, D. J. Hoffman, E. F. Jaeger, C. C. Klepper, D. A. Rasmussen, P. M. Ryan, C. E. Thomas, J. B. Wilgen, D. C. Stallings, J. Rogers, J. R. Wilson, B. Beaumont, A. Becoulet, D. Guilhem, A. Grosman, H. Kuus, and B. Saoutic, "Three Dimensional Modeling of Phased Antennas"

American Physical Society Division of Atomic, Molecular, and Optical Physics (1994 Joint April Meeting of the American Physical Society and the American Association of Physics Teachers), Crystal City, Virginia, April 18–22, 1994. Abstracts published in *Bull. Am. Phys. Soc.*

M. E. Bannister, X. Q. Guo, and T. M. Kojima, "Electron-Impact Single Ionization of Kr^{4+}, Kr^{5+}, and Kr^{7+} Ions"

L. Folkerts, M. A. Haque, and C. C. Havener, "Low-Energy Electron Capture Cross Sections for N^{4+} + H Collisions Using Merged Beams"

L. Folkerts and F. W. Meyer, "Below-Surface Auger Electron Emission from Collisions of Ar^{17+} and Ar^{18+} with Au(011)"

D. R. Schultz and D. H. Madison, "Lattice Approach for Fully Correlated Two-Electron Systems"

J. Sheffield, "Fusion Energy and Technology Development"

J. L. Shinpaugh, F. W. Meyer, A. Basalaev, and S. Datz, "Charge Transfer in Multiply Charged Ion-Ion Collisions"

J. S. Thompson, A. M. Covington, and C. C. Havener, "Low-Energy Electron Capture Cross Sections for Heavy Multicharged Ion Collisions with Hydrogen Using Merged Beams"

Presentation at CIEMAT, Madrid, Spain, April 1994

B. A. Carreras, "Dynamics of the L to H Transition"

B. A. Carreras, "Technology 2000"

B. A. Carreras, "The ORNL R&D Strategic Plan"

B. A. Carreras, D. E. Newman, and P. H. Diamond, "Spatially Propagating Transition Fronts"

Oral Presentation at Universidad Carlos III, Madrid, Spain, April 18–22, 1994

B. A. Carreras, "Confinement Improvement in Fusion Experiments"

International Symposium on Decontamination and Decommissioning, Knoxville, Tennessee, April 25–29, 1994

P. W. Fisher and C. A. Foster, "Centrifugal Cryoblaster for Decommissioning and Decontamination"

T. L. White, C. R. Schaich, C. T. Wilson, and D. Foster, Jr., "Phase II Results Microwave Concrete Decontamination"

May

ITER Steering Committee, U.S. (ISCUS) Committee Meeting, Princeton, New Jersey, May 3–4, 1994

B. A. Carreras, "Transport Task Force"

Presentation at Princeton Plasma Physics Laboratory, Princeton, New Jersey, May 4, 1994

J. Sheffield and J. Galambos, "Fusion, the Competition and the Need for Realistic Fusion Research"

10th Topical Conference on High-Temperature Plasma Diagnostics, Rochester, New York, May 8–12, 1994. Proceedings published

G. R. Hanson, J. B. Wilgen, T. S. Bigelow, I. Collazo, A. C. England, M. Murakami, D. A. Rasmussen, and J. R. Wilson, "Differential Phase Reflectometry for Edge Profile Masurements on TFTR"

G. R. Hanson, H. K. Park, J. B. Wilgen, and M. Murakami, "Integrating Reflectometer Edge Profile Data with Multichannel Interferometric Measurements"

C. H. Ma, D. P. Hutchinson, R. K. Richards, J. Irby, and T. Luke, "A CO_2 Laser Polarimeter for Measurement of Plasma Current Profile in Alcator C-Mod"

D. A. Rasmussen, C. E. Thomas, D. W. Swain, D. B. Batchelor, J. B. Caughman, R. J. Colchin, R. H. Goulding, G. R. Hanson, D. J. Hoffman, R. C. Isler, E. F. Jaeger, and J. B. Wilgen, "Possible Integrated Diagnostic Set for Ion Cyclotron Heating for the Tokamak Physics Experiment (TPX)"

R. K. Richards, D. P. Hutchinson, and C. H. Ma, "Design of a CO_2 Laser Thomson Scattering Ion Tail Diagnostic for Alcator C-Mod"

M. G. Shats, K. M. Likin, J. B. Wilgen, J. H. Harris, K. A. Sarksyan, L. R. Baylor, J. D. Bell, T. S. Bigelow, J. L. Dunlap, R. C. Goldfinger, and C. H. Ma, "Microwave Scattering Diagnostic on the ATF Torsatron"

C. E. Thomas, J. H. Harris, G. R. Haste, M. Kwon, R. H. Goulding, D. J. Hoffman, B. Saoutic, A. Becoulet, D. Fraboulet, L. Ladurelle, and J. Y. Pascal, "The Tore Supra Fast Reciprocating ICRF Probe"

J. B. Wilgen, G. R. Hanson, T. S. Bigelow, I. Collazo, M. Murakami, D. A. Rasmussen, and J. R. Wilson, "Differential Phase Reflectometry for Edge Profile Measurements on TFTR"

Symposium on Two-Center Effects in Ion-Atom Collisions, Lincoln, Nebraska, May 13–14, 1994. Proceedings published by AIP Press, New York, 1994

D. R. Schultz, C. O. Reinhold, and R. E. Olson, "Two-Center Effects in the Ejected-Electron Spectra in Ion-Atom Collisions"

NSRP Panel SP-3 Surface Preparation & Coating Meeting, Kenner, LA, May 16–17, 1994

C. A. Foster and P. W. Fisher, "Advanced Turbine/CO_2 Pellet"

1994 Department of Defense (DoD)/Industry Advanced Coatings Removal Conference, New Orleans, Louisiana, May 16 or 17–19, 1994

C. A. Foster and P. W. Fisher, "Advanced Turbine/CO_2 Pellet Accelerator"

Paralell Virtual Machine (PVM) Users' Group Meeting, Oak Ridge, TN, May 19–20, 1994

V. E. Lynch, B. A. Carreras, J. B. Drake, and J.-N. Leboeuf, "Using PVM for Fusion Energy Turbulence Calculations"

11th International Conference on Plasma Surface Interactions in Controlled Fusion Devices, Ibaraki-ken, Japan, May 23–27, 1994. Proceedings published in *J. Nucl. Mater.* **220–222** (1995)

J. T. Hogan, P. K. Mioduszewski, D. Guilhem, A. Seigneur, and W. Hess, "Modeling of Impurity Generation and Transport at the Large Area Inner-Wall Limiter of Tore Supra"

C. C. Klepper, J. T. Hogan, S. Tobin, D. Guilhem, W. Hess, and P. Monier-Garbet, "Measurements and Modeling of Impurity Source Distributions from the Tore Supra Outboard Pump Limiter"

L. W. Owen, R. Maingi, J. T. Hogan, P. K. Mioduszewski, D. L. Hillis, M. R. Wade, D. R. Baker, A. W. Leonard, M. A. Mahdavi, J. W. Cuthbertson, and C. J. Lasnier, "Transport Modeling of Divertor D_α Radiation and Core Fueling in DIII-D"

R. Maingi, P. K. Mioduszewski, J. W. Cuthbertson, D. N. Hill, D. L. Hillis, J. T. Hogan, C. C. Klepper, C. J. Lasnier, D. K. Lee, A. W. Leonard, M. A. Mahdavi, R. A. Moyer, L. W. Owen, M. J. Schaffer, R. D. Stambaugh, M. R. Wade, and J. G. Watkins, "Effect of Low Density H-Mode Operation on Edge and Divertor Plasma Parameters"

R. Maingi, P. K. Mioduszewski, J. W. Cuthbertson, D. L. Hillis, J. T. Hogan, C. C. Klepper, C. J. Lasnier, A. W. Leonard, M. A. Mahdavi, R. A. Moyer, L. W. Owen, M. J. Schaffer, M. R. Wade, and J. G. Watkins, "Effect of Particle Exhaust on Edge and Divertor Plasma Parameters"

P. K. Mioduszewski, "Steady State Particle Handling in Tokamaks with Controlled Particle Exhaust"
C. E. Thomas, J. H. Harris, G. R. Haste, C. C. Klepper, J. T. Hogan, S. Tobin, F. W. Baity, M. D. Carter, D. J. Hoffman, P. M. Ryan, B. Saoutic, B. Beaumont, A. Becoulet, H. Kuus, D. Fraboulet, A. Grosman, D. Guilhem, J. Walter, T. Loarer, M. Chatelier, and Equipe Tore Supra, "First Results from Experimental Measurements of ICRF and Edge/SOL Plasma Interactions on Tore Supra"
T. Uckan, B. Richards, A. J. Wootton, R. D. Bengtson, B. A. Carreras, G. X. Li, P. Hurwitz, W. L. Rowan, H. Y. W. Tsui, J. R. Uglum, and D. Winslow, "Feedback Control and Stabilization Experiments on the Texas Experimental Tokamak (TEXT)"
M. R. Wade, D. L. Hillis, J. T. Hogan, R. Maingi, C. C. Klepper, W. P. West, A. Mahdavi, K. H. Burrell, G. L. Jackson, and N. H. Brooks, "Helium Exhaust Studies in ELMing H-mode Plasmas in DIII-D"
M. R. Wade, J. T. Hogan, D. L. Hillis, M. A. Mahdavi, R. Maingi, W. P. West, N. H. Brooks, K. H. Burrell, D. F. Finkental, R. J. Groebner, G. L. Jackson, C. C. Klepper, G. L. Laughon, M. M. Menon, P. K. Mioduszewski, and the DIII-D Team, "Helium Exhaust Studies in the DIII-D Tokamak"

June

Collaboration on Transport Status and Modeling, Moscow, Russia, June 6–11, 1994
B. A. Carreras, "Dynamics of the L to H Transition"
B. A. Carreras, "Transport Task Force Modeling Working Group"

1994 Science and Technology Advisory Council Meeting, June 7, 1994
A. W. Trivelpiece and J. Sheffield, "ITER Site in Tennessee"

Workshop on Transport in Fusion Plasmas, Göteborg, Sweden, June 14–17, 1994
B. A. Carreras, "Dithering Transitions"
B. A. Carreras, "Transport Task Force Workshop 1994"

11th Topical Meeting on the Technology of Fusion Energy, New Orleans, Louisana, June 19–23, 1994. Proceedings published in *Fusion Technol.*
J. D. Galambos and Y-K. M. Peng, "Comparison of Standard and Spherical Tokamak Volume Neutron Sources (VNS)"
J. Galambos, Y-K. M. Peng, J. R. Haines, and J. Sheffield, "Minimun Size Q = 1 and Ignited Spherical Tokamak Devices"
W. A. Houlberg and S. E. Attenberger, "Evaluation of Current Drive Requirements and Operating Characteristics of a High Bootstrap Fraction Advanced Tokamak Reactor"
W. A. Houlberg and S. E. Attenberger, "Evaluation of Pumping and Fueling Requirements for the ITER EDA"
D. C. Lousteau, "The ITER In-Vessel System"
M. J. Rennich and B. E. Nelson, "TPX Remote Maintenance and Shielding"
J. Sheffield and J. D. Galambos "Prospects for Toroidal Fusion Reactors"
D. W. Swain, P. L. Goranson, W. M. Nevins, P. Bonoli, M. Porkolab, A. von Halle, S. Bernabei, and N. Greenough, "Heating and Current Drive Systems for TPX"
N. A. Uckan, J. T. Hogan, W. A. Houlberg, J. D. Galambos, L. J. Perkins, S. W. Haney, S. Kaye, and D. E. Post, "ITER Design: Physics Basis for Size, Confinement Capability, Power Levels and Burn Control"
M. R. Wade, D. L. Hillis, J. T. Hogan, R. Maingi, C. C. Klepper, P. K. Mioduszewski, W. P. West, M. A. Mahdavi, K. H. Burrell, G. L. Jackson, and N. H. Brooks, "Helium Transport and Exhaust Studies in DIII-D"

Presentation at the University of Electronic Science and Technology of China, Chengdu, Sichuan, China, June 20, 1994
D. J. Hoffman, "ICRF Technology Development in the United States"

Third International Symposium on Fusion Nuclear Technology, Los Angeles, California, June 27, 1994. Abstracts published

Y-K. M. Peng, M. A. Abdou, and E. T. Cheng, "Small Spherical Tokamaks for Nuclear Applications"

21st European Physics Society (EPS) Conference on Controlled Fusion and Plasma Physics, Montpellier, France, June 27–July 1, 1994. Proceedings published in *EPS Conference Proceedings*

G. R. Hanson, D. A. Rasmussen, J. B. Wilgen, A. E. England, M. Murakami, T. S. Bigelow, D. J. Hoffman, D. B. Batchelor, D. C. Stallings, E. F. Jaeger, M. D. Carter, P. M. Ryan, J. H. Rogers, J. R. Wilson, R. Majeski, G. Schillings, and J. Stevens, "Edge-Density Profile Measurements and Antenna Coupling During ICRF Heating on TFTR"

G. R. Hanson, J. B. Wilgen, T. S. Bigelow, I. Collazo, M. Murakami, D. A. Rasmussen, J. R. Wilson, and H. K. Park, "Microwave Reflectometry for Edge Density Profile Measurements on TFTR"

J. H. Harris, C. E. Thomas, Jr., J. T. Hogan, G. R. Haste, S. Tobin, C. C. Klepper, B. Saoutic, B. Beaumont, A. Becoulet, H. Kuus, D. Fraboulet, A. Grosman, D. Guilhem, and J. Walter, "Experimental Measurements of ICRF and Edge Plasma Interactions on Tore Supra"

R. C. Isler, A. P. Post-Zwicker, S. F. Paul, W. Tighe, M. Ono, B. P. LeBlanc, R. Bell, and H. W. Kugel, "Impurity Behavior During Ion-Bernstein Wave Heating in PBX-M"

C. C. Klepper, R. C. Isler, S. J. Tobin, J. T. Hogan, and W. R. Hess, "Determination of Ion Temperatures from Zeeman Broadened Spectral Lines in the Edge of Tore Supra"

J. F. Lyon, S. L. Painter, L. M. Kovrizhnykh, and K. Gulec, "Stellarator Transport Optimization with Self-Consistent Electric Fields"

M. G. Shats, J. H. Harris, K. M. Likin, J. B. Wilgen, L. R. Baylor, J. D. Bell, C. H. Ma, M. Murakami, K. A. Sarksyan, S. C. Aceto, T. S. Bigelow, G. L. Bell, R. J. Colchin, R. A. Dory, J. L. Dunlap, G. R. Dyer, A. C. England, G. R. Hanson, D. P. Hutchinson, R. C. Isler, T. C. Jernigan, R. A. Langley, D. K. Lee, J. F. Lyon, A. L. Qualls, D. A. Rasmussen, R. K. Richards, M. J. Saltmarsh, J. E. Simpkins, K. L. Vander Sluis, J. J. Zielinski, "Drift-Wave-Like Density Fluctuations in the Advanced Toroidal Facility (ATF) Torsatron"

July

14th IMACS World Congress on Computational and Appliled Mathematics, Atlanta, GA, July 11–15, 1994. Proceedings published

L. Dresner, "Nonlinear Partial Differential Equations Invariant to a One-Parameter Family of Stretching Groups"

Second Energy Research Power Users Symposium II (ERPUS II), Rockville, MD, July 12, 1994. Proceedings posted electronically at NERSC (http://www.nersc.gov/doc/Quick_Help/ERSUG/ERPUS/leboeuf.html)

J.-N. Leboeuf, B. A. Carreras, L. A. Charlton, J. B. Drake, V. E. Lynch, D. E. Newman, K. L. Sidikman, and D. A. Spong, "Parallel Plasma Fluid Turbulence Calculations"

14th International Conference on Atomic Physics, Boulder, Colorado, July 31–August 5, 1994

L. Folkerts, S. Schippers, and F. W. Meyer, "Neutralization of Multicharged Oxygen and Argon Ions during Surface-Channeling Interactions with Au(110)"

August

10th International .Workshop on Ion Surface Collisions, Grand Targhee, Wyoming, August 8–12, 1994. Proceedings to appear in *Nuclear Instruments and Methods in Physics Research B*

F.W. Meyer, L. Folkerts, and S. Schippers, "Angular and Charge State Distributions of Highly Charged Ions Scattered during Low-Energy Surface-Channeling Interactions with Au(110)"

Aerospace Environmental Technology Conference, Huntsville, Alabama, August 10–11, 1994. Abstracts published

C. A. Foster, P. W. Fisher, W. D. Nelson, and D. E. Schechter, "A Centrifuge CO_2 Pellet Cleaning System"

C. C. Tsai, W. D. Nelson, and D. E. Schechter, "A Microwave Plasma Cleaning Apparatus"

10th International Heat Transfer Conference, Brighton, England, August 14–18, 1994. Proceedings published

W. Li, M. A. Ebadian, T. L. White, R. G. Grubb, and D. Foster, Jr., "Temperature and Pore Pressure Distribution in a Concrete Slab During the Microwave Decontamination Process"

Gordon Research Conference on Laser Interactions with Surfaces, Colby-Sawyer College, New London, New Hampshire, August 14–19, 1994

K. R. Chen, C. L. Liu, J. M. Donato, D. B. Geohegan, J-N. Leboeuf, A. A. Puretzky, and R. F. Wood, "Dynamic Modeling of Laser-Ablated Materials"

18th Symposium on Fusion Technology, Karlsruhe, Germany, August 21 or 22–26, 1994. Proceedings published by Elsvier Science

R. W. Callis, F. W. Baity, W. P. Cary, J. S. deGrassie, S. W. Ferguson, D. J. Hoffman, R. C. O'Neill, C. C. Petty, R. D. Phelps, R. I. Pinsker, D. B. Remsen, and D. J. Taylor, "4 MW Fast Wave Current Drive Upgrade for DIII-D"

S. K. Combs, L. R. Baylor, P. W. Fisher, C. A. Foster, C. R. Foust, M. J. Gouge, T. C. Jernigan, S. L. Milora, A. L. Qualls, D. E. Schechter, D. O. Sparks, and C. C. Tsai, "Pellet Injector Research and Development at ORNL"

D. W. Swain, S. E. Attenberger, P. Bonoli, W. A. Houlberg, and W. M. Nevins, "Operating Points and Feedback Control of Plasma Characteristics in Tokamaks with Full Current Drive"

International Symposium on Safety of Superconductors and Related Heat Transfer at Low Temperatures, Fukuoka, Japan, August 28–31, 1994. Abstracts published

L. Dresner, "Summary of Research During the Period August 1991 to August 1994"

September

Presentation to the National ITER Siting Meeting, San Diego, California, September 7, 1994

J. Sheffield, "Status of Planning for ITER Site on the Oak Ridge Reservation"

15th International Conference on the Numerical Simulation of Plasmas, Valley Forge, Pennsylvania, September 8, 1994

J. W. Cobb and J.-N. Leboeuf, "A Syncopated Leap-Frog Algorithm for Orbit Consistent Plasma Simulation of Materials Processing Reactors"

Fusion Power Associates Annual Meeting and Symposium, San Diego, California, September 8, 1994. Proceedings published

J. Sheffield, "Magnetic Fusion Commercial Power Plants"

Plasma Edge Turbulence Meeting, CIEMAT, Madrid, Spain, September 19–21, 1994

B. A. Carreras, "Radiation-Driven Turbulence at the Plasma Edge"

IEA Technical Workshop on the International Fusion Materials Irradiation Facility, Karlsruhe, Germany, September 26–29, 1994

T. E. Shannon, "Proposed Organization and Work Breakdown Structure"

15th International Atomic Energy Agency (IAEA) International Conference on Plasma Physics and Controlled Fusion, (Seville) Madrid, Spain, September 26–October 1, 1994. Proceedings published

R. D. Bengtson, G. X. Li, H. Lin, M. Meier, B. Richards, H. Y. W. Tsui, J. Uglum, A. J. Wootton, B. A. Carreras, T. Uckan, and A. Sen, "Edge Turbulence and its Control in TEXT"

P. H. Diamond, V. B. Lebedev, Y.-M. Liang, A. V. Gruzinov, I. Gruzinova, M. Medvedev, B. A. Carreras, D. E. Newman, L. Charlton, K. L. Sidikman, D. B. Batchelor, E. F. Jaeger, C. Y. Wang, G. G. Craddock, N. Mattor, T. S. Hahm, M. Ono, B. Leblanc, H. Biglari, F. Y. Gang, and D. J. Sigmar, "Dynamics of the L → H Transition, VH-Mode Evolution, Edge Localized Modes and RF Driven Confinement Control in Tokamaks"

L. Garcia, B. A. Carreras, V. E. Lynch, and P. H. Diamond, "Dithering Transitions in Resistive Pressure-Gradient-Driven Turbulence"

C. Hidalgo, T. Estrada, E. Sanchez, B. Branas, I. Garcia-Cortes, R. Balbin, M. A. Pedrosa, J. Sanchez, B. A. Carreras, S. Aceto, G. R. Hanson, J. H. Harris, T. Uckan, L. Garcia, H. J. Hartfuss, L. Giannone, G. Tynan, L. Schmitz, and the PBX-M Team, "Nonlinear Phenomena, Turbulence and Anomalous Transport in Fusion Plasmas"

G. Janeschitz, H. Nakamura, K. Borrass, J. Dietz, D. Hillis, J. Hogan, W. Houlberg, Y. Igitkhanov, A. Kukushkin, R. Maingi, R.R. Parker, D. E. Post, A. Pozharov, P. Stangeby, M. Sugihara, A. Taroni, G. Vlases, and M. R. Wade, "Physics Basis of Power and Particle Control in ITER"

G. Janeschitz, H. Nakamura, A. Antipenkov, M. Araki, C. Baxi, J. Brooks, S. Chiocchio, J. Dietz, G. Federici, M. J. Gouge, W.A. Houlberg, S. L. Milora, J. R. Haines, P. Ladd, E. Martin, R. Matera, R. R. Parker, D. Post, P. H. Rebut, R. Tivey, M. Ulrickson, and the ITER Joint Central and Home Teams, "The Design of the ITER Divertor and Pumping, Fueling System"

E. A. Lazarus, A. W. Hyatt, T. H. Osborne, S. E. Attenberger, M. E. Austin, K. H. Burrell, T. A. Casper, M. S. Chu, J. W. Cuthbertson, E. J. Doyle, P. Gohil, J. M. Greene, C. M. Greenfield, R. J. Groebner, W. A. Houlberg, C.-L. Hsieh, G. L. Jackson, J. Kim, S. Konoshima, L. L. Lao, C. Lasnier, A. W. Leonard, S. I. Lippmann, M. A. Mahdavi, R. Maingi, R. A. Moyer, C. L. Rettig, B. Rice, M. J. Schaffer, D. P. Schissel, R. T. Snider, R. D. Stambaugh, R. E. Stockdale, T. S. Taylor, A. D. Turnbull, M. R. Wade, R. Wood, D. Wroblewski, "The Role of Shaping in Achieving High Performance in DIII-D"

J. F. Lyon, J. A. Rome, P. R. Garabedian, D. T. Anderson, and S. L. Painter, "Physics Assessment of Stellarators as Fusion Power Plants"

T. E. Shannon, F. Cozzani, D. H. Crandall, F. W. Wiffen, K. Ehrlich, H. Katsuta, T. Kondo, V. Teplyakov, and L. Zavialsky, "The International Fusion Materials Irradiation Facility"

D. A. Spong, B. A. Carreras, C. L. Hedrick, J.-N. Leboeuf, and A. Weller, "Energetic Particle Destabilization of Shear Alfvén Waves in Stellarators and Tokamaks"

October

ITER Workshop on Confinement Data Bases and Modeling, Seville, Spain, October 3–4, 1994

W. A. Houlberg, "Summary of U.S. 1-D Modeling Efforts"

45th Aeroballistic Range Association Meeting, Huntsville, Alabama, October 10–14, 1994

S. K. Combs, M. J. Gouge, L. R. Baylor, P. W. Fisher, C. A. Foster, C. R. Foust, S. L. Milora, and A. L. Qualls, "Recent High-Speed Ballistics Experiments at ORNL"

1994 Applied Superconductivity Conference, Boston, Massachusetts, October 16–21, 1994 Proceedings published in *IEEE Transactions on Applied Superconductivity*, May 1995

L. Dresner, "The Effect of Stability and Thermal Hydraulic Quenchback of Perforating the Jacket of a Cable-in-Conduit Conductor"

M. S. Lubell, J. W. Lue, et al., "Structure and Cost Scaling for Intermediate Size Superconducting Magnetic Energy Storage (SMES) Systems"

J. W. Lue, "Review of Stability Experiments on Cable-in-Conduit Conductors"

J. W. Lue, L. Dresner, S. W. Schwenterly, D. Aized, J. M. Campbell, and R. E. Schwall, "Stability Measurements on a 1-T High Temperature Superconducting Magnet"

S. W. Schwenterly, J. W. Lue, M. S. Lubell, M. S. Walker, D. W. Hazelton, P. Haldar, J. A. Rice, J. G. Hoehn, Jr., and L. R. Motowidlo, "Performance of Multiple In-Hand Ag/BSSCO Pancake Coils in Static and Ramped Magnetic Fields"

41st National Symposium and Topical Conference of the American Vacuum Society (AVS), Third International Conference on Nanometer-Scaled Science & Technology, Denver, Colorado, October 24–28, 1994. Papers published in *J. Vac. Sci. Tech.* 13(3, Pt. 1)

J. B. O. Caughman, "The Ion Energy Distribution at the Substrate Surface in a RF Induction Plasma Source"

W. L. Gardner, "Sensor for Measuring the Atomic Fraction in Highly Dissociated Hydrogen"

M. M. Menon, G. J. Laughon, R. Maingi, M. R. Wade, D. L. Hillis, and M. A. Mahdavi, "Pumping Characteristics of a Cryopump with Ar Sorbent in He and in D_2/He Mixture"

November

U.S.–Japan Workshop on Bootstrap Current in Tokamaks and Stallarators, Lake Lanier, Georgia, November 2–4, 1994

W. A. Houlberg and S. E. Attenberger, "Advanced Tokamak Operation with High Bootstrap Fraction"

Second Specialists' Meeting on Codes for Simulating Collective Fast Particle Effects, Minneapolis, Minnesota, November 6, 1994

K. R. Chen, D. B. Batchelor, and J. G. Leboeuf, "PIC Simulation of Alpha Particle Dynamics Due to Self-Driven Relativistic Lower-Hybrid Cyclotron Waves"

Transport Task Force Core Group Meeting, Minneapolis, Minnesota, November 7, 1994

D. E. Newman, B. A. Carreras, and P. H. Diamond, "Theoretical Model of VH Mode Evolution"

Thirty-Sixth American Physical Society (APS) Annual Meeting, Division of Plasma Physics, Minneapolis, Minnesota, November 7–11, 1994. Abstracts published in *Bull. Am. Phys. Soc.*

S. E. Attenberger and W. A. Houlberg, "Simulation of Current Profile Control in DIII-D Using Pellet Fueling and RF Heating"

S. E. Attenberger, W. A. Houlberg, S. P. Hirshman, S. Krasheninnikov, and D. J. Sigmar, "Modelling Impurity Parallel Transport in the Scrape Off Layer"

L. R. Baylor, T. C. Jernigan, S. K. Combs, C. R. Foust, W. A. Houlberg, S. L. Milora, M. R. Wade, J. C. Phillips, and D. P. Schissel, "Initial Results from Deuterium Pellet Injection Experiments in DIII-D"

G. L. Bell, J. M. Lohr, J. B. Wilgen, M. E. Austin, and C. B. Forest, "Initial ECE Radiometer Electron Temperature Measurements on DIII-D"

T. S. Bigelow, C. R. Schaich, C. T. Wilson, and J. White, "ATF ECH System Long Pulse Operation"

J. B. O. Caughman, G. L. Bell, W. L. Gardner, and D. J. Hoffman, "The Effects of RF Sheaths on the Erosion of Faraday Shield Coatings"

L. A. Charlton, J.-N. Leboeuf, B. A. Carreras, and A. A. Martynov, "Ideal MHD Stability Properties of Small Aspect Ratio Tokamaks"

M. D. Carter, D. B. Batchelor, D. C. Stallings, C. Wang, D. J. Hoffman D. Rasmussen, and P. M. Ryan, "Phased Array Antennas for Fast Wave Current Drive and Heating"

K. R. Chen, D. B. Batchelor, and J.-N. Leboeuf, "Alpha Particle Dynamics Due to Self-Driven Relativistic Lower-Hybrid Cyclotron Waves"

K. R. Chen, J.-N. Leboeuf, D. B. Geohegan, R. F. Wood, J. M. Donato, C. L. Liu, and A. A. Puretzky, "Dynamic Modeling of Laser-Ablated Plasmas"

J. W. Cobb, J.-N. Leboeuf, L. A. Berry, and E. F. Jaeger, "Orbit Consistent Plasma Processing Simulations"

R. J. Colchin, J. D. Galambos, S. P. Hirshman, and J. A. Rome, "Plasma Voltages, Flux Consumption, and Neutral Beam Calculations for START"

N. Dominguez, K. C. Shaing, M. Yokoyama, M. Wakatani, and C. T. Hsu, "Approximate Analytic Expressions for Plasma Viscosity and Neoclassical Flows and Fluxes in Finite Aspect Ratio Tokamaks"

A. C. England, J. B. Wilgen, G. R. Hanson, D. A. Rasmussen, M. Murakami, D. C. Stallings, J. H. Rogers, and J. R. Wilson, "Reflectometer Measurements of Edge-Density Profiles at an ICRF Antenna on TFTR"

R. H. Goulding, G. L. Bell, D. J. Hoffman, P. M. Ryan, V. Bhatnagar, M. Bures, J. A. Dobbing, B. Fechner, D. F. H. Start, and T. J. Wade, "Initial FWCD Results using the JET A2 Antenna Arrays and Experience with Phased Operation"

G. R. Hanson, A. C. England, J. B. Wilgen, D. A. Rasmussen, M. Murakami, M. D. Carter, D. C. Stallings, J. H. Rogers, and J. R. Wilson, "Results from the ORNL Two-Frequency Differential-Phase Reflectometer on TFTR"

G. R. Hanson, J. B. Wilgen, E. J. Doyle, K. W. Kim, C. L. Rettig, E. De La Luna, and J. Sanchez, "Edge Density Profile Measurements on DIII-D Using an AM Reflectometer"

D. L. Hillis, G. Mank, K. H. Finken, H. Euringer, U. Samm, B. Unterberg, M. R. Wade J. T. Hogan, A. Post-Zwicker, J. A. Boedo, D. S. Gray, A. M. Messien, G. van Oost, J. Ongena, G. Van Wassenhove, and P. Dumortier, "Helium Transport and Exhaust in the Presence of a Neon Radiating Boundary with the ALT-II Pump Limiter in TEXTOR"

S. P. Hirshman, W. A. Houlberg, S. E. Attenberger, S. I. Krasheninnikov, D. J. Sigmar, and D. Knoll, "Reduced Impurity Flow Modeling of the Scrape-Off Plasma"

W. A. Houlberg and S. E. Attenberger, "Isotopic Tailoring of Fuel Density Profiles Using Auxiliary Fueling Sources and Pumping"

E. F. Jaeger, L. A. Berry, J. S. Tolliver, and D. B. Batchelor, "Power Deposition in High Density Inductively Coupled Plasma Tools for Semiconductor Processing"

T. C. Jernigan and the ATF Team, "Long Pulse Experiments on the ATF Stellarator"

G. R. Hanson, J. B. Wilgen, E. J. Doyle, K. W. Kim, C. L. Rettig, E. de la Luna, and J. Sanchez, "Edge Density Profile Measurements on DIII-D Using an AM Reflectometer"

C. C. Klepper, N. H. Brooks, S. Tugarinov, A. W. Leonard, W. P. West, "Measurements of the CIII Emission Distribution and Ion Temperature in Radiative Divertor Experiments"

J.-N. Leboeuf, C. L. Hedrick, V. E. Lynch, K. L. Sidikman, D. A. Spong, and R. D. Sydora, "Nonlinear Calculations of Core Fluctuations with Gyro-Landau Fluid Models"

J.-N. Leboeuf, K. R. Chen, J. M. Donato, D. B. Geohegan, C. L. Liu, and R. F. Wood, "Two-Dimensional Modeling of Plume Dynamics in Laser Ablation Processes"

V. E. Lynch, B. A. Carreras, and J.-N. Leboeuf, "The Performance of Fluid Codes on Parallel Computers"

J. F. Lyon, S. L. Painter, L. M. Kovrizhnykh, and K. Gulec, "Stellarator Transport Optimization With Self-Consistent Electric Fields"

M. Murakami, D. B. Batcherlor, A. C. England, G. R. Hanson, E. F. Jaeger, D. A. Rasmussen, C. Wang, J. B. Wilgen, M. G. Bell, R. Budny, E. Fredrickson, J. C. Hosea, R. Majeski, H. Park, C. K. Phillips, J. H. Rogers, G. Schilling, S. C. Scott, J. E. Stevens, G. Taylor, J. R. Wilson, and M. C. Zarnstorff, "Modulated ICRF Heating and Transport in DT TFTR Plasmas"

D. E. Newman, B. A. Carreras, and P. H. Diamond, "A Computational Study of the Dynamics of Hydrodynamic Trapped Ion Temperature Gradient Driven Turbulence"

L. W. Owen, R. Maingi, D. K. Lee, P. K. Mioduszewski, D. L. Hillis, J. T. Hogan, M. R. Wade, D. R. Baker, and G. L. Jackson, "Modeling of Global Particle Confinement in L-Mode and ELM-Free H-Mode Plasmas in DIII-D"

Y-K. M. Peng, C. L. Hedrick, K. Erents, D. Goodall, J. Hugill, and A. Sykes, "MHD Ballooning Stability Limit for Scrape-Off Layer Thickness"

D. A. Rasmussen, R. Kumazawa, K. Nishimura, S. Masuda, T. Mutoh, F. Shimbo, T. Seki, T. Watari, R. Akiyama, A. Ando, A. Ejiri, H. Idei, K. Ida, H. Iguchi, S. Kubo, K. Matsuoka, T. Morisaki, S. Morita, S. Okamura, T. Ozaki, S. Sakakibara, C. Takahashi, T. Kawamoto, K. Tanaka, J. Xu,

H. Yamada, I. Yamada, M. Murakami, D. J. Hoffman, and E. F. Jaeger, "Ion Cyclotron Heating in the Compact Helical System (CHS)"

J. A. Rome and the SPPS Team, "Stellarator Power Plant Study"

P. M. Ryan, D. W. Swain, R. H. Goulding, M. D. Carter, D. J. Hoffman, and D. B. Batchelor, "Phase Control System for the TPX ICH Antenna Arrays"

K. C. Shaing and C. T. Hsu, "Poloidal Flow and E × B Flow in H-Mode"

K. L. Sidikman, C. L. Hedrick, J.-N. Leboeuf, and V. E. Lynch, "Characteristics of Dissipative Trapped Electron Mode Turbulence Calculated from a Gyro-Landau Fluid Model"

D. A. Spong, C. L. Hedrick, and B. A. Carreras, "Gyrofluid Models of Fast Ion-Driven Shear Alfven Instabilities in Tokamaks and Stellarators"

D. C. Stallings, D. B. Batchelor, C. Y. Wang, and M. D. Carter, "Determination of the Plasma Surface Impedance for Low Frequency Current Drive"

D. W. Swain, F. W. Baity, D. B. Batchelor, S. C. Chiu, J. Degrassie, E. J. Doyle, G. R. Hanson, K. W. Kim, R. I. Pinsker, C. C. Petty, C. L. Rettig, and J. Wilgen, "DIII-D FWCD Antenna Operating with No Faraday Shield"

T. Uckan, M. Chatelier, A. Grlsman, T. Loarer, P. K. Mioduszewski, and L. W. Owen, "Power and Particle Handling Studies for the Tore Supra Toroidal Belt Pump Limiter"

M. R. Wade, J. T. Hogan, D. L. Hillis, R. Maingi, W. P. West, D. F. Finkenthal, K. H. Burrell, R. J. Groebner, M. A. Mahdavi, M. M. Menon, and the DIII-D Team, "Helium Transport and Exhaust Studies in Enhanced Confinement Regimes in Enhanced Confinement in DIII-D," invited

M. Wakatani and K. C. Shaing, "Shock Formation in Poloidally Rotating Helically Symmetric Plasmas"

C. Y. Wang, D. B. Batchelor, and E. F. Jaeger "Parallel Forces Induced in Ion Cyclotron Range of Frequency"

J. B. Wilgen, A. C. England, T. S. Bigelow, G. R. Dyer, D. E. Greenwood, M. Murakami, C. R. Schaich, J. A. White, and J. L. Yarber, "ECE Radiometer Measurement of Electron Temperature on the ATF Stellarator"

1994 American Society of Mechanical Engineers (ASME) Annual Winter Meeting, Chicago, Illinois, November 13–18, 1994. Proceedings published in *J. Heat Transfer* **207** (1994)

L. E. Lagos, W. Li, M. A. Ebadian, T. L. White, D. Foster, R. G. Grubb, "Heat Transfer within a Radioactively Contaminated Concrete Slab with a Temperature Dependent Dielectric Properties"

W. Li, M. A. Ebadian, T. L. White, and R. G. Grubb, "Heat Transfer Within a Radioactive Contaminated Concrete Slab Applying a Microwave Heating Technique"

High Performance Computing and Communications (Supercomputing '94), Washington, D.C., November 14–18, 1994. Proceedings published as *Proceedings of Supercomputing '94*

V. E. Lynch, B. A. Carreras, and J.-N. Leboeuf, "Distributed Computing for Fusion Energy Turbulence Calculations"

International Symposium on Evaluation of Current Trends in Fusion Research, Washington, D.C., November 14–18, 1994

J. F. Lyon, "Stellarator Research"

Fall Meeting of the Materials Research Society, Boston, Massachusetts, November 28–December 2, 1994. Proceedings published by Materials Research Society

C. L. Liu, J.-N. Leboeuf, R. F. Wood, D. B. Geohegan, J. M. Donato, K. R. Chen, and A. A. Puretzky, "Modeling of Thermal, Electronic, Hydrodynamic, and Dynamic Deposition Processes for Pulsed-Laser Deposition of Thin Films"

Sixth International Toki Conference on Plasma Physics and Controlled Nuclear Fusion, Toki-city, Japan, November 29–December 2, 1994. Proceedings published

M. Murakami for the TFTR Group, "ICRF Heating and Transport of DT Plasmas in TFTR," invited

M. Murakami, T. C. Jernigan, T. S. Bigelow, R. J. Colchin, G. R. Dyer, A. C. England, C. C. Klepper, C. R. Schaich, D. A. Rasmussen, J. E. Simpkins, J. A. White, J. B. Wilgen, J. L. Yarber, A. Komori, S. Morimoto, O. Motojima, A. Sagara, M. Sato, H. Yamada, "The ATF Finale—Long Pulse Experiments"

H. Yamada, M. Murakami, T. C. Jernigan, T. S. Bigelow, R. J. Colchin, A. C. England, A. Komori, S. Morimoto, O. Motojima, A. Sagara, M. Sato, J. B. Wilgen, "Control and Effect of Long Pulse Discharge in ATF"

1994 REPORTS

ORNL Reports

J. Sheffield, C. C. Baker, M. J. Saltmarsh, and Fusion Energy Division Staff, *Fusion Energy Division Progress Report, Period from January 1, 1990, to December 31, 1991*, ORNL-6714, February 1994

ORNL Technical Memoranda

T. S. Bigelow, *ITER ECH Launcher Options for Start-Up Assist, Bulk Heating, and EC Current Drive Experiments*, ORNL/TM-12658, March 1994

L. Dresner, *Design and Construction of the Astronautics Refrigerator Magnet*, ORNL/TM-12757, 1994

D. C. Gregory and M. E. Bannister, *Electron-Impact Ionization of Multicharged Ions at ORNL: 1985–1992*, ORNL/TM-12729, Martin Marietta Energy Systems, Inc., Oak Ridge Natl. Lab., July 1994.

J. D. Galambos, L. J. Perkins, S. Haney, and J. Mandrekas, *The Impact of Improved Physics on Commercial Tokamak Reactors*, ORNL/TM-12483, January 1994

C. C. Klepper, J. T. Hogan, S. J. Tobin, R. C. Isler, D. Guilhem, W. R. Hess, and P. Monier-Garbet, *Measurements and Modeling of Impurity Source Distributions from the Tore Supra Outboard Pump Limiter*, ORNL/TM-12795, August 1994

J. F. Lyon, K. Gulec, R. L. Miller, and L. El-Guebaly, *Evaluation of Torsatrons as Reactors*, ORNL/TM-12670, March 1994

C. C. Tsai, H. H. Haselton, W. D. Nelson, D. E. Schechter, V. B. Campbell, A. L. GLover, J. M. Googin, and L. M. Thompson, *Plasma Surface Cleaning in a Microwave Plasma Source*, ORNL/TM-12495 March 1994

T. Uckan, B. Richards, A. J. Wootton, R. D. Bengtson, R. Bravenec, B. A. Carreras, G. X. Li, P. D. Hurwitz, P. E. Phillips, W. L. Rowan, H. Y. W. Tsui, J. R. Uglum, Y. Wen, and D. Winslow, *Feedback Control and Stabilization Experiments on the Texas Experimental Tokamak (TEXT)*, ORNL/TM-12757, June 1994

Reports Published by Other Institutions

D. K. Lee, S. P. Hirshman, M. Okabayashi, M. F. Reusch, and Y. C. Sun; *Method of Rapid Determination of MHD Equilibrium Properties with the Modified Version of the SURFAS Code*, PPPL-2939 Princeton Plasma Physics Laboratory, Princeton, N.J., 1994

D. R. Mikkelsen, K. M. McGuire, G. L. Schmidt, S. J. Zweben, S. E. Attenberger, W. A. Houlberg, and S. L. Milora, *Core Fueling to Produce Peaked Density Profiles in Large Tokamaks*, PPPL-2997, Princeton Plasma Physics Laboratory, Princeton, N.J., 1994

1994 CONGRESSIONAL TESTIMONY

C. C. Baker for the U.S. ITER Home Team, Testimony for Congressional Hearings on Fusion Energy Concepts held by the House of Representatives Committee on Science, Space, and Technology, April 1994

T. E. Shannon, Testimony for Congressional Hearings on Fusion Energy Concepts held by the House of Representatives Subcommittee on Energy, August 1994

Appendix 2

Abbreviations and Acronyms

ACRONYMS

1-D	one-dimensional
1.5-D	1.5-dimensional
2-D	two-dimensional
3-D	three-dimensional
ADI	alternative direction implicit
ALT-II	Advanced Limiter Test II
ARIES	Advanced Reactor Innovation and Evaluation Studies
ASC	American Superconducting Corporation
ATF	Advanced Toroidal Facility
AVS	Advanced Visual Systems
CADW	configuration-average distorted-wave
CCD	charge-coupled device
CD	compact disk
CDA	conceptual design activity
CDR	Conceptual Design Review
CER	charge-exchange recombination
CFADC	Controlled Fusion Atomic Data Center
CHS	Compact Helical System
CIEMAT	Centro de Investigaciones Energéticas, Medioambientales, y Tecnológicas
CLR	Coherent Laser Radar
COE	cost of electricity
CRADA	Cooperative Research and Development Agreement
CSEWG	Cross-Section Evaluation Group
CTMC	classical trajectory Monte Carlo
cw	continuous wave
D-D	deuterium-deuterium
D-T	deuterium-tritium
DEH	direct electron heating
DID	Design Integration Division
DOE	Department of Energy
dpa	displacements per atom
DTEM	dissipative trapped electron mode
ECE	electron cyclotron emission
ECH	electron cyclotron heating
ECR	electron-cyclotron resonance
EDA	engineering design activity
ELM	edge-localized mode
EMF	electromagnetic field
ENDF/B	Evaluated Nuclear Data File
ENEA	Ente per le Nuove Tecnologie L'energia e L'ambiente
EOL	Electro-Optics Laboratory

ES&H	environmental, safety, and health
ETD	Engineering Technology Division
ET/FE DPO	Engineering Technology/Fusion Energy Division Publications Office
ETG	El Toro Grande
Euratom	European Atomic Energy Community
FAR	Finite Aspect Ratio
FBL	feedback launcher
FDDI	fiber-distributed data interface
FED	Fusion Energy Division
FENDL	Fusion Evaluated Nuclear Data Library
FLR	finite Larmor radius
FM	Frequency Modulated
FPCC	Fusion Power Coordination Committee
FWB	first wall and blanket
GAE	global Alvfén eigenmode
GB	gigabyte
GLOSI	Global and Local One-Dimensional Solution for ICRF heating
HF	helical field
HFIR	High Flux Isotope Reactor
HIP	hot isostatic pressing
HPCC	High-Performance Computing Center
HTL	Home Team Leader
HTS	high-temperature superconducting
HVPNS	high-volume plasma neutron source
HVPNS	high-volume, plasma-based neutron source
IAEA	International Atomic Energy Agency
IBW	ion Bernstein wave
ICH	ion cyclotron heating
ICRF	ion cyclotron range of frequencies
ICRH	ion cyclotron resonance heating
IEA	International Energy Agency
IPMS	Integrated Process Management System
IR	infrared
ISTC	International Science and Technology Center
ITER	International Thermonuclear Experimental Reactor
JCT	Joint Central Team
JET	Joint European Torus
JILA	Joint Institute for Laboratory Astrophysics
LANL	Los Alamos National Laboratory
LH	lower hybrid
LHCD	LH current drive
LHD	Large Helical Device

LHH	LH heating
LLNL	Lawrence Livermore National Laboratory
M&S	Magnetics and Superconductivity
MAST	Mega-Ampere Spherical Tokamak
MATF	modular ATF
MB	megabyte
MHD	magnetohydrodynamic
MHH	modular helias-like heliac
MIT	Massachusetts Intstitue of Technology
MRFI	measured rf input
MSE	motional Stark effect
MSS	Management Services Section
NB	neutral beam
NBI	NB injection
NEA	Nuclear Energy Agency
NERSC	National Energy Research Supercomputing Center
NGS	neutral gas shielding
NIFS	National Institute for Fusion Science
NPDES	National Pollutant Discharge Elimination System
NSTX	National Spherical Tokamak Experiment
ODE	ordinary differential equation
OFE	Office of Fusion Energy
OMA	optical multichannel analyzer
OPL	outboard pump limiter
ORNL	Oak Ridge National Laboratory
OSP	outer strike point
PBX-M	Princeton Beta Expmeriment—Modified
PC	personal computer
PEP	pellet-enhanced performance
PF	poloidal field
PIC	particle-in-cell
PICES	Poloidal Ion Cyclotron Expansion Solution
PPPL	Princeton Plasma Physics Laboratory
PVM	parallel virtual machine
QA	quality assurance
R&D	research and development
RB	removable beryllium
rf	radio frequency
RFTF	Radio-Frequency Test Facility
RGA	residual gas analyzer
RH	remote handling
RIED	radiation-induced electrical degradation
RLW	Rebut-Lailla-Watkins

RLWB	Rebut-Lallia-Watkins-Boucher
ROM	read-only memory
RSIC	Radiation Shielding Information Center
SAIC	Science Applications International Corporation
SOL	scrape-off layer
SPI	Superconducting Partnership Initiative
SPP	special parallel processing
SPP	Superconducting Partnership Program
ST	spherical tokamak
START	Small Tight Aspect Ratio Tokamak
TAE	torroidal Alvfén eigenmode
TEM	transverse electromagnetic
TEXT	Texas Experimental Tokamak
TEXTOR	Tokamak Experiment for Technology Oriented Research
TF	toroidal field
TFTR	Tokamak Fusion Test Reactor
THQ	thermal hydraulic quenchback
TPOP	tritium proof-of-principle
TPX	Tokamak Physics Experiment
TSA	Technology and Science Applications
TSC	Tokamak Simulation Code
TSTA	Tritium Systems Test Assembly
UCLA	University of California at Los Angeles
UCSD	University of California at San Diego
USC	User Service Center
UT	ultrasonic testing
VDE	vertical displacement event
VF	verticle field
VLSI	very-large-scale integrated
VNS	volumetric neutron source
XPS	X-ray photoelectron spectroscopy

Appendix 3

FED Organization Chart

ORNL
FUSION ENERGY DIVISION

APRIL 1995

ORNL-DWG 95-2545R FED

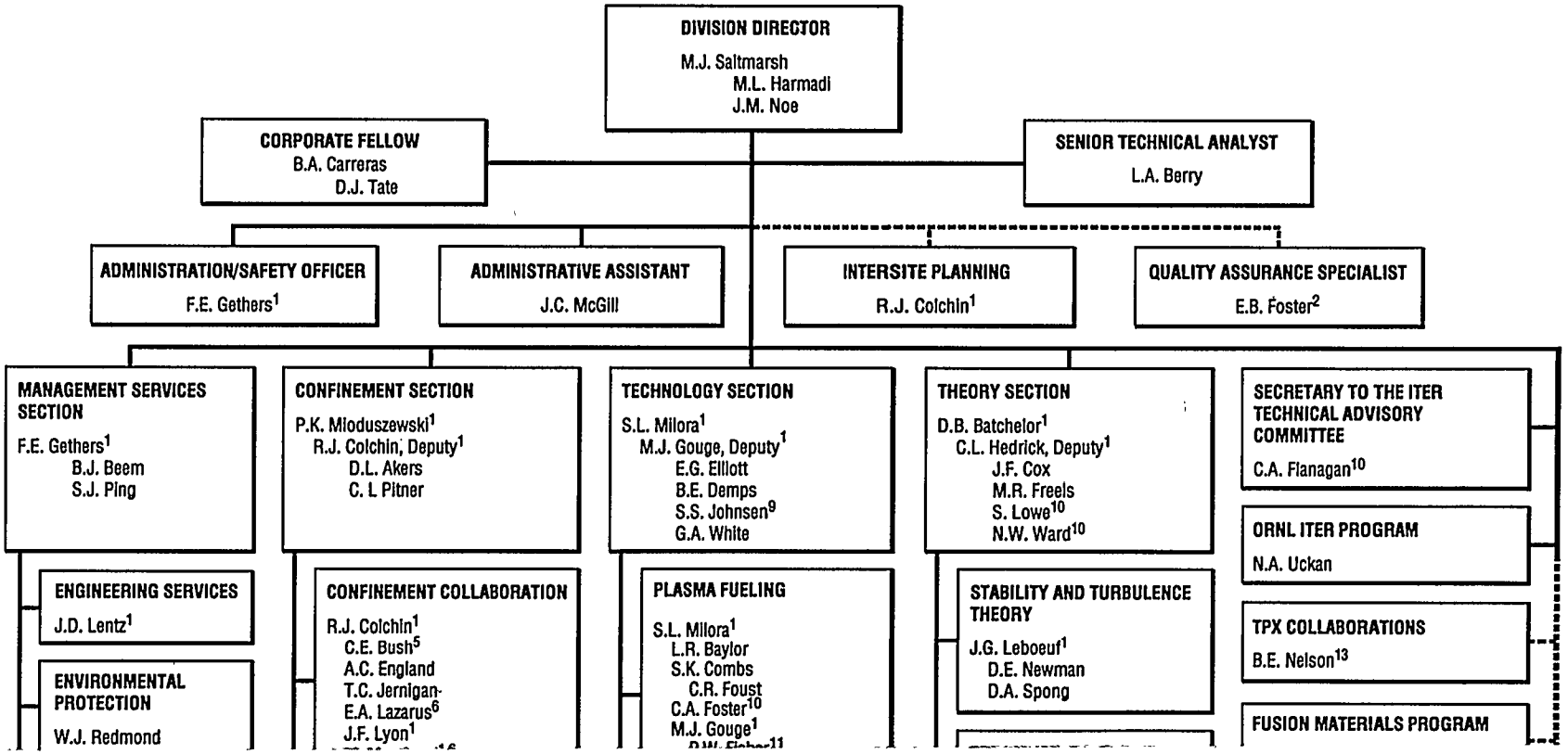

PROCUREMENT
M.E. Disney
J.O. Richardson

TRAINING
J.D. Lentz[1]

FINANCE OFFICE
L.J. Hickey[3]
S.B. Armstrong
K.A. Ensey

FED LIBRARY
L.W. Foley[4]

J.B. Wilgen

EDGE PHYSICS AND PARTICLE CONTROL
P.K. Mioduszewski[1]
D.T. Fehling
J.H. Harris[1,7]
G.H. Henkel
D.L. Hillis[1]
R.C. Isler
C.C. Klepper
R. Maingi[8]
A. Post-Zwicker[8]
T. Uckan
M.R. Wade[6]

DIII-D PROGRAM
M. Murakami[1,6]

JET/TEXTOR/AUG PROGRAM
D.L. Hillis[1]
R.H. Goulding[1]
D.J. Hoffman[1]

TFTR PROGRAM
S.L. Milora[1]

TPX PHYSICS PROGRAM
G.H. Neilson[5]

TORE SUPRA PROGRAM
J.H. Harris[1,7]

STELLARATOR PROGRAM
J.F. Lyon[1]

D.E. Schechter[1]
C. Tsai[1]

RF PLASMA HEATING
D.J. Hoffman[1]
F.W. Baity
J.B. Caughman
G.R. Haste
A. Fadnek
S.C. Forrester
G.C. Barber
D.O. Sparks
T.S. Bigelow
C.R. Schaich
G.L. Bell[12]
W.L. Gardner[1]
R.H. Goulding[1]
D.A. Rasmussen
P.M. Ryan
D.W. Swain[1]
H. Zhang[8]

TECHNOLOGY AND SCIENCE APPLICATIONS
J.R. Haines[1]
W.L. Gardner[1]

MAGNETICS DEVELOPMENT
M.S. Lubell
E.C. Jones[8]
J.W. Lue
S.W. Schwenterly

SPHERICAL TOKAMAK PROGRAM
Y-K. M. Peng

WASTE PROCESSING DEVELOPMENT
T.L. White

ITER/TPX HEATING TECHNOLOGY
D.W. Swain[1]

ION SOURCE APPLICATIONS
C. Tsai[1]
D.E. Schechter[1]

IFMIF PROGRAM
J.R. Haines[1]

EDGE/DIVERTOR THEORY
C.L. Hedrick[1]
S.P. Hirshman
J.A. Rome

RF THEORY
D.B. Batchelor[1]
M.D. Carter
E.F. Jaeger
C. Wang[8]

PLASMA MODELING
W.A. Houlberg
J.T. Hogan
K-C. Shaing

PLASMA PROCESSING
J.G. Leboeuf[1]
K.R. Chen[8]
J.W. Cobb[8]

COMPUTING
D.R. Overbey
C.E. Gibson

E.E. Bloom[14]

ATOMIC PHYSICS PROGRAM
F.W. Meyer[15]

[1] Dual Capacity
[2] Office of Quality Programs and Inspection
[3] Finance and Business Management
[4] Leased Personnel
[5] Assignment, Princton Plasma Physics Laboratory
[6] Assignment, General Atomics
[7] Assignment, Tore Supra
[8] Postdoctoral Research Participant
[9] MMES Clerical Assignment Group
[10] Part-Time Employee
[11] Chemical Technology Division
[12] Assignment, JET
[13] Engineering
[14] Metals and Ceramics Division
[15] Physics Division

Special Assignments:
Computer Security Officer - D.R. Overbey
Environmental Protection Officer - W.J. Redmond
Radiation Control Officer - W.J. Redmond
Work Force Diversity Representative - J.C. McGill

ORNL-6879
Dist. Category UC-420

INTERNAL DISTRIBUTION

1. D. B. Batchelor
2. L. A. Berry
3. E. E. Bloom
4. T. D. Burchell
5. B. A. Carreras
6–7. R. J. Colchin
8. F. E. Gethers
9. M. J. Gouge
10. J. R. Haines
11. D. J. Hoffman
12. W. A. Houlberg
13. P. W. King
14. J.-N. Leboeuf
15. M. S. Lubell
16. J. F. Lyon
17. C. H. Ma
18–24. J. C. McGill
25–26. F. W. Meyer
27. S. L. Milora
28–29. P. K. Mioduszewski
30. M. B. Nestor
31. D. R. Overbey
32–33. J. C. Parrott
34. Y-K. M. Peng
35. G. W. Roupe
36. A. F. Rowcliffe
37. M. J. Saltmarsh
38. D. R. Schultz
39. B. J. Smith
40. J. O. Stiegler
41. A. W. Trivelpiece
42. C. C. Tsai
43. N. A. Uckan
44. J. E. White
45–46. Laboratory Records Department
47. Laboratory Records, ORNL-RC
48. Central Research Library
49. Document Reference Section
50. Fusion Energy Division Library
51. ORNL Patent Office

EXTERNAL DISTRIBUTION

Office of Fusion Energy, Office of Energy Research, 19901 Germantown Road, Germantown, MD 20874-1290

52. S. E. Berk
53. R. A. Blanken
54. C. Bolton
55. M. Cohen
56. R. Dagazian
57. N. A. Davies
58. W. F. Dove
59. T. V. George
60. J. Hoy
61. A. Katz
62. W. Marton
63. R. H. McKnight
64. G. R. Nardella

65. D. B. Nelson
66. E. Oktay
67. A. Opdenaker
68. R. E. Price
69. W. Sadowski
70. C. Sege
71. H. S. Staten
72. F. W. Wiffen
73. J. W. Willis

Lawrence Livermore National Laboratory, P.O. Box 5511, Livermore, CA 94550

74. S. Allen (General Atomics)
75. J. Denavit, L-18
76. R. F. Post
77. K. I. Thomassen, L-637

Los Alamos National Laboratory, P.O. Box 1663, Los Alamos, NM 87545

77. J. L. Anderson
78. C. W. Barnes
79. J. D. Rogers
80. K. F. Schoenberg
81. G. A. Wurden

National Institute of Standards and Technology, University of Colorado, Campus Box 440, Boulder, CO 80309

82. V. D. Arp
83. A. Clark
84. G. H. Dunn
85. A. V. Phelps
86. F. R. Fickett

Naval Research Laboratory, Washington, DC 20375

87. B. Hui
88. B. H. Ripin
89. A. Robson, Code 4760

Oak Ridge Institute for Science and Education, DOE/Oak Ridge Associated Universities, P.O. Box 117, Oak Ridge, TN 37831-0117

90. A. M. Weinberg, IEA
91. University Programs Department

92. Institute for Energy Analysis
93. Information Center/EES (attention H. T. Burn)

Pacific Northwest Laboratories, Battelle Boulevard, P.O. Box 999, Richland, WA 99352

94. D. A. Dingee
95. B. F. Gore
96. L. L. Schmid

Princeton Plasma Physics Laboratory, P.O. Box 451, Princeton, NJ 08543

97. R. C. Davidson
98. N. Fisch
99. R. J. Goldston
100. R. Hawryluk
101. P. Heitzenroeder
102. W. Lang
103. D. M. Meade
104. P. H. Rutherford
105. N. Sauthoff
106. J. A. Schmidt
107. J. Sinnis
108. M. Williams
109. K. Young

Sandia National Laboratories, P.O. Box 5800, Albuquerque, NM 87185

110. M. Ulrickson
111. F. L. Vook, Org. 1100
112. J. B. Whitley, Div. 6248

Bechtel Corp., Bechtel Research and Development, P.O. Box 193965, San Francisco, CA 94119-3965

113. E. von Fischer
114. H. K. Forsen, Advanced Technology Division

EG&G ORTEC, 100 Midland Road, Oak Ridge, TN 37830

115. J. Ayers
116. D. A. Gedcke

General Atomics, P.O. Box 85608, San Diego, CA 92186-9784

117. D. E. Baldwin
118. V. Chan
119. R. L. Freeman
120. R. Harder
121. C. Moeller
122. T. Simonen
123. R. D. Stambaugh
124. T. Tamano

General Dynamics-Convair Division, P.O. Box 85377, San Diego, CA 92138

125. R. F. Beuligmann
126. D. S. Hackley
127. R. A. Johnson, MZ 16-1070

Grumman Corporation, Electronics Systems Division, M/S B 29-25, Bethpage, NY 11714-3588

128. R. Botwin
129. T. Favale

TRW, Inc., 1 Space Park, Redondo Beach, CA 92078

130. J. Gordon
131. J. A. Maniscalco

Westinghouse Electric Corporation, Advanced Reactors Division, P.O. Box 158, Madison, PA 15663

132. A. Anderson
133. G. G. Gibson

Atlanta University, Atlanta, GA 30314

134. R. E. Mickens

Auburn University, Auburn, AL 36849-3511

135. M. S. Pindzola, Physics Department
136. D. G. Swanson
137. R. F. Gandy, Physics Department

Columbia University, New York, NY 10027

138. G. A. Navratil

Denison University, Granville, OH 43023

139. W. A. Hoffman
140. R. R. Winters

University of California at Los Angeles, Los Angeles, CA 90024

141. M. Abdou

University of California at San Diego, La Jolla, CA 92093

142. T. Amano
143. C. C. Baker
144. R. W. Conn
145. P. H. Diamond
146. F. Najmabadi
147. M. N. Rosenbluth

Georgia Institute of Technology, Atlanta, GA 30332

148. J. N. Davidson
149. R. K. Feeney, School of Electrical Engineering
150. W. M. Stacey, School of Nuclear Engineering
151. E. W. Thomas, School of Physics

University of Illinois, Urbana, IL 61801

152. K. K. Kim, Department of Electrical Engineering
153. G. Miley
154. W. Sutton, Department of Nuclear Engineering

University of Maryland, College Park, MD 20742

155. V. L. Granatstein, Electrical Engineering Department
156. H. R. Griem, Laboratory for Plasma and Fusion Studies
157. C. S. Liu, Department of Physics and Astronomy

Massachusetts Institute of Technology, 77 Massachusetts Ave., Cambridge, MA 02139

158. G. Bekefi, 36-213
159. D. R. Cohn, NW16-140

160. B. Coppi, 26-217
161. J. P. Freidberg, NW16-240
162. I. Hutchinson, NW17-186
163. D. B. Montgomery, NW17-288
164. M. Porkolab, NW16-106B
165. J. Schultz, NW17-225
166. D. Sigmar, NW16-250

Rensselaer Polytechnic Institute, P.O. Box 2000, Troy, NY 12181

167. W. C. Jennings
168. D. Steiner

University of Tennessee, Knoxville, TN 37996

169. I. Alexeff, Department of Electrical Engineering
170. E. G. Harris, Department of Physics
171. J. R. Roth, Department of Electrical Engineering
172. T. E. Shannon, Department of Nuclear Engineering

University of Texas, Austin, TX 78712

173. H. L. Berk, Institute for Fusion Studies
174. D. W. Ross, Department of Physics
175. H. H. Woodson, Department of Electrical Engineering
176. A. J. Wootton, Fusion Research Center

University of Wisconsin, Madison, WI 53706

177. J. D. Callen, Department of Nuclear Engineering
178. J. R. Conrad, Department of Nuclear Engineering
179. G. Kulcinski
180. D. C. Larbalestier
181. S. Prager
182. J. L. Shohet, Torsatron/Stellarator Laboratory
183. J. C. Sprott, Department of Physics

Research School of Physical Sciences, Australian National University, P.O. Box 4, Canberra, A.C.T. 2601, Australia

184. Plasma Research Laboratory

Plasma Research Section, Physics Division, Forskningscenter, Risø, P.O. Box 49, DK-4000 Roskilde, Denmark

185. C. T. Chang
186. V. O. Jensen
187. O. Kofoed-Hansen

JET Joint Undertaking, Abingdon, Oxon OX14 3EA, United Kingdom

188. J. G. Cordey
189. K. J. Dietz
190. D. Düchs
191. A. Gibson
192. L. D. Horton
193. M. Keilhacker
194. J. Jacquinot
195. P. E. Stott
196. E. Thompson
197. Library

UKAEA, Culham Laboratory, Abingdon, Oxon OX14 3DB, United Kingdom

198. R. Hancox
199. T. C. Hender
200. M. Keilhacker
201. Library
202. M. W. Lomer
203. D. C. Robinson
204. D. R. Sweetman
205. J. B. Taylor
206. T. Todd

CEN/Cadarache, B.P. 1, F-13108 Saint-Paul-lez-Durance, France

208. M. Chatelier
209. D. Escande
210. Bibliothèque

CEN/Saclay, B.P. No. 2, F-91191 Gif-sur-Yvette, France

211. H. Desportes, STIPE
212. J. C. Lottin

IPP/KFA Jülich, Postfach 1913, D-5170 Jülich 1, Federal Republic of Germany

212. Bibliothek
213. K.-H. Dippel
214. E. Hintz
215. H. Euringer
216. K.-H. Finken
217. A. Rogister
218. G. Wolf

Forschungszentrum Karlsruhe GmbH, Postfach 3640, D-7500 Karlsruhe 1, Federal Republic of Germany

219. O. Hagena, Nuclear Engineering Institute
220. W. Klose, Division of New Technology and Basic Research
221. P. Komarek, Institute for Technical Physics
222. A. Ulbricht, Institute for Technical Physics
223. J. E. Vetter, Nuclear Fusion Project
224. Bibliothek

Max-Planck Institut für Plasmaphysik, D-8046 Garching, Federal Republic of Germany

225. Bibliothek
226. G. von Gierke
227. G. Grieger
228. J. Junker
229. M. Kaufman
230. A. Knobloch
231. K. Lackner
232. L. L. Lengyel
233. D. Pfirsch
234. K. Pinkau
235. H. Renner
236. A. Schlüter
237. F. Wagner

ENEA Centro di Frascati, C.P. 65, I-00044 Frascati (Roma), Italy

238. R. Andreani, Fusion Department
239. H. E. Knoepfel
240. N. Sacchetti, Technology Division
241. G. Sacerdoti
242. M. Spadoni, Fusion Reactor Engineering Project

International Centre for Theoretical Physics, P.O. Box 586, I-34100 Trieste, Italy

243. A. M. Hamende
244. Library

National Institute for Fusion Science, Chikusa-ku, Nagoya 464-01, Japan

245. M. Fujiwara
246. K. Husimi
247. A. Iiyoshi
248. H. Ikegami
249. S. Okamura
250. Research Information Center
251. T. Uchida
252. Library

Japan Atomic Energy Research Institute, Naka Fusion Research Establishment, Naka-machi, Naka-gun, Ibaraki-ken 311-01, Japan

253. S. Shimamoto
254. K. Tomabechi
255. M. Yoshikawa
256. Library

Plasma Physics Laboratory, Kyoto University, Gokasho, Uji, Kyoto 531, Japan

257. Library
258. M. Wakatani
259. T. Obiki

Plasma Research Center, University of Tsukuba, Sakura-mura, Niihari-gun, Ibaraki Japan

260. Y. Kiwamoto
261. S. Miyoshi

FOM-Instituut voor Plasmafysica, Rijnhuizen, Postbus 1207, NL-3430 BE Nieuwegein, The Netherlands

262. M. J. van der Wiel
263. Library

Division de Fusion Termonuclear, EURATOM/CIEMAT, Avenida Complutense 22, 28040 Madrid, Spain

264. C. Alejaldre
265. C. Hidalgo
266. B. Zurro

Centre de Récherches en Physique des Plasmas, Ecole Polytechnique Fédérale de Lausanne, 21 Avenue des Bains, CH-1007 Lausanne, Switzerland

267. Bibliothèque
268. F. Troyon

Paul Scherrer Institute, CH-5234 Villigen, Switzerland

269. Library
270. G. Vécsey

I. V. Kurchatov Institute of Atomic Energy, P.O. Box 3402, 123182 Moscow, Russia

271. G. A. Eliseev
272. V. D. Shafranov

Institute of General Physics, Russian Academy of Sciences, Ulitsa Vavilova 38, 1779246 Moscow, Russia

273. I. S. Danilkin
274. L. M. Kovrizhnykh
275. I. Shpigel

Kharkov Physico-Technical Institute, Ukranian Academy of Sciences, 310108 Kharkov, Ukraine

276. A. Y. Omelchenko
277. O. S. Pavlichenko

278. R. E. Aamodt, Lodestar Research Corporation, 2400 Central Ave., Boulder, CO 80301
279. E. Anabitarte, Avenida de los Castros s/n, Dpt. Fisica Aplicada, Universidad de Cantabria, 39005 Santander, Spain
280. M. P. G. Avanzini, NIRA S.p.A., C.P. 1166, 16100 Genova, Italy
281. W. Bauer, Dept. 8340, Sandia National Laboratories, P.O. Box 969, Livermore, CA 94550
282. P. R. Bell, 132 Westlook Circle, Oak Ridge, TN 37830
283. K. H. Berkner, B50 Rm 150, Lawrence Berkeley Laboratory, Cyclotron Road, Berkeley, CA 94720
284. R. A. Berry, Varian Associates, Inc., 611 Hansen Way, Palo Alto, CA 94303

285. G. Bohner, Forschungslaboratorien, Siemens AG, Postfach 325, D-8520 Erlangen 2, Federal Republic of Germany
286. R. A. E. Bolton, IREQ Hydro-Quebec Research Institute, 1800 Montée Ste.-Julie, Varennes, P.Q. JOL 2PO Canada
287. M. H. Brennan, Australian Atomic Energy Commission, Lucas Heights Research Laboratories, New Illawara Road, Lucas Heights, Private Mail Bag, Sutherland, N.S.W., Australia 2232
288. G. Briffod, CEN/Grenoble, B.P. 85X, F-38041 Grenoble, France
289. R. N. Cherdack, Burns & Roe, Inc., 700 Kinder Kamack Road, Oradell, NJ 07649
290. E. W. Collings, Battelle Memorial Institute, 505 King Ave., Columbus, OH 43201
291. J. G. Crocker, EG&G Idaho, Inc., Idaho National Engineering Laboratory, Idaho Falls, ID 83401
292. F. L. Culler, Electric Power Research Institute, P.O. Box 10412, Palo Alto, CA 94303
293. S. O. Dean, Fusion Power Associates, Inc., 2 Professional Drive, Suite 248, Gaithersburg, MD 20879
294. H. W. Deckman, Advanced Energy Systems Laboratory, Exxon Research and Engineering Company, P.O. Box 8, Linden, NJ 07306
295. Department of Nuclear Engineering Sciences, 202 Nuclear Science Center, University of Florida, Gainesville, FL 32611
296. Director, Technical Library, Defense Atomic Support Agency, Sandia Base, Albuquerque, NM 87185
297. T. J. Dolan, Department of Nuclear Engineering, University of Missouri, Rolla, MO 65401
298. G. W. Donaldson, School of Electrical Engineering, University of New South Wales, P.O. Box 1, Kensington, N.S.W., Australia
299. D. A. Dreyfus, Gas Research Institute, 1331 Pennsylvania Ave., N.W., Suite 730N, Washington, DC 20004-1703
300. E. Dullni, NB-05/639, Experimentalphysik, Ruhr-Universität Bochum, D-4630 Bochum, Federal Republic of Germany
301. W. G. Ellis, DP-20, U.S. Department of Energy, Washington, DC 20545
302. W. R. Ellis, Ebasco Services, Inc., 2 World Trade Center, New York, NY 10048
303. T. K. Fowler, University of California at Berkeley, Berkeley, CA 92740
304. H. B. Gilbody, Department of Pure and Applied Physics, Queens University, Belfast BT7 1NN, Northern Ireland, United Kingdom
305. R. W. Gould, California Institute of Technology, Building 116-81, Pasadena, CA 91125
306. D. C. Griffin, Rollins College, Winter Park, FL 32789
307. R. A. Gross, Department of Applied Physics & Nuclear Engineering, Columbia University, New York, NY 10027
308. T. G. Heil, Department of Physics and Astronomy, University of Georgia, Athens, GA 30602
309. J. P. Holdren, Energy and Resources Group, Building T-4, Room 100, University of California, Berkeley, Berkeley, CA 94720
310. W. R. Husinsky, Technical University of Vienna, Karlsplatz 13, A-1040 Vienna, Austria
311. S. Ihara, Central Research Laboratory, 8th Department, Hitachi Ltd., Kokubunji, Tokyo 185, Japan

312. M. Iwamoto, Central Research Laboratory, Mitsubishi Electric Corporation, 80 Nakano, Minamishimizu, Amagasaki, Hyogo 661, Japan
313. Japan Atomic Energy Research Institute, 1825 K Street, Washington, DC 20006
314. C. K. Jones, Cryogenic Research Laboratory, Westinghouse Electric Corporation, Research and Development Center, 1310 Beulah Road, Pittsburgh, PA 15235
315. R. W. Jones, Physics Department, Emporia State University, 1200 Commercial, Emporia, KS 66801
316. R. Jones, Department of Physics, National University of Singapore, Bukit Timah Road, Singapore 10.25
317. D. Klein, Westinghouse Electric Corporation, Strategic Operations Division, P.O. Box 598, Pittsburgh, PA 15230
318. A. C. Kolb, Maxwell Laboratories, Inc., 9244 Balboa Avenue, San Diego, CA 92123
319. K. Koyama, Electrotechnical Laboratory, 1-1-4 Umezono, Sakura-mura, Niihari-gun, Ibaraki-ken 305, Japan
320. N. A. Krall, Krall Associates, 1070 America Way, Del Mar, CA 92014
321. A. H. Kritz, LeHigh University, Bethlehem, PA 18015
322. K. Kuroda, Central Research Laboratory, 1-280, Higa Shiko Igakubo, Kokubumji, Tokyo 185, Japan
323. Laboratorio Associado de Plasma, Instituto Nacional de Pesquisas Espaciais, Caixa Postal 515, 122201, Sao Jose dos Campos, SP, Brazil
324. Laboratory for Plasma and Fusion Studies, Department of Nuclear Engineering, Seoul National University, Shinrim-dong, Gwanak-ku, Seoul 151, Korea
325. Laser Fusion Group, Department of Mechanical and Aerospace Science, River Campus Station, University of Rochester, Rochester, NY 14627
326. P. C. Liewer, MS 198-231, Jet Propulsion Laboratory, 4800 Oak Grove Dr., Pasadena, CA 91109
327. C. M. Loring, Varian Associates, Inc., Microwave Tube Division, 611 Hansen Way, Palo Alto, CA 94303-1031
328. V. A. Maroni, CEN 205, Argonne National Laboratory, Argonne, IL 60439
329. A. Maschio, Istituto Gas Ionizzati, Corso Statti Uniti 4, I-35020 Padova, Italy
330. E. A. Mason, Brown University, Providence, RI 02912
331. D. G. McAlees, Advanced Nuclear Fuels Corporation, 600 108th Ave., NE, Bellevue, WA 98009
332. R. L. McCrory, Jr., Laboratory for Laser Energetics, University of Rochester, 250 East River Road, Rochester, NY 14623-1299
333. O. Mitarai, Department of Electrical Engineering, Kumamoto Institute of Technology, Ikeda 4-22-1, Kumamoto 860, Japan
334. F. Moon, Department of Theoretical and Applied Mechanics, Cornell University, Ithaca, NY 14850
335. T. J. Morgan, Physics Department, Wesleyan University, Middletown, CT 06457
336. K. G. Moses, JAYCOR, 2811 Wilshire Boulevard, Suite 690, Santa Monica, CA 90403
337. N. F. Ness, Bartol Research Institute, University of Delaware, Newark, DE 19716
338. C. Oberly, Aero Propulsion Laboratory, Power Distribution Branch, Wright-Patterson Air Force Base, OH 45433

339. T. Ogasawara, Department of Physics, College of Science and Technology, Nihon University, Kanda-Surugadai, Chiyoda-ku, Tokyo 101, Japan
340. H. Ogiwara, Toshiba Research and Development Center, 1 Komukai Tsohiba-cho, Saiwai, Kawasaki, Kanagawa 210, Japan
341. R. J. Onega, Nuclear Engineering Group, College of Engineering, Virginia Polytechnic Institute and State University, Blacksburg, VA 24061
342. B. Outten, Jr., Western Metal Products Company, 1300 Weber Street, Orlando, FL 32803
343. D. Palumbo, via Gabriele d'Annunzio 52, Palermo I-90144, Italy
344. K. Prelec, Brookhaven National Laboratory, Upton, NY 11973
345. F. C. Rock, Plasma Physics Laboratory, Department of Physics and Astronomy, Brigham Young University, Provo, UT 84602
346. R. H. Rohrer, Department of Physics, Emory University, Atlanta, GA 30322
347. M. Rosenbaum, Director, Nuclear Science Institute, Universidad Nacional Autonoma de Mexico, Circuito Exterior, Ciudad Universitaria, Delegación Coyoacán, Apartado Postal 70-360, 04510 Mexico D.F.
348. P. A. Sanger, Airco, 600 Milik St., Carteret, NJ 07008
349. S. St. Lorant, Stanford Linear Accelerator Center, P.O. Box 4349, Stanford, CA 94305
350. M. M. Satterfield, The Nucleus, 761 Emory Valley Road, Oak Ridge, TN 37830
351. Y. Sawada, Heavy Apparatus Engineering Laboratory, Toshiba Corp., 2-4 Suehirocho, Tsurumi-ki, Yokohama 230, Japan
352. J. H. Schneider, Joint Research Centre, Ispra Establishment, I-21020 Ispra (Varese), Italy
353. G. R. Siegel, Tennessee Valley Authority, 25 33A Missionary Ridge Place, Chattanooga, TN 37402
354. P. Staudhammer, Vice President and Director, Center for Automative Technology, TRW, Inc., Bldg. E1, Room 2091, One Space Park, Redondo Beach, CA 90278
355. Z. J. J. Stekly, Magnetics Corporation of America, 47 Hartz St., No. 2, Gloucester, MA 01930
356. U. Stiefel, Eidg. Institut für Reaktorforschung, CH-5301 Wurenlingen, Switzerland
357. K. Tachikawa, Chief, Electric Materials Laboratory, National Research Institute for Metals, 3-12, 2-Chome, Nakameguro, Meguru, Tokyo, Japan
358. R. J. Taylor, Center for Plasma Physics and Fusion Engineering, University of California, Los Angeles, CA 90024
359. D. P. Tewari, Department of Physics, Indian Institute of Technology, New Delhi 110016, India
360. M. Thumm, Institut fur Plasmaforschung, Pfaffenwaldring 31, D-7000 Stuttgart 80, Federal Republic of Germany
361. J. F. Traexler, Westinghouse Electric Corp., Quadrangle 2WII-203, Orlando, FL 32817
362. G. Vahala, Department of Physics, College of William and Mary, Williamsburg, VA 23185
363. T. C. Varljen, Westinghouse Hanford, P.O. Box 1970, Richland, WA 99352
364. R. Varma, Physical Research Laboratory, Navrangpura, Ahmedabad 380009, India
365. C. Walters, Technology Division, Building R25, Rutherford Laboratory, Chilton, Didcot, Oxon OX11 OQX, United Kingdom
366. C. N. Watson-Munro, University of Sydney, Wills Plasma Project, Sydney, N.S.W., Australia

367. H. Weitzner, Courant Institute for Mathematical Sciences, New York University, 251 Mercer St., New York, NY 10012
368. J. T. Woo, Interscience, 105 Jordan Road, Troy, NY 12180
369. S. B. Woo, Department of Physics, University of Delaware, Newark, DE 19711
370. H. Yoshikawa, Manager, Materials Engineering, Hanford Engineering Development Laboratory, P.O. Box 1970, Richland, WA 99352
371. V. A. Glukhikh, Scientific-Research Institute of Electro-Physical Apparatus, 188631 St. Petersburg, Russia
372. D. D. Ryutov, Institute of Nuclear Physics, Siberian Branch of the Academy of Sciences, Sovetskaya St. 5, 630090 Novosibirsk, Russia
373. Deputy Director, Southwestern Institute of Physics, P.O. Box 15, Leshan, Sichuan, China (PRC)
374. Library, The Institute of Plasma Physics, Academia Sinica, P.O. Box 1126, Hefei, Anhui, China (PRC)
375. M.-L. Xue, Institute of Mechanics, Academia Sinica, Beijing, China (PRC)
376. Office of Assistant Manager for Energy Research and Development, U.S. Department of Energy, Oak Ridge Operations Office, P.O. Box 2001, Oak Ridge, TN 37831-8705
377–390. Given distribution as shown in DOE/OSTI-4500/R75, Energy Research (Category UC-420, Magnetic Fusion Energy) (13 copies)

*U.S. GOVERNMENT PRINTING OFFICE: 1995-650-187/20001